Lawrence Livermore National Laboratory

Laboratory Directed Research and Development

FY2002 Annual Report

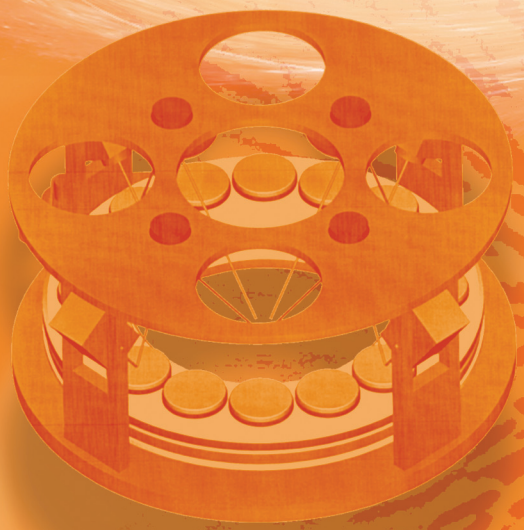

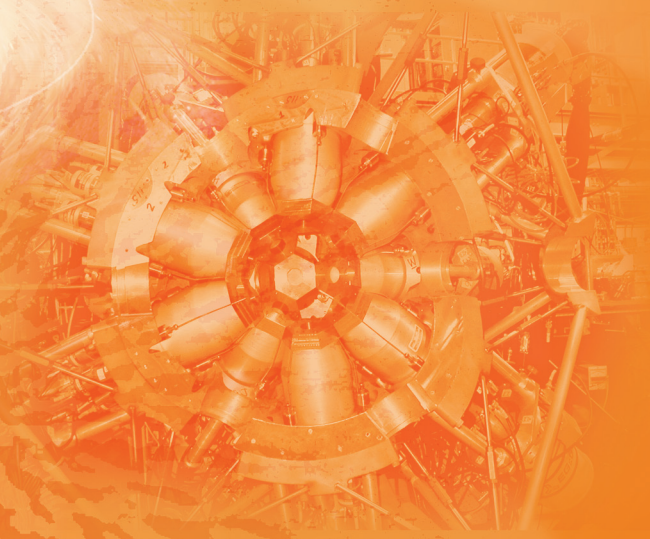

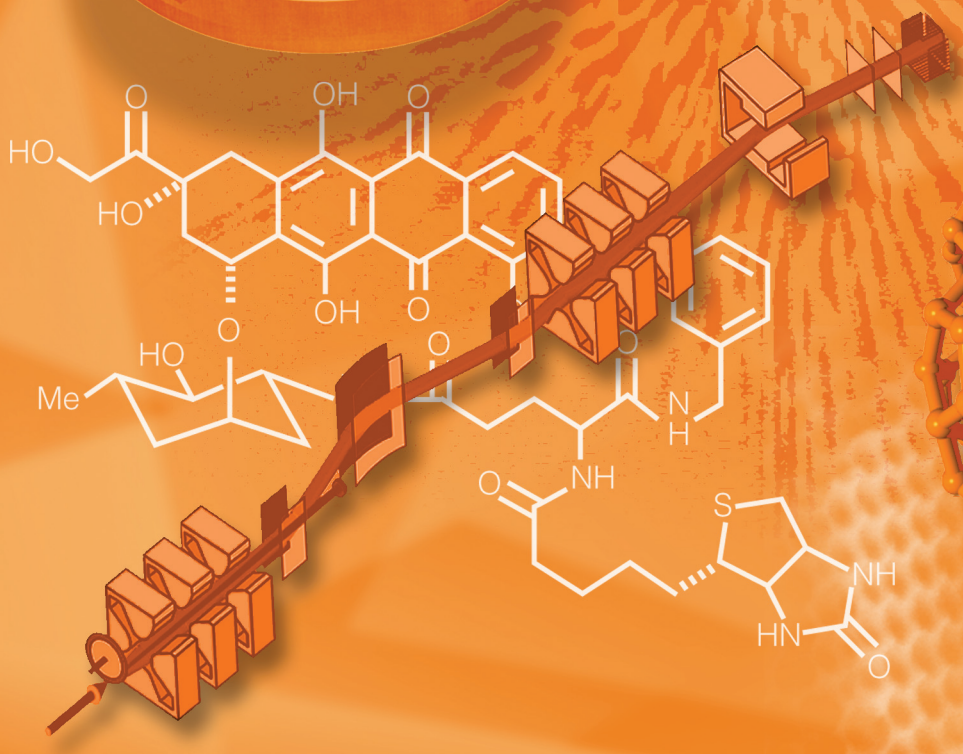

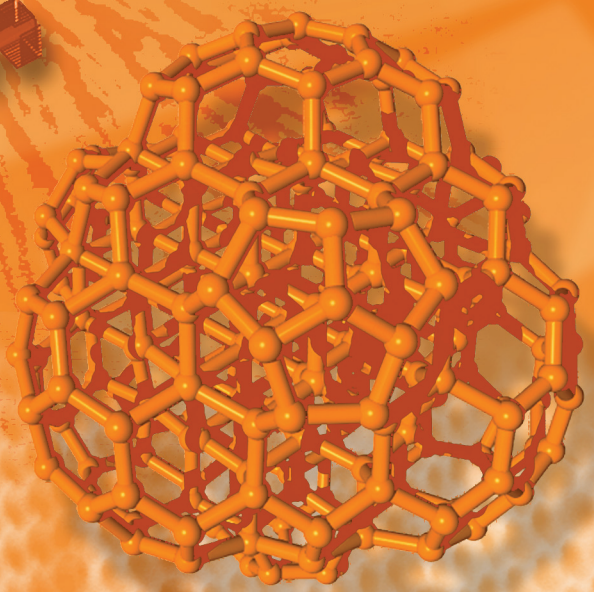

This work was performed under the auspices of the U.S. Department of Energy by University of California Lawrence Livermore National Laboratory under contract No. W-7405-Eng-48.

Lawrence Livermore National Laboratory

Laboratory Directed Research and Development

FY2002 Annual Report

UCRL-LR-113717-02

Acknowledgments

This Annual Report provides an overview of the FY2002 Laboratory Directed Research and Development (LDRD) Program at Lawrence Livermore National Laboratory (LLNL) and presents a summary of the results achieved by each LDRD project. At LLNL, Laboratory Director Michael Anastasio and Deputy Director for Science and Technology Harold Graboske are responsible for the LDRD Program and delegate responsibility for the operation of the Program to the Associate Deputy Director for Science and Technology and the Director of the Laboratory Science and Technology Office (LSTO), Rokaya Al-Ayat. The LDRD Program at LLNL is in compliance with Department of Energy (DOE) Order 413.2 and other relevant DOE orders and guidelines.

The LDRD Program extends its sincere appreciation to the principal investigators of the FY2002 projects for providing the content of the Annual Report and to the publications team. For their technical review, a special thanks goes to Craig Smith and to Kenneth Jackson and Karl van Bibber of the LSTO staff. The Program also thanks the following members of the LSTO team for their many contributions to this publication: Carol Booth, administrative specialist; Mary Callesen, administrator; Nancy Campos, database administrator; and Cathleen Sayre, resource manager.

Scientific Editor

Rokaya Al-Ayat

Publication Editor

Karen Kline

Publication Designer

Daniel Moore

Publication Staff

Paul Kotta, editor
Steven Knecht, designer

Credits

p. 8. Heller, A. " A giant leap for space telescopes." *LLNL Science & Technology Review*. March 2003. UCRL-5200-03-3.

Contents

Section 2 Biological Sciences

Section 3 Chemistry

Section 4 Earth and Space Science

Section 5 Energy Supply and Use

Section 6 Engineering and Manufacturing Processes

Section 7 Materials Science and Technology

Section 8 Mathematics and Computing Sciences

Section 9 Nuclear Science and Engineering

Section 10

Appendix

Director's Statement

Michael R. Anastasio, Director

The Laboratory Directed Research and Development (LDRD) Program, authorized by Congress in 1991 and administered by the Laboratory Science and Technology Office, is our primary means for pursuing innovative, long-term, high-risk, and potentially high-payoff research that supports the Laboratory's and the Department of Energy and National Nuclear Security Administration's missions in national security, energy security, environmental management, bioscience and technology to improve human health, and breakthroughs in fundamental science and technology. The accomplishments described in this *Annual Report* demonstrate the strong alignment of the LDRD portfolio with these missions and contribute to the Laboratory's success in meeting our goals.

The LDRD budget of $62.8 million for Fiscal Year 2002 sponsored over 200 projects. These projects were selected through an extensive peer-review process to ensure the highest scientific quality and mission relevance. Each year, the number of deserving proposals far exceeds the funding available, making the selection a tough one indeed.

Our ongoing investments in LDRD have reaped long-term rewards for the Laboratory and the Nation. Many Laboratory programs trace their roots to research thrusts that began several years ago under LDRD sponsorship. Recent events underscore the importance of LDRD investments to national security. For example, most of the counterterrorism technologies fielded by the Laboratory after September 11, 2001 began as LDRD-funded projects. In addition, many LDRD projects contribute to more than one mission area, leveraging the Laboratory's multidisciplinary team approach to science and technology.

The LDRD Program is a success story. Our projects continue to win national recognition for excellence through prestigious awards, papers published in peer-reviewed journals, and patents granted. With its reputation for sponsoring innovative projects, the LDRD Program is also a major vehicle for attracting and retaining the best and the brightest technical staff and for establishing collaborations with universities, industry, and other scientific and research institutions.

By keeping the Laboratory at the forefront of science and technology, the LDRD Program enables us to meet our mission challenges, especially those of our ever-evolving national-security mission.

Overview

About the FY2002 Laboratory Directed Research and Development Annual Report

The *FY2002 Laboratory Directed Research and Development (LDRD) Annual Report* provides a summary of LDRD-funded projects for the fiscal year and consists of three parts:

Overview: An introduction to the LDRD Program and the LDRD portfolio-management process, as well as highlights of the FY2002 LDRD portfolio and recent Program accomplishments.

Project Summaries: A one-page article, submitted by the principal investigator, for each project in the FY2002 portfolio. Articles summarize the project scope, motivation, goals, relevance to Department of Energy/National Nuclear Security Administration and Lawrence Livermore National Laboratory mission areas, and the progress achieved in FY2002. Articles are arranged in sections by research category (in alphabetical order). Within each section, articles are organized by project category—Strategic Initiative (SI), Exploratory Research (ER), Laboratory-Wide Competition (LW), and Feasibility Study (FS). Within each category, the projects are listed in order of their project tracking code, a unique identifier that consists of three elements. The first element is the fiscal year the project began, the second element is the LDRD project category, and the third element identifies the serial number of the proposal for the fiscal year. For example:

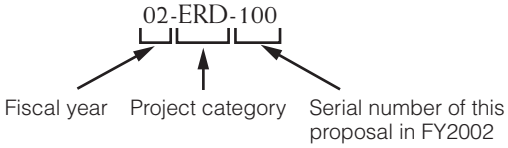

Appendix: A compilation of LDRD-research-generated publications, a principal-investigator index, a project-title index, and an index of projects by tracking code.

Introduction

Laboratory Directed Research and Development Program

Established by Congress in 1991 at Lawrence Livermore National Laboratory (LLNL) and all the Department of Energy (DOE) national laboratories, the Laboratory Directed Research and Development (LDRD) Program provides the Laboratory with the flexibility to invest in long-term, high-risk, and potentially high-payoff research and development (R&D) activities that support the DOE and National Nuclear Security Administration's (NNSA's) evolving national-security missions. By funding innovative R&D at up to 6% of the total Laboratory budget, the LDRD Program develops and extends the Laboratory's intellectual foundations and maintains its vitality as a premier research institution. As proof of the Program's success, many of the research thrusts that started ten years ago under LDRD sponsorship are at the core of today's programs.

The LDRD Program, which serves as a proving ground for innovative ideas, is the Laboratory's most important single resource for fostering excellent science and technology for today's needs and tomorrow's challenges. Basic and applied research activities funded by LDRD enhance the Laboratory's scientific strength, driving its technical vitality and creating new capabilities to meet DOE/NNSA and national-security needs. The Program also plays a key role in building a world-class multidisciplinary workforce by engaging the Laboratory's best researchers, recruiting its future scientists and engineers, and promoting collaborations with all sectors of the larger scientific community.

The LDRD Portfolio Management Process

The LDRD management process at LLNL has four major components that ensure the quality of the year's portfolio: (1) a top-level strategic planning process to identify strategic science and technology areas for LDRD investment, (2) a call to the Laboratory scientific and technical community for innovative and relevant proposals within the NNSA mission areas, (3) a scientific peer-review process to select an LDRD portfolio from these proposals, and (4) rigorous technical and financial management.

The NNSA oversees LLNL's LDRD Program to ensure that it accomplishes its objectives. This oversight includes field and headquarters reviews of both technical content and management processes. In an independent FY2001 report to Congress,[1] the General Accounting Office stated,

> All the LDRD projects we reviewed at the…laboratories we visited met DOE's guidelines for selection [and] had created the internal controls necessary to reasonably ensure compliance with DOE's guidelines. The key controls in place included using DOE's guidelines to control and conduct the project-selection process…and ensuring appropriate DOE oversight and review of the results of the process.

About Lawrence Livermore National Laboratory

A premier applied-science laboratory, Lawrence Livermore National Laboratory (LLNL or the Laboratory) has at its core a primary national-security mission—to ensure the safety, security, and reliability of the nation's nuclear weapons stockpile without underground nuclear testing and to prevent and counter the spread and use of weapons of mass destruction: nuclear, chemical, and biological.

The Laboratory uses the scientific and engineering expertise and facilities developed for its primary mission to pursue advanced technologies for other important national-security needs—homeland defense, military operations, and missile defense, for example—that evolve in response to emerging threats. In terms of broader national needs, the Laboratory executes programs in energy security and long-term energy needs, environmental assessment and management, bioscience and technology to improve human health, and breakthroughs in fundamental science and technology. With this multidisciplinary expertise, the Laboratory serves as a science and technology resource to the U. S. government and as a partner with industry and academia.

One of three Department of Energy (DOE) National Nuclear Security Administration (NNSA) laboratories, LLNL has been managed since its inception in 1952 by the University of California (UC). This half-century association with UC has enabled the Laboratory to establish an atmosphere of intellectual freedom and innovation that attracts and maintains the world-class workforce needed to meet challenging national missions.

[1] U.S. General Accounting Office. (2001). *Report to Congressional requesters: National Laboratories oversight of Laboratory Directed R&D Program.* (OUO). GAO-01-927. p. 3.

Structure of the LDRD Program

Project Categories

The LDRD Program at LLNL consists of three major project categories: Strategic Initiative (SI), Exploratory Research (ER), and Laboratory-Wide (LW) Competition. Throughout the year, the Program also funds a few projects in a fourth category, Feasibility Studies/Project Definition (FS).

Strategic Initiative

The SI category focuses on innovative R&D activities that are likely to set new directions for existing programs, help develop new programmatic areas within LLNL's mission responsibilities, or enhance the Laboratory's science and technology base. Projects in this category are usually larger and more technically challenging than projects funded in other categories. An SI project must be aligned with the strategic R&D priorities of at least one of the four Laboratory Strategic Councils: (1) the Council on Bioscience and Biotechnology, (2) the Council on Energy and Environmental Systems, (3) the Council on National Security, and (4) the Council on Strategic Science and Technology.

Exploratory Research

The ER category is aligned with the strategic R&D needs of a Laboratory Directorate (ERD) or Institute (ERI). Typically, fewer than half of the proposals that researchers submit to their Directorates and Institutes are forwarded to the ER selection committee for review.

Laboratory-Wide Competition

Projects in the LW category emphasize innovative research concepts and ideas and undergo limited management filtering. The LW competition is open to all LLNL staff in programmatic, scientific, engineering, and technical-support areas. Researchers submit their project proposals directly to the LW selection committee. The number of projects selected in this category ranges from one-third to one-fifth of those submitted.

Feasibility Studies/Project Definition

This special project category, FS, provides researchers with the flexibility to define and develop potential projects in the other three categories. To increase its responsiveness to Laboratory scientists and engineers, the LDRD Program funds FSs throughout the year. Individual FSs are limited to a maximum duration of 12 months and a budget not to exceed $75K.

Project Categories

Although LDRD projects often address more than one scientific discipline, each project is classified into one of ten research categories that are relevant to NNSA and Laboratory missions. The ten categories are:

- Advanced Sensors and Instrumentation
- Biological Sciences
- Chemistry
- Earth and Space Sciences
- Energy Supply and Use
- Engineering and Manufacturing Processes
- Materials Science and Technology
- Mathematics and Computing Sciences
- Nuclear Science and Engineering
- Physics

The FY2002 LDRD Portfolio

Investing in the future of national security

Portfolio Structure

The FY2002 LDRD portfolio was carefully structured to continue the Program's vigorous support for the strategic vision and long-term goals of NNSA and LLNL. The FY2002 projects described in this Annual Report have undergone a stringent selection process and ongoing management oversight.

In FY2002 the Program funded 205 projects. Figure 1 shows the number of projects in each of the four categories.

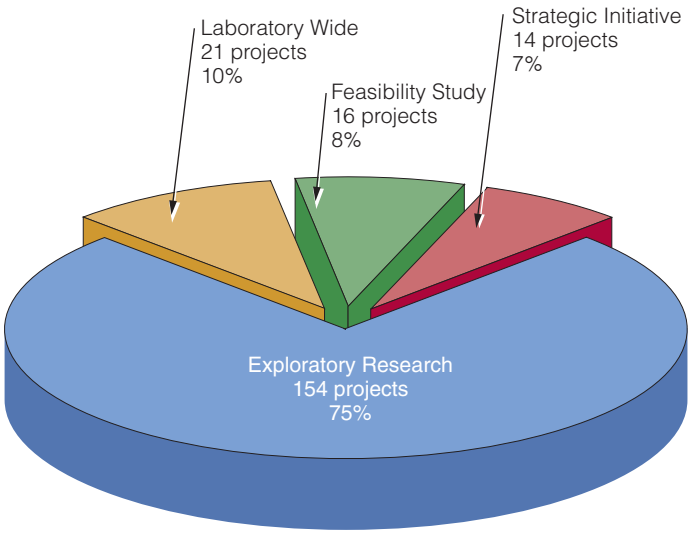

Figure 1. Number and percentage of LDRD projects in each project category in FY2002.

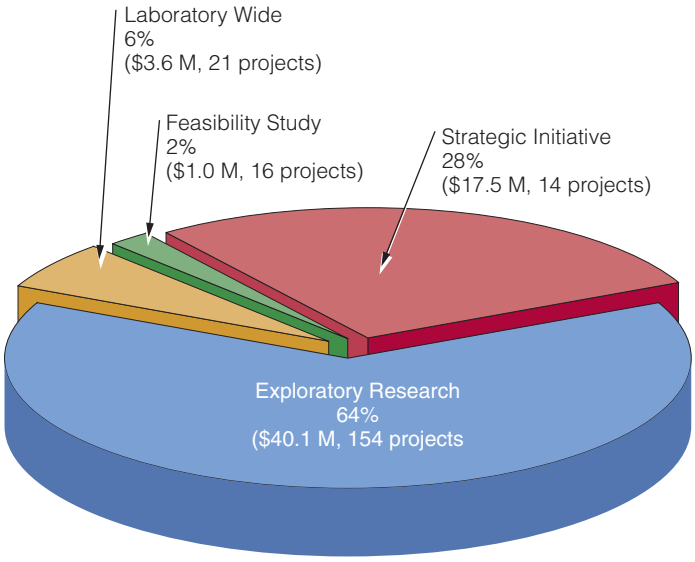

Figure 2. Distribution of funding (in $ million) among the four LDRD project categories. Total funding for FY2002 was $62.8M.

Strategic Initiative

The LDRD Program funded 14 SI projects in FY2002. The SI category represents 7% of the total number of LDRD projects for FY2002. Projects in this category range from research in computational biology to earth and space science.

Exploratory Research

In FY2002, 154 ER projects were funded. The largest project category, ERs account for 75% of LDRD projects for the fiscal year. Examples of projects in this category include global and climate simulations, research on remote detection of bioaerosols, and ultrafast production of highly stable nanostructures on semiconductors.

Laboratory-Wide Competition

Twenty-one LW projects were funded in FY2002, which represents 10% of LDRD projects for the year. Projects in this category range from applying adaptive optics to extend the range of human visual acuity to x-ray lasers to probe the properties of high-density plasmas.

Feasibility Study

In FY2002, the Program funded 16 FS projects, or 8% of the projects for the year.

Portfolio Funding

In FY2002, the DOE authorized the LDRD Program to fund $62.8M for projects: approximately 64% was allocated for ERs, 28% for SIs, 6% for LWs and 2% for FSs. Figure 2 shows the distribution of funding among the four LDRD project categories.

Projects vary in size, with 31 projects receiving less than $100K and 9 receiving more than $1M. The average funding for an LDRD project in FY2002 was $306K. Figure 3 shows the number of projects in various levels of funding.

Figure 4 shows the percentage of Program funding that each competency area received in FY2001. Consistent with the Laboratory's strategic needs, Physics projects received the most funding, 21%, and account for the largest number of projects, 46, while Nuclear Science and Engineering received about 2% of the funding for 5 projects. Figure 4 shows that the Laboratory has invested its FY2002 LDRD funds in research categories that are essential to its future strategic needs. This investment strategy enables the Laboratory to meet its special responsibility for nuclear weapons research, including advanced simulation and computing, the prevention and counterproliferation of weapons of mass destruction, homeland security, international security, arms control, and energy and environmental management.

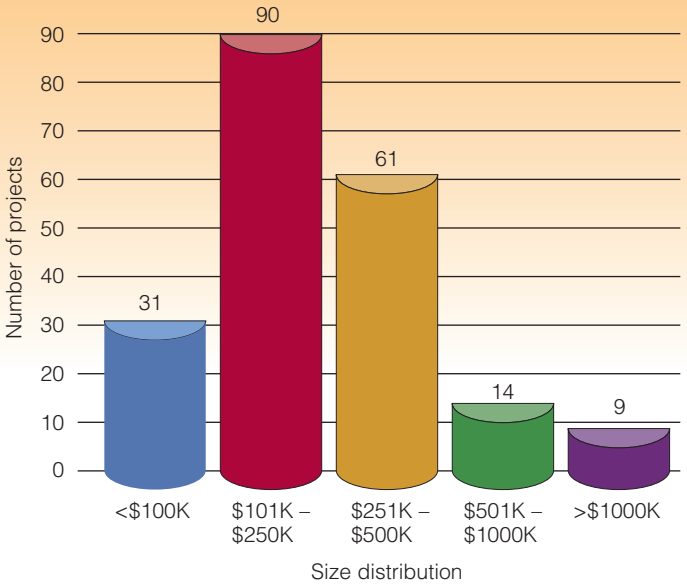

Figure 3. Number of projects and levels of funding (in $ thousand). The average funding level for an LDRD project in FY2002 was $306K.

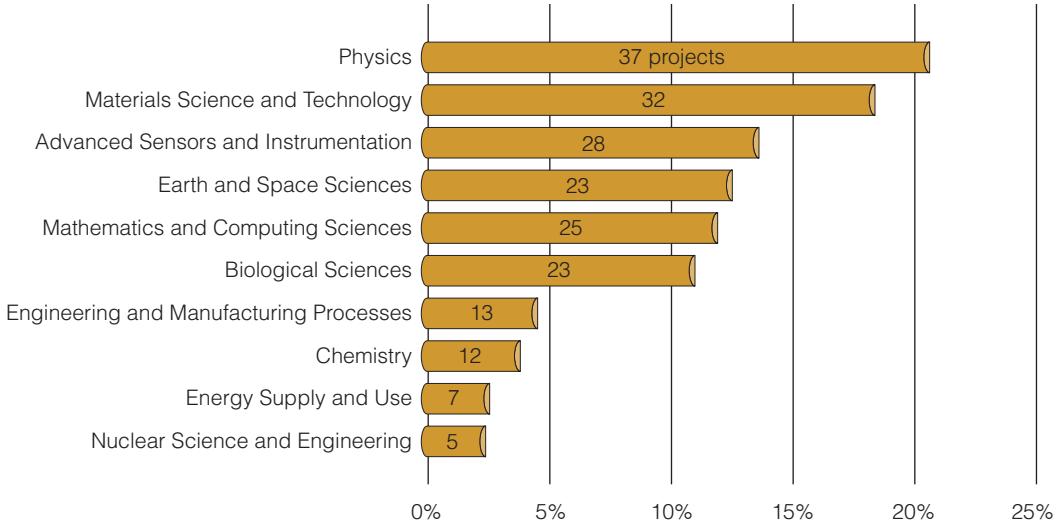

Figure 4. Percentage of LDRD funding and number of projects in each research category in FY2002.

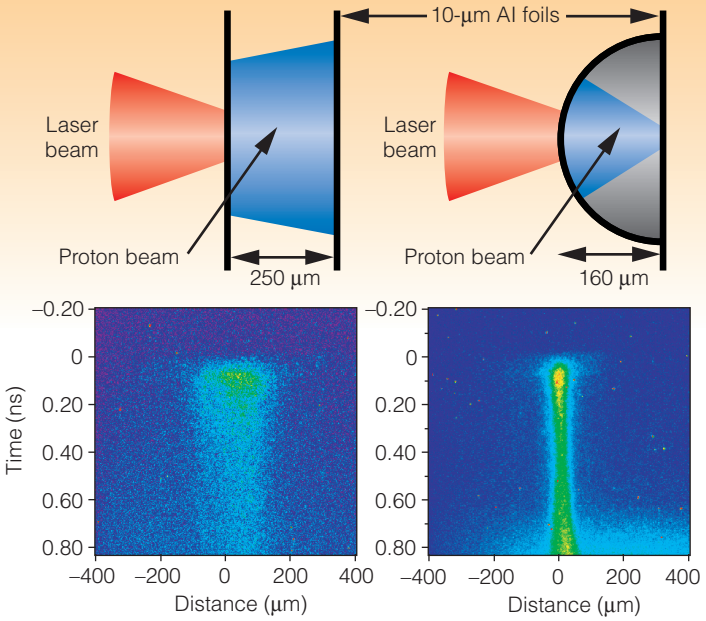

02-SI-004

Portfolio Highlights

Six FY2002 projects—two projects each from the SI, ER, and LW categories—highlight the diverse scope of LDRD research. These projects demonstrate the Program's emphasis on science and technology R&D to meet the evolving needs of the NNSA's national-security mission.

Strategic Initiative

Short pulse: An initiative to enable relativistic applications for advanced inertial confinement fusion and stockpile stewardship

M. Key, Principal Investigator (02-SI-004, p. 10–2)

This project aims to develop technologies to generate high-energy petawatt (HEPW) laser pulses of 5 kJ energy and 5 ps pulse duration. Such lasers will be able to heat solid-state media to extreme temperatures and densities needed for research in the Stockpile Stewardship Program (SSP), inertial-fusion-energy science, and laboratory-based astrophysics. These lasers will also extend the scope of radiographic measurements used in SSP experiments at the National Ignition Facility.

Work in FY2002 included research and development in HEPW-enabling technologies, short-pulse optical-damage studies, and evaluation of HEPW science opportunities. Significant breakthroughs include developing damage-resistant diffraction gratings for multikilojoule-pulse compressors; conducting preliminary damage tests to verify initial models for short-pulse damage; inventing a new, folded-compressor design that reduces overall compressor dimensions by 50%; and demonstrating—at LLNL's Janus ultrashort-pulse laser facility—the first ballistic focusing and isochoric heating by laser-generated protons.

In FY2003, the project will research technologies for scaling HEPW components to the meter-scale dimensions required to support multikilojoule pulses, develop new broadband seed-pulse technologies, and continue to evaluate advanced radiographic and dense-plasma applications of HEPW pulses.

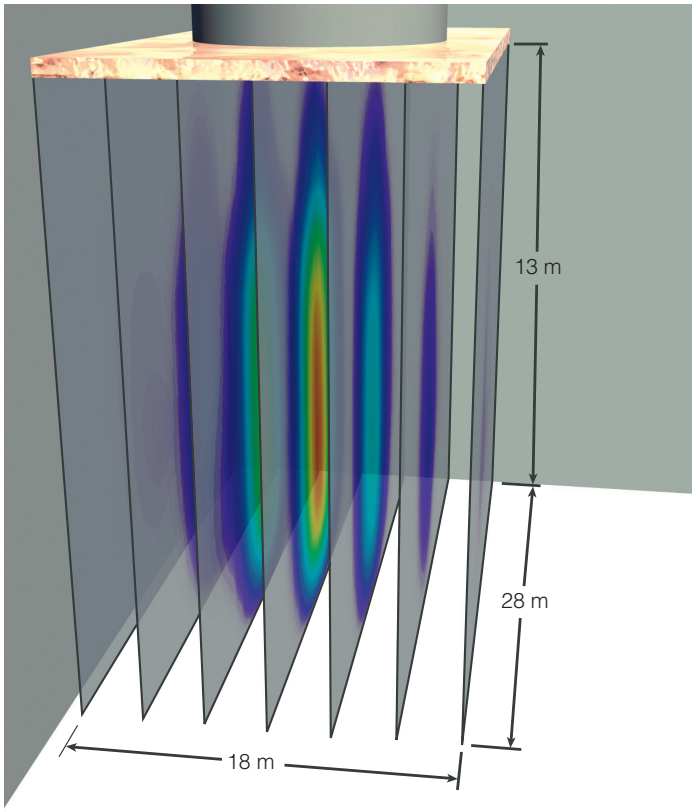

01-SI-003

The stochastic engine: Improved accuracy in predicting the behavior of unobservable features in geologic environments

R. Aines, Principal Investigator (01-SI-003, p. 8–2)

Computer simulations must often rely on sparse data to investigate complex issues, such as determining the underground movement of contamination and analyzing diverse intelligence data. In this project, we are developing a combination of probabilistic and deterministic approaches—called the "stochastic engine"—that uses all available data in these problems by integrating accurate simulators with a probabilistic method that accounts for error in data and models. The root technology is importance-based Monte Carlo sampling, which rapidly chooses among a very large number of hypothesized system states.

This methodology allows decision makers to weigh various courses of action, and will find applications in LLNL's environmental-restoration, antiterrorism, nonproliferation, and stockpile-stewardship programs.

In FY2002, we produced three-dimensional probabilistic imaging of an experimental leak at a test facility using tomography data with pressure- and moisture-sensor data. In FY2003, this concept will be used to find the location of underground facilities and tunnels. Demonstrations will be conducted that apply the stochastic engine to intelligence-data interpretation and structural-flaw analysis of complex mechanical devices.

Exploratory Research

Designer diamond anvils for novel, high-pressure experiments: Magnetic susceptibility experiments on actinides to multimegabar pressures

S. T. Weir, Principal Investigator (01-ERD-036, p. 7–12)

A better understanding of complex electron–electron interactions in magnetic materials is important for developing better models of magnetic materials and materials with strong electron-correlation effects (e.g., actinides).

This project is performing ultrahigh-pressure magnetic-susceptibility experiments to provide a strong foundation for developing better actinide equations-of-state and high-pressure phase diagrams for stockpile stewardship.

To perform high-sensitivity magnetic experiments to ultrahigh static pressures, the project team is using specially fabricated diamond anvils with diamond-encapsulated, thin-film metal microcircuits. The magnetic properties of the sample are measured under these conditions using a diamond-encapsulated 5-turn microcoil. The proximity—just a few micrometers—of this magnetic sensing loop to the high-pressure sample enables extremely high signal sensitivities with very low background levels.

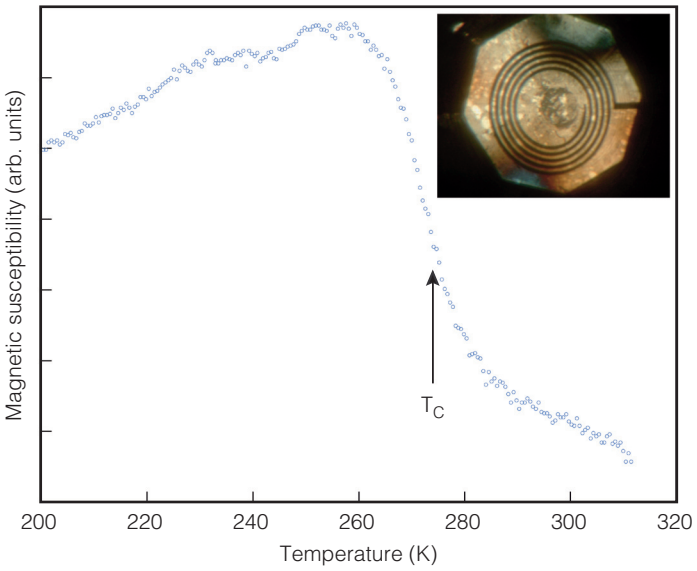

01-ERD-036

During FY2002, the team performed high-pressure (16 kbar) magnetic-susceptibility experiments on gadolinium, observing its transition to a ferromagnetic state when cooled below about 275 K. Next year, the team plans to start experiments on the actinide elements, including uranium and plutonium, to characterize their magnetic behaviors over a wide range of pressures and temperatures.

Disposable polymerase chain reaction device

E. Wheeler, Principal Investigator (01-ERD-009, p. 1–6)

The anthrax scare that followed the September 11, 2001 terrorist attack demonstrated the threat posed by biological weapons. To take appropriate action, first responders to a biological attack must identify the specific organism used in the release. Polymerase chain reaction (PCR) assays enable pathogen identification by amplifying a target segment of the pathogen's DNA. However, these sophisticated tools are both expensive and require highly trained individuals to operate them.

The goal of this project is to design and demonstrate a compact, low-cost, easy-to-use PCR device based on a convective thermal cycler. The device will allow first responders to quickly identify the nature and extent of an attack. This project leverages LLNL's competencies in microtechnology and instrumentation and supports LLNL's homeland security mission.

During FY2002 the project team used the thermal cycler to successfully amplify a 90-base-pair segment of a DNA plasmid—one of the first times DNA amplification has been accomplished using convective forces. Work also began to design a sample-preparation system based on a pillar chip, which captures DNA on silica pillars.

In FY2003, the team will continue optimization of the cycler and begin incorporating all components into an integrated, easy-to-use, low-power, robust PCR device for first responders.

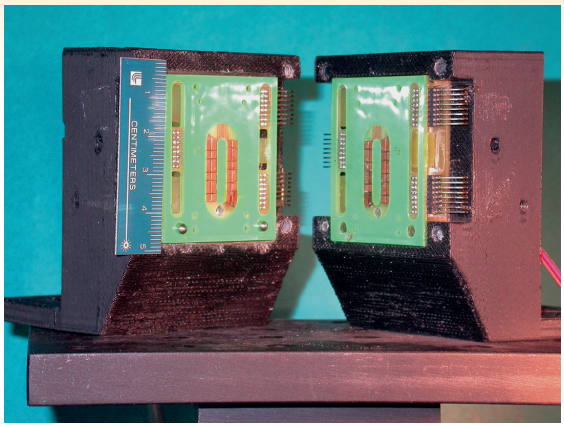

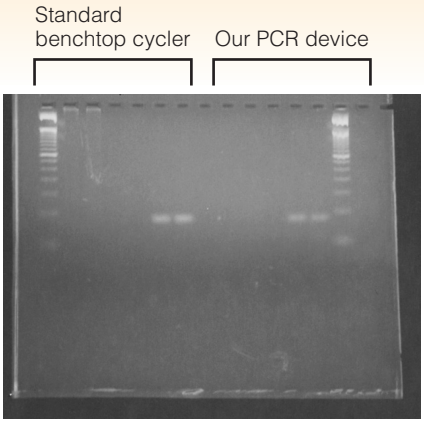

01-ERD-009

Laboratory-Wide Competition

Diffraction-limited adaptive optics and the limits of human visual acuity

S. Olivier, Principal Investigator (01-LW-036, p. 1–20)

Visual acuity of the normal human eye is limited by significant high-order optical aberrations that cannot be corrected by standard corrective eyewear. Adaptive optics (AO), a technology used in astronomy to correct for image blurring arising from atmospheric turbulence, can compensate for these aberrations and provide normal eyes with supernormal vision.

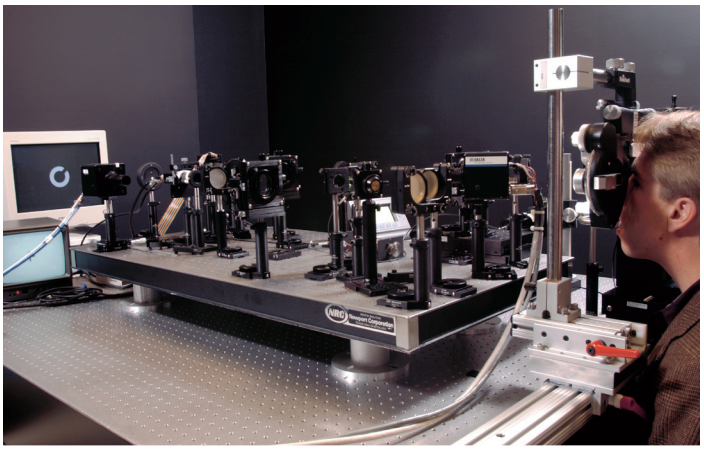

01-LW-036

This project has designed and constructed an AO system for human vision correction using new, liquid-crystal, spatial light modulator technology. The system senses and corrects the aberrations present in the human eye.

This work will advance next-generation corrective eyewear and surgical procedures and will also have direct application in developing (1) supernormal vision capabilities that support the Laboratory's national-security mission, and (2) advanced clinical ophthalmic instrumentation for diagnosing and treating diseases that cause human blindness.

In FY2002, initial experiments on human subjects were performed, and the results were analyzed to optimize the system for correcting aberrations in the human eye. In FY2003, this completed system will be used to perform initial clinical trials of human visual acuity improved by correcting the subjects' ocular aberrations.

Origami in Orbit—Foldable Space Optics

Sending telescopes into space, thus liberating them from the constraints of earthbound observation like bad weather and pollution, brings the promise of astounding new knowledge of our own Solar System, the cores of distant galaxies, and edges of the universe. The National Aeronautics and Space Administration (NASA) has announced plans to field a progression of giant space telescopes, with apertures of 25 m and more, over the next two decades. But the challenges of designing large-aperture space optics that are both optically precise and can meet the size and weight requirements practical for launch and deployment are formidable.

Livermore physicist Rod Hyde heads a team that has developed a radically new concept to overcome the difficulties inherent in building and fielding a high-quality space telescope far larger than ever deployed. The concept, called Eyeglass, uses diffractive optics instead of mirrors or conventional glass lenses. Diffractive optics, also called Fresnel lenses, are flat on one side and ridged on the other with a series of concentric grooves that are etched into a thin sheet of glass, silica, or plastic to bend and focus light. The design for Eyeglass, inspired by origami, the ancient Japanese art of paper folding, allows a large lens to be made up of individual thin-glass panels about 30-nm thick. Lithographic surface patterning and high-precision assembly make each panel act as a segment of the overall diffractive lens. The panels are seamed together with flexible joints so that the lens can be folded into a neat package that fits into a space launch vehicle.

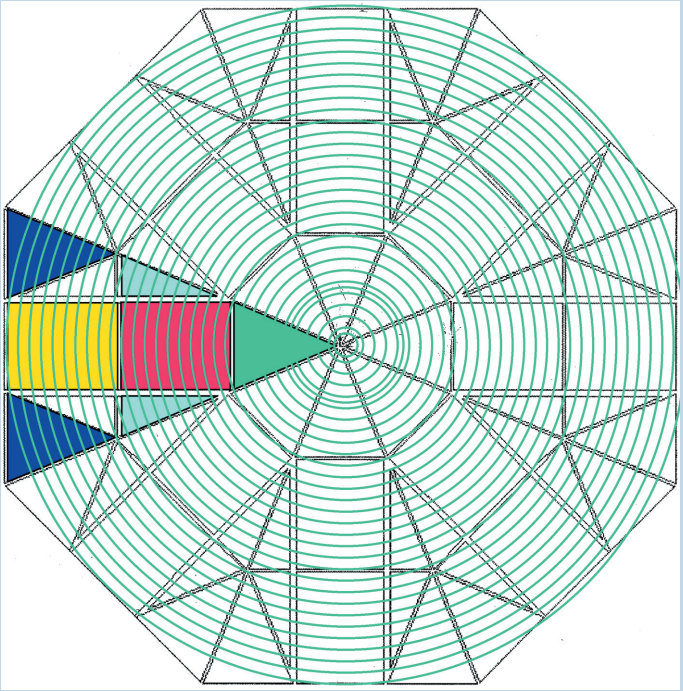

The final 5-m lens is composed of 72 segments: 16 rectangles, 32 right triangles, and 24 isosceles triangles. The segments are grouped into eight "petals," each covering 45 ° or one-eighth of the complete lens. One of the petals is highlighted. The concentric circular lines suggest some of the 19,105 circular etched grooves that focus the light.

In FY2002, under LDRD funding (see article on p. 4–1) and with support from federal agencies, the team built and tested the largest optical-quality lens in the world—a 5-m diffractive Eyeglass lens assembled from 72 thin-glass panels. The lightweight, foldable high-resolution lens, twice the diameter of the primary mirror for the Hubble Space Telescope yet 10 times lighter, could be deployed in space for surveillance and scientific uses within two to three years, says Hyde.

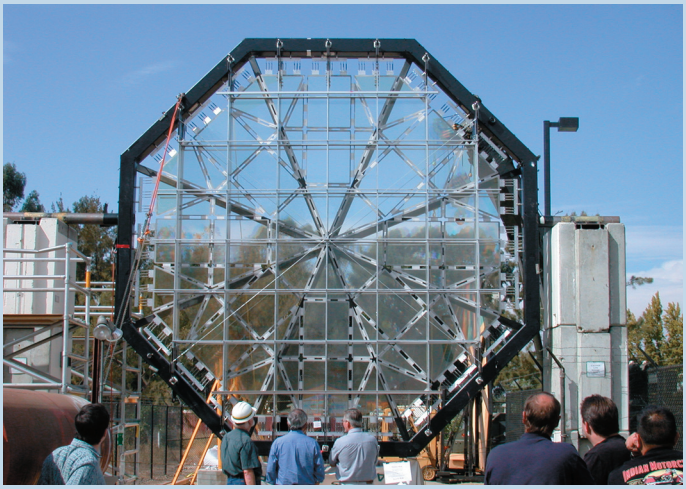

The 5-m lens mounted in a frame and ready for optical testing.

Single-molecule techniques for advanced in situ hybridization
C. Hollars, Principal Investigator (01-LW-062, p. 1–22)

Researchers have only just begun to understand the relationships between the human genome and gene and protein expression in the body's millions of highly specialized cells. Analysis of gene and protein expression in situ has been progressing at an extremely slow pace because current methods, which rely on catalytic chemical amplification to raise the selected signal above the background autofluorescence, can evaluate only a few expression points per tissue sample.

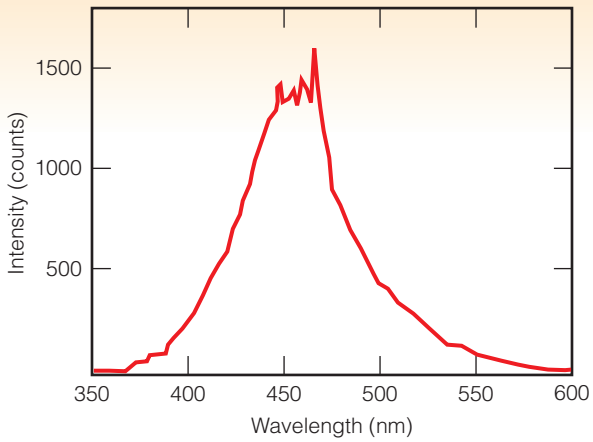

01-LW-062

In FY2002, this project used new optical techniques and instrumentation with single-target sensitivity to detect low levels of gene-probe response in situ, without the need for amplification. These advancements will enable precise, simultaneous localization of the expression points of multiple genes or proteins in a cell, which is crucial to discovering new pharmacological agents for treating disease.

Work in FY2002 focused on developing a plasmon-resonant particle (PRP) fabrication protocol based on a gold-seeding and silver-enhancement procedure. To determine particle size and shape, the project team constructed a system combining atomic-force microscopy with measured spectral response. In situ PRP hybridization experiments conducted on the Peg3 gene showed promise for refining the fabrication protocol.

Recent LDRD Program Accomplishments

Over the years, LDRD-sponsored projects have realized major scientific and technical breakthroughs that have been widely reported in the scientific community. Highlighted here are a few of the achievements of recent LDRD projects.

Patents

The table below shows the number of patents resulting from LDRD-funded research since 1996. Projects sponsored by LDRD consistently account for a large percentage of the patents issued for LLNL research, especially considering that the LDRD Program funding represents 6% of the total LLNL budget, with the exception of FY2000, when the Program received only 4% of the budget.

	1996	1997	1998	1999	2000	2001	2002
Total LLNL patents	83	64	78	84	93	89	97
LDRD patents	35	29	39	45	35	42	27
LDRD patents as percentage of total	42	45	50	54	38	47	28

Awards

R&D 100 Awards

In 2002, LLNL won six R&D 100 awards. Of these, two awards were earned for innovative technologies developed through LDRD-funded research.

Solid-State Heat Capacity Laser

The Solid-State Heat Capacity Laser can produce up to 13,000 W in a single, high-quality beam with output-pulse energies of more than 600 J, making it the most powerful solid-state laser in the world. The system's solid-state heat-capacity design paves the way for a laser, now under development, that will produce 100,000 W in a single beam and opens up a range of applications for industrial materials processing and military defense.

Silicon Monolithic Microchannel (SiMM) Cooled Laser Diode Array

A silicon monolithic microchannel (SiMM) cooling system makes possible the smallest, most powerful, and least expensive laser-diode pumps ever. On each SiMM, a tiny package of ten diode bars can be combined with as many microlenses—which collimate the laser light—to create a unit from which large diode arrays can be built. The microlenses attached to each package, developed and patented by Livermore scientists, give unsurpassed optical brightness. These powerful arrays measure only 10 × 18 cm but can produce 45 kW of power. From delicate surgical procedures to cutting and welding metals, diode-pumped solid-state lasers offer a wealth of applications.

LLNL FY2002 Science and Technology Awards

Both of LLNL's FY2002 Science and Technology Awards went to teams whose research was conducted with substantial LDRD support.

Rapid development of nucleic acid diagnostics

Team members: J. Patrick Fitch, Shea Gardner, Thomas Kuczmarski, Paula McCready, Linda Ott, Thomas Slezak, Elizabeth Vitalis, Adam Zemla

With LDRD funding, the team designed and implemented a computer-assisted process that begins with DNA-sequence information and yields highly specific, sensitive, and robust pathogen signatures. When combined with polymerase chain reaction instrumentation, the resulting diagnostics are both rapid and robust. Applications for this technology range from countering bioterrorism to detecting naturally occurring diseases.

Discovery of CP violation in the B-meson system

Team members: Douglas Wright, David Lange, Richard Bionta, Marshall Mugge, Karl van Bibber

Cosmological models of the early universe require a charge/parity (*CP*) violating process to produce our matter-dominated universe; however, a plausible source for this *CP*-violating effect has yet to be discovered. Current particle physics theory contains such a process, but it does not resolve the cosmology problem, and until recently could not be experimentally tested. This team, supported by LDRD funding, made significant contributions to the discovery of *CP* violation in the B-meson system as part of the BaBar collaboration with the Stanford Linear Accelerator Center and Lawrence Berkeley National Laboratory.

LLNL Teller Fellow FY2003

Fred Milanovich, chief scientist in R Division of the Nonproliferation, Arms Control, and International Security Directorate was selected as one of two 2003 Teller Fellows for his work on biodectors for homeland security, much of which was performed with LDRD funding.

Advanced Sensors and Instrumentation

Section 1

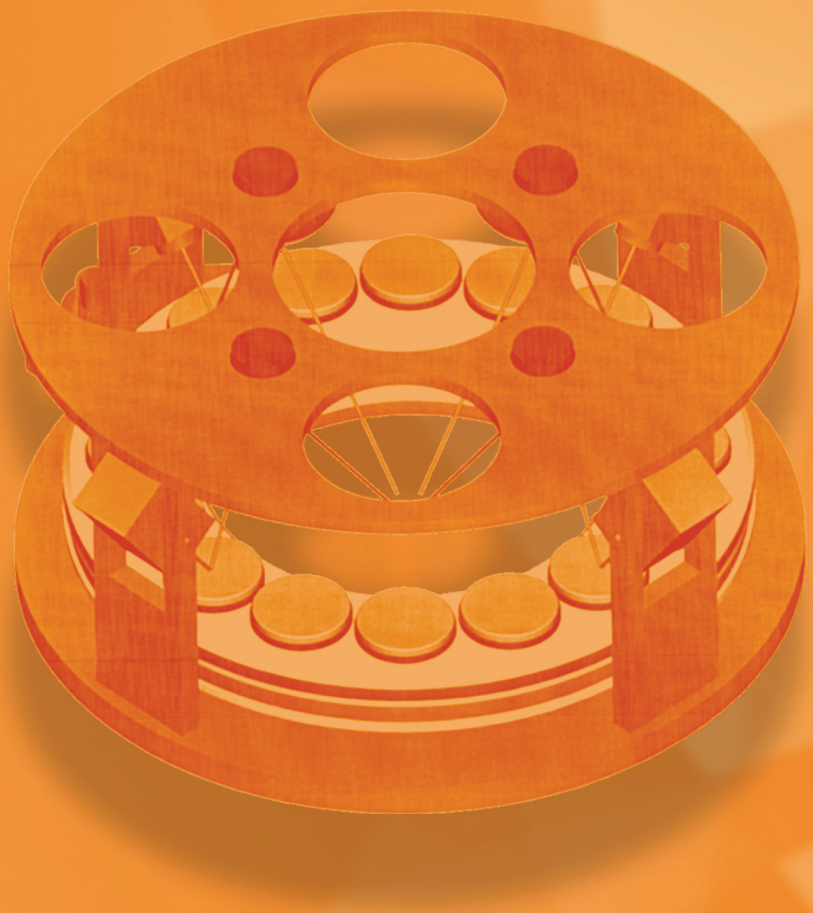

Section 1 — Advanced Sensors and Instrumentation

Secure air–optic transport and routing network

A. J. Ruggiero

Although new generations of U.S. sensor systems insure our technological edge in surveillance by enabling unprecedented quantities of data to be collected, communication bottlenecks limit timely data synthesis and interpretation. Overcoming such bottlenecks—and maintaining our information dominance—requires secure, high-capacity communications networks capable of seamlessly routing data between permanent fiber infrastructures and deployable infrastructures, including mobile and temporary platforms. Open-air laser communication (lasercom) links have the potential to provide the communication networks that are essential to national security.

Although the concept of free-space and air–optic lasercom has been around since the early 1960s, the functional use of lasercom is in its infancy. Commercial "last mile" lasercom links have recently demonstrated availabilities and bit-error rates (BERs) comparable to those of fiber internets, but only over ranges of 100 to 500 m. To develop a long-range (tens of kilometers) lasercom technology, difficulties with optical-beam propagation through weather and turbulent atmospheric conditions must be overcome.

The objective of this Secure Air–Optic Transport and Routing Network (SATRN) project is to develop and demonstrate technologies for long-range, secure, high-capacity, high-availability air–optic lasercom links. Through a series of system-level, horizontal-path link demonstrations, we are establishing the viability of our concepts and techniques. Air–optic data from our horizontal lasercom demonstration testbed are being used to calibrate performance models and simulations of terrestrial links to airborne intelligence, surveillance, and reconnaissance platforms. This project will further LLNL's national-security mission by providing advanced communications technologies for surveillance and intelligence applications.

The portable transceiver system of the Secure Air–Optic Transport and Routing Network (SATRN) in position on Mt. Diablo. One of the longest high-capacity terrestrial links ever achieved, SATRN established a 28.2-km laser-communications link from Mount Diablo to LLNL at a single-channel data rate of 2.488 Gbit/s. This is equivalent to ~1600 conventional T1 data lines, 400 TV channels, or 40,000 simultaneous phone calls.

The key elements of this project are development and testing of (1) adaptive-optics (AO) receivers based on microelectromechanical systems (MEMS) and other advanced technologies; (2) forward error-correction coding; (3) high-power, fiber-based transmitters; (4) custom transceiver components; (5) atmospheric and system-performance modeling; and (6) fiber Internet and radio-frequency, wireless interfacing.

In FY2002, we developed a portable lasercom terminal and established a long-range laser communications testbed (see Figure). A 28.2-km lasercom link from LLNL to Mount Diablo was successfully established at a single-channel data rate of 2.488 Gbit/s—the equivalent of ~1,600 conventional T1 data lines, 400 TV channels, or 40,000 simultaneous phone calls. This is one of the longest high-capacity terrestrial links ever established. Bit error rates for this first attempt were 10^{-4} to 10^{-5}, which is good for an unoptimized system without forward error correction. The link subsequently achieved an aggregate data rate of 10 Gbit/s in both directions simultaneously using four, 2.488-Gbit/s channels at different optical wavelengths.

Other accomplishments include (1) completing preliminary air–optic gigabit Ethernet experiments on our 1.3-km outdoor building-to-building testbed; (2) optimizing single-channel transceiver sensitivity; (3) developing, assembling, and testing customized error-coding hardware; (4) developing a photonic-crystal-fiber amplifier and MEMS AO modeling capability; (5) fabricating and testing nonlinear AO; and (6) developing and implementing a path-averaged turbulence-measurement capability based on a Shack-Hartmann sensor.

In FY2003, we will focus on using our air–optic testbeds to further develop and evaluate advanced, new technologies, including technology to improve the availability and reduce the error rate of the 28.2-km link and enable operation in accordance with long-range Gigabit Ethernet and Fibre Channel protocols. Long-range experiments with data rates up to 100 Gbit/s are planned, along with completion of an end-to-end modeling capability that includes atmospherics, boundary-layer effects, and pointing and tracking.

Presymptomatic detection and containment of infectious biological agents

F. P. Milanovich, K. W. Turteltaub, A. A. Quong, R. G. Langlois, S. L. McCutchen-Maloney, B. Colston

After a half-century of vaccine and antibiotic successes, infectious diseases are again the leading cause of human mortality worldwide. In addition, the anthrax attacks of 2001 exposed our nation's vulnerability to the covert introduction of harmful biological agents. Natural epidemics overseas—such as foot-and-mouth disease in the U.K. and the outbreak of mad cow disease throughout Europe—have shown the potential for serious economic and political harm.

Current disease surveillance-and-response systems rely on postsymptomatic reporting. However, many infectious agents such as smallpox have a long latency period, eluding early detection and resulting in widespread infection. The emergence of West Nile virus in New York in 1994, for example, was not identified until 14 days after the first case.

The goal of this one-year project was to develop the technology for a sustainable, continuous, and comprehensive nationwide early-warning system based on medical surveillance and designed for the timely detection of covert biological attacks or naturally occurring pandemics. The two major milestones to this work are to (1) identify specific presymptomatic or precontagious biomarkers for a select number of pathogens that provide unambiguous warning of disease and (2) design and demonstrate the technology for a continuous, nationwide surveillance architecture for the presymptomatic detection of infectious disease in the U.S. This work supports LLNL's missions in national security—by developing means to prevent the spread of biological weapons of mass destruction—and in bioscience to improve human health.

Our approach to identify molecular biomarkers specific to individual diseases involved designing innovative detection technologies; performing clinical trials utilizing blood, urine, nasal and skin swabs, and exhaled air; performing research to understand the interaction of pathogens with immune components; and developing strategies for a national medical-surveillance network. Potential sources of these samples include blood banks and military personnel.

In FY2002, we substantiated the feasibility of routine medical surveillance for infectious agents. Using a statistical model, we determined that if a dangerous pathogen were to infect 500 people, monitoring a fifth of the donated blood supply in the U.S. would provide a >99% chance of detection.

To develop the biomarkers for use in our monitoring strategy, we established two key collaborations, one in gene expression analysis and a second in proteome analysis; began routinely receiving blood samples from a broad spectrum of patients at a local clinic; and began creating a database of the results of sample analysis. In work to characterize host–pathogen interactions as another means to identify biomarkers for presymptomatic detection, human macrophage cells were exposed to *Yersinia pestis*, which causes plague. We have identified over 30 proteins that are differentially expressed in macrophage cells after *Y. pestis* exposure (see Figure).

To facilitate the further discovery of biomarkers, we developed computational models for analyzing data such as those obtained in this project. Our models can be used to predict other potential biomarkers based on comparisons between initially defined markers and their known relationship to metabolic pathways contained in the model.

In summary, this one-year project confirmed that a combined proteomic and genomic approach holds great promise for presymptomatic detection. It has set the stage for a discovery-based research program that could enable a national surveillance system for detecting bioterrorist attacks and natural pandemics in the early stages.

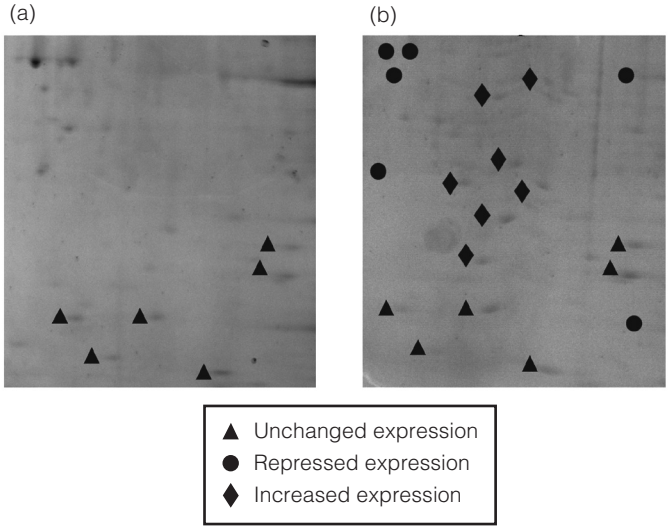

Proteins expressed differentially after exposure to viral or bacterial agents can be used as biomarkers to enable rapid detection of those agents. The photographs show human proteins (a) before and (b) after exposure to Yersinia pestis. *The proteins exhibiting a post-exposure increase (diamond shapes) are potential biomarkers.*

Structural characterization of noncovalent interactions between biomolecules

S. J. Shields

To counter bioterrorism and understand, treat, and prevent human disease by developing antibodies for pathogens, we must be able to interrogate protein conformation, characterize protein–ligand noncovalent interactions, and determine protein conformation changes induced by ligand binding. Characterizing and understanding the cascade of biomolecular interactions is at the heart of biomolecular sensor development. Research by LLNL and DOE includes the design, synthesis, and characterization of small-molecule ligands that noncovalently bind to, and inhibit the function of, biological toxins such as tetanus, botulinum, and cholera by blocking the protein's active site.

Noncovalent interactions are energetically weak associations between molecules (1 to 5 kcal/mole) and consist of (1) hydrophobic interactions, in which nonpolar functional groups interact based on their repulsion from water; (2) electrostatic interactions, in which oppositely charged atoms interact; (3) hydrogen bonds, in which a hydrogen atom is shared between two electronegative atoms; and (4) van der Waals interactions. Because noncovalently bound complexes are weak, and their nature depends on the solvent involved, it is difficult to detect them and to determine regions of interaction. The ability to detect and characterize these interactions would further LLNL's national-security mission by aiding in developing molecules to inhibit protein functions involved in human disease from naturally or intentionally released pathogens. For instance, experimentation to determine where and how small molecules bind to the surface of proteins is critical to developing biological sensors based on molecular recognition.

This project is aimed at developing mass spectrometry (MS) methods to structurally characterize noncovalent interactions in protein–ligand complexes. The project has focused on the complex between the tetanus toxin c-fragment protein (TTc-F) (MW 51.8 kDa) and doxorubicin (MW 0.543 kDa). Although the binding of doxorubicin to a specific region on the TTc-F surface had been computationally predicted previously, our time-resolved limited proteolysis experiments on TTc-F:doxorubicin complexes determined, for the first time, two potential doxorubicin-binding regions.

In FY2002, time-resolved limited proteolysis experiments using multiple enzymes for proteolysis determined that doxorubicin does not bind to the same location on the surface of TTc-F as the gangliosides—physiological binding molecules. Instead, doxorubicin induces a conformational change in the protein's tertiary structure during complex formation, inhibiting the ganglioside's ability to recognize TTc-F. This result was significant because it invalidated two previous assumptions: (1) doxorubicin interacts solely with the protein surface, with no structural change in TTc-F and (2) the gangliosides all bind to the same site on the protein.

We also used the MS methods developed to interrogate a larger, more complex biomolecular system—a complex between the protein XPA (MW 34 kDa) and a benzo[a]pyrene-adducted DNA molecule. This protein–DNA complex is involved in the repair of damaged DNA. However, our investigation was hindered because XPA was not very stable under the experimental conditions required for MS. For example, XPA lyophilized in preparation for MS would aggregate, forming irreversible self-complexes.

After obtaining appropriate conditions for the MS applications, we began proteolysis experiments as we had in the TTc-F–ligand studies. However, data interpretation proved challenging because the protein–DNA interface was much more extensive than in the other studies. For instance, the binding-site information was difficult to distinguish from possible conformation changes induced by binding. However, future experiments involving hydrogen–deuterium exchange and chemical crosslinking could aid in distinguishing the two.

The unique MS methods developed in this project resulted in invited presentations and publications and have been incorporated into other LLNL projects to characterize protein–surface interactions for biosensor development.

Smart membranes

T. van Buuren, S. Létant, A. Vance

Biological membranes such as cell walls can selectively filter ions, molecules, and biomaterials. Artificial membranes have been unable to replicate this selectivity—most select molecules according to their size only and have no chemical selectivity. An artificial membrane able to mimic the selectivity of a biological membrane would enable a new class of highly specific biosensors capable of detecting specific microorganisms, such as biowarfare agents or other pathogens in body fluids.

The goal of this project is to create a smart, selective membrane by controlling (1) the pore size of the membrane and (2) the chemical groups coating the inside surface of the pores. Such membranes will be able to act either as a passive filter—to select molecules according to size and coarse chemical properties—or as a highly specific filter to immobilize, concentrate, and analyze selected biomolecules or entire microorganisms, such as bacteria and viruses.

This research will enhance LLNL's capability in nanotechnology and bioscience in support of our biological-weapon detection programs, furthering the national security mission.

To create a rigid membrane with a narrow pore-size distribution, we are prepatterning silicon wafers on both sides using standard photolithography techniques. The top pattern was achieved in FY2001 and consists of inverted-pyramid-shaped indentations, which allow precise positioning of the pores. The back pattern comprises 25 windows—formed by thinning the silicon wafer from 500 to 50 μm. This provides membrane rigidity by maintaining a thick silicon grid to support the thin membrane area and allows control and tunablility of the membrane thickness. The pores are etched using an electrochemical technique that allows formation of pores between 300 nm and 3 μm in diameter, with a narrow size distribution (<50 nm).

In FY2002, the last year of the project, the back pattern was successfully fabricated (see Figure). We then functionalized the silicon membrane by coating the pore surfaces with biotin, which was anchored using a covalent silicon–carbon bond attachment technique coupled with crosslinking chemistry. The presence of biotin and its linker in the pores was verified by energy-dispersive x-ray spectroscopy of the pores.

To demonstrate capture of an organism, membranes with biotin-coated pores 1 μm in diameter were tested with a solution containing polystyrene beads 200 nm in diameter—roughly the size of a large virus. Some beads were coated with streptavidin, which simulates proteins on the surfaces of various microorganisms and which specifically binds to biotin. Other beads were left uncoated to check for nonspecific adsorption. Because of their rigidity, the membranes were mounted in a standard Luer syringe, and the solution was flowed through the membrane by pushing the plunger. Fluorescence assays showed that the membrane passed through almost all of the uncoated beads while trapping 40% of the streptavidin-coated beads. Because pore size was 5 times larger than the bead diameter, we can conclude that bead capture was due to surface functionalization only.

This project has shown that this smart-membrane technology can be used to create detectors able to analyze, in situ and in real time, the type and amount of microorganisms trapped in the pores. Such sensors could be used in counterterrorism applications to detect biological threats, as well as medical applications to detect pathogens in body fluids.

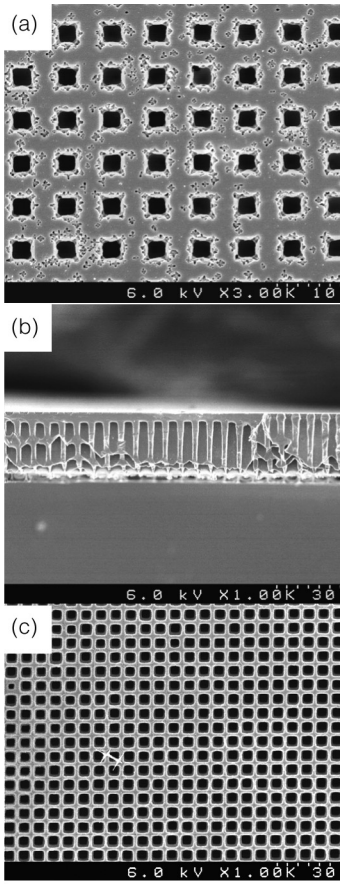

Scanning electron micrograph of a 15-μm-thick silicon membrane with a pore diameter of 2 μm: (a) top view, (b) cross section, and (c) bottom view. The inside surface of the pores can be coated with a chemical group to create a smart, selective membrane. Such membranes can act as a highly specific filter to immobilize, concentrate, and analyze selected biomolecules or entire microorganisms, such as bacteria and viruses.

Cooperative mobile sensing networks

R. S. Roberts, K. A. Kent, E. D. Jones, G.H. Armstrong

Low-cost, high-endurance unmanned air vehicles (UAVs) are now practicable for autonomous sensing and data collection over wide areas. The UAVs can collect data either with onboard sensors or by receiving and relaying data from ground-based sensors. Using a network of UAVs to collect sensor data would provide advantages such as quicker data collection and the ability to adapt to the loss of an individual UAV. Applications of UAV networks include providing communication services to isolated ground sensors, aerial monitoring of national borders and seaways for homeland security, and air sampling for atmospheric modeling.

Our project investigated two fundamental requirements for using UAV networks to autonomously collect sensor data: (1) route optimization—constructing efficient routes that allow the UAVs to collect data without duplicating effort or interfering with one another—and (2) control architectures for network adaptation—allowing a network of UAVs to optimally adapt to exceptional events, such as the loss or addition of UAVs to the network or changes in the priorities of subregions in the area covered. By potentially enabling data collection by UAVs, this project supports LLNL's missions in national security and environmental management.

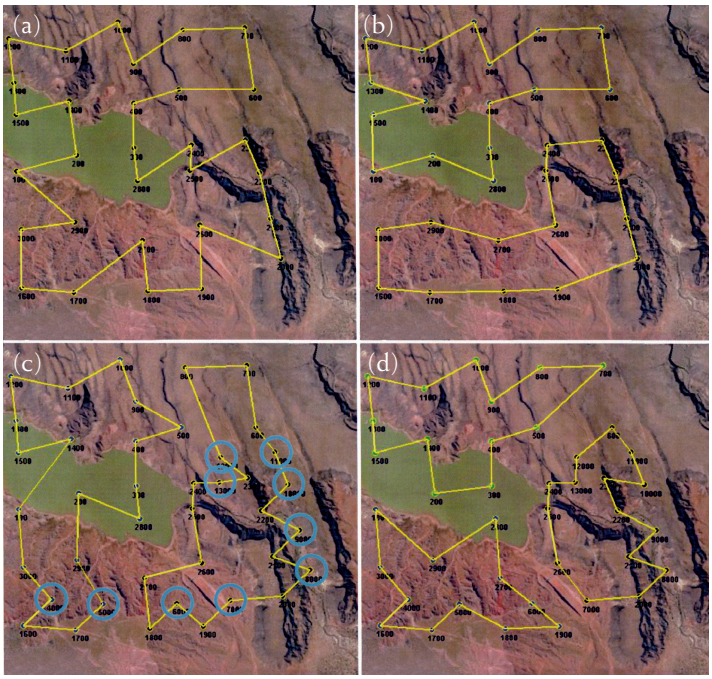

An example of adaptability in a network of unmanned air vehicles (UAVs) controlled with the simulation, tactical operations, and mission planning (STOMP) tool. (a) First, an area is covered by one UAV collecting data at sensing points along a route. (b) A second UAV is added, and the area is divided into two routes for faster data collection. (c) Surveillance resolution is increased by adding sensing points. (d) A third UAV is added.

In FY2002, we completed our investigation into UAV control architectures and network adaptation schemes, including improving our route-optimization algorithm to better process information about sensing cost—the effort required for a UAV to complete a data-collection route. Cost information is regularly estimated by each UAV and shared throughout the network. This work resulted in control architectures based on hierarchical or distributed control. In the hierarchical architectures, network adaptation is initiated by one lead UAV, which can be replaced by any other UAV should it be disabled. This architecture is useful in small networks requiring quick adaptation. In the distributed architectures, UAVs cooperatively perform network adaptation by individually optimizing sensing costs for their subregions. These architectures are useful in large networks in which subregion sensing costs can change abruptly—for instance, if a UAV had to remain over a specific location to video a convoy of vehicles.

In collaboration with the University of California, Davis, we continued developing a software tool called STOMP, which stands for simulation, tactical operations, and mission planning. STOMP implements the control architectures described above to simulate, control, and communicate with UAVs used in sensing applications. The Figure gives an example of network adaptability when increasing the number of UAVs and sensing points in a network. The capabilities of STOMP include simulations in which real UAVs and sensors interact with the virtual UAVs and sensors. This capability enables experiments to determine whether a sensing task requires more sensors and UAVs than are on hand.

Finally, we conducted several experiments in which an airborne UAV collected imagery from unattended ground sensors and transmitted the data to a ground station. These experiments allowed us to test the communications modules developed during FY2000 and refine the data-transfer techniques developed during FY2001. The results of these experiments were applied to the design of the STOMP communications objects. In summary, we developed a data-collection architecture in which UAVs collect data adaptively and cooperatively. Results of this project are already being applied to remote-sensing applications in the DOE complex.

Disposable polymerase-chain-reaction device

E. K. Wheeler, W. Benett, K. Ness, P. Stratton, A. Chen, A. Christian, J. Richards, T. Weisgraber

The September 11, 2001 attack on the United States and the subsequent anthrax attack have raised antiterrorist vigilance to new heights. Although the September 11 attack was orchestrated with hijacked planes, the next threat could be nuclear, chemical, or—as evidenced by the anthrax attack—biological. Many countries that may support terrorist activities are likely to have biological weapons capabilities; biological weapons may also be available on the black market and accessible to domestic terrorists. Planning and equipping for a biological attack requires detection devices that are robust in the field, easy to use, and relatively inexpensive. This project will leverage LLNL's competencies in microtechnology and instrumentation and will provide new capabilities in support of LLNL's homeland security mission.

To take appropriate action, first responders to a biological attack (local emergency response personnel, military, or intelligence personnel) must identify the specific organism used in the release. For this purpose, polymerase-chain-reaction (PCR) assays are becoming increasingly important because they can amplify a target segment of DNA (by thermal cycling of the necessary reagents) and enable identification of pathogens. However, the sophisticated tools needed to assess a potential biological release not only are unaffordable to many first-response agencies, but also require highly trained operators.

In this project, we are designing and demonstrating a compact, easy to use disposable PCR unit based on a novel thermal cycler [Fig. (a)]. The PCR device will allow first responders at the scene of a biological attack to quickly identify the nature and extent of the attack. By building on LLNL's success in designing portable PCR units, we are seeking to develop low-cost, disposable PCR units to be used by first responders. Authorities looking for the source of contamination in food or water will also benefit from this device.

During FY2002 we focused on improving and testing our novel convective PCR thermal cycler, which uses the thermal convective forces created by fixed, non-fluctuating, hotter- and cooler-temperature regions to thermally cycle the sample fluid to achieve amplification. The advantage of this approach is its lower power requirements, increasing the probability that small batteries will suffice as the system's power source. We used our thermal cycler to successfully amplify a 90-base-pair, multiple-cloning site segment of a DNA plasmid—one of the first times DNA amplification has been accomplished using convective forces [Fig.(b)].

Successful DNA amplification requires an optimum temperature profile in the thermal cycler—for example, its heaters must not produce local hot spots. We fabricated several types of heating systems and achieved one that satisfied this and other thermal requirements; a patent application was filed for this heating scheme.

Sample fluid velocity was also addressed. Because the DNA amplicon—the amplified segment of DNA—in a sample fluid doubles each time the fluid cycles through the PCR unit, greater fluid velocity reduces the time needed for detectable amplification, further lowering power requirements. Measurements made with digital particle image velocimetry during test cycling yielded a fluid velocity of 1.6 to 2.4 mm/s—in excellent agreement with the velocity (2.8 mm/s) predicted as necessary with models in FY2001.

In addition, we began designing a sample-preparation system based on a pillar chip—a device that captures DNA on silica pillars while inhibitors are removed, after which a series of wash steps releases the DNA from the pillars for thermal amplification.

In FY2003, we will continue thermal optimization of the cycler and begin work to incorporate sample preparation and the pillar chip with the thermal cycler—crucial for an integrated, easy-to-use, low-power, robust, and disposable PCR device.

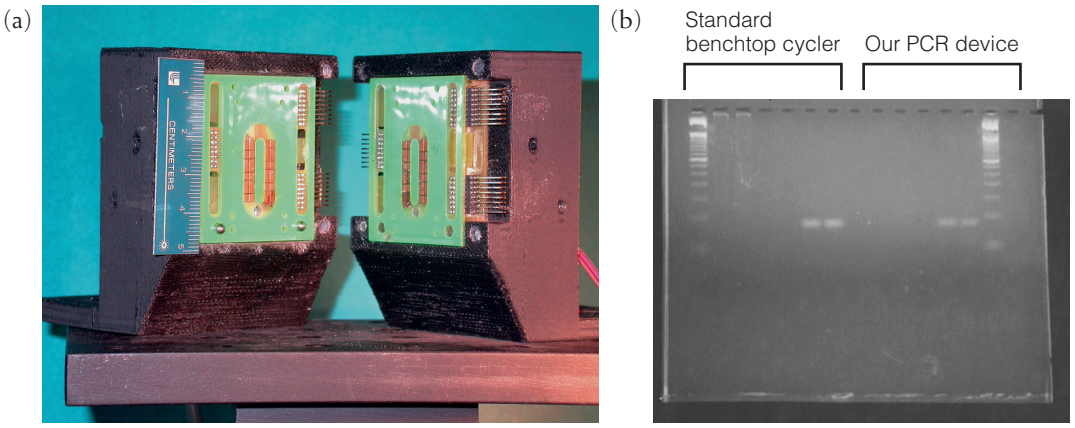

(a) The convectively driven polymerase-chain-reaction (PCR) thermal cycler developed in this project. (b) Gel detection showing successful amplification of a 90-base-pair, multiple-cloning-site segment of plasmid DNA using our device, compared to amplification with a standard benchtop thermal cycler.

Ultrawideband communications

F. Dowla, A. Spiridon, D. Benzel, T. Rosenbury

National-security operations require short-range communications systems capable of collecting data rapidly and transmitting it reliably with minimal interference to other communication devices. Such systems must be robust; have a low probability of detection and intercept; employ low-power, small-size hardware; and interface easily with other systems for analysis or to establish long-distance links. Commercial communication systems operate in fixed-frequency bands, are easily detectable, and are prone to jamming by the enemy, among other shortcomings.

We are focusing on the three key operational modes for the Department of Defense and the wireless sensor network community: (1) secure sensor and voice communications over a 1-km range; (2) ground-to-ground and air-to-ground data channels needed for small, unmanned air vehicles; and (3) network communication for large numbers of sensors in a local area, including multipath and extremely low-altitude operations.

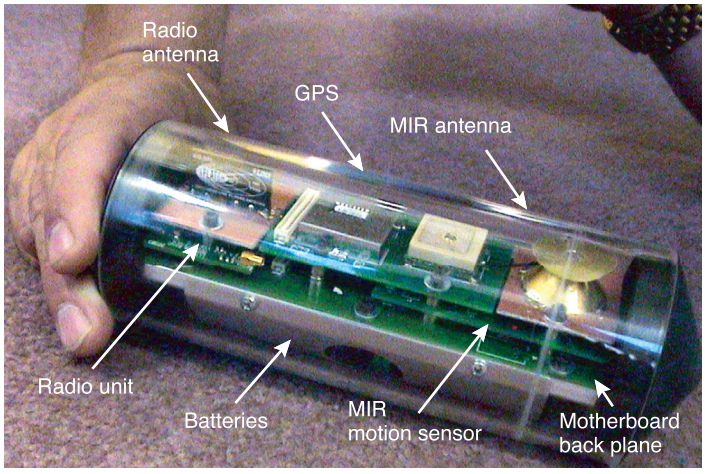

An ultrawideband (UWB) radio integrated into a compact sensor node, which is also equipped with an antenna, global positioning system (GPS), UWB radar, micropower impulse radar (MIR), processing unit, and batteries. Network protocols were developed to interface with our UWB radio design. Sensor radio nodes of this type will play a critical role in modern wireless sensor networks for intelligence and battlefield applications.

The goal of this project is to develop and demonstrate (1) ultrawideband (UWB) communication with a capacity of 5 Mbps and a range of 1 km, (2) multichannel capability with sensors, (3) a testbed for application development, and (4) performance standards for bit error rate and low probabilities of detection and intercept.

In FY2002, we built several UWB communication transceivers for voice, video, and digital-data communications for intelligence applications (see Figure). We also performed modeling and propagation analyses with multiple channels and developed (1) a UWB radio with a capacity of 2 Mbps, a range of 160 m, two channels, and a power requirement of <1 W; (2) a graphical user interface for these models; (3) an interface for real-time applications; and (4) a network and architecture design. In addition, arrays of transmitters for communications were computationally modeled and simulated, and preliminary testing of the UWB communications device was conducted.

For FY2003, we plan to (1) complete the modeling and propagation analysis for mobility and multipath capabilities; (2) design and implement a reconfigurable, integrated network for ten UWB radios, including the application-layer infrastructure; (3) further refine our robust 5-Mbps, 1-km-range system to operate on <0.5 W with 10 channels, including a mobile channel; and (4) develop a transmitter array using high-capacity and noninterfering wireless communications;—our novel synchronization technique will provide no interference in the same channel on other communication systems. We also plan to submit papers on propagation, architecture, and performance to peer-reviewed publications.

A highly efficient fast-neutron threshold detector

P. L. Kerr, T. M. Tillotson, J. F. Poco, S. P. Swierkowski

In this project, we investigated two new concepts for a fast-neutron threshold detector. The objective was to produce a detector prototype with higher fast-neutron detection efficiency than existing fast-neutron threshold detectors by incorporating the thorium (Th) threshold reaction of the Th fission chamber. This new detector, which would be used in conjunction with the active-neutron-interrogation technique, would provide an improved tool to search for shielded highly enriched uranium in support of the Laboratory's national-security missions in counter- and nonproliferation.

As with a threshold fission chamber, both of the detector designs are based on the technique of detecting fission fragments from an actinide that has a sharp rise in neutron fission cross section near 1 MeV. The innovation in our designs is the use of a liquid or solid to detect fission fragments instead of a gas. The greater fission-fragment stopping power of a liquid or solid detection medium allows higher Th density, thereby increasing detection efficiency. The first design uses a Th sol-gel infused with liquid scintillator. The gel is contained in a metal cell with a glass window coupled to a photomultiplier tube. The Figure illustrates this design. The second design uses a slotted-silicon surface-barrier detector filled with a solid thoria aerogel. The silicon diode, an efficient, charged-particle detector, detects fission fragments directly.

A prototype of the sol-gel detector was produced first, and FY2002 research focused on this design. A multiparameter data-acquisition system was installed to acquire pulse height and rise time information simultaneously from the scintillator signal. In principle, this system, along with pulse-shape discrimination (PSD) properties of scintillators, should allow separation of gamma-ray, neutron, and alpha-particle signals from the fission fragment counts.

In the first year of the project, the first 100% thoria sol-gel was produced. This sol-gel prototype had good light transmission, but not PSD properties. A series of experiments were conducted with Th dissolved in a liquid scintillator to simplify the chemistry. We found that thorium nitrate was a good Th carrier. Initially the light collection and PSD properties were poor also, but the addition of ethanol in proportion to the thorium nitrate improved the PSD properties. Another problem was peeling of the reflective coating in the scintillator cells due to the thorium nitrate–scintillator solutions reducing the adhesive properties. This coating is important for good light collection, detector efficiency, and energy resolution. After trials with other reflective material, a set of cups was designed and procured as a retrofit to the original coating. The cups were coated using a new process and have been robust to date. The effect of the reflector cups improved the pulse-counting efficiency and energy resolution by a factor of 2.

Samples of 1%, 5%, and 10% of thorium nitrate were prepared, purged with nitrogen to remove oxygen, and exposed to neutron fluxes to evaluate the energy calibration and neutron response. Subtraction of cell background was necessary due to gamma-ray and alpha-particle production from the natural decay of Th. Spectra to date indicate the fission fragment region may not be well separated from the gamma-ray and neutron regions. In addition, as the thorium nitrate concentration was increased, the increased gamma-ray and alpha-particle activity adversely affected the ability to separate the particle groups using PSD, thus limiting the Th concentration that could be used.

Solution to these issues could involve investigation of other fissionable isotopes with lower specific activities. Additional work with the second (silicon) design is planned and may be more promising, since PSD is not necessary in Si because of the direct detection of fission fragments.

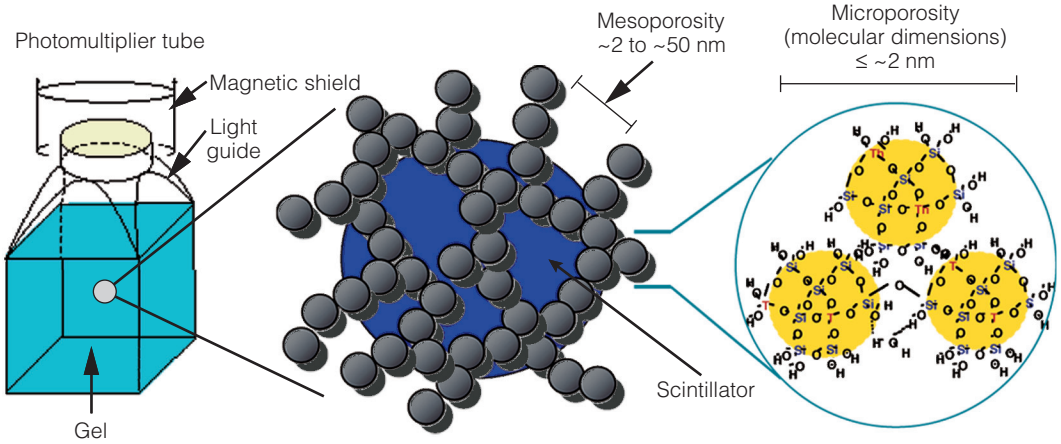

Diagram of the thoria sol-gel liquid scintillator neutron detector, showing successive magnification: (left to right) Full detector, sol-gel lattice filled with liquid scintillator, and molecular structure of the gel.

Geolocation using passive synthetic apertures

M. R. Portnoff

Accurately determining the geographic location of a source of radio-frequency energy on the Earth's surface is needed for a variety of civil and national-security applications, including search and rescue, delivery of emergency services, support to military operations, and other surveillance needs. Traditional geolocation methods typically require two or more widely separated sensors. The signals received by the individual sensors are jointly processed using a triangulation algorithm to determine the location of their common origin. Traditional methods present two significant problems: (1) they require multiple platforms, which are both expensive and in high demand, and (2) practical deployments often deliver less than desirable geolocation accuracy.

Our new approach overcomes these problems by moving airborne or spaceborne sensor platforms to synthesize a very large antenna aperture capable of high spatial resolution. This concept, passive-synthetic-aperture (PSA) processing, illustrated in Figure (a), differs from the current practice of using multiple receivers to collect the same signal at different locations, or a single receiver taking "snapshots" at different locations and times. Unlike traditional methods, our approach can provide highly accurate results using only a single sensor with a modest-size antenna. Our goal is to develop and characterize PSA signal-processing algorithms that provide an order-of-magnitude accuracy improvement over traditional methods.

This project is applicable to several of LLNL's national-security missions, including counter- and nonproliferation, support to military operations, and other surveillance needs.

During FY2002, we developed and implemented a PSA processing algorithm designed to accurately geolocate a continuous-wave (CW) emitter using the signal received by a single, moving sensor. The algorithm "spatially focuses" the received signal to produce a two-dimensional geographic map of emitted energy with a spike at the location of the emitter. Because the processing is linear, by superposition, multiple co-channel sources will be focused to multiple spikes at their corresponding locations on the output map. The resolution depends on the extent of the synthetic aperture.

To test the algorithm, we carefully simulated the signal that would be received from a remote CW source by a moving sensor, then focused the data with our PSA algorithm. The resulting impulse response was virtually identical to the theoretical optimum we derived in FY2001 using mathematical analysis. Figure (b) illustrates the amplitude of such an impulse response. The scale factors depend on the source–receiver geometry, the source wavelength, and the synthetic aperture.

A directly implemented PSA algorithm is computationally very intensive. To reduce the computational burden, we developed and incorporated mathematical approximations with approximation errors comparable to the level of the computer's floating-point round-off noise. We also developed a fast recursive algorithm for the inner loop of the PSA processing and have parallelized the overall code to obtain a 200-to 300-fold processing speedup on our 8-processor workstation. Small test cases now run in 1 to 2 min rather than several hours.

Future goals include testing and characterizing the PSA algorithm on real data, extending and exploring its application to multiple sensors, and developing a much faster, fast-Fourier-transform-based algorithm suitable for processing very large data sets.

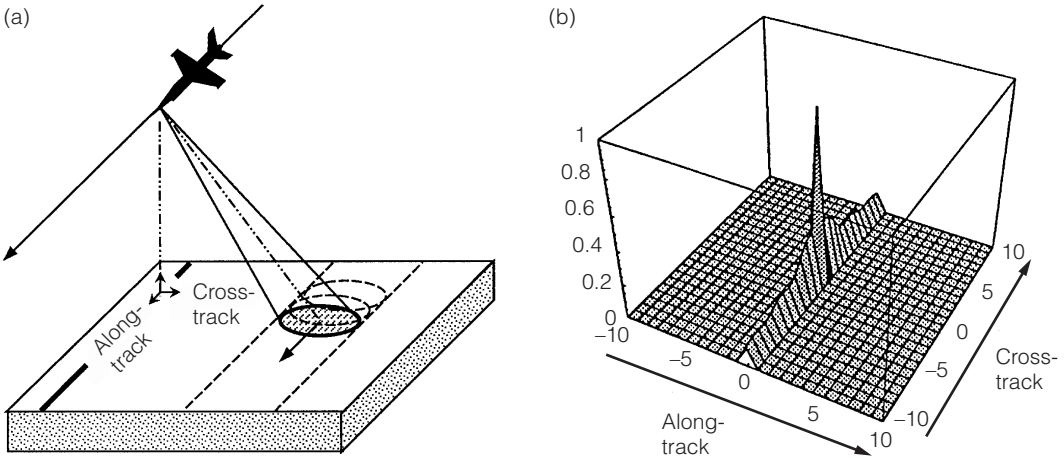

(a) Passive-synthetic-aperture (PSA) processing maps the locations of radio-frequency emissions by continuously processing signals picked up by a moving receiver. The effective aperture is the segment of the flight path for which a point source is in the field of view of the receiver's antenna. (b) Two-dimensional amplitude response of the PSA processing algorithm for a point source. The scale factors for the axes depend on the source–receiver geometry, the source wavelength, and the source aperture length.

Stroke sensor development using microdot array sensors

C. Carter, B. Colston, M. McBride, T. Wilson, R. Alvis, D. Gutierrez

Stroke is a major cause of mortality and the primary cause of long-term disability in the U.S. A recent study of stroke incidence suggests that over 700,000 people annually in this country will have a stroke. Of these, approximately 400,000 will be left with a significant impairment. Thus, the annual target population of this research is greater than 400,000 individuals.

The intent of this project is to provide clinicians with a new diagnostic tool for making enzyme, blood/gas, and ion measurements related to stroke. Our goal is to develop and demonstrate a reproducible, minimally invasive, optical-fiber-based sensor for rapid, in vivo measurements of stroke biomarkers using inkjet printing technology. We have coined the acronym, MiDAS (microdot array sensors) for this new sensor-fabrication methodology.

Biosensor development is an important capability needed to meet national gaps in our ability to detect and mitigate the effects of emerging infectious diseases. Fiber-based microdot array sensors, along with other multianalyte detection methods, will be the future, practical embodiment of the pathomics initiative at LLNL in support of its mssion in biotechnology. This sensor will also have direct application to the Laboratory's national security and environmental missions.

We are using inkjet printing technology for printing indicator chemistries on image guide fibers, as the Figure shows. This unique technology allows the creation of chemical sensors designed to detect and quantify one or more analytes of interest in a fluid or airborne medium. The indicator chemistry contains one or more dyes that absorb energy from light. The dye's optical characteristics change in response to the target analyte. By spectrally monitoring these changes using fluorescence spectroscopy, we can make highly sensitive detection and quantitation of the analyte. If multiple ligand-specific indicator chemistries are printed in a known pattern, simultaneous detection and measurement of these analytes can be accomplished using optical imaging techniques to register each microdot spatially.

One of our major accomplishments of FY2002 was the completion of an instrument capable of printing on optical fibers. Its key features include robotic motion control of the printing mechanism, a custom vision system allowing real-time viewing of the printing process, and a custom fiber positioner that uses feedback from an optoelectrode. This is a unique and new technology at LLNL. We also completed all chemistry work on our second-generation pH sensor, including a major change in the polymer matrix and a modification to the pH indicator dye, which increased the dynamic range of the sensor.

Considerable progress has been made in the solution-based phase for our enzyme biomarkers. Presently, we are testing our chemistries within the photopolymerized polymer matrix required for printing on fibers. We anticipate additional modification/reformulation before proceeding to fiber-based work.

For FY2003, we plan to publish our results; complete chemistries for an oxygen sensor and demonstrate a pH, enzyme, and oxygen multianalyte imaging sensor; and design and build a clinically practical imaging system.

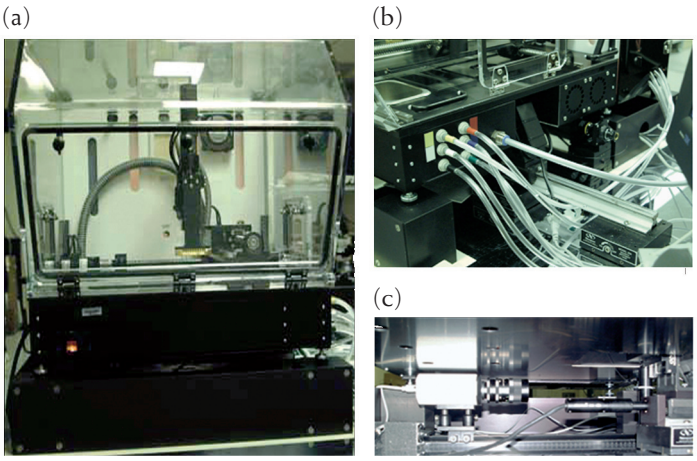

(a) Front view of fiber printer atop the support base, which houses (b) the fiber positioner and (c) the vision system

Retrospective plutonium biodosimetry by modeling urinary plutonium-239 from archived occupational samples

K. T. Bogen, D. P. Hickman, T. A. Brown, T. F. Hamilton, A. A. Marchetti

Uncertainty about patterns of plutonium (Pu) excretion by the human body limits retrospective Pu dosimetry, ^{239}Pu detection for national security, and other uses of emerging ultrasensitive Pu-detection technology. This project has demonstrated the feasibility of using one such technology—accelerator mass spectrometry (AMS)—to analyze archived alpha spectrometry (AS) plates and reveal previously undetectable patterns of low-level urinary Pu excretion.

Archived data on LLNL Pu workers monitored from 1981 to 2001 include AS plates and dosimetry records. In FY2002 we continued to study AS plates of urinary Pu from one worker exposed through a puncture wound (Worker 1) and two exposed by inhalation (Workers 2 and 3), as well as blank control plates from the same period. Records were searched for corresponding data on Pu-recovery efficiency (F_r), dosimetry, and other information. The plates contained electroplated ^{239}Pu, along with ^{242}Pu spikes used to determine F_r. The plates were prepared for AMS analysis by standard radiochemical purification and were also recounted by AS, but none exceeded ~130 μBq, the minimum amount of ^{239}Pu detectable by AS. Total Pu isotopes were determined using the original ^{242}Pu spike information. Uranium (U) plates were also included on each AMS sample wheel for detection of possible background contribution from ^{238}U. Background levels of less than 1 million atoms (<0.9 μBq) of ^{239}Pu were observed routinely, without interference from up to 10^{13} coprocessed U atoms.

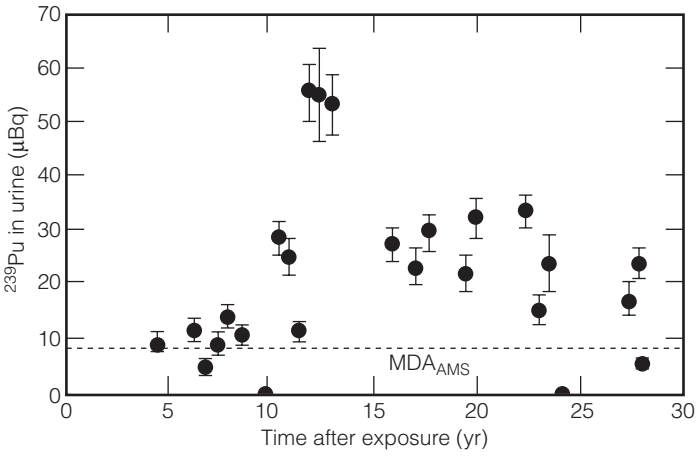

Accelerator mass spectrometry (AMS) measurements of plutonium-239 (^{239}Pu) in archived urine-sample plates prepared for a worker exposed to <370 μBq of ^{239}Pu more than 25 yr ago. Alpha spectrometry had failed to detect any urinary ^{239}Pu beyond 10 days after exposure. AMS detected elevated ^{239}Pu in nearly all the archived samples, in which the minimum detectable amount (MDA_{AMS}) was 15-fold lower than achievable by AS.

In FY2002, 57 AS plates spanning 1981–2001 were evaluated: 45 plates for Workers 1–3 and 12 blank control plates. AMS detected ^{239}Pu in most plates. Results indicate that AMS can detect amounts of ^{239}Pu as low as ~8 μBq, which is ~15-fold more sensitive than AS. (AMS sensitivity could have been ~150-fold greater if ^{239}Pu separated directly from urine were measured.)

Results for Worker 1 confirmed a nearly linear increase in urinary ^{239}Pu levels, consistent with an accidental ^{239}Pu injection undetected for 20 yr. Such increases are not predicted by current Pu biokinetic models. Results for Worker 2 reveal a significant, previously nondetectable increase in urinary ^{239}Pu, consistent with two suspected respiratory exposures, only the first of which had been documented. Analysis for Worker 3—exposed more than 25 yr ago to <370 μBq of ^{239}Pu by inhalation (see Figure)—detected persistently elevated levels of urinary ^{239}Pu in samples spanning two decades. No excessive ^{239}Pu had previously been detected by AS.

Such results demonstrate that AMS is a better method for characterizing human Pu excretion and support its application in occupational safety and nuclear security. At least one case seemed inconsistent with current biokinetic models. This new method should be able to evaluate dosimetry reconstruction based on assumptions and exposure records.

In FY2003, we will extend our analyses to additional Pu workers at LLNL to reduce uncertainties about long-term Pu excretion and biokinetic modeling. This ultrasensitive LLNL AMS Pu-detection technology eventually will be made available to other DOE sites, the Department of Defense, and other agencies.

Single-cell proteomics with ultrahigh-sensitivity mass spectrometry

E. E. Gard, M. Frank, D. Fergenson, H. Tobias, M. Pitesky, P. Steel, J. Horn

Fundamental understanding of biological systems requires new tools for the analysis of single cells, the building blocks of biological systems. Such tools will better equip us to understand, detect, and curtail the spread of disease either under natural conditions or due to the intentional use of biological weapons.

Our objective is to develop a new technique to analyze the molecular composition of single cells in real time for application to both biological defense and biomedical research. Bio-aerosol mass spectrometry (BAMS) is a high-throughput, real-time, reagentless, single-cell analysis technique for measuring proteins and other biomolecules in a single spore or cell to identify the cell or to study the molecular changes that occur during normal and abnormal cell growth and death. Based on laser-ionization time-of-flight mass spectrometry (TOF-MS), BAMS uses a novel combination of advanced laser desorption and ionization techniques with mass spectrometry to achieve sensitivities two to three orders of magnitude better than laser ionization techniques routinely used for biological analysis.

Applications for national security include bio-agent detection (see Figure). Medical applications include clinical biopsy for cancer detection and analysis of respiratory effluent (cough or sneeze) for noninvasive, symptomatic and presymptomatic diagnoses.

In FY2002, we demonstrated that unique molecular signatures could be obtained with BAMS from single bacterial spores in the *Bacillus* genus, allowing discrimination between bacteria and background aerosols. In collaboration with researchers at Lawrence Berkeley National Laboratory (LBNL), a two-step infrared laser desorption and ultraviolet–vacuum ultraviolet (UV–VUV) ionization setup was implemented to explore sensitivity improvements. Initial results indicate that the UV–VUV setup is capable of the large increase in ion generation needed to achieve the required two-order-of-magnitude increase in sensitivity. We also began optimizing the system for more precise measurement of VUV power. As a result of these demonstration experiments, the Department of Defense has shown interest in the technology for bio-aerosol detection.

In FY2003, we will use BAMS to (1) increase the sensitivity of mass spectrometry to measure moderately abundant proteins and other cellular components in single cells, (2) demonstrate the utility of single-cell mass spectrometry for studying cellular processes, (3) identify biological aerosols and study the molecular changes in individual cells during normal and abnormal cell growth and cell death, (4) develop a novel combination of aerosol mass spectrometry with advanced laser-desorption and ionization techniques to increase the sensitivity of TOF-MS, (5) study the relationship between mass signatures and cell viability as affected by radiation damage, and (6) expand our studies of the influence of laser wavelength on signatures to include short-pulse lasers with 100-fs pulse width.

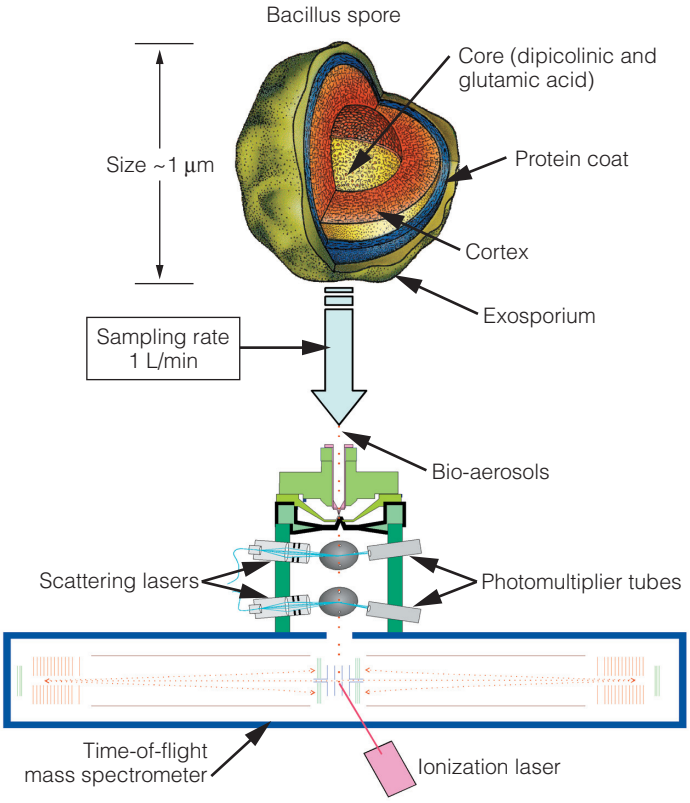

A schematic of a bio-aerosol mass spectrometry (BAMS) system being used to analyze a bacterial spore. BAMS has the potential to identify bio-agents, such as anthrax, from only a single spore or cell and to elucidate the molecular changes that occur in normal and abnormal (e.g., cancerous) cells. The signature molecules in this example are relatively small biological molecules unique to, and located in the core of, Bacillus *spores.*

Ultrasonic nondestructive evaluation of multilayered structures

M. J. Quarry, K. Fisher, J. L. Rose

Multilayered structures, such as weapons assemblies and aircraft wings, pose challenges for nondestructive evaluation (NDE) techniques—to detect a cracked ceramic or void in a multilayered weapons system, for instance—because of inaccessible areas and close interfaces. We are developing two approaches for overcoming these difficulties: (1) guided-wave modes and (2) beam steering of bulk waves.

The first approach involves using the wave-guide structure of a multilayered medium to send wave modes along the structure into inaccessible areas and requires the ability to preferentially excite modes in which most of the energy exists in the layer of interest. A novel phased-array method is being developed under this project to find such guided-wave modes experimentally. Most guided-wave research has been limited to single layers, such as aluminum plates in aircraft or steel piping. Investigating guided waves in multilayered media will extend guided-wave techniques into many new applications.

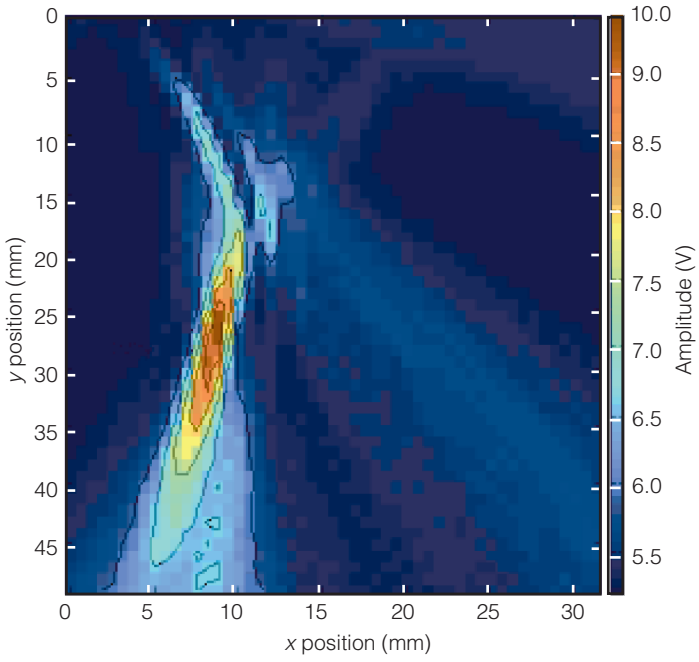

An imaged section of an aluminum block with a 1-mm-diam side-drilled hole obtained by a 20° ultrasonic steered beam.

The second approach steers and focuses ultrasonic bulk waves into layers of interest to find voids in a sublayer. Steering the beam enables areas up to ~40 cm to be scanned from a single position. Focusing increases resolution and improves minimum flaw-size detection.

Our project will develop advanced technologies for inspecting weapons systems in support of LLNL's stockpile stewardship mission and will establish the science base for using guided-wave-based NDE for multilayered mesoscale targets, such as the National Ignition Facility target.

In FY2002, a model of guided-wave mode generation by phased array was developed. Results of analysis using this model showed the need to maximize array length, minimize the effect of element spacing, and maximize the number of elements. We designed an array based on this analysis and used it to detect successfully a 30% through-wall notch in a 1/8-in.-thick aluminum plate, although sensitivity was ~33% less than that of traditional ultrasound.

We developed a software interface for steering a phased array of ultrasonic beams for single-layer media. In addition, a time-delay beam-image reconstruction algorithm previously developed at LLNL for steered-beam data was modified and used to image a 1-mm-diam hole in an aluminum block—achieving our goal of detecting flaws 1 mm in diameter. The area of the block shown in the Figure was imaged by focusing the 20°-off-axis beam at the center of the area.

In FY2003, we will advance from single-layer to multilayered media and (1) perform proof-of-concept testing of guided waves and bulk waves for the NDE of multilayered structures by detecting programmed flaws in multilayered structures, (2) develop array input parameters for beam steering in multilayered media, (3) modify image reconstruction codes for multilayered media, and (4) improve axial distortion in images.

Development of ultrasensitive, high-speed biological assays based on two-dimensional flow cell detection of single molecules

C. Hollars, O. Bakajin, T. Huser

Present immuno- and DNA assays not utilizing amplification methods are generally limited to detection concentrations in the nanomolar (10^{-9}) to picomolar (10^{-12}) range. A few research groups have attempted to improve the limits of detection by several orders of magnitude with newly developed, single-molecule optical-detection methods. Such attempts have been only partially successful; the detection results are largely limited by nonspecific binding for surface-based analysis and impractically long analysis times for solution-based approaches. This project is in the process of developing a device that combines microfluidics and total internal reflection (TIR) microscopy to provide a generalized biological assay with better than femtomolar (10^{-15}) sensitivity. This device will have from a thousand to ten thousand times greater throughput than previous one-dimensional microstream devices, and will allow rapid (<10 min) immuno- and DNA assays at ultralow concentrations.

Once developed, the planar, microchannel-fluidics TIR microscope device will be used to demonstrate ultrasensitive assays of biological species which are relevant to pathogen detection in biological warfare applications. This technology will support Livermore's homeland security mission and will improve healthcare by advancing medical, drug, and basic scientific research.

The project uses a general immunoassay scheme with two or more distinct antibodies or target-complementary oligonucleotides (short fragments of single-strand DNA), chosen for their capability to bind to a specific target. These are labeled with spectrally distinguishable fluorescent markers and then incubated in a solution with the sample to allow them to attach to the target. This solution is analyzed in a 0.5 × 100 × 100-mm microfluidic device providing a two-dimensional flow stream. The flowing solution is imaged with a dual-channel TIR microscope equipped with a video-rate, amplified, charge-coupled-device camera. A coincidence event in each channel is used to indicate the concentration of target in the sample.

During FY2002, we constructed a dual-channel TIR imaging system demonstrating single fluorescent molecule sensitivity (see Figure) and successfully fabricated microfluidic devices with dimensions consistent with those cited above. The completed system was tested and optimized using fluorescent molecules immobilized on glass substrates as well as dye-loaded microspheres flowing in the microfluidic device. Furthermore, we have submitted a patent application covering the planar-microchannel–imaging system.

In FY2003, we plan to continue optimizing the planar-microchannel–imaging system and demonstrate the ultralow (femtomolar) level analysis of biomolecular species. During this time, we plan to publish the results of ultrasensitive, high-speed analysis of biological molecules and the study of nanoscale biomolecular dynamics.

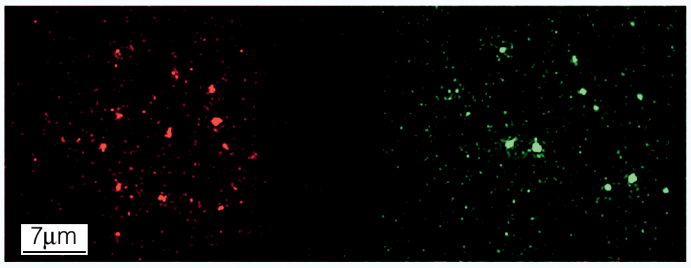

Simultaneously collected red and green (false color) fluorescence images of targets detected by two labeled oligonucleotides that were dispersed onto a solid substrate.

Development of a fast microfluidic mixer for studies of protein-folding kinetics

O. Bakajin

We are designing and fabricating a laminar-flow microfluidic mixer, a microscale device for observing single protein molecules and elucidating the mechanisms of protein folding. The mechanisms by which proteins fold into their biologically active structures is of great importance because misfolded proteins cannot perform their function and sometimes cause disease. Understanding this mechanism requires a detailed knowledge of the sequence of conformational events that leads from a denatured random coil to a unique native protein. In the mixer, the protein-folding reaction is triggered by rapidly mixing a chemically denatured protein solution with a buffer that dilutes the denaturant—the chemical agent that prevents the protein from folding. As the denaturant is diluted, folding occurs. The kinetics of folding is monitored using optical spectroscopic methods, such as fluorescence resonance energy transfer (FRET).

The mixer will be robust; will have low power consumption, short dead time, and better time resolution than commercially available mixers; and will be compatible with various spectroscopic methods. The mixer uses a laminar flow—instead of a turbulent flow—made thin enough through hydrodynamic focusing for diffusion to occur on a short time scale. The microfluidic capabilities this mixer provides will be applicable to the study of other biological systems and to many other microfluidic projects, including national-security-relevant work such as detecting low concentrations of toxins. In addition, this work is aligned with the Laboratory's long-term objective of developing new bioscience and healthcare capabilities and will also help attract the next generation of scientific staff to LLNL.

In FY2002, we set up a microfluidics characterization laboratory equipped for basic device assembly, for characterization using visible laser excitation [Fig. (a)], and for flow control using a customized, computer-controlled pressure regulator system. We made progress in modeling and fabrication of the mixer, and, in collaboration with National Institutes of Health (NIH) scientists, performed actual measurements on a protein system. Recently obtained software for simulating flows and diffusion in user-defined structures is being applied to mixer optimization. Fig. (b) shows the modeled concentration of a protein denaturant.

We are developing processes for the fabrication of fused silica, whose high transmission makes it a suitable material for the mixer, and have also completed all the processes necessary for fabricating the mixer itself, e.g., mastering glass-to-glass fusion bonding in a cleanroom, setting up a microblaster system for making small holes in fused silica, and successfully etching the mixer structures using reactive-ion etching [Fig. (c)].

In the meantime, we have also begun designing a silicon-based mixer. Although limited to a narrower range of spectroscopic observation methods than with fused silica-based devices, silicon-based devices have been used in other protein-folding reaction studies because of their ease of fabrication. In collaboration with a group from NIH, we used a silicon-based device to perform, for the first time, the measurement of protein-folding kinetics using the single-molecule FRET technique.

In FY2003, we will continue to develop the laminar-flow microfluidic mixer and to collaborate with other institutions in measuring protein-folding kinetics.

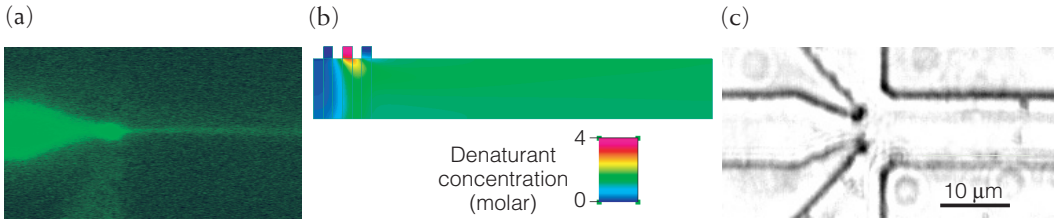

This work has resulted in a laminar-flow microfluidic mixer that will help explain the mechanism of protein folding. (a) A stream of fluorescein can be seen in the mixer during single-molecule fluorescence resonance energy transfer (FRET) measurement of protein-folding kinetics. (b) Simulation of a mixer for single-molecule protein-folding studies. Protein folding is initiated at the point of equilibrium concentration of the denaturant, and changes in the FRET signal along the stream determine the degree of folding. (c) A mixer made of fused silica. A mixture of protein and denaturant is inserted through the middle inlet while the buffer is inserted from the side. As the solutions flow, the denaturant diffuses out of the protein stream, triggering the folding reaction. We can monitor kinetics of folding because different points along the stream correspond to different times after the initiation of the reaction.

Novel application of fiber-optic sensors for characterizing real-time contaminant transport in rapid storm runoff

C. G. Campbell, J. Richards, P. Stratton, M. Zavarin

Lake, river, and stream water quality are all affected by industrial, urban, and rural land-use activities. Many pollutants in these environments, including metals (e.g., mercury) and organic compounds like polychlorinated biphenyls (PCBs), dioxins, and pesticides, are likely to be adsorbed to suspended sediments, which can result in physical and chemical pollution in surface runoff. Because methods to measure the total mass of suspended sediment mobilized in storm water runoff are inadequate, it is not possible to accurately estimate the total load of the contaminants transported with the sediments.

Environmental management of contamination is a major goal at DOE sites. As a result, an important component of our Laboratory's mission is providing better tools for environmental management and long-term stewardship of contaminated sites.

In response to this challenge, our project developed a fiber-optic in-stream technology (FIT) for continuous measurements of suspended sediment load in surface waterways. Our research goals were to (1) assemble and test the FIT to measure light absorbance intensity of solutions, (2) adapt the probe design to measure suspended sediment loading and address calibration issues, (3) examine various portable and stationary field measurement designs, and (4) perform field investigations of sediment and contaminant fate and transport in various surface waters at the Livermore site and Site 300.

Since mid-year FY2002 funding, we (1) designed a prototype for the FIT [Fig. (a)], (2) constructed sediment-mixing microcosm for proof-of-concept and calibration tests, (3) designed and initiated studies to test the FIT and compared it to other available technologies, and (4) developed and tested a digital data detection and collection system.

The proof-of-concept studies examined using a low-energy light source—a red laser diode—connected to a linear fiber-optic array to measure suspended sediments in a simulated laboratory bench-top installation, the storm water simulator. The approach was successful, with a large linear measurement area and high signal-to-noise ratio. By using light intensity and adjusting the source-detector spacing, the design provides a wider linear measurement range and simpler device-calibration procedures. This versatile design makes it possible to optimize the various components of the FIT to produce an accurate, simple system to measure suspended sediments.

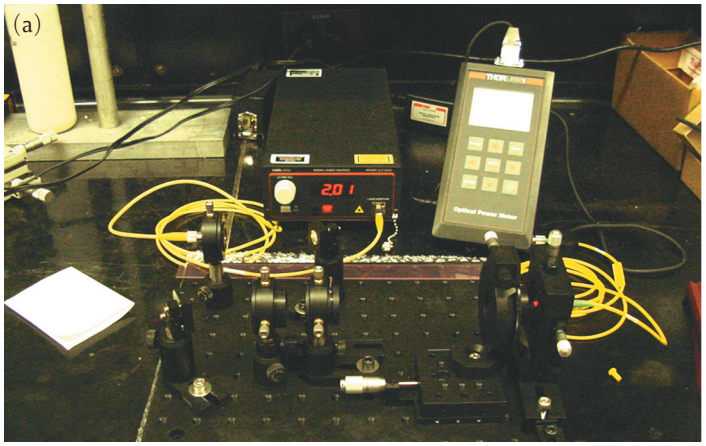

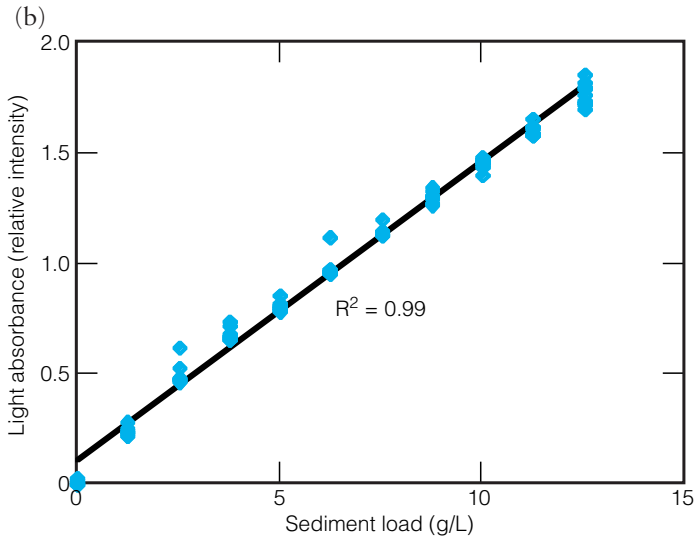

(a) Prototype fiber-optic in-stream technology (FIT) provides versatility for testing various sensor designs. (b) Light absorbance measurements made with the linear fiber-optic array while a known mass of sediment was suspended in water in the storm water simulator. The results demonstrate that the fiber-optic device can be used for direct measurements of suspended sediment at the kind of sediment loadings observed in streams during storms.

Development of a quantum-limited microwave amplifier using a direct-current superconducting quantum-interference device

S. D. Kinion

Experiments in many scientific fields rely on ultralow-noise microwave amplifiers, yet the noise temperatures of traditional transistor-based amplifiers remain an order-of-magnitude higher than the limit imposed by the Uncertainty Principle of quantum mechanics. Reaching the quantum limit would be a major scientific and technological achievement and lead to rapid progress in many areas, including radio astronomy, particle astrophysics, spin measurement, and quantum information processing.

The goal of this project is to fabricate and demonstrate the first quantum-limited microwave amplifier using a dc superconducting quantum interference device (dc SQUID). One of the first applications will be to combine the amplifier with a single-electron transistor (SET) to achieve a quantum-limited electrometer. With a suitable spin filter, the SET + SQUID electrometer will enable rapid, single-spin measurements needed for basic scientific research and for viable implementation of quantum computation.

Success will give LLNL a substantial role in the quantum information and quantum computation fields and could lead to revolutionary techniques for secure information communication networks for the Laboratory's national-security missions. Other applications include efficient data mining and encryption techniques for homeland defense. This project builds upon an ongoing collaboration with Professor John Clarke at the University of California, Berkeley.

The dc SQUID consists of two Josephson junctions—the most sensitive magnetic flux detectors available—in a superconducting loop. When properly biased, they act as very-low-noise amplifiers at frequencies from a few kilohertz to ~10 GHz. The Figure shows a schematic (a) and microphotographs (b) and (c) of a typical square-washer SQUID amplifier. The SQUID loop is formed by the washer and counter electrode separated by two Josephson junctions with external shunt resistors. The input signal is applied to the input coil, which acts as a microstrip resonator. The output signal is the voltage between the counter electrode and the washer. Present devices are an order-of-magnitude quieter than the best transistor-based amplifiers and within a factor of 2 to 3 of the quantum limit. Previous measurements suggest that the noise temperature was limited by hot-electron effects in the shunt resistors. By reducing this effect with a design modification, SQUID amplifiers should reach the quantum limit.

In FY2002, we implemented a controllable, reliable fabrication process for Josephson junctions and fabricated prototype dc-SQUID amplifiers. The gain of these devices, measured at 4.2 K, was found to be greater than 20 dB, slightly better than devices fabricated earlier.

FY2003 should bring the first demonstration of a quantum-limited microwave amplifier. When the largest obstacle—cascading two of these devices without sacrificing gain—is overcome, the prototype devices will be tested at 25 mK. After one or two rapid design iterations, we expect to achieve the standard quantum limit.

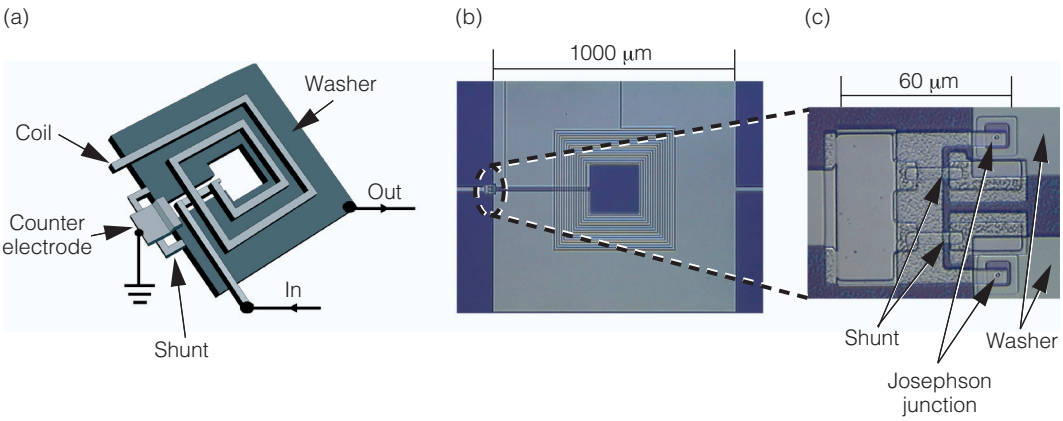

(a) Schematic of a square-washer SQUID, with integrated spiral coil electrically insulated from it. (b) Microphotograph of square-washer SQUID with 15-turn input coil. (c) Conter electrode. The two small dots are the Jospehson junctions, consisting of an aluminum oxide layer sandwiched between the niobium (Nb) washer below and the Nb counter electrode above. The normal metal shunt resistors are visible as two horizontal strips above and below the middle of (c).

Probing the properties of cells and cell surfaces with the atomic force microscope

M. McElfresh, R. Rudd, J. Belak, R. Balhorn

In the past decade, rapid development of atomic force microscopy (AFM) has made possible nanometer-scale-resolution imaging of biological materials ranging in size from single molecules to intact cells. By monitoring the deflection of chemically functionalized cantilevers during approach-retraction cycles (i.e., force volume curves), the unbinding forces have been determined for various ligand receptor pairs. It is now possible to use a single receptor molecule bound to the tip of an AFM cantilever to map the locations of ligands bound to solid surfaces.

In this project, we are developing a new recognition-mapping method that will provide real-time response measurements of individual living cells to a range of perturbations. The properties of living cells change in response to a wide variety of external stimuli, ranging from chemical and thermal changes in the environment to their response to infection or poisoning by bacteria and toxins such as those manifested by biological and chemical warfare agents. Our technique will allow detection of resulting changes in the properties of the cell membrane at the nanoscale. This project support the laboratory's counter proliferation and homeland security missions.

We are also developing an experimental technique to measure living cells and a computational model to distinguish the mechanical response of the cell from local surface interactions, with subsequent application of these concepts to a well-known cell system. Local surface interactions include recognition (or binding) events between molecules bound to an AFM tip (e.g., an antibody) and molecules or receptors on the cell surface (e.g., the respective antigen).

During FY2002, nanostamped patterns of specific self-assembled-monolayers (SAMs) were fabricated, and AFM tips functionalized (a process that allows the attached molecule to react with specific molecules on the surface) with Concanavalin-A (Con-A) were used to test the binding of the target molecules between an AFM tip and rigid, surface-bound molecules on the SAMs. The Con-A tips were then used to study living cells prior to and after the acrosomal reaction—a natural process in which the sperm cell sheds part of its outer membrane in preparation for fertilization—and recognition events were observed for cells for which the acrosomal reaction had been induced (see Figure). We also obtained unprecedented topographic images of the post-acrosomal cell that show a dramatic change in the shape of the cell, and we used theoretical modeling to incorporate constitutive properties of the membrane to produce a more realistic cell model.

In FY2003, we will quantify recognition events being observed on both rigid surfaces and the cell surface and use the theoretical model to analyze measurements of cells to improve our understanding of the target molecule in its membrane environment. The bovine sperm-cell model will be refined to include a realistic model of the cell's content to gain a better understanding of currently unexplained features in the force–distance curves and to provide a platform for integrating and analyzing measurements on local membrane properties.

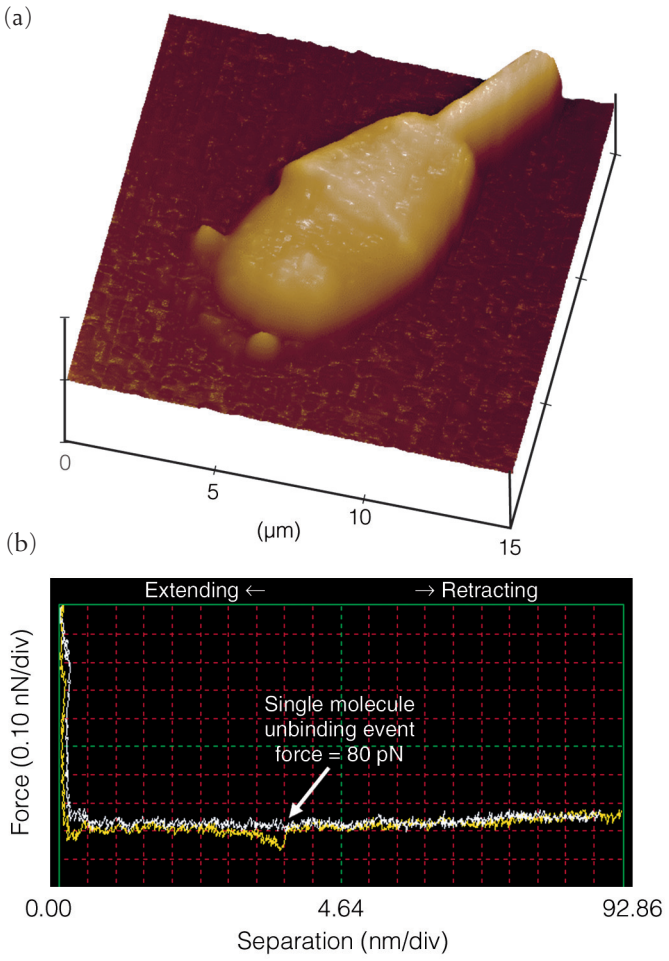

Topographic atomic force microscopy (AFM) image of (a) a bovine sperm cell and (b) a force–distance curve showing an "unbinding" event between the AFM-bound Con canavalin-A tips and the receptor on the cell.

Surface-enhanced Raman spectroscopy with high spatial resolution

T. Huser

Identifying individual molecules and determining how they interact with their environments are critical steps toward a better understanding of complex organic systems. Although optical detection techniques have always played a key role in the nondestructive and noninvasive analysis of complex materials, until recently optical microscopy has lacked the sensitivity to study biomolecular processes at the molecular scale.

The recent development of novel light-detection techniques—such as highly quantum-efficient photon detectors—is enabling researchers to probe optically biomolecular processes at the single-molecule level by observing the fluorescence of specific marker molecules. However, this approach has limited application because it requires (1) a priori knowledge about the system under investigation and (2) the use of marker molecules, which alter the system in undesirable ways. Raman scattering is one of few optical techniques that can identify molecular bonds by observing their distinct vibrational fingerprints, but it is orders of magnitude weaker than fluorescence.

In this project, we are developing new optical probes that enable nondestructive characterization and identification of organic and inorganic matter at the nanometer scale by combining surface-enhanced Raman spectroscopy (SERS) with gold- or silver-coated scanning-probe microscope (SPM) tips. The scanning SERS probe generates an image of the physical structure of a sample together with detailed chemical information about its composition.

This work will enhance LLNL's capabilities to characterize materials at the nanometer scale, which is very important to potential applications such as (1) identifying spurious amounts of biological and chemical warfare agents, (2) identifying nanometric laser damage-initiation sites in optical materials for high-power lasers, and (3) conducting genomics and proteomics research at the single-molecule level, in support of LLNL's mission in national security and basic science.

In FY2002, we conducted experiments on single, isolated gold and silver nanoparticles to which just one or a few molecules were adsorbed. Our first experiments were conducted with organic molecules, such as amino acids, in an effort to establish the limits of detection with our instrumentation. In the next phase, single molecules of 4-mercaptopyridine were adsorbed to isolated silver particles. The characteristic intermittent emission from single, isolated particles proved that only signals from single molecules were observed. We also applied single-molecule SERS to protein folding by conducting proof-of-principle studies of DNA hairpin loops adsorbed to isolated silver particles.

To combine SERS with SPM, we produced SERS tips by sputter-depositing silver thin films onto commercially available silicon and silicon nitride SPM tips, then used these tips to study single bull-sperm cells. The images (see Figure) revealed significant Raman enhancement and local differences in the local composition of the samples.

In summary, this project achieved the identification of single molecules using SERS on colloidal noble-metal nanoparticles. This technology was then combined with atomic-force microscopy to chemically distinguish differences in the composition of individual biological cells.

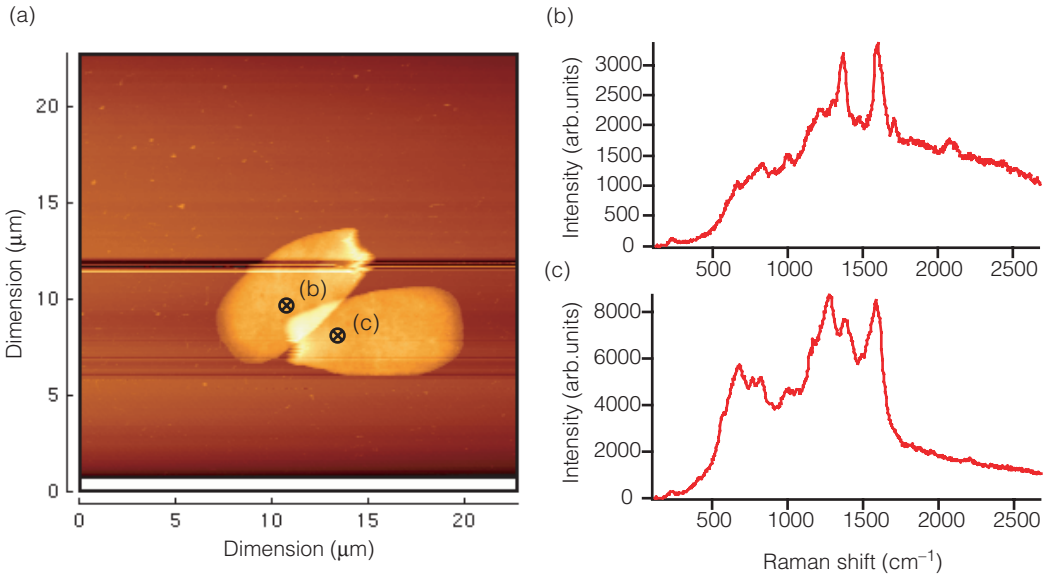

The results of surface-enhanced Raman spectroscopy using gold-coated scanning-probe microscope tips. (a) Topographic image of two bull sperm cells. Differences in spectra indicate (b) local protein abundance and (c) locally increased DNA content.

Diffraction-limited adaptive optics and the limits of human visual acuity

S. S. Olivier, A. A. S. Awwal, B. J. Bauman, D. T. Gavel

Visual acuity of the normal human eye is limited by significant high-order optical aberrations that cannot be corrected by standard corrective eyewear. Adaptive optics (AO), a technology used in astronomy to correct for image blurring arising from atmospheric turbulence, can compensate for these aberrations and provide normal eyes with supernormal vision.

In collaboration with the Department of Ophthalmology at the University of California, Davis (UCD), we are using LLNL's unique expertise in high-resolution optical wavefront control with liquid-crystal spatial-light modulator devices to carry out detailed studies of the visual performance benefits of improved ocular aberration correction for the general population. This project seeks to determine the ultimate resolution of the human eye and the ideal optical correction, considering wavefront aberrations and neurological factors.

Beyond the fundamental contribution to basic vision research, this work will advance next-generation corrective eyewear and surgical procedures designed to take the general population beyond the "20/20" visual acuity standard. This work will also have direct application in developing (1) supernormal vision capabilities that support LLNL's national-security mission and (2) advanced clinical ophthalmic instrumentation for diagnosing and treating the diseases that are the primary causes of human blindness, in support of LLNL's mission in science to improve human health.

In an earlier LDRD project (98-ERD-061), we developed expertise in using high-resolution liquid-crystal wavefront-control technology to provide high-precision beam control for high-power laser systems. In the present project, we are applying that expertise to high-precision correction of optical aberrations in the human eye. This high-precision capability will be critical in reaching our objective of using AO to enable assessment of the ultimate physiological and neurological limits of human visual acuity.

We have designed and constructed an AO system (see Figure) for human vision correction using new liquid-crystal, spatial-light modulator technology. The system senses and corrects the aberrations present in the human eye.

First, a dim beam of infrared light is directed into the eye and focused onto the retina. A small fraction of this light is reflected from the retina and serves as a "beacon" for sensing aberrations in the eye. The light from this beacon is relayed to the liquid crystal and then to a wavefront sensor that determines the residual aberrations. This wavefront information is used to calculate signals that are sent to the liquid crystal to compensate for the aberrations. Simultaneously, the subject can look through the system, off the face of the spatial light modulator, to a computer monitor that displays a visual acuity target. By varying the characteristics of this target and recording the subject's perceptions, we can study the limits of human visual acuity.

In FY2002, we transferred the AO system to a laboratory at the UCD Medical Center. Initial experiments on human subjects were performed, and the results were analyzed to optimize the system for correction of aberrations in the human eye.

In FY2003, this completed system will be used to perform initial clinical trials of human visual acuity improved by correcting subjects' ocular aberrations.

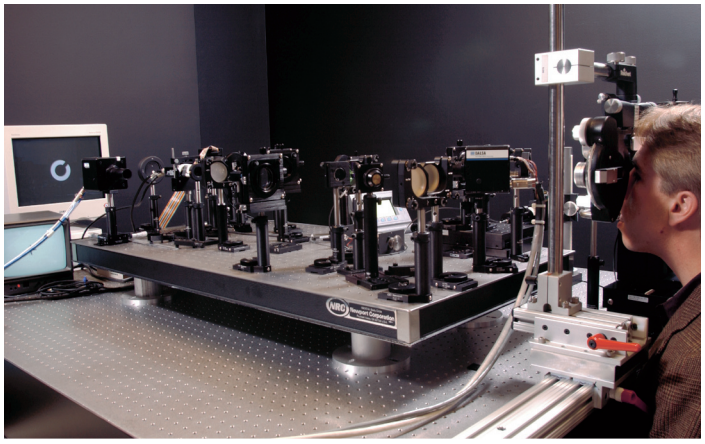

High-resolution liquid-crystal adaptive-optics system for human vision correction now in use at the University of California, Davis, to study the limits of human visual acuity.

A high-speed photon-counting camera for the detection of extrasolar planets

T. Miyazaki, J. N. Ullom, M. F. Cunningham, B. Macintosh, S. E. Labov

The search for extrasolar planets—planets orbiting stars outside our Solar System—is motivated by the desire to discover small planets similar to Earth.

However, directly observing an extrasolar planet from Earth is challenging because of the relative proximity of the planet to its parent star. Although a large, terrestrial telescope can provide the angular resolution necessary to visually separate the planet from the star, atmospheric turbulence limits the telescope's performance. In addition, the parent star appears much brighter than the planet. Adaptive optics (AO) can increase a planet's brightness, but they have little effect on residual star glare.

To overcome these difficulties, we are developing a high-speed, photon-counting camera that is sensitive to individual optical and infrared photons. This camera, which brings together cryogenic sensing elements and cryogenic digital electronics, will integrate sensors with a novel read-out multiplexer that allows the response of many sensors to be measured by a relatively small number of amplifiers. The camera will capture a series of images, taking each frame during the short timescale (~100 ms) when star glare consists of discrete speckles of light. In any given frame, some pixels may have speckles, while others may be speckle-free. The speckle-free pixels can then be combined to build a final image uninterrupted by star glare and atmospheric turbulence.

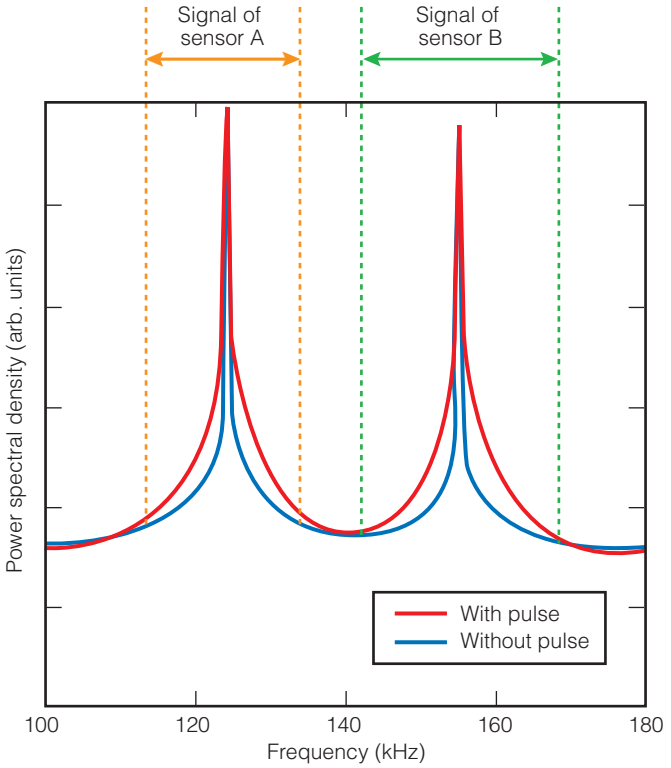

Output power spectrum of the two sensors for our high-speed, photon-counting camera. The signals of the sensors are modulated at different frequencies and read by a single amplifier.

The project builds on existing LLNL expertise in AO and cryogenic photon sensors and, if successful, will make it possible to acquire and process data from arrays containing thousands of pixels. Results will provide the proof-of-concept needed for LLNL to build larger instruments for major observatories and space-based missions. In addition, we are using the new read-out technology to develop detectors that perform high-resolution spectroscopy of fissile material at about five times the spectral resolution of existing equipment. The ability of these detectors to discern the presence of nuclear material has potential applications that in support of LLNL's nuclear nonproliferation mission.

Our progress during FY2002 includes developing a multiplexed read-out system. This system sums signals from two gamma-ray sensors, which have an energy resolution of approximately 60 eV for 60-keV photons and a superconducting transition temperature of 0.12 K. An ac bias current, instead of the traditional dc bias current, is applied to modulate the signals of both sensors at bias frequencies of 125 and 155 kHz—fast and well separated relative to the sensor-decay time constant (~1 ms) and the signal bandwidth, respectively (see Figure). The signal is demodulated with a commercial lock-in amplifier. Under ac bias multiplexed read-out, the system showed the same performance as under conventional dc bias read-out.

We also made progress in sensor-noise analysis by creating a sensor model that combines the thermal and electrical properties of the sensor and that explains most of the sensor noise observed. This model can be used to optimize both sensor performance and the read-out electronics.

In FY2003, we will (1) improve the read-out system to demodulate multiplexed signals from more than two sensors, (2) demonstrate the system's performance, (3) improve the sensor model, and (4) optimize the sensors and read-out system for optical and infrared photons.

Single-molecule techniques for advanced in situ hybridization

C. W. Hollars

Researchers have only begun to understand the relationships between the three-billion-nucleotide genetic code described in the human genome and the regulation and control of gene and protein expression within each of the millions of different types of highly specialized cells. Analysis of gene and protein expression in situ is progressing at an extremely slow pace because the methods used typically involve gene-probe complexes used in combination with catalytic chemical amplification or avidin–biotin amplification. Amplification is necessary to raise the selected signal above the background autofluorescence; however, only a few targets per tissue section can be evaluated.

This project used new optical techniques and instrumentation with single-target sensitivity to detect low levels of gene-probe response in situ, without the need for amplification. These advancements will enable precise, simultaneous localization in a cell of the expression points of multiple genes or proteins in a single sample. Information regarding the precise timing and location of gene expression is a crucial component in the discovery of new pharmacological agents for the treatment of disease. By developing technologies that accelerate the analytical process, this project supports LLNL's mission in bioscience to improve human health.

During FY2002 we focused on developing a plasmon-resonant-particle (PRP) fabrication protocol capable of generating multiple distributions of particles with a narrow size distribution using a gold-seeding and silver-enhancement procedure. We successfully fabricated three distributions consistent with particles exhibiting blue, green, and red scattering cross sections.

Although these results show great promise in using PRPs in a multiplexed assay, the fabrication protocol was irreproducible. The dependence of several experimental factors in the silver-enhancement process were explored to no avail. We then examined factors affecting scattering properties, including particle size—widely known to affect spectral response—as well as particle shape and nanocrystal defects. To evaluate these factors, we constructed a microscope capable of determining the size and relative shape using atomic-force microscopy combined with the measured spectral response of single nanocrystals (see Figure).

We also continued PRP in situ hybridization experiments on the Peg3 gene, focusing on reducing nonspecific binding and background scatter from the surrounding tissue. The results of these experiments are promising; future work to enable demonstration of multiplexed PRP in situ hybridization experiments includes completion of the refined fabrication protocol.

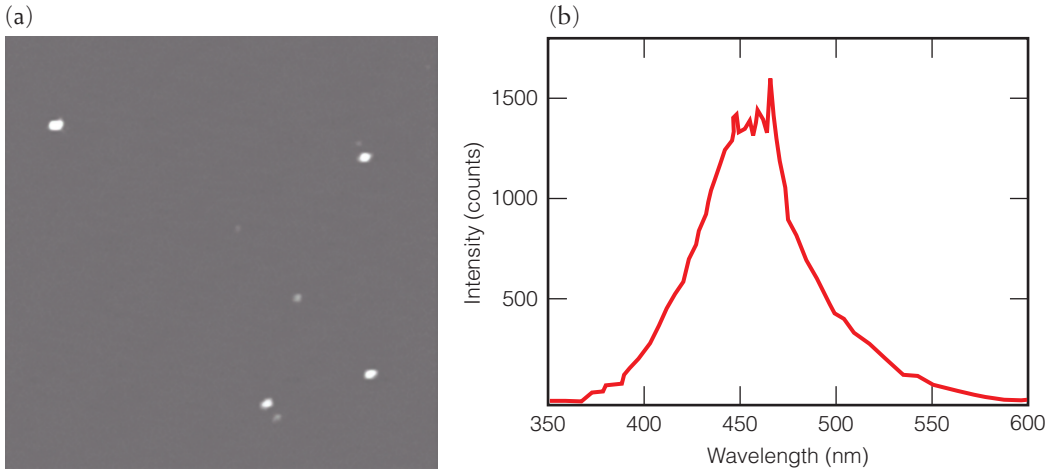

(a) An atomic-force microscopy image (4 μm × 4 μm) of 60-nm plasmon-resonant particles dispersed onto a glass substrate. (b) A representative single-particle scattering spectrum.

Generation of single-cycle light pulses

B. C. Stuart, I. Jovanovic, J. P. Armstrong

Most optical pulses, even at the 10-fs timescale, consist of several oscillations of the electric field. Our research proposes to produce and amplify an ultrabroadband continuum to produce single-cycle (<3 fs) optical pulses. This will require pulse compression to <3 fs with subfemtosecond accuracy. Production of these single-cycle pulses will lead to new generations of experiments in the areas of coherent control of chemical excitations and reactions, high-order harmonic generation for probing materials and fast processes, and three-dimensional (3-D) micrometer-scale material removal and modification.

Several groups have demonstrated pulse generation in the 5 to 10-fs regime. These pulses are typically very low energy—in the nanojoule range. Our objective is to generate the extremely short pulses and to amplify them to useful levels—in the microjoule to millijoule range. An optical parametric amplifier (OPA) is one way to accomplish this because it can support amplification of extremely broad bandwidths. Optical parametric amplification is a phase-matched, nonlinear process in which energy from a pump beam is transferred to an amplified signal beam within a nonlinear crystal or structure. Along with the amplified beam, an idler beam is created at a given wavelength and angle to conserve energy and momentum.

(a)

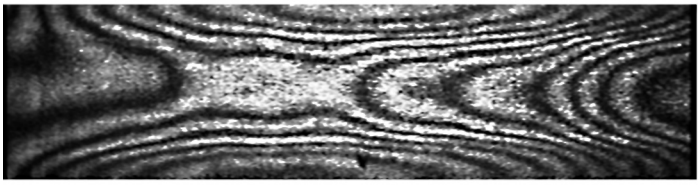

(b)

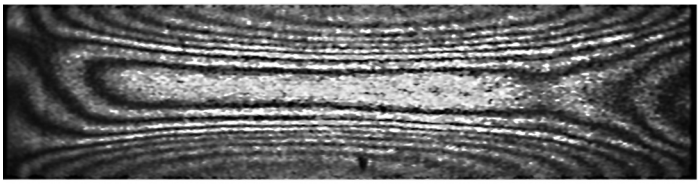

The genetic algorithm flattens (a) an initially distorted 19-element micromembrane deformable mirror. (b) The same mirror flattened by the genetic algorithm along the central horizontal stripe. Along this line, the mirror is flat over 70% of its length, with two to three waves of error at each end, which were due to the way the mirror was manufactured and its limitations in stroke for correcting the initial aberrations.

Our project goals include (1) constructing an 8-fs oscillator, (2) amplifying pulses from several oscillators, (3) splitting off some of the pulses to generate a broadband continuum, (4) using the rest of the pulses to pump a novel OPA, and (5) using adaptive control of a deformable mirror to achieve pulse compression to the single-cycle regime.

Completion of this project will create a new DOE capability in materials probing and manipulation on extremely fast timescales, which is important for many applications that support the Laboratory's stockpile-stewardship mission: controlled excitation and detection of chemical compounds, submicrometer 3-D machining, and subfemtosecond extreme ultraviolet generation for materials probing.

A genetic algorithm—called "genetic" because it operates on analogy with the natural-selection process—has been activated to control the first deformable mirror for pulse shaping and optimization. The Figure shows interferograms of a distorted 19-element micromembrane mirror [Fig. (a)] that was flattened along its central horizontal strip [Fig. (b)] by the genetic algorithm.

In FY2002, our first pulse diagnostic, the spectral phase interferometry for direct electric-field reconstruction (SPIDER), was constructed and initial testing begun. We pursued two alternate paths to seed generation: an argon-filled hollow capillary and a shorter-pulse (8-fs) oscillator. A novel approach to the amplification stage was designed, and the OPA amplification hardware ordered.

In FY2003, we will (1) compress amplified pulses to 3 fs by using an optical configuration that includes adaptive phase control of both the input to the fiber continuum generator and the continuum compression, (2) measure the continuum intensity and phase through frequency-resolved optical gating and SPIDER, and (3) apply the amplified pulses to selectively excite materials, initially, diatomic or other small molecules. Phase control of the final output pulse will also allow for the manipulation of excitations in atoms and molecules. The pulses will be amplified using the OPA, and carrier-envelope phase control will also be investigated.

Photoluminescent silica sol-gel nanostructured materials designed for molecular recognition

S. J. Shields, J. G. Reynolds, B. Clapsaddle

To counter bioterrorism, rapid detection and structural characterization of biologically relevant molecules are critical. However, difficulties detecting biological molecules (e.g., proteins, metabolites and DNA) arise from the complex nature of the cellular or environmental matrix that lead to interferences in many detection methods. In addition, complex mixtures of molecules purified from the environmental matrix often leads to the inability to detect all species present, by masking the target molecule. Separation methods such as chromatography and electrophoresis fractionate complex mixtures into simpler mixtures, thereby increasing the likelihood for detection of low-abundance molecules. However, these separation methods can be very expensive, difficult, time consuming, and disruptive to the native structural motif of biological molecules. The prefered experimental configuration is to isolate and detect biomolecules as quickly as possible.

In the last decade, mass spectrometry (MS) technology has taken the lead in biomolecule-detection schemes, becoming a viable method for studying large, labile molecules, such as proteins and DNA. The success of MS is partly due to the advent of ultraviolet matrix-assisted laser desorption ionization (MALDI), which uses a matrix to absorb the energy at the wavelength of the laser. Desorption occurs when analyte molecules entrained in the matrix crystal lattice are vaporized from the solid state to the gas phase. Two limitations of MALDI MS for rapid detection of biological molecules are extensive sample preparation requiring a matrix, and interferences in ionization by cellular constituents.

In an attempt to circumvent the limitations of MALDI MS, this project is aimed at developing silica sol-gel nanostructured materials to function as separations media directly on MALDI sample plates (see Figure). Several properties of the silica sol-gel materials, including their ability to photoluminesce and separate, make them unique to the application of MALDI for rapid separations of biomolecules. Photoluminescent properties allow the material to replace the matrix. These materials can be designed to have various chemical and physical attributes—such as acidity, hydrophobicity, and pore size—that will selectively bind specific molecular compositions from complex mixtures. This partitioning of molecules is then detected by observing different molecular mass signatures in the MALDI MS experiment.

During FY2002, we focused our research on developing sol-gel materials for MALDI MS experiments. The synthesis procedures we designed produced silica sol-gels and aerogels of varying porosity and densities. Our sample plate-coating techniques produced coatings of low porosity (spin and dip coat), to high porosity (spray coat). Properties of the sol-gels and aerogels associated with analyte interactions were varied by incorporating different organic compounds into the silica framework. For example, a triphenyl functionality was added to the silica framework to increase hydrophobic character, thereby increasing the hydrophobic interactions of biomolecules with the surface.

Preliminary results by MALDI MS and surface infrared spectral analysis indicate that several of the materials bind target biomolecules too tightly to be viable because the material features are too porous or have selected chemical functionality that suppresses volatility of the target molecules. However, when selected organic compounds, such as the triphenyl functionality, are incorporated into the material, volatilization and ionization of the analyte occurs, producing quality MS spectra without addition of normal MALDI matrices. This is a significant advance in the development of these materials to act as in situ ionization tool.

In FY2003, we will continue to develop materials that function as a matrix and further explore the separations capability of the materials by using a variety of spectroscopic tools to elucidate the nature of biomolecular interaction with these materials.

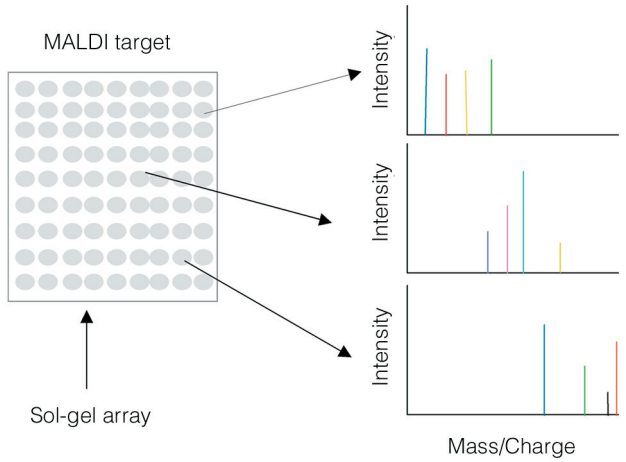

(left) Ultraviolet matrix-assisted laser desorption ionization (MALDI) sample plate with coating of sol-gel materials of varying pore sizes and chemical compositions. The sol-gel coating eliminates the need for matrix application and simultaneously separates biomolecules by selectively binding specific molecular compositions from complex mixtures. (right) Separated molecules are detected by observing their molecular mass signatures using MALDI mass spectrometry.

Micro-airships for sensing and imaging

J. Marion, J. Trent, B. Anderson, A. Grossman, L. Wood

The U.S. relies on intelligence gathered from space and from high-altitude aircraft to assess a potential adversary's activities. In this study, we examine the feasibility of performing certain surveillance functions from airships that are orders of magnitude smaller than current ones, such as commercial blimps. Superpressure micro-airships, with or without self-propulsion, can be fitted with modern miniaturized imaging and sensing payloads for applications such as information collection over specific locales. Because imaging payloads can be assembled from commercial technology, these airships can be low cost and disposable in nature.

This study examines some key elements of the feasibility of using micro-airships charged with helium gas and deployed upwind from the target by ground, ship, or aircraft. First, we examine airship size scaling, then the feasibility of a smart, Global Positioning Satellite- (GPS-) based, on-board navigational system that permits each airship to autonomously seek a windborne path to a target by a set of altitude changes. Optional self-propulsion using battery-powered propellers will also be considered as a course-modification capability to more exactly overfly the target. Successful completion of this study could enable the rapid (<1 yr) development of a mission-capable constellation of these sensing platforms. By providing a rapidly deployable, less costly method of surveillance, this work supports LLNL's missions in national security.

The nominal payload envisaged for a wind-propelled airship consists of an imager and sensor package; control processor; and data-storage, GPS, communications, and energy-storage systems. In the most elementary imaging application, the airship wind drifts under variable altitude control to specific GPS coordinates, then generates and transmits several images. The simplest communications package is a satellite telephone, which has a low payload mass but only a modest bandwidth (2900 bps). Our baseline design accommodates a payload mass of 500 to 1000 g, depending on the level of integration, although applications requiring higher-resolution cameras would involve greater payload mass.

In FY2002 we first examined airship size requirements for the nominal payload as a function of altitude, generating a range of potential operational possibilities. For example, a 1.3-m airship could lift a 500-g payload to an altitude of 10 km. Studies of capabilities for correcting an airship's course as it drifts downwind found that a 100-km cross-range capability would require a modest mass increase, which could be accommodated with a slight increase in airship size. Station keeping—maintaining a stationary position over a target—is viable for short times in modest winds, but all-weather station keeping would require very large airships.

To examine the prospects for purely windborne navigation, we created a model that demonstrates the flight paths of windborne objects launched at various altitudes to see whether there exists a specific path whereby an airship could, by altitude changes alone, navigate eastward from a specific site to a second specific site. Our study shows that for most eastward paths GPS-based navigation would often permit overflight of a specific target. Autonomous navigation appears feasible; adding the course-correction option significantly enhances this capability.

This project demonstrated that a mission-capable constellation of these sensing platforms could be developed rapidly (<1 yr). The system could provide a new and potentially less costly way of performing surveillance for national- and homeland-security applications.

Gigapixel surveillance camera

R. E. Marrs and C. L. Bennett

The threats of terrorism and proliferation of weapons of mass destruction require new techniques for surveillance and intelligence collection. The U.S. faces a serious and growing threat from adversaries who locate key facilities underground, hide them within other facilities, or otherwise conceal their location and function. Reconnaissance photographs are one of the most important tools for uncovering the capabilities of adversaries. However, current imaging technology provides only infrequent static images of a large area or an occasional video of a small area.

This project proposes to add a new dimension to reconnaissance imaging by developing a gigapixel video surveillance camera for high-altitude aircraft. This camera, combined with a motion-detection algorithm, would make it possible to track every vehicle in a 1,000-km^2 area, roughly the size of the Livermore–Amador Valley. The tracking information will help find and characterize hidden facilities by identifying vehicle movement that links them to other facilities. In a different mode of operation, a gigapixel camera could provide real-time surveillance for tactical operations.

During our FY2002 Feasibility Study, we developed a design for a 500-megapixel, flight-capable camera and determined that the design can be scaled to over 10 gigapixels. Reliable vehicle tracking requires a ground resolution of 0.5 to 1 m and a framing rate of approximately two frames per second (fps). From aircraft platforms, this resolution can be achieved with aperture diameters of a few centimeters. Our design uses commercial camera lenses with focal lengths between 150 and 1000 mm. The light sensor is an 8-megapixel CMOS focal plane array with a read-out rate of 30 fps.

The key innovation in this design is multiplexing several fields of view into the same sensor by using a rotating mirror wheel that holds 16 small-angle, 3-in.-diam tip-tilt mirrors, each of which can be tilted out of the plane of the wheel by about 3 deg. With a readout rate of 30 fps, the sensor can look at 16 different fields of view approximately twice per second. Since the lenses required for this application are relatively small, using multiple lenses and sensors increases the field of view even more. Our 500-megapixel design uses four, 8-megapixel sensors, each of which can look at the 16 adjacent fields of view provided by the tip-tilt mirrors (see Figure).

The area of coverage for a gigapixel camera is so large that computer processing is required to locate and track moving vehicles. We have developed and tested a motion-detection algorithm that works by comparing the intensity of each pixel in each frame to the running average of the intensity at the same location in the preceding and following frames. The algorithm, which flags any vehicle-sized cluster of pixels that deviates from the average intensity, was able to find all moving vehicles in a video of a freeway interchange and discriminate them from most artifacts such as the apparent motion of the tops of tall buildings caused by changing camera position.

Results from this Feasability Study have already benefited projects now funded by the DOE. When additional funding becomes available, the next step will be to construct a prototype camera, which includes 16-fold multiplexing, to demonstrate the value of gigapixel surveillance data for intelligence collection.

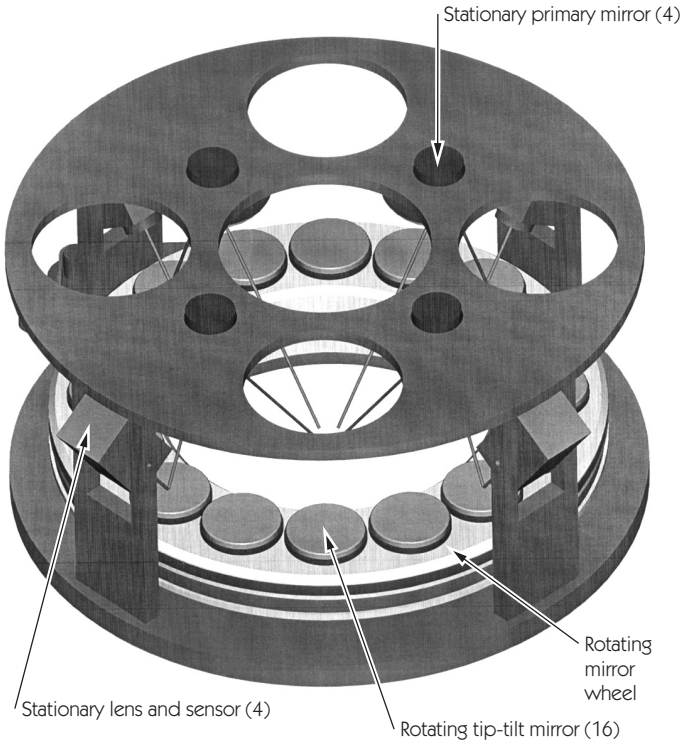

In this 500-megapixel multiplexing camera design, each of four sensors can look at 16 adjacent fields of view—provided by the16 tip-tilt mirrors on the rotating mirror wheel—approximately twice per second.

Rapid, single-spore identification using micro-Raman spectroscopy

C. E. Talley

Highly sensitive, rapid methods for identifying potential biological warfare (BW) agents are a pressing national-security issue. No current method of identifying bacterial spores is both rapid and sufficiently accurate. For instance, techniques based on polymerase chain reaction (PCR) are extremely accurate but take 12 to 24 h. to determine the presence of pathogenic spores. For more rapid detection, antibody-based techniques are typically used. These techniques can identify the presence of spores within minutes but require a minimum of ~10,000 spores and are prone to false positives.

The goal of this project is to develop an accurate and rapid technique for detecting bacterial spores by exploring the possibility of using micro-Raman spectroscopy—using a microscope to focus a laser beam to a diffraction-limited spot (typically 0.5 μm in diameter) on the sample, recording the sample's spectrum, and identifying the molecules in the sample by comparing the spectrum with the previously recorded spectra of known materials. The sequence of work in this project is to (1) obtain spectra for a variety of spore species; (2) identify the chemical components that are responsible for the specific spectroscopic features observed; (3) characterize the effects of bacterial growth conditions on the Raman signal; and (4) combine micro-Raman with surface-enhanced Raman spectroscopy (SERS), in which gold or silver nanoparticles are attached to the spore surface to increase the Raman signal by several orders of magnitude and identify unique, species-specific chemical features on the outer layer of the spore.

During FY2002, we collected the Raman spectra of individual spores for four species of *Bacillus* spores: *B. subtilis, B. cereus, B. thuringiensis*, and *B. megaterium*. These spectra were dominated by calcium dipicolinate (see Figure), which is present in the cortex of the spore and which interfered with species identification by overwhelming Raman signals from the proteins, lipids, and other species-specific molecules that would have enabled identification. Spores from bacteria grown in different media were spectroscopically analyzed to investigate the possibility of identification based on detecting the type of media used to culture the bacteria, but again, the calcium dipicolinate dominated the spectra and overshadowed any subtle spectral changes caused by the type of growth media.

We investigated the effect of attaching SERS particles to the outside of the spores before analysis. The SERS particles circumvented the problem of signal saturation by calcium dipicolinate by allowing the field to penetrate only a few nanometers into the spore. Unique spectra were obtained for *B. cereus* and *B. subtilis* spores, demonstrating that the Raman spectra acquired using SERS can be used to identify the spore species and distinguish between spore species. Future work in this area will focus on providing a more reproducible means of attaching the SERS particles to the spores and identifying the SERS components of spectroscopic features.

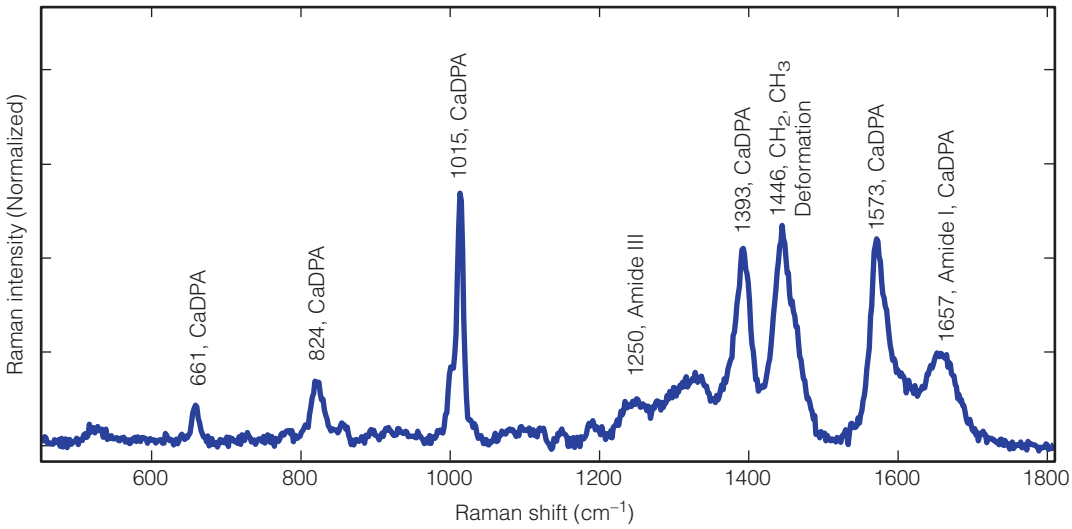

The Raman spectrum from a single Bacillus cereus *spore illustrating that the Raman signal is dominated by calcium dipicolinate, found in the spore cortex.*

A phase-conjugate resonator for solid-state heat-capacity lasers

M. D. Rotter

The conventional approach to improve beam quality in heat-capacity lasers is to use a deformable mirror in the cavity, but this method is mechanically and operationally complicated. Optical phase conjugation (OPC) is a much simpler and less expensive method. In OPC, the phase of a laser beam is reversed so that upon propagation through the distorting system, the aberrations—which can be thought of as variations in beam phase—are "unwound," resulting in an essentially aberration-free beam. However, it is not known whether solid-state heat-capacity lasers are capable of initiating OPC, given their low intracavity intensity and large Fresnel number—which is beam area divided by the product of the light wavelength and cavity length.

The goal of this project was to determine, using computer modeling, the suitability of a three-slab heat-capacity neodymium–glass (Nd:glass) laser for OPC experiments. This particular laser was chosen because many of its characteristics are similar to those of a full-scale heat-capacity laser. An immediate application of this technology is in high-average-power (100-kW class) heat-capacity lasers for tactical short-range air defense systems, in support of LLNL's national security mission. This work is also of value to laser research in general and could enable radically different, greatly improved designs for high-average-power laser systems for numerous DOE and DoD programs, such as the Future Combat System program.

As a first step, in FY2002, we developed a computer model that calculates the energetics of a laser resonator having an OPC mirror. The code couples, in a self-consistent manner, laser oscillation dynamics with time- and space-dependent stimulated Brillouin scattering (SBS), which is the nonlinear process responsible for OPC.

Initial calculations on our three-slab test bed showed that the Stokes intensity—the intensity of light reflected back into the laser cavity—was extremely small, on the order of a few milliwatts, indicating a very low level of phase conjugation. The main cause of the weak Stokes intensity was the broad (25.5-nm) fluorescence line width of the Nd:glass laser medium. Gain narrowing was insufficient to achieve the long coherence length needed to generate high levels of Stokes radiation.

Our next-generation heat-capacity laser will use Nd-doped gadolinium–gallium–garnet (Nd:GGG) crystals, which have a substantially narrower fluorescence line width, as the laser media. Calculations showed that gain narrowing in the pulse should be sufficient to obtain a long coherence length and, therefore, generate sufficient Stokes radiation. In our calculations, the laser output with SBS [Fig. (a)] exhibited the spikes in intensity characteristic of SBS, whereas output without SBS [Fig. (b)] exhibited relaxation oscillations characteristic of normal laser operation.

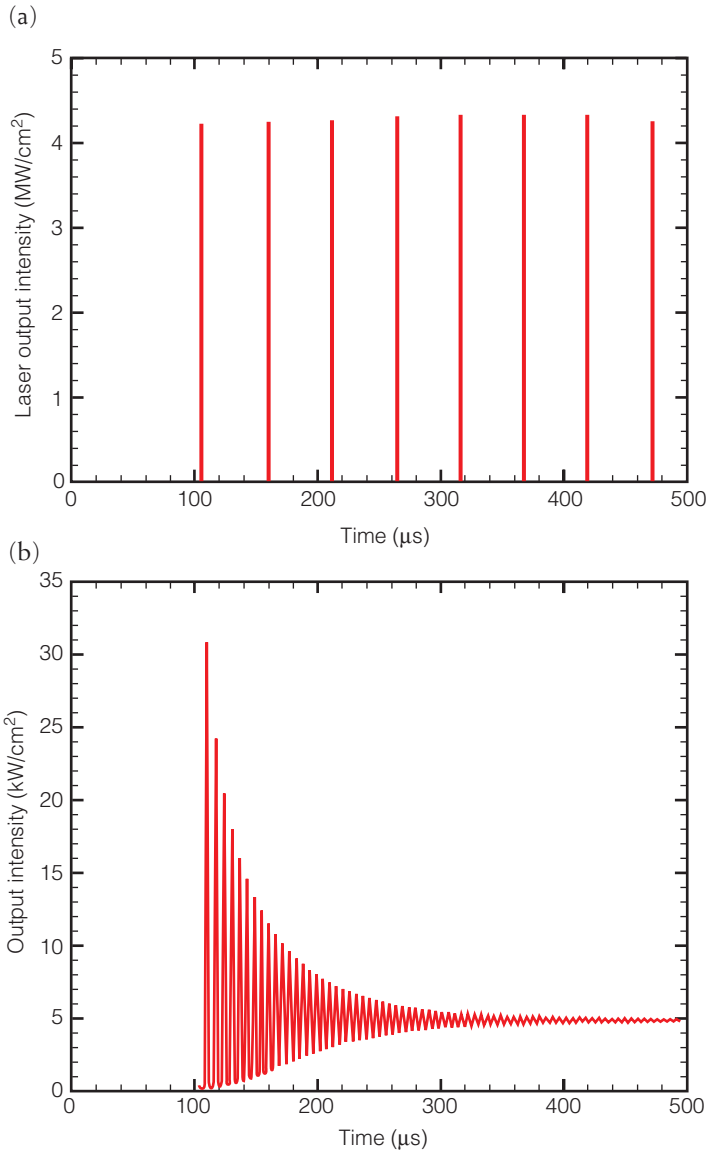

Calculated output intensity of a neodymium-doped gadolinium–gallium–garnet (Nd:GGG) heat-capacity laser under (a) stimulated Brillouin scattering (SBS) conditions and (b) non-SBS conditions. The presence of SBS suggests the possibility of improving beam quality in heat-capacity lasers using optical phase conjugation.

Biological Sciences

Section 2

Biological Sciences — Section 2

Pathogen pathway project

J. P. Fitch, S. L. McCutchen-Maloney, E. Garcia, V. Motin

The deliberate or accidental exposure of hundreds or thousands of people to pathogens could result in significant loss of life, with high economic and social costs. Addressing the threat of bioterrorism requires improved understanding of the mechanisms by which pathogens harm humans.

This project identifies and characterizes the genes and proteins involved in the virulence mechanisms of pathogenic bacteria and in the response of the host organism. We expect to find traits that could lead to new strategies for detecting genetically engineered organisms. We initially focused on the plague bacterium, *Yersinia pestis*, a potential biowarfare agent with virulence mechanisms that can be induced in vitro. These mechanisms are found in other human pathogens with significantly different clinical manifestations, so our work will apply to other microbes, including *Salmonella* and *Y. pseudotuberculosis*.

The goal of this project is to develop high-throughput, broadly applicable methods for improving our understanding of pathogens and to apply the methods to *Y. pestis*. Integrating knowledge obtained from genomic and proteomic tools could help create new classes of detectors, vaccines, and treatments, furthering LLNL's national-security mission.

In FY2002, genomic activities continued to refine microarray designs for all genes of *Y. pestis* and *Y. pseudotuberculosis* and to use the arrays to discover additional new genes related to pathogenicity. Modeling approaches to elucidate biomolecular processes have been used, including fuzzy restricted-logic biomodels and integrating modeling with indexed experiments.

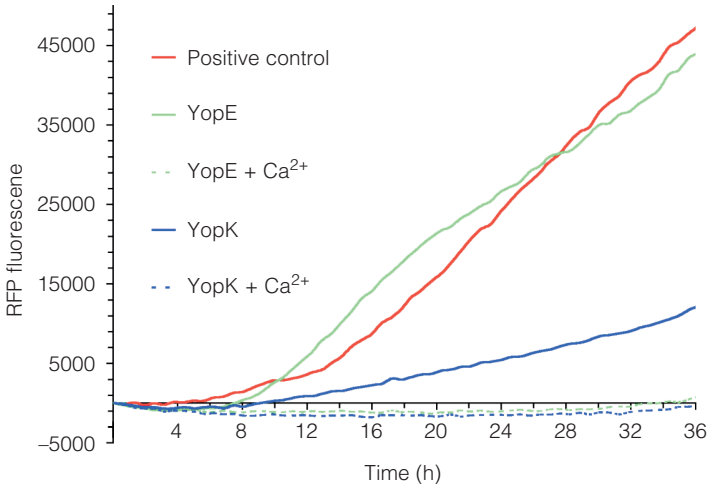

Expression of a protein (YopE) and virulence factor (YopK) for Yersinia pestis *was measured with red fluorescent protein (RFP) fluorescence. Solid lines indicate expression under conditions simulating those of the bacteria's human host (37°C, low calcium levels); dashed lines, under conditions of the flea vector (26°C, high calcium levels). These results indicate that* Y. pestis *virulence proteins are differentially expressed according to surrounding conditions.*

Proteomic efforts focused on identifying *Y. pestis* proteins that are differentially expressed according to the different temperatures and calcium levels in the flea vector (26°C, high calcium levels) and the human host (37°C, low calcium levels). To identify proteins in each environment, we used separation methods consisting of fast protein liquid chromatography, including ion exchange and hydrophobic interaction, followed by sodium dodecyl sulfate–polyacrylamide gel electrophoresis. Separated proteins were removed from gels, analyzed by mass spectrometry, and identified by database searches. Dozens of differentially expressed proteins were identified. So far, over 40% of the predicted *Y. pestis* proteome has been identified.

We also demonstrated—with the LacI protein as a model system—a new method that uses custom arrays to capture transcription factors and novel mass-spectrometry detection to identify them, and began characterizing expression cascades of virulence factors using a fluorescent reporter system to monitor real-time expression in living cells (see Figure). This platform enables more precise measurements of expression patterns, including temporal distributions. In addition, genomic and proteomic host–pathogen interaction studies were begun using two-dimensional gel separations and mass-spectrometry identification; initial application to the response of human cells to multiple *Yersinia* species was completed. Such experiments are critical to what we term pathomics—the comprehensive understanding of the cause of disease.

This project has already resulted in spinoffs: biomarkers for early detection for the NNSA's Office of Nonproliferation Research and Engineering (NA-22); application of the genomic methods to other pathogens, also for NA-22; basic *Yersinia* biology for the National Institutes of Health; computational signature discovery for bacteria and viruses (for NA-22) and its application to the foot-and-mouth disease virus (with University ofCalifornia, Davis and for the U.S. Department of Agriculture) and the smallpox virus (for the Centers for Disease Control and Prevention).

In FY2003, we plan to integrate fuzzy logic and differential equation modeling; expand host–pathogen interaction experiments, data analysis, and modeling; and publish the results of whole-genome transcript profiling.

Strategic Initiative in applied biological simulations

M. E. Colvin, G. Galli, D. Barsky, F. C. Lightstone, E. Schwegler, C. Venclovas, C. Mundy

The continuing goal of this project is to apply advanced molecular simulations to biological research areas important to LLNL missions and to the broader scientific community through collaborations with experimental biologists both at LLNL and at universities. Areas of research include studies of the enzymes that repair DNA damage, DNA-binding anticancer drugs, food-borne cancer-causing chemicals, the multiprotein "machines" that replicate DNA, and protein–molecule interactions relevant to new cancer treatments and autoimmune diseases. The simulation capabilities used in the project have broad application to other DOE missions, including biodefense and environmental cleanup.

The project has built a productive collaboration with the University of California, Davis, Cancer Center on a new type of cancer radioimmunotherapy. In this approach, four antibodies are linked together on a molecular scaffold; two of these antibodies bind to the surface of prostate cancer cells and two others bind to subsequently administered radionuclides that are bound in chemically linked chelators. We have used protein structure prediction methods to model the antibodies, classical molecular dynamics (MD) to study the conformational distributions of the linked chelators, and quantum chemistry to model the chelation of radionuclides. These simulations suggest new chemical structures to be synthesized and evaluated by our collaborators.

In FY2002, we modeled enzymes that recognize and repair DNA damage. Using MD simulations, we analyzed mutants of human apurinic/apyrimidinic endonuclease that increase cancer risk, and extended our studies to include the Rad51 family of proteins that repairs DNA double-strand breaks. Molecular modeling provided structural predictions of several Rad51 proteins and complexes and guided several experiments to determine how these proteins form a complex. The Figure shows our models of the Rad51B/Rad51C complex (left) that were used by our collaborators to design yeast two-hybrid experiments and create specific mutations (blowup at right) that affect the protein complex formation. In FY2003, we will extend our model to include other key proteins binding to the Rad51B/Rad51C complex.

We made considerable progress in our first-principles MD (FPMD) simulations of nitrogen mustard anticancer drugs. These simulations involve very accurate dynamical simulations using quantum mechanical force fields of each step in the activation reaction path. In FY2002, we simulated the intramolecular cyclization reactions of an important cancer drug metabolite, phosphoramide mustard. In FY2003, we will simulate an inactive ester form of phosphoramide mustard to identify chemical differences related to anticancer activity. These results will be valuable in validating other, less computationally costly simulation methods and in helping design new anticancer drugs.

In FY2002, we completed studies of the reaction mechanisms for the oxidation of DNA bases by the chemical radicals formed from ionizing radiation. Using both static quantum chemical methods and FPMD methods, we investigated and identified transition states and reaction mechanisms for an isolated guanine interacting with hydroxyl radical. In collaboration with researchers at Princeton University, we extended our study to the DNA base thymine, also implicated as a DNA base that will undergo damage.

Using protein modeling, in FY2002 we generated all-atom models to structurally characterize individual subunits that comprise the eukaryotic replication factor C (RFC) protein complex, a protein that loads a torus-shaped protein (PCNA) onto DNA, a step critical in the replication of genomic DNA. These detailed models allowed us to propose a functional mechanism by which RFC interaction with PCNA can be regulated in the cell cycle. Our modeling-based study provided both a structural framework for interpretation of existing experimental data and reported a number of novel findings that can be subjected to direct experimental testing. In FY2003, we will be modeling two alternative RFC complexes that are believed to have alternative functions within the cell.

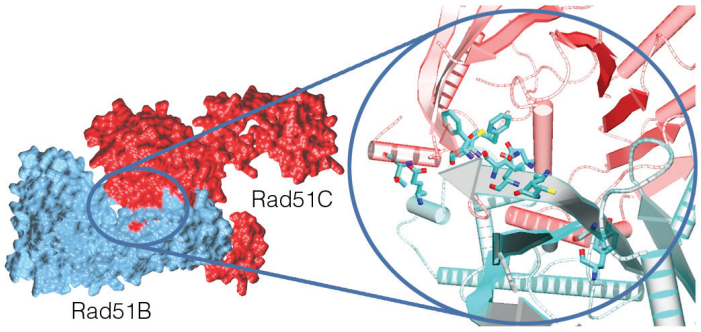

(left) Initial models of Rad51B/Rad51C complex were used to design yeast two-hybrid experiments, revealing which regions of the proteins are in contact. (right) Details of the modeled interactions allowed specific mutations to be tested.

Structural genomics of human DNA repair and microbial proteins

M. A. Coleman, B. W. Segelke, P. T. Beernink

The growing number of genes identified in human, animal, and microbial genomics projects challenges us to understand their biological function. The new research field called proteomics aims to elucidate protein structure and function, which are unknown for most of the newly discovered genes. Proteomics projects using high-throughput structure determination, or structural genomics, have run into significant bottlenecks in protein production, purification, and crystallization. Most proteins do not express well and have only moderate solubility, making them poor candidates for structural studies.

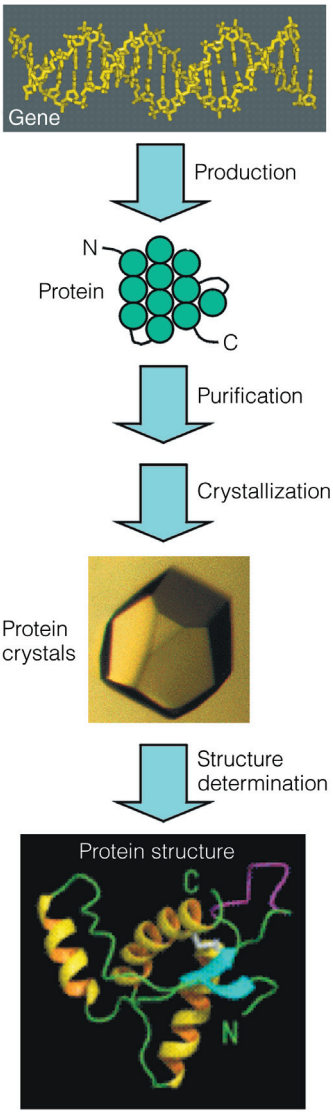

Process steps in structural genomics. This project has laid the groundwork for an efficient, automated crystallization facility.

The objective of this project is to overcome these bottlenecks by developing techniques for the rapid production, screening, and functional analysis of cell-free proteins. By using methods to increase the protein solubility, we can make many more proteins candidates for crystallization. The efficient, automated crystallization screening protocol we are developing—called CrysTool—allows us to screen many more proteins for crystallization, increasing the likelihood of successful structure determination.

This project used information from microbial sequencing and gene-array experiments, as well as LLNL's Integrated Molecular Analysis of Genome Expression (IMAGE) gene library, for selecting protein targets of interest. In addition, we developed novel procedures and technologies that constitute significant intellectual property of interest to pharmaceutical, structural genomics, and other biotechnology companies.

Our research has increased the value of genomic information generated at LLNL for the DOE's Human Genome Project by providing novel screening, production, and crystallization technologies. By focusing on microbial pathogens and human DNA repair processes, this project has also furthered LLNL's missions in national security and bioscience to improve human health, as is evident from the number of human diseases associated with pathogens and defects in DNA repair pathways.

In FY2002, we (1) continued to develop our pipeline for protein production; (2) targeted an additional 192 genes of interest from *Yersinia pestis*, which causes bubonic plague; (2) continued examining some 80 genes from IMAGE; (3) identified > 63 expressed proteins that are suitable for large-scale protein production; (4) purified 25 proteins to homogeneity; and (5) developed several screening techniques for cell-free protein production. Using a standard fluorescence-based protein-folding assay, we distinguished soluble proteins, which can be purified, from insoluble proteins, which will need further engineering before purification. Crystallization trials of the soluble proteins yielded five crystals, of which two are ready for x-ray diffraction studies.

We also configured a liquid-handling robot with custom components and interfaced the robot with CrysTool for automated crystallization design, setup, and data acquisition, with a throughput of >4000 experiments per day.

This project has laid the groundwork for an efficient, automated crystallization facility. Remaining issues include miniaturization of crystallization screening.

The structure and function of regulatory DNA: A next major challenge in genomics

L. Stubbs

The biology of gene regulation is a rapidly growing field with applications ranging from human susceptibility to managing microbes in the environment. Previous research has revealed some of the basic mechanisms of gene control, which are fundamentally similar in all life forms from microbes to man. Gene "control switches" are DNA sequences that serve as docking sites for specific activating or silencing proteins. However, very few of these regulatory DNA sequences have been identified, and most details of their function remain unknown.

The DNA sequences of human, mouse, and other species provide a large new set of raw material for regulatory element (RE) sequence discovery and analysis. Discovery of gene regulation mechanisms is a high-priority goal for the DOE and National Institutes of Health genomics efforts. In the past year, we have succeeded in establishing the basic technical foundations for regulatory genomics research at LLNL.

In this project, we developed high-throughput methods for identifying RE sequences in the human genome and used these methods to verify 20 different predicted REs for genes located on human chromosome 19 (HSA19). Only about 5% of the human DNA sequence is functional, and finding these important DNA elements against a background of genomic "junk" is a significant challenge to the genome community.

The best way to find these important sequences depends on computational alignment and sequence comparisons between large segments of human DNA with genomes of distantly related species. Although "junk" DNA can change rapidly without consequence, genes and REs cannot; DNA sequence change generally leads to loss of function. As a result, evolution has preserved these important sequences as islands of similarity that stand out against the background of junk DNA when two genomes are aligned, as illustrated in the Figure.

In FY2002, we used several different computational methods developed by others to compare related regions of human, mouse, and chicken DNA sequence. We compiled the results of different methods to find the most probable locations of gene (protein coding) sequences from potential REs. We also developed high-throughput experimental approaches to test the validity of both protein coding and regulatory elements in human DNA. We completed computational analysis of three different one-megabase regions of HSA19, and tested our experimental pipeline on a set of 20 genes and REs contained in one of the regions. With this new technology in hand we are set to apply the approach to study global mechanisms of gene regulation in humans.

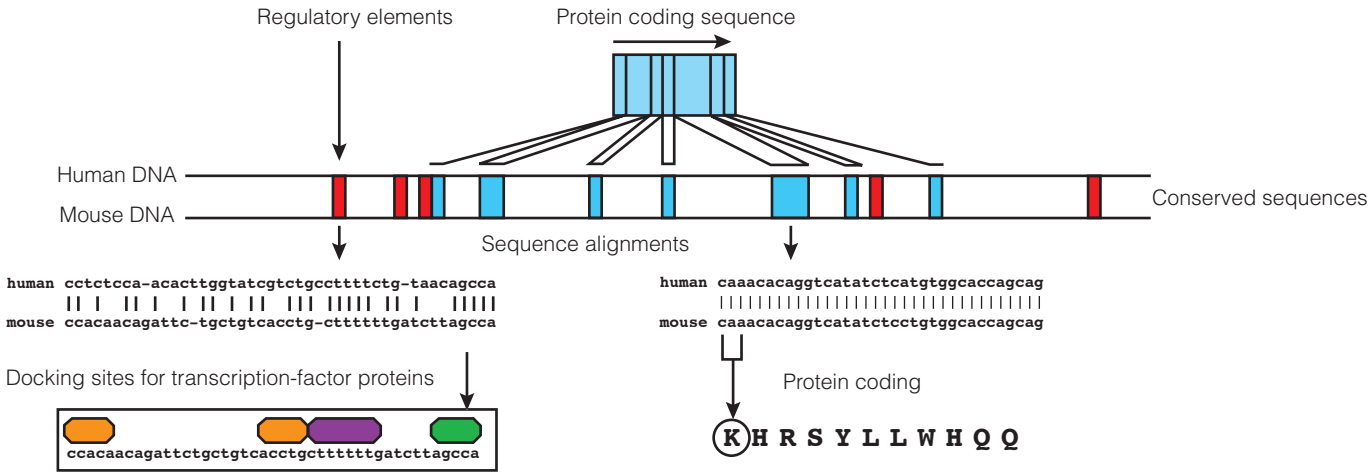

Aligning human DNA sequence regions with comparable regions from species distantly related to humans, such as the mouse, identifies functional sequences because their structure has been conserved over evolutionary time. These conserved sequences comprise most of the protein-coding components of genes (blue), as well as the regulatory elements (REs) (red) that control the timing, cell locations, and levels of gene activity. The REs, which serve as docking sites for specific regulatory proteins—called transcription factors—do not follow a strict sequential code and therefore are more tolerant of DNA sequence changes acquired over evolution than protein-coding (gene) sequences, which are more tightly conserved because the three-letter code for amino acids that comprise proteins is relatively strict and must remain in register to function.

Development of synthetic antibodies

J. Perkins, R.L. Balhorn, M. Cosman, F.C. Lightstone, L.C. Zeller

Much of what we know about molecular targeting is based on lessons learned from the immune system, an elegant, highly successful mechanism for detecting and eliminating molecular and microscopic foreign entities from the human (or animal) body. Central to the immune system's operation are antibodies—macromolecules designed to recognize and target foreign molecular structures. Antibodies enable vast, microscopic, seek-and-destroy operations that serve to fight off infections, cancer, and many other diseases. We believe that it is now possible to develop molecular targeting agents that improve upon the characteristics of natural antibodies and directly deliver lethal substances to cancer cells. The concept of molecular recognition can also be extended to developing powerful new detectors for biological-warfare (BW) agents. Like the natural immune system, detectors relying on molecular-recognition concepts promise to simultaneously detect numerous types of harmful biological agents within a single, compact instrument.

The aim of this project is to develop synthetic high-affinity ligands (HALs), which are synthetic molecules designed to bind to target proteins with high affinity and specificity. The targets of interest are HLA-DR10, a protein expressed on the surface of non-Hodgkins lymphoma (NHL), and the toxins of the tetanus and botulism bacteria—potential BW agents. A HAL for NHL would be an effective delivery device for radionuclides that would shrink or destroy cancer cells. This project is being carried out in collaboration with the University of California, Davis Cancer Center, where researchers have already used natural antibodies as radiation-delivery agents. A synthetic counterpart could solve some of the problems associated with the injection of a natural antibody into the body. A HAL for tetanus or botulinum toxin could be used as an inhibitor for the toxins or as part of a sensory device. This project supports LLNL's missions in national security and bioscience to improve human health.

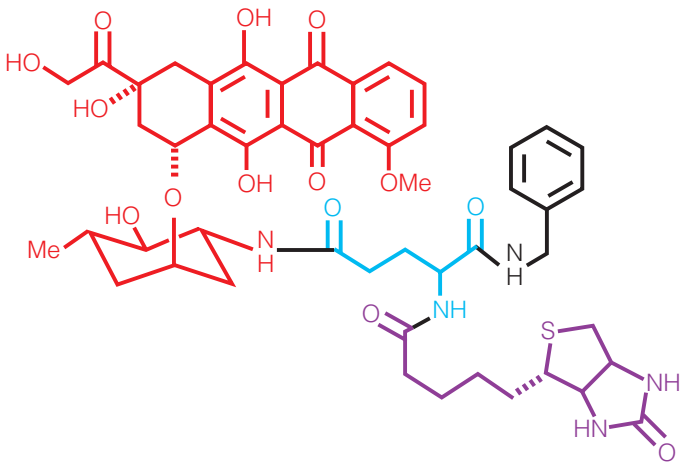

One of two synthetic high-affinity ligands (HALs) developed for the tetanus toxin. HALs can be used as an inhibitor for the toxins or incorporated into a sensory device.

In FY2002, a series of commercially available compounds were identified by a computational docking routine as binding to two unique, predetermined sites on HLA-DR10. Approximately 50 such compounds were then acquired and experimentally screened using nuclear magnetic resonance spectroscopy (NMRS) to determine their binding to the protein in solution. The result was a list of compounds that bind to each site on the protein. Two molecules, one from each list, were then chemically linked with a lysine scaffold to form a potential HAL, which is being investigated to determine its affinity for target protein.

We also synthesized two potential HALs for the tetanus toxin, each consisting of biotin and doxorubicin linked with lysine. An x-ray crystal structure of a tripeptide bound to the tetanus toxin was successfully obtained by our collaborators at Brookhaven National Laboratory. This result, coupled with our prior knowledge about the binding of doxorubicin to tetanus, enables us to initiate the synthesis of a new set of ligands.

Work proposed for FY2003 includes determining the specific binding affinity of the HAL that binds to HLA-DR10 and continuing to carry out NMRS screening for other compounds that bind to HLA-DR10. We will continue to synthesize the tetanus ligands and determine the binding constants and specific binding affinity between the ligands and their respective protein targets. This will require incorporating biotin into the HALs. By the end of FY2003, we hope to have in place a proof of principle for the design and realization of HALs.

Imaging of isotopically enhanced molecular targeting agents

J. N. Quong

The goal of radiation therapy is to kill only cancer cells while minimizing radiation damage to normal cells. Current methods for radiation dose estimation are based on crude, whole-body measurements and centimeter-scale dose averaging, neither of which addresses how radiation is deposited at the cellular level.

One approach to delivering radiation therapy more accurately is using targeted radiopharmaceuticals (TRPs) to seek out cancer cells via cancer-specific targets on the cell surface. However, the distribution of TRPs in tumor and normal cells is currently not known. Chemical imaging at the cellular level can determine TRP distribution and provide information about the interaction between TRPs and cells, leading to more effective cancer treatment while minimizing damage to healthy tissue.

We are developing a secondary-ion mass spectrometry (SIMS) imaging system to determine the distribution of isotopically enhanced TRPs in normal and cancer cells at the microscopic level. Our goal in this project is to develop an integrated imaging–simulations system to characterize the distribution of TRPs in biological tissue and to simulate dose distributions at the microscopic level. To do this, we must (1) determine a biological sample-preparation technique that does not alter the biochemical distribution and composition of the sample while preserving microstructure and morphology; (2) develop standards for each isotope of interest for quantitative SIMS measurements for input into the dose-estimation software program; and (3) extend PENELOPE—a well-tested and validated Monte Carlo photon- and electron-transport code—to calculate 3-D radiation-dose deposition from the measured, internal, source-drug distribution.

This project builds on LLNL's capabilities in radiation and analytical chemistry and supports LLNL's mission in bioscience and technology to advance human health, as well as its strategic alignment with the University of California, Davis (UCD) through the Joint UCD/LLNL Cancer Center.

Work in FY2002 focused on studying the distribution of isotopically labeled antibody-based anticancer agents using stable surrogates yttrium-89 (^{89}Y) and iodine-127 (^{127}I) in normal and cancer cells. We began (1) developing concentration standards for ^{89}Y and ^{127}I to enable relative quantification from signal intensities in the SIMS images and (2) studying the distribution of ^{89}Y and ^{127}I in kidney, liver, and tumor samples of mouse B-cell lymphoma. The Figure shows accumulation of an ^{89}Y-labeled antibody, which represents a radiopharmaceutical, in kidney tubules.

Work in FY2003 will include further analysis of treated samples to determine the cellular distribution of various TRPs as the basis for determining (1) effectiveness in treating tumor cells and (2) toxicity to normal organs. We will also look for correlations between differences in the processing by tumors and normal tissue of TRPs labeled with isotopes for which published variations in observed toxicity to tumors and normal organs are available.

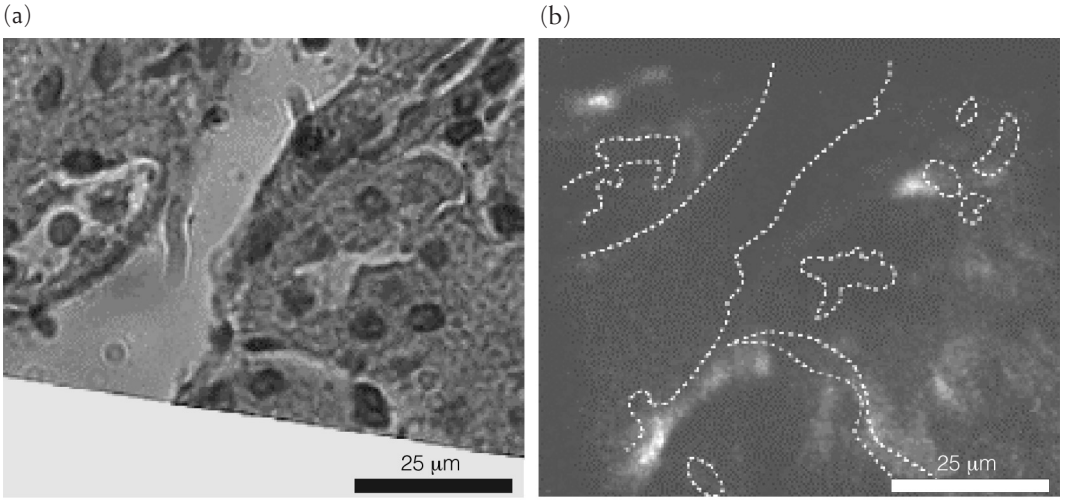

Tubules seen in (a) a bright-field image of a mouse B-cell lymphoma sample and (b) demarcated by dotted lines in an image of yttrium-89 (^{89}Y) concentration in the same sample obtained with our secondary-ion mass spectrometry imaging system. Understanding how targeted radiopharmaceuticals—represented by ^{89}Y—are distributed in cells can lead to more effective cancer treatment.

Measuring DNA repair pathway function: A step toward determining health risk from radiation

I. M. Jones, D. O. Nelson, H. W. Mohrenweiser

Although it has been known for decades that human exposure to ionizing radiation increases the incidence of cancer, predicting which individuals are at most risk from radiation exposure is still a distant goal. Such predictive ability is needed to guide policies that regulate radiation exposure and ensure that medical treatments provide maximum benefit with minimum risk.

Differences between people in susceptibility to radiation are largely based on genes inherited from their parents. Among the important genes in this connection are those that produce proteins that repair DNA damaged by radiation. These proteins are of two types: base excision repair (BER) proteins that repair single-strand breaks and oxidized bases in DNA, and double-strand break repair proteins that repair broken chromosomes. This study focused on the BER pathway. The BER genes are known, variants of the genes have been identified at LLNL, and LLNL has recently developed an assay for BER function using white blood cells.

Using technologies and information from the Human Genome Project, we had determined before beginning this project that the DNA sequence of DNA repair genes varies within the human population. For each of 37 genes studied, an average of three to four different variants that affect the protein were found. The average frequency of these variants is 5%. Given the many genes in each DNA repair pathway and their many variants, our technical ability to determine an individual's repair genotype greatly exceeds our ability to interpret the information.

A long-term goal of this project is to relate DNA repair genotypes to health risk from radiation. The goal of our initial effort was to begin developing pilot data and identifying statistical methods that could be used to test the hypothesis that many different genotypes have similar DNA repair capacity phenotypes (functions). Relations between genotype and phenotype could then be used to group genotypes with similar phenotypes and ultimately test the association of groups of genotypes with health risk from radiation. Genotypes with reduced repair function are expected to increase risk of radiation-induced health effects. By enhancing our scientific basis for understanding the exposures and risks to humans from low-dose radiation, the work supports LLNL's mission in bioscience and technology to improve human health.

In FY2002, analysis of the cell lines of 81 people for the capacity to repair DNA damage in the absence of radiation was completed by assaying single-strand DNA breaks using single-cell gel electrophoresis and image analysis. We also assembled genotype information for these people and the predicted functional impact for 86 inherited variants of 25 BER genes and began analyzing the relationship between this phenotype and BER pathway genotype. Preliminary analyses identified seven variants that together explain 16% of the individual variation in the damage in unirradiated cells. This successful analysis of a very complex data set demonstrates the promise of our approach to relating genotype at many related genes to the ability to repair DNA damage. A pilot study has been funded by the National Cancer Institute to investigate the association of this repair phenotype with cancer risk in occupationally exposed radiological technicians.

In addition, we completed studies with human blood lymphocytes and found that cryopreserved cells, after thawing, retained the capacity of repairing radiation-induced damage and that this capacity was higher in thawed and incubated cells than in cells taken directly from blood. The oxidative stress of cell culture may lead to better repair function. We also refined an assay for estimating the rate of repairing DNA damage induced by ionizing radiation and applied the assay to cell lines from 31 people whose BER genotype was known.

Proposals were submitted to fund follow-on work that will focus on finishing our analysis of the association between genotype and damage in unirradiated cells for 86 BER variants, completing application of our rate-of-repair assay to cell lines from 81 individuals, and analyzing the association of this second BER phenotype with BER genotype.

A three-dimensional model of signaling and transport pathways in epithelial cells

A. A. Quong, C. J. Mundy, A. Kubota, A. Golumbfskie, A. Nichols

The emergence of many new technologies for measuring biological data, including whole-genome sequencing, DNA- and protein-expression arrays and imaging technologies for in vivo chemical measurement, makes quantitative modeling of cell function a realistic possibility. The near-term goal of such modeling will be to validate and integrate empirical data about cell function, but the long-term goal will be to study the effect of cellular signaling on pathogen–host interactions, which have critical impact on human and animal health.

Epithelial cells represent the body's interface with the outside world, including pathogens. Epithelial function depends on the transport of both water and ions. Knowledge of the signaling pathways, connected with one another and with a multitude of other signaling and metabolic pathways, is vital to a scientific understanding of the pathogen–host interaction. Understanding the complexity of ion transport in airway epithelial cells is important for developing new strategies for the treatment of diseases such as cystic fibrosis. This project supports LLNL's national-security mission by developing a model that can be used to study issues related to biosecurity and health.

To understand the complexity of epithelial signaling and transport systems, we have developed a fully three-dimensional (3-D) model of calcium (Ca) signaling in epithelial cells. This model includes ion diffusion and active transport within the cell and across membranes as well as structural predictions and molecular simulations of the proteins responsible for metal ion chelation and transport processes. The model is based on fundamental chemistry and uses experimental data at the largest length scale for model validation. We will also use experimental data to determine the structural components of our 3-D model. The computational model is based on a set of reaction-diffusion equations that are solved on a large-scale finite-element code in 3-D (ALE3D). We have explicitly included the major compartments in the cell: the membrane, cytosol, nucleus, and gap junctions.

During FY2002, we implemented a diffusion-reaction model within ALE3D that involves Ca^{2+}, inositol triphosphate (IP3), endogenous buffer, the dye Fura-2, and the green fluorescent protein, and we have begun using this model to study the dynamics of Ca and IP3 in cells. At this point, our model gives us qualitative agreement with experimental data (Hirose, 1999), which is illustrated in Fig. (a). Figure (b) shows the results of our simulation in a simplified geometry of a Ca^{2+} wave initiated with IP3 spike. This is the first attempt at building a 3-D model, although the approach has been used before in simplified geometries.

In FY2003, work will focus on developing a validated 3-D model of the epithelial cell by using both published data and by performing a set of experiments using cell lines to measure the geometrical parameters for our model. We plan to determine structural parameters, perform additional measurements to validate our model, and compare our results with published experimental data to validate the model and determine its diffusion parameters.

(a) (b)

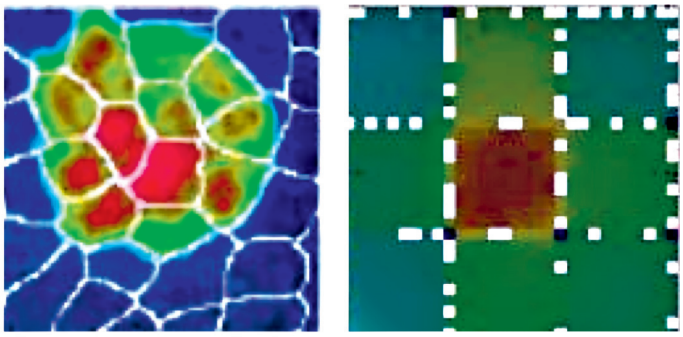

Experimental image of calcium-2+ (Ca^{2+}) in kidney epithelium (a) compared with simulation and (b) in a simplified geometry. Red and blue represent high and low Ca concentrations, respectively.

Tailored assays for the detection of viral agents

P. McCready

Bioterrorists targeting livestock or other agricultural assets in the U.S. could have major economic consequences. One of the most serious crises that the U.S. Department of Agriculture (USDA) could face is an outbreak of a foreign animal disease—a disease not currently found in the U.S., such as foot and mouth disease (FMD), shown in the Figure—because of the absence of a rapid, validated, and widely available diagnostic for detecting and identifying many such pathogens.

The rapid spread of diseases such as FMD has prompted the international community to require that infected animals and those within a three-mile radius of the initial infection be destroyed within 24 hours of initial diagnosis. However, in an epidemic, the large numbers of disease samples to diagnose can overwhelm a nation's diagnostic laboratories. For instance, during the FMD outbreak in the U.K., the turnaround time for laboratory diagnostics was approximately 30 days, forcing the U.K. and neighboring countries to rely on observation of clinical symptoms.

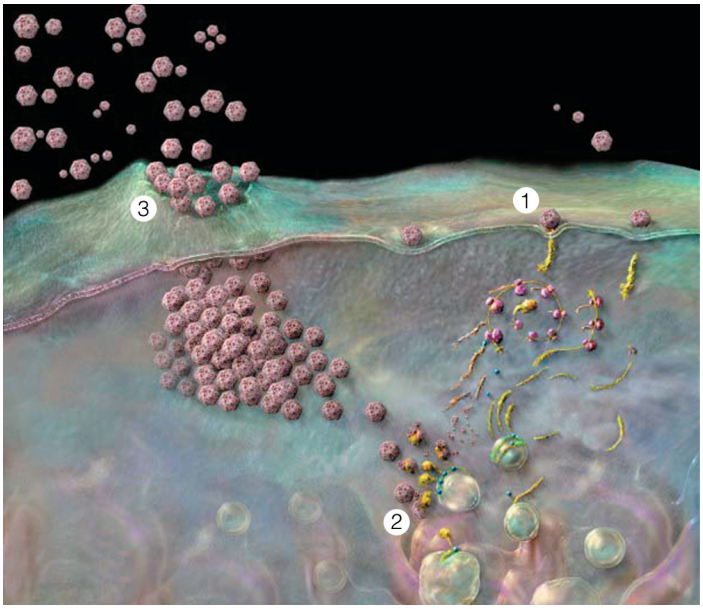

The foot and mouth disease (FMD) virus (1)enters a cell and replicates in the cytoplasm. (2) The cell's chromosome is used to make new copies of the virus , eventually destroying the cell (3) and releasing new virus particles to infect other cells. This research has produced assays that enable the rapid, reliable detection of foreign animal diseases such as FMD.

Because many viral diseases exhibit initial symptoms similar to those of FMD, U.K. authorities destroyed any herd exhibiting FMD-like symptoms, as well as adjacent herds. Unfortunately, subsequent analyses indicated that most of the animals destroyed actually had non-FMD infections. In the future, a widely available, rapid, and accurate test would ensure that decisions of such tremendous impact are based on objective data.

The goal of this project is to establish a process at LLNL that would allow the rapid development of new diagnostics for viral pathogens such as FMD. In FY2002, computational tools and DNA sample archives necessary for viral-assay production were developed and implemented to produce assays for five viruses. These assays were extensively screened for sensitivity and specificity.

Three of the assays, combined in a single tube form, were tested with freshly collected field samples at the California Animal Health and Food Safety Laboratory. This testing included benchmarking the new test against "gold-standard" assays for two indigenous viruses. The results show that our assay test works better and faster than current diagnostics. In testing at Plum Island, New York, the only facility in the U.S. where testing for FMD is allowed, the assays far surpassed our expectations for sensitivity and specificity, outperforming all other tests currently in use. This FMD assay test is currently being field tested in Indonesia by the U.S. Department of Agriculture. In addition, viral assays were generated to detect the West Nile and St. Louis encephalitis viruses. These two tests are currently undergoing extensive testing with the State Department of Health in Texas, New York, and California.

In FY2003, follow-on work will begin at LLNL with joint funding from DOE's Chemical and Biological National Security Program and the USDA's Agricultural Research Service. The project entails bringing together researchers and diagnosticians from around the country to fortify our nation's capability to generate assays rapidly and distribute them nationwide in an emergency. This capability will enable the rapid identification of foreign animal disease outbreaks that would threaten our country's stability and security.

Rapid assay development for biological-weapon-agent detection and surveillance

K. Turteltaub

The use of biological agents as a weapon of terror on U. S. soil is now a reality and threatens our security as a nation. Mitigating the effects of a biological-agent attack requires early detection, identification of the agent, and assessment of options for decontamination and treatment. Over the last decade, LLNL has demonstrated the usefulness of DNA diagnostics for detecting and identifying selected threat organisms. Most recently, a "pipeline" approach to producing DNA-based diagnostics for threat organisms was created, offering us the ability to produce diagnostics in a high-throughput fashion as new threats arise. The "pipeline" has resulted in high-confidence nucleic acid identification for 15 high-priority bioterrorism agents.

This project has begun an effort to use the same large-scale, whole-genome approach for identifying pathogen-specific DNA signatures to develop a "protein pipeline" for identifying pathogen-specific protein signatures. Such a capability would provide reagents that could be used to detect and identify highly mutable viruses, such as Venezuelan equine encephalitis (VEE), for which it will not be feasible to develop DNA-based Taqman assays, and for genetically modified organisms.

In FY2002, the first step in the protein pipeline development process was completed. This included developing a prototype protein-signature-identification pipeline that could be used to identify organism-specific protein signatures. The process identifies amino-acid sequences that are conserved among strains of the organism, but unique to the species. We have applied the process to several bacterial and viral genomes.

To test our prototype protein pipeline, we examined each of the genes present in the West Nile virus (WNV) to identify optimal targets for protein signature development. Three of the ten WNV genes were found to code for protein sequences that were sufficiently similar to proteins with known structures that homology models could be created using the AS2TS automated protein-modeling system (see Figure). One of these, a viral coat protein sharing ~38% sequence identity with the coat protein of the tick encephalitis virus, was selected for more detailed signature analysis and monoclonal antibody production.

A comparison of the sequence of the WNV gene producing this glycoprotein with the genes of all other organisms, including closely related viruses, revealed that the WNV gene contained nine unique DNA sequences, of which eight yielded peptides containing four to twelve amino acids. These sequences were mapped on the homology model of the protein produced using the known crystal structure of the tick encephalitis virus coat protein as a template, and six sequences were chosen for monoclonal antibody production based on their predicted surface exposure.

Each of the peptide sequences was synthesized, conjugated to a larger protein to stimulate the immune response, and a set of six mice were immunized with the conjugated peptides. Following the first immunization, each mouse was screened for its serum titers of antibody using the purified peptides, and a subset of the mice was used to produce hybridomas for signature sequences exhibiting sufficient antibody titers. The remaining mice were immunized a third time to increase the titers of antibodies recognizing the remaining peptides prior to hybridoma production.

In follow-on work, hybridomas will be produced using mice exhibiting high serum titers to the most reactive peptide. Three clones producing an antibody that recognizes each sequence will be selected; the clones will then be grown up and retested for antibody production. Arrangements have been made with the Laboratory of Vector Borne Disease at the University of California, Davis to conduct testing of antibodies from each clone using a panel of WNV strains and nearest neighbors.

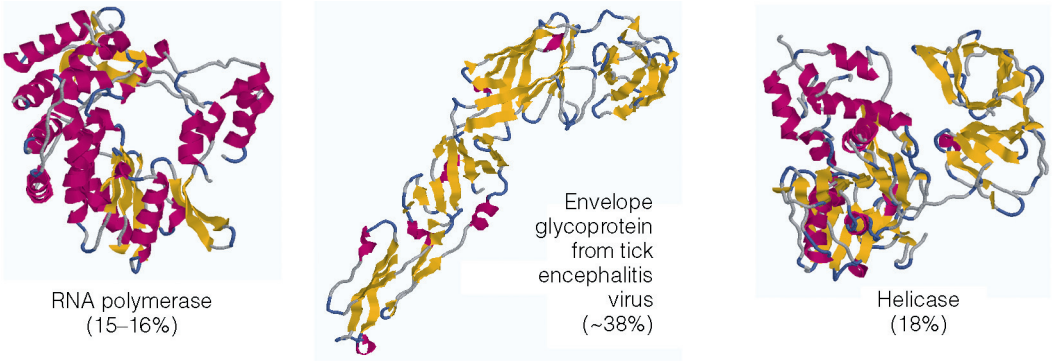

Structures of three West Nile virus (WNV) proteins predicted using the AS2TS automated protein modeling system developed at LLNL. These proteins models were developed by comparing the WNV proteins to similar proteins of known structure. The numbers in parentheses represent the similarity between the compared proteins

Advanced filtration and separation technologies based on nanoporous and aerogel technologies

A. J. Makarewicz

This project proposes to carry out the enabling research and development for advanced filtration and separation technologies that are based on LLNL's nanoporous and aerogel technologies. Rugged, lightweight and regenerable devices for separating and sequestering biological solutes could have applications to critical national needs in biowarfare defense, biosciences, and human health. Components of this research will include advanced-filtration devices, dialysate-regeneration devices, and portable fluidics systems. Upon success of this first phase of research, the components will be integrated into a proof-of-concept wearable artificial kidney, as an example of an application that improves human health.

Dialysis is the standard treatment for lost kidney function, currently used by nearly 400,000 patients in the U.S. During dialysis, blood high in toxins, which are normally removed by healthy kidneys, is filtered across a membrane. Through two processes, convection and diffusion, the membrane exchanges toxins with a clean dialysate fluid. Normal treatment involves three, 4-h sessions each week. Toxins build up between sessions, but no dialysis technology is currently available that can clean the blood continuously, as do the natural kidneys. Higher doses of dialysis delivered continuously would provide a boon to the patient's quality of life and improve patient's overall outcomes. To develop continuous dialysis, new technology is need that can offer more selective filtration and regenerate ultrapure dialysate solutions.

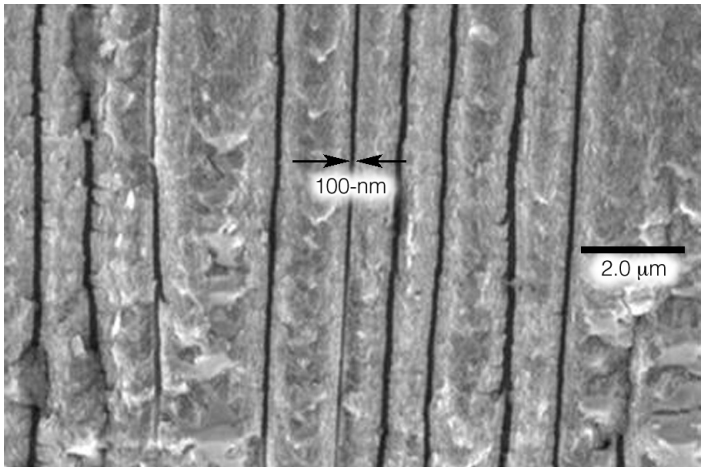

Cleaved section of nanoporous silicon with 100-nm pores, achieved using a photolithography etch technique.

The primary goal of this project is to form highly uniform pores of silicon with diameters of about 50 nm by electrochemical etching. This nanoporous material will allow the fractionation of medium to large proteins via a staged filtration approach. Using this approach, removal of harmful proteins and retention of beneficial proteins can be achieved. This capability alone could prove very powerful in controlling the protein composition of dialysis patients' blood.

By improving the etching process in silicon, we have reduced the practical silicon pore size from 300 nm to 100 nm during the last six months. Further improvement is expected in the near future. This technical achievement was the most significant challenge for our advanced filtration component. Experiments are ongoing to determine the mass-transport capabilities of the advanced filter.

A second goal is to optimize the removal of ions from aqueous solutions using carbon aerogels in fluid flow regimes and at solute concentrations not studied in previous proof-of-concept work. Experiments are ongoing to characterize the ionic trapping of the carbon aerogel capacitor.

During FY2003, research will focus on further testing the carbon aerogels for separation of biological solutes utilizing solute charge, diffusion kinetics, and molecular trapping. By the end of the project, we expect to have a prototype blood-plasma processing system ready for testing with human dialysate.

Modeling the novel *Yersinia pestis* toxin that resembles *Bacillus anthracis* edema factor

V. Motin, A. Zemla, D. Barsky, E. Garcia

Plague has had a devastating effect in human history. Although plague is not a public health problem in most parts of the world, its potential for contagion, the lack of an effective vaccine, and the recent emergence of multiple antibiotic-resistant strains make this organism a potential candidate for use in bioterrorism.

Although studied for more than five decades, the acute nature of plague infection is poorly understood. The complete genome sequence of *Yersinia pestis* (strain CO92), the causative agent of bubonic and pneumonic plague, has been recently deposited in GenBank (a public gene database) by researchers at the Sanger Centre in the U. K. Our analysis (unpublished observations) of this genome revealed that the chromosome of the plague microbe contains a gene that resembles the gene that produces an edema factor (EF) in *Bacillus anthracis*. The EF is one of the two major anthrax toxins. However, this putative function was missed by the Sanger Centre researchers. The structure of the anthrax EF was recently determined and released to the public, creating an opportunity for LLNL scientists to perform biochemical characterization and homology modeling on the *Y. pestis* toxin to determine the similarities between the two toxins.

The project's goal is to investigate the functionality of the novel *Y. pestis* toxin, which we hypothesize significantly contributes to the virulence of this dangerous microbe. The results could lead to an important connection between plague and anthrax and thereby strengthen the nation's ability to detect and counter bioterrorism.

In FY2002 we began both experimental and computational studies of the toxin. To investigate distribution of the putative EF gene among different *Y. pestis* strains, toxin-specific primers were designed and tested against a collection of plague isolates of different geographical origins. All strains except two possessed the toxin genes. Chromosomal mapping of both toxin-negative isolates showed deletion not only of the toxin gene but also its neighboring region. The effect of this deletion on the virulence of the plague microbe is unknown and should be further investigated. In addition, we found that the domains (functional parts) of the putative toxin on the chromosome of *Y. pestis* CO92 corresponded to two open reading frames (ORFs), which are where a gene starts and stops on the DNA chain. The physical separation of the two parts of the toxin was identical among 22 other plague isolates we tested.

Using our newly developed AS2TS homology-modeling protein structure prediction system (02-LW-003), we created a working model of the putative *Y. pestis* toxin from the published anthrax EF toxin structure, as the Figure illustrates. Two domains in the *Y. pestis* toxin are disjoined at what corresponds to the separation of the ORFs (green region). Both domains appear to be involved in binding to adenosine-triphosphate (ATP), with the domain in purple binding the purine molecule and the domain in gray binding the phosphate molecules in ATP. This model strongly supports our assertion that these ORFs may represent a viable toxin in *Y. pestis*. We have cloned and expressed the putative plague EF toxin in *E. coli*, and its sequence has been verified. The toxin has been purified using affinity chromatography, and testing its activity is under examination.

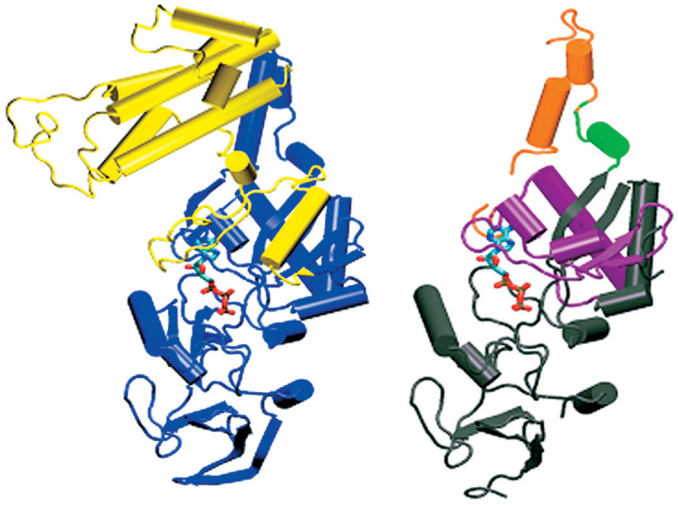

At left is a blue-and-yellow model of anthrax edema factor toxin binding to a molecule of adenosine-tri-phosphate (in red). At right is a similarly shaped model of a toxin produced by Y. Pestis*; the purple and gray regions are two separate functioning parts, and the orange and green regions represent the flexible parts.*

Dynamic simulation tools for the analysis and optimization of novel filtration, sample collection, and preparation systems

D. S. Clague, T. H. Weisgraber, K. D. Ness

Heightened attention on chemical and biological early-detection systems has increased the need for high-efficiency filtration, collection, and sample-preparation systems. To study and understand the physics governing such systems, optimize these critical operations, and characterize system efficiencies based on the details of the microstructure and environmental (temperature) effects, we are developing advanced computational analysis tools—new lattice Boltzmann (LB) simulation capabilities. These tools will be used to study fluid behavior not by tracking individual fluid molecules, but by tracking a probability-distribution function that represents the collective behavior of fluid molecules in local regions. This new simulation capability will be validated with experimental data.

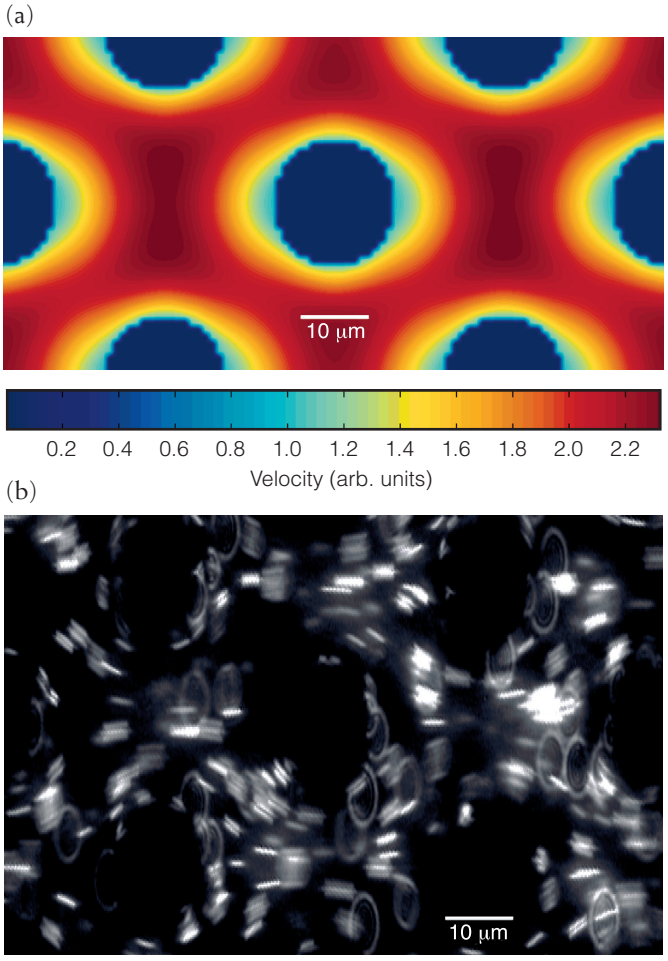

(a) Lattice Boltzmann simulation of fluid velocity through a pillar array. (b) Experimental image of particles flowing though the pillar array.

The new simulation tools will have a direct impact on filtration, collection, and sample-preparation systems that support the Laboratory's chemical and biological counterproliferation and homeland-security missions.

In FY2002, we developed an input module for ordered arrays of cylinders to replicate the microstructure of a novel DNA purification device, the pillar chip. Because this device, in which DNA is preferentially trapped on the pillar surfaces, has received wide acceptance here at LLNL, design and analysis tools to optimize chip performance are crucial.

Initial LB simulations were performed to analyze velocity and shear stress through different pillar arrangements with various cross sections. The goal is to maximize the available surface area for capture by characterizing fluid velocity and shear stress at pillar surfaces for various proposed designs. An example velocity field is shown in Fig. (a) for a periodic pillar array in a 50-μm-deep channel. The Reynolds number based on the 8-μm-diam pillars was 0.026. Both velocity and shear stress exhibited strong gradients due to the close packing of the cylinders, which will strongly influence species transport and capture in the device.

To validate the LB capability, digital particle-image velocimetry experiments were conducted to measure the velocity profile through the pillars [Fig. (b)]. We also developed theory to incorporate electrostatic and van der Waals interactions between suspended species and pillars; these colloidal interactions were incorporated into the LB method. These new capabilities are directly relevant to ongoing research efforts that use the pillar chip.

In FY2003, we will develop (1) a generalized porous media generation module that includes pillar geometries, porous membranes and fibrous filters; (2) colloidal-interaction theory specific to porous membranes; (3) a novel approach to incorporate Brownian motion; (4) a coupled-energy equation to account for environmental effects; and (5) a characterization of species-transport properties through, and capture efficiencies in, a pillar chip with and without environmental effects.

Discovering the unknown mechanisms of virulence in a Class A biological warfare agent

P. S. G. Chain, E. Garcia

The post-September 11 anthrax attacks have forced us to re-examine our biological warfare (BW) vulnerabilities and improve our understanding of the most serious BW organisms. The Centers for Disease Control and Prevention has categorized four microbial organisms [*Yersinia pestis* (the plague), *Bacillus anthracis* (anthrax), *Francisella tularensis* (tularemia), and *Clostridium botulinum* (botulism)], along with the smallpox virus (*Variola major*) and the hemorrhagic fever virus families (filoviruses and arenaviruses), as Category A agents, that pose a risk to national security. Of the four Category A microbial agents, *F. tularensis* is one of the least understood. For instance, the mechanism of action against its host remains unknown. Although the ulceroglandular form of the disease is rarely fatal (mortality rate is 3 to 10%), typhoidal or pneumonic tularemia has a mortality rate of 30 to 80%. This, along with its extreme infectivity and ease of dissemination, makes *F. tularensis* one of the most dangerous potential BW agents, as evidenced by U.S. and Soviet stockpiling in the 1950s and 1960s of aerosolized, antibiotic- and vaccine-resistant *F. tularensis* strains.

The goal of this research is to work toward identifying and characterizing the *F. tularensis* virulence genes. This work will combine genome sequencing, genome analysis, and comparative genomics (between pathogenic and nonpathogenic strains) to provide great insight into the biology of this lethal organism, particularly how it affects its human and other mammalian hosts. The knowledge achieved in this proof-of-principle investigation will enable future efforts to devise diagnostics (species- and strain-specific signatures), prophylaxes (vaccines), and treatments (targeting virulence factors). Such results are highly supportive of NNSA's national-security mission area of biodefense and countering bioterrorism.

Previously, we began to sequence a strain of the *F. tularensis* subspecies *tularensis* in an ongoing project with the Walter Reed Army Institute of Research, the Swedish Defense Research Agency, and the U.K.'s Defense Science and Technology Laboratory in Porton Down. We then generated a rough-draft sequence for *F. philomiragia* and the *F. tularensis* subspecies *holartica* and *novicida*, all three of which cause a much less life-threatening form of disease than does the subspecies *tularensis*, the highly virulent human pathogen.

In FY2002, we completed the draft phase of sequencing for a *holartica* strain and began the more difficult task of finishing and gap closure (Figure 1). We resolved 90% of the repeat elements and gaps, reducing the number of contigs (groups of cloned nucleotide sequences that are contiguous) to 18. We compared this genome with that of the subspecies *tularensis* and found fourteen regions, varying in size from one to ten kilobases, that appear to be unique to this subspecies. From these regions, we generated a list of genes (including some putative membrane proteins) that are potentially involved in the subspecies *tularensis* virulence process and that may enable this organism to produce the acute form of tularemia.

Because these data have been obtained from unfinished sequencing data, we plan to refine and augment the list of potential virulence factor candidates by comparing complete and annotated genomes. In FY2003, we will finish the genomes of all three *Francisella* strains and perform genome-to-genome comparisons to identify all the differences between them. These differences will prove very useful for identification purposes (i.e., signature development) and will open avenues for future virulence studies, such as gene knockouts—studies in which an organism is bred with a targeted gene inactivated, or "knocked out." Differences between that organism and normal specimens help reveal the role that the gene plays in the organism's disease process.

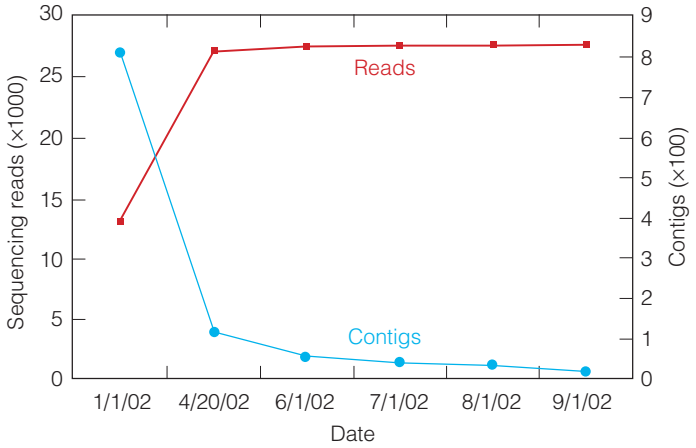

The finishing process for the Francisella tularensis *live vaccine strain has resolved many misassemblies (due to the presence of two repeated insertion sequences) and has reduced the number of Contigs to <20. Polymerase chain reaction products cover nearly all of the remaining gaps.*

Accelerator analyses for protein research

J. S. Vogel, P. G. Grant, G. Bench, N. M. Palmblad, D. J. Hillegonds

Genome sequences are the blueprints of life, which are executed in the form of the proteins encoded by individual genes and generated in living cells. Proteins serve many functions, from providing a cell's structural integrity to acting as hormonal messengers between distant organs or tissues. These functions require interactions with biological macromolecules or response to chemicals in their immediate surroundings. Health and disease both involve protein interactions with nutrients, toxins, drugs, and the myriad biomolecules within us.

Protein research, including proteome studies employing extensive data from the Human Genome Project, requires accurate quantitation—determining the exact mass or concentration of a protein in a solution. Because toxins and drugs, for example, take effect by producing or interacting with specific proteins, the potency of new drugs and the danger of toxic agents—including biological and chemical weapons, which affect human health at very low concentrations—can be estimated reliably only by finding the quantities of proteins directly affected by these compounds.

In this project, we are quantifying proteins and their interactions using physical analytical methods based on accelerated ions to gain sufficient sensitivity for exploring life on a cellular level and for discovering the detailed effects of very potent toxins or drugs. This project brings the precise, nondestructive tools of nuclear technology to biological defense studies, health research, and basic investigations of life sciences in support of LLNL's national security and bioscience missions.

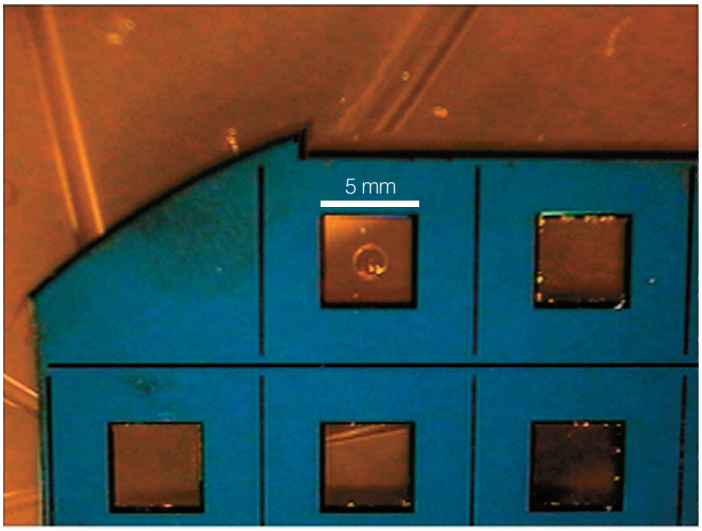

Photo of several silicon nitride windows. The upper left window contains a 5-μg spot of protein on it. The energy losses of the protons, alpha particles, and oxygen nuclei passing through the protein samples were measured to determine the amount of protein on the window.

The objective of our project is to explore three techniques that use accelerated ions: (1) measuring a mass of biomolecules by determining the physical loss of energy of accelerated ions passing through that mass, (2) quantifying elemental abundance by measuring the distinctive x-rays emitted by metals in that mass when exposed to accelerated ions, and (3) direct counting of isotope-labeled compounds bound to a quantified mass. Protein separation techniques are also used to detect these binding proteins at low levels. For all three techniques, the samples to be analyzed relate to studies of the causes of cancer and the toxic mechanisms of environmental or antagonistic chemicals.

In FY2002, the quantitation of protein in amounts from a few nanograms to hundreds of micrograms was shown to be a linear function of the average energy loss of high-energy ions from either accelerators or radioactive sources. The proteins were spotted onto think silicon nitride windows (see Figure). Next, the energy losses of the protons, alpha particles, and oxygen nuclei passing through the windows and protein samples were measured to determine the amount of protein on the window. This technique was combined with mass spectrometry for protein identification and accelerator mass spectrometry (AMS) for measuring isotope-labeled chemicals bound to the spotted proteins. We were able to measure the amount of toxin bound to a protein from a sample 1,000 times smaller than with sophisticated AMS techniques alone. An efficient routine for gel-based protein separations for AMS measurement was developed, for rapid surveys of very-low-level protein binding and is being applied to understand protein targets of toxins.

In FY2003, we will study the roles of heavy metals in certain cancer cells, quantifying their incorporation in identified proteins; quantify inhaled toxin interactions with lung proteins to pinpoint differences in target proteins as functions of dose and time after exposure; and use archived tissues to document the particular levels of protein damage in brain and liver of mice exposed to a wide dose range of a nerve agent simulant.

Solid-state, nuclear-magnetic-resonance methods for structural characterization of membrane proteins: Applications to understand multiple sclerosis

R. S. Maxwell, M. Cosman, A. Tran, J. Ulloa

Myelin oligodendrocyte glycoprotein (MOG), a 26-kD to 28-kD glycoprotein, is an integral membrane protein of the central nervous system, which is implicated as a target for autoaggressive antibodies in multiple sclerosis (MS). MOG is thought to be comprised of a region outside the cellular membrane (the extracellular domain) and a region that spans the membrane wall (transmembrane domain). Such multiple-domain proteins are difficult to study using traditional methods, e.g., solution-state, nuclear magnetic resonance (NMR) and x-ray diffraction. Moreover, the conformation of MOG associated with the myelin membrane is unknown, and the exact nature of interactions between this protein and disease-inducing immune responses have not been determined. Thus, there is a critical need to develop new structural characterization tools for this important class of biomolecules.

In this project, we propose to develop new, proof-of-principle solid- and solution-state NMR methods to study membrane proteins such as MOG to better understand how they function in their environment and therapeutics to inhibit the antigen–antibody interaction and thus prevent demyelination in MS patients. This effort will have a significant impact on fundamental biochemical research and development worldwide by facilitating further investigation of difficult-to-study proteins and other high-molecular-weight macromolecules. In addition, solid- and solution-state NMR methods developed in this project will have application to broader fields of study such as protein reactions relevant to bioremediation of contaminated sites, bone growth, prosthetic rejection by living tissue, biomolecular engineering, and the detection and decontamination of toxins.

In FY2002, we completed expression and purification of both the extracellular domain and full-length MOG, developed and tested solid-state NMR methodologies on small, molecular-weight peptides, began solution-state NMR experiments of the extracellular domain, and obtained nitrogen-15 isotopically enriched MOG. Computer simulations of nitrogen-proton two-dimensional heteronuclear correlation spectrum [polarization inversion spin exchange at the magic angle (PISEMA)] were performed based on homology modeling [Fig. (a)] and the results compared to experimental data. PISEMA experiments provide detailed structural data by measuring orientation-dependent NMR observables for membrane proteins aligned in the NMR spectrometer. Figure (b) shows the first proton detected two-dimensional homonuclear correlation NMR spectrum of the extracellular domain of MOG ever obtained. These data are providing key insight into the structure of the transmembrane domain of MOG—insight previously unobtainable by other methods.

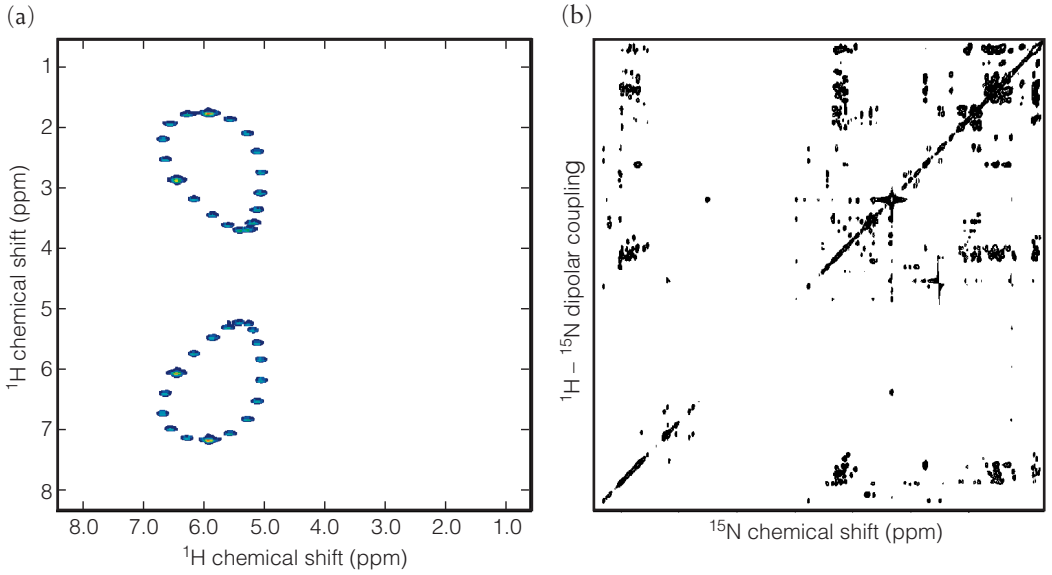

(a) Hydrogen-1–nigtrogen-15 heteronuclear-dipolar-coupling–chemical-shift-correlation solid-state NMR spectral simulation of aligned MOG. (b) Hydrogen-1 homonuclear correlation spectrum These spectra provide insight into the structure of the transmembrane domain of myelin oligodendrocyte glycoprotein (MOG).

Automated three-dimensional protein structure predictions based on sensitive identification of sequence homology

A. T. Zemla, D. Barsky, D. Sawicka, T. R. Slezak

Genome sequencing projects require the characterization of many new proteins in terms of their structure and biochemical function, but the cost and time to experimentally characterize such proteins are prohibitive. Computational methods based on amino-acid sequence similarities (homology) between proteins hold great promise for uncovering the structure and function of new proteins.

This project proposes to (1) develop and package a method for characterizing newly sequenced proteins in terms of their three-dimensional (3-D) structure and function into a Web-based interactive system; and (2) apply this system to open questions in biology. We are using a novel approach to predict protein structure by identifying unique folds, i.e., distinct conformations, that are well conserved throughout all living organisms and combine sequence and structure searches of existing databases to identify structural homologs of proteins for which sequence similarity alone is insufficient. This project builds on LLNL's capabilities in bioinformatics and high-speed computing, and, if successful, will boost biodefense capabilities at the Laboratory by providing automated identification of bacterial toxins and virulence factors. This capability could also make possible better genomic annotation for the many microbes being sequenced at the DOE's Joint Genome Institute.

During FY2002, we developed and applied a Web-based protein-structure prediction system in both cancer research and biodefense work. In particular, we generated a preliminary series of 3-D models for the Rad51 DNA repair proteins and provided structural predictions for experiments that, in turn, used our models to determine how the Rad51 family of proteins forms a complex (see Figure). We also predicted the structure and function of several potential virulence proteins of *Yersinia pestis*, including the difficult-to-predict, low-homology protein orf38. Based on our models, this protein is hypothesized to bind small molecules—likely amino acids—and may play a transport role in the virulence of this pathogen.

In FY2003, we will develop methods for identifying and analyzing the structural similarities of proteins that have less amino-acid sequence similarity by including sequence-structure patterns, secondary structure information, and intermediate sequence-search techniques. This work will significantly improve the process of fold recognition and more-distant homolog detection, and enhance the quality and accuracy of the final 3-D protein models produced, especially when small signature fragments of proteins need to be modeled. Through experimental collaborations, we will continue to test our hypotheses on the Rad51 and *Y. pestis* proteins to improve our modeling system.

(a)

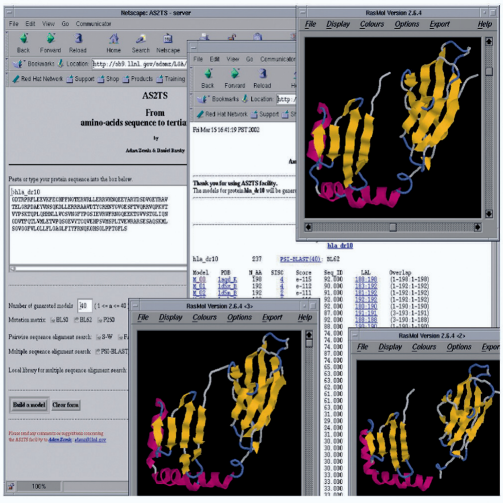

(b)

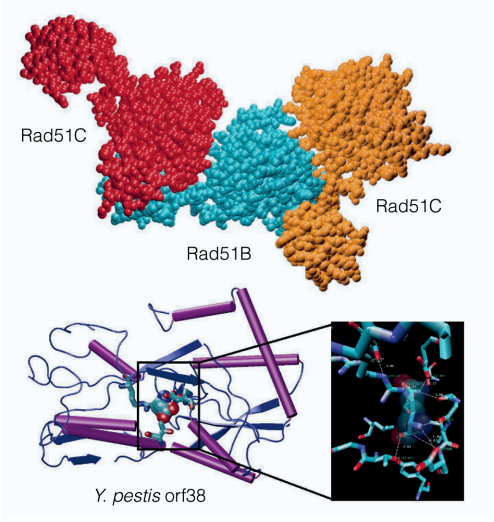

(a) Screen shots of the AS2TS Web-based protein prediction system. (b) Homology model of DNA repair proteins Rad51C and Rad51B. (c) Model and active site analysis for Yersinia pestis *orf38 protein.*

Alterations in cell-signaling pathways in breast cancer cells after environmental exposure

K. Kulp, J. Montgomery, E. R. Latham, L. M. Bennett

Understanding the biologic impact of exposure to a lifetime of complex environmental mixtures is a major human health challenge. An environmental exposure that upsets normal cell growth regulation may have important ramifications for disease development by changing the expression of genes and proteins that have a role in growth regulatory pathways. Characterizing the consequences of exposure to complex environmental mixtures is essential for developing strategies that minimize risk from exposure.

This project supports the DOE mission to improve human health and NNSA missions in counterterrorism and homeland security by improving our understanding of real-life exposure to complex environmental mixtures. The methods developed here can be directly applied to other defense-related biological research, including cellular response to infection.

We are investigating diet-related compounds that induce cell proliferation in breast-cancer cell lines. The genotoxic heterocyclic amine 2-amino-1-methyl-6-phenylimidazo[4,5-b]-pyridine (PhIP) is a naturally occurring mutagen that is formed in well-cooked muscle meats. The PhIP mutagen consistently causes dose-dependent breast tumor formation in rats, and consumption of well-done meat has been linked to increased risk of breast cancer in women. Flor-EssenceÆ and EssiacÆ Herbal Tonics, complementary and alternative medicines, are self-administered by women who have been diagnosed with breast cancer as an alternative therapy for disease treatment and prevention.

The purpose of our project is to determine how exposure to these dietary compounds alters cell growth pathways in the human MCF-7 breast-cancer cell line. We plan to use functional cell proliferation and reporter assays in combination with new macroarray technology. Our objective is to quantify exposure-induced alterations in RNA and protein expression and relate them to the cell-proliferation experiments.

During FY2002 we determined that these compounds have a pronounced effect on breast cancer growth control (see Figure). Treatment with PhIP resulted in a statistically significant increase in estrogen-dependent cell growth pathways compared to untreated cells, which is a novel finding for a mutagen that was previously known primarily for causing DNA damage . Cell-proliferation assays demonstrated a 20 to 30% increase in cell number after PhIP treatment, comparable to the increase seen when the cells are treated with estrogen. The herbal tonics, which contain extracts of herbs known or suspected to be estrogenic, stimulated cell growth as much as twofold and increased estrogen receptor activity four- to fivefold. Co-incubating the cells with PhIP and Flor-essenceÆ produced an additive response that increased estrogen-receptor response sixfold.

Attempts to relate the results from these functional assays to the array technology were not as successful. Although the array experiments were repeated several times, the results were variable. More work is needed to refine this innovative technology.

Because estrogen and estrogen-like compounds (xenoestrogens) are known risk factors for breast cancer, our results show that these dietary compounds stimulate cell growth through an estrogen receptor-dependent pathway. These results may have important implications for breast cancer survivors that use herbal tonics while continuing to eat overcooked meats. Further research is needed to determine how these environmental exposures may modulate the expression of genes and proteins involved in growth regulation and how this may contribute to the initiation, promotion, or progression of disease.

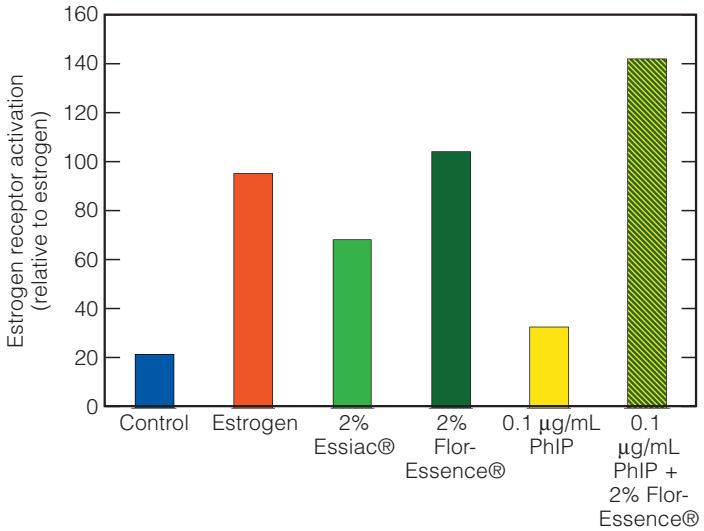

Effect of the herbal tonics Flor-EssenceÆ and EssiacÆ and the food mutagen PhIP on estrogen receptor activation in MCF-7 human breast-cancer cells.

Feasibility study of passive particulate samplers

G. A. Keating, W. Bergman

This study will establish the feasibility of using passive samplers to collect biological and nonbiological aerosols. A passive sampler is like flypaper for particles: it collects airborne particles without a pump. Such a collector would benefit many LLNL missions, including homeland security, counterterrorism, counter- and nonproliferation, environmental monitoring, and atmospheric-effects simulations, by providing the capability to measure airborne particles over a wide area or a large number of locations at a small fraction of the current cost. For example, hundreds of samplers could be dispersed over miles to provide the National Atmospheric Release Advisory Center (NARAC) with particle-disperal data for validating model calculations. Samplers could also replace or supplement the very expensive BASIS sampling system used for detecting bioaerosols. The samplers could be sent and returned by mail to thousands of homes to assess various environmental and ecological hazards and would allow extremely large-scale environmental measurements in future bioaerosol programs.

The goal of the project is to establish a preliminary relationship between particles collected by the passive sampler and the air concentration for key parameters of the sampler (exposure time, surface charge, particle sticking coefficient, and water adsorption), particles (size, density, charge, and water adsorption), and the environment (relative humidity, wind speed, and turbulence). Experiments using model aerosols (both biological and nonbiological) generated in an instrumented test chamber will compare the particle-collection efficiency of various passive samplers to that of conventional filters, aerosol-monitor instruments, and conventional surface swipes. A limited matrix of test parameters will be selected to demonstrate feasibility.

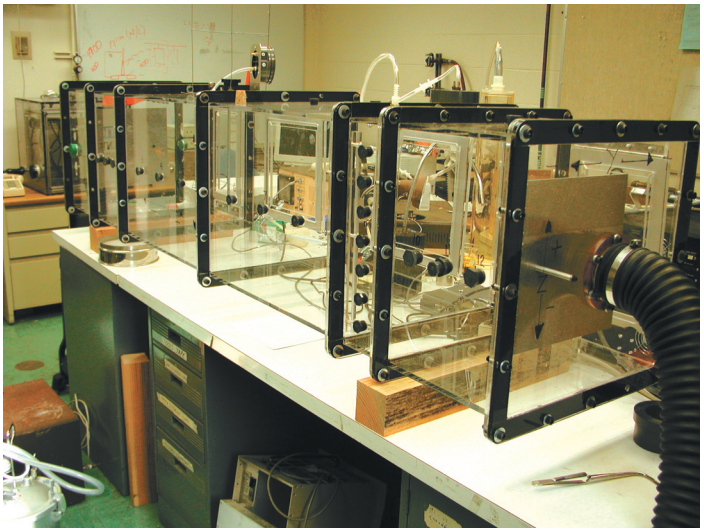

Test chamber used to evaluate the passive-sampler concept. Doors and ports provide access for air-sampling instrumentation and chamber decontamination.

In FY2002, construction and instrumentation of the test chamber were completed. The chamber (Figure 1), measuring $2.4 \times 0.6 \times 0.6$ m, is fitted with multiple access doors and sampling ports to facilitate placement of air-sampling equipment and decontamination of the chamber. Supply and exhaust are HEPA-filtered and wind speeds ranging 3 to 30 cm/s can be achieved within the chamber. These speeds represent the range of indoor and ambient wind speeds for passive sampling; homogeneity of wind speeds and turbulence in the chamber is adequate for representative air sampling using standard methods. Different methods for aerosolizing test particles have been demonstrated to produce adequate atmospheres for testing. Protocols for the collection and analysis of monodisperse particles using conventional filter samples and passive samplers have been developed. These protocols are currently being evaluated with various test particles and environmental parameters.

Approval for the aerosolization of *Bacillus globigii* (BG) spores and other biowarfare simulants (RNA bacteriophage and ovalbumin) in the test chamber has been received from the LLNL Institutional Biosafety Committee (IBC). Although BG spores, commonly used as a simulant for biowarfare agents, are categorized by the Centers for Disease Control as Risk Group 1 agents, aerosolization of BG spores elevates the agent to Risk Group 2. Additional safety controls have been implemented to the test chamber and the surrounding laboratory.

In FY2003, the study will proceed to evaluate the collection of BG spores with conventional filter samplers and passive samplers. The BG spores collected on the passive samplers will be identified indirectly by particle counting and directly using fluorescent antibodies. These data will establish if passive samplers provide a potential alternative to conventional sampling methods.

Evaluation of endocrine disruptor compounds from nonpotable reuse of municipal wastewater as a tracer for groundwater source

A. Grayson, B. Hudson, H. Beller, S. Burastero, C. Campbell, S. Kane

Water is a finite resource and recycling wastewater is an attractive option for enhancing water supply worldwide. Projects designed to treat wastewater to high purity standards for indirect potable reuse have met with significant public opposition throughout the U. S. These projects are often labeled "toilet to tap" by project opponents. At the same time, water-recycling projects for nonpotable reuse, such as landscape irrigation, that use water treated to lower standards have been widely accepted and implemented. In these nonpotable reuse projects, wastewater is filtered and disinfected but most dissolved compounds are not removed, including endocrine-disrupting compounds (EDCs), which alter the normal functioning of the endocrine system in humans and animals. Endocrine-disrupting compounds found in wastewater include natural and synthetic hormones and compounds associated with alkylphenol ethoxylate surfactants, which are widely used in commercial products like laundry detergents.

This study examined one of the environmental impacts of irrigation with recycled water by evaluating the fate and transport of EDCs at a golf course in Livermore, CA, where treated wastewater has been used for landscape irrigation over the past 25 yr. Two features make this an interesting site for examining the impacts of irrigation with recycled water. First, LLNL has regularly released small amounts of tritium to the sewer system, which provide a tracer for wastewater (discharges were in compliance with a permit and DOE orders). Second, both the recycled water and the shallow groundwater have been carefully monitored for the past 25 yr. This study supports the LLNL mission by contributing to environmental regulation in the area of emerging contaminants and water supply.

In FY2002, we sampled the treated wastewater being used for irrigation and several strategically selected groundwater wells. In addition, we collected and evaluated soil cores for subsurface transport of EDCs. For the groundwater samples, we used tritium and its daughter, helium-3, to establish sample chronology and the stable isotopes of oxygen and hydrogen, along with sample chemistry, to estimate effects of evaporation and dilution.

The treated wastewater and groundwater samples were analyzed for nonylphenol (NP), a metabolite of alkylphenol ethoxylate surfactants and an EDC that is commonly detected in treated wastewater. To carry out NP analyses for this project, we developed a highly sensitive (detection limit ~11 ng/L for a 0.5-L sample) and specific analytical method that involves solid-phase extraction combined with liquid chromatography/tandem mass spectrometry using selected reaction monitoring. In addition to analyzing NP in groundwater and effluent, we also analyzed total estrogenic activity present in these samples with a state-of-the-art bioassay technique that provides a measure of estrogenic potencies of mixtures containing unknown compounds. The method is based on interaction with estrogen receptors (3xERE) in a human breast-cancer cell line. A dual-luciferase assay system allows for internal control and normalization of response data.

Our study detected NP at tens to thousands of nanograms per liter in treated wastewater and groundwater. Bioassays of the same samples showed that samples with higher NP concentrations also had the highest estrogenic activities. Results suggest that NP can account for a significant portion of the total estrogenic activity found in the treated wastewater and groundwater samples. The Alameda County Zone 7 Water Agency has committed to installing additional monitoring wells for this project.

A follow-on study could expand the scope of our investigation by including additional EDCs and more sampling sites and by examining other bioassay techniques.

Carbon nanotube array microfluidics

A. Noy, O. Bakajin, N. Ben-Barak, J. Peng

Small detection devices that rapidly identifiy potential biowarfare agents would be a boonto the war on bioterrorism by s. An essential part of any such device is an effective mechanism for molecular separation and concentration, because high-resolution detectors require relatively clean samples. Microfabrication techniques promise mass-production of small, low-cost devices for field use. Although current techniques can provide robust channel networks designed to transport, mix, and test sample solutions, no technique exists to easily and reliably fabricate separation and concentration elements having patterned materials of predetermined surface properties, geometry, and porosity at the scale of the molecules to be detected. Unconventional materials and fabrication techniques are needed for further refinement and miniaturization.

Carbon nanotubes, because of their enormous surface-to-volume ratio and high mechanical resilience, form the foundation of a new generation of integrated microfluidic filtration, concentration, separation, and detection systems for chemical and biological agents. For example, nanotube arrays have potential use as miniature, efficient on-chip chromatography columns.

In this project, catalytic chemical vapor deposition is used to grow nanotube arrays, and spatially control the placement of the arrays by prepatterning the nanotube growth catalyst in the prefabricated microfluidic channel. The goal of this project is to create patterned arrays of carbon nanotubes as separation and concentration elements that could be easily incorporated as a filter into microfabricated gas- or liquid-phase detection devices. With potential application in the detection of biowarfare agents, these microfluidic technologies will further LLNL's national security mission.

By the end of FY2002, we accomplished all of the project goals, refining our fabrication procedures to produce a prototype nanotube array device [Fig. (a)]. We used a solution of latex beads to confirm that the device can be used as a filter [Figure (b)], and demonstrated chromatographic separation with the device by using different solvents to capture and release latex beads on the nanotube mesh. We also explored another application for our nanotube arrays—solid-probe microextractor (SPME)—by fabricating and successfully testing a prototype SPME consisting of freestanding nanotube arrays. These results led to two provisional patent applications and indicate that freestanding carbon nanotube arrays have great potential as a novel nanostructured collection-and-separation medium.

(a)

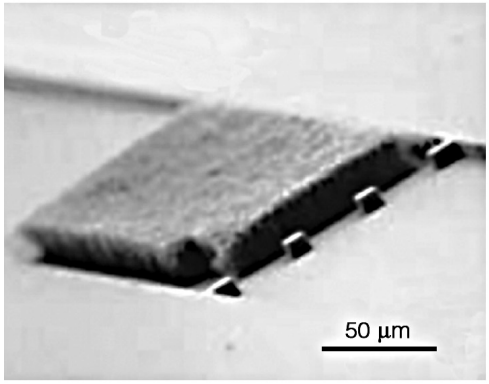

(b)

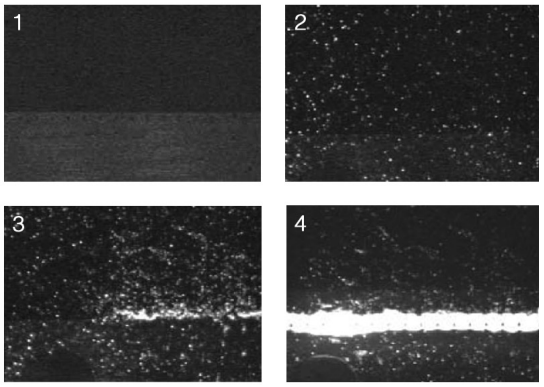

We developed carbon nanotube arrays as separation-and-concentration elements for applications such as detectors capable of rapid identification of biowarfare agents. Array placement is controlled by prepatterning the nanotube growth catalyst in a prefabricated microfluidic channel. (a) A single carbon nanotube array. (b) Time-lapse images showing a test mixture of latex beads flowing through the channel and collecting in front of the nanotube array.

A high-throughput microenvironment for single-cell operations

A. T. Christian

The Instrumented Cell (IC) initiative being developed at LLNL promises to develop models of chemical interactions within and among cells, following perturbations made within the cell and to the cell environment. One important aspect of the IC initiative is to develop a way to sample the cytoplasmic contents of individual cells continuously and nondestructively, while varying their environment. Sampling will allow precise research on internal cellular activities following such events as pathogen infection. The technology currently exists to sample single cells using a microscope-mounted microinjection device, but not to control and vary the environment of the cell while simultaneously injecting and sampling fluids. In addition, the microinjection platform is not scalable for throughput, though scalability is of the essence: dozens or even hundreds of individual cells must be sampled to obtain meaningful and timely data.

This project aims to provide the IC initiative with an automated, high-throughput microenvironment for isolating large numbers of individual cells to facilitate various types of environmental changes and intracellular measurements. Our goal is to discover a way to isolate individual cells and impale them on a nanopipette or microneedle so that samples could be introduced into and removed from a cell. The traditional means of obtaining cell cytoplasm is to hold a cell with one pipette, using negative pressure, and move another pipette toward the cell while using visual aids. We hope to replace this manual, time-consuming method with an automated, high-throughput process.

In FY2002, we examined dielectrophoresis—movement caused by an electrical field generated by a pair of electrodes—as a means of attracting cells toward, and impaling them on, nanopipettes to automate the procedure, allowing multiple cells to be sampled. However, dielectrophoresis drew too many cells toward the single nanopipette, and generated insufficient force to impale the cells.

Next we developed a two-part process in which the cells are first trapped in capture wells and then impaled using a microneedle. An array of capture wells (see Figure) was fabricated by making a mold of SU-8—a photo-patternable epoxy spun on a flexible glass wafer—then using the mold to make the well array in silicone. Individual cells caught in the wells could then be impaled on the microfabricated silicon needle by deflecting a glass membrane.

The results of tests showed that the wells were effective in capturing cells. Although further optimization is needed, our well design is viable and has the advantage over pipettes of allowing both free-floating and medium-attached cells to be examined. This prototype can be further developed to serve as a platform for the single-cell analyses for the IC initiative.

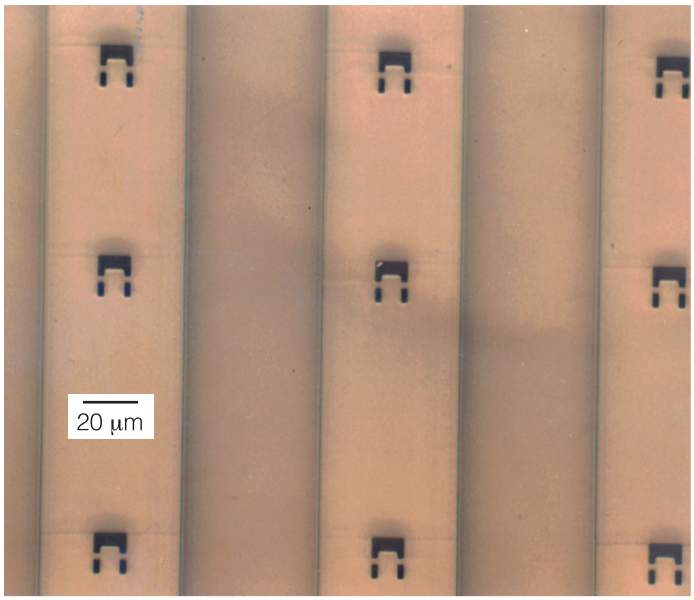

Top view of capture wells (approximately 20 × 20 μm), each with approximately a single-cell capacity. The wells are the basis of a high-throughput process for isolating individual cells and injecting and sampling cellular fluids while controlling and varying the environment of the cells.

Chemistry

Section 3

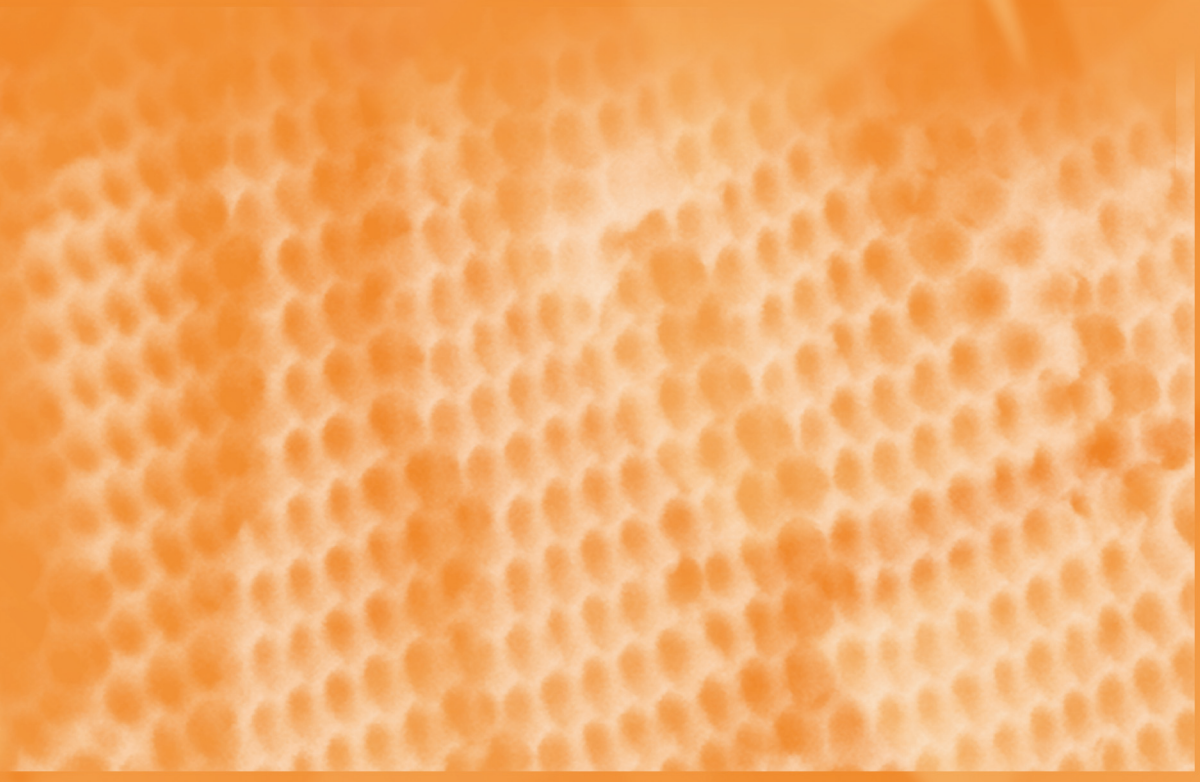

Section 3 — Chemistry

Novel approaches for monitoring intrinsic bioremediation

H. R. Beller

Because engineering approaches to groundwater cleanup at civilian and military sites would cost billions of dollars nationally, intrinsic bioremediation is increasingly viewed as a favorable, cost-effective option for restoration of groundwater contaminated with organic pollutants. A primary impediment to intrinsic bioremediation is the difficulty of demonstrating that decreases in the concentrations of contaminants truly represent biological metabolism of the compounds rather than abiotic processes such as dilution or dispersion.

Using microbial studies and chemical analyses of groundwater from contaminated sites, we are identifying and testing the usefulness of unique metabolites as distinctive indicators of in situ biodegradation of specific contaminants. The contaminants, which are of concern at LLNL and many other DOE and Department of Defense facilities, include high explosives (HE) [such as RDX (hexahydro-1,3,5-trinitro-1,3,5-triazine)] and certain aromatic hydrocarbons [benzene, toluene, ethylbenzene, and xylenes (BTEX)] found in gasoline.

The project is contributing to our understanding of the biological fate of HE compounds underground and could dramatically enhance the effectiveness of in situ monitoring for BTEX degradation by taking advantage of recent groundbreaking findings in anaerobic hydrocarbon biochemistry. This research supports LLNL's environmental remediation mission by investigating cost-effective remediation of HE contamination at Site 300 and developing knowledge that is relevant nationwide.

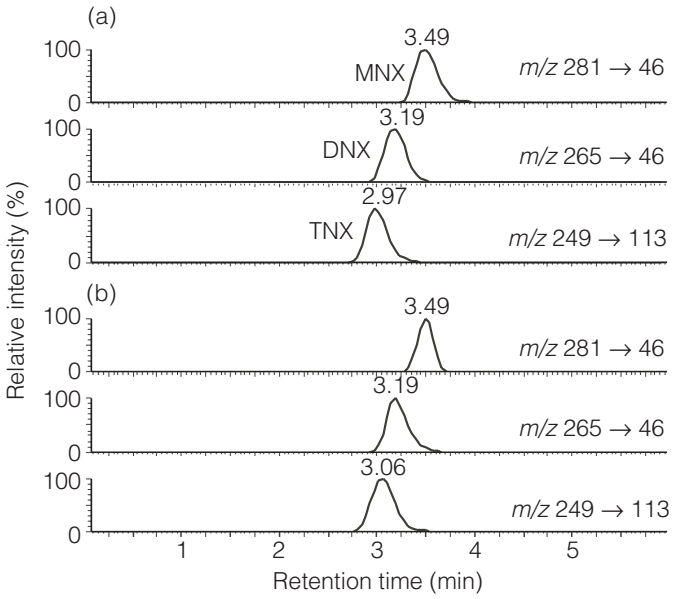

Liquid chromatography/tandem mass spectrometry chromatograms of adducts of three distinctive RDX metabolites (mono-, di-, and trinitroso-RDX; MNX, DNX, and TNX, respectively) in (a) a standard and (b) a contaminated groundwater sample.

The project has resulted in significant findings concerning anaerobic RDX metabolism by bacteria in aquifers. Fields tests are using a state-of-the-art analytical method developed for this project—based on liquid chromatography/tandem mass spectrometry (LC/MS/MS) and having a proven detection limit of ~100 ng/L. In FY2001 and FY2002 we detected three distinctive nitroso-substituted RDX metabolites in numerous groundwater samples from an Army ammunition plant. The presence of these metabolites, confirmed by the appropriate mass/charge (m/z) ratios and chromatographic retention times (see Figure), provides strong evidence of in situ RDX transformation.

Notable results were obtained from laboratory studies of anaerobic RDX metabolism by bacteria enriched from LLNL Site 300 aquifer material. The primary finding was that RDX can be transformed in a simple growth medium having hydrogen as the sole electron donor. Past studies have typically involved complex, undefined media with multiple potential electron donors and acceptors. With hydrogen as the sole electron donor, we observed transient formation of the same metabolites detected in groundwater from the Army ammunition plant. In FY2002, the physiology of the Site 300 bacteria was further studied, including the effects of nitrate on RDX transformation.

For monitoring of in situ BTEX degradation, we developed an LC/MS/MS method for a distinctive class of metabolites (benzylsuccinates). The method was validated in studies with groundwater and proved to be sensitive and accurate. In FY2002 field studies, strong correlations between concentrations of benzylsuccinates and their parent compounds were found in groundwater samples. In addition, we performed biochemical (in vitro) studies to show that these metabolites are relevant to a diverse range of aquifer bacteria. Four articles describing our work were published in refereed journals. In FY2003, we plan to study metabolites from anaerobic TNT degradation and further assess the applicability of nitroso-substituted RDX metabolites and BTEX metabolites as indicators by performing LC/MS/MS analyses on groundwater from multiple contaminated sites.

Chemical deactivation of reactive uranium

D. Gates-Anderson

The U.S. Department of Transportation strictly controls the transport of pyrophoric materials, which are not accepted at disposal sites for hazardous, low-level, and mixed waste. LLNL has an inventory of waste-containing pyrophoric depleted-uranium (DU) metal waste of at least 11,700 kg (with a total volume of about 33 m^3) that requires treatment to render it suitable for disposal. An additional inventory of more than 40,000 kg of pyrophoric DU waste across the DOE complex requires treatment.

Developing a technology to treat pyrophoric DU metal waste is essential for DOE sites to remain in compliance with regulatory agreements. The objective of this project is to develop an integrated process to convert pyrophoric DU metal wastes to a nonpyrophoric waste that is suitable for disposal.

In FY2002 we studied in detail two systems—a mixture of sulfuric acid (H_2SO_4) and nitric acid (HNO_3) and a mixture of hydrochloric acid (HCl) and phosphoric acid (H_3PO_4)—that prior screening studies had demonstrated to deactivate pyrophoric DU at ambient temperature. In addition to optimum treatment conditions (acid concentration, liquid-to-mass ratio, and temperature), we investigated the kinetics and thermodynamics of the reactions involved. Complete dissolution of DU was accomplished in less than 20 min with a solution of 7.5-molar H_2SO_4 and 1.0-molar HNO_3 at a ratio of 20 mL solution per gram of DU. The resulting solution, which contains uranyl sulfate and nitrate complexes, is very acidic and would require pH adjustment and solidification prior to disposal.

Treatment with the HCl/H_3PO_4 mixture resulted in the formation of a solid that may be easier to process for disposal than the acidic uranyl solutions. Complete transformation, without the presence of free liquid upon completion, was achieved in less than 4 h with a solution of 3-molar HCl and 1-molar H_3PO_4 used at a ratio of 10-mL acid solution per gram of DU. The solids formed were characterized using extended x-ray absorption fine structure (EXAFS) spectroscopy, energy-dispersive x-ray analysis (EDXA), x-ray absorption near-edge structure (XANES) spectroscopy, and x-ray diffraction analysis. This characterization—important because of the limited existing literature on U(IV)/phosphate/chloride solids—is needed to determine the reaction mechanism and understand the solids' long-term stability and disposal characteristics. The U(IV) phosphate solid formed may slowly oxidize to uranyl phosphate if oxygen is present, which is not a disposal concern, because both U(IV) and U(VI) phosphate solids are sparingly soluble. Data from XANES revealed U(IV) in all of the solids analyzed, whereas EXAFS data indicated U(VI) in one sample. It is uncertain whether the U(VI) was formed during the chemical transformation or was already present in the waste sample prior to treatment.

An important requirement for processing DU into solid form is avoiding the presence of chloride, which requires more expensive process equipment and final storage containers. Our EXAFS and EDXA data indicate that a solid free of chloride can be formed under certain conditions (see Figure).

During FY2003, we will (1) use the methods described above and other common analytical techniques (e.g., elemental analysis and infrared) to investigate the reaction kinetics and thermodynamic characteristics of the selected dissolution systems by determining key data such as the molar heat of reaction, activation energy, rate, reaction order, and scaling factors; (2) determine the best unit operations for a full-scale process, including pre-washing, dissolution, and stabilization; and (3) complete full characterization of the final disposal product.

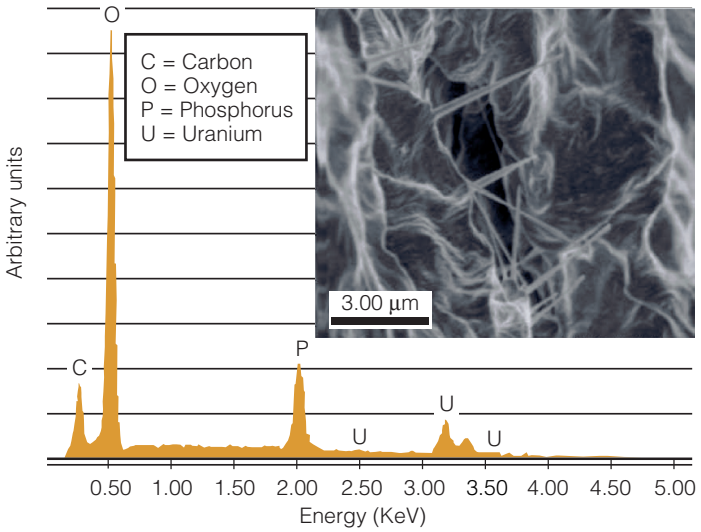

(a) Energy-dispersive x-ray analysis spectrum of the solid formed in the treatment of depleted-uranium (DU) waste with 1-molar phosphoric acid and 3-molar hydrochloric acid. These results show that our technique can produce a chloride-free solid, an important requirement for processing DU into a stable waste form. (b) Scanning electron microscope image of the solid's physical structure.

Mesochem: Chemical dynamics on a mesoscopic scale

L. E. Fried, R. H. Gee, C. J. Wu

Most chemically stable organic materials age through changes on the mesoscopic scale (from 10 nm to 10 mm). Examples include the slow crystallization of polymers, changes in particle-size distributions with age, and the swelling of pressed powders. We are developing a new mesoscopic modeling capability for organic materials, including polymers, molecular crystals, and filled polymer composites. Our goal is to develop and validate novel mesoscopic modeling techniques that are well suited for materials of interest to LLNL's national-security mission, such as high explosives, binding agents, and foams.

Although LLNL has a world-class ability to model material properties on the atomic and macroscopic scales, the structures characteristic of soft matter occur at the mesoscopic scale, between these two limiting regimes. Our current ability to model the aging and dynamical properties of mesoscopic systems is quite limited. In this project, we are developing flexible models of organic matter on the mesoscopic scale. This will help LLNL to better achieve a wide range of programmatic goals, while generating a scientifically unique model of mesoscale matter.

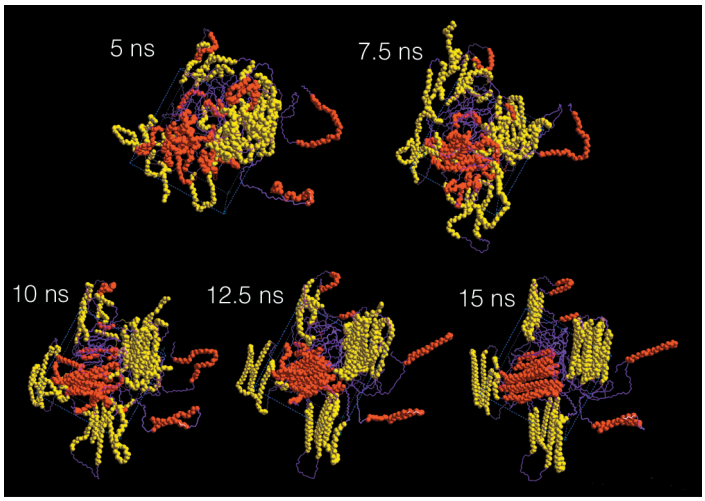

Time evolution of polyvinylidene fluoride crystal nucleation and growth. This is the first time that bulk polymer crystal formation has been observed in a molecular simulation.

The complex structure characteristic of soft matter leads to material behavior on a variety of timescales that are much longer than the 10-ns practical time-scale limit of molecular dynamics. To create a framework to address this wide range of problems, we are expanding upon a recently proposed method called dissipative particle dynamics" (DPD), an intermediate-length-scale approach to dynamics. Dissipative particle dynamics uses equations of motion similar to molecular dynamics to propagate "blobs" of material and uses transport equations based on nonequilibrium statistical mechanics to exchange mass, momentum, and energy between the particles. The equations are chosen so that the correct macroscopic hydrodynamics is obtained at large length and time scales.

In this project, we are developing methods to determine an accurate mesoscopic representation of a system based on underlying microscale calculations by combining electronic structure and molecular dynamics simulations to derive effective DPD interactions. If successful, the project will produce the first truly multiscale approach to DPD.

Our work in FY2002 has centered on developing mesoscopic models of polymer crystallization, pressed powder swelling, and recrystallization of volatile solids. The crystallization of polymers has a strong effect on their mechanical properties and can be responsible for changes in polymer mechanical properties with age. Having conducted extensive ordinary molecular dynamics studies of crystallization in vinylidene fluoride, we discovered that vinylidene fluoride forms ordered crystals within 10 to 20 ns when cooled extremely rapidly from the melt. This is the first time that bulk, three-dimensional polymer crystallization has been calculated through molecular dynamics. The Figure shows the crystallization event as it occurs in our simulations. The DPD models of polymer crystallization are also in development.

In FY2003, we plan to develop a mesoscopic model of polymer crystallization that is closely based on the atomistic model of vinylidene fluoride. Mesoscopic simulations of crystallizing polymers will then be carried out on microsecond time scales that are not accessible via atomistic simulations.

Chemical reactions controlling the mobility of uranium in ground- and surface-water systems with an emphasis on apatite

M. J. Taffet, B. K. Esser, E. Nelson, K. Roberts, B. E. Viani, P. Zhao

Uranium (U) contamination of groundwater is common at U mining, processing and disposal sites, and other DOE sites. Apatite minerals remove dissolved U from water and form the basis for a promising remediation technology. However, optimizing removal from water requires knowledge of the kinetics and thermodynamics of the dominant reactions. Currently, we do not have a quantitative understanding of what conditions lead to removal mediated by a surface process or when precipitation of an insoluble phase (e.g. autunite) dominates U removal at the low concentrations typical of groundwater and drinking water standards.

Our research goals are to achieve a mechanistic understanding of U removal by apatite using batch and column experiments, geochemical modeling, and solid-phase characterization to identify controlling species and phases, characterize thermodynamics and kinetics of the dominant reactions, and determine effective lifetimes of apatite-containing reactive barriers and filters as limited by aging, capacity, and porosity. The laboratory experiments involve quantifying the effects of dissolved U/apatite ratio, pH, carbon dioxide, common aqueous ions, and apatite composition and surface area. X-ray diffraction and x-ray absorption spectroscopy (XAS) are used to constrain the structure and speciation in fresh and aged U solid phases. This project supports the Laboratory's environmental management mission.

During FY2002, we conducted batch experiments with crystalline hydroxylapatite pre-equilibrated with buffer solution for several days. Experiments ran for 10 d at initial U concentrations of 0.7 to 10 ppm. Sorption of U on crystalline apatite was observed to be reversible, indicating that sorption of U to this apatite may be an equilibrium process. The experiments also indicated that precipitation can dominate above 50 ppb U.

We used XAS to investigate the oxidation state and coordination of sorbed U. Near-edge data indicate that U on crystalline apatite remains in the U(VI) oxidation state, so sorption does not involve a redox process. Figure (a) depicts Fourier transforms of the U L_{III} absorption edge, extended x-ray adsorption fine structure (EXAFS) data for three apatites from batch experiments (8.3 ppm initial U). These data show uranyl ions (UO_2^{2+}) bound to phosphate as a surface complex, and possible uranyl phosphate precipitates.

To investigate the competing processes of autunite precipitation and surface complexation on the apatite surface, samples with high and low concentrations of U were prepared. The high-concentration sample (17 wt% U) has nearly identical EXAFS to a reference autunite. The low-concentration samples were prepared by addition of U onto crystalline apatite for 4 wk while maintaining solution U concentrations at less than 10 ppb. The XAS data indicate that at up to several thousand parts U per million parts apatite, surface complexation is the predominant process.

We recently began sorption-edge experiments from pH 4 to pH 10 with crystalline apatite and initial U concentrations of 1, 2, and 10 ppb. Preliminary results indicate no appreciable difference in sorption of U to apatite across the pH range.

During FY2003, we will use reactive transport simulations to design column studies and batch experiments. Total carbonate concentrations and pH will be varied to characterize solid phases and adsorbed species. Data from these experiments will be used to refine kinetic and thermodynamic data used to characterize the transport properties of U in aqueous solutions.

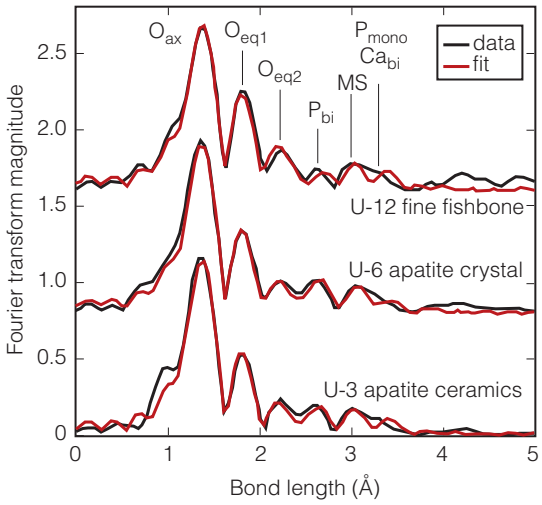

(a) Uranium (U) L_{III} absorption edge, extended x-ray adsorption fine structure data for three apatites from batch experiments (8.3 ppm initial U), showing similar fits for each of the apatite surfaces. [O_{ax} refers to peak for U bound to axial oxygens (O), O_{eq1} and O_{eq2} to U bound to equatorial oxygens, P_{bi} to bidentate bonding of U to phosphorus (P), MS to multiple scattering due to axial oxygens, P_{mono} to monodentate bonding of U to P, and bidentate calcium (Ca_{bi}) to bidentate bonding of U to Ca.]

Computational actinide chemistry at mineral interfaces and in colloids

K. Balasubramanian, V. Wheaton

Investigations of aqueous actinide complexes are central to understanding the mechanism by which radionuclides in high-level radioactive wastes migrate through soil to the groundwater. [Such studies can also provide the needed capabilities for actinide chemistry in uranium (U) corrosion modeling for the aging of nuclear materials.] In the environment, some actinides appear to be sorbed by geological interfaces, plants, or bacteria. The sorption reactions of actinides on these interfaces play a major role in the distribution and migration of actinides in the environment. However, the nature of the chemical reactions, coordination chemistry, and geometries of the sorbed actinide complexes at the mineral interfaces are poorly understood. In fact, there are several conflicting interpretations and models of the observed data.

Our project focuses on new computational actinide chemistry capabilities for modeling uranyl complexes at geological and biological interfaces. We have investigated the minimum energy geometries (i.e., bond distances and bond angles), vibrational frequencies, thermodynamic properties (enthalpies and Gibbs energies), bonding features, and spectroscopic properties of the actinide sorption complexes on geological and bacterial interfaces. The focus of work is U(VI) complexes of carbonates and silicates at interfaces and in solution.

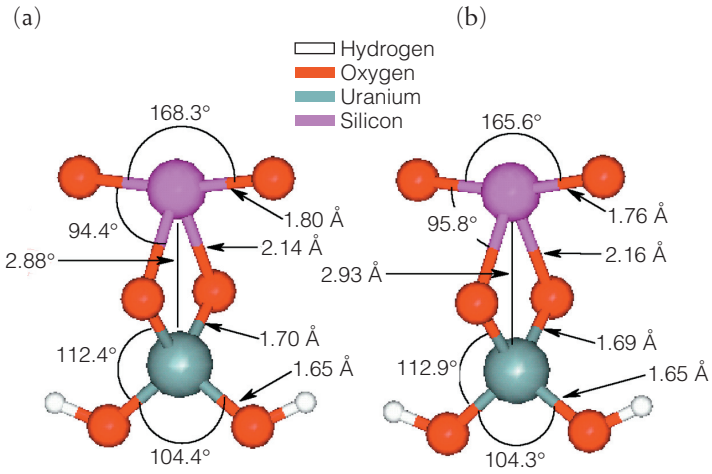

Structure of uranyl silicate found at low uranium loading on silica gel as determined with the (a) MP2 and (b) B3LYP computational methods. Our computationally determined optimized structure is the first ever to match accurately the experimentally observed monosilicate bridged structure of uranyl silicate as identified in extended x-ray absorption fine structure analysis.

Because of the large number of protons (92) in U, the speeds of the inner electrons can approach the speed of light, making relativistic effects extremely important. Consequently, neglecting relativistic effects in actinide-containing species can alter bond lengths by 0.3 to 0.4 Å, bond angles by up to 25°, and bond energies by a factor of 2. To reduce such errors to 0.02 to 0.04 Å in bond lengths and 5° in bond angles, our computational approach employs state-of-the-art, first-principles, relativistic quantum-chemical techniques. In addition, the project is enhancing existing computer codes to perform the required computations for actinide complexes in solution and at interfaces.

This work is applicable to nuclear-material aging studies in support of stockpile stewardship. The computational models will support DOE environmental missions by providing new insight into actinide migration and speciation in natural groundwater to improve environment management of high-level radioactive wastes.

Focusing on U(VI) complexes with carbonates at interfaces and in aqueous solution, in FY2002 we completed computations of uranyl silicate complexes that occur in colloids and silica gel, and performed benchmark calculations to validate our technical approach. We computed the energies, bond lengths, and bond angles of uranyl carbonates (in solution and at interfaces) and of uranium oxides, for which a great deal of experimental data exist. A computational method of ours, termed the complete active space–relativistic configuration interaction (CAS–RCI) method, reproduces experimental energies with errors of only 0.1%—something no other method can do—and transition energies that match experimental data within a few percentage points.

In addition, our work determined, for the first time, the geometries of uranyl silicate complexes in silica gel and silicate colloids. Consistent with the results of an extended x-ray absorption fine structure study of U(VI) sorption onto silica gel, we explained the origin of two types of bridged structures of uranyl silicates: a monosilicate bridged structure observed at low U loadings (see Figure) and a bisilicate structure observed at higher U loadings. Our work optimized the geometries of hydrated uranyl carbonates in solution and resulted in three publications. In FY2003, we will extend these results by completing calculations of the bond energies for U(VI) monosilicate complexes. These results should provide valuable insight into the mechanisms responsible for sorption of U(VI) onto geologic materials.

Modern chemistry techniques applied to metal chelation with medical and environmental applications

M. Sutton, S. R. Burastero

The number of reported cases of occupational chronic beryllium (Be) disease (CBD) is increasing, but currently no cure exists for CBD. Beryllium body burden has been identified in many CBD patients and may play a role in CBD pathogenesis. Chelation therapy—removal with an intravenously administered compound that binds with Be, which is then flushed out in urine—has been suggested as a potential therapeutic treatment for the reduction of Be body burden. Alternatively, the chelator can be administered directly into the lungs.

This project aims to modernize the scientific approach to developing metal chelators using analytical, synthetic, and combinatorial chemistry coupled with thermodynamic and structural modeling. The goal is to develop a specific screening process and use the process to choose the most promising metal chelators based on factors such as chemistry, environmental and medical feasibility, toxicology and pharmacology data, usefulness to the DOE complex, and importance to public health. Preliminary synthesis of specific chelation agents will also be performed for medical and environmental decontamination.

This work supports the Laboratory's missions in health care and environmental management by advancing the study of possible chelation therapy for CBD and the management of Be and other metals (lead, mercury, and arsenic) with medical, industrial, and environmental importance. To leverage Laboratory expertise in chemistry, biology, and medical and environmental application, this project is performed in collaboration with the University of California, San Francisco.

In FY2002, we assessed a large number of possible chelators and developed a ranking system based on the effectiveness of the chelator in dissolving Be particles and competition for metal chelation with other chemical systems in the body. This has led to the selection and development of three candidates for selective and effective chelators for futher study: sulfonaphthoic acids, diphosphonic acids (see Figure), and disulfonic acids. We also studied Be solubility and speciation in a number of simulated body fluids, allowing us to better understand the chemistry of Be as it travels through the body and reacts with elemental constituents.

Work planned for FY2003 includes (1) using chemical thermodynamics, quantum molecular dynamics, and structure investigation to develop a full-suite database for modeling Be chelation in biological systems; (2) studying the chemistry and thermodynamics of metal chelation in conditions mimicking human physiology while using animal models to study Be decorporation with new, effective chelators; (3) combining selected chelators with inert solid support (e.g., polystyrene, silica beads, and aerogel) and physical applications such as ion extraction systems, and possibly incorporating the chelating agent into a spray or absorbent material for cleaning Be-contaminated equipment, areas, and coolant fluid; and (4) publishing the results of our work.

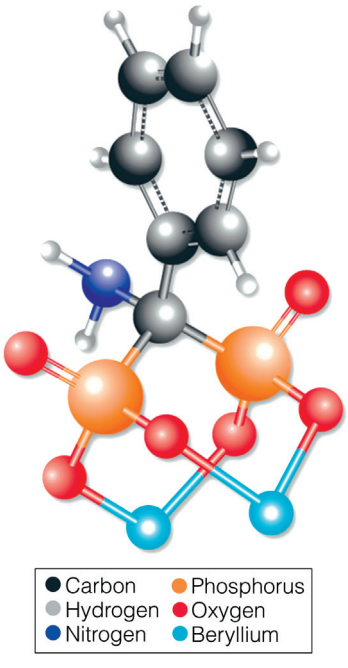

A chelate complex of beryllium (Be) and diphosphonic acid, which we identified as one of three candidates for selective and effective chelators. Diphosphonic acid enables Be removal through electrostatic attraction between its negatively charged oxygen molecules at the positively charged Be ion ($Be2^{+}$). Such chelators have applications in chelation therapy—reducing Be body burden—and in environmental decontamination.

Local-scale atmospheric reactive-flow simulations

C. K. Westbrook, R. L. Lee

Possible atmospheric releases of chemically reactive materials include fires, chemical spills at refineries or on railroads, and the accidental or intentional release of chemical or biological warfare agents. In all of these scenarios, the need exists to predict where the material will go and how it will evolve chemically as it is transported in the atmosphere. Such predictions can be used to assess health risks and are more vital for public safety than ever before. However, existing atmospheric-simulation models do not include reactions involving chemicals and aerosols transported by air, although such species can be highly affected by local conditions of humidity and sunlight and by other airborne chemicals.

We are developing computer models to describe the coupled chemical reactions and spatial transport of a wide variety of gases and aerosols by building on existing capabilities in atmospheric-flow simulations, including those used in regional-scale atmospheric-release modeling and studies of the chemical kinetics of hydrocarbons and other chemicals. The resulting model will be valuable to LLNL's nonproliferation, homeland security, and environmental programs.

Three separate but interconnected activities are required to provide this computational analysis tool: (1) modifying an existing atmospheric flow code to include time-dependent chemistry and aerosol changes, together with the associated submodels to compute those changes for toxic airborne chemicals; (2) devising submodels for particulate or liquid aerosols; and (3) modifying an existing regional-scale fluid-mechanics model based on FEM3MP—a finite-element, three-dimensional code—to compute the time variation in the atmospheric transport of chemicals and particulate aerosols due to reactions. This will be done by adding subroutines to simulate gas-phase chemical reactions and aerosol–surface reactions of species that are being carried along by airflow. Effects of humidity, sunlight, temperature, and concentrations of other chemical species on these reaction rates will be included in the evolution submodels.

In FY2002, significant progress was made in developing the submodels for calculating the chemical reactions of aerosols and gaseous species of interest. The nerve-gas sarin was selected for study because its chemical similarity with other organophosphorus compounds (OPCs) with which we had considerable kinetic-modeling experience. Kinetic modeling identified the major steps in sarin decomposition as molecular reactions producing propene and hydrofluoric acid [Fig. (a)]. This analysis also identified other OPCs that react in much the same manner as sarin and showed that common OPCs used to simulate the reactions of sarin actually react much more slowly than sarin and should not be used as chemical surrogates.

In addition, the FEM3MP code was modified, tested, and used to perform a simulation of a gas release [Fig. (b)]. Theoretical analysis of condensation of water vapor on surfaces of aerosols also progressed and should lead to a multiphase model of wet chemistry on the surfaces of these solid particles.

Work planned for FY2003 will integrate the different submodels to investigate scenarios involving the release of toxic chemicals into populated urban areas. The detailed chemical model for sarin will be simplified using knowledge about its most important reactions, and the results will be incorporated into the FEM3MP framework. Simulations of related aerosol transport and reactions will also be pursued, although the detailed aerosol chemistry model is not yet as well developed as chemical models of toxic gases.

(a)

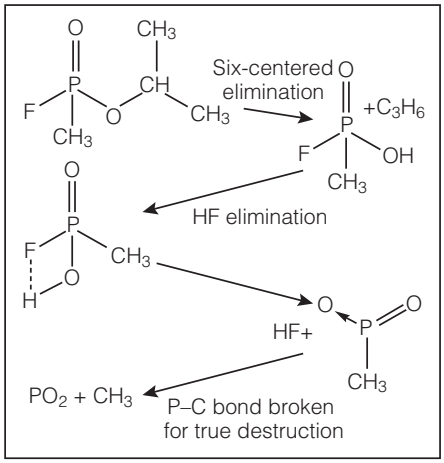

(b)

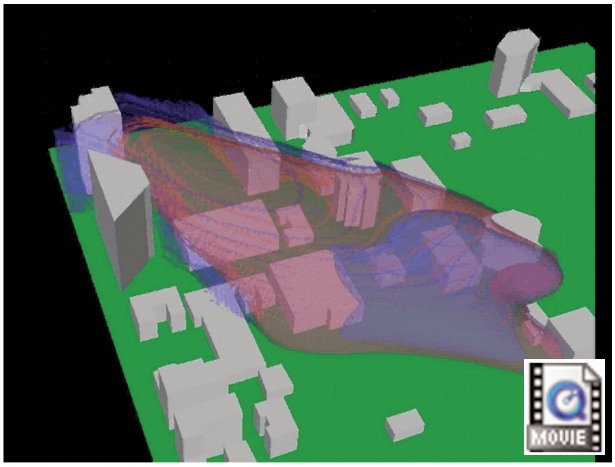

(a) The major chemical steps in the destruction, by thermal decomposition, of the nerve-agent sarin as a series of molecular elimination reactions. Our analysis showed that common organophosphorus compounds used to simulate the reactions of sarin actually react much more slowly than sarin and should not be used as chemical surrogates.
(b) Simulation of a reactive-gas plume spreading through a city. Contours show varying gas concentrations as the chemical is degraded by reactions with the atmosphere. To perform this simulation, we modified a fluid-mechanics model based on the FEM3MP code to include time variation in atmospheric transport caused by gas–atmosphere reactions.

Transport and biogeochemical cycling of iodine-129 from nuclear fuel reprocessing facilities

J. E. Moran

Reprocessing spent nuclear fuel is a comparatively straightforward way of obtaining fissionable material. However, reprocessing results in the airborne or waterborne release of several volatile radioactive species. Of the volatile species emitted, iodine-129 (^{129}I) is the most effective tracer of radioactive emissions from reprocessing facilities, owing to the very low level of naturally occurring ^{129}I and the large amounts of it released during reprocessing.

Tracing ^{129}I requires determining how it is transported and its ultimate fate in the environment, which is a significant challenge for three reasons. First, several chemical forms of iodine are found in environmental samples because of their thermodynamic stability in the atmosphere and hydrosphere. Second, iodine is involved in active biological and chemical cycles. Third, both ^{129}I and ambient ^{127}I are found in only very small amounts in environmental samples.

The primary goal of this research is to provide the scientific basis for interpreting ^{129}I/^{127}I ratios in soil, water, and biological materials by determining, for the first time, all major chemical forms of iodine present in environmental samples; detecting low amounts of ^{129}I; and interpreting the results of measurement, i.e., the concentration of ^{129}I and the ratio of ^{129}I to ambient ^{127}I in samples.

The ability to interpret ^{129}I concentrations and ^{129}I/^{127}I ratios depends on having a framework for predicting the chemical transformations that ^{129}I undergoes after release from a reprocessing facility. By experimentation, we are testing the hypothesis that ^{129}I from nuclear fuel reprocessing facilities is transported in a different chemical form than is either residual ^{129}I from atmospheric weapons testing or ambient, stable ^{127}I. Characterizing these different chemical forms and transformations will enable the tracing of ^{129}I, which supports (1) the national-security mission by allowing development of tools for detecting clandestine nuclear fuel reprocessing activity, and (2) national efforts to trace radioactive emissions from domestic reprocessing plants and address the radioactive legacy at contaminated sites.

In FY2002, we used synchrotron x-ray techniques [e.g., x-ray absorption near-edge structure and extended x-ray absorption fine structure (EXAFS)] to determine directly the oxidation state, bond length, and near-neighbors (elements or functional groups next to which iodine is found in environmental samples) of the major forms of iodine in solid and aqueous materials. Although accelerator mass spectrometry is the established method for measuring exceedingly small ^{129}I/^{127}I ratios, we have focused on a much faster, more versatile method—multicollector inductively coupled plasma (MC-ICP) mass spectrometry. Previously, an impediment to using this method was isobaric interference from xenon-129 (^{129}Xe). However, we found that using oxygen in the hexapole collision cell of our MC-ICP mass spectrometer avoids this interference, thereby allowing a significantly lower detection limit than was previously possible (see Figure).

In FY2003, we will carry out bench-top soil column experiments using XAFS to determine the degree and mechanism of the sorption of iodine by solids. These experiments will provide the basis for predicting the environmental transport and fate of ^{129}I, which is especially important for DOE legacy sites where the transport of radionuclides into groundwater is occurring. Another major area of effort will be using on-line species separation by ion chromatography, in conjunction with MC-ICP mass spectrometry, to simultaneously determine the chemical form and concentration of ^{129}I in aqueous samples, such as rainfall and groundwater.

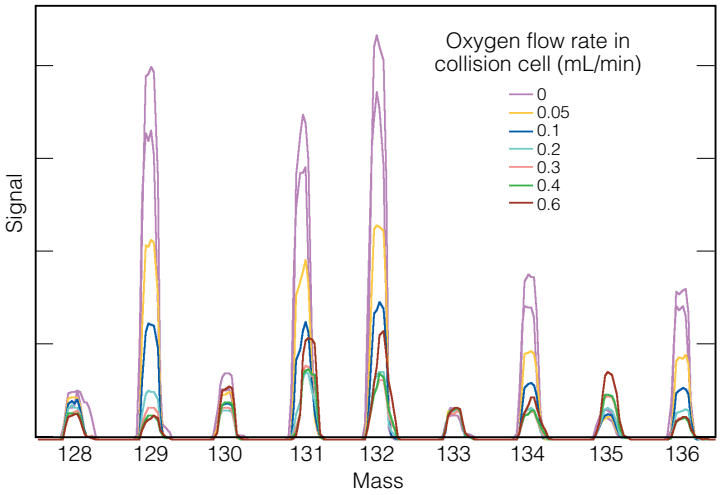

Seven of the nine stable isotopes of xenon (Xe), including abundant isotope ^{129}Xe, are present in a plasma gas and interfere with low-level detection of iodoine-129. Reaction with oxygen in the collision cell suppresses formation of Xe ions—an effect that is optimized at an oxygen flow rate of about 0.4 mL/min.

Exploring the linkage between impurities and optical properties in rapid growth of crystals

R. Hawley-Fedder

Impurities play a key role in crystal growth and affect properties such as shape, homogeneity, optical breakdown, and optical transmission. Understanding the physics and chemistry of crystal growth from solution has broad application to a wide range of technologies, including crystal engineering, protein crystallization, biomaterials engineering, and optical materials development. Future advances require increasingly sophisticated approaches for understanding the link between optical properties and growth conditions.

While potassium dihydrogen phosphate (KDP) is considered to be an archetypical solution-grown optical crystal, understanding how impurities influence crystal growth and the resulting optical performance in KDP will have broad-reaching implication on the development of crystalline materials for optical components and photonics applications worldwide. LLNL has a well-established reputation in key areas of crystal growth—impurity-step interactions, solution crystallization, biomineralization, and simulations—and is also well recognized internationally for its work in rapid solution growth of very large (1 m) crystals. Continued research in these areas supports the Laboratory's science and technology mission and will enhance our ability to produce large KDP crystals for a variety of applications, including components of high-power optics systems.

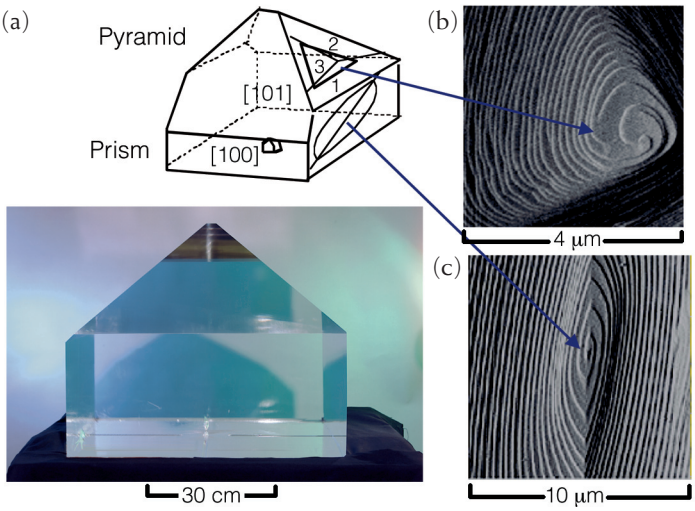

(a) KDP crystal grown at LLNL showing growth structures on the (b) pyramid [101] and (c) prism [100]. Prism faces are strongly influenced by impurities; pyramid faces are not.

In this project, we will investigate a new approach to eliminate the source of impurities (e.g., water soluble, usually multivalent metal cations) in crystal vessels and determine the factors affecting incorporation of impurities into the crystal lattice and the impact on the final shape of crystals of preferential incorporation into prismatic versus pyramidal material (see Figure). The first step is redesigning current crystal-growth systems to include engineered barriers that control the release of aluminum (Al) and other impurities from the walls of glass vessels used to grow crystals. Next, we will systematically control the concentration of specific impurities (e.g., Al^{3+}) in the growth solution, use three-dimensional (3-D) modeling to predict the effect of rotation regimes on growth, and simulate heat transport in the system. Advanced hardware and software will be implemented to monitor and control conditions within the growth tank system.

During FY2002, two candidate materials—Halar and FEP, which are both fluoropolymers similar to Teflon—were identified, tested, and found to be stable inert barrier materials. Controlled impurity addition (Al^{3+}) to a deuterium potassium dihydrogen phosphate (DKDP) solution did not affect shape as expected based on similar data using the KDP solution. A 3-D model was developed to simulate the effect of rotation rate on mass transfer to the crystal and used to minimize turbulent flow while maximizing the mass transport ("feeding") of the crystal faces. We completed fabrication and testing of a new system that incorporated automated controls for temperature, solution level, and pumping speed. These enhancements greatly increased the stability of the system during a crystal growth run.

In FY2003, we plan to expand our efforts to understand the effects of temperature, composition (deuterium vs. hydrogen), impurity composition, and impurity incorporation in both prismatic and pyramidal crystal faces by linking experimental results with modeling of impurity/crystal interactions. We will use modeling to predict the exact chemical composition that the impurities take when interacting with the crystal surface and the effect of that interaction on crystal growth. Atomic force microscopy will allow us to probe the interactions of these impurities on the nanometer scale at the crystal surface. Crystal growths from 0.1 to 1 m will provide sufficient information to determine the amount of impurity incorporated into the crystal.

Toward applications of quantum dots: Surface modification and novel electronic properties

L. J. Hope-Weeks, B. R. Taylor

Nanometer-size semiconductor particles, often called quantum dots or nanocrystals, have interesting and unusual properties that differ from those of the bulk material. The interesting properties of these materials arise from the fact that the number of atoms at or near their surface is far greater than in the bulk material. As a result, the surface of quantum dots plays a large role in their electrical and optical properties, whereas in the bulk material, the surface plays a very minor role. Our project covers some of the initial work needed to bring the advantages that these properties offer to applications that support LLNL missions, for example, biological tags and sensors for missions in nonproliferation, counterterrorism, and biotechnology.

Quantum confinement, which occurs when the quantum dot is smaller than the radius of a bound electron hole pair, changes the dot's electronic properties. Because most or all the atoms interact with the surface, any charge carriers also interact strongly with the surface. Therefore, controlling the surface chemistry changes both the physical and electronic properties of the dot. The surface termination chosen protects the dots from oxidation, permits them to form stable suspensions in organic solvents, and improves their luminescent efficiency by tying up dangling bonds.

Modifications of the surface will permit chemical attachment of quantum dots to surfaces and proteins, and may eventually permit electrical connections to them. Due to the large surface area per unit volume, appropriate functionalization may permit the development of a sensitive sensor for pathogens or chemical agents, a possibility that is clearly relevant to the DOE's nonproliferation and counterterrorism missions.

During FY2002, we continued to investigate effects on surface chemistry of both silicon (Si) and germanium (Ge) quantum dots. Our work with Ge has focused on improving the size distributions by using the traditional metathesis reaction. When studied by x-ray absorption spectroscopy (XAS), Ge nanoclusters show a blue shift of the conduction band edge, consistent with quantum confinement theory.

Silicon nanocrystals are extremely hard to synthesize, and size selection via the metathesis route has proven extremely difficult. We optimized the conditions of this reaction to give the best possible yields of nanocrystals and demonstrated the ability to chemically modify the surface. To improve the size selectivity of the nanocrystals, we focused our attention on other methods for nanocrystal production. By modifying procedures that involve the reduction of Si(IV) starting materials, we produced nanocrystals with hydride-terminated surface. We also demonstrated the ability to modify the hydride surface to attach functional groups without affecting their desirable luminescent properties. Atomic force microscopy has shown that size control can result from varying the conditions under which the nanocrystals are produced (see Figure).

In this project, we have demonstrated that the surface of Si and Ge nanocrystals can be readily modified with a variety of novel organic groups that renders them resistant to oxidation.

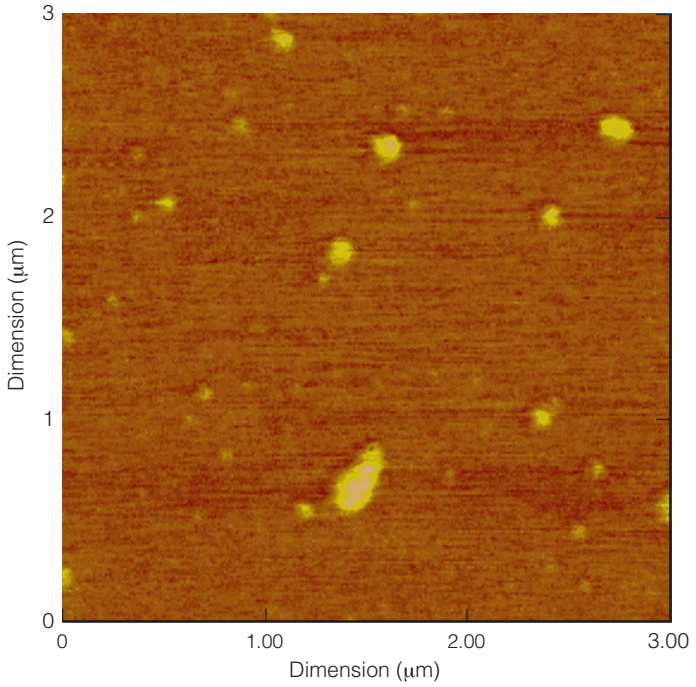

Atomic force microscopy image of silicon quantum dots showing particles with an average size of 2 nm. The average size of nanocrystals can be controlled by varying the reaction conditions that produce them.

Surface attachment of mechanically interlocking molecules

A. L. Vance, T. van Buuren

In recent years, interest in mechanically interlocking molecules, known as catenanes and rotaxanes, has grown significantly—primarily because of their potential as building blocks of molecular-scale devices. Catenanes consist of interlocking molecular rings, whereas rotaxanes are assembled by threading a linear molecule through a ring and capping both ends with "molecular stoppers" to prevent dethreading. Free (i.e., not surface-attached) molecules of this type are well documented, but the incorporation of mechanically interlocking molecules on surfaces is an area that remains virtually unexplored. Very few examples of surface-attached catenanes or rotaxanes have been reported in the literature to date.

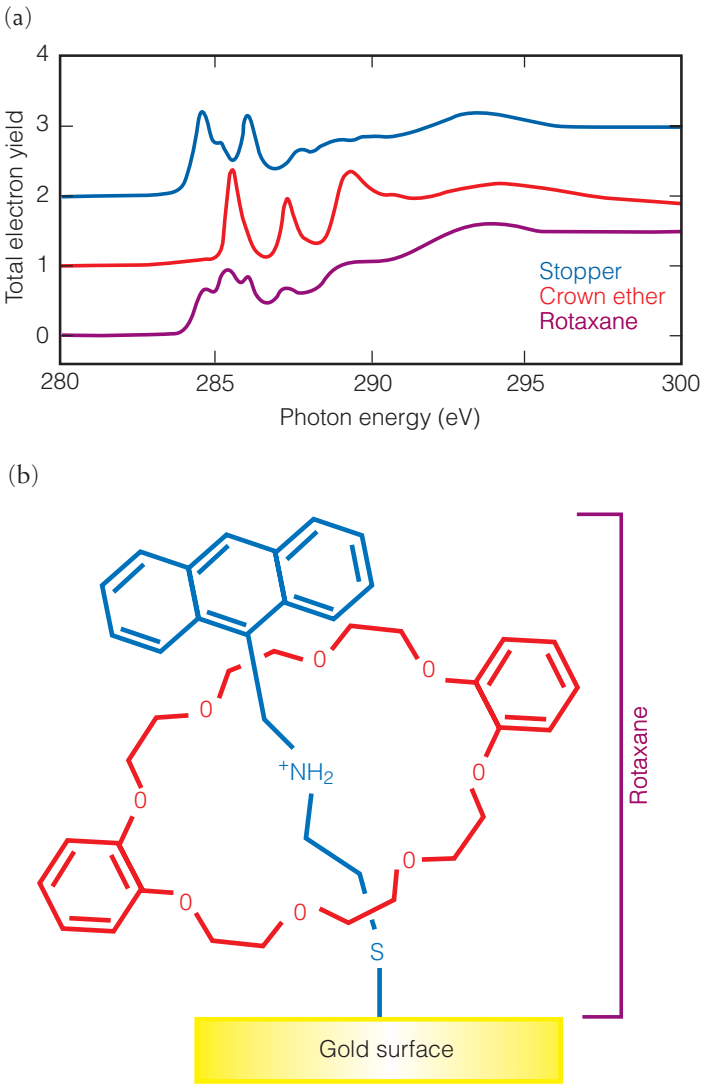

(a) Carbon K-edge x-ray absorption spectra and (b) molecular diagram of a surface-attached rotaxane (on a gold surface) and its separate components—a thiol stopper and crown ether ring. The low electron yield shows the rotaxane to be a gold-bound interlocking molecule, which has potential applications such as sensors with properties that can be controlled at the molecular level.

We are working to develop new mechanically interlocking molecules for the formation of multifunctional and tunable self-assembled monolayers. Our long-term goal is to create sensors with properties that can be controlled at the molecular level. These sensors will exploit three anticipated properties of surface-attached mechanically interlocking molecules: (1) molecular recognition can occur within the pocket created by linking two molecular rings, (2) recognition elements can be placed on the exterior of the movable ring for tunable properties, and (3) terminal receptors can be combined with a molecular shuttle whose location on the surface-attached chain generates a unique signal. By using mechanical linkages in the monolayers, recognition can be switched on or off, which allows sensing to be controlled by changes in the configuration of the surface-attached species. With the design flexibility inherent in these systems, detection can be carried out through a variety of methods such as electrochemistry or fluorescence.

This project expands efforts at LLNL to develop new types of self-assembled monolayers for improved detection and separation technologies and has the potential for making a significant impact on LLNL's nonproliferation and environmental missions.

During FY2002, we focused on preparing and characterizing surface-attached rotaxanes. Monolayers on gold(111) were prepared from an anthracene-stoppered thiol thread, a pseudorotaxane obtained by mixing the thiol with dibenzo-24-crown-8, and a disulfide-containing [3]rotaxane. X-ray absorption spectroscopy and x-ray photoemission spectroscopy showed clear distinctions between the constituent monolayers, allowing identification of spectral contributions from the separate components (see Figure). The spectroscopic data clearly showed that only the [3]rotaxane yields the desired gold-bound interlocking molecule. This work highlighted important considerations for researchers interested in pursuing molecular-scale devices.

Highly ordered, three-dimensional nanoscale structures with controlled surface chemistry

T. F. Baumann, J. H. Satcher, Jr., B. R. Hart

Ordered porous solids are an area of active research and are being investigated for a wide range of applications, including catalysis, separation technology, photonic crystals, and nanoelectronics. One method of forming highly ordered, three-dimensional (3-D), porous nanoscale materials is the template approach, in which (1) close-packed arrays of monodisperse spheres of a material such as latex are formed as a template; (2) the interstitial regions are infused with a reaction solution of the material that will eventually comprise the replicate structure; and (3) the template is removed either chemically or thermally, yielding a porous replicate solid with periodic voids 0.1 to 1 μm in diameter.

The goal of this project is to use organic sol-gel chemistry for the template-assisted preparation of 3-D ordered porous solids with controlled surface chemistry. Using organic sol-gel chemistry allows us to tailor both the composition and textural properties of the replicate surfaces and control the bulk optical, mechanical, and chemical properties of the porous solids. If successful, this approach could provide important new materials that are applicable to nonproliferation and environmental programs.

In FY2002, we developed a general procedure for the synthesis of ordered porous organic and carbon aerogels in which colloidal crystals of polystyrene spheres were used as templates. Formation of an organized 3-D template was achieved through filtration of a dilute solution of monodisperse polystyrene particles (290 nm in diameter) through a smooth, narrow-pore membrane. Once assembled, the interstitial regions of the template were infiltrated with an organic sol-gel solution using filtration. After the sol-gel material gelled, the resulting composite was washed with toluene to remove the latex template. Finally, the replicate solid was processed to afford an organic aerogel.

The 3-D ordered array of spherical cavities within the organic aerogel were confirmed using scanning electron microscopy. Micrographs show that the hexagonal symmetry of the template has been preserved in the ordered pore structure of the replicate solid (see Figure). These ordered lattices of voids are responsible for the brightly colored opalescence observed in the organic replica. The organic aerogel material can be carbonized (heated) in an inert atmosphere to yield a carbon aerogel that retains the ordered macroporous structure. Carbonization is an important process that allows us to modify the chemical and conductive properties of the replicate solid.

Future issues to address include controlling the surface properties of these novel porous materials, which can be accomplished using our demonstrated techniques for incorporating specific organic and inorganic species into the organic aerogel framework through functionalized sol-gel precursors.

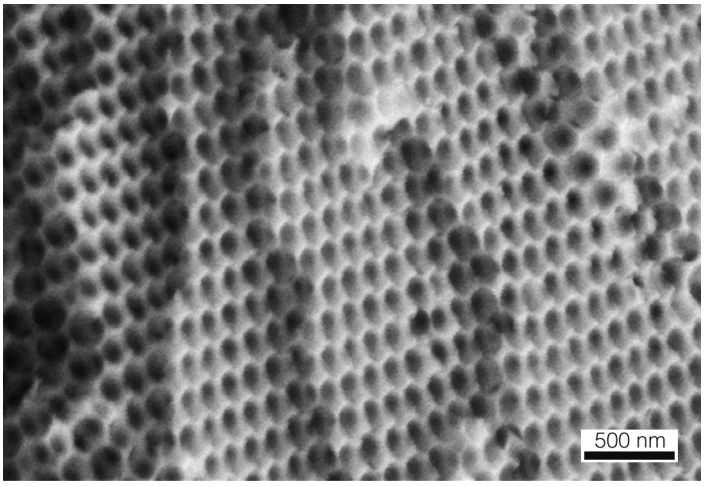

Scanning electron micrograph showing the hexagonal symmetry of the ordered pore structure of an aerogel prepared using a template of ordered latex spheres.

Earth and Space Sciences

Section 4

Section 4 — Earth and Space Science

Large-aperture, lightweight space optics

R. A. Hyde, S. N. Dixit, A. H. Weisberg

Large, lightweight optics are important for many space-related missions. To develop such optics, this research project has proposed a radically different approach for making them using diffractive optics instead of mirrors or conventional lenses. The goal of this project is to fabricate a thin, 5-m-aperture diffractive lens that is lightweight, foldable, of high resolution, and the size class of lenses used in the Palomar and Hubble telescopes. By providing such an optic for surveillance and scientific uses in space, this project supports LLNL's missions in national security and basic science.

In FY2002, the final year of this project, our primary goal was to fabricate, assemble, and test a large, optical-quality, diffractive lens using the techniques developed in previous years. The basic approach for building the lens was to assemble it by seaming together multiple thin-glass panels. This multipanel approach splits lens fabrication into two separate and feasible tasks: optical engineering to create meter-scale lens panels and mechanical engineering to align and join panels across the full 5-m aperture. Accomplishing these tasks required a number of innovations in metrology and optical-component fabrication.

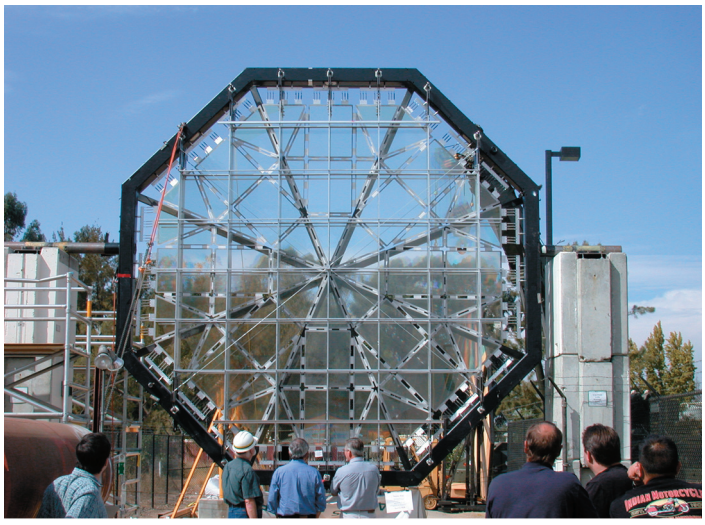

A 5-m diffractive lens assembled from 72 lens panels. Lithographic surface patterning and high-precision assembly make each panel act as a segment of the overall diffractive lens. The result is a lightweight, foldable, high-resolution lens that can be deployed in space for surveillance and scientific uses.

To make the lens panels, we need meter-sized sheets of thin glass, each smoothed to an identical, uniform thickness and patterned with the proper diffractive surface profile. We accomplish this with a two-stage smoothing process based on spatially controlled wet etching. First, initial smoothing is performed by a line etcher—already built and tested—that smoothes the full-size (80-cm) panels along a one-dimensional (1-D) reference line to a thickness of ~30 nm. Next, a second-pass etcher removes any residual 2-D surface ripples. After the lens panels are smoothed, lithographic surface patterning makes each panel act properly as a segment of the overall diffractive lens.

Assembly of the full suite of 72 lens panels into a complete lens involves accurately placing each one at its proper site and then joining them together on a semi-automated work station we designed. Its work surface is 6 × 6 m in size and is thermally and vibrationally controlled. Each panel is aligned to its neighbors, first by monitoring fiducials along the common borders, and then applying the proper 3-degrees-of-freedom adjustment to its position with a precision nudger. Once the panel is in the proper location, it is joined to its neighbors with foldable metal seams.

In FY2002, we built and tested the second-pass etcher and largely completed the semi-automated work station. However, because our glass-smoothing processes was not sufficiently well advanced to smooth all 72 lens panels needed for the 5-m lens, the lens was built with unsmoothed lens panels. Although the unsmoothed glass precluded diffraction-limited levels of performance, we were nevertheless able to build an operational 5-m lens comprised of diffractively patterned lens panels. Because the unsmoothed glass obviated closed-loop alignment accuracy, a simpler, open-loop assembly process was used.

The lens was mounted outdoors at LLNL and optically tested at three different wavelengths. For each color, the lens delivered a harmonic series of tight focal spots. This is the largest high-quality diffractive lens ever fielded and has performed very well. With further refinements, this capability is expected to find important applications in research and surveillance.

Djehuty: A next-generation stellar-evolution code

D. S. Dearborn, P. P. Eggleton

Stars provide the fundamental quantitative units for measuring the universe, such as determining distances and ages and the factories driving chemical evolution. Stars continue to be used as physics laboratories for constraining the properties of fundamental particles (e.g., cross sections and masses) and hot plasmas [e.g., opacities and equations of state (EOS)].

Current practices in stellar evolution employ one-dimensional (1-D) calculations that quantitatively apply to only a minority of the observed stars—single nonrotating stars and well-detached binaries. Even in these systems, astrophysicists depend on models of complex 3-D processes such as convection. With the advent of massively parallel computers and the development of codes to use them, LLNL is uniquely situated to move the calculation of stellar properties to the next level of physical understanding.

This project leverages abilities from across the Laboratory to develop a 3-D stellar-evolution code, called Djehuty, that operates on massively parallel computers with the best available physical data (e.g., opacities and EOS). Our code will be a test-bed to validate—using astronomical observations—the physical data and advanced numerical algorithms being developed for the Stockpile Stewardship Program, in support of LLNL's national security mission.

In FY2002, Djehuty became an operational code and was used to perform stellar simulations. These calculations include the first 3-D simulation of a type II supernova (see Figure). A goal was to investigate how the silicon-burning region of a supernova produces nickel, an important energy source in the observed light curves. Our calculations showed development of instability that caused tendrils of nickel to extrude into surrounding material at an early stage, in agreement with observations of Supernova 1987A. Previous 1-D simulations had predicted extrusion occurring much later.

We also performed the first simulation of a nova—an explosive event in which hydrogen is torn from a normal star in a binary-star system and deposited on its white-dwarf companion. According to our 3-D calculation, hydrogen ignition propagates from a number of ignition points and creates a shock that accelerates the surface to nearly 3000 km/s. Upon emerging at the surface, the shock is heated to temperatures greater than 1 keV, creating an x-ray pulse. However, the calculated white-dwarf mass was somewhat smaller than those thought appropriate for most novae, and the hydrogen accretion was symmetric over the surface of the star. Future work includes achieving a more realistic hydrogen distribution, in which the material settles onto the star as a high-velocity stream.

Other results in FY2002 include developing, for our 4-solar-mass main sequence model, new boundary conditions that seem to resolve numerical-stability problems that previously precluded runs of more than a few thousand cycles; serving on the organizing committee for a very successful conference on 3-D simulations of stars at the University of California, Davis; and giving an invited colloquium at the University of Texas at Austin. In addition, a postdoctoral researcher involved in this project was hired at LLNL.

This project has provided a tool—Djehuty—that combines precise observation with analysis to study nature at scales from a gigaparsec to less than a nanometer. By linking high-energy-density research to observations of objects close to the beginning of time, Djehuty provides a natural link between astrophysics and national security.

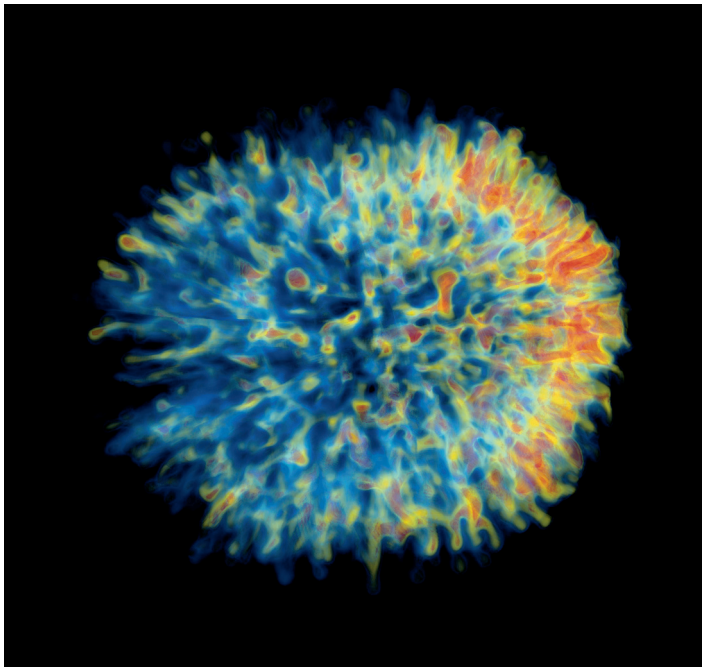

The first 3-D simulation of a type II supernova, showing radioactive nickel being produced in the silicon-burning region of the supernova. Our calculations indicated development of instability that caused tendrils of nickel to extrude into surrounding material at an early stage, in agreement with observations of Supernova 1987A.

An integrated climate- and carbon-cycle model

S. L. Thompson

Coupled climate- and carbon-cycle modeling is required to understand and predict the future environmental impacts of fossil-fuel burning. At present, atmospheric carbon dioxide (CO_2) concentrations are prescribed, not simulated, in large climatic models. To produce credible simulations of the entire climatic system that predict time-evolving atmospheric-greenhouse forcing, manmade emissions must be the fundamental input.

Predicting atmospheric CO_2 concentrations represents a substantial scientific advance because of the large natural sources and sinks of carbon that are likely to change as a result of climate change. Estimates of the amount of manmade CO_2 that will accumulate in the atmosphere depend on understanding the carbon cycle. For this reason, models that use CO_2 emissions as input must directly address greenhouse-related questions of interest to policymakers—such as the amount of CO_2 we can emit before causing a dangerous level of climate change.

The goal of this project is to develop a global-scale, integrated climate- and carbon-cycle (INCCA) model to (1) predict the fate and climatic effect of fossil-fuel-derived CO_2 and aerosols and (2) evaluate the climatic impact of proposed energy policies. INCCA requires models of the global climate to be coupled with terrestrial and oceanic ecological and biogeochemical components. Our approach relies on using existing models of the atmosphere, ocean, land surface, and aerosol chemistry that are well developed and published. Where necessary, we are modifying codes for use on terascale, high-performance computers and for coupling into a comprehensive simulation system.

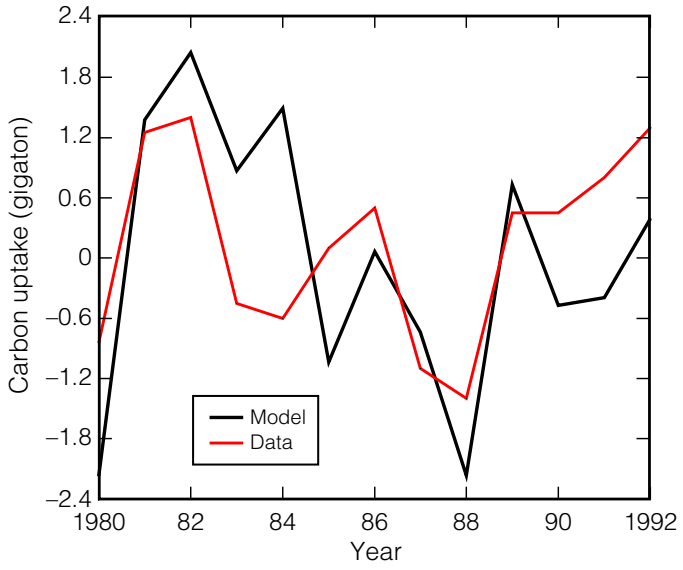

Year-to-year variability in terrestrial carbon uptake as simulated by integrated climate- and carbon-cycle modeling (black line) and as estimated from observations (red line). Agreement between the two indicates that our model can help us understand how the global biosphere reacts to climatic change.

In this high-priority area of global-change prediction, this project leverages previous and ongoing LLNL developments in climatic science and terascale parallel computing. Two current initiatives launched by the White House—the U.S. Climate Change Research and Climate Change Technology—both highlight the need for an improved climate-carbon prediction capability. By contributing to these initiatives, INCCA supports LLNL's mission in environmental management.

During FY2002, we completed our analysis of 16 multiyear simulations with a coupled climatic and vegetation model subset of INCCA and demonstrated that the model can reproduce observed interannual variability of CO_2 uptake by plants, which is caused by climatic variations. The Figure illustrates agreement between observed and simulated time series of terrestrial carbon uptake. Model results such as these will help us understand how the global biosphere reacts to climatic change, which is difficult to do from observations alone.

We also completed and tested a fully comprehensive climate- and carbon-cycle model combining ocean, atmosphere, sea ice, terrestrial biosphere, and marine biogeochemical components. A starting point for this model was created—an equilibrium, preindustrial state corresponding to the year 1870. A stabilized, postindustrial, enhanced-greenhouse state was also completed for comparison with the preindustrial state. Results from both simulations compare favorably with those of other models, indicating our new model is now ready for predictive simulations.

In FY2003, we will run the full INCCA model from the year 1870 to produce simulations of the twentieth and twenty-first centuries. Using historically observed and projected greenhouse gas emissions, the model will produce climates and greenhouse gas concentrations that can be compared to observations and used to improve our understanding of future interactions between climate and the carbon cycle.

An imaging Fourier transform spectrometer for astronomy

R. Wurtz, E. Wishnow, K. Cook, S. Blais-Ouellette

Experience has shown that the most efficient use of the photons striking a telescope's aperture would be to produce true three-dimensional imaging—a hyperspectral data cube, consisting of two spatial dimensions and one spectral dimension—that could later be investigated in detail.

An imaging Fourier transform spectrometer (IFTS) observation yields a spectrum for every spatially resolved element (pixel) in its field of view, which offers an exciting multiplex advantage over a dispersive spectrograph for astronomical imaging ranging from studying the dark matter distribution in galaxies and clusters of galaxies, to studying the convective mixing of nucleosynthetic products in the later stages of stellar evolution.

Livermore's pioneering hyperspectral infrared imaging spectrometer (HIRIS) obtains datacubes by means of an IFTS in the thermal infrared. In this project, we are extending hyperspectral imaging to faint megapixel objects that are emitting visible light. The project advances the Laboratory's skill and knowledge base for remote sensing in support of NNSA's nonproliferation mission. Furthermore, the IFTS has generated significant interest among astrophysicists and has attracted post-doctoral researchers and university collaborators. The success of this LLNL project will demonstrate the viability of IFTS for astronomy and lead to the implementation of IFTS for first-rank ground-based and space-based optical and infrared telescopes.

In FY2002, the final half-year of the project, we completed instrument development and check-out observations. Instrument checkout entailed an observing run during "bright-time"—when the moon is up—in early December 2001 at the 3.5-m telescope at the Apache Point Observatory (APO), New Mexico. Because of this third successful checkout, we were awarded coveted APO "dark time" to acquire science-grade data of faint objects in March 2002.

Based on the bright-time data we had obtained in June, we made two presentations to the community, which included a datacube of an emission-line object that nearly fills our field of view and multicolor imaging of a cluster containing tens of thousands of stars of different spectral types (see Figure). These demonstrations led to the California Institute of Technology's instrument scientist for the 30-m CELT telescope joining our collaboration and offering us the use of the 5-m Hale telescope at the Palomar Observatory for further observing. In addition, our small, fieldable spectral-imaging instrument found application at LLNL for diagnostics of re-entry vehicles.

At the conclusion of this project, we have the only astronomical instrument of its kind in the world. This project succeeded in turning astronomical IFTS into a proven and mature technology for upcoming hyperspectral astronomical instruments, on which LLNL will take a central role in both instrument design and data handling.

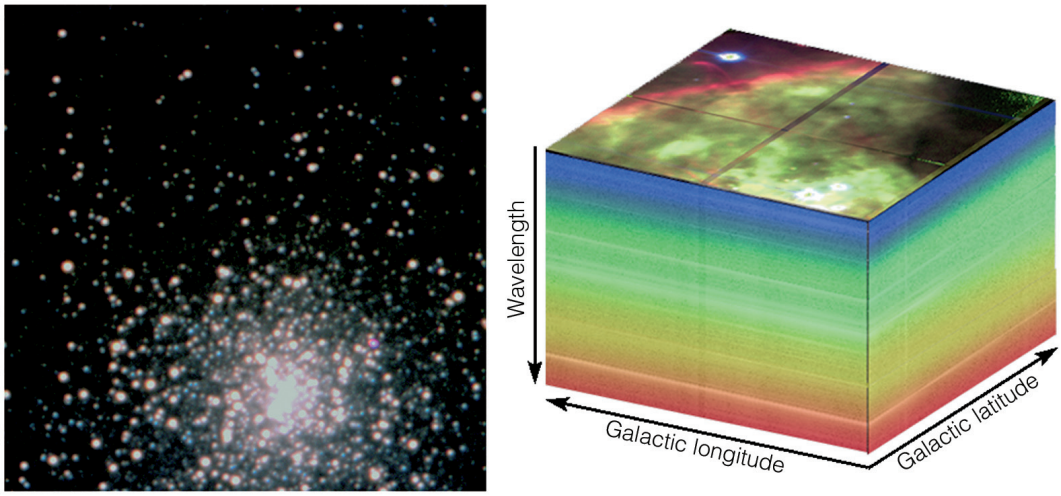

Imaging Fourier transform spectrometer images: (left) an inventory of astronomical types by color in a star cluste, and (right) chemical regions in a datacube of an interstellar cloud.

Colloidal transport of actinides in the vadose zone

P. Zhao, M. Zavrin, P. G. Allen, E. Sylwester, R. Maxwell

Toxic contaminants generated during the nuclear weapons program have resulted in more than 6 billion m^3 of contaminated soil and rock at DOE facilities. Some 60 million m^3 of soil and rock within the vadose zone (between the land surface and the underlying groundwater aquifers) are contaminated with radioactive waste or mixed low-level radioactive waste. Cleaning up the contaminated subsurface is a DOE responsibility. A better understanding of contaminant migration in the vadose zone will enable better, more effective, and less costly cleanup and containment.

Because of laboratory observations that plutonium (Pu) and americium (Am) attach strongly to the rock surface and do not readily dissolve in groundwater, it has long been thought that such radionuclides do not migrate in the subsurface. Our earlier field studies suggest, however, that these radionuclides are in fact transported in groundwater. We detected Pu in groundwater more than 1 km downgradient from its source, the location of an underground nuclear test at the Nevada Test Site (NTS).

The Pu and other radionuclides (Am, europium, and cesium) were associated with the colloidal fraction of the groundwater. Colloids, naturally occurring submicrometer particles found in almost all surface water and groundwater, are formed through the weathering of rocks, soils, and plants; because colloids are so small, they can be transported in groundwater. Determining how colloids may transport low-solubility radionuclides is critical for developing reliable conceptual models for predicting contaminant transport. Models based solely on solubility measurements could underestimate the transport of low-solubility radionuclides.

In this project, we are studying geochemical controls on colloid-facilitated transport of actinides in the vadose zone at the NTS. We will integrate field and laboratory studies into a reactive-transport model of subsurface transport, with the ultimate objective of developing a framework for predicting when colloid-facilitated transport of actinides may occur, to quantitatively describe these results and to develop a flow and transport model based on our experimental results.

In FY2002, water containing Pu was collected from the fracture-flow vadose zone at the NTS. We found that the detected Pu was associated with the colloidal and not the dissolved fraction of the groundwater, which supports our hypothesis that colloid-facilitated transport is the dominant transport mechanism for low-solubility Pu and other radionuclides in fracture-flow groundwater conditions (see Figure).

These field results provided the framework for experimental studies on the sorption and desorption of Pu of several mineral colloids observed at the NTS. We focused on Pu(IV) and Pu(V), the dominant oxidation states of Pu under equilibrium conditions at the NTS. The major findings were that (1) Pu sorbed to all minerals investigated, although the extent, rates, and mechanisms were mineral dependent; (2) sorption of Pu(IV) on zeolite (clinoptilolite) was rapid and extensive (70 to 90%) and desorption was low (2 to 5%); and (3) according to x-ray absorption near-edge spectroscopy, Pu ended up as Pu(IV) on all mineral surfaces, regardless of the initial oxidation state of Pu in solution.

These results demonstrate, for the first time, that Pu strongly sorbs to common minerals and reduces to Pu(IV) on mineral surfaces, regardless of its original oxidation state in solution; and that, based on the low desorption rate on clinoptilolite, the majority of sorbed Pu(IV) will remain on the mineral surface, available for transport.

We incorporated our field and experimental results into a single-fracture colloid transport model. Results obtained with the model show that Pu(IV) transport is very fast—consistent with experimental observations—but that Pu transport is ultimately limited by the colloid load in solution.

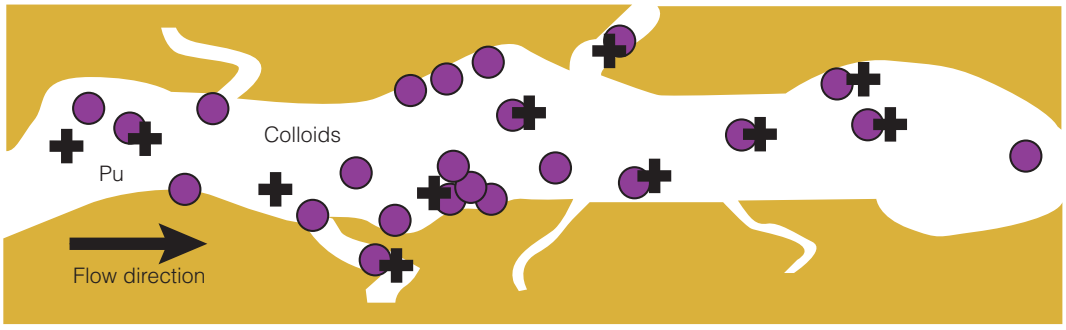

Cartoon depicting naturally occurring colloids (purple circles) and plutonium (black plus signs) in a fractured rock. Plutonium is attached to the mineral colloids, which can either become immobilized by attaching to the host rock wall or migrate through the fracture.

Recreating planetary cores in the laboratory

G. Collins

In planetary and stellar interiors, material compression occurs from gravitational force, creating states that lie on an isentrope (ignoring phase separation) from the low-density atmosphere to the ultrahigh-density core. For instance, the core of a giant planet such as Jupiter is thought to reach pressures of ~80 Mbar, densities of ~70 g/cc, and temperatures of ~20,000 K. At these extreme densities, materials are predicted to have quite unearthly properties, such as high-temperature superconductivity and low-temperature fusion.

The key to a credible planetary model is an accurate equation of state (EOS) for the planet's constituent materials at extreme conditions. However, experimental validation of high-pressure (>few Mbar) EOS has been carried out on only a few materials, and even then only on the principal Hugoniot—the locus of all final states achieved behind a single shock wave passing through a material from an initial state. In addition, work on inertial-confinement fusion (ICF) and stockpile stewardship requires accurate EOS data at densities higher than are achievable on the principle Hugoniot.

This project is using high-energy laser facilities to produce and characterize material states at densities even more extreme than those achievable with single-shock techniques. Our goal is to measure Hugoniot and off-Hugoniot properties of materials to provide stringent tests of the materials database needed for stockpile stewardship, ICF, and planetary models, in support of LLNL's missions in national security, energy, and fundamental science.

In FY2002, we used the Vulcan laser facility (in the U.K.) and a diamond anvil to perform precompressed hydrogen experiments with a maximum energy of a few hundred joules. The Figure is a pressure–temperature phase diagram for hydrogen, showing calculated Hugoniot lines for the uncompressed and precompressed initial states achieved. The data show a continuous trend from single-shock principal Hugoniot data to reverberating gas-gun data—very different from a previously proposed semiconducting model. Such data will help us understand the magnetic field of Jupiter, which has perplexed planetary scientists for years. Typically, planetary isentropes can only be compared against gravitational moment and magnetic-field data from space probes, planetary radius, and spectroscopy of the upper atmosphere. This new body of data will provide rigid constraints on planetary models and have a significant impact on a broad community of planetary and condensed-matter scientists, as well as our fundamental understanding of the giant planets.

In this project, we have mapped the single-shock, ultrahigh-pressure EOS and transport properties of hydrogen—a primary constituent of extrasolar and solar giants—and water and carbon, which are primary constituents of Neptune, Uranus, and most known comets. These experiments determined the ionic-to-electronic phase boundary of water, the melt transition of diamond, and the metal insulator transition of hydrogen on the principal Hugoniot. In addition, by combining dynamic-compression techniques using large lasers with static-compression techniques using diamond anvils, we created—for the first time—material states that previously existed only at the core of giant planets or low-mass stars. In addition to creating extreme-density states of hydrogen, water, helium, and other materials, this technique enables production of planetary mixtures, such as helium and dihydrogen, which have never been studied at high pressures and temperatures.

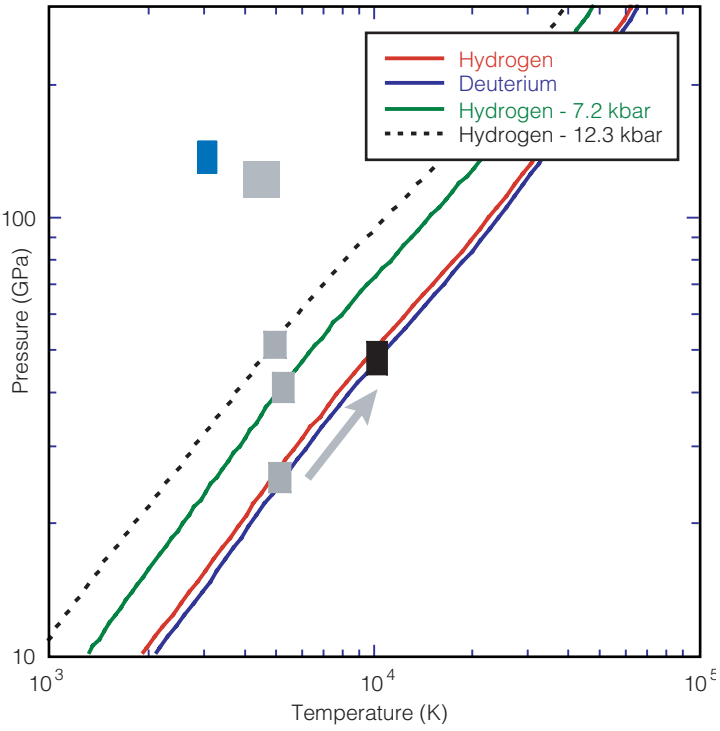

A pressure–temperature phase diagram for hydrogen showing calculated Hugoniot lines for uncompressed and precompressed initial states. The grey points show regions of constant reflectivity (10%) on Hugoniots with different initial densities as measured in this work; the black point shows where the reflectivity for hydrogen saturates at a high value on the principal Hugoniot; and the blue point shows the transition to a minimum conductor from previous gas-gun research. The data suggest a continuous trend from single-shock principal Hugoniot data to reverberating gas-gun data—very different from the previously proposed semiconducting model.

Nearby active galactic nuclei

C. E. Max

In some galaxy cores, a region well less than a cubic parsec in size—known as the Active Galactic Nucleus (AGN)—emits up to 10,000 times the normal luminosity of an entire galaxy. The high luminosity, small volume, and nonthermal spectra of AGNs have led to the hypothesis that their energy is provided by accretion onto supermassive black holes (mass more than a billion times that of the Sun).

For more than 30 yr, DOE labs have researched the physics of black holes. DOE computer simulations were the first to describe how black holes form. However, only recently has direct evidence of supermassive black holes emerged via astronomical observations with very high spatial resolution.

In this project we are using adaptive optics (AO) and laser guide stars—developed using LLNL and DOE technology on telescopes at Lick and Keck Observatories—to measure properties of AGNs. Adaptive optics are now used with virtually all new DOE high-power lasers and are important to national security applications involving imaging or laser propagation through the turbulent atmosphere. This project enhances DOE's expertise in AO, precision optics, and controls in support of LLNL's missions in national security and fundamental science.

In FY2002, we completed work on a new control system for the laser guide star at Lick Observatory; the entire laser system is now operated remotely by a laser technician from the main telescope control room. Performance of the Lick laser guide star remains the best in the world, and commissioning of a second-generation laser at Keck Observatory was begun. The laser and AO systems at Lick and Keck have enabled us to observe 16 AGNs to address one of the outstanding questions in AGN research—the mechanism by which matter "falls into" the black hole, entering its accretion disk.

An example of our exciting results is shown in the Figure. Fig. (a) is a new high-energy x-ray image, taken with the Chandra observatory, of the core of the active galaxy NGC 6240. The center of this galaxy, known to be undergoing a major merger event, contains two black holes, which presumably were each already present in the nuclei of the merging galaxies. Fig. (b), an image we obtained using the AO system on the 10-m Keck II telescope at a wavelength of 2.2 μm, resolves nuclear star clusters immediately surrounding the two black holes. Each of the nuclear clusters is elongated, a result of dynamical stripping of the star clusters by motion of the black holes through background galactic stars.

Fig. (c) is a Keck AO image of the core of NGC 6240 in the light of a strong molecular hydrogen emission line. At this specific wavelength, we see regions where the interstellar medium is being penetrated by shock waves resulting from the violent merger. Such shocks provide significant dissipation of energy and angular momentum, allowing shocked gas to fall in towards the dual black holes.

This project, using AO and laser guide stars, has made very significant contributions to our understanding of violent events in the cores of active galaxies and to application of AO technology to high-power lasers.

(a) (b) (c)

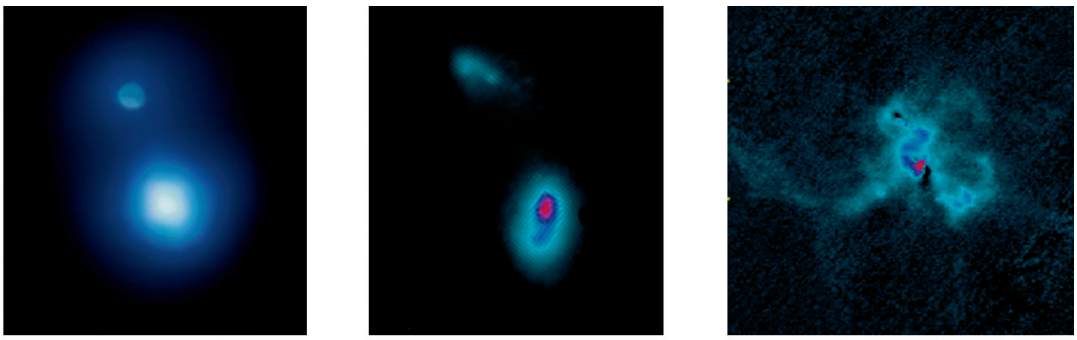

Twin active galactic nuclei (AGNs) in merging galaxy NGC 6240: (a) an x-ray image from Chandra spacecraft; (b) a Keck adaptive optics (AO) image at a wavelength of 2.2 μm; and (c) a Keck AO image—at a larger scale—in a molecular hydrogen emission line, showing shocked interstellar gas.

Adaptive optics imaging and spectroscopy of the Solar System

S. G. Gibbard, B. A. Macintosh, C. E. Max, A. Grossman, I. de Pater

This project focuses on using adaptive optics (AO) imaging and spectroscopy at the 10-m W. M. Keck Observatory to investigate the planets Uranus and Neptune, and Saturn's moon, Titan. These bodies share a common type of atmosphere, one that is rich in methane and has a hydrocarbon haze layer produced by methane photolysis. Neptune and Uranus have atmospheric features that change on short time scales; we are investigating their altitude, composition, and connection to events occurring deeper in the planets' tropospheres. The composition of Titan's surface, located under its dense atmosphere, is still quite uncertain. With spectra that sample the surface and the vertical structure of Titan's atmosphere, we are determining its surface reflectivity and atmospheric composition. In addition to the stunning images produced by Keck AO, Keck's near-infrared spectrograph, NIRSPEC, offers high spectral resolution and can be used in conjunction with the AO system.

This project will result in the continued development of AO technology (e.g., new tools for high-precision optical characterization), which can be applied to other optical systems at LLNL, including AO systems and sensors for high-power lasers and all-optical, free-space communication networks and long-range surveillance capability in support of LLNL's nonproliferation mission. In addition, success in this work will position LLNL as a world leader in observing and modeling giant planets and will support DOE's science mission by expanding basic scientific knowledge.

During FY2002, we obtained images of Neptune and Uranus in July and August using the new NIRC2 camera, which allows us to get high signal-to-noise images with a field that is wide enough to capture the Uranus ring system in a single image. These images clearly demonstrated the superiority of AO over conventional infrared imaging; our spectacular images of the Uranian ring system (see Figure) are the first Earth-based detection of individual rings on Uranus.

The NIRC2 camera also has a spectrograph that we used to obtain spectra of individual bright "storm" features on the disk of Neptune. This spectroscopy allows us to determine the altitude of these features and thus to construct a three-dimensional (3-D) map of Neptune's atmosphere and its variation in time.

In FY2002, our efforts on Titan focused on three fronts: determining the surface albedo, analyzing spectra to determine atmospheric structure, and developing a 3-D radiative transfer code for Titan's atmosphere. Our analysis of Titan spectra indicates that Titan's southern hydrocarbon haze may be dissipating from the outer atmosphere inwards as Titan's seasons change from southern summer to southern winter. A 3-D radiative transfer model, ARDRA, currently in use at LLNL, is being adapted to perform radiation-transport calculations for Titan's atmosphere. The ARDRA model uses a combination of discrete ordinate and spherical harmonic methodologies to calculate spherical radiation intensities and is capable of using LLNL parallel computation architecture

During FY 2003, we expect to complete our analysis of Neptune and Uranus spectra to determine the altitudes of infrared bright features seen on these planets. We will also continue our study of the dynamics of Neptune's clouds and attempt to image Neptune's very faint ring system. We plan to complete calibrated surface maps of Titan at 1.6 and 2 μm and continue our analysis of Titan spectra to determine the location of haze layers in Titan's atmosphere and possibly the existence of methane clouds. Our efforts will continue on developing a full 3-D radiative transfer model to simulate the nonsymmetric features in Titan's atmosphere.

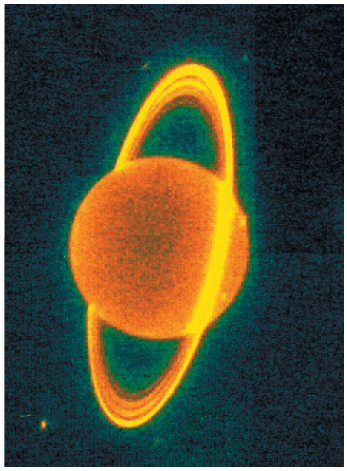

Near-infrared adaptive optics image of Uranus and its ring system obtained with the 10-m Keck Telescope.

Constraining nucleosynthesis models: Mapping titanium-44 in Cassiopeia A

W. W. Craig, K. Gunderson

Supernovae produce and disseminate most of the elements in the universe. Supernova explosions are also among the most energetic in the universe, and the amount of light they emit has recently been established as an extremely sensitive measure of the size and geometry of the universe.

The study of supernova remnants using the light from radioactive isotopes has long been a goal of astrophysics and is now recognized as one of the highest-priority scientific objectives for high-energy astrophysics in the next decade. Radioactive titanium-44 (^{44}Ti) (half-life of 52 yr) is perhaps the most important isotope available for the postmortem analysis and study of the events that occur during a supernova. This element is produced at the boundary between the material ejected during the explosion and the material that falls back into the neutron star or black hole left behind when a massive star explodes; its distribution is an ideal diagnostic of the details of the supernova event.

Cassiopeia A (Cas A), the remnant of a supernova that occurred 300 yr ago at a distance of 9000 light yr, is an ideal object in which to study ^{44}Ti. Cas A has been the subject of intense study over the last 20 yr because its ^{44}Ti emission is expected to be strong due to its age and proximity to the Earth. Modeling programs have made great progress and have made very specific predictions of the ^{44}Ti mass fraction and its spatial distribution in Cas A. Makeing the crucial next step in our understanding of supernova—actually measuring and creating the first-ever map of the ^{44}Ti distribution in a remnant—is the ultimate goal of this research project.

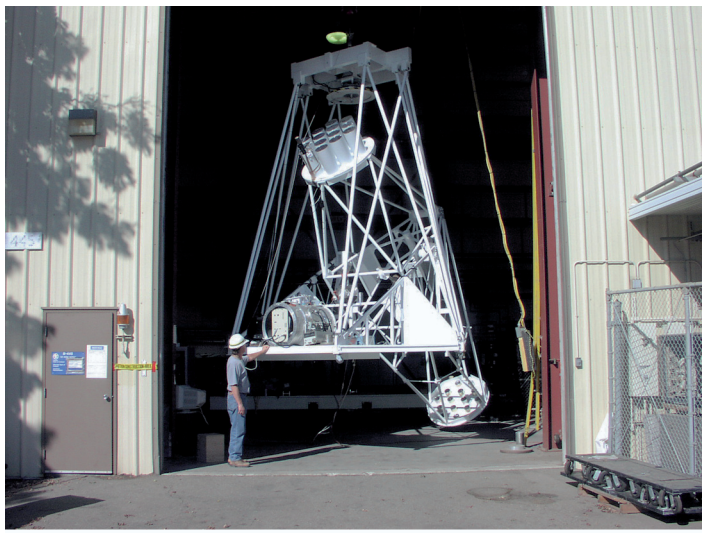

The High-Energy Focusing Telescope (HEFT) balloon gondola during final testing at LLNL. The gondola will point HEFT at Cassiopeia A to a precision of 10 arcseconds.

Our work builds on decades of LLNL expertise in supernova modeling and will provide the first true experimental verification of the details of these models. The grazing-incidence, multilayer-coated hard-x-ray optics that make the observations possible also have potential applications in laser–plasma diagnostics and are now being developed to produce highly sensitive instruments for radionuclide imaging in medical applications. Such applications support LLNL's missions in national security and bioscience to improve human health.

Our observations of Cas A will be made possible by a new generation of instruments capable of sensitive measurements of nuclear line emission for the first time. Of these new instruments, only the High-Energy Focusing Telescope (HEFT), a collaboration with the California Institute of Technology (Caltech) and others, will have the angular resolution required to measure the Cas A ^{44}Ti distribution.

As originally planned, the HEFT platform would be incapable of the proposed ^{44}Ti observations, which require a very long exposure time and unprecedented pointing stability for the gamma-ray telescope. Neither the 24-h flight nor the 10-arcsecond pointing required for a Cas A map was possible with the original HEFT gondola design. Our goal is to completely redesign and build a new kind of gondola to improve the pointing accuracy by a factor of 3 and to develop a system to permit accurate daytime pointing by designing and building an extraordinarily sensitive, dual-camera, daytime star-tracking system.

During FY2002, we completed construction of the balloon gondola and demonstrated 10-arcsecond tracking. The first of two star trackers, consisting of high-performance cameras and baffle systems, was completed, tested, and shown to meet all flight specifications.

In FY2003, we will finish integrating all flight systems, including optics from Columbia University and detectors supplied by Caltech, and will also complete the flight plan for the scheduled FY2003 flight.

Micro- and nanodeformation of aqueous films for seismic applications

D. L. Farber, B. P. Bonner, M. Balooch, B. Viani, W. Siekhaus, J. Berryman

Seismology—in the broadest sense, the study of Earth's dynamical response to mechanical stimuli—is a singularly powerful tool for investigating a wide variety of scientific, technical, and environmental problems. Seismic research impacts an extraordinarily wide range of human activities, including earthquake hazard mitigation, tracking movement of pollutants underground, and hydrocarbon exploration. The LLNL mission addresses nontraditional but critical seismic problems, such as predicting the ground response to explosive or earthquake loading at locations that have no local calibration, and forensic seismology, the detection of clandestine explosions.

This project addresses the most fundamental and long-standing problem in seismic remote sensing of the Earth: the role fluids play in transmission, modulation, and dissipation of seismic energy. This project has used emerging technologies, developed at LLNL for materials and geochemistry studies based on atomic force microscopy (AFM) and nano-indentation, to attack this problem at the nano- and microscales where the critical physical mechanisms operate. Our results directly are relevant to issues related to several LLNL missions, including the Ground Based Nuclear Explosion Monitoring Program (GNEM), prediction of weapons effects on the surface and underground, fossil energy programs, and environmental stewardship.

During FY2002, we continued to use depth-sensitive nanoindentation and AFM force measurements to study aqueous films in and on the surface of nano- and macrocrystals. Many layered silicates confine extremely thin water layers (2.5 Å per layer) between silicate sheets making up the crystallites, presenting opportunities to study the effect of bound water on physical properties. At ambient temperature, the number of water layers intercalated by surface forces can be controlled by modulating the activity of water. Suspensions of a swelling clay, montmorillonite, were evaporated onto optically flat fused-silica substrates to create thin films in which the sheets are oriented parallel to the substrate. Samples were tested in dry nitrogen and ~30% relative-humidity air to determine the effect of a single molecular layer of water on the mechanical response. Young's modulus (the stiffness in compression) decreased from ~11 to 4 GPa with hydration. Force modulation experiments (Figure) indicate that strong frequency-dependent damping increases dramatically for the hydrated sample. Molecular dynamics simulations of hydration in montmorillonite from the literature (Karaborni et al., 1996) predict that water molecules can occupy either of two nearly equally probable sites as hydration proceeds. The hypothesis that movements between the two sites are the mechanism for the large damping observed in the experiments can be tested by examining the dependence of damping on water content.

We made AFM measurements of force distance curves for vermiculite, phlogopite, and muscovite to observe how force distance curves depend on location and mineralogy. The simplified contact-adhesion hysteresis model advanced by Sharma et al. (1994) as a potential seismic-attenuation mechanism does not explain the observed surface interactions in all the systems we have investigated to date. Indeed, while the Sharma et al. model suggests that all the energy dissipation should occur at separation distances between 30 and 70 nm, we see hysteretic effects at length scales at least an order of magnitude greater than this.

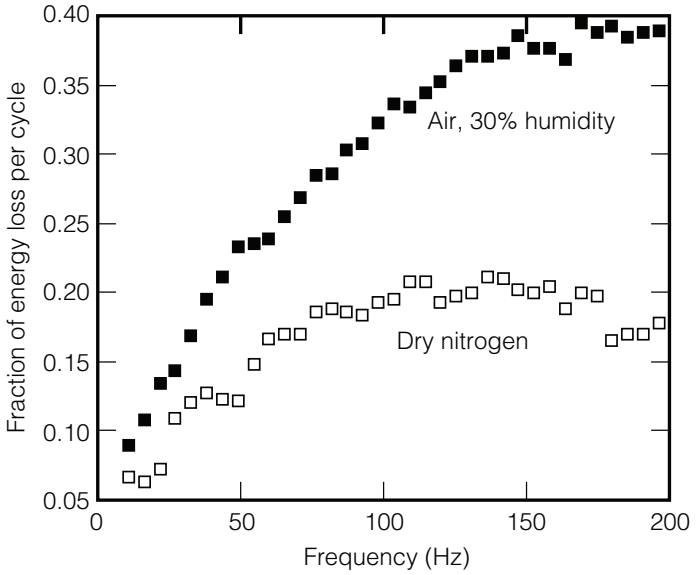

Frequency-dependent energy dissipation for hydrated (filled squares) and dry (open squares) montmorillonite, which shows the effects of a single molecular layer of water on mechanical response.

Evaluation and optimization of methyl-*tert* butyl ether biodegradation in aquifers

S. R. Kane, T. C. Legler, C. J. Koester, W. J. Wilson

Methyl *tert*-butyl ether (MTBE), a fuel oxygenate added to gasoline to decrease carbon monoxide emissions, has become a major threat to drinking-water supplies because of its release at numerous leaking underground fuel tank (LUFT) sites, its high mobility in groundwater, and its recalcitrance to biodegradation. Nationwide, an estimated 250,000 of the approximately 385,000 confirmed LUFT releases have contained MTBE, a suspected carcinogen. In addition, its primary metabolite, *tert*-butyl alcohol (TBA), is a known carcinogen. Although scheduled to be phased out as a fuel additive beginning in late 2003, MTBE will continue to impact groundwater for years to come. Optimal remediation of MTBE-contaminated sites requires filling the gaps in knowledge concerning MTBE biodegradation, including the (1) distribution of and factors controlling aerobic MTBE degradation; (2) occurrence and activity of MTBE-degrading bacteria; and (3) effect of dissolved gasoline components—most notably benzene, toluene, ethylbenzene, and xylenes (BTEX).

This project aims to define site-specific factors that determine whether aerobic degradation occurs in situ and characterize microorganisms responsible for MTBE degradation. Our focus is on aerobic conditions, under which degradation rates are much more rapid than under anaerobic conditions. Using purge-and-trap gas chromatography/mass spectrometry, we are analyzing MTBE degradation activity in microcosms containing sediment and groundwater from contaminated LUFT sites. Molecular biology approaches such as denaturing gradient gel electrophoresis (DGGE) are being used to characterize the microorganisms present in MTBE-degrading microcosm and enrichment cultures. Results will allow the optimization of biotreatment approaches and the prediction of where aerobic bioremediation may be successful in support of DOE's mission in environmental restoration and management.

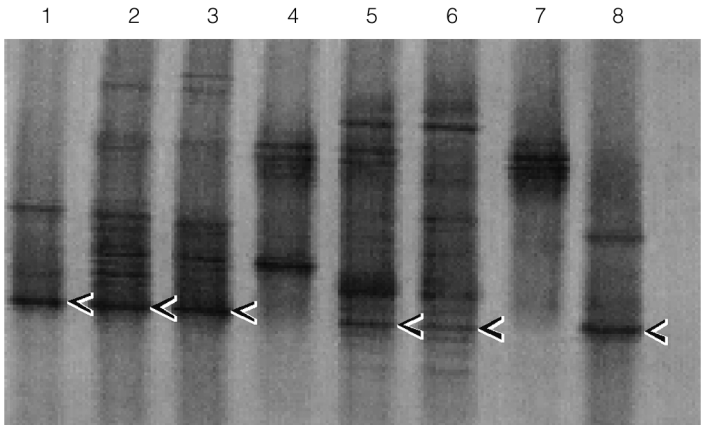

One goal of this project is to characterize microorganisms that degrade methyl tert-butyl ether (MTBE), a major threat to drinking-water supplies. Using denaturing gradient gel electrophoresis, we examined the gene sequences of microbial cultures found to actively degrade MTBE (lanes 1–3, 5, 6, and 8; lanes 4 and 7 are from sterilized control dishes). The arrows denote bands with similar sequences to a known MTBE-degrading strain, PM1.

In FY02, we assessed the aerobic MTBE degradation potential in sediments from an additional four LUFT sites in California, for a total of eight sites so far. Of these, sediments from only three sites exhibited MTBE degradation—MTBE added to the sediment was consumed at a rate of ~0.8 mg/L/d after a lag period of 4 to 19 d. When radiolabeled MTBE was added, ~50% was completely degraded to carbon dioxide. No degradation of MTBE was observed in sediments from the other sites after 200 d, although aerobic conditions were maintained.

For sediments in which no MTBE degradation occurred, addition of MTBE-degrading microorganisms resulted in MTBE removal, whereas addition of growth medium had no effect, suggesting that the factor limiting MTBE removal was biological rather than chemical. Molecular phylogenetic analyses of MTBE-degrading sediments using DGGE detected species closely related to a known MTBE-degrading bacterial strain, PM1 (Figure); those strains were not detected in sediments lacking MTBE degradation activity. At one of three sites, the presence of dissolved gasoline components significantly inhibited MTBE degradation and led to more pronounced accumulation of TBA. Sediments collected at sites where gasoline components had been present did not show inhibition of MTBE degradation.

Work in FY2003 will be to begin to identify the genes involved in aerobic MTBE degradation using classical mutagenesis techniques—screening mutants for loss of MTBE degradation activity—with pure-culture strains already isolated. Using the sequence data, we can then develop primer and probe sets that specifically target genes involved in MTBE degradation to predict the MTBE degradation potential at a specific LUFT site. These quantitative detection methods can then be validated using DNA extracts from sites with and without MTBE degradation activity. Sequence data could also be used to develop reporter gene fusions for evaluating how MTBE degradation genes are expressed, with the ultimate goal of optimizing MTBE degradation activity.

Electromagnetic imaging of carbon dioxide sequestration at an enhanced oil-recovery site

B. Kirkendall, J. Roberts

A potentially effective means of decreasing the surface-warming effects of increased levels of carbon dioxide (CO_2) is to sequester CO_2 in the subsurface. Moreover, the petroleum industry uses CO_2 to recover heavy oil—an abundant petroleum compound that is also expensive to recover—more efficiently than other techniques can in enhanced oil-recovery (EOR) efforts.

In this project, we are combining laboratory and field research to (1) image CO_2 injection and long-term sequestration at an EOR site using an electromagnetic (EM) imaging technique previously developed at LLNL, (2) improve and understand data processing in CO_2 studies by coupling field results with laboratory measurements, and (3) explore new techniques for imaging sequestrated CO_2. Our goal is to develop the ability to image subsurface injected CO_2 during EOR while discriminating between the injected CO_2 and pre-existing petroleum and water deposits. This work addresses LLNL's energy-security mission by developing field and laboratory techniques to improve in situ analysis of oil- and gas-enhanced recovery operations and also by providing a tool for in situ analysis of CO_2 sequestration.

Our imaging technique calculates two-dimensional images of subsurface electrical conductivity at the EOR site. Because core samples saturated with brine, oil, and CO_2 have distinct electrical signatures, EM images at appropriate frequencies should identify the different components. In the laboratory, we subject samples to similar reservoir temperature and pressures under controlled conditions. These results, in addition to numerical processing techniques under development, provide a better understanding of CO_2 behavior and improve interpretation of field images.

During FY2002, we (1) acquired two sets of multiple-frequency field data 6 mo apart, (2) developed a data-processing software package—based on the MATLAB computational environment—to speed calculation of field images; (3) developed a multiple-frequency step-inversion technique to decrease the error in image development; and (4) developed a geochemical electrical conductivity prediction code to help quantitatively understand the chemical and physical changes in core samples flooded with CO_2 during laboratory measurements. Multiple-frequency images in the Figure indicate the frequency dependence of CO_2, the understanding of which is contributing to improved resolution and interpretation of such images.

In FY2003, we will focus on laboratory data, processing techniques, and image resolution. In the laboratory, we will complete the CO_2 injection experiments with core samples, including how resistivity varies over time and according to pore-saturating fluid. Numerically, we will examine the feasibility of creating broadband-frequency images from single-frequency images, continue to develop a step approach to process data more accurately and at higher frequencies, work on multi-frequency optimization of finite-difference mesh grids, and develop a technique for estimating oil and gas saturation.

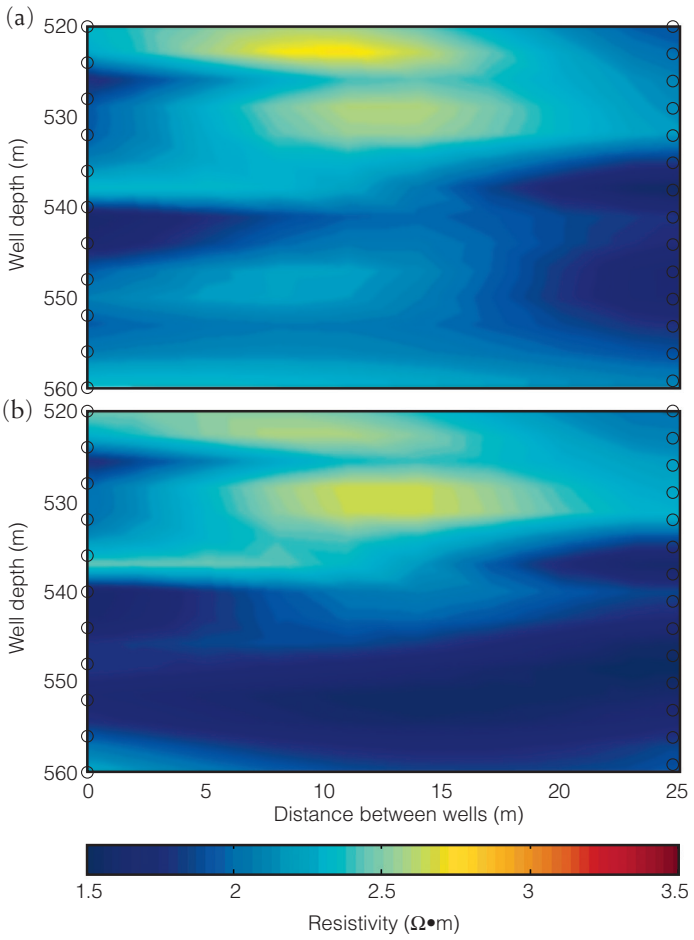

Two-dimensional electromagnetic images of subsurface electrical resistivity—obtained at (a) 4.0 and (b) 6.0 kHz—between two observation wells at an enhanced oil-recovery site where carbon dioxide (CO_2) was injected. The circles represent (left) receiving and (right) transmitting antennae (left and right, respectively). Understanding CO_2 frequency dependence, as seen in the difference between the two figures, is leading towards improved resolution and interpretation of images of subsurface injected CO_2.

Accelerated carbonate dissolution as a carbon dioxide separation and sequestration strategy: Continued experimentation and simulation

K. Caldeira, K. Knauss, G. H. Rau

Burning coal, oil, natural gas, and other fossil fuels adds carbon dioxide (CO_2) to the atmosphere and the oceans. In the atmosphere, this added CO_2 may significantly impact global climate and, in the ocean, may adversely affect marine biota. For instance, simulations of global warming indicate that unabated release of CO_2 could increase global land temperatures an average of 8°C by the end of the century. This creates a pressing national need to understand ways to mitigate the adverse affects on the climate and ocean chemistry of CO_2 released by fossil-fuel use.

Carbonate dissolution—a natural process in which CO_2 combines with limestone and another carbonate minerals to produce bicarbonate ions—naturally contributes to removal of this added carbon from the atmosphere over many thousands of years, buffering it in the ocean in a relatively benign form. The carbonate-dissolution method of ocean CO_2 disposal is technically, geochemically, and environmentally advantageous. The method uses existing technologies, abundant carbonate minerals, and seawater to neutralize CO_2 acidity and convert CO_2 to a form that does not readily exchange with the atmosphere. The bicarbonate-containing wastewater generated by the this method would be relatively benign and could be released into near-shore ocean waters.

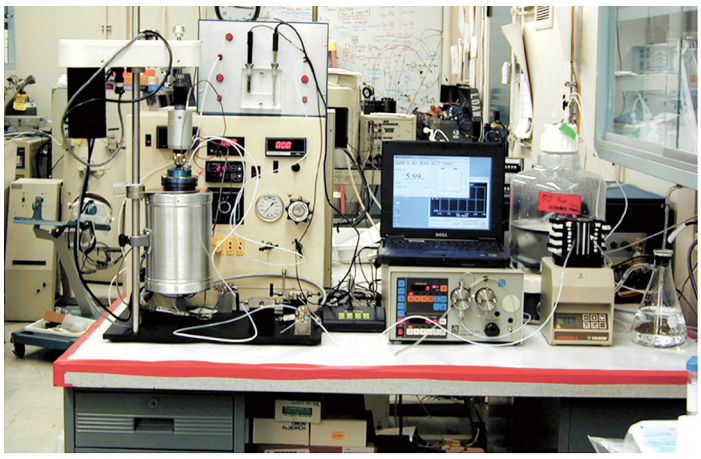

An experimental apparatus for accelerated carbonate dissolution at the bench-top scale. We are investigating carbonate dissolution—a natural process in which carbon dioxide combines with a carbonate mineral (in this case, limestone) to produce bicarbonate ions—as a low-environmental-impact method of sequestering atmospheric carbon produced by fossil-fuel use. Limestone dissolution occurs in the metallic cylinder to the left.

Our goals are to (1) demonstrate that this natural process can be accelerated by a factor of one million or more, so that CO_2 generated from burning fossil fuels can be stored in the ocean without significant adverse consequences for either climate or marine biota; and (2) determine whether this method can be applied economically on a large scale. While no single approach is likely to solve the entire CO_2 problem, the carbonate-dissolution technique for sequestering fossil-fuel carbon could contribute significantly to global carbon management.

This work will directly contribute to the LLNL missions of energy security and environmental management by developing environmentally acceptable ways of supplying the energy needed by our economy.

Preliminary cost estimates for this process are as low as $68 /ton of carbon sequestered, as compared to >$170/ton for other approaches to CO_2 separation with geologic or deep-ocean storage. Recently, engineers at McDermott Technologies independently estimated the cost of our proposed technique and concluded that our cost estimates were at the high end of the likely range.

In FY2002 we (1) performed computer simulations of the carbonate-dissolution process, (2) completed initial computer simulations of the fate of the wastewater after it is released in the ocean, (3) set up an experimental apparatus to measure rates of relevant reactions (see Figure), and (4) began laboratory carbonate-simulation experiments.

In FY2003, we will test various experimental parameters to determine optimum plant design and operations so that the basic viability of carbonate dissolution can be evaluated. Laboratory experiments will examine such questions as the impact of flow rate, reactor residence time, bubble size, and mixing rate on the rate of carbonic acid formation; the impact of particle size and the influence of inhibitors or catalysts on the rate of calcite dissolution; the effect of acidification, degassing, and dilution on other seawater solutes; and the maximum degree of supersaturation achievable during partial degassing prior to carbonate precipitation. To study the long-term effectiveness of the technique, we will also simulate the fate of wastewater generated by the process after release in the ocean as a function of the chemistry of the effluent and of location and depth of release.

Developing smart seismic arrays: A simulation environment, observational database, and advanced signal processing

P. E. Harben, D. B. Harris, S. C. Myers, S. C. Larsen, K. E. Nelson

Seismic imaging and tracking methods have important potential intelligence and surveillance applications, such as tracking vehicles and detecting tunnels. However, current seismic technology cannot handle unknown geologic heterogeneity—such as variation in bedrock and soil composition—or gather and analyze data rapidly (in hours or even seconds). This project is using seismic arrays capable of determining sources of continuous seismic energy and hence is applicable to situations in which distinct seismic waveform features cannot be identified by all sensor elements. These seismic arrays will be combined with an advanced data-processing system that characterizes geologic heterogeneity for rapid analysis in the field.

The goal of this project is to develop analysis and processing systems for seismic arrays and test the systems in tracking vehicles and imaging tunnels and other underground structures. Such capabilities will have direct application in surveillance, battlefield management, finding hard and deeply buried targets, and portal monitoring. This project benefits the U.S. military and intelligence community in support of LLNL's national-security mission.

Detection is accomplished by determining the best fit between field data and precomputed data spanning a range of expected geologies. This strategy enables rapid analysis in the field and characterization of the influence of random geological heterogeneity. In vehicle tracking, all propagation paths to the arrays are characterized with observed data, then matched to field data to determine the best fit. In underground imaging, LLNL's total wave field modeling code—named E3D—is run for all expected tunnel configurations and expected geological heterogeneity, which are then matched to the field data for a best fit.

In FY2002, we tested the data-processing strategy for vehicle tracking. At a test site at LLNL, three seismic arrays were used to track a tank in real time. The results demonstrated that three arrays could track a tank from as far as a few miles away. This aspect of the project will be spun off in FY2003 and supported by the Department of Defense. We also used the data-processing system in imaging underground structures at the Nevada Test Site (see Figure). The results demonstrate that our methodology has promise in tunnel detection. Late in FY2002, much more extensive testing was conducted at a mine-safety laboratory in Lake Lynn, Pennsylvania, to attempt detection of a deeper tunnel in a more realistic and difficult environment. Results will be available in FY2003.

In FY2003, we will test our data-analysis methodology by generating data with E3D for many geological realizations and matching the E3D data with field data from the Lake Lynn site. Other objectives include analyzing past data from tunnel explosions at Lake Lynn to determine whether our seismic arrays and data-processing methodology can determine the origins of simultaneous, noncoincident ordnance detonations.

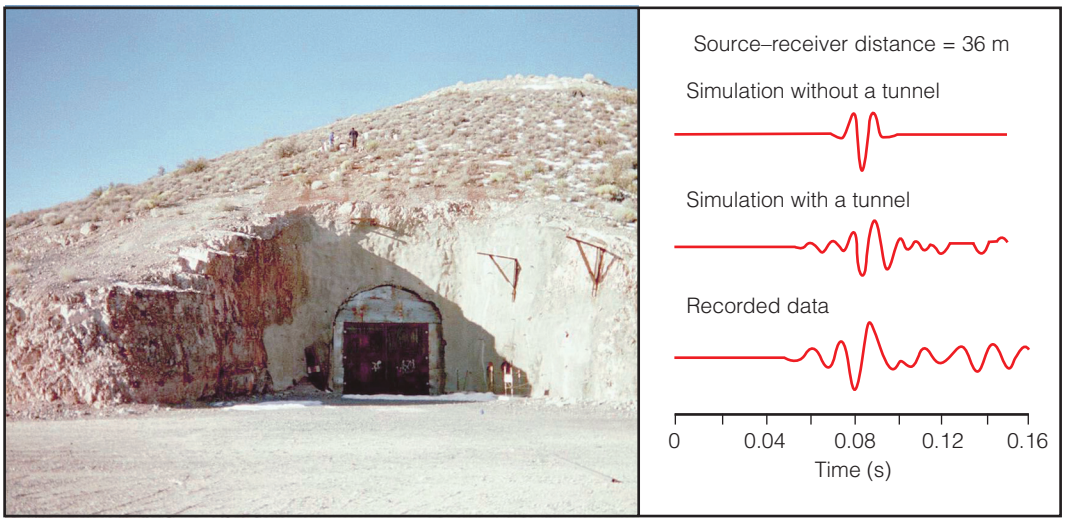

Seismic arrays and data-processing technology developed in this project were tested in detecting a tunnel at the Nevada Test Site. LLNL's total wave field modeling code—E3D—is run for all expected tunnel configurations and expected geological heterogeneity, then compared with field data to find the best fit. (a) The tunnel over which field data was recorded. (b) Results of E3D simulations conducted with and without a tunnel. The model simulation with a tunnel best agrees with the field data, demonstrating the effectiveness of our seismic-array system.

Near-real-time assessment of health risks from simulated-contaminant wet deposition using real-time rainfall and geographic-information-system databases

R. T. Cederwall, G. A. Loosmore, J. H. Shinn, J. R. Kercher

Hazardous materials may be released to the atmosphere through industrial accidents or terrorist attacks. Accurately predicting the fate of such material and assessing health risks are more vital for public safety than ever before. This project will develop (1) a first-of-its-kind capability for assessing, in near real time, the potential health risk of hazardous material deposited on the ground by rain following an atmospheric release and (2) the capability for incorporating, for the first time, the effects of rainfall into computational predictions of hazardous-material plumes. These capabilities will be used in LLNL's National Atmospheric Release Advisory Center (NARAC), whose functions include providing predictions of hazardous-material plumes to emergency responders. By further enhancing NARAC's predictions, this project will support LLNL's homeland-security mission.

Removal of airborne material by rain is hundreds of times more effective than dry removal and must be included in calculations to produce accurate predictions when rainfall occurs near a release. Our work will enable NARAC's current system to utilize the near-real-time, spatially varying rainfall data that are available hourly for the entire U.S. at 4-km resolution.

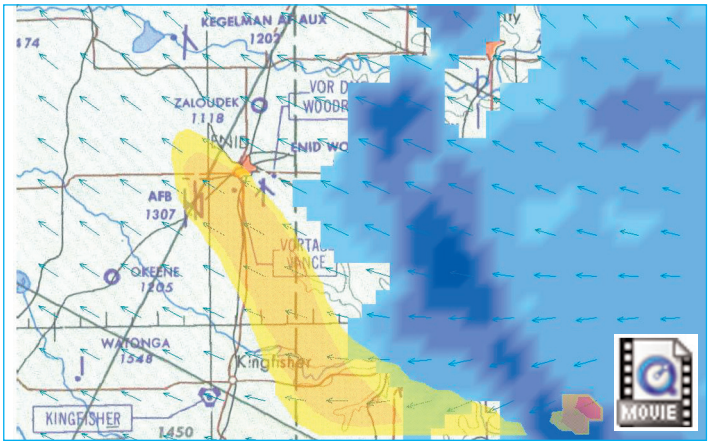

A computational simulation of a plume of hazardous airborne material (yellow and orange) being removed by rainfall (blue) as the rain cloud passes over the plume. The algorithms developed in this project incorporate rainfall in such simulations for the first time.

In this project, we will (1) develop a wet-deposition algorithm incorporating real-time rainfall data, (2) develop a health-risk assessment system for identifying the geographic area where the concentration of a hazardous material on the ground exceeds a specified level, and (3) validate aspects of the algorithm by comparison to measurements.

During FY2002, we finished developing a wet-deposition algorithm and began testing it in the NARAC dispersion code using observed winds and spatially resolved rainfall for a hypothetical release of hazardous material in a case-study area in Oklahoma. The Figure, an example of our simulation of the case study, shows the removal of airborne material by rain in an intense summer storm. This simulation is the first combination of hourly 4-km-resolution rainfall data with a dispersion model. The algorithm is very sensitive to the hazardous material's particle size and the rainfall rate. We improved the treatment of rainfall rate in the algorithm and began incorporating the effects of in-cloud processes that increase particle size.

In FY2002, we also developed a health-risk assessment model, compiled the necessary geographical information, and tested the model. The results showed that geographical patterns of dose levels were strongly affected by wet deposition. We also enhanced the health-risk assessment model by including radionuclides with short half-lives. The result was a geographical area of specified risk levels that was twice as large as previously predicted.

In FY2003, we will evaluate the wet-deposition algorithm against field data, perform sensitivity analyses, and quantify uncertainty in the wet-deposition estimates. We will incorporate dynamic aspects, such as time-varying meteorology and seasonal variation of surface characterization, into the dose model to provide more accurate estimates of health risks. By the end of FY2003, we will deliver a tested prototype system that will give NARAC a unique capability to respond to airborne hazardous releases under a full range of weather conditions and provide emergency agencies with a complete assessment of health risks immediately after a release and during post-release mitigation.

Infrastructure response to ground motion: High-performance computing and distributed sensing for regional-scale prediction and response

D. B. McCallen, S. C. Larsen, A. J. Rodgers

Earthquakes and underground nuclear explosions disperse tremendous energy into geologic strata. This energy propagates large distances in the form of traveling seismic waves, which shake the ground surface and can present a serious hazard to manmade structures. Measurements of ground motions from earthquakes and nuclear tests indicate that the strength of these motions varies greatly with location. Shaking intensity at any site is a complex function of the energy source mechanism, the geologic path along which the seismic waves propagate, and the soil conditions below the site. The direct relationship between the vibrational characteristics of a particular structure and the frequency content of the ground motion controls how much a particular structure is shaken.

Until recently, scientists and engineers have relied on relatively simple empirical relationships to estimate the motions that a structure will undergo. However, this approach often requires generalization and extrapolation from the existing knowledge base and is limited because of the complexities of wave propagation in the heterogeneous earth. While such approaches might be adequate for basic structure design information, they do not provide detailed information for a specific earthquake that might occur.

Massively parallel computers now can simulate the physics of energy propagation from the source through the earth and into a structure, making it possible to generate more realistic site-specific motions that account for the propagation path, local soil response, and interaction between the seismic waves and the structure. In this project, a regional combined geophysics–structural model is under development. The Southern Nevada region encompassing the Las Vegas Valley and the Nevada Test Site (NTS) (see Figure) is serving as a case study for the model development. The research results will provide a tool for the NNSA to assess nuclear-test readiness and to understand the seismic hazard to the rapidly growing Las Vegas Valley in the event that testing resumes. In addition to supporting this national-security mission, the research will spin off the tools and knowledge needed to predict earthquake hazards and to enhance earthquake safety.

The regional model framework, called NEVADA, includes a finite-difference wave-propagation code coupled to a special-purpose structural finite-element program that permits linear and nonlinear analysis of building systems. Once a source of ground motion at the NTS is defined, the regional model propagates seismic energy into the Las Vegas Valley and analyzes the response of a specified structure at preselected locations throughout the Valley.

In FY2002, we successfully developed the geophysics model of the Southern Nevada region, created the special structural modeling code, coupled the codes on Livermore's Advanced Simulation and Computing (ASCI)-level compute engines, and demonstrated the coupled simulations on the ASCI Blue computer. Our geology characterization was completed in close collaboration with University of Nevada researchers. As a result of basin-amplification effects, parametric simulations with the regional model indicate dramatic variations of ground motion and structural response across the Las Vegas Valley, which correlates with the legacy nuclear-test data indicating that ground-motion amplitude across the Valley varies by factors of 10 to 20.

In FY2003, we intend to complete additional parametric studies of regional response to determine the degree to which observed ground-motion variabilities are controlled by basin topography or by local soil site response. These parametric studies will also validate the simulation models by comparison with actual ground-motion data.

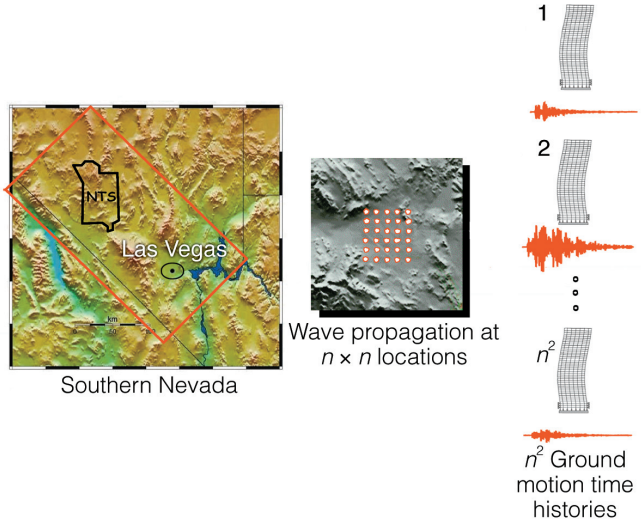

A geophysical model (~ 400 million zones) of the 45,000-km2 Southern Nevada region that encompasses the Las Vegas Valley and the Nevada Test Site is combined with wave-propagation and structural models of buildings to simulate the propagation of seismic energy from the ground to the structure.

Carbon dioxide drawdown through silicate chemical weathering

C. I. Steefel

Chemical weathering of silicate rocks contributes to the drawdown of atmospheric carbon dioxide (CO_2) over geologic time through reactions in which CO_2 (a weak acid) and rock-forming minerals (e.g., feldspar) are consumed at the expense of secondary phases (e.g., clay and bicarbonate). While the importance of this process is widely recognized, overall controls on the rate of silicate weathering are still not completely understood. Thus, it is difficult to evaluate hypotheses such as those recently advanced that claim enhanced weathering resulting from the uplift of the Himalayas contributed to CO_2 drawdown and global cooling during the Cenozoic geologic era.

We conducted a field study on the Precambrian Guayana Shield (see Figure) in South America to improve our understanding at a mechanistic level of the controls on the rate of silicate chemical weathering. The Precambrian Guayana Shield is a geologic province greater than 1 billion yr old that covers portions of Venezuela, Guyana (the country), Surinam, French Guiana, and Brazil. It is the oldest active weathering surface on Earth with very low physical-erosion rates, thus providing an end-member case that can be compared with weathering rates in actively eroding mountain belts. Study of weathering on this extremely old erosion surface can provide parameterization of weathering rates as a function of tectonic uplift and physical erosion rates and supports the Laboratory's environmental assessment and management mission.

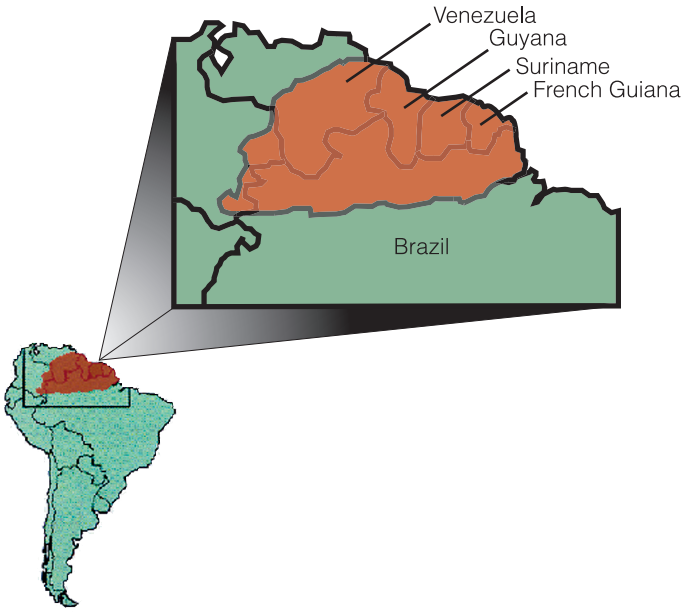

Location of the Precambrian Guayana Shield.

Our original plan was to study the portion of the Precambrian Guayana Shield located at the Los Pijiguaos bauxite mine in Venezuela in collaboration with colleagues at the Universidad Central de Venezuela. However, due to political instability in the region, we were unable to go to Los Pijiguaos during the 6 mo of the project. Instead, we decided to focus our study on the portion of the shield located in Guyana, immediately to the east of Venezuela.

In FY2002, our colleagues in Venezuela provided samples from the Los Pijiguaos for beryllium-10 analysis, an isotopic technique used for quantifying physical erosion rates, and for uranium series disequilibria analysis, another isotopic technique used for quantifying the rate of movement of the weathering front. Los Pijiguaos has the advantage of being well exposed to mining operations and is located on a topographic high where the dissolved solute load from chemical weathering is not obscured by contributions from rock types other than granite. We also examined deep weathering profiles (laterites) on the portion of the Guayana Shield located in Guyana and concluded that it was not suitable to study silicate chemical weathering because (1) the extensive cover by younger sediments provided additional inputs to the dissolved load in streams, thus obscuring the weathering of the basement granitic rock, and (2) exposure is poor due to the lack of topographic relief and the thickness of the jungle vegetation.

Three-dimensional astronomy: Scientific observations with the Livermore imaging Fourier transform spectrograph

R. Wurtz, E. Wishnow, K. Cook, S. Blais-Ouellette, B. Holden

The objective of this project is to determine the total light and mass in clusters of galaxies. Such observations determine the dark matter content of the clusters, which in turn provides information about the mass density of the universe, a fundamental cosmological parameter. Clusters provide the primary measurement of dark matter, independent of dark energy arising from the recently revived cosmological constant—a parameter describing the energy density of the vacuum (empty space), and a potentially important contributor to the dynamical history of the universe.

Currently, because of the limitations of conventional astronomical instruments, cluster measurements of dark matter rely on imaging and then selecting a subsample of bright red galaxies for spectroscopic observations. This two-pass method measures the brighter and redder objects, but the behavior of the rest of the cluster members must be inferred. The precision of dark-matter measurements using this biased method is doubtful. Groups using this method in recent years have obtained a large range of values for the mass of the universe.

The astronomical visible imaging Fourier transform spectrometer (IFTS), developed at LLNL and the only instrument of its kind, offers an exciting multiplex, three-dimensional advantage over a dispersive spectrograph. In addition to acquiring imaging data in two dimensions, the IFTS introduces a third dimension by obtaining a spectrum for every one of hundreds of thousands of spatial pixels in the field of a cluster, thus avoiding the need to infer properties of unobserved cluster members. By using the IFTS to make a full, unbiased inventory of luminosity and dynamics for members of approximately ten clusters, this project will obtain the most direct measurement ever made of cluster mass and light using an optical spectroscopic technique.

This project builds on LLNL and DOE's expertise in optics, control systems, and hyperspectral data acquisition and analysis to study dark matter, one of the premier questions in physics today, and advances the skill and knowledge base for remote sensing in support of NNSA's nonproliferation program. These high-profile activities have attracted first-rank postdocs and university collaborators to LLNL and will influence the next generation of astronomical instruments.

In FY2002, we performed our first observations of faint objects with IFTS at the Apache Point Observatory 3.5-m telescope in March (see Figure). An observation of a galaxy cluster provided data for building the cluster data analysis pipeline and expanding existing analysis tools. We assembled a team of galaxy cluster observers from inside and outside LLNL to interpret existing data and to plan for observing time at the Palomar Observatory on the 5-m Hale telescope, which has twice the collecting area of Apache Point. Special optics were designed and fabricated to adapt the IFTS to the Palomar Observatory. A first observation produced a spectacular interferogram movie of the planet Saturn. (click on icon to view movie).

In addition to our observation work, members of the team supported the design of a fieldable hyperspectral imager for nonproliferation remote-sensing applications. This was a programmatic spinoff of our LDRD work, which enhances the Hyperspectral Infrared Imaging Spectrometer (HIRIS) Program, itself a programmatic spin-off of an LDRD project. Furthermore, we fielded a simple hyperspectral imaging camera for re-entry vehicle diagnostics in ballistic missile testing.

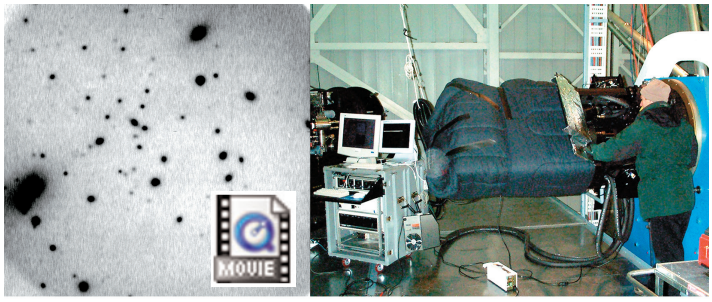

(left) A galaxy cluster observed by the Livermore astronomical imaging Fourier transform spectrograph, (right) shown mounted on the Apache Point Observatory 3.5-m telescope.

Surveying the Outer Solar System with robotic telescopes

S. Marshall, K. Cook, R. Porrata

The region of the Solar System beyond the orbit of Neptune has been an area of increasingly active research since 1992, when the first trans-Neptunian object (TNO) was detected. Today, hundreds of members of a disk-like population of remnants, known as the Kuiper Belt, have been cataloged. The region contains preserved clues about the early Solar System and is the source reservoir for short-period comets. The distribution of orbits, sizes, and physical properties of this population provide valuable insights relevant to planetary system physics.

We have developed two novel surveys for TNOs. The Southern Edgeworth Kuiper Survey (SEKS) is carrying out a very wide-area search for large (bright), but correspondingly rare, TNOs. The Taiwanese-American Occultation Survey (TAOS) seeks to detect very small (faint), but numerous, TNOs. These surveys are complementary to existing observations. Our work enhances LLNL's competency in several national-security mission support areas: advanced sensors, system integration, and processing large data sets.

The SEKS employs the 1.3-m Macho Telescope System in Canberra, Australia.* The survey probes for objects larger than 200 km in diameter and as large as Pluto (2300 km). With it, we can search the wide area necessary to detect large TNOs. Work to automate the telescope began in FY2000 and by the end of FY2002, useful 3-epoch observation sets covering 2400 square degrees near the ecliptic plane have been obtained. Observations are processed by an automated pipeline that measures sources in the images and places the results into a photometry database.

Lulin peak in central Taiwan is approximately 2835 m above sea level. The small clamshell domes in the center house two of four TAOS telescopes.

*All of the telescopes on Mt. Stromlo in Canberra were destroyed in a brushfire on 18 January, 2003.

Candidate moving objects are obtained by applying a set of filters for direction, velocity, brightness, angle to the ecliptic plane, and straight-line motion. Approximately 20% of the candidates are artificial TNOs added for efficiency determination. The remaining objects are mostly spurious detections resulting from chance positioning of faint stars, bleeding of flux from overexposed bright stars, and stars that are distorted during periods of bad seeing. Actual detections will represent a very small fraction of the candidate objects. At the end of FY2002, this pipeline has been completed and is being run in reverse chronological order on the existing observations. As interesting objects are found, possible orbits are fitted and checked against known objects at the Minor Planet Center (MPC). They will be re-observed in follow-up mode to confirm the detection.

The Taiwanese-American Occultation will probe for TNOs that are much smaller than in previous surveys. By detecting brief occultations of bright background stars, TAOS will detect TNOs down to 2 km in diameter. To carry out the survey, TAOS has constructed an automated observatory in the mountains of central Taiwan. Three of four planned 0.5-m f/1.9 wide-field telescopes equipped with thinned, back-illuminated, 4-megapixel-CCD cameras have been installed. Computer, networking, and software systems have been developed to operate the system autonomously. The system will monitor approximately 2000 stars simultaneously at 5 Hz. When a TNO passes in front of a monitored star, the telescope array will detect the brief (0.2-s) reduction in stellar brightness. Coincident detection by multiple telescopes will eliminate false positives due to atmospheric fluctuations, random noise, or terrestrial sources. A real-time analysis system will detect and archive these occultations. Observations are expected to begin during fall 2003. Current models of the Kuiper Belt predict as few as ten and as many as thousands of detections per year.

Results from these two surveys will be significant. Bright TNOs can be studied spectroscopically to determine composition. The shape and extent of the Kuiper Belt can be traced by obtaining enough large TNOs. Determining the number of small TNOs will lead to a better understanding of the formation and collisional evolution in the region as well as a more accurate prediction of the threat of comet collisions with the Earth.

Satellite-based observation of the tectonics of southern Tibet

F. J. Ryerson, R. C. Finkel, P. Tapponnier, M. Chevalier, J. Van der Woerd, L. Benedetti

The Tibetan Plateau represents an area comparable in size to the western U.S., but with an average elevation close to 5000 m above sea level. Understanding the timing and mechanisms responsible for uplifting such a huge region remains one of the outstanding problems in continental geodynamics. The Plateau is surrounded by large strike-slip faults oriented at high angle to the direction of convergence between India and Asia. At one extreme, these faults have been viewed as the geodynamically unimportant byproduct of distributed ductile deformation in the lower crust and mantle. At the other, the faults are interpreted as localized, lithospheric shear zones that are absorbing large motions between relatively rigid blocks. The resolution of this issue requires quantitative information on the rates of slip along these faults. Low slip rates (millimeters per year) would be compatible with distributed deep deformation, whereas fast rates (centimeters per year) rule it out.

In this project, we have been determining the slip rates of the Karakorum Fault (KKF), the Karakorum–Jiali Fracture Zone (KJFZ), the Jiali Fault, the Altyn Tagh Fault (ATF), and the Red River Fault using a combination of satellite-image interpretation, field mapping, and cosmogenic (cosmic-ray exposure) dating. The work will lead to a better understanding of the mechanical properties of the Earth's crust, with implications for the earthquake cycle, monitoring nuclear tests, and resource recovery in support of LLNL's missions in national security and basic science.

In FY2002, we continued investigating the slip rate of the KKF, the major strike-slip fault in southwestern Tibet. If the KKF is the kinematic southern boundary of this zone and is the only feature accommodating eastward extrusion of Tibet, its slip rate should be similar to that of the ATF in the north. One method for determining slip rates is to measure and date river offsets—the distance between a flowing and a dry river formerly connected but separated by movement along a fault crossing the river. Offsets along the KKF ranging from tens of meters to kilometers were mapped using satellite imagery and field mapping, and sample ages were determined by cosmogenic dating. In the Gar Valley, a river channel in glacial sediments had an offset of 1750 m (see Figure) and an age of 283,000 yr, equivalent to a slip rate of 6 mm/yr. Smaller, terrace-riser offsets (tens of meters) on the India–China border were also sampled. However, mixing of cobbles between the different levels prevented dating with sufficient accuracy.

Taken together with results from previous years, the data indicate that the slip-rate on individual strands of the KKF are typically less than 10 mm/yr. Relative to the ATF, these slip rates for the KKF are thus lower than expected. Because our measurements cover almost the entire length of the KKF, the disparity cannot be attributed to along-strike variation in the rate. This suggests that either (1) features other than the KKF contribute to the deformation of southern Tibet or (2) the KKF is, relative to the ATF, an unstable feature in which deformation is accommodated by a number of subparallel strands of the fault, which may shift the locus of deformation over time. Future work to resolve these issues includes further investigating the distribution of faults in the KKF system, along with other faults in southern Tibet.

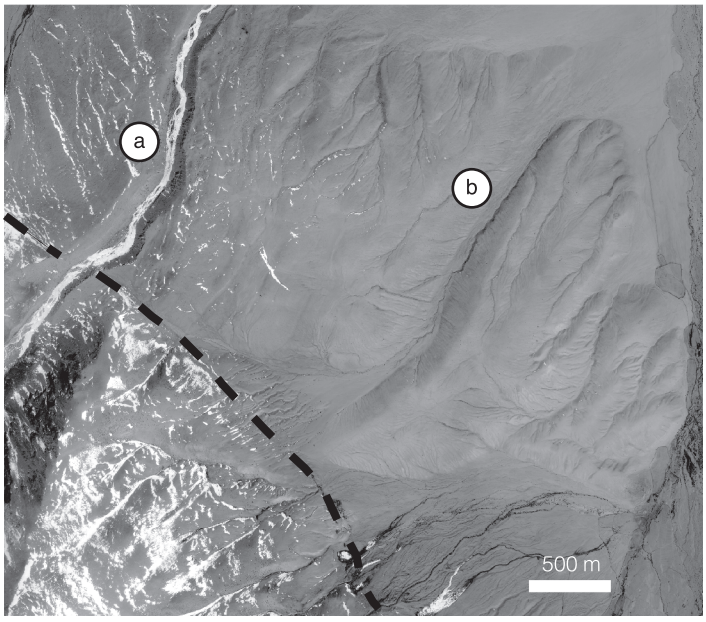

Satellite image of a 1750-m offset between a river (a) and dry channel (b) separated by movement of the Karakorum Fault (dashed line), a strike-slip fault in southern Tibet. Cosmogenic dating showed this offset to be 283,000 yr old, equivalent to a slip rate of 6 mm/yr.

Stuffing carbon away: Mechanisms of carbon sequestration in soils

P. J. Reimer, C. A. Masiello, J. S. Southon

As humans continue to add the greenhouse gas carbon dioxide (CO_2) to the atmosphere, understanding the processes that can be used to sequester carbon becomes increasingly important. Such studies must focus on carbon reservoirs that are large enough to receive significant quantities of CO_2 and stable enough to retain the CO_2 for many years.

Soils are a promising natural reservoir for carbon storage because the soil carbon pool is approximately twice the size of the atmospheric carbon pool. Limited measurements on radiocarbon (^{14}C) in soil show that some soils are excellent at removing carbon from the atmosphere, retaining high organic-carbon concentrations for hundreds to thousands of years, while other soils return their organic matter to the atmosphere within decades. This project is the first to use the carbon-cycle analytical strength of ^{14}C to approach problems of mineral-carbon storage in nonvolcanic soil systems. By identifying some of the conditions under which soil carbon storage is maximized, this study will contribute useful knowledge to inform land-use planning to enhance sequestration beyond current levels (for example, by returning agricultural land to forest or pasture).

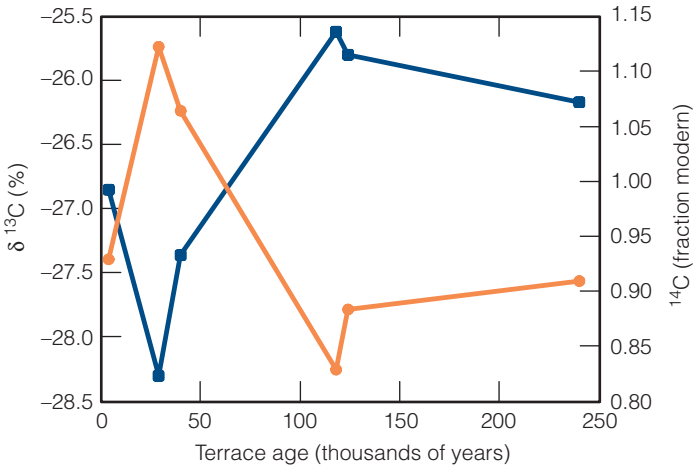

Content of delta-carbon-13 ($\delta^{13}C$, blue line) and ^{14}C (red line) vs terrace age in upper soil layers of coastal terraces in Eureka, California. The intermediate-aged terraces have the lowest ^{14}C content, indicating the longest carbon turnover time. The change in $\delta^{13}C$ indicates either preferential storage of specific compound classes, such as lipids and polysaccharides, or fractionation during microbial respiration.

This research supports the DOE's terrestrial carbon-sequestration program through better understanding and improved models of how various soils store carbon. Collaborators include researchers at the University of California, Santa Barbara; the University of California, Irvine; Lawrence Berkeley Laboratory;, and the U.S. Geological Survey.

Coastal California soils provide excellent field sites for studying soil mineralogy and precipitation, two potential controls on carbon storage. Our field sites are two sets of California coastal soil terraces, one near Eureka and another near Santa Cruz. Within each set of terraces, only soil mineral development varies; all other pertinent parameters (rainfall, plant systems, and soil parent material) are nearly constant. Precipitation at Santa Cruz is half that at Eureka, allowing us to create a two-dimensional matrix of soil properties. We are using radiocarbon to determine the turnover time of soil organic matter on each of these terraces. These data will be used to quantitatively improve the conceptual model for carbon in the terrestrial environment by providing a set of mineralogical proxies for the turnover rate of organic carbon in soil.

In FY2002 we finished field sampling at the Santa Cruz sites, installed lysimeters to collect water for measuring dissolved organic carbon, and used soil carbon concentration and radiocarbon measurements to determine the capacity of the soils to hold organic carbon. At the Eureka site, we found a strong correlation between the soil mineralogy and the organic carbon turnover. The lowest ^{14}C content, which indicates the longest carbon turnover time, was observed for the intermediate-aged terraces (see Figure), which also had the highest pyrophosphate-extractable aluminum and iron contents. The changes in delta-^{13}C ($\delta^{13}C$) with terrace age indicate either preferential storage of specific compound classes, such as lipids and polysaccharides, or fractionation during microbial respiration. Carbon-13 nuclear magnetic resonance would help to characterize the carbon compounds. In addition, a comparison between sites showed that the higher precipitation resulted in organic carbon being transported more quickly to deeper levels. Soil mineralogy, which can be influenced by changes in climate and hydrology, is a key parameter in estimating the carbon turnover time for soils along the California coast.

Lithic astronomy: Absolute chronometers and correlated isotopic anomalies in meteorites

I. D. Hutcheon, R. W. Williams, F. J. Ryerson, P. K. Weber, J. C. Gezo, K. D. McKeegan, A. N. Krot

Major rock-forming elements such as oxygen, magnesium, and silicon have isotope abundances that vary significantly in different kinds of primitive Solar System materials. These isotope anomalies are most pronounced in the calcium–aluminum-rich refractory inclusions (CAIs) found in chondritic meteorites, the oldest known solid objects in our Solar System. Despite their important implications for the evolution of the Solar System, the origin of isotope anomalies is highly controversial. Two competing models are (1) solar-nebula seeding by ejecta from a nearby supernova and (2) the production of exotic nuclear species through irradiation by cosmic rays in the X-wind from the protosun. The goal of this project is to obtain new constraints to assess these two models.

In FY2002, in collaboration with three universities, we developed, and began to apply, a new radiochemical dating scheme to determine small differences in age between early Solar System materials such as CAIs and chondrules. Our results will allow us to narrow the time frame of the formation of the first solid bodies in the Solar System and to constrain models for the evolution of other sun-like stars. This project uses unique LLNL capabilities in mass spectrometry and microanalysis and will extend the Laboratory's competencies in advanced instrumentation and nuclear chemistry, areas critically important to stockpile stewardship in that results published in the open literature are stringently reviewed by experts. Procedures thus validated can then be applied to similar problems—such as reanalysis of radiochemical tracers used as diagnostics, archived nuclear tests, and future test readiness.

Our dating system takes advantage of the fact that CAIs and chondrules, millimeter- to centimeter-size rock spherules found in primitive meteorites [see Fig. (a)], contain both relatively short-lived radionuclides (e.g., beryllium-10, aluminum-26, and calcium-41) and the long-lived isotopes of uranium. By accurately measuring small variations in isotope ratios, such as those of magnesium or lead, we determine the initial abundance of the parent isotope and thereby the object's age. In FY2002, we used this system to demonstrate chondrules in Acfer 059 to be 4564.7 million yr old and CAIs in Efremovka to be 4567.2 million yr old [Fig. (b)]. This age difference of ~2.5 million yr implies that CAIs and chondrules formed at different times, and that the condensation and melting that gave rise to them persisted for at least 2 million yr. This time span, much longer than predicted by the X-wind model, strongly supports the supernova ejecta model.

In FY2003, we will use a state-of-the-art ion microprobe to investigate radionuclide distribution in CAIs and chondrules with unprecedented 50-nm spatial resolution and resolve uncertainty surrounding the metamorphic reprocessing and redistribution of daughter nuclides among coexisting minerals. This will allow better assessment of models for the evolution of sun-like stars.

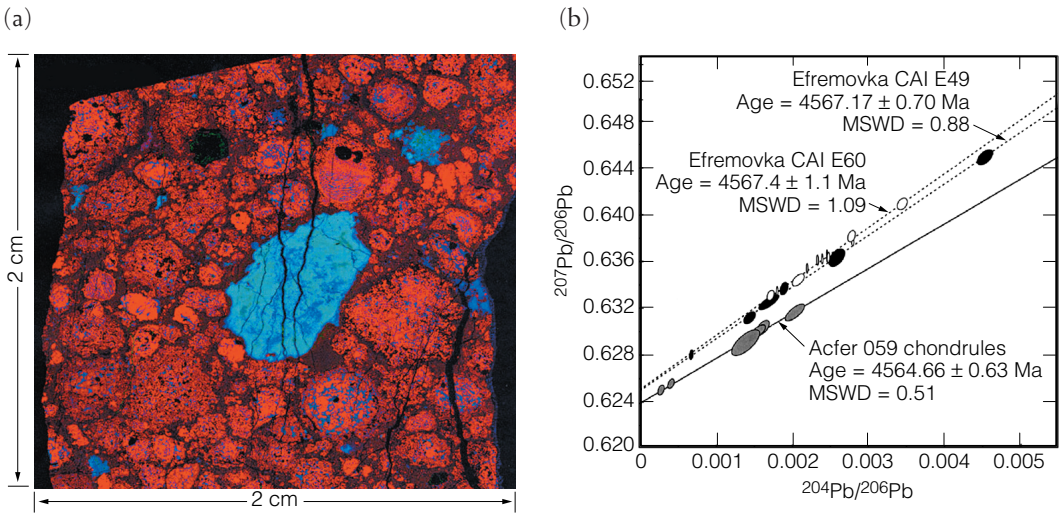

(a) A false-color x-ray element map of a calcium–aluminum-rich refractory inclusion (CAI), colored blue, and chondrules (red) in the Leoville meteorite. Isotope anomalies in CAIs and chondrules reveal age differences to constrict the time frame of the formation of the first solid bodies in our Solar System. (b) Isochron diagram of lead isotope ratios for chondrules from Acfer 059 (solid line) and CAIs from Efremovka (dashed lines). The slope difference corresponds to an age difference of ~2.5 million years. Mean square weighted deviation (MSWD) indicates data dispersion.

Natural variability and anthropogenic influence on climate: Surface water processes in the Indonesian Seas over the last 120 years

T. P. Guilderson, K. Caldeira, S. Fallon, and M. Kashgarian

The intimate coupling of the surface ocean and the overlying atmospheric boundary layer implicitly links variations in atmospheric characteristics to the underlying sea-surface temperature field. The Indonesian Seaway is a conduit for cross-equatorial, transoceanic exchange between the western Pacific and Indian Oceans and is recognized as an important contributor to the global thermohaline circulation and global climate. Vertical mixing in the Indonesian Seas drives large fluxes of heat and freshwater into the water column, which is ultimately incorporated into the Indonesian through-flow (ITF) and contributes to the regional freshwater and heat budget. This redistribution of heat and salt, in concert with regional or basin-scale processes such as the El Niño Southern Oscillation, sets the stage for the global thermohaline circulation.

The goal of this project is to determine the variations of radiocarbon (^{14}C) in surface water over the last approximately120 yr and how such variations relate to the transfer of water and heat through the Indonesian Seaway. We will use a series of model-sensitivity tests and detailed data-model comparisons to document the processes governing water mass mixing and movement in the Indonesian Seas. This project supports the Laboratory's environmental assessment and management mission.

During FY2002, high-resolution, coral-^{14}C time-series data [Fig. (a)]—including stable isotope analyses—were generated from the Langkai in the Makassar Straits to independently derive the ^{14}C age model. We performed four related simulations to determine the effects of vertical-mixing parameterizations. Our first, "basic," simulation specified vertical mixing ranging from 0.2 cm^2/s at the surface to 10 cm^2/s in the deepest ocean. The second, "enhanced upper-ocean-mixing," simulation was identical to the basic simulation, except that mixing was increased to 1 cm^2/s between the upper two layers, effectively deepening the ocean mixed layer to approximately 50 m. The third, "K-profile parameterization (KPP) mixed-layer," simulation incorporates the KPP ocean mixed-layer model into a simulation that is otherwise identical to the enhanced upper-ocean-mixing simulation. This model computed ocean mixed-layer depth from the physical state of the ocean and applied winds and buoyancy forcing. The fourth, "dynamic interior vertical-mixing" simulation is similar to the KPP mixed-layer simulation, except that the vertical-mixing coefficients in the ocean interior were dynamically computed rather than specified. Computation of the vertical-mixing coefficient incorporates components associated with vertical stability (1 over Brunt Vaisala number mixing) and shear forces in relation to vertical stability (Richardson number mixing). Interestingly, model spin ups with these significantly different vertical-mixing schemes yield similar surface coral-^{14}C values [Fig. (b)].

The results of our high-resolution, coral-^{14}C and modeling activities were presented at the American Chemical Society's annual meeting, the American Geopysical Union and American Society of Limnologists and Oceanographers biannual meeting, and the 9th International Accelerator Mass Spectrometry Conference.

In FY2003, we will complete coral-^{14}C measurements from Bunaken, Padang Bai, and Langkai; conduct analyses at Pombo Island; study the effect of wind-forcing time step (daily vs. monthly); and explore the time-varying differences between observations and simulated fields, air-sea exchange parameterizations, and particle tracking schemes.

(a)

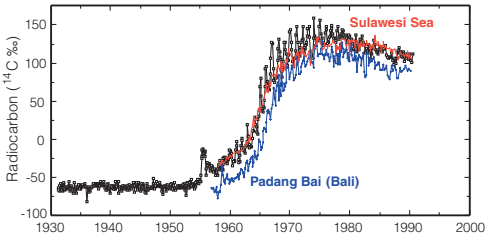

(b)

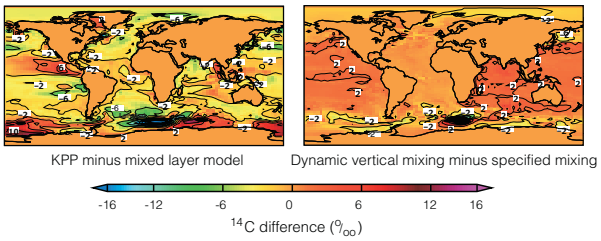

(a) High-resolution coral–carbon-14 (^{14}C) in the Indonesian Seas and (b) surface ^{14}C as expressed in four sensitivity experiments.

Direct imaging of warm extrasolar planets

B. A. Macintosh

One of the most exciting scientific discoveries in the final decade of the twentieth century was the detection, via spectroscopy, of planets orbiting other stars. However, spectroscopy can only detect planets close to their parent star, and all the planetary systems found thus far are very different from our own, with giant planets located in what would be the inner part of our Solar System. Such systems have overturned the conventional paradigm of planet formation but have no room in them for Earth-like worlds where we would expect them to orbit.

A powerful complement to spectroscopic detection of extrasolar planets will be direct imaging of the planets themselves. This technique will allow photometric measurements of planet properties and is most sensitive to planets in wide orbits. However, direct detection is extremely challenging because , for example, Jupiter is a billion times fainter than our Sun. Two techniques are proving helpful to overcome this contrast and see giant planets directly. The first is adaptive optics (AO). The second technique is looking for young planets by searching in the infrared for companions to young stars. Infrared searching reveals the thermal emission from planets that are still warm with the heat of their formation.

Adaptive optics is a key technology for a wide variety of LLNL applications including high-power laser systems for stockpile stewardship and remote surveillance in support of nonproliferation. Pushing the technology to its limits in projects such as this is helping researchers to design the next generation of AO systems for astronomical and other projects. This project is carried out in collaboration with a University of California, Los Angeles team that leads the field in young-star identification.

In FY2002, we continued development of our image-processing algorithms and software to enhance and identify faint candidates and to resolve them from artifacts in the image. Using the Keck Observatory AO system, we conducted a systematic search for young planetary companions to 80 stars.

These stars include barely-formed stars, less than 2 million yr old, in the Ophiucus cloud; "adolescent" stars that are 10 to 50 million yr old; and very close mature stars that are surrounded by thick dust disks that serve as signposts of planetary systems. The search identified several exciting candidate planetary companions, and we performed a preliminary analysis to assess the significance of their signals; the Figure shows one of these. If true planets, these would have masses three to five times greater than Jupiter and would be located in an orbit five times wider than the edge of our Solar System. Discovering very large planets at the edge of a solar system would challenge conventional planet-formation models.

In FY2003, we will continue our survey and carry out follow-up spectroscopic observations to determine whether we have detected true planets or merely background stars. We are also developing advanced image-processing techniques, based on previous LLNL work, to improve our ability to detect faint companions against the highly correlated noise caused by light scattered by imperfections in the telescope and AO system.

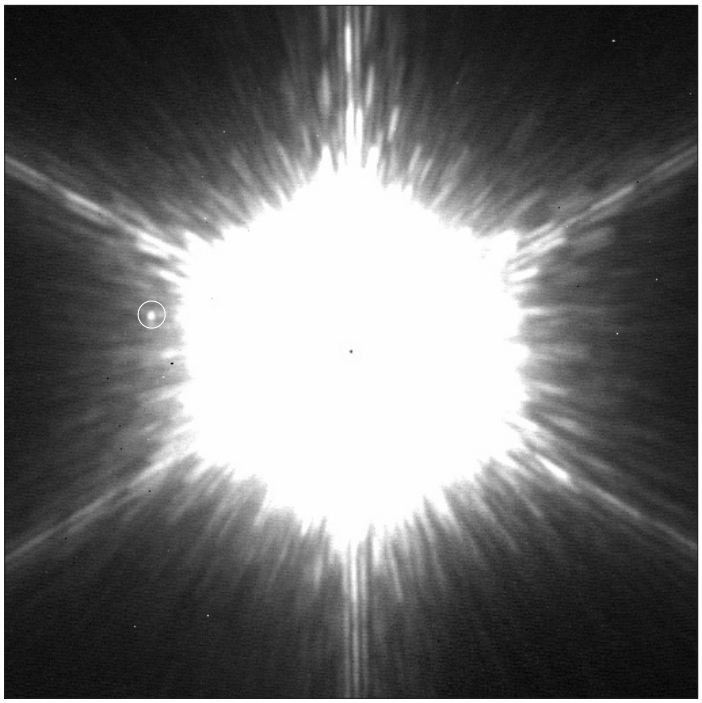

A candidate planetary companion (marked with a circle) near a young star. The pattern of sharp diffraction spikes is caused by the telescope's primary mirror.

Hadean oceanography: Experimental constraints on the development of the terrestrial hydrosphere and the origin of life on Earth

F. J. Ryerson, T. M. Harrison, P. Weber

The period of ~4.5 billion yr between accretion and preservation of the oldest rocks is known as the Hadean Period. In 2001, two research groups reported geochronological and oxygen isotopic evidence from detrital zircons ($ZrSiO_4$) that suggested the presence of a Hadean hydrosphere. The quartzitic gneisses that contain these zircons are 3 billion yr old, but the zircons themselves yield uranium–lead ages as old as 4.4 billion yr, about 400 million yr older than the oldest preserved whole rocks.

The oxygen isotopic composition of these zircons, which varies between 5.4‰("light") and 15.0‰ ("heavy"), is used to infer the isotopic compositions of their original host rocks, which have been destroyed by erosion. Heavy oxygen isotopic compositions require a source that once experienced equilibration between clay minerals and liquid water, implying the presence of liquid water at the Earth's surface 4.4 billion yr ago. This observation has important implications for the development of the Earth's continental crust and chemical differentiation of the mantle, and by extension, the suitability of the early Earth for the development of life.

The inferred composition of the zircon source rock depends on the oxygen isotopic fractionation between zircon and melt and between zircon and water, but these fractionation factors have not been determined experimentally, which constitutes the weak link in this argument. This project has conducted a series of experiments to measure these fractionation factors by partially equilibrating finely powdered quartz, polished single crystals of zircon, and isotopically perturbed water. As the quartz–water fractionation factors are known, the coexistence of quartz, zircon and water will allow us to calculate zircon–water fractionation without analysis of water, which is often lost at the end of the experiment.

In FY2002, the experiments on single crystals of zircon were run in a solid-media piston cylinder apparatus at 6 kbar and temperatures of 600 to 1000°C [Fig. (a)] with run durations up to 500 hr. Under these conditions, zircon should only partially equilibrate with the fluid, producing an oxygen isotopic diffusion profile perpendicular to the surface [see Fig. (b)]. The diffusion profiles in zircon can be extrapolated back to the sample surface to obtain the isotopic compositions of zircon in equilibrium with water.

Determining surface oxygen isotopic compositions has been hindered by two factors. At temperatures above 900°C, the depth profiles are extremely short, and the steep isotopic gradient near the surface precludes confident extrapolation to the surface with the depth resolution currently attainable. Below 900°C, the zircon surface becomes armored with quartz, which prevents direct contact between the zircon and the fluid. Another series of experiments with both zircon and quartz slabs and zircon powder has begun with the goal of ameliorating these factors.

The results of this work provide information on the environmental conditions existing on the early Earth and whether such conditions were conducive to the development of rudimentary life forms. This work has implications for LLNL's biological security mission and maintains LLNL's microanalytical capabilities and high-pressure and -temperature experimental techniques that are applicable to security- and energy-related missions.

(a) (b)

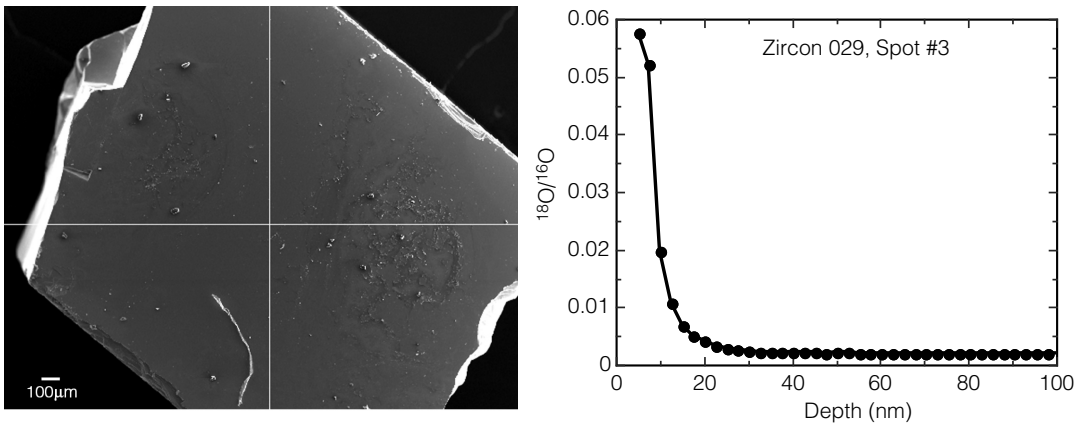

(a) Scanning electron microscope image of a zircon recovered from a 900°C sample and (b) the ratio of $^{18}O/^{16}O$ in the zircon determined by ion probe as a function of depth perpendicular to its surface. The total profile is less than 20-nm deep due to slow diffusion of oxygen and surface dissolution.

Energy Supply and Use

Section 5

Section 5 — Energy Supply and Use

Research concerning the direct conversion of carbon into electricity

N. Cherepy

Fossil fuels comprise 80% or more of the U.S. energy supply and will likely continue to do so for at least the next 20 yr. The objective of this project is to develop a carbon fuel cell to convert carbon directly into electricity at high efficiency and practical rates. The carbon fuel cell has many advantages over other fossil-fuel technologies, including potentially very high efficiency—up to 80% of fuel enthalpy—due to (1) the near zero entropy change of carbon and oxygen to carbon dioxide ($C + O_2 \rightarrow CO_2$) and (2) full utilization of the carbon fuel. No regulated emissions are released, only pure CO_2, which may be used for various industrial processes or sequestered. The fuel cell is very safe, because no compressed or explosive gas mixtures are required, and environmental impact is minimal, because no moving parts or cooling water are required. The carbon fuel cell may be able to provide low-cost, clean electricity from abundant domestic coal; use carbons from oil, methane, and biochar; and potentially raise the fossil-fuel-to-electricity conversion efficiency from ~50%—that of direct methane fuel cells and combined-cycle plants—to >70%, meeting DOE's 21st Century Fuel Cell Program target and supporting LLNL's energy security mission.

Carbon fuels are prepared by low-cost purification of coal, biochar, or petroleum coke or by pyrolysis of methane, which produces carbon and hydrogen much more efficiently than steam-reforming methane—methane enthalpy loss is only 3% instead of 28%. The carbon fuel cell generates electricity by reacting particulate carbon at the anode with air at the cathode, using a molten carbonate electrolyte at a temperature of 700 to 850°C. A porous ceramic separator allows carbonate transport, the cathode reaction ($O_2 + 2CO_2 + 4e^- = 2CO_3^{2-}$), and the anode reaction ($C + 2CO_3^{2-} = 3CO_2 + 4e^-$); the net reaction is $C + O_2 = CO_2$, with an electrochemical potential $E \approx 1.0$ V.

In FY2002, we continued exploring the relationship between the structure and electrochemical reactivity of carbon fuels and found that the least crystalline carbons—carbons with the lowest graphitization, such as biochars—are the most reactive, discharging at rates of 80 to 120 mA/cm^2 of electrode area at 0.8 V (see Figure). However, even graphite particles produce ~40 mA/cm^2 at 0.8 V, and inexpensive petroleum cokes with high sulfur content may be used but require a sulfidation-corrosion-resistant anode. We tested two advanced cathodes: (1) a proprietary cathode from Fuel Cell Energy and (2) a new LLNL-fabricated cathode. Both were shown to provide stable power (100 mW/cm^2), sufficient for utility power applications. We also tested small prototypes extensively and built 60-cm^2 and 1000-cm^2 fuel cell units.

This project has demonstrated that carbon fuel cells for power-plant applications can provide lower-cost power (~$300/kW) than other high-temperature fuel cells. Development of the carbon fuel cell, for which multiple patent applications have been submitted, will continue at LLNL. Other potential applications include auxiliary power units for long-haul trucks, work on which has already begun under a separate project.

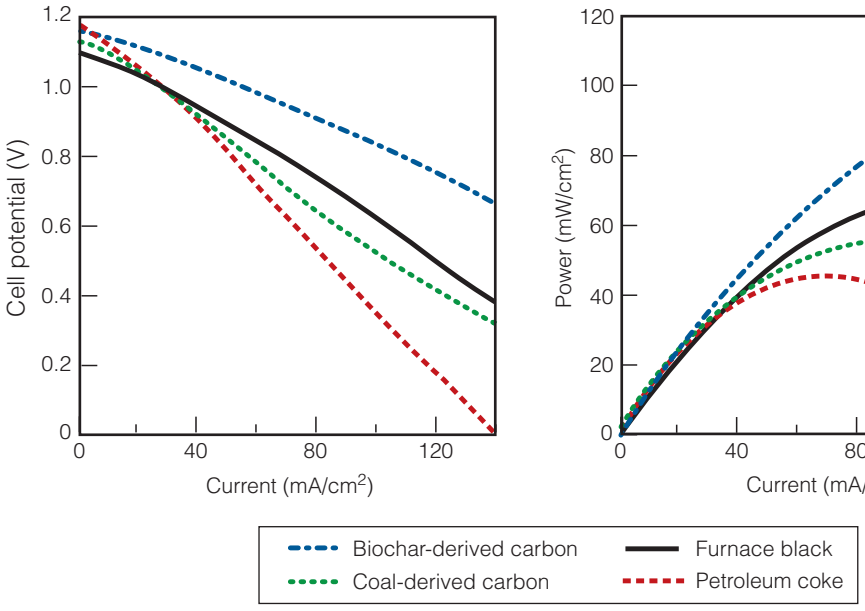

Our direct carbon conversion cell can produce electricity from carbon derived from biomass, furnace oil, coal, and petroleum coke at more than twice the efficiency of coal–steam power plants. We obtained the highest discharge rate, 100–125 mA/cm^2 at 0.8 V, with biochar-derived carbons, the materials with the lowest crystallinity.

Ultrahigh-power inorganic liquid laser

E. R. Ault, B. J. Comaskey

Neodymium (Nd) and other metal ions embedded in a variety of glassy and crystal hosts have been the mainstay of commercial lasers and fusion lasers for decades. However, the results have been disappointing when these devices are applied to multikilowatt applications. Despite the development of many complex and expensive systems, practical operation at greater than 1 kW with beams near the diffraction limit has not been demonstrated. This complex problem is an issue of thermal management. Solids must have the heat conducted away. At high heat loads, this leads to unavoidable temperature gradients that destroy optical-beam quality and can lead to fracture of the media. When a fluid medium gets hot, it can be removed from the optical path and cooled. Rare-earth ions imbedded in a fluid have the same laser kinetic advantages as their solid-state counterparts. What is needed is a way to use a host for rare-earth ions that has the advantages of a fluid that stores optical energy.

This project is developing inorganic-liquid lasers containing Nd ions that are optically pumped with semiconductor diode bars. Work focuses on elucidating the scaling parameters and numerical models that will allow the design of 100-kW-class lasers. To verify our efficiency and beam quality projections, the goal of this project includes completing and testing a demonstration prototype at a power level determined by the availability of laser diodes.

High-average-power, high-optical-quality lasers are a critical need of the fusion-energy program and could be an attractive option for a photon collider. More importantly, high-average-power lasers have many Department of Defense applications for battlefield, theater, and ballistic missile defense.

In FY2002, our Laboratory successfully produced Nd chloride solutions in thionyl chloride. Solution-absorption spectroscopy and lifetime measurements agree with or exceed published values. Several host systems are being studied, but thionyl chloride is the front runner at this time.

Key to our effort is modeling the laser performance and optical quality of the laser medium. To support this work, we have a thermal-loading testbed based on Nd-alcohol solutions. Experiments have conclusively shown that our optical-aberration cancellation scheme works as predicted at pump power levels appropriate to high-power laser operation, as the four-part Figure shows. In (d), when a pair of flow cells has opposite flow directions, the low-order optical aberrations cancel. The cells are power loaded with pump laser light to achieve a temperature rise of about 1° C. This temperature difference is the figure of merit that allows scaling to high-power operation. Increasing the pump power and increasing the flow speed accordingly while maintaining the same temperature rise allow the laser to achieve high-power operation while maintaining the same optical-path difference or the same high beam quality.

Once measured, the optical performance is established and scaling to higher power by increasing the flow speed is a linear relationship. The cancellation of thermally induced aberrations is quite good. The remaining cylindrical error is easily corrected with a low-order deformable mirror. Furthermore, our modeling shows that with a zigzag configuration, we can achieve near-diffraction-limited optical performance at high power loadings. Laser experiments with the thionyl chloride system, intended for photophysical measurements rather than a power demonstration, have reached 1.2 W of output power. We believe this is the first time a continuous-wave liquid laser has been demonstrated.

In FY2003, we plan to build a several-watt demonstration laser using existing laser diodes. We will continue to increase our knowledge of the chemistry and thermal performance of the inorganic hosts.

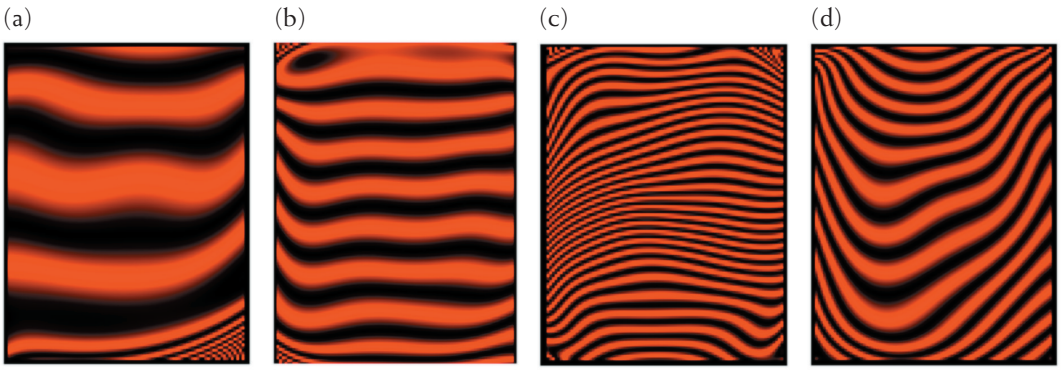

Interferograms each show two flow cells that are optically in series. (a) and (b) show the optical distortion for steady flow with no addition of heat from laser diodes. In (c), the flow directions of the two cells are parallel and heat from laser diodes has been applied. Note the marked increase in optical distortion caused by the deposited heat. In (d), the cells are under the same thermal conditions as (c) but with one of the flow directions reversed. Note the much smaller distortion produced by cancellation of the optical aberrations.

FLIRT: A magnetic field topology diagnostic for spheromaks and other self-organized, magnetically confined plasmas

H. S. McLean, H. Chen, D. D. Ryutov

Tangled magnetic field lines are common in laboratory and space plasmas, but determining the geometrical structure of magnetic fields in the presence of plasma is a difficult and still unresolved problem. To address this open question, we are developing and testing a new technique for measuring the magnetic field-line topology in magnetically confined plasmas. Our field-line tracing diagnostic (FLIRT) (see Figure) uses a high-power, short-pulse laser to launch a burst of energetic (~100 keV) electrons from a target passing through the plasma. These electrons generally follow magnetic-field lines until they strike a solid surface, where a burst of x rays is produced. The field-line connection length can be determined from the time delay between the laser pulse and the burst of x rays. The topology of the field lines can be inferred by measuring the connection length as a function of initial target location inside the plasma. Measuring the spatial distribution of x-ray production provides further information on the field topology, including the effects of magnetic-field fluctuations and stochasticity.

This research includes testing the appropriate x-ray detectors; measuring the background x-ray emission in a spheromak plasma and the energetic electron production by a short-pulse, high-power laser; and making preliminary measurements of the edge field line topology in the Sustained Spheromak Physics Experiment (SSPX). A pulsed electron-beam source is the prototype for a laser-based source. If successful, this technique will have broad application to a variety of plasma configurations and provide physics data applicable for magnetic-confinement fusion and space plasmas relevant to the DOE's fusion energy science program and the Laboratory's energy mission.

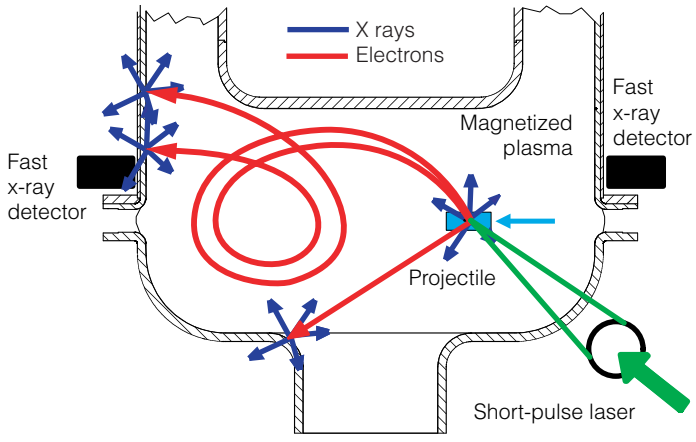

Electrons generated by a high-power laser inside a magnetized plasma are confined to magnetic fields lines and eventually strike the walls, producing x rays.

In FY2002 we (1) confirmed that the background x rays will not interfere with the expected x-ray signals, (2) constructed an electron gun system that produces the pulse width (~10 ns) and energy spectrum (10 to 100 keV) necessary to simulate the laser-produced electrons, and (3) constructed and tested a fast detection system that can easily resolve line lengths of <0.70 m. Tests on SSPX injecting electrons into a plasma showed that further work was required to separate the x-ray pulse generated by the electron gun from x rays generated by electrons hitting the walls of the device.

The absence of large background x-ray signals in SSPX was supported by analytical calculations showing that high-energy (>100 keV) runaway electrons can be formed only if very long flux tubes exist, making at least 5000 turns around the geometrical axis. Three-dimensional magnetohydrodynamic computer simulations showed such conditions are met only sporadically in SSPX, and high-energy x rays will have a character of short bursts, leaving long "quiet" intervals suitable for the FLIRT measurements. Another analytical study predicted the characteristic shapes of the x-ray pulse produced by mirror-trapped electrons, electrons injected on the rational flux surfaces, and untrapped electrons injected on the open field lines. The role of electron drift and field-line stochasticity was also evaluated.

This project has demonstrated the basic principles of the technique and justification for continued work. The laser power to produce sufficient electrons is modest, the x rays from these electrons are detectable, and the x-ray signals can be interpreted to provide information about the magnetic structure within the plasma. The next steps in pursuing this method include targeting a projectile with a laser and refining the detection system to include better imaging of the x-ray strikepoints.

Active load control and mitigation using microtabs: A wind-energy application

D. Nakafuji

National policies and funding are focusing on renewable energy generation to improve the reliability of our country's electrical infrastructure and increase our self-reliance on natural, renewable resources, such as wind. In fact, industry and DOE projections indicate that wind energy will be our greatest source of renewable energy. However, fundamental research has not kept pace with development needs, including new technologies to increase turbine life spans and reduce costs.

Promising technologies include active load control and load-alleviation systems, which mitigate peak loads to prevent damage to turbine components. This project addresses the science and engineering challenges of developing active load control using microtabs—small (~1% of the chord length of the blade), retractable tabs placed along the trailing edge of a wind-turbine blade in the spanwise direction (see Figure). When extreme bending moments are detected by sensors located throughout the blade, the microtabs are deployed, either on the upper or lower surface, at a rate much faster than possible with conventional control techniques. The microtabs reduce bending moments on the blade by either increasing lift (lower-surface tabs) or decreasing lift (upper-surface tabs) on the blade. By making wind turbine technology more reliable and cost effective, this project contributes to decreasing U.S. dependence on foreign fuel sources and increasing energy reliability through fuel-resource diversity—without contributing to greenhouse gas emissions—in support of LLNL's energy security mission.

The scope of this project encompasses (1) experiments, including wind-tunnel experiments to understand governing unsteady and turbulent-flow physics and structural interactions at the microscale and the mesoscale; (2) computations to analyze microtab effectiveness as load controllers and mitigators; (3) fabrication and demonstration of microtab devices; (4) design and integration of robust, miniature actuators, sensors, and controllers that can withstand actual operating environments; and (5) developing practical devices to meet industry needs. For instance, the design of microtabs will require sophisticated codes and modeling capabilities for two-dimensional (2-D) and 3-D flows in steady and unsteady analysis, and the design of robust actuators for the microtabs will require new microelectromechanical (MEMS) approaches.

Accomplishments to date in FY2002 include (1) completing numerous upgrades to a wind-tunnel facility at the University of California, Davis, to enable detailed analysis for the project; (2) completing detailed drag studies based on 2-D experimental results; (3) establishing a collaboration with NASA Ames staff to receive support with Overflow, a 3-D code for numerical simulations; (4) completing 3-D grids for simulations and design studies; (5) designing a prototype actuator; and (6) collaborating with the National Renewable Energy Laboratory to conduct acoustic testing of microtab geometries.

In FY2003, we plan to (1) characterize microtab flow physics and actuator response for wind-energy applications using numerical simulations and wind-tunnel experiments; (2) quantify the response frequency and load changes needed for turbine load mitigation; (3) continue 3-D numerical analysis to gain insight on physics and flow structures generated by the microtabs; (4) build experimental platforms to provide guidance for feedback control and logic; and (5) complete acoustic testing and analysis on preliminary microtab geometries.

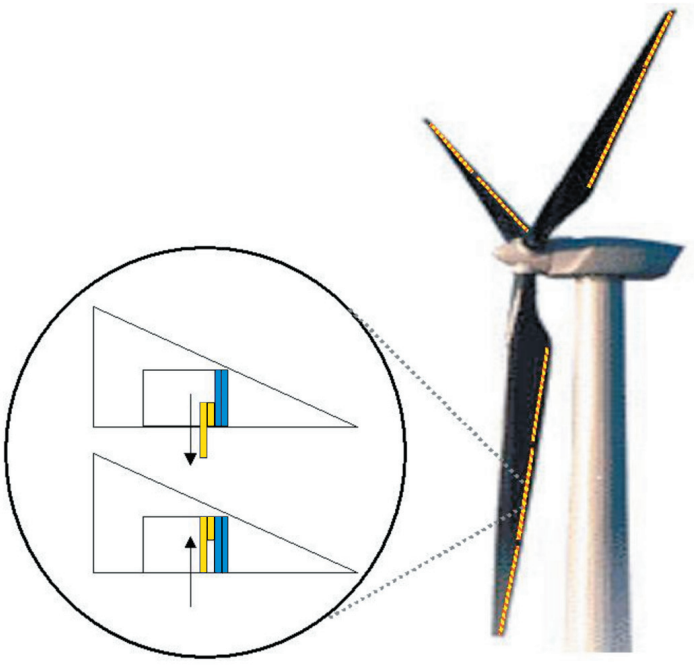

The microtab active load mitigation concept includes rows of small (~1% of the chord length of the blade), microelectromechanical tabs (microtabs) built into the trailing edge region of wind turbine blades. When unfavorable loading conditions are sensed, the microtabs are actively deployed on either the upper or lower surface (inset top) by microactuators to enhance lift or decrease lift on the blades to help mitigate extreme load conditions and prevent damage.

Isotopic tracing of fuel components in particulate and gaseous emissions from diesel engines using accelerator mass spectrometry

B. A. Buchholz

Environmental and health concerns over engine emissions influence increasingly stringent emissions standards and drive research into the use of nonconventional, cleaner-burning fuels. Adding oxygenates to diesel fuel reduces particulate emissions, but the mechanisms responsible for the reductions are not understood. Measurement of particulate matter (PM), unburned hydrocarbons (HC), and carbon monoxide (CO) are routine, but determining the origin of the carbon atoms that make up these undesired emissions is difficult. In this project, we are using the subattomole sensitivity of accelerator mass spectrometry (AMS) for measuring carbon-14 (^{14}C) to trace the carbon atoms from specific fuel components to soot or gaseous emissions. Radioactive materials are not required because contemporary carbon (e.g., ethanol from grain, biodiesel) has 1000 times more ^{14}C than petroleum-derived fuels. The specificity and sensitivity of ^{14}C -AMS make the technique a powerful tool in acquiring data for validating combustion modeling.

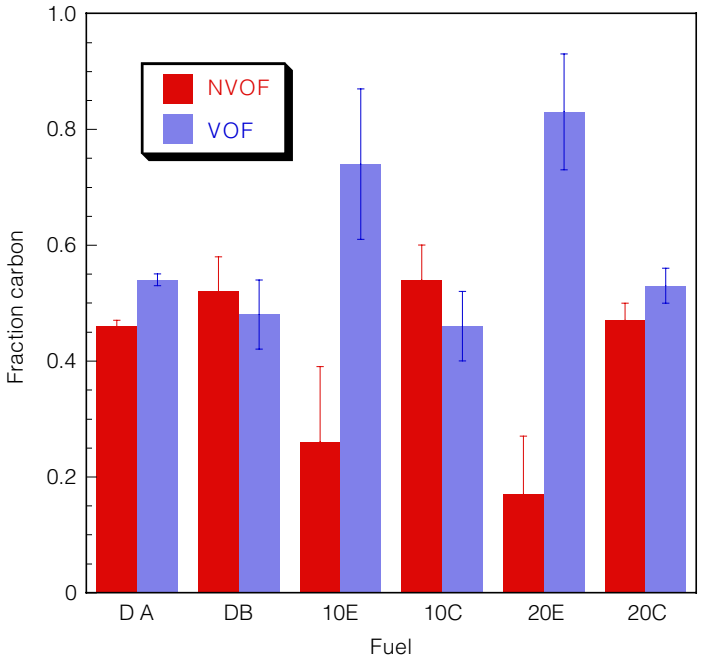

Partitioning of carbon between volatile organic fractions (VOF) and non-volatile organic fractions (NVOF) on filters loaded with particulate matter from various fuel formations: diesel (DA, DB), emulsified diesel-ethanol blends (10E, 20E) and cosolvent diesel–ethanol blends (10C, 20C).

Beyond emissions concerns, U.S. dependence on the supply of imported oil makes transportation fuel a national-security issue. Substituting renewable bioderived fuels for petroleum products will reduce dependence on foreign oil and slow the transfer of deep-reservoir carbon to greenhouse gases. The data acquired in this project validate combustion models and create insights into which chemical structures within fuels and additives most greatly influence emissions.

The test engine, a 6-cylinder, 6-L 1993 Cummins diesel, was operated at steady-state conditions of 1600 rpm and 210 ft-lb. Particulate matter was collected on quartz filters following a minidilution tunnel. Blends of diesel–biodiesel and ethanol-in-diesel were run since it is likely that bioderived fuels will supplement petroleum fuels rather than replace them. Particulate matter was separated into volatile and nonvolatile organic fractions (VOF and NVOF) for AMS analysis (see Figure). Fuel formulations such as the emulsified ethanol–diesel blends that shift PM to the VOF while reducing total PM mass are preferred since the VOF is easily treated with current exhaust catalyst technology. The Figure shows diesel fuel and 10% and 20% ethanol–diesel cosolvent blends (10C, 20C) with similar VOF/NVOF partitioning while 10% and 20% ethanol–diesel emulsified blends (10E, 20E) shift the carbon to the VOF.

The biodiesel–diesel blends tended to decrease CO and HC as biodiesel increased. Particulate matter production varied little between the diesel and biodiesel–diesel blends (20%, 50%, and 100% biodiesel by volume), but fuel consumption increased with biodiesel fraction. The difference in ^{14}C content between 100% biodiesel and traditional lubrication (lube) oil was exploited to measure the contribution of lube oil to PM. Although proportionately small by mass, the relatively high sulfur levels of conventional lube oil can lead to catalyst fouling. Our technique for directly measuring lube-oil transport into the cylinder and out the exhaust port is directly applicable to all diesel platforms.

In FY2003, we plan to study mechanisms of operation of simple nitrous oxide traps. By using contemporary carbon compounds to regenerate the traps, we will learn how the chemical reactions occur on the surfaces. Since all the carbon leaving the exhaust catalysts is fully oxidized, an atomic rather than molecular tracer is required.

The kinetic stabilizer: A route to a simpler magnetic-fusion system

R. F. Post, J. A. Byers

The project, motivated by the country's pressing need for a simpler, smaller, quicker-to-implement approach to fusion power, involves theoretical and computational studies of a new stabilization technique, called the Kinetic Stabilizer (K-S), for magnetic-confinement fusion systems. The K-S is applicable to "magnetic mirror" confinement systems with axisymmetric fields, (i.e., fields generated by circular magnet coils having a common axis). Mirror experiments dating back to the 1960s showed that axisymmetric fields can confine plasmas in a near-quiescent state where cross-field transport is not enhanced by turbulence. However, such fields are prone to magnetohydrodynamic (MHD) instabilities, resulting in rapid plasma loss across the confining field.

Theory, confirmed by experiments, shows that MHD-unstable axisymmetric mirror systems can be stabilized by the presence of a low-density plasma in the expanding-field region outside the mirrors. In a mirror fusion system, the density of the effluent plasma leaking through the mirrors would be below the density required to stabilize the confined plasma. The K-S solves this problem by injecting ion beams directed up the magnetic gradient outside the mirrors. Magnetic compression and stagnation/reflection of these beams then forms a localized plasma peak, which stabilizes the interior, confined plasma.

Calculations show that the beam power required by K-S would be small compared to the fusion power. By using the K-S, the full potential of magnetic confinement can be exploited, something not possible with today's mainstream approaches where transport is dominated by turbulence, which requires scaling up to large size (and cost) to yield net fusion power.

In FY2002, the study met all three of its objectives: (1) employ analysis to define suitable configurations and parameters for the K-S; (2) update FLORA, LLNL's legacy MHD-stability code, for operation on modern workstations; and (3) benchmark FLORA against the analytical results, in preparation for extending the computations to fusion-relevant cases that are beyond the present capabilities of the analytical approach.

The Figure shows one practical implementation of the K-S concept that would not require the continuous use of ion sources to produce the stabilizer plasma. Assuming that ion beams have been used to allow the buildup of a stable hot plasma in a tandem-mirror system, at a point outside the mirror where the confining potential has fallen to 1.0 kV, directed low-density gas jets would be turned on. The gas molecules of these beams would be ionized by the plasma and accelerated down the magnetic gradient in the expander, producing and accelerating ions and electrons, which would then take over the stabilizing function so that the ion sources could be turned off. In preliminary studies, calculations indicated that the power drain caused by accelerating ions formed from the gas jets was only about 200 kW in a tandem-mirror system producing hundreds of megawatts of fusion power.

Plans for FY2003 include extending the FLORA K-S studies to fusion-relevant parameters, employing Fokker-Planck computer codes to generate plasma distributions for FLORA that model those in a tandem-mirror fusion system, and investigating the plasma conditions required to avoid non-MHD instability modes, such as drift-rotational modes. These analyses and computer calculations will help us to form a much more comprehensive visualization of a full-scale K-S-stabilized tandem-mirror fusion power system.

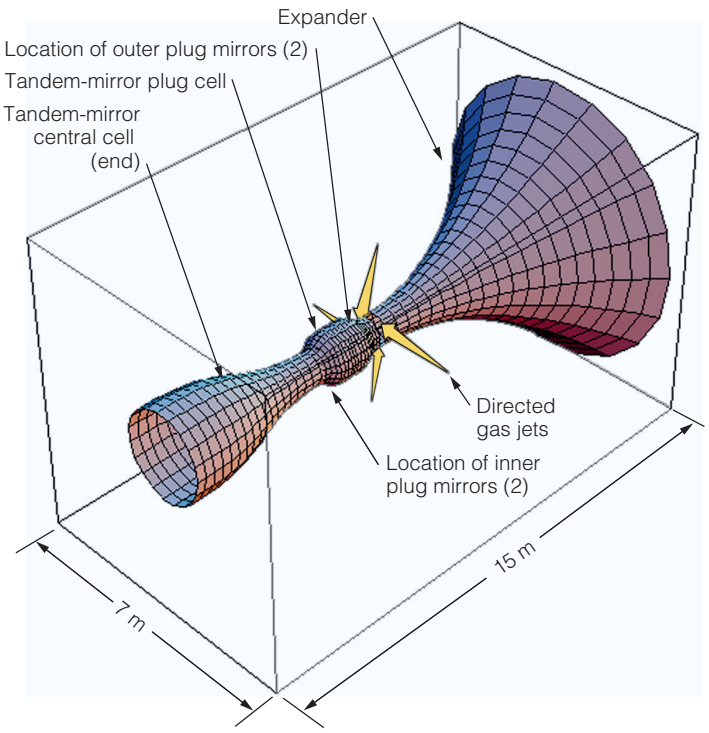

Schematic of the magnetic flux surface of a kinetically stabilized, tandem-mirror system shows (from the left) the end of the central cell; the small-volume, high-magnetic-field "plug" region with two mirrors at each end; and the expander field, where the flux surface flares out. The gas jets take over the stabilizer function, following buildup of the plasma and its stabilization by ion beams (not shown), which would be located near the outermost part of the expander flux surface and aimed inward at small angles to the direction of the field lines.

Potential new anode materials for solid-oxide fuel cells

O. E. Kesler, R. L. Landingham

Solid-oxide fuel cells (SOFCs) using pure hydrogen as fuel have the potential for the highest efficiency among the different fuel cell types and are attractive candidates for applications in both transportation and stationary power generation. However, widespread commercialization remains limited because of materials-related challenges posed by the high-temperature (600 to 1000°C) operating environments. Differential thermal expansion and sintering shrinkage in the fuel-cell material layers lead to thermal stresses that limit cell lifetime and reliability. Residual stresses also lead to cell curvature, which impedes stack assembly and increases maximum deflection as a larger cell area is used for greater stack power.

The objective of this project is to improve the mechanical behavior of SOFCs and to reduce thermal stresses and curvature in the cells by more closely matching the thermal expansion of the different material layers. We examine anode-supported cells and study the effect of doping nickel–yttria-stabilized zirconia (Ni–YSZ) cermet—the traditional SOFC anode material—with aluminum oxide (Al_2O_3) to better match the thermal properties of the anode with that of the electrolyte coating.

This research supports LLNL's energy security mission by working toward (1) the increased commercial availability of clean, efficient, secure, and renewable sources of electrical energy and (2) greater energy diversity, which increases the nation's energy security by making the U.S. energy infrastructure less susceptible to power crises or terrorist attacks.

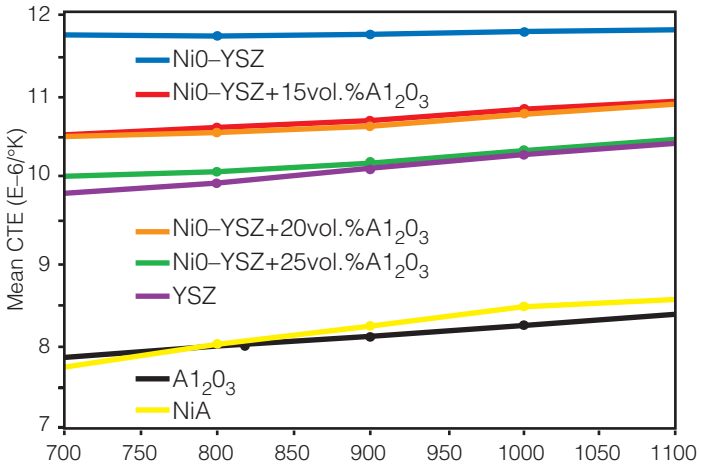

Coefficient of thermal expansion (CTE) from 20°C for various anode and electrolyte compositions for solid-oxide fuel cells. This shows that adding aluminum oxide (Al_2O_3) to the nickel oxide–yttrium-stabilized zirconia anode decreased the CTE. Close CTE matching between the anode and electrolyte was possible with a 25% volume fraction of added Al_2O_3, which should improve cell lifetime and reliability.

In FY2002, various anode compositions were investigated. Dilatometry, sintering shrinkage, scanning electron microscopy, four-probe electrical conductivity, and reduction studies were performed to correlate the microstructure, thermomechanical and electrical properties, and composition. Experimental results were used to select a composition leading to low overall cell curvature and improved mechanical behavior with respect to standard SOFC anode cermet materials.

We added Al_2O_3 in varying amounts to powders of nickel oxide (NiO) and zirconium dioxide (ZrO_2) with 8 mole% yttrium oxide (Y_2O_3), with the volume fraction of NiO in the powders held constant at 51%. The resulting changes in coefficient of thermal expansion (CTE) are shown in the Figure, which demonstrates that increasing the quantity of Al_2O_3 decreased the CTE, and that close CTE matching between the NiO–YSZ-based anode and the YSZ electrolyte occurred with a 25% volume fraction of Al_2O_3 added to the NiO–YSZ.

Although adding Al_2O_3 to the standard NiO–YSZ anode material reduced or eliminated the CTE mismatch between the anode and electrolyte reaction of Al_2O_3 with NiO, forming nickel aluminate ($NiAl_2O_4$) upon high-temperature sintering reduces the overall Ni content of the post-reduction anode material because the $NiAl_2O_4$ does not reduce to Ni and Al_2O_3 in typical in situ stack reduction conditions. Additional NiO can be added to the original mixture to maintain a constant volume fraction of Ni in the cermet after reduction—a trade-off between anode conductivity and the stress and curvature resulting from CTE mismatch between the anode and electrolyte layers. We found that an added Al_2O_3 volume fraction of 24% was sufficient to reduce the overall cell curvature to less than 0.5-mm deflection for a large-area (>10 cm on each side) cell while still retaining a percolated conductive Ni network in the reduced material.

Long-term testing is still needed to determine whether the reduced volume fraction of Ni will cause the conductivity to drop over time. However, because microstructure strongly effects anode conductivity and mechanical behavior, factors such as particle size and pore-former content can be adjusted to control overall porosity and obtain a more optimal combination of mechanical behavior and electrical conductivity in anodes with added Al_2O_3.

Engineering and Manufacturing Processes

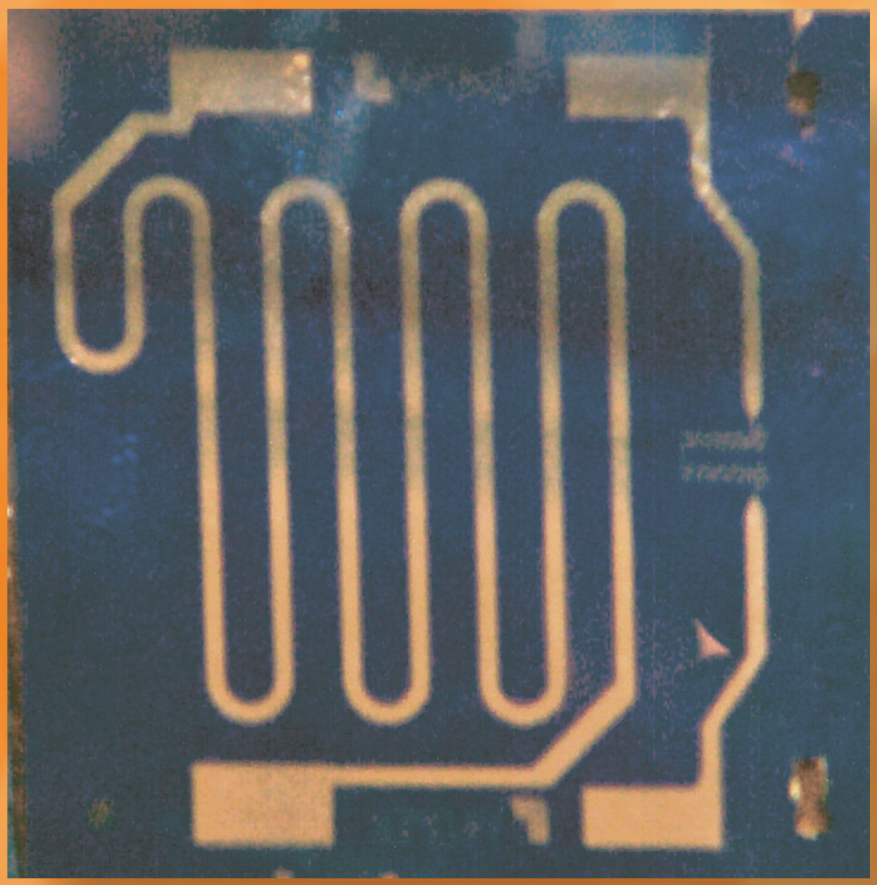

Section 6

Section 6 — Engineering and Manufacturing Processes

Higher-order, mixed finite-element methods for time-domain electromagnetics

N. K. Madsen, D. A. White, N. J.Champagne

Time-domain computational electromagnetic (CEM) modeling is the most cost-effective approach for electromagnetic design and analysis for problems that are electromagnetically very large or nonlinear and transient in nature. However, no stable, higher-order, conservative methods—such as those that exist for computational fluid dynamics and other disciplines—exist for time-domain CEM, largely because of the unique characteristics possessed by Maxwell's equations, which are typically solved with a set of low-order, Cartesian-grid methods. These simple, stable methods work well for rectangular geometries but require prohibitively large meshes for quantitative field predictions on electrically large problems and produce inconsistent solutions for nonorthogonal geometries. In addition, finite-volume schemes, which are often considered as an alternative, suffer from numerical instabilities, lack of conservation, and low accuracy.

To overcome these limitations, this project is investigating higher-order, mixed finite-element methods (MFEM)—a new methodology for solving partial differential equations on three-dimensional (3-D), unstructured grids. Our goal is to develop a stable, conservative, higher-order, and accurate simulation code for Maxwell's equations and related equations of electromagnetism. Our MFEM methodology builds on LLNL's competency in computational engineering and will (1) enable engineers to perform electromagnetic simulations on unstructured grids, and (2) provide a coupled electrothermalmechanical modeling capability, both in support of the Laboratory's national security mission.

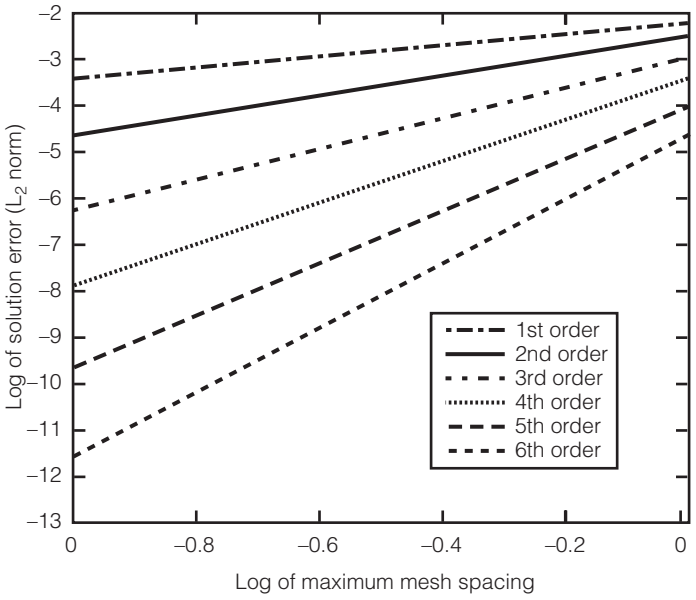

To demonstrate the accuracy of our higher-order, mixed finite-element methods (MFEM) for time-domain computational electromagnetic modeling, we used MFEM methods of various orders to solve the vector Helmholtz equation for a resonator. The Figure shows that the rate of error decreases as mesh spacing is refined, and that the sixth-order method achieves almost 12 digits of solution accuracy.

Accomplishments in FY2002 include (1) making progress on the core higher-order numerical components of our simulation code, such as integration rules, basis functions, and the hexahedron, tetrahedron, and prism elements; (2) collaborating with a consulting firm to develop software components for assembling and solving, in parallel, the global linear systems; and (3) using these software components to demonstrate the efficacy of higher-order methods and perform a time-dependent simulation using higher-order time-integration methods.

To demonstrate accuracy, we used MFEM methods of various orders to solve the vector Helmholtz equation for a resonator. The Figure shows the rate of error decreasing as the mesh spacing is refined. The sixth-order method achieves, for the first time at LLNL, almost 12 digits of solution accuracy. We also studied using adaptive Runge-Kutta schemes for time-dependent problems and tested our high-order basis functions in the parallel assembly of mass and stiffness matrices for arbitrary-order, finite-element discretization.

Our work in FY2003 will focus on (1) completing our prototype parallel, higher-order electromagnetic-application code; (2) further evaluating this code by comparing computed results to well-known solutions; (3) preparing and submitting journal articles about our underlying numerical methods; (4) modifying our software to improve parallel efficiency, scalability, and ease-of-use; and (5) demonstrating our technology by simulating important, longstanding issues in CEM—such as absorbing boundary conditions, mesh refinement, and material models—that existing methodologies cannot effectively simulate.

Further development of wet-etching tools for precision optical figuring

S. N. Dixit, M. R. Rushford, J. A. Britten, C. Hoaglan

The four most common approaches for figuring large-aperture optics—grind-and-polish, small-tool figuring, magnetorheological finishing, and plasma etching—involve large capital investment. A high degree of optical finish (transmission wavefront of the order of λ/10 or better) is needed for applications in high-power lasers and high-resolution imaging. Large apertures are also required in high-power lasers to minimize the laser damage and in space telescope applications to enhance the signal-to-noise ratio.

In this project, we are developing a low-cost etching process for figuring large-aperture, very thin (<1 mm) optic plates that cannot be processed by any other means. A patent on wet-etch figuring is pending. These techniques will enable the fabrication of continuous-phase plate, diffractive optics, and disposable debris shields for the National Ignition Facility being built by DOE's Stockpile Stewardship Program. This technology will be transferred to industry for use in low-cost production of high-quality optics for various national security and commercial applications.

The process involves the controlled application of a hydrofluoric acid etchant to the glass surface being figured. The etchant is pumped through a narrow tube and flows back down along the outer surface of the tube because of gravity. The tube is surrounded by an alcohol-containing region. Slight absorption of the alcohol in the etchant reduces the surface tension between the etchant and the glass surface—known as Marangoni confinement—which contains the etch footprint. An in situ interferometer monitors the optical thickness in real time.

We previously developed and demonstrated a point etcher and a one-dimensional (1-D) linear etcher. Although successful in producing complex surface figures on thin glass substrates, such etching tools are slow when figuring large areas. The next step is developing a parallel etch process for simultaneously etching the entire 2-D surface, which should reduce surface-figuring time by orders of magnitude. Parallel 2-D etching requires simultaneously etching different areas of the 2-D surface at different etch rates. Because etch rate doubles with a 10° increase in etchant solution temperature, we are focusing on using temperature to differentially control local etch rates.

In FY2002, we experimentally examined several methods, such as locally heating the solution with electrical wires and through a gray-scale mask. Initial results were promising—the required thermal gradients were achieved—although the gray-scale mask technique required a very-high-power light source.

To enable rapid, in situ gathering of the surface wavefront data needed for active feedback during 2-D etching, we built a large-aperture Fizeau interferometer capable of measuring the surface wavefront of thin sheets of glass as large as 1 m across. A large-aperture, Fresnel lens collimates light from a laser and focuses it on the glass [Fig. (a)]. Light reflected from the top and bottom surfaces creates Fizeau fringes [Fig. (b)], which are captured as fringe maps at four wavelengths using a frequency-scanning laser and then converted to a wavefront map [Fig. (c)].

In addition to wet etching, we also examined electrolytic differential etching using fluorine ions. The etch differential is controlled by adjusting individual electrodes in the array. This technique achieved etch rates of >100 nm/min with very modest (~10 V) voltages, but its drawbacks are generation of particulate precipitates and erosion of the electrodes.

In FY2003, we will continue to examine other methods for parallel optical figuring, such as differential heating of the glass with hot-air jets and differential heating of the etchant with a rastered infrared laser beam or an independently addressable 2-D array of resistors.

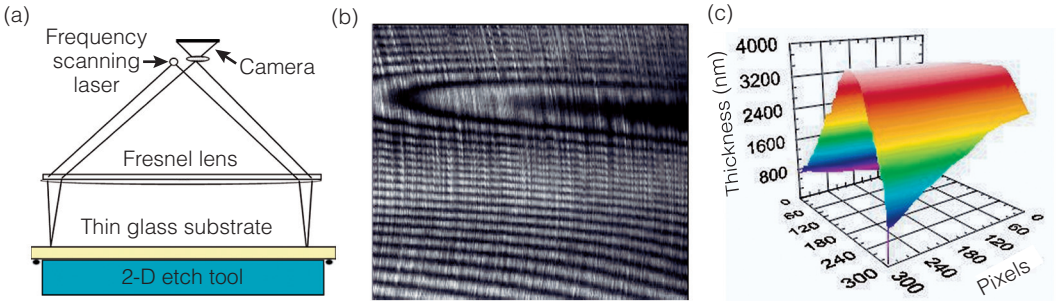

(a) A Fizeau interferometer developed in this project for measuring the wavefront of a thin glass substrate during two-dimensional (2-D) etching. This device enables the rapid, in situ conversion of (b) Fizeau fringe patterns into the (c) surface wavefront data needed for active feedback during 2-D etching.

Integrated microfluidic fuel processor for miniature power sources

R. S. Upadhye, J. D. Morse, A. F. Jankowski, M. A. Havstad

Improving portable power sources is critical for the military, weapons-testing monitors, and the intelligence community. Commercially available batteries are inadequate for advanced applications in remote reconnaissance, intelligence gathering, and telemetry—applications that require lighter-weight, longer-lasting power sources. Current proton-exchange membrane (PEM) fuel cells are limited to 3 to 15% methanol solution, which restricts power and energy density. We are developing a PEM fuel cell with a separate microreactor that converts the methanol to hydrogen, thus exploiting the very high energy densities of methanol and other liquid fuels.

The objective of this project is to demonstrate the feasibility of a packaged microfluidic fuel processor with improved catalyst and integrated thermal management for waste-heat recovery or heat conservation through improved arrangements of heat exchanger and insulation. The project combines experimentation with theoretical and numerical analysis, design, and development and leverages LLNL's expertise in microfluidic devices, microfabrication techniques, and materials science. By delivering a reliable, long-lasting, miniature power source for applications such as sensors—a field in which long-lasting power sources are greatly needed—this work supports LLNL's national security mission. Farther in the future, applications could include long-lasting, lightweight power sources for consumer electronics products such as cell phones and laptop computers.

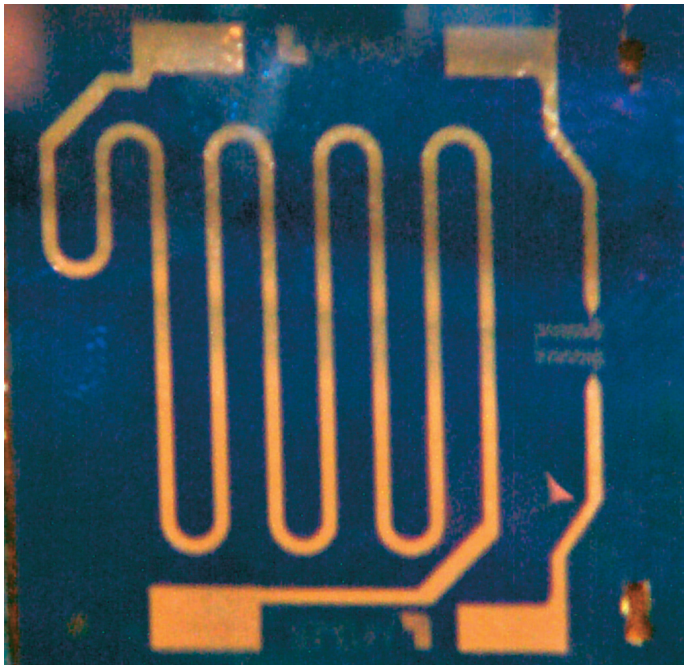

Photograph of a microreactor (approximately 1 in. square) capable of converting a liquid fuel such as methanol to hydrogen. Using a commercially available copper oxide–zinc oxide catalyst, we achieved energy conversion rates of 80 to 96% at 250 to 300°C, which corresponds to electrical power of 500 to 1000 mW.

Our power supply is a catalytic microchannel reactor based on the steam reforming of methanol, in which a mixture of water (H_2O) and methanol (CH_3OH) is heated to produce hydrogen gas (H_2) and carbon dioxide (CO_2) at ~300°C in the following reaction: $CH_3OH + H_2O \rightarrow CO_2 + 3\ H_2$. [Some methanol decomposes into carbon monoxide and hydrogen ($CH_3OH \rightarrow CO + 2\ H_2$), but a goal of catalyst optimization is to minimize decomposition.] The hydrogen fuel and the O_2 byproduct are then delivered to the fuel cell manifold by microfluidic interconnects. With adequate catalyst surface area and applied heat, the microfluidic reformer produces hydrogen with only minimal power needed to sustain the reaction. This system is an integrated solution that solves the issues of fuel storage, processing, and delivery.

In FY2002, we developed reactor models based on published kinetics, achieving excellent agreement with our data. Experiments using our microreactor (see Figure) with two commercial catalysts containing copper oxide (CuO) and zinc oxide (ZnO) on alumina achieved methanol conversion rates of 80 to 96% at 250 to 300°C, which corresponds to electrical power of 500 to 1000 mW. We successfully deposited sputter-coated nickel (Ni) and CuO catalysts on microchannels and nanoporous membranes, and built and operated a PEM fuel cell fed directly by the reformate hydrogen gas and yielding up to 150 mW of electrical power—our goal is >500 mW. Byproducts of this work include techniques for depositing active catalyst on microdevices and metallic sponges with very high surface area, which may be excellent catalysts for some applications. The results of this project were featured in two conference presentations, will soon appear in several peer-reviewed journals, and are expected to lead to one or more patents.

Our key objective for FY2003 is to determine the best components and design for our microfluidic fuel processor so that a preprototype power module can be developed. For example, the appropriate catalyst (Ni or CuO/ZnO) and reactor configuration (microchannel, nanoporous membrane, or a combination of the two) will be chosen. Our project will also investigate how best to thermally integrate the reactor inlet and the outlet, as well as how to integrate our microreactor with an operating fuel cell.

Femtosecond laser synthesis of multi-element nanocrystals

L. N. Dinh, M. Balooch, T. Trelenberg, B. Torralva

The goals of this project are to achieve a complete scientific understanding of the physical and chemical properties involved in the femtosecond synthesis of nanocrystals and a computational modeling capability for predicting nanocrystal properties. Our research has applications that benefit various NNSA/DOE missions: energy (solid-state fuel cells), nonproliferation (sensors), and biotechnology (molecular targeting and drug delivery).

In FY2002,we investigated the conditions under which short-pulsed laser-deposited (PLD) stoichiometric multi-element nanocrystals of major classes of materials are formed. Studies were performed on gallium arsenide (GaAs), indium phosphide (InP), cobalt-platinum alloy (CoPt) and inconel, an alloy of chromium, iron, and nickel. The properties of the PLD nanoclusters and the irradiated targets were investigated as a function of the laser pulse length (150 fs to 500 ps) and the inert background gas pressure in the synthesis chamber (microtorr to hundreds of torr). The size distributions, morphologies, and structures of PLD nanoclusters were obtained by scanning electron microscopy, atomic force microscopy (AFM) and x-ray diffraction (XRD). Nanocluster compositions were probed by XRD, Auger electron, x-ray photoelectron, and x-ray fluorescence spectroscopies. The thickness of the nanocluster films was measured by AFM and profilometry. Passivation of the surfaces of semiconductor nanoclusters from oxidation was done in situ. The ablated targets were subjected to similar studies.

Our results reveal that the formation of stoichiometric GaAs nanocrystals [Fig. (a)] required ablating a GaAs target with a < 25-ps laser in >100 mTorr of inert background pressure. For InP, a mixture of stoichiometric InP and In nanocrystals with an InP/In ratio of ~1 resulted when ablating an InP target in argon (Ar) at 1 Torr. This InP/In ratio increased to ~5 when ablating the InP target in an Ar pressure of 750 Torr [Fig. (b)]. Upon air exposure, these semiconductor nanocrystals developed a ~2-nm-thick oxide outer layer.

Passivation of the semiconductor nanocrystal surfaces with sulfur gas (in the synthesis chamber prior to air exposure) failed to prevent the surface oxidation due to the poor vacuum level in the experimental apparatus (microTorr). In the case of the CoPt alloy, the stoichiometry in the target was not reflected in the collected nanocluster films, independent of the background gas pressure. Even in a vacuum, the stoichiometry of the target was found in the collected nanocluster films when an inconel target was ablated by a femtosecond laser; the constituents of inconel have similar vapor pressures while Co and Pt do not.

Our experimental results suggest that the stoichiometries of the PLD multi-element nanoclusters are closer to those of the targets when shorter than 25-ps lasers are used. However, this does not imply that simply irradiating a multi-element target in vacuum with a shorter than 25-ps pulse laser would automatically result in the formation of stoichiometric nanocrystals. Preserving the stoichiometry of the irradiated target and forming stoichiometric semiconductor nanocrystals require ablating the targets with a shorter than 25-ps laser in a background gas. The minimum background gas pressure is materials dependent. For metal alloys, the stoichiometry of the ablated target cannot be found in the collected nanocluster films if the constituent elements have widely different vapor pressures.

On the computational front, we have successfully used density-functional-based tight-binding potentials to study the material-removal process as a result of femtosecond laser–GaAs target interaction [Fig. (c)]. This code work can be extended to other multi-element compounds and alloys.

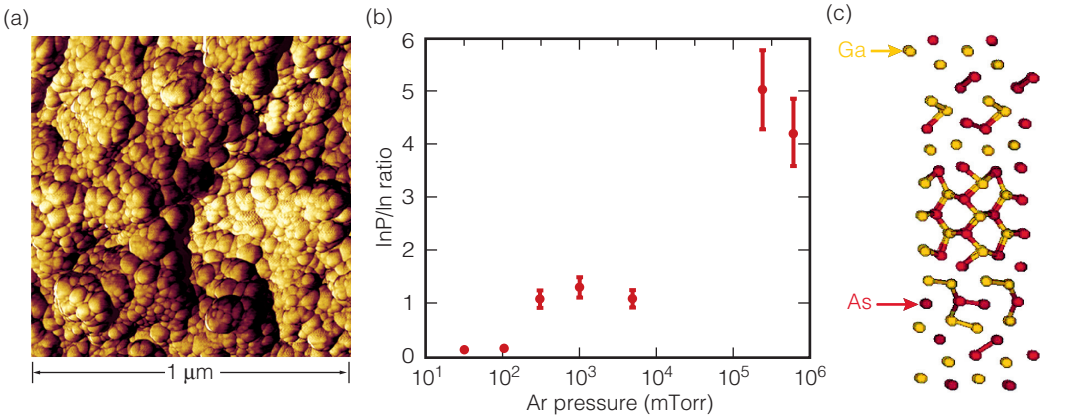

These three panels show the dependence of nanocrystal stoichiometry on the target composition and processing conditions (a and b) experimentally and (c) computationally. (a) Atomic-force microscopy image of GaAs nanocrystal film; (b) Indium phosphide/indium ratio in short-pulsed laser deposited films vs. inert background pressure; (c) computer model of gallium arsenide nanocrystal film1 ps after the onset of a 150-fs laser pulse.

High-accuracy x-ray imaging of high-energy-density-physics targets

W. Nederbragt, D. Schneberk, T. Barbee, J. Klingmann, S. Lane, J. Jackson

High-energy-density experiments play an important role in corroborating the improved physics codes that underlie LLNL's stockpile stewardship mission. Conducting these experiments will require improvements in diagnostics, in fabrication techniques, and especially in characterizing the target assemblies, which have millimeter-sized components with micrometer-sized features.

X-ray microscopy and tomography is one technique that holds promise for characterizing the internal structure of target assemblies. Submicrometer spatial resolution has been demonstrated using a synchrotron x-ray source, but that approach does not accommodate LLNL's requirements for a high-throughput, low-cost approach for characterizing production quantities of target assemblies.

This project is conducting the research and development of an x-ray microscope that uses a replicated multilayer Wölter Type-I optic. The fabrication of the optic is the key to the project's success. The replication technique coats a superpolished mandrel (see Figure) with reflective multilayer materials. The multilayers are covered with a 1- to 2-mm-thick layer of nickel to provide structural rigidity. The Wölter optic is then separated from the mandrel. This results in an optic with nearly the same figure and roughness as the mandrel. If successful, this microscope will provide high-throughput and high-resolution x-ray imaging of target assemblies in a laboratory setting. Moreover, this instrument would bring a new capability to the Laboratory that will have application to stockpile stewardship and a variety of other mission areas.

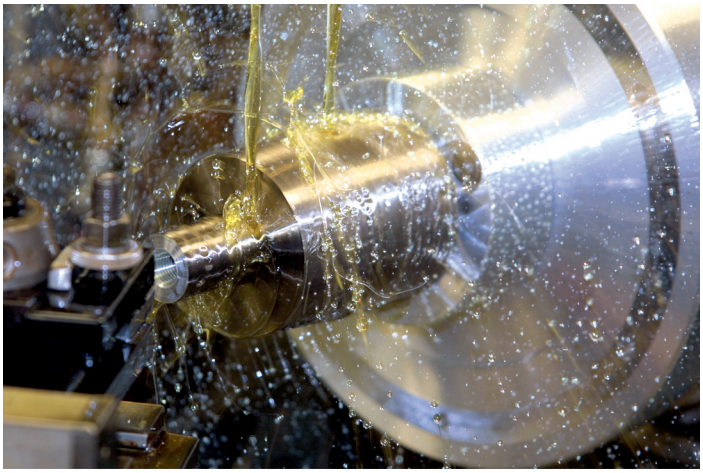

Diamond turning of the high-accuracy mandrel.

During FY2002, we designed the optical system, simulated the three-dimensional x-ray imaging properties of our optical design, and fabricated mandrels for creating the optics.

The optical design involved an extensive parameter study to determine the best design for our needs. Parameters included the maximum reflection angle, length, magnification, and collection efficiency (photon throughput) of the instrument. The maximum reflection angle was influenced by the use of multilayer technology, which was incorporated into our optical design. The result of the optical analysis was a microscope design with a length of 5 m, a magnification of 12×, and a solid collection angle of 0.0019 sr.

With the optical design complete, we constructed a test mandrel for testing and adjusting the multilayer coating process. Several more test mandrels were fabricated and used to test the mandrel–optic separation process.

The super-polished mandrel has been fabricated, coated with nickel, and diamond-turned to get the surface figure to less than 25 nm. After completing the diamond-turning process, the mandrels were superpolished to 3 to 5 Å. One mandrel can be used to fabricate several optics.

In FY2003, we will complete the mechanical design of the prototype microscope, fabricate several optics using the superpolished mandrel, construct the prototype microscope, and test the microscope using phantoms (test parts) and real target assemblies. If the project succeeds, this instrument will lead to the construction of a production microscope.

Precision hole drilling with a polychromatic, bimodal laser approach

H. W. Friedman

Rapid, precise drilling of submillimeter holes with a high aspect ratio is needed for many national security applications and industrial products, including turbine blades, aircraft wings, and fuel injectors. In addition, applications such as x-ray pinholes and neutron masks for the National Ignition Facility require 20-μm holes in millimeter-thick, high-*Z* metals. Ultrashort-pulsed lasers show promise but currently deliver poor beam quality, involve unexplained phenomena, are difficult to scale to high average powers, and require large, expensive vacuum chambers. Ultraviolet eximer lasers with lithographic imaging can achieve small features but lack the necessary throughput.

This project uses results obtained with inexpensive diode-pumped solid-state lasers (DPSSLs) that operate in the near infrared (1.06 nm) and the second harmonic (532 nm) to drill precision submillimeter holes with arbitrary shapes in metal and ceramic substrates.

These lasers operate in the ablative regime (flux from 0.1 to 1 GW/cm^2)—which enables short pulse duration (<100 ns) to minimize the heat-affected zone (HAZ)—and at high average power (300 W at 10 kHz) to achieve 1-s drilling times in millimeter-thick substrates. Drilling is bimodal, involving two lasers in separate steps. First, the infrared beam, sized roughly to the hole diameter, rapidly removes the bulk of the material and allows an escape path for debris. The second step uses a "trepanning" laser—a much lower power, but near-diffraction-limited (and therefore more precise) laser beam operating at the second harmonic wavelength and focused to one-tenth the infrared beam diameter. The trepanning beam cleans, shapes, and polishes the sides of the hole, so that both shape and cross section can be cut to the desired dimensions while maintaining a minimum HAZ. In this project, we have already demonstrated that with an infrared power level of 250 W at 13 kHz, a 250-μm hole can be drilled in a 1.5-mm substrate in ~1 s, with no measurable HAZ. If successful, this project will yield an improved technique for laser hole drilling that will produce high-quality holes with precise dimensions more quickly, cheaply, and reliably than previous methods. The techniques demonstrated in this project will find widespread use in LLNL's national security programs and in the aerospace industry.

In FY2002, we achieved second-harmonic generation with the frequency needed for trepanning laser operation, producing 20 W of 532-nm light at 13 kHz with a beam quality of less than three times the diffraction limit, sufficient for making holes a few hundred microns in diameter. Using a diffraction-limited beam expander and F2 lens, we focused the beam to a 20-μm diam with a power density of 5 GW/cm^2—much greater than the minimum for ablation.

With this beam, we demonstrated trepanning by drilling 20-μm holes with aspect ratios as high as 50 in several metals, including stainless steel, nickel, platinum, and tantalum. Drilling times were ~1 s, and metallographic studies indicated negligible HAZ (see Figures).

This project demonstrated the basic processes needed for the bimodal approach to precision hole drilling. The infrared and trepanning lasers were used to drill precise, submillimeter holes with a large aspect ratio in millimeter-thick substrates. Each step required only 1 s and resulted in no HAZ. The remaining work is to combine the two drilling processes with common-axis delivery optics to demonstrate precision hole drilling with a total process time of several seconds.

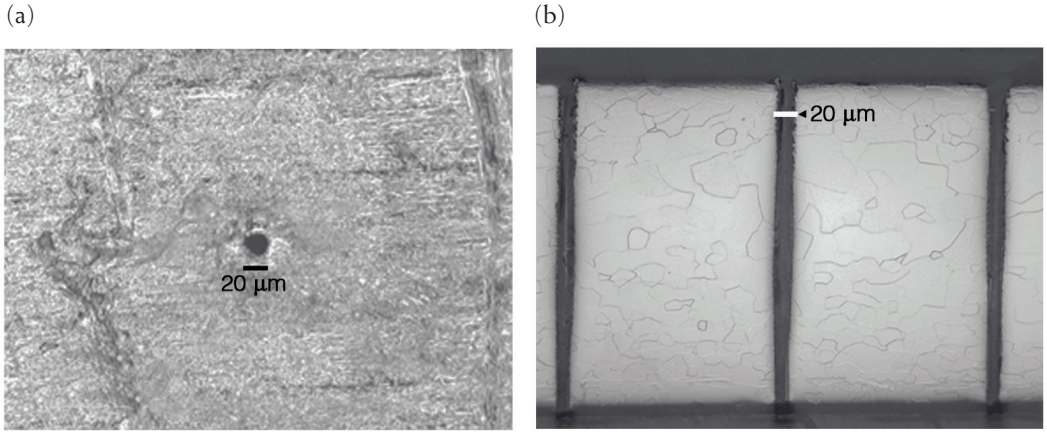

Using diode-pumped solid-state lasers operating in the near infrared and the second harmonic, we drilled precision submillimeter holes in metal and ceramic substrates. Drilling is a two-stage process, in which an infrared laser drills a hole slightly small than the final hole diameter, after which a narrower "trepanning" laser beam performs finishing. (a) Top view and (b) cross section of 20-μm precision holes drilled in a 0.75-mm-thick tantalum substrate with the trepanning laser. Drilling resulted in no heat-affected zone. Together, the high-power infrared beam and high-precision trepanning beam promise rapid, precise drilling.

A compact accelerator for proton therapy

G. J. Caporaso, J. Sullivan

Proton therapy as a treatment for cancer is superior to x-ray therapy. Because of Bragg-peak energy deposition, protons and other ions deposit most of their energy in the targeted tumor, rather than in healthy surrounding tissue. In contrast, x rays deposit more energy in healthy surrounding tissue than in the tumor. However, proton therapy is practiced at only four locations in the U.S. because of the large size and high cost of existing proton facilities. A compact, high-voltage, short-pulse proton accelerator being developed as a flash-x-ray radiography source for the Stockpile Stewardship Program could potentially be used in proton therapy, but obstacles include the need for an electrical closing switch that can operate at a high electric field stress, close rapidly, and last for many shots. The nonlinear, lateral, gallium arsenide (GaAs), photoconductive, semiconductor switch (PCS) is an attractive candidate for the closing switch in the compact proton accelerator application due to its small size, rapid closure, high gradient, and short pulse capability.

The goal of this project is to develop a PCS that would enable this type of proton accelerator—relatively inexpensive and small enough to fit in a single room—to be used medically. By potentially leading to the widespread use of proton therapy, this work supports LLNL's mission in bioscience and technology to improve human health.

The nonlinear, lateral, GaAs PCS is switched on by the optical generation of electron-hole pairs in the volume of the GaAs located between anode and cathode electrodes. The advantage of operating the GaAs PCS in the nonlinear mode is that a low-energy optical pulse of a few microjoules switches the device on. A disadvantage of operating the GaAs PCS in the nonlinear mode is that the switch current flows in constricted filaments. The high current density of the constricted current filaments damages the GaAs and the contact metallization at the GaAs/contact interface. The damage/erosion that accumulates at this interface during repetitive switching operations eventually leads to failure of the PCS. We adapted and proposed to extend techniques developed at Sandia National Laboratory to increase the lifetime of the nonlinear, GaAs PCS. The GaAs PCS lifetime can be increased by incorporating n- and p-type doped layers just below the cathode and anode metallizations. The doped layers force the current filaments to diffuse, lowering the current density at the GaAs/electrode interface.

Work in FY2002 focused on fabricating and testing a doped GaAs PCS. Standard microelectronic planar processing techniques were used to thermally diffuse silicon (Si) and zinc dopants below the electrodes on 2-in.-diam GaAs wafers. The diffusion patterns were defined by a mask. The result was two sets of PCS electrodes with shallow (~100 nm) diffused layers and ohmic contacts [Fig. (a)]. The Rogowski-profiled electrodes had a width and gap of 1.2 and 0.2 mm, respectively.

The GaAs PCS was tested with two 50-Ω transmission lines [Fig. (b)]. One line was pulse-charged to several kilovolts and sent a wave to the second line when the GaAs PCS was triggered by a high-power laser diode. Maximum voltage gradient was 52 kV/cm, meeting our goal of 50 to 100 kV/cm. Peak current was 112 A but was limited by transmission line impedance. Future work will improve the gradient by submerging the switch in a liquid dielectric and test the PCS at much higher currents.

(a) (b)

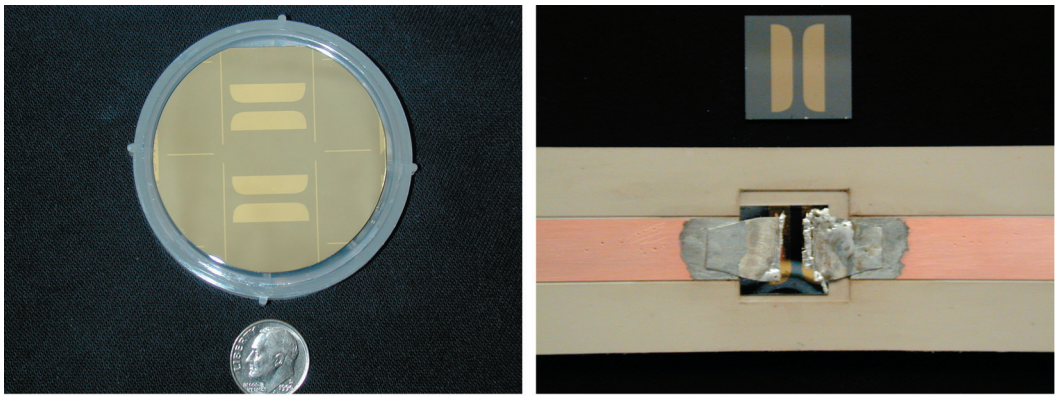

This project fabricated and tested a photoconductive switch (PCS) that could allow a compact, high-voltage, short-pulse proton accelerator to be used in proton therapy for cancer patients. (a) Two sets of PCS electrodes formed on a gallium arsenide wafer. (b) A PCS mounted between two 50-Ω transmission lines.

Extremely high-bandwidth, diamond-tool axis for weapons-physics-target fabrication

R. C. Montesanti, D. L. Trumper, J. L. Klingmann

Our project will enable the fabrication of high-contour-accuracy and low-roughness three-dimensional (3-D) target features for weapons-physics experiments using high-power lasers by expanding the bandwidth of a fast-tool-servo (FTS) axis to 10 kHz. This work will build on recent research efforts in the area of rotary-motion FTSs. Current capabilities are limited for fabricating 3-D target features, which are used to investigate weapons performance characteristics. At present, ultraprecise, single-point diamond-turning machining methods are the most accurate and efficient approach for fabricating certain target features, such as the longest spatial wavelengths of surface contours. These methods also offer the lowest risk for implementation.

This project proposes to develop a 10-kHz FTS—a short-stroke, fast machine axis that can be coupled with precision machines to create a unit that will enable us to use single-point machining to produce higher spatial-frequency surfaces while maintaining very high accuracy rates. A rotary FTS design was chosen because the reaction time is more easily managed than a linear force equivalent.

Initially we plan to develop a 2-kHz prototype FTS that will include a commercially available actuator. This approach will allow us to address high-risk controller issues associated with cutting dynamics and provide a system for target fabrication early in the project cycle. Once this new unit meets our desired specifications (a 10-kHz bandwidth with accurate motion control to 0.5 μm and high stiffness of 18 N/μm), knowledge gained from this work, and from ongoing research on three other FTS designs at the Precision Motion Control Laboratory at the Massachusetts Institute of Technology (MIT), will enable us to fabricate physics-target components that are beyond the reach of current fabrication technology. In addition, by expanding the bandwidth of this type of mechatronic device, our new unit will advance the state of the art in the precision-motion-control field.

During FY2002 we designed and operated the 2-kHz FTS in a closed-loop manner. The system includes an innovative (patent application in process) rotary architecture that minimizes disturbance forces and torques on diamond-turning machines used for target fabrication and a device that provides guided motion for the FTS while maintaining the stiffness needed for diamond turning. We also ordered fabrication of all parts, purchased a 2-kHz commercial galvanometer integrated with a digital controller, and developed a detailed design package for the 2-kHz FTS and sophisticated control algorithms.

In FY2003, we will assemble and integrate the mechanism for the 2-kHz system with the galvanometer and digital controller, refine the control algorithms, integrate the system with a diamond-turning machine at MIT to produce test parts, and develop an advanced actuator. The system will be transferred to LLNL by the end of the year.

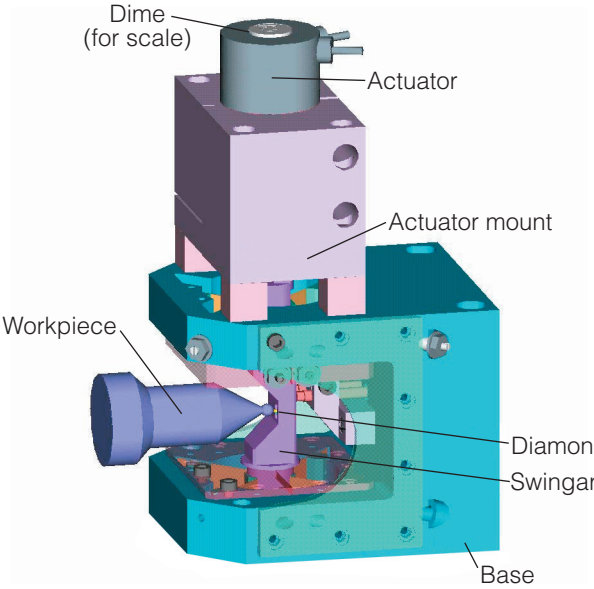

Computer-aided design of the 2-kHz fast-tool servo.

Nanoscale fabrication of mesoscale objects

R. P. Mariella Jr., A. Rubenchik, G. Gilmer, M. Shirk

High-energy-density experiments (HEDE) are expected to play an important role in corroborating the improved Advanced Simulation and Computing (ASCI) physics codes that underlie the Stockpile Stewardship Program. To conduct these experiments, several improvements are needed—both in the diagnostics for measuring experimental results and in target fabrication. This project is working on a new LLNL capability for improving fabrication and characterization of mesoscale (millimeter size) objects with micrometer-size features at nanometer-scale accuracy for HEDE targets. Other applications include pinholes required for a phase-shifting diffraction interferometer, microporous electrodes in miniature fuel cells, remote sensors, and medical technologies. To create a fabrication capability that is deterministic, this research combines modeling and experiments.

This project leverages LLNL expertise in modeling, simulation, and laser–surface interactions to develop a new capability for fabricating and characterizing mesoscale targets for weapons physics experiments in support of LLNL's stockpile stewardship mission.

In FY2002, we successfully combined three-dimensional (3-D) molecular dynamics (MD) modeling with the 1-D hydrocode, HYADES, to take advantage of the strengths of each approach. First, the laser–material interaction is tracked with HYADES. Then, well after laser pulse termination and the relaxation of the electron subsystem, the density, velocity, pressure and temperature profiles are passed on as initial conditions for the MD simulator. For 150-fs laser pulses on copper, this approach predicts void nucleation to occur within about 20 nm of the surface.

Experimentally, our studies included single-shot and multiple-shot ablation of single-crystal and polycrystalline, copper and gold targets, using 150-fs laser pulses at 800-nm wavelength. For laser pulses only slightly above the threshold for ablation, results show that the residual surface roughness is relatively independent of the total depth of the ablation crater. [Figs. (a) and (b)]. We have also observed that initial surface scratches, like those in Fig. (c), tend to be nucleation sites for the micropits that are formed during ablation. During FY2003, we plan to continue exploring the possibility of using submicrometer-spaced ridges, made by diamond turning of the surface prior to laser ablation, to "seed" and control the growth of these features.

Laser "polishing" could reduce the amplitude of submicrometer surface perturbations caused by ablation, without affecting the longer-length-scale pattern formed by this process. Using a Monte Carlo model of the crystal surface structure, we studied the effect of laser-heating the object to temperatures near the melting point. Though effective, the time required was too great for efficient processing. However, by modeling laser pulses that produce a transient liquid layer of controlled thickness (surface melting), we predict that the time required to smooth the surface could be reduced dramatically. The trade-off between the smoothening and freezing times determines the duration, period, and intensity of the polishing pulses.

In FY2003, we plan to use diamond-turned copper, gold, and nickel substrates to study the smoothening processes experimentally with excimer laser pulses at 193 nm.

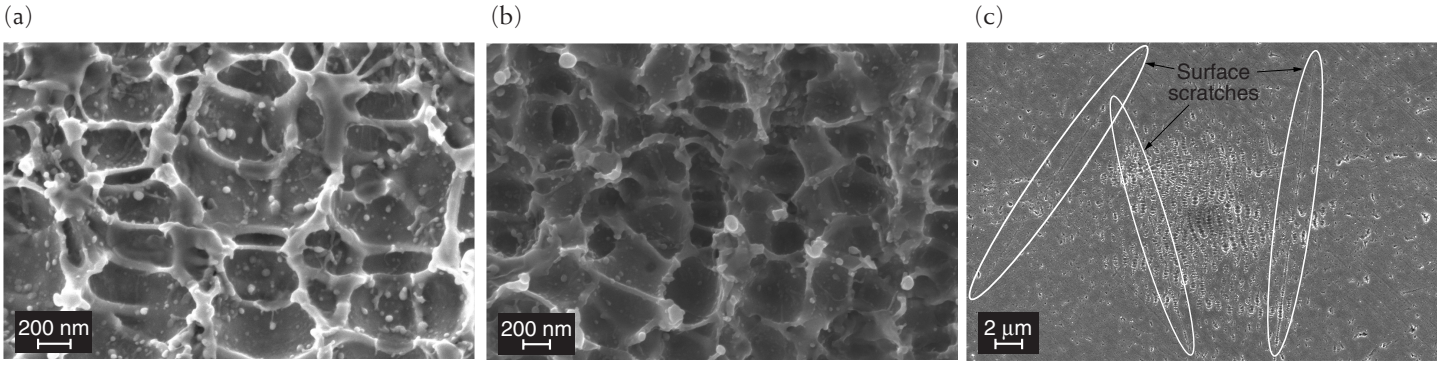

Photomicrographs of copper surfaces show little difference in surface roughness after ablation with (a) 5 and (b) 100 150-fs laser pulses at 800 nm. Microscale pock marks are seen in (c), some nucleating on initial surface scratches (circled areas).

Concealed-threat detection at multiple frames per second

S. G. Azevedo, J. Chang, R. L. Leach, C. Romero, J. E. Hernandez, V. R. Algazi (U.C. Davis)

In this project, we will investigate the efficacy of real-time imaging (10 to 30 frames/s) produced by an array of detectors using radar, acoustics, or another technology as a method for rapidly detecting hidden threats, such as weapons concealed under clothing or people hiding behind a wall, door, smokescreen, or fog. Security personnel attempting to detect such threats must make very fast assessments using minimal information. This project aims to develop a prototype of a detector-array-based system that will provide both the speed and specificity (i.e., a high probability of detection and low false-alarm rate) needed to respond quickly and appropriately to concealed threats.

Current detection technologies offer either speed or specificity, but not both. Devices in the first category (e.g., metal detectors, listening devices, and through-wall radars) notify the user immediately that a potential threat exists in a general area but cannot pinpoint the threat. However, after detecting the threat the user can move the instrument around that area to narrow down the search.

The second category of devices (e.g., x-ray backscatter, sniffers, and tomographic electromagnetic imagers) are much more discriminating and specific: they provide the precise location of the threat, with a low rate of false alarms. However, such devices are slow, complex, bulky, and require considerable computational resources. Their principal disadvantage is long processing times for acquiring and processing data into a high-definition image of a scene, which precludes a quick threat assessment.

The array-based detection system we envisage combines the benefits of both categories of devices: real-time (high-frame-rate) visual display; specificity; nonintrusiveness, i.e., causing no impediment to normal movement and traffic flow; ruggedness and portability; low-to-moderate cost; safety to users and the public, with no emission of ionizing radiation; automated detection of specific weapons or other threats; and audio feedback for the user.

This project focuses on radar, which penetrates all materials except solid-metal barriers and water. Virtually any object of any material that radar can penetrate will provide a radar image, although the backscattered intensity also depends on geometry and composition. Previous attempts to use radar detectors have produced single-element systems that provide either real-time but nonspecific scope traces or images that are detailed but that take time to reconstruct. Our approach will provide images in real time, allowing the user to detect a threat visually or aurally. The Figure shows an example of such a system—a real-time radar array detecting people inside a building.

In this first half-year of this project, we have shown, by simulated examples and statistical analyses, that real-time techniques measurably enhance detection. Our data-processing methodologies that incorporate novel array beam-forming hardware and software assist users to perceive threats in real-time and are applicable to real-time imaging.

Beginning in FY2003, we plan to design, assemble, and test a prototype detector array (radar-based or acoustic) that will demonstrate full-field imaging with an improved detection capability. We will also continue to develop simulation capability, algorithms research, and methods to deploy the system for field use. Studies will include standard analyses of image quality, the limitations of this technique due to electronic noise, clutter, etc., and time sensitivity. In conjunction with our collaborators at the University of California, Davis, we plan to conduct cognitive studies of human visual perception in relationship to array-based radar imaging.

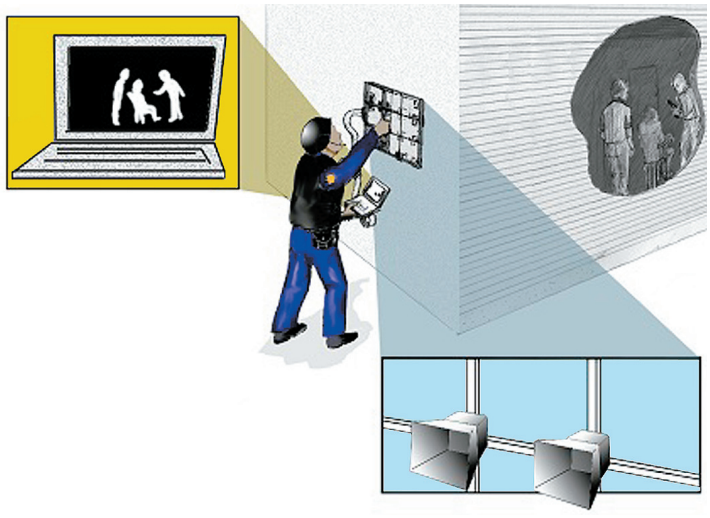

Concept drawing of a portable real-time radar array being used by security personnel in a hostage situation. When the portable array of radar detectors is held against a building's exterior wall, the handheld imaging unit provides a real-time image of the people located inside. Insets show (left) a close-up of the image display and (bottom) the detector array.

Low-voltage spatial light modulator

A. P. Papavasiliou

Spatial light modulators (SLMs) are electro-optic devices for modulating the phase, amplitude, or angle of light beams. Applications for arrays of SLMs include turbulence correction for high-speed optical communications, imaging through distorting media, input devices for holographic memories, optical manipulation of DNA molecules, and optical computers. Devices based on microelectromechancial systems (MEMS) technology have recently attracted special interest because of their potential for greatly improved performance at a much lower cost than liquid-crystal-based devices. The new MEMS-based SLM devices could have important applications in high-speed optical communication and remote optical sensing in support of DoD and DOE national security missions.

Present MEMS SLMs are based on parallel-plate capacitors, in which an applied voltage causes a suspended electrode to move towards a fixed electrode. They require relatively high voltages, typically on the order of 100 V, resulting in (1) large transistor sizes, which are available only from specialized foundries at significant cost and which limit the amount and sophistication of electronics under each SLM pixel; and (2) large power dissipation per area, which requires heat removal due to the optical precision required (~1/50th of a wavelength).

This project studied the feasibility of a three-electrode actuator technology that promises to reduce the switched voltage requirements and linearize the response of spatial light modulators. By adding a third electrode and the ability to tune nonlinear springs, our SLM design can reduce the required switched voltage and increase the linearity of the voltage-displacement response.

In FY2002, we achieved three major technical goals: (1) developed computer models that demonstrate substantial advantages offered by this technology [Fig. (a)], (2) determined a fabrication method and optimal designs for test devices, and (3) fabricated and tested those devices. Figure (b) is a microphotograph of the three-electrode actuator.

The computer models we developed demonstrate the advantages of the three-electrode actuator in comparison to the conventional parallel-plate actuator. Displacements comparable to the conventional actuator are possible with less than one-third of the switched voltage, and the voltage-displacement characteristics are significantly more linear. Using the computer model and optimal design techniques, we created designs for test structures that maximize linearity and can be fabricated in a standard MEMS foundry process. We had parts fabricated and tested those parts. The results show that the actuators behave as predicted: increasing bias voltage on the third electrode increases linearity and reduces required switched voltage.

(a)

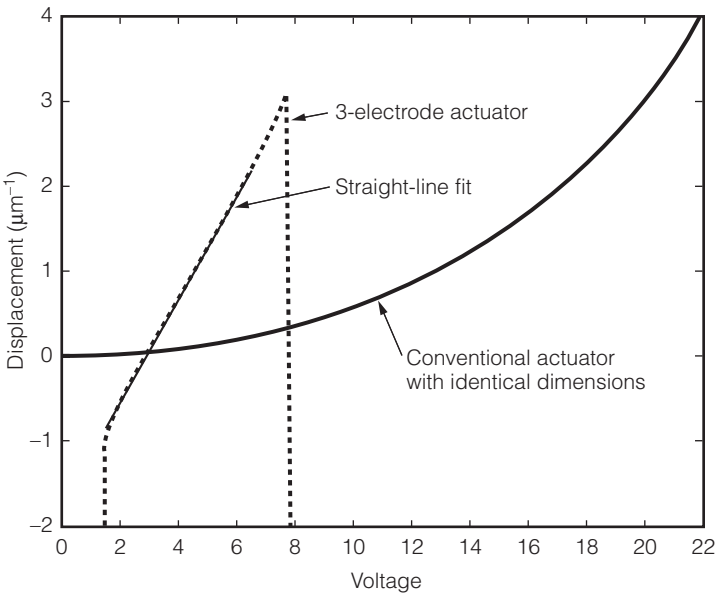

(b)

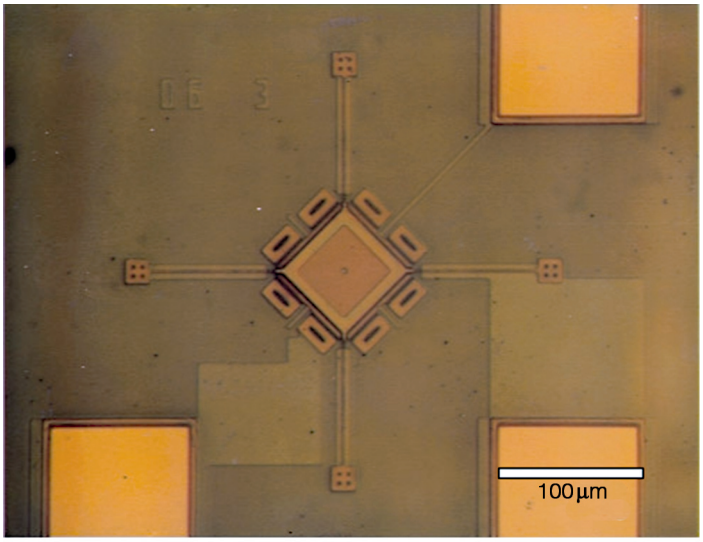

(a) Plot of simulated actuator response; (b) photograph of actuator.

Materials Science and Technology

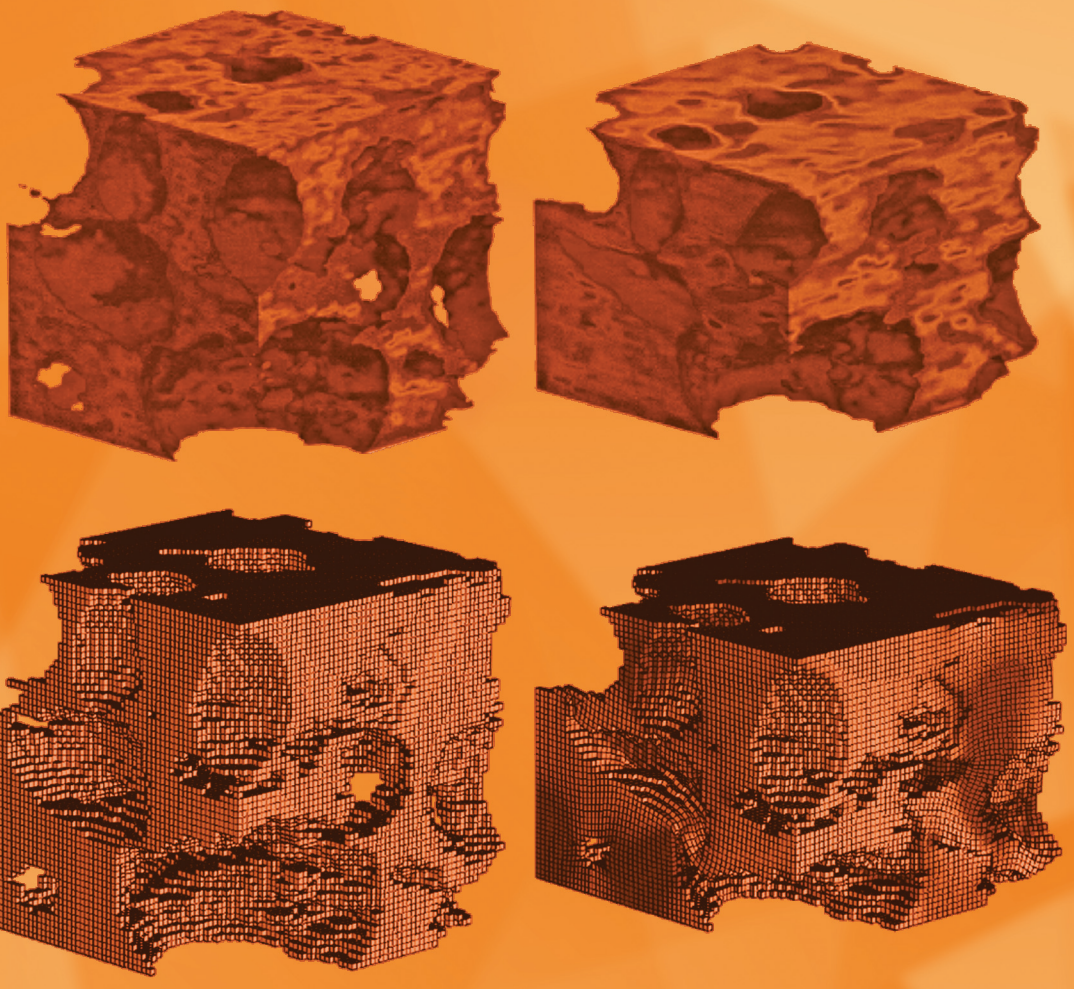

Section 7

Section 7 — Materials Science and Technology

Material strength at high pressure

D. H. Lassila, B. P. Bonner, V. V. Bulatov, J. U. Cazamias, E. A. Chandler, D. L. Farber, J. A. Moriarty, J. M. Zaug

Various aspects of the Laboratory's stockpile stewardship mission depend on accurate computer code simulations of plastic flow (i.e., nonreversible deformation) under high hydrostatic pressures. Current strength models cannot be extrapolated to high pressure because they are not based on the underlying mechanisms of plastic deformation.

The principal mechanism of plastic deformation in metals is the generation, motion, and interaction of dislocations (line defects) in the crystal lattice. The primary goal of LLNL's multiscale modeling effort is to account for the mechanisms associated with dislocation motion, multiplication, and interaction in strength models used in computer code simulations.

Multiscale modeling uses the results of simulations of mechanisms that occur at small length scales, e.g., dislocation mobility, as input to simulations of plastic deformation at larger length scales. Dislocation dynamics simulations are the critical links that make this connection possible.

This research project focuses on new developments of physics-based dislocation dynamics simulation capability for predicting the strength of body-centered-cubic (bcc) metals under high pressure. This work involves coordinated modeling, simulation, and experimental studies of physics associated with dislocation phenomena at high pressures and high strain rates.

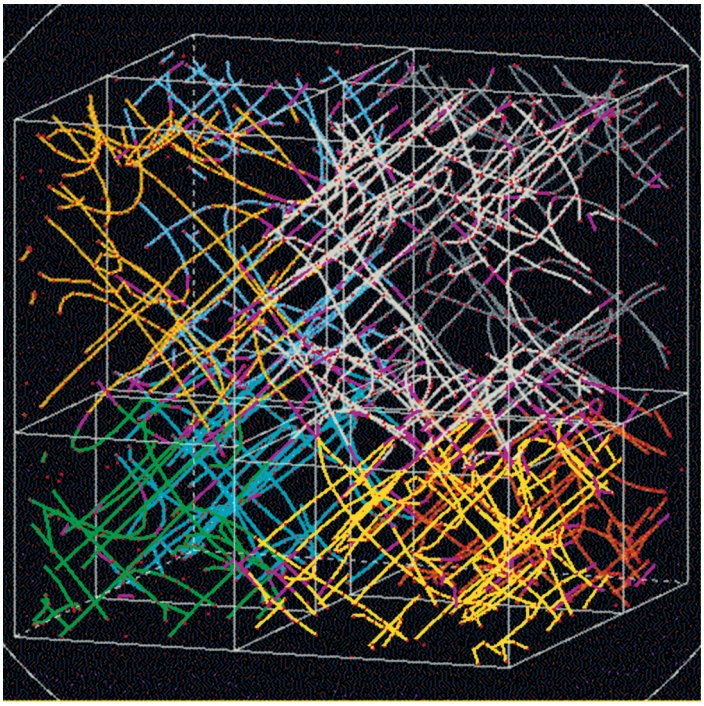

Three-dimensional atomistic simulations provide detailed information on dislocation mobility and associated defect production. This information is used in higher-length-scale dislocation dynamics simulations of plastic flow.

Although the fundamental nature of plastic deformation of metals at high pressure is similar to that at low pressure, involving the generation, motion, and interaction of dislocations, these unit mechanisms can be substantially different at high pressures and high strain rates. As part of our research, we are examining various dissipative mechanisms of dislocation mobility over a range of pressures in full atomistic detail.

Results in FY2002 include new information on the effect of the atomic structure of the dislocation core and state of stress on dislocation mobility at high velocities (on the order of 1000 M/s). Some of the most recent atomistic simulations make use of recently developed interatomic potentials that include pressure dependence.

The first ever, all-parallel dislocation dynamics code is now running on the latest parallel computing platforms at LLNL. In FY2002, the code framework was completed and a simulation (see Figure) with over 1 million dislocation segments—a critical milestone—was run.

All of our experimental work is being performed using high-purity oriented single crystals. In FY2002 we performed an initial set of experiments to probe the effects of high pressure and high strain rate on the strength properties of molybdenum and tantalum crystals. These experiments include diamond anvil cell (DAC) "stack" experiments, dynamic gas gun, and Hopkinson bar experiments. One of our notable achievements was the creation of a new Bridgman cell capability named "tri-anvil." This experiment can provide critical data on the effect of pressure (up to 50 GPa) on the work hardening of bcc metals.

In FY2003 we plan to complete our experimental capability developments of the DAC stack and tri-anvil experiments. However, a substantial effort will be devoted to measurement of strength at high pressure and to determine deformation-induced dislocation structure for validation of dislocation dynamics simulations. We plan to develop and carry out deformation experiments to measure material strength to validate simulation results, including deformation-induced dislocation structures. A 100 to 700-kbar DAC, a 30 to 400-kbar Bridgman cell, and gas-gun experiments will be used to determine yield strength.

Ultrafast materials probing with the Falcon linac–Thomson x-ray source

P. T. Springer

The goal of this project is to enable unprecedented dynamic measurements in matter by developing the Picosecond Laser Electron Interaction for Dynamic Evaluation of Structures (PLEIADES), a novel x-ray source based on Thomson scattering of short laser pulses from relativistic electron bunches. PLEIADES will use the interaction between ultrashort light pulses from the 35-fs Falcon short-pulse laser and a cosynchronous, tightly focused electron beam from LLNL's 100-MeV linear accelerator (see Figure) to produce tunable, ultrafast, hard (10 to 200 keV) x-ray pulses that greatly exceed existing third-generation synchrotron sources in speed (100 fs to 1 ps), brightness (10^{20} photons/mm^2/s/mrad^2, 0.1% bandwidth, and $>10^9$ photons/pulse), and simplicity.

Our research will demonstrate this new Thomson x-ray source as an enabling technology for ultrafast x-ray probes of material dynamics, a next-generation experimental capability for the Stockpile Stewardship Program (SSP). For example, this new, ultrafast x-ray source will have sufficient intensity to enable time-resolved pump-probe experiments to examine the time-dependent behavior—e.g., equations of state, phase-transition dynamics, structure, melting, and recrystallization—of laser-excited materials of interest to the SSP. PLEIADES will also establish LLNL's leadership in advanced laser and accelerator research and development.

FY2002 accomplishments include (1) producing and demonstrating a 100-MeV electron beam capable of a 1000-A current, a 1-ps pulse duration, and a 10-μm focal-spot radius; (2) completing and commissioning the beam line; (3) completing the integrated modeling of beam performance; and (4) beginning initial interaction experiments to demonstrate and characterize x-ray production at 10 to 200 keV.

Research proposed for FY2003 will involve a series of applications experiments that will take advantage of the unique characteristics of the Thomson source—the large single-pulse flux, ultrafast time resolution, and narrow spectral bandwidth. Two experiments that have scientific and stockpile-stewardship applications will be conducted: (1) a dynamic diffraction experiment involving bismuth, a high-Z metal that has numerous phase transitions in the 100-kbar range associated with changes in crystal structure and volume collapse; and (2) a spectroscopy experiment to examine the phase transition and volume collapse associated with changes in the electronic structure and localization of praseodymium, used because its electronic effects in the phase diagram are similar to those of plutonium, a metal of keen interest for stockpile stewardship.

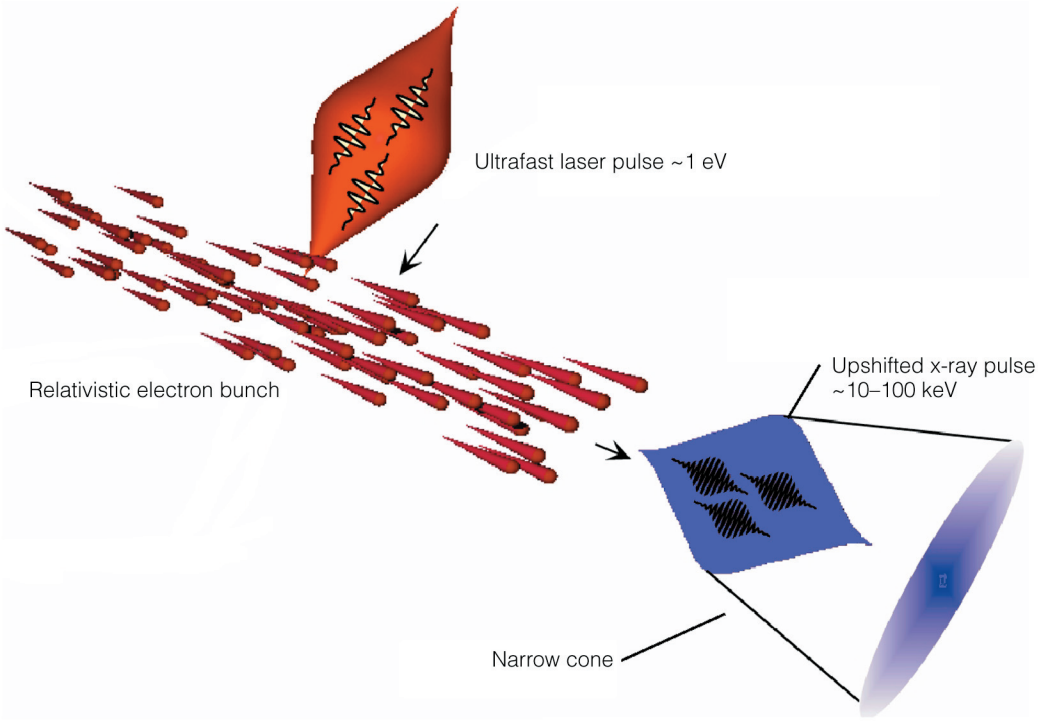

Scattering a short-pulse laser from a relativistic electron beam generates an ultrafast x-ray beam for dynamic materials experiments. The narrow cone concentrates the x rays into a small area.

Reconfigurable, optical code-division multiple access for fiber-optic networks

S. W. Bond, I. Y. Han, C. V. Bennett , E. M. Behymer, V. R. Sperry, S. J. Yoo

High-speed, high-capacity fiber-optic communications networks, which allow multiple users to access the same network simultaneously by sharing the same transmission medium, have proliferated for long-distance, metropolitan, and local-area communications systems. Recently, a rapid expansion has begun into wavelength-division multiplexing (WDM) systems, which use multiple wavelengths to increase capacity. In addition, code-division multiple-access (CDMA) techniques, which were originally developed for wireless communications, can also be used to further increase the number of channels on an optical fiber.

This project entails the development of advanced technologies that have potential applications to national security—such as secure, high-speed transmissions—and that will enhance LLNL's competencies in optoelectronics and high-speed communications.

By applying innovations in WDM-component technology, we are developing a compact optical CDMA encoding and decoding device that would handle large code sizes, be remotely reconfigurable by a network operator, and be compatible with commercial fiber-optic infrastructures. The device, which would be comprised of two indium phosphide (InP) arrayed waveguide gratings (AWG) and an array of InP phase modulators, would allow each user of a network to spectrally phase-modulate (encode) a broadband, ultrashort, transmitted optical pulse. Only the intended recipient, in possession of the correct complementary phase code, would be able to decode the transmitted information. The use of InP enables single-chip integration of active and passive components for operation at telecommunication wavelengths of ~1550 nm, which is not possible with other semiconductor materials.

(a) (b)

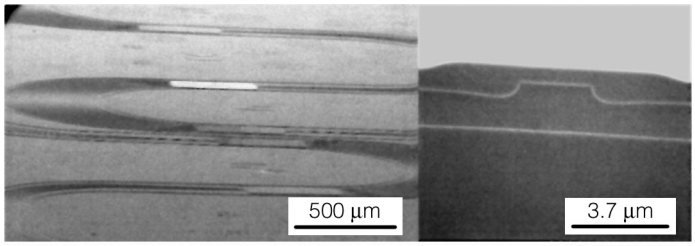

Scanning electron microscope photographs of indium phosphide (InP) components fabricated for a compact optical code-division multiple-access device: (a) An arrayed waveguide grating created by wet-etching InP material grown by metal–organic chemical vapor deposition (MOCVD). (b) InP top cladding material regrown on a rib waveguide using MOCVD.

Our approach uses broadband, ultrafast (300-fs) pulses from an actively mode-locked, erbium-doped, fiber-ring laser operating at 1.55 µm with a 2.488-GHz repetition rate, which is equivalent to a SONET OC-48 rate. These pulses are spectrally phase-encoded by transmitting them through the monolithically integrated semiconductor device. In this process, the input AWG, functioning as a diffraction grating, spectrally slices the input pulse. Next, the spectral components are phase delayed by an electrically controlled waveguide phase modulator and then recombined by the output AWG for insertion into the network. This device allows a network operator or user to change the transmitted or received code at very high speeds by phase-trimming each spectral slice of the optical pulse.

In FY2002, we (1) utilized the waveguide and device designs made in FY2001 to grow InP material for the AWGs using metal-organic chemical vapor deposition; (2) demonstrated wet-etched fabrication of an AWG device [Fig. (a)]; (3) developed InP regrowth techniques for creating an upper cladding material for some waveguide designs [Fig. (b)]; and (4) installed an electron cyclotron resonance (ECR) dry-etching facility for improved curved waveguide fabrication.

In FY2003, we plan to complete fabrication of the InP-based integrated device using the ECR dry-etching facility and to demonstrate spectral phase coding of a 300-fs optical broadband pulse.

Shock recovery of organic liquids: From the origin of life to the defense of the Nation

J. G. Blank

The origin of life on Earth remains one of the key questions in modern science, with far-reaching implications not only for our own origins but also for the prospects of life on other planets. The defense of the nation against ballistic missiles carrying chemical or biological agents is a major national-security objective involving a multiyear investment of more than $100 billion. Ironically, these two disparate subjects are connected at a fundamental level by questions concerning the fate of organic liquids subjected to strong shock compression.

In this project, we are defining a new scientific niche, that of high-pressure-shock organic chemistry, with relevance to issues of national defense, public curiosity (as related to life's origins), and basic scientific research. This project allows direct assessment of organic chemistry occurring under extreme pressures and temperatures relevant to cometary impacts. It also provides, for the first time, laboratory simulations directly applicable to real conditions of a missile interception and allows us to gauge chemical evolution of warheads interrupted en route to their target.

The scope of our project is deceptively simple: shock organic liquids to extreme pressures, recover these liquids, and characterize their resulting chemistry as a function of pressure, temperature, and duration of the high-pressure pulse. Our objective is to determine the survivability of (a) organic compounds delivered to Earth or other terrestrial bodies via a cometary impact and (b) chemical weapon (CW) simulants released when a ballistic missile is intercepted. Based on the results of our impact experiments using aqueous solutions doped with amino acids as a comet proxy, we constrain models for the flux of organic compounds to the early Earth. Analogous experiments on CW simulants will determine whether part of a deadly payload may be rendered inert by shock and whether chemical byproducts might be suitable for remote sensing of successful intercepts.

In FY002, 16 shock-recovery experiments were conducted using a 6.5-m two-stage light gas gun, and we achieved the major milestone of bringing shocked-liquid recovery capability to LLNL. Additional accomplishments in FY2002 include: (1) successful impact loading of a liquid solution up to 40 GPa in a stainless steel capsule; (2) retrieval of up to 95% of the shocked liquids using a novel metal-piercing device; (3) quantitative measurement by liquid chromatography and mass spectrometry of two-amino-acid aqueous solutions and identification of dipeptides produced from shock (see Figure); and (4) verification of chemical change in shocked di-isopropyl methyl phosphonate and 2-di-isopropyl aminoethanol in experiments using these CW analogs. We also began a complementary quantum simulation of dipeptide formation in aqueous solutions to investigate the pressure dependence of the rate of peptide formation.

In FY2003, we are in production mode and will apply our method to suites of liquids subjected to an array of shock conditions. We will enlarge our numerical modeling to address amino acid polymerization and CW analog breakdown via shock processing.

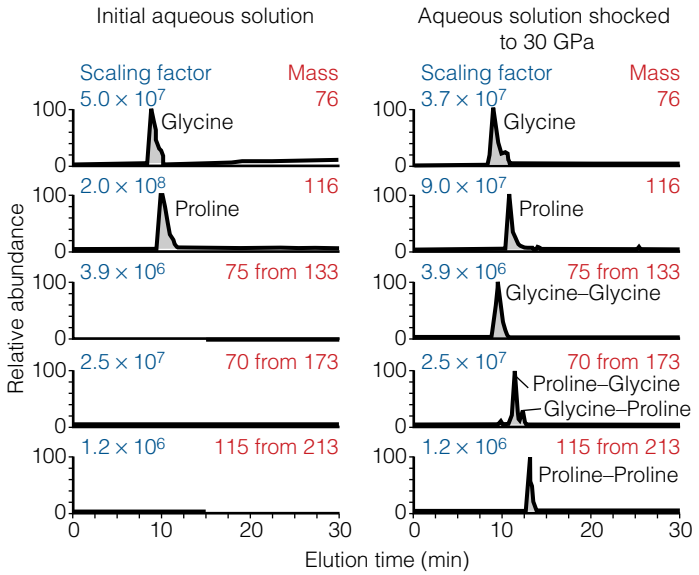

Comparison of an aqueous solution before and after shocking reveals the production of dipeptides (glycine–glycine, glycine–proline, proline–glycine, and proline–proline) as well as persistence of a fraction of the initial amino acids glycine and proline.

Microstructural origins of dynamic fracture in ductile metals

J. Belak, J. Cazamias , M. Fivel, D. Haupt, J. Kinney, M. Kumar, R. Minich, R. Rudd, A. Schwartz

From the formation of microscopic cracks in the fuel pipe liner of the Space Shuttle to the safety of roadway bridges, the fracture of materials has enormous implications throughout our society. The ability to assess and design safe engineering structures requires a detailed knowledge of this failure process. The fracture process depends on both the loading history and the detailed microscopic structure (microstructure) of the material. Weak points, such as inclusions and grain boundary junctions, are the locations from which microscopic fractures (voids and cracks) originate. Once nucleated, these fractures quickly link together to form a macroscopic crack. Despite this qualitative understanding, little is known about void nucleation, plastic deformation in the surrounding material, and the mechanisms of linking.

Central to stockpile stewardship is an understanding of shock loading of materials. During the passage of a shock wave, the material is compressed at a high rate. This compression produces a high density of dislocation defects and other changes to the microstructure that are poorly understood. When the shock wave reflects from a free surface, the compression is rapidly released and extreme tension is produced inside the material. If this tension exceeds the internal rupture strength, microscopic fractures form and link up to create a spallation layer—a thin scab that separates from the bulk of the material.

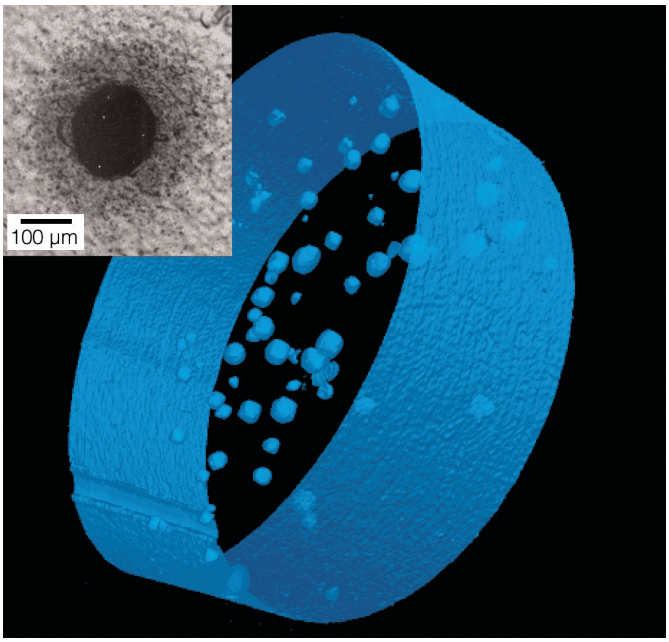

A three-dimensional tomographic image of incipient spallation in 6-mm-diam piece of single-crystal aluminum. The insert shows the halo of dislocation pits surrounding one of the voids.

In this project, we use LLNL's gas gun to produce a planar stress pulse with controlled duration and amplitude. The sample is carefully captured in soft foam while measuring the free-surface velocity profile. The amount of change in the surface velocity during release is related to the spallation strength. We study light metals—aluminum (Al), vanadium (V), titanium (Ti), and copper (Cu)—with known initial microstructure: single crystal, polycrystalline, and single crystal with engineered inclusions. Light metals enable direct measurement of the three-dimensional (3-D) distribution of damage using x-ray tomography. After the tomography experiment is complete, the samples are sliced and analyzed using 2-D metallography.

During FY2002, we continued our study of polycrystalline Al and completed a study on pure single-crystal Al. These samples were scanned at the Stanford Synchrotron Radiation Laboratory and 3-D x-ray tomographic images were produced. The image of single-crystal Al shocked at 166 m/s along the [011] direction is shown in the Figure. In contrast to our polycrystalline studies, in which the void size distribution is represented by an exponential function, the distribution in this single-crystal study required a Gaussian function in addition to the exponential one, indicating a bimodal distribution of void. Many of the voids are faceted, consistent with our direct numerical simulations of void growth. Shown in the figure inset is a 2-D metallographic image of one of the large voids. The halo in the metal surrounding the void is revealed by the surface preparation process. The surface etches at a greater rate near a dislocation core, resulting in a surface pit. The halo is a cloud of surface pits that demonstrate the high density of dislocations in the region surrounding the incipiently grown void. This is the first direct measurement of the plastically deformed zone in void growth. We have further analyzed this zone with orientational imaging microscopy to reveal the direction of slip and with nanoindentation to reveal the enhanced hardness inside the zone. Research using transmission electron microscopy to reveal details of the dislocation structure is currently under way.

In FY2003, we will complete our study in body-centered-cubic C, hexagonal-close-packed Ti, and face-centered-cubic Cu with nanoscale (20-nm) inclusions to make direct overlap with our numerical simulations.

Shear localization and fracture in shocked metals

G. H. Campbell, F. X. Garaizar, J. M. McNaney, D. P. Trebotich, M. Kumar

Metals are used in structural-engineering applications because they yield and deform before they break. However, under certain conditions of dynamic loading, metals can fail prematurely. This behavior is often associated with shear localization phenomena, in which a shear band acts as a precursor to crack formation. These phenomena have been observed in metals for some time; however, modeling this behavior in a continuum-simulation code has met with very limited success. In this project, we are pursuing a series of model experiments closely linked to new model development to gain a fundamental understanding of shear localization and fracture.

Many NNSA- and DoD-related missions require modeling and simulation of the response of metals to high-explosive (HE) loading to determine whether those metals fail or fracture. High-explosive loading differs from the loading experienced by a specimen in a traditional engineering application. In HE loading, detonation causes a strong shock to pass through the metal. This shock completely changes the microstructure of the metal by inducing intense dislocation multiplication, sometimes accompanied by the formation of deformation twins. This change in microstructure strongly modifies the mechanical response of the metal, changing its yield strength, work hardening rate, and strain to failure. Only after this complete change of microstructure does the metal start to deform due to the velocity imparted by the shock and the further acceleration from the high-pressure HE detonation gases.

Our multidisciplinary approach couples experiments with the development of a new simulation capability aimed at capturing the important physics involved with failure and fracture. The experimental approach is to break down the process into two steps, first by creating microstructures in our test specimens that are representative of the shocked state, and then performing the mechanical and fracture tests.

The preshocked microstructure is induced by laser-shock processing (LSP). This method is considerably easier and less expensive than recovering material from HE-driven experiments. The first year of the experimental effort was spent in determining the appropriate LSP conditions for the materials of interest. The mechanical properties were measured by tensile tests at differing strain rates. The microstructures were characterized before and after deformation, and the differing mechanical response could be explained based on the differing microstructural evolutions observed. The second year, FY2002, was spent developing the fracture-toughness testing methodology that would be most appropriate for the 1-mm-thick specimens needed for LSP. The choice was an elastoplastic analysis of the critical strain energy release rate to characterize the fracture toughness.

In FY 2002, the modeling and simulation effort has centered on building a simulation capability suited to the unique challenges posed by fracture and failure. The large strains associated with ductile failure dictates the use of an Eulerian code. Our approach incorporates explicitly conservative schemes in the quantities of energy, density, and momentum to predict wave structures accurately. The code will be inherently three dimensional, parallel in implementation, and incorporate adaptive mesh refinement. These capabilities are enabled by building the code with the SAMRAI toolbox developed at LLNL. A working version of the code produced the simulation shown in the Figure.

In FY2003, the project will concentrate on characterizing the process zone surrounding the tip of a propagating crack. We will measure the fracture energy of pristine and LSP material. Interrupted tests will allow us to investigate the crack-tip process zone by cross-sectioning techniques. The picture of the crack-extension process through void nucleation, growth, and linkage will allow us to develop a micromechanics model of the crack-tip process zone.

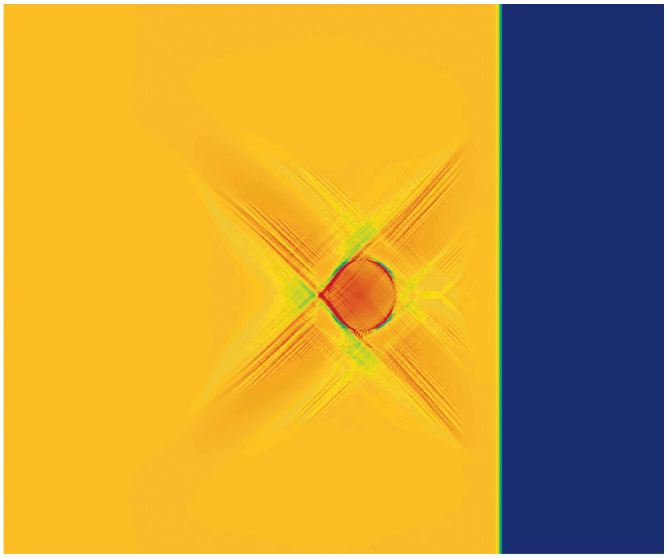

Simulation of a shock interacting with a soft inclusion in copper. The shock front (vertical line moving from left to right) has passed through the inclusion, and colors indicate levels of plastic strain. The yellow material is shocked and at a high level of strain, while the blue material is as yet unshocked and has a zero level of strain.

Life performance, including long-term aging of polymer systems with significant microstructure

G. B. Balazs, S. J. deTeresa, H. E. Martz, E. J. Kokko, J. M. Caruthers

Polymeric components and systems, although often required to function for many years, can exhibit significant degradations in performance from factors like chemical reactions, thermal stresses, and vibration-induced fatigue. It is impractical to performance test materials and components for their design lifetimes and impossible to do so for new materials that have only been available for a fraction of their design lifetime. Models that predict the aging behavior of polymer systems are needed, but currently available models typically extrapolate from historical data with the hope that the aging process is linear. Rational models that acknowledge the underlying chemical and physical processes of aging are needed.

The development of rational models for complex polymeric materials has enormous technological implications. These materials are (a) critical in a variety of current systems relevant to LLNL national security missions, (b) employed in numerous DOE and Department of Defense applications, and (c) currently used in industrial and consumer applications worth hundreds of billions of dollars each year. The main goal of this project is to develop a methodology for integrating polymer-aging parameters into modeling codes for component lifetime predictions that are applicable to all polymer systems.

In FY2002, we continued our multidisciplinary work on bridging the molecular (i.e., chemistry and materials science) to continuum (i.e., mechanical engineering) domains. Having completed the preparation matrix of virgin and controlled-damage samples for our material of interest—a silica-filled silicone foam, a solid polymer—we completed the mechanical, chemical, and microstructural characterization of this material.

This work included using solid-state nuclear magnetic resonance to perform further measurements of the effect of gamma radiation on the solid polymer's motional dynamics, and completing all of the uniaxial and biaxial (disc inflation) tests of material that was irradiated in a stress- and strain-free state. Additionally, we quantified the amount of tensile and compressive "set" exhibited by this material after irradiation in a stressed state; this data will be incorporated into the hyperelastic constitutive models being developed by our collaborator at Purdue University.

For the macroscopic domain, we refined our analysis methods for the transformation of computed tomography (CT) image data on the polymer foam into meshes suitable for finite element analyses (FEA). We designed, built, and collected image data using a fixture to compress the samples while under irradiation, and took images of the foam before and after compression, and before and after irradiation and compression. A remarkable aspect of these data is the lack of elastic rebound on unloading but with no evidence of visible degradation in the specimen. We believe this is due to the permanent set effect noted above. The Figure shows an example of a reconstruction of image data of the foam, along with the associated FEA meshes.

This project made substantial advances in the development of constituitive equations that describe the mechanical properties of an aging polymer system. However, despite the apparent simplicity of this goal, it is an enormous technological modeling problem that has never been solved, even for simpler systems such as crystalline (metal) structures. We demonstrated that computed tomography imaging could be used to provide the input mesh for FEA codes, and that (simplified) equations could be inserted into these models for testing, with the ultimate "age-aware" models that can be incorporated later.

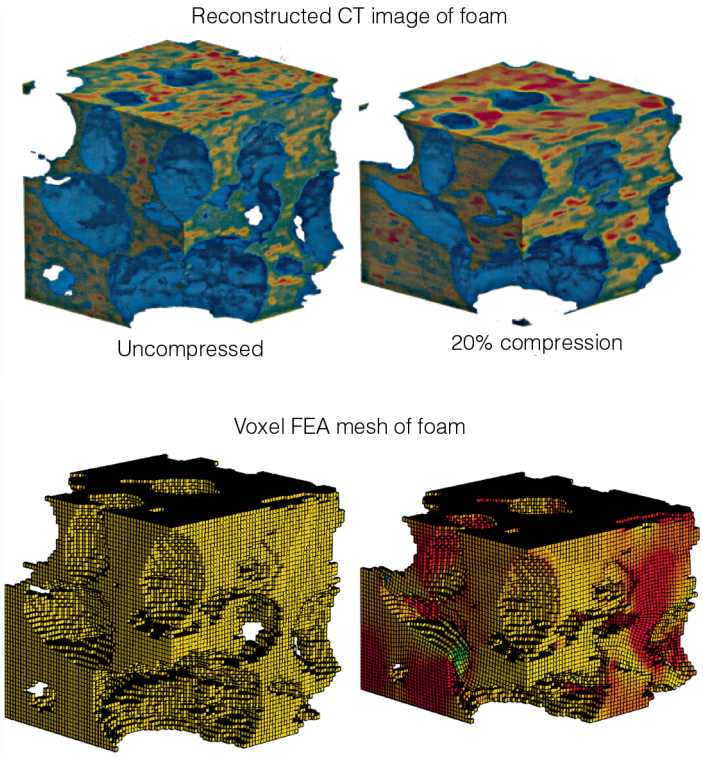

(top) Reconstructed computed tomography images (left) uncompressed and (right) under 20% compression; (bottom) corresponding voxel representation of finite element analysis (FEA) under the same deformations.

Metastability and delta-phase retention in plutonium alloys

A. J. Schwartz, K. J. Blobaum, J. J. Haslam, C. R. Krenn, M. A. Wall, W. G. Wolfer, J. Wong

The displacive martensitic phase transformation is one of the most challenging problems in physical metallurgy and requires simultaneously treating thermodynamics and kinetics controlled by materials properties. An extreme example is delta-stabilized plutonium (δ-Pu) alloys. Here, the δ-to-α' phase transformation results in a density change of ~20%, indicating that stress and plastic accommodation play central roles. By investigating this problem, we expect significant progress in dealing with similar issues in other important areas, including long-term storage of nuclear waste and reactor and fusion-energy materials, as well as aging problems of interest to stockpile stewardship. An important result will be a deeper understanding of the role of microstructure, solute content, and stress in the stabilization of the δ phase and development of the scientific basis for future stockpile stewardship in support of LLNL's national-security mission.

Our goal is to develop the physical framework to describe and predict important features of the transformation, such as martensite start temperature and hysteresis width. Our approach uses experience with other metastable alloy systems undergoing martensitic transformations but recognizes the unique physics of Pu. Our plan involves the experimental measurement, microstructural characterization, and predictive modeling of the thermodynamics and kinetics.

In FY2002, we complemented our resistivity, optical microscopy, and transmission electron microscopy (TEM) capabilities with differential scanning calorimetry (DSC), x-ray diffraction (XRD)—including time-resolved XRD for in situ observation of the low-temperature δ-to-α' transformation—and extended x-ray absorption fine-structure (EXAFS) analysis. We determined a reproducible martensite start temperature and transformation hysteresis for our reference alloy based on resistivity; performed quenching experiments to explore the effect of transformation temperature on microstructure; and conducted initial EXAFS experiments, which successfully identified both the α' and δ phases in one of these quenched alloys. In addition, a three-dimensional simulation code obtained in collaboration with Rutgers University was used on LLNL supercomputers to model the growth of α' plates (see Figure) and was extended to include the effects of plasticity that may occur during transformation.

In FY2003, the focus will be on optical and TEM microstructural characterization of quenched specimens; resistivity and DSC measurements of the three alloys; and XRD and EXAFS characterization of the α' phase. We will also use our simulation codes to determine the effect of microstructure on the total volume fraction of α' produced during transformation and to model a series of complete hysteresis loops, which will be validated using our experimental data.

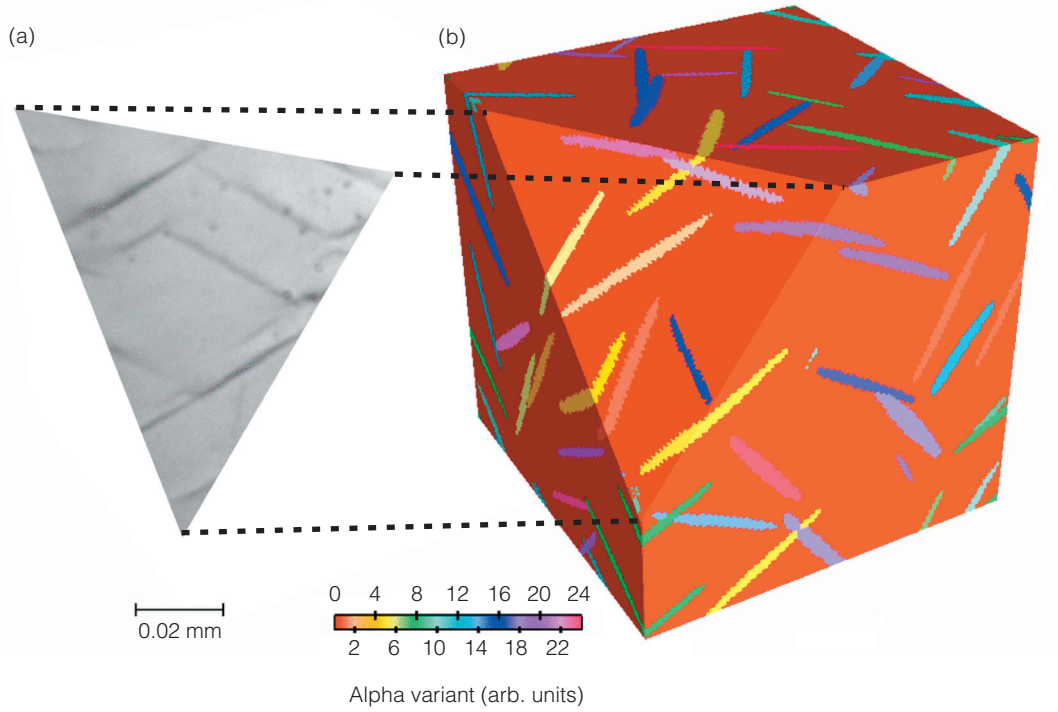

The project aims to elucidate martensitic phase transformation, particularly in delta-phase plutonium (δ-Pu). (a) Optical micrograph of δ-Pu. (b) Three-dimensional simulation of martensitic transformation in a similarly shaped sample of Pu. The δ phase is colored dark red. The α' phase is indicated by rods.

Thermodynamics and structure of plutonium alloys

P. G. Allen, P. E. A. Turchi, T. H. Shen, G. F. Gallegos

Understanding the effects of impurities in plutonium (Pu) alloys is important for predicting long-term phase stability, yet the role of iron (Fe) and nickel (Ni) impurities in gallium- (Ga-) stabilized delta (δ) Pu is poorly understood. These elements may segregate at grain boundaries or within the grains, where they can induce secondary phase formation or possible precipitation, which can change mechanical behavior and influence long-term stability. Because these effects have implications for all existing or future Pu-Ga materials, it is important to understand and verify the thermodynamic behavior of Pu alloys through theoretical modeling and experimental techniques.

This project, which coordinates experimental and theoretical approaches, focuses on (1) binary and ternary alloy synthesis (i.e., PuGa, PuFe, and Pu-Ga-Fe systems) by melting; (2) crystallographic characterization by microscopy, x-ray diffraction, and x-ray absorption spectroscopy; and (3) thermochemical measurements using differential scanning calorimetry (DSC). The experimental results will confirm or clarify regions on the binary and ternary phase diagrams. Our theoretical approach includes simulating alloy formation thermodynamics by coupling experimental information on alloy energetics to the calculation of phase diagrams (CALPHAD) approach.

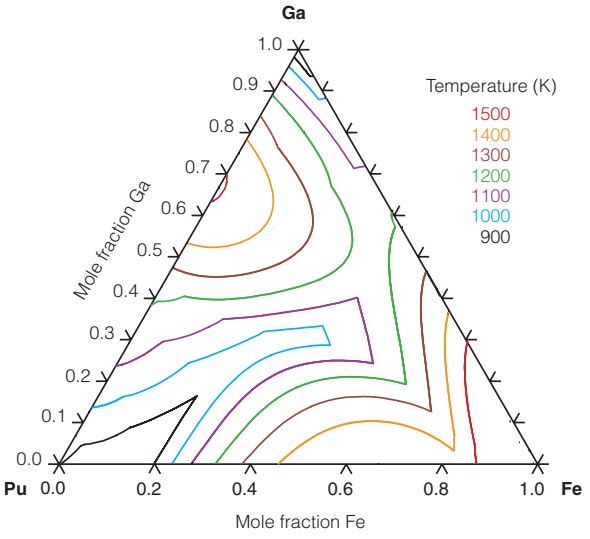

First theoretical assessment for the ternary plutonium-gallium-iron (Pu-Ga-Fe) system displaying isothermal solid–liquid concentration boundaries— liquidus lines.

This work forms a scientific foundation in actinide metallurgy for studying important aspects of metal dynamics and aging in support of the Laboratory's stockpile stewardship mission. The project will yield valuable information concerning the role of impurity atoms on the thermodynamics, secondary phase formation, and local structure in Pu alloys. The long-term benefit is the development of state-of-the-art experimental and theoretical tools for studying nuclear materials and forms the basis for future predictive work to assess the impact of alloy impurities on Pu mechanical behavior.

During FY2002, the CALPHAD modeling confirmed the existence of a low-lying eutectoid between the alpha (α) phase of Pu, the δ-based solid solution and the low-temperature Pu_3Ga compound at 59.5°C and 7.8 at% Ga, a result similar to that suggested in the Russian phase diagram (97°C and 7.9 at% Ga). We completed full assessments of the Pu-Ga, Pu-Fe, and Fe-Ga binary phase diagrams that allowed us to construct the first-ever isothermal sections of the ternary Pu-Ga-Fe phase diagram (see Figure). A small-scale Pu melting furnace was developed and tested for small (~3g) sample synthesis. This facility provides controlled heating up to 1600°C in an inert atmosphere. Using this capability, we successfully synthesized bulk samples of Pu_3Ga, Pu_6Fe and PuNi. Our DSC workstation for Pu thermochemistry was successfully commissioned, and the first set of samples were analyzed. Experimental data on the heats of formation for α Pu, Pu_3Ga, Pu_6Fe, and PuNi were obtained and analyzed.

In FY2003, we plan to conclude our research in the following areas: (1) detailed theoretical assessment of the ternary Pu-Ga-Fe and Pu-Ga-Ni phase diagrams and of their thermochemistry, (2) analysis of the results of kinetic studies on phase decomposition (i.e., eutectic decomposition of face-centered cubic-based Pu-Ga into α Pu and Pu_3Ga), (3) experimental verification and validation of theoretical assessments through complete thermochemical (DSC) and structural (SEM, XRD) analysis of binary and ternary compounds, and (4) complete XAS and microscopic investigations on selected binary and ternary samples. As was also performed in FY2001, our FY2003 work includes complete temperature-dependent analysis to quantify lattice vibrational modes.

Modeling and characterization of recompressed damaged materials

R. Becker

Ductile metals subjected to shock loading can develop internal damage through nucleation growth and coalescence of voids. The extent of damage can range from a well-defined spall plane induced by light shocks to more widespread damage caused by strong shocks. Because damaged materials are often part of a dynamic system, significant additional deformation and recompression can occur in the damaged region. To represent material behavior correctly in simulation codes for applications such as stockpile stewardship calculations, both the damage and the recompression processes must be modeled accurately. Currently, no experimentally based models of recompression behavior are available for use in numerical simulations.

The goals of this project are to (1) perform recompression experiments on samples containing controlled and well-characterized damage, (2) develop a model that captures the recompression behavior and residual strength based on the experimental data and micromechanical models, and (3) implement the model in the Advanced Simulation and Computing (ASCI) code ALE3D. The recompression model, together with failure models based on underlying physical mechanisms, will provide a more accurate representation of the behavior of explosively loaded materials. Accurate modeling of the deformation of severely damaged materials is important for stockpile stewardship simulations and DoD applications.

The experiments involve creating a controlled level of damage inside material specimens in the form of spall-induced porosity. The material is then compressed to close the porosity and subsequently tested to determine the strength of the recompressed material. Samples are taken from each stage of the process to observe the damage level through standard metallographic techniques. For the experiments conducted in FY2002, the spall damage was introduced in the copper specimens through impact experiments conducted on a light gas gun. The damaged material was recovered and compressed 15% at quasistatic strain rates and in a split Hopkinson bar at dynamic strain rates of 3000/s. Following recompression, tensile specimens were machined and tested to assess the residual strength of the material.

The strength of the damaged region during compression was unexpectedly high. Although the spall-related porosity accounted for a significant fraction of the total area on the spall plane, the strength of the damaged region in compression was high enough to resist deformation while the surrounding material deformed. A large fraction of the 15% compressive deformation occurred outside of the damaged region. Our results indicate that this is due to the significant strain hardening of the highly strained material surrounding the voids.

Additional experimental and simulation work is planned for FY2003 to better define and characterize the material response during recompression. Simulations will be used to determine the role of strain hardening on the void closure behavior. Recompression experiments will be pursued using higher pressures available with a gas gun and lasers. The laser experiments are particularly interesting since they access a much higher pressure and strain-rate regime. The additional data will provide more confidence in the model when it is applied to simulating materials under extreme conditions.

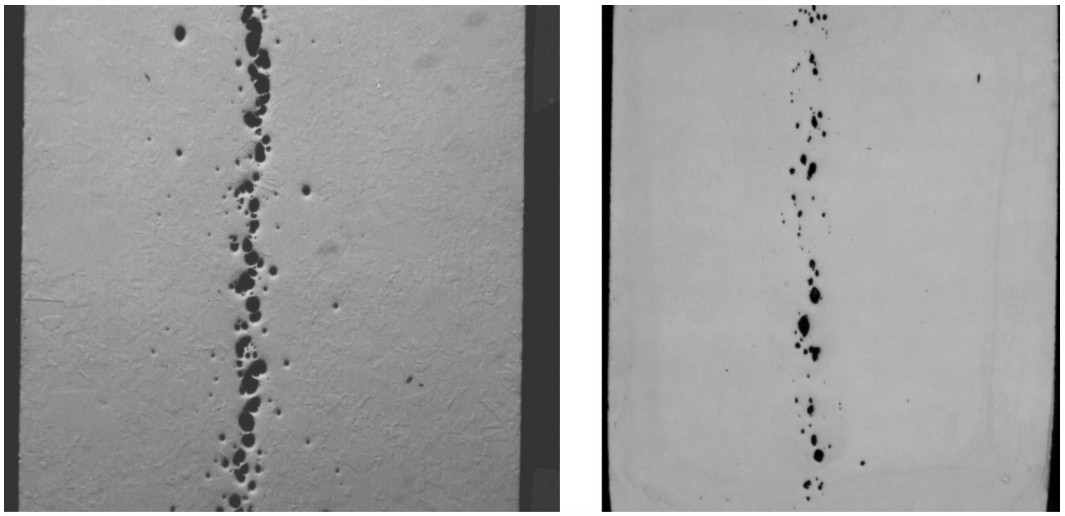

Spall damage in copper specimen (left) before and (right) after 15% compression. Significant compression has occurred outside of the damaged region.

The Deformation DIA: A novel apparatus for measuring the strength of materials at high strain to pressures at elevated temperature

W. B. Durham, S. Mei

The goal of this project is to develop and demonstrate the Deformation DIA (D-DIA), a new experimental capability for validating models for material strength as a function of temperature, pressure, and plastic strain. The D-DIA measures the strength of materials at confining pressures as high as 15 GPa under conditions that have been heretofore unobtainable in a laboratory. By enabling the study of material properties at extreme conditions—of central importance to the Stockpile Stewardship Program—this project supports LLNL's national security mission.

The D-DIA is a solid-medium press that applies a mechanical load to a 1-mm^3 single- or polycrystalline sample. The key feature of the D-DIA is the coupled inward motion of deformation anvils, which move against the sample, and the outward motion of side anvils, which constrain the soft pressure medium to keep the pressure constant. Measuring material rheology (flow) under such conditions requires state-of the-art x-ray and neutron sources, which are available at DOE facilities at Argonne, Brookhaven, and Los Alamos National Laboratories. The x rays provide high-resolution direct imaging of materials deforming under high pressure, allowing rates of deformation to be measured. In addition, x-ray diffraction reveals the state of elastic distortion and hence the state of stress that drives deformation, enabling characterization of the relationship between stress and deformation rate at fixed conditions of pressure and temperature.

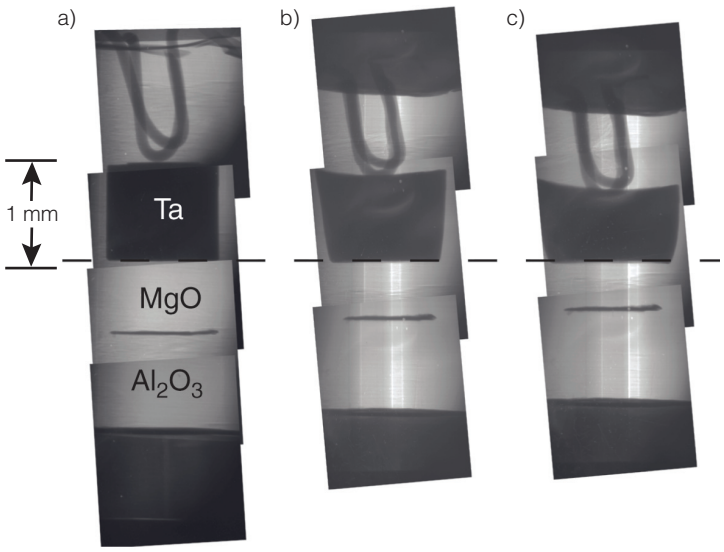

The Deformation DIA (D-DIA) enables study of material properties at conditions heretofore unobtainable in a laboratory. X radiographs show tantalum (Ta), molybdenum (Mo), and aluminum oxide (Al_2O_3) inside the D-DIA (a) before deformation and after deformation at (b) 3 GPa and (c) 6 GPa and at 500°C.

This project is experimentally testing the Steinberg-Guinan-Lund model by deforming polycrystalline samples of molybdenum (Mo) and tantalum (Ta) to strains approaching 1 at pressures up to 15 GPa and temperatures up to 1700 K. This is possible with the D-DIA because of its ability to deconvolve the effects of plastic strain and pressure—something difficult to do with instruments such as a gas gun or diamond anvil cell.

In FY2002, the D-DIA was constructed at LLNL and used in measurement with synchrotron x rays at the National Synchrotron Light Source (NSLS) at Brookhaven and at Argonne's Advanced Photon Source (APS), in which it functioned perfectly. To demonstrate the control possible, we pressurized a 1-mm-long Ta cylinder (see Figure) and a magnesium oxide (MgO) cylinder to 3 GPa (30,000 atm) at 500°C, shortening the cylinder approximately 9% at constant deformation rate over 1 hr, then increased the pressure to 6 GPa for 30 min, shortening it another 10%. The MgO deformed less—and is therefore stronger—than the Ta at 3 GPa but deformed approximately the same amount at 6 GPa.

Work in FY2003 will focus on measuring stress in the D-DIA and defining rheological laws for Ta and Mo using x-ray sources at APS and NSLS and x-ray-transparent cubic boron nitride anvils already installed.

Designer diamond anvils for novel, high-pressure experiments: Magnetic susceptibility experiments on actinides to multimegabar pressures

S. T. Weir, D. Jackson, C. Ruddle, V. Malba, J. Akella

Magnetism and magnetic order are manifested in a wide variety of materials. In materials exhibiting magnetic order, the order may assume one of a number of different forms such as ferromagnetic ordering, antiferromagnetic ordering, and spin-density wave states. This rich variety of possible magnetic orders reflects the competing and often subtle electron–electron interactions at play in many materials. However, despite the widespread technological use of magnetic materials today, our current understanding of the basic physics of magnetism and magnetic order is very far from complete, primarily because of the theoretical complexities associated with the electron–electron interactions.

Developing a better understanding of these electron–electron interactions is important not only for developing better models of magnetic materials, but also for developing better models of materials (e.g., the actinide elements) that exhibit strong electron correlation effects. The information gathered by our ultrahigh-pressure magnetic-susceptibility experiments provides a strong foundation for developing better actinide equations-of-state and high-pressure phase diagrams in support of the Stockpile Stewardship Program.

To perform high-sensitivity magnetic experiments to ultrahigh static pressures, we are making use of a new high-pressure technology—designer diamond anvil technology—that was developed at LLNL in collaboration with the University of Alabama. Designer anvils are specially fabricated diamond anvils with diamond-encapsulated, thin-film metal microcircuits. Our fabrication tools include three-dimensional optical lithography, metal sputter deposition, and epitaxial diamond chemical vapor deposition (CVD). For this project, we are fabricating designer anvils with multiple-turn microloops on the 300-μm-diam tip of the anvil. The Figure inset shows a small gadolinium (Gd) sample under high pressure in a diamond anvil cell. The magnetic properties of the sample are measured under these conditions using the diamond encapsulated 5-turn microcoil shown. The line width of the microcoil is 5 μm. Because of the proximity—just a few microns—of this magnetic sensing loop to the high-pressure sample, we can achieve extremely high signal sensitivities with very low background levels.

During FY2002, we performed high-pressure magnetic susceptibility experiments on Gd and made appropriate design modifications to our microcoil anvils to improve their electrical performance. The Figure shows a plot of the output voltage from a multiloop anvil that is examining a tiny sample of high-pressure Gd about 75 μm in diameter. At this pressure (16,000 atm) the transition to a ferromagnetic state is seen to occur when the sample is cooled below about 275° K.

In the coming year we plan to continue ultrahigh-pressure magnetic susceptibility experiments on several lanthanide f-electron elements, including Gd and Sm. Gadolinium is particularly interesting because it undergoes a pressure-induced structural phase transition at 61 GPa in which the volume suddenly collapses by 10%. This collapse is probably caused by the sudden delocalization of the f electrons; if so, we hope to confirm this by detecting the magnetic signature that should accompany the electronic delocalization. We also plan to start experiments on the actinide elements, including uranium and plutonium, to characterize their magnetic behaviors over a wide range of pressures and temperatures.

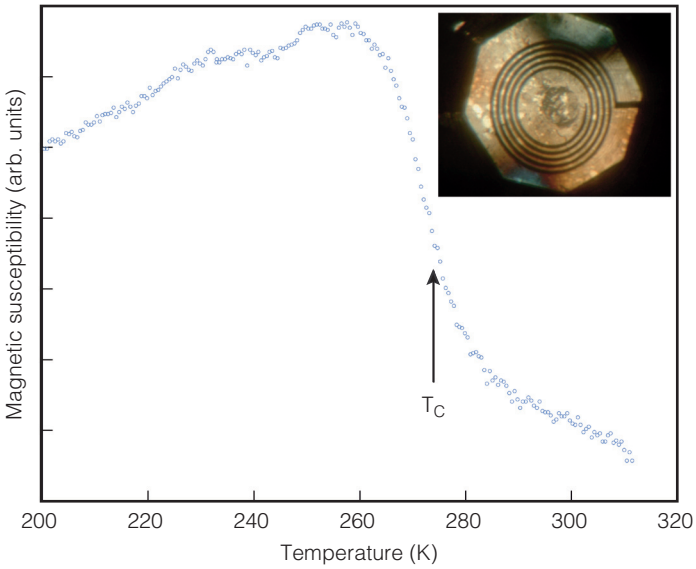

Plot of magnetic susceptibility signal vs temperature for gadolinium at high pressure (16,000 atm) measured with a multiloop anvil (inset). Ferromagnetic transition (T_C) occurs at about 275° K.

Nuclear reactor lifetime extension: A combined multiscale-modeling and positron-characterization approach

B. D. Wirth, P. Asoka-Kumar, A. Denison, S. C. Glade, R. H. Howell, J. Marian, G. R. Odette, P. A. Sterne

Increasing U.S. and worldwide demand for electricity and the desire to reduce greenhouse-gas emissions make it important to maintain and extend the operating lifetime of nuclear reactors safely and reliably. Maintaining the integrity of structural materials, including the reactor pressure vessel (RPV), whose properties are degraded as a result of neutron- and gamma-ray exposure, is one of the major challenges. Predictions of safe operating lifetimes require fundamental understanding of the chemistry and structure of nanometer-scale features that form in steels during irradiation.

In this project, we combine molecular dynamics modeling of defect production in high-energy displacement cascades with kinetic Monte Carlo simulations of the long-time defect evolution. The combination provides a multiscale model for predicting the formation of nanometer features in multicomponent ferritic steels. These features are characterized at the LLNL positron facility by measuring the positron lifetime, which allows us to identify the defect type and size, and the orbital electron momentum spectrum, which provides information about the chemical composition of the defect. The integration of modeling predictions with experimental characterization gives a validated, atomistic picture of the character and composition of the nanometer features and forms the basis for predicting mechanical property changes and thus safe operating lifetimes.

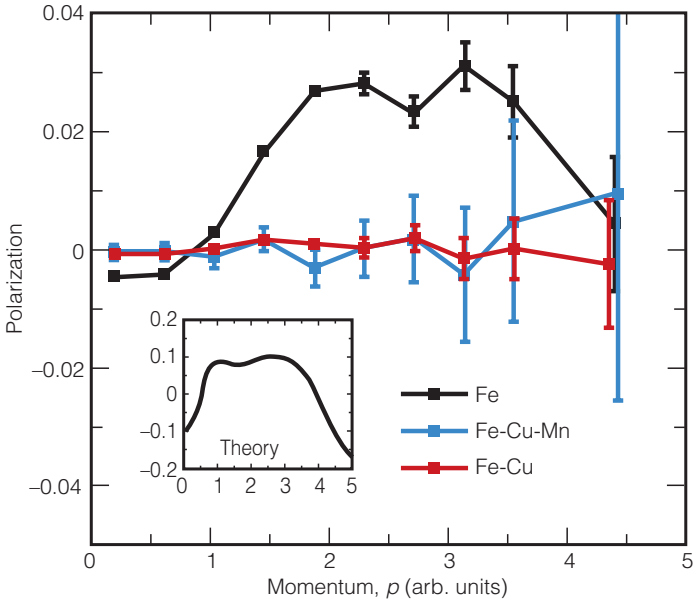

Electron polarization spectrum as a function of orbital electron momentum in solution-annealed iron (Fe), thermally aged iron-copper (Fe-Cu) and 288°C neutron-irradiated iron-copper-manganese (Fe-Cu-Mn). The inset shows the ferromagnetic Fe curve predicted by theory, which closely matches the measured curve of the solution-annealed Fe.

Our work will enhance the Laboratory's capability to characterize nanometer-scale features responsible for strength in structural steels and will contribute to the Laboratory's work in nuclear energy technology and stockpile stewardship.

During FY2002, we developed and applied a positron-annihilation spectroscopy technique to probe the magnetic character and chemical composition of the nanometer copper-manganese (Cu-Mn) precipitates. This represents the first application of spin-polarized, magnetic positron-annihilation measurements of the orbital electron momentum spectra of embedded nanoprecipitates.

The Figure shows the polarization spectra as a function of orbital electron momentum, measured with spin-polarized positrons and associated magnetic field reversal. The inset shows the corresponding theoretical curve in ferromagnetic iron (Fe), which is in qualitative agreement with the measured shape of the solution-annealed Fe, but not scaled to account for the partial positron beam polarization. For the thermally aged and neutron-irradiated Fe-Cu-Mn alloys, the data points all lie close to 0.0, which indicates that positrons are annihilating within nonmagnetic regions of the sample, unaffected by the applied magnetic field. The small deviation from 0.0 is comparable to bulk Fe deviations. The results confirm that the nanometer-size precipitates in thermally aged Fe-Cu and 288°C neutron-irradiated Fe-Cu-Mn alloys are nonmagnetic, with a bulk Cu-like character of the nanometer precipitates formed in the these alloys. The practical consequence of this result is that the Cu precipitate contribution to RPV steel embrittlement is not expected to contribute to further increases in embrittlement during extended reactor lifetimes.

In FY2003, plans include (1) extending our modeling and positron characterization capability to multicomponent RPV steels and weld material, and (2) continue to investigate the atomic structure and composition of the nanometer features, including identification of features expected to form at very high radiation exposures.

Nanoscience and nanotechnology in nonproliferation applications

J. G. Reynolds, B. R. Hart, T. M. Tillotson, S. E. Letant, S. R. Kane, M. Z. Hadi

Chemical and biological weapons (CW and BW) are now recognized as major threats to national safety and security. One approach to combat CW and BW is to monitor clandestine production activities through sample collection and detection. Commercial, polymer-utilizing tools developed for CW field collections have good selectivity. However, such tools must be sensitive enough to detect trace (parts per billon) or ultratrace (parts per trillion) levels of CW- and BW-related materials in the environment. Specific selectivity is necessary to distinguish CW and BW agents from naturally occurring compounds.

Nanostructured materials—materials that have surface features and pore structures on the nanometer scale—can potentially be more specific, yet more versatile, than traditional polymers. Materials attractive for this use are silica sol-gels, carbon nanotubes, and porous silicon. In this project, we are tailoring—through chemical and surface modification—these nanostructured materials to be the new generation of highly efficient, small collectors and sensors for CW and BW compounds.

During FY2002, we made further progress in developing collectors based on silica sol-gels and carbon nanotubes and detectors based on porous silicon. Silica sol-gels were modified to provide designed pores and binding sites that increase specificity for target CW compounds. For example, we synthesized pores of specific size in the nanostructured framework by first incorporating organic substituents and then removing them by air oxidation. To increase the selectivity of these pores for CW compounds, we designed binding sites by incorporating europium and terbium into the silica framework through alkoxide condensation reactions. For better selectivity in aqueous environments, fluorinated groups were incorporated into the sol-gel matrix, making the material hydrophobic.

Using commercially available, single-wall nanotubes, we developed new activation techniques that enhance collection. Initial test results with these modified nanotubes in unique collection configurations demonstrated an activity 3 to 4 times greater than that of Carboxen—a polymer that is the industry standard for collection of CW-related compounds. We also used silicon polymers as binders to develop coatings that contain these materials; such coatings are important for the ultimate, real-time application of nanostructured collectors.

Our efforts in using modified porous silicon as a detector focused on developing methods to attach CW-active enzymes to a photoluminescent, porous silicon surface. The photoluminescent properties of porous silicon enable CW and BW detection because the silicon's photoluminescence spectrum changes when the receptor compound on the silicon's surface binds to the target CW or BW compound. We developed a process for producing photoluminescent, porous silicon, and synthesized and attached several different linkers. The linker shown in the Figure was formed through Lewis-acid-catalyzed hydrosilylation of nitrile-terminated alkynes, followed by reduction and attachment using protein cross-linker chemistry. These linkers were used to attach potential BW detectors—such as streptavidin—without losing the photoluminescence of the porous silicon.

In FY2003, we will continue to enhance the sol-gel materials by determining systematic parameters for controlling binding sites and pore size, then test the materials on surrogates for CW agents. For porous silicon, we will structurally characterize the binding of selected common enzymes to the surface; determine the effects of binding on enzyme activity and silicon photoluminescence; attach a CW-active enzyme (organophosphate hydrolase); and test the enzyme's activity utilizing a flow cell that we designed specially for photoluminescent interrogation.

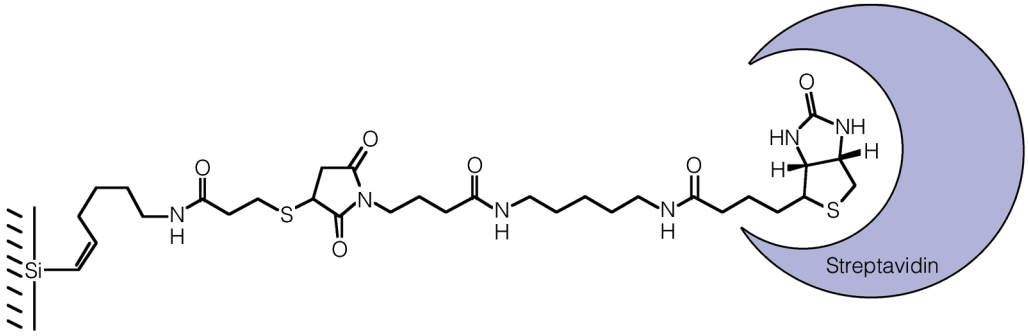

A chemical and biological weapon detection scheme based on the binding of streptavidin to porous silicon utilizing a new chemical linker

Materials-processing technology for vertically integrated random-access memory

S. P. Vernon

Over the next decade, the computational demands of stockpile stewardship and other applications of national interest, such as computational biology, will far exceed the capabilities of the Advanced Simulation and Computing Program, with its goals of 100 teraflop/s computing speeds. New technologies that circumvent current limitations are key to narrowing the gap between computational demands and speeds.

Current integrated-circuit technology is two-dimensional (2-D). Circuits are formed in the near-surface regions of a single-crystal semiconductor material, usually silicon (Si). Lithography and ion implantation are used to form n- and p-type regions. However, significant performance gains are needed for 3-D architectures, in which multiple memory layers are stacked directly on top of a microprocessor. With increased volumetric density and reduced signal paths, such architectures could achieve nearly optimal data-processing speeds but involve layer-by-layer circuit construction. Thin-film deposition is used to grow individual layers, which are doped and activated using the low-temperature techniques needed to avoid disrupting the underlying layers. Furthermore, the interconnect structure must provide access to each layer. Consequently, at least some of the circuitry must be formed on a thin-film metal underlayer.

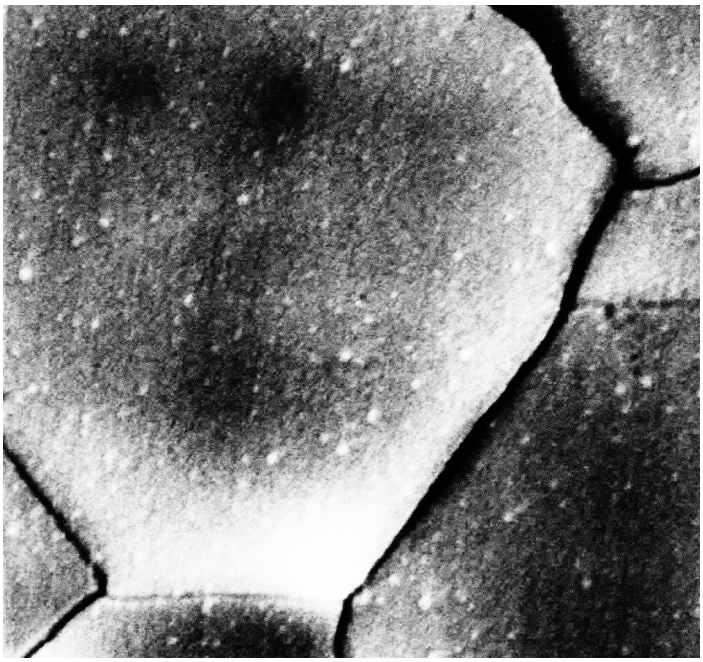

Plan-view micrograph of polycrystalline silicon film prepared by ultraviolet-laser-recrystallization of amorphous silicon The film is comprised of individual hexagonal crystallites approximately 1 μm in diameter.

Previously, we developed physical vapor-deposition processes for the fabrication of amorphous Si (a-Si) thin films and proof-of-concept excimer-laser processing protocols for a-Si recrystallization and dopant activation. Laser processing permits local deposition and absorption of optical energy in the near-surface region and therefore minimal disruption of the underlying structure. This work supports LLNL's national security mission by developing technology that will enable faster computational speeds for science-based stockpile stewardship and other applications.

In FY2002, we improved the laser crystallization process by replacing the xenon–chlorine (308-nm) excimer source with a frequency-tripled (355-nm) neodymium–yttrium-aluminum-garnet system, improving homogeneity of illumination and decreasing optical-pulse duration by an order of magnitude. Experiments focused on issues associated with designing and fabricating vertically-integrated, polycrystalline Si (p-Si), Schottky barrier, and p–n junction diodes formed by laser-processing a-Si films on a refractory molybdenum underlayer. Chemical composition, interface morphology, and crystalline grain size were studied using techniques such as Rutherford backscattering, surface-ion mass spectroscopy, and sputter Auger electron spectroscopy.

Laser-recrystallization experiments were performed to determine fluences for building vertically integrated test structures and identify optimized laser-processing parameters. At low fluences, a-Si was converted to small-grain p-Si with good interface morphology and negligible intermixing but high grain-boundary density. We successfully fabricated p–n and Schottky-barrier structures with significant nonlinearity and diode-like anisotropy in current-voltage (IV) characteristics. However, the devices' electrical properties were unsuitable for array fabrication. The on/off ratio was ~10^3, whereas vertically integrated memories will require ratios of 10^9.

In this project, vertical p–n junction and Schottky-barrier p-Si diodes were successfully fabricated on metal underlayers using laser processing. Despite the diodes' suboptimal electrical performance, insertion of a conductive thin-film diffusion barrier—such as indium tin oxide—between the metal and Si may mitigate the problems, allowing production of large-grain p-Si.

Warm dense matter with energetic materials

J. D. Molitoris, W. M. Howard, R. W. Lee, J. W. Forbes, L. E. Fried, M. W. McElfresh

Understanding properties of materials at high density and temperature is important to LLNL's stockpile stewardship mission. One of the least understood areas of the density–temperature phase space is the transition region between solids and plasmas. This warm dense matter (WDM) regime is where standard theories of condensed matter physics and plasma statistical physics are invalid. In this regime, very little experimental data are available on materials, and the sensitivities of materials important to stockpile stewardship are unknown.

The scope of this project was to determine the WDM phase space accessible with energetic materials and its impact on understanding WDM. In this project, we developed a new experimental technique to investigate WDM. This experimental technique combines the use of custom nanocomposite materials, dual detonations for colliding-shock compression, and simultaneous fast radiometric imaging and streak spectrometry.

Our colliding-shock technique is capable of producing a range of temperatures and densities within the WDM regime. Two identical cylindrical masses of LX-10 explosive are simultaneously detonated, which compress and heat the SiO_2 aerogel from both ends. The heating and compression is maximized when the shocks ultimately collide, which forms a plane of WDM. This technique allows clear side views of the WDM plane for several microseconds. The SiO_2 aerogel material is compressed at densities of 100 and 300 mg/cc. By varying the initial density, the temperature–density range can be expanded to the extreme limits. A range of materials of interest, including Be, Al, Fe, Cu, Ta, and U, can be placed in the aerogel. With the colliding shock technique, these materials can be shock heated, compressed, and studied. Relevant properties to explore for WDM include ionization state, opacity, and equilibrium conditions.

In FY2001, we performed a series of experiments validating the effectiveness of single- and double-shock techniques to produce WDM conditions. The lower end of the WDM temperature spectrum (<1.0 eV) can easily be achieved, but temperatures of a few electronvolts are required for WDM to become plasma-like. Radiance diagnostics start to fail around 1 eV, so to explore the upper end of the temperature spectrum required a new diagnostic. In FY2002 we developed a streak spectrometer and imaging system capable of simultaneously imaging the shock collision and measuring spectrally and temporally resolved resolved line emission. Such line emission is characteristic of the temperature. The Figure shows a streaked Si emission spectrum for double-shocked 300-mg/cc aerogel. The temperature associated with this emission approaches 3 eV. An independent calculation with the Cheetah/ALE code is consistent with this result and calculates a temperature of 2.8 eV.

The ultimate achievable density with this technique has not been determined. Radiography indicated that densities greater than solid can be achieved, but how much greater and how the density varies as a function of time remain open questions. To answer these will require the use of a high-energy heavy-ion diagnostic to validate radiographic measurements performed at LLNL. This diagnostic has been made available to us through a collaboration with the German Institute for Heavy-Ion Science in Darmstadt. By using independent diagnostics, we hope to cross-validate the measurements and establish that absolute densities can be determined via radiography.

This project explored and developed several advanced diagnostics and experimental techniques important to small-scale experimental support for LLNLs stockpile stewardship mission. In follow-on work to this project, we are poised to perform sensitivity measurements on a range of materials to understand how the transition through the WDM regime affects the final extreme state of matter produced.

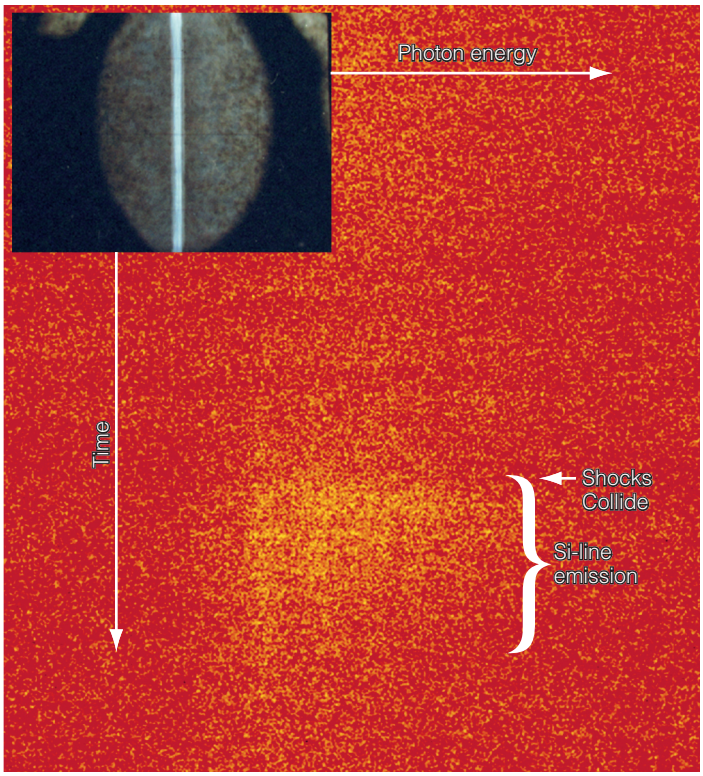

Streak spectrometer data showing silicon (Si) line emission after shock collision. Inset shows hot, plasma-like region formed on the collision plane.

Enhancement of strength and ductility in bulk nanocrystalline metals

T. G. Nieh, C. A. Schuh, W. E. King

Nanocrystalline materials are expected to have high strength and ductility, perfect for structural applications. However, experimental results of hardening and plasticity in nanocrystalline materials often appear difficult to compare or contradictory, which could be due to microstructural features that have yet to be considered in sufficient detail.

The large interfacial area-to-volume ratio of nanocrystalline materials poses many challenges for the design and synthesis of nanostructured and interfacial materials and for the characterization or assessment of their mechanical response, performance, and thermal stability under complex service conditions in structural components.

In response to these challenges, this project is developing a robust scientific and technological framework for designing high-strength, -ductility, and -toughness nanocrystalline and interfacial materials that would have direct benefit to understanding DOE mission-relevant stockpile material performance. For example, resistance to radiation damage and improved plasticity under dynamic conditions are important characteristics for stockpile materials. This research couples theory and experiments with an emphasis on materials of macroscopic dimensions (in the millimeter to centimeter range) that are composed of nanoscale (<100 nm) grains.

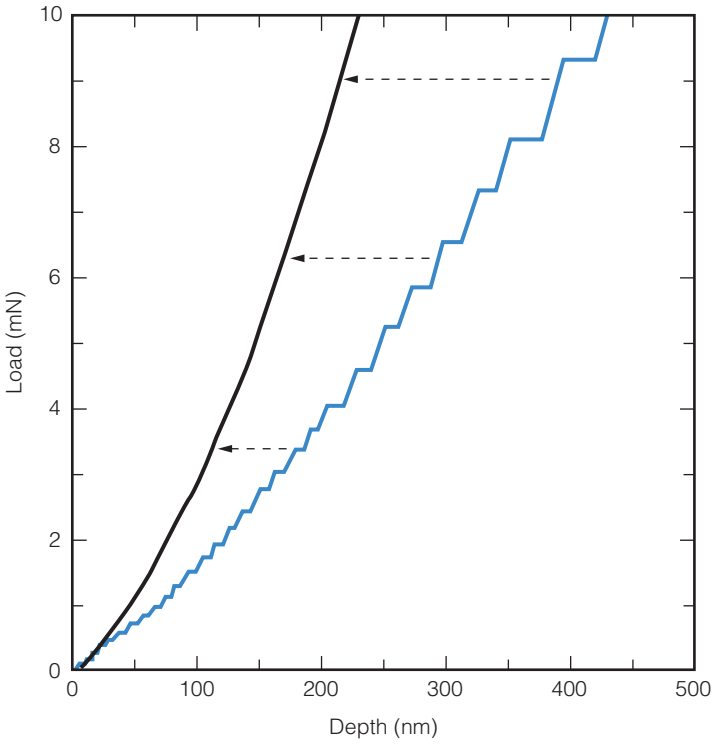

Plasticity occurs in a series of discrete steps, as the serrated load-depth curve for an amorphous metal ($Pd^{-30}Cu^{-10}Ni^{-20}P$) shows. After removal of the serration discontinuities, a smooth, consolidated elastic curve results (denoted by the arrows).

During FY2002, we accomplished several experiments and simulation tasks. Using electrodeposited nanocrystalline nickel (Ni) with grain size ranging from 12 to 25 nm, we observed breakdown in Hall-Petch (H-P) hardening at the finest grain sizes studied (12 to 14 nm). This breakdown of H-P hardening was also manifested during abrasion wear tests. In seeking for the dominant deformation mechanism in the inverse H-P hardening region, we examined the plasticity in bulk amorphous metals using instrumented nanoindentation. We found that plasticity occurs in a quantized manner, as the serrated line shows in the Figure. The mechanics of plasticity depend strongly on the indentation loading rate. For sufficiently slow indentations, we found that plastic deformation becomes completely quantized in a series of discrete yielding events. As the loading rate is increased, a transition from discrete to continuous yielding is observed. Although the underlying mechanism is still unclear, quantized plasticity was observed for the first time ever.

We used molecular dynamics simulations to study the effect of texture on the deformation mechanisms of nanocrystalline Ni, and found that the strength of the material is strongly dependent upon grain size. Also, dislocation activity reduces as grain size decreases, pointing towards a possible change in mechanism of deformation dominated by dislocations to grain boundary processes.

In FY2003, we plan to produce nanocrystalline copper (Cu), gold (Au), and Cu–Au with various grain sizes ranging from 5 to 100 nm using electrodeposition technique. The mechanical properties, in tension, compression, and creep, will be conducted at different strain rates and temperatures to probe the deformation mechanism and examine possible yield asymmetry. To understand the quantization phenomenon, we propose to study the deformation behavior of amorphous silicon and boron. This study will shed light on the fundamental mechanisms operating in the inverse H-P region.

Dip-pen nanolithography for controlled protein deposition

J. J. De Yoreo, J. A. Camarero, C. L. Cheung, B. Weeks, M. C. Bartelt

The ability to organize macromolecules and nanoparticles deterministically on surfaces is a major goal of nanoscience and will benefit materials science, synthetic chemistry, biology, and medicine. However, no practical methods for achieving this goal currently exist. This project combines our capabilities in atomic force microscopy (AFM) with advances in protein engineering and surface chemistry to create new technology for trapping, detecting, and assembling proteins, which will assist LLNL's biological nonproliferation and proteomics in support of the national-security and basic-science missions.

Detecting biological agents and investigating protein–protein interactions will be advanced by the ability to fabricate ultrasmall, highly selective protein chips. Creating ordered layers of proteins will eliminate the need to crystallize proteins—an obstacle to protein-structure determination. Creating colloid and quantum-dot arrays will enhance LLNL's ability to investigate particle-interaction physics at the nanometer scale.

In this project, we are using dip-pen nanolithography (DPN) to create chemical patterns with feature sizes of 10 to 100 nm. In DPN, the atomic force microscope is used like a fountain pen. The tip is "dipped" into a reservoir of a chemical compound (the "ink"), then moved across the surface along a predetermined path to create the pattern. The compound consists of long-chain molecules, at one end of which is the base group, which binds strongly to the surface. Binding forms a self-assembled monolayer in which the ink molecules pack closely together and stand up, exposing the group at the other end of the chain, known as the head group. By designing the head group to bind preferentially to certain sites on specific macromolecules, DPN patterns can be used to control the location and orientation with which those molecules bind to the surface. This chemistry and its application to formation of crystalline macromolecular arrays are unique, and a provisional patent application has been filed.

In FY2002, we focused on developing generic inks usable with virtually any protein, virus, or antibody. Inks with two different base groups were developed for use on either gold or silicon oxide substrates. Using a novel solid-phase synthesis technique, four different head groups were then added: cysteinyl, which binds to proteins with a thioester group at one end; ONH_2, which binds to glycoproteins; amine, which binds electrostatically to virus particles; and tri-ethylene glycol (TEG), which passivates the substrate's unpatterned portion. The Figure demonstrates the high degree of control over the location of virus adsorption using the amine-terminated ink for patterning and TEG for passivating the background. We also developed a physical model for controlling humidity and writing time for DPN features; the ability to fabricate carbon nanotube AFM probes to image deposited single proteins; and statistical simulations of protein-layer growth using kinetic Monte Carlo (KMC) methods.

In FY2003 we will use our inks in the template deposition of a series of viruses and proteins into crystalline arrays, using the KMC codes to simulate first-layer deposition, then mapping the adhesion force between the macromolecules and the patterned surfaces. These macromolecular arrays will then be analyzed for their degree of order using surface x-ray scattering techniques.

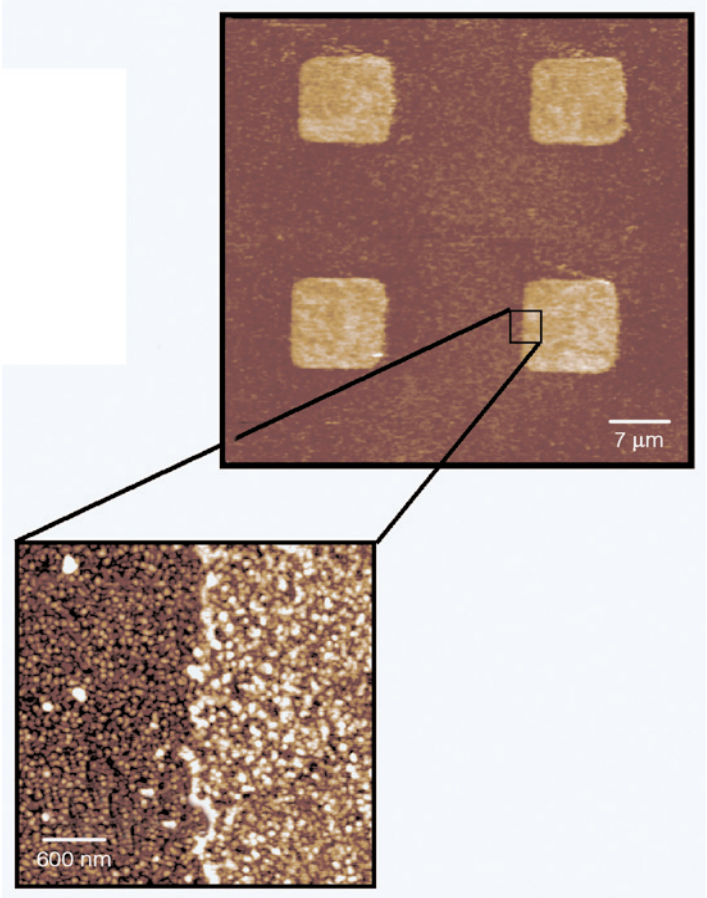

Preferential adsorption of the cow pea mosaic virus on the carboxyl-functionalized area (light brown) of a template with a triethylene glycol background (dark brown), which repels the virus so that virus coverage is restricted to the carboxyl-functionalized areas. Both compounds were deposited with a dip-pen nanolithography technique developed in this project.

Spectroscopy of shock-compressed deuterium

N. C. Holmes, G. W. Collins

The compression properties of dense, fluid hydrogen and deuterium(D_2) have been a topic of intense scientific interest since our earlier shock-temperature measurements and subsequent disagreement between measurements of compression on the Hugoniot using laser drive at Nova and magnetically-driven flyers at Sandia's Z machine. In recent measurements of sound velocities aimed at helping understand this problem, we uncovered a set of unusual effects in shocked D_2 at the relatively low pressures below 13 GPa. These effects include apparently anomalous absorption, sound speed, and optical emissivity. In a regime for which we expected shocked D_2 to be transparent, it behaves like a shiny metal. Since we think the fluid is molecular in this pressure and temperature region, we proposed experiments in this project to understand the measurements we made on the bulk fluid by using spectroscopy.

The experiments we propose will be the first to directly test and challenge the predictions of first-principles theory and simulations on the molecular structure, and the first experiments to measure the optical properties of shocked D_2. The techniques used in these experiments, fundamental for understanding explosives and the destruction of chemical weapons, will support the Laboratory's national-security mission. They also support LLNL's science and technology mission by providing a new ability to perform Raman and absorption spectroscopy under shock compression in fluid systems at high temperature and pressure.

In these experiments, we are using spontaneous Raman spectroscopy to look at molecular vibrations, and absorption spectroscopy to observe changes in optical properties. We think these arise from unexpected strong molecular interactions in the fluid. Our experiments look for evidence of these interactions by observing the shape of the D_2 stretch vibrational spectrum. The width and symmetry of the spectrum provide clues to the molecular structure. If stable clusters exist, then low-frequency vibrations might be seen. Furthermore, the width of the vibrational spectrum may tell us about the lifetime of the molecules, thus providing a direct test of molecular dynamic simulations. Since the optical properties provide a basis for understanding electronic changes in the fluid, optical absorption is the best way to observe them. The experiments will be carried out at LLNL's large two-stage gas gun using a single-pulse, 532-nm, 300-mJ laser pulse for the Raman work, and a long-pulse white-light source for the absorption experiments. This light source was designed after the mid-year start.

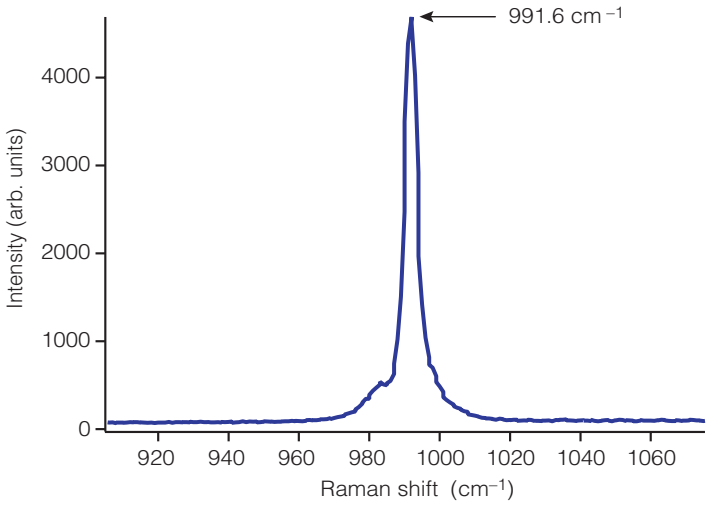

A test Raman spectrum (at approximately 992 cm^{-1}) of the ring-breathing mode of benzene. This spectrum was recorded in 160 ns using a succession of pulses.

With a mid-year FY2002 start, our goal was to get the Raman system running and initial work completed on the optical system and target design. The new laser, which replaced the one we had planned to use, produces 300-mJ, 8-ns pulses at 532 nm at 10 pulses/s. With this laser, our first test looked at the Raman spectrum of the ring-stretch mode of benzene, which provides a very strong and simple Raman spectrum, at roughly 992 cm^{-1} frequency. The Figure shows a spectrum from this test. The weak line on the shoulder of the main vibration peak may be evidence of photochemistry, since we find the benzene decomposes after many shots. This work gives us a basis to test improvements in optical sensitivity, effects of timing jitter, and so forth.

We had initially surmised that the strong change in optical opacity was due to D_2 clusters forming in the shocked fluid. Our first guess was that these were trimolecular clusters—three D_2 molecules forming a nearly hexagonal "ring." This is probably not the case based on our recent configuration interaction calculations. In these calculations, we vary the distance and position of the molecules and find the change in the optical properties. Even at compressions well beyond our experiments, this geometry will not make the D_2 opaque. Our calculations did suggest a structure that would: a parallel set of molecules squeezed tightly together will absorb visible light strongly.

In FY2003, design work will continue on an improved cryogenic system for the first shock experiments in fluid nitrogen-2, to be followed by experiments in D_2. Nitrogen is used for the first tests because it is much simpler, and also is scientifically interesting in the dissociation regime. The flash-lamp system for absorption measurements has been designed.

Using an aerogel composite to remove metals from groundwater

S. J. Coleman, P. R. Coronado, J. G. Reynolds, V. L. Dias, E. C. Ramon, R. W. Williams, M. J. Taffet

Contaminated groundwater is a problem at many DOE and other governmental and industrial sites. At LLNL we have a regulatory requirement to clean up contaminated groundwater at both the Livermore Site and at Site 300. If successful, the technology developed in this project will offer a practical means for reducing the cost of cleaning up contaminated groundwater at LLNL and other sites.

This research project supports the Laboratory's environmental-management mission by providing potentially efficient and cost-effective materials to remove metals from groundwater. These materials have the potential to benefit DOE and other governmental (e.g., DoD) or commercial sites with similar groundwater contamination issues. A secondary goal is to produce materials that can quickly be disseminated through technology transfer and employed at sites using granular activated carbon (GAC), which is commonly used in groundwater and drinking water treatment and is an excellent adsorbent of volatile organic compounds

Our research in FY2002 consisted of the continued preparation and testing of hydrophobic silica-aerogel–GAC composites (Composites) with phosphate functional groups that adsorb uranium (U). We also produced separate Composites with functional groups for hexavalent chromium [Cr(VI)] and arsenic (As). Additionally, in FY2002 we submitted a patent application and presented our research results at three conferences.

Preparation of the Composite materials for U begins with varieties of hydrophobic silica aerogel that had been modified with phosphate functional groups. These aerogels were then individually combined with GAC to produce composite samples. The modified materials were formed by mixing tetra methoxysilane [$(CH_3O)_4Si$] with the hydrophobic sol-gel precursor, $(CH_3O)_3SiCH_2CH_2CF_3$. The phosphorus was added during the aerogel reactions by using different phosphorus-containing precursors. A similar process was used to prepare composite materials for Cr(VI) and As adsorption with the exception of the functional groups.

The Composites were put into vials with laboratory-prepared simulated groundwater and actual groundwater from Site 300 for batch testing. Batch tests have been completed for U and begun for Cr(VI). We analyzed the treated waters using inductively coupled plasma mass spectrometry and calculated the amount of contaminant that was adsorbed by each Composite. The Composites were superior to GAC alone in removing U and Cr(VI) from solution.

The most promising Composites for U adsorption capacity were then used in flow-through column tests with solutions of 100 pCi/L of U. Column tests further demonstrated that U adsorption quickly occurred onto a Composite. As the Figure shows, the Composite in the column sustained greater than 90% reduction of the column influent concentration of 100 pCi/L of U using 50 g of a Composite material and a flow rate of 5 mL/min. The effluent from the column had a maximum U concentration of 8 pCi/L and an average concentration of 5 pCi/L without breakthrough occurring. These results show that Composites can form superior materials for adsorption of aqueous-phase U.

In FY2003, we plan to prepare two separate Composites with functional groups that have an affinity for Cr(VI) and As, bench-scale test both, column and field test the composite for Cr(VI), document our results, and submit them to a peer-reviewed journal. In addition to exploring the potential adoption of this technique at LLNL's Site 300, discussions have begun with potential commercial licensees.

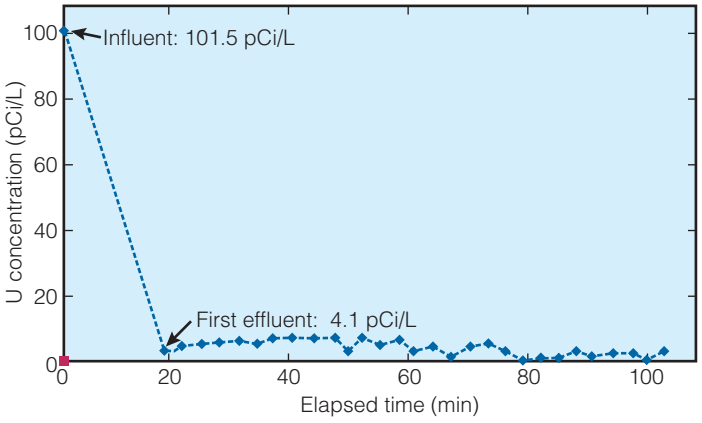

Column test results for uranium adsorption using 50 g of aerogel–granular-activated carbon composite show that such composites can form superior materials for adsorption of aqueous-phase uranium.

The properties of actinide nanostructures

A. V. Hamza, J. G. Tobin, P. A. Sterne, T. W. Trelenberg, S. C. Glade

We will obtain a detailed predictive description for the relationship between the structural and electronic properties of actinide materials—a key area of science-based stockpile stewardship. To accomplish this goal, we need a detailed experimental benchmark of the band structure theory (e. g. bandmapping). Actinide nanostructures provide a key to meeting this goal. To date, the lack of single-crystal samples of the actinide metals has made experimental band-structure determination impossible. We plan to provide two-dimensional (2-D) and 1-D quantum-confined, crystalline structure with macroscopic nonconfined dimensions, allowing for conventional band-structure determination with photoemission techniques. A structural and electronic description of the actinides requires determining the balance of 5f electron correlation effects, including Coulomb energy, electron exchange correlation, spin-orbit coupling, and crystal field effects. Coulomb energy is inversely proportional to the size of the sample, whereas the electron exchange correlation is inversely proportional to the square or cube of the size. We will use photoemission and bandmapping as a function of size on the nanometer scale to separate the correlation effects experimentally and benchmark and guide the band-structure theory.

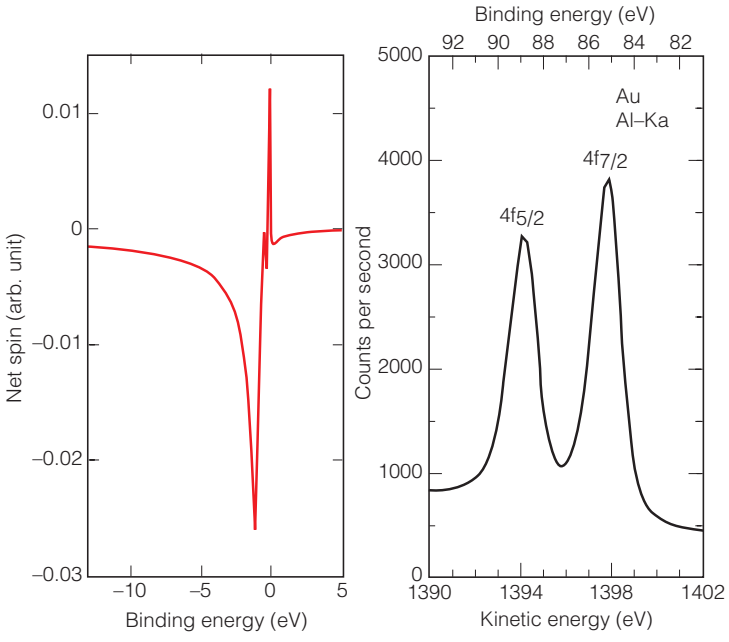

(a) Plutonium dichroism due to internal spin structure predicted with a model that includes spin and spin–orbit splittings in descriptions of 5f states. (b) Performance of our working photoelectron spectrometer with Al–K-alpha for a gold surface.

The properties of the 5f elements and compounds are quite complex because of their correlated electron behavior. The results of this project will help define the balance of the various electron correlation effects and will therefore support stockpile stewardship, which requires a fundamental understanding of the structure–property relationship for actinides.

Density-functional calculations will determine the electronic density of occupied and unoccupied states for comparison with the results of photoemission and scanning tunneling spectroscopy. In addition, the calculations can also incorporate matrix-element effects associated with photoemission to provide a more direct comparison between theory and experiment.

In FY2002, our angle-integrated investigation of alpha plutonium (α-Pu) and δ-Pu has led to a new paradigm for interpreting photoemission spectra of uranium (U), neptunium (Np), α-Pu, δ-Pu and americium (Am). Our approach is founded on a model that includes spin and spin-orbit splittings in the picture of the 5f states and on the observation of chiral and spin-dependent effects in nonmagnetic systems. Including spin and correlation effects has lead to a remarkable agreement between results calculated with the model and the measured angle-integrated spectra of U, Np, Pu (particularly δ-Pu), and Am, and to a prediction of what we might expect to see in future spin-resolving experiments on single-crystal samples.

The reactive nature of actinide surfaces requires stringent, ultrahigh-vacuum (UHV) conditions to determine experimentally the electronic structure of clean surfaces. We have added a cryogenic shroud in our UHV analysis chamber for producing extremely low partial pressures of oxygen and water, the impurities that most quickly contaminate the surface. The upgraded system has achieved 2×10^{-10} Torr vacuum, affording more than 10 h to perform measurements before the samples are contaminated. We have also installed and operated the in situ angle-resolved photoemission spectrometer for bandmapping, and constructed and installed a vacuum suitcase to safely handle Pu and to deposit clean actinide layers by pulsed-laser deposition.

In FY2003, we will produce 2-D samples of ^{238}U on silicon templates by pulsed laser deposition, then perform scanning tunneling microscopy to determine the atomic structure and in situ bandmapping to determine the electronic structure. Two-dimensional Pu samples will also be produced and characterized using the same techniques.

Nanofilters for metal extraction

W. L. Bourcier, S. K. Roberts, A. Wallace, Sonia Letant

Energy-efficient water-purification technologies will play a key role in water and waste treatment in the coming decades. As water resources are depleted and populations increase, the availability of clean, abundant water resources will become a national security issue. We propose to develop a silicon nanofilter to remove specific metal elements from water by coating the walls of through-going nanopores in silicon wafers with a compound that selectively bonds with the target element, drawing it into and through the pores. The nanopores will be electrochemically etched through the silicon wafer in a hydrogen fluoride-alcohol-water solution. Pore diameter, which can be as small as 1–2 nm, is controlled by current density and composition of the etching solution.

If successful, the filter could be used to concentrate elements for use in sensors or to remove toxic, radioactive, or valuable elements from water. As an initial step in developing this technology, we have chosen to use the silicon nanofilter in a sensor for arsenic (As). Arsenic limits for potable water in the U.S. have recently been reduced from 50 to 10 parts per billion, creating a demand for inexpensive methods for monitoring As content in water supplies. For this use, the nanopores will be coated with an ethylenediamine–copper compound shown to have high selectivity for As ions. We expect this step will result in the prototype of a useful As sensor and demonstrate proof of principle for additional applications of the filter to other metals.

This project will contribute to several laboratory missions: (1) development of an As sensor will be an enabling technology in the area of environmental assessment, particularly in response to lower limits for As in drinking water; (2) processing brines is a key component of the economics of energy production from geothermal systems in support of the energy-security mission; and (3) turning nonpotable water into potable water could play a significant role in the long-term security of the nation and in the management of natural resources.

In FY2002 we set up a laboratory for porous silicon wafer fabrication and made silicon nanofilters with through-going monodisperse pores 1–2 nm in diameter. This optimized diameter is large enough to accommodate both the element-specific compound coating and passage of arsenic through the pores, and small enough to retain selectivity.

Work in FY2003 will continue our efforts to functionalize and test the filters. Our goal is to produce a working prototype As sensor that is thousands to millions of times more sensitive than those currently available.

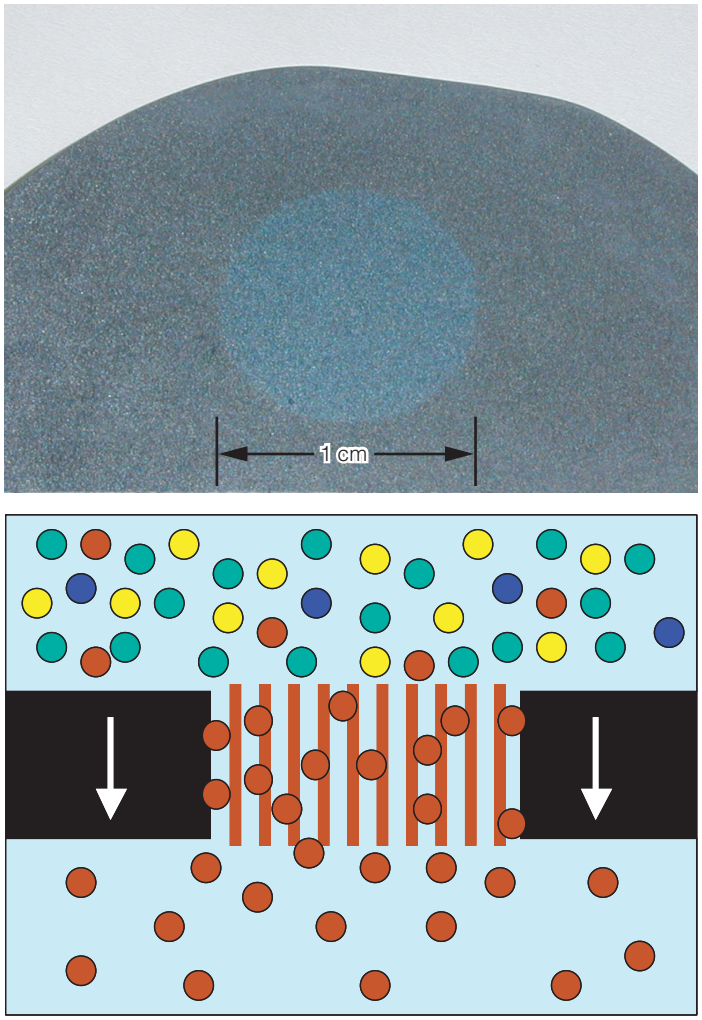

(a) Bluish circle, approximately 1 cm in diameter, marking a region of through-going nanopores etched into a silicon wafer. (b) Schematic showing how nanopores in the filter selectively remove targeted metal element (red) from a solution. Arrows indicate the direction of element transport.

Rapid resolidification in metals using dynamic compression

F. H. Streitz

The purpose of this project is to develop an understanding of the kinetics of phase transitions at high temperature and pressure. Kinetic limitations are known to play a large role in the dynamics of solidification at low temperatures, determining, for example, whether a material crystallizes upon freezing or becomes an amorphous solid. The role of kinetics is not understood in transitions at high temperature when extreme pressures are involved. We propose to investigate the effect of kinetics on the rapid resolidification of metals by (a) designing isentropic compression experiments using density-graded flyers as impactors to control the experimental time scale, (b) developing novel time-resolved diagnostic tools for use with the light gas gun facilities, and (c) applying these tools in a series of dynamic shock-compression experiments specifically designed to enable direct comparison with simulation while (d) performing atomic-scale simulations of the process, using the experimental results.

The primary deliverable associated with this project will be the creation of two new capabilities which enhance our core competency in support of stockpile stewardship: (1) the ability to experimentally control pressure-loading rates by designing and using novel impactors whose density is graded across the thickness of the flyer, and (2) the ability to characterize in situ the behavior of a metal as it follows a carefully prescribed thermodynamic path. These two capabilities substantially broaden both the range of phase space that can be accessed and the amount of information that can be gained with dynamic compression experiments. This project addresses important basic science issues concerning our understanding of equation-of-state experiments, and will yield an unprecedented view into the dynamic nature of melting and resolidification under conditions of pressure and temperature that are relevant to our national defense.

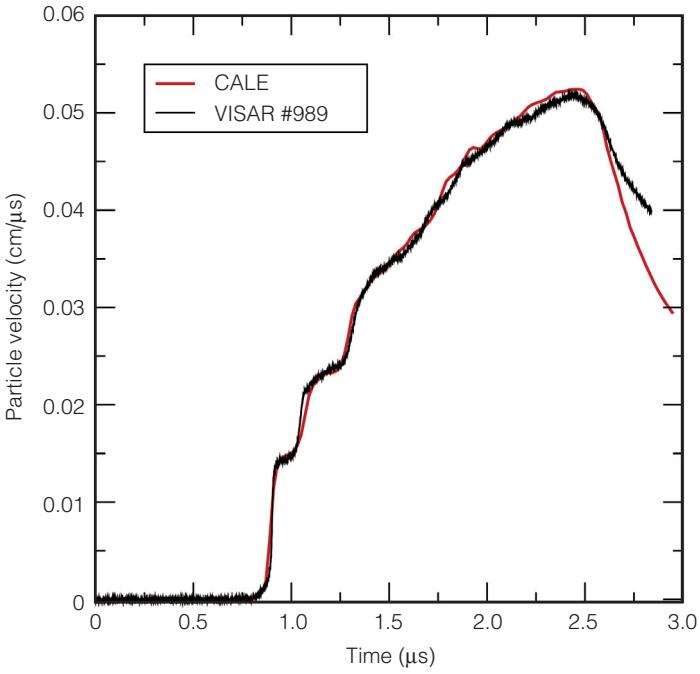

Velocity interferometry (VISAR) data (blue) showing response of copper to impact from a density-graded flyer. The results of a hydrodynamic calculation (CALE) simulating the impact closely match the VISAR data.

In FY2002 we made substantial progress in developing layered impactors. Our design, using powdered metals in a resin matrix, has proven capable of producing nearly isentropic pressure ramps in liquid and solid metals such as copper (Cu) (see Figure). A redesign of the target produced an adhesiveless assembly, which successfully seals against molten bismuth (Bi). This design has been tested in the gun chamber both with single-density flyers, which produced simple shocks, and with our graded impactors, which produced near-isentropic compression. Additionally, we have upgraded our diagnostic capabilities by utilizing a second interferometer probe during the experiment, which allows us to measure phenomena such as the material response of both liquid Bi and solid Cu under identical loading conditions. Preliminary shots using this geometry have yielded the first evidence of resolidification under dynamic compression in molten Bi.

In FY2003, we will continue our experimental effort by beginning a study of rapid resolidification in molten Bi, utilizing our graded-density flyers to produce near-isentropic compression. By using our dual-probe setup and a specially designed sample geometry, we can make measurements from which to build a strength-of-material model applicable to metals under extreme conditions of pressure and temperature. Additionally, we will continue to improve the design of the impactor (or bullet), concentrating on reducing the magnitude of the small shock originating from the initial impact of the bullet.

Effect of grain-boundary character on high-temperature dimensional stability of materials

C. A. Schuh

Although individual grain boundaries in polycrystalline materials are very complex, a full grain-boundary network displays traits that are universal to self-assembled systems. The goal of this research is to establish, for the first time, a scientific understanding of the effect of grain-boundary networks—crystallography and topology—on the high-temperature viscous deformation of the material. Experimentally, the work will seek a correlation of high-temperature deformation and failure mechanisms with detailed microstructural observations of the grain-boundary crystallography in two pure metals studied as model systems, as well as in Inconel 600, a nickel-based engineering alloy of interest to energy applications. Theoretically, the prevailing physical models of high-temperature deformation will be adapted to consider the effect of boundary structure, with particular emphasis on the dominant atomic-level mechanisms of deformation. The ultimate goal is to explain why crystallographically "special" grain boundaries—such as low-misorientation-angle boundaries—can impart substantial improvements in high-temperature strength.

If successful, this project will advance grain-boundary engineering technology to improve the operating efficiency of high-temperature power plants—both conventional and nuclear—in support of LLNL's mission in energy security.

In FY2002, orientation-image microscopic experiments were performed to obtain data on grain-boundary networks in a variety of materials. Custom software was written to analyze in detail the connectivity and percolative properties of the boundaries, classified as either crystallographically special or random. This analysis package was used to systematically study how thermomechanical processing can influence the grain-boundary network in Inconel 600.

A Monte Carlo-based computational model was also developed to simulate grain-boundary networks and how their connectivity and clustering properties change with crystallographic constraints. This model revealed that crystallography changes the percolation threshold for grain-boundary networks. This result has broad implications for the prediction of failure in metals by intergranular mechanisms like corrosion, cavitation, or cracking. In addition, an analytical model was developed to describe the essential effects of crystallography on the constraint of grain boundary networks.

In summary, this project has provided the first-ever quantitative analysis of grain-boundary network topology; identified critical underlying physics that govern many intergranular-failure mechanisms; and performed the modeling required to understand these phenomena in terms of the grain-boundary network.

Magnetic transition metals and oxides at high pressures

V. Iota, J.-H. Park, C.-S. Yoo

Understanding the role of magnetic interactions in the phase stability of solids is a fundamental issue in condensed-matter physics, and determining the magnetic properties of 3d-band transition metals—iron (Fe), cobalt (Co), and nickel (Ni)—and their oxides at Earth-core conditions (150–300 GPa, 2000–5000 K) is key to understanding the Earth's magnetic field. This research will investigate the electronic and magnetic properties at high pressures of 3d-band transition metals and their oxides. In these metals, electronic and magnetic properties are greatly influenced by the spatial arrangement of atoms in their solid phases, and phase stability and atomic structure are determined largely by spin interactions. This strong magnetism–structure correlation is believed to account for the stability of nonstandard structures in Fe, Co, and Ni at ambient conditions. This project supports the stockpile stewardship mission in the study of metals and actinides.

A goal of this project is to develop reliable in situ magnetic probes by combining (1) a side-access diamond anvil cell (DAC), which generates high pressures (see Figure); (2) high-resolution x-ray emission spectroscopy (XES) to determine electronic structure; and (3) x-ray magnetic circular dichroism (XMCD), which determines magnetic properties by measuring the difference in absorption between right and left circularly polarized photons at the 1s–3d (K-beta) transition. Previously, such spectroscopy for samples at high pressure was limited by the strong absorption of the DAC below ~12 keV. We use beryllium gaskets (which transmit x rays) and measure K-beta emission (~7 keV) in a radial geometry (hence the name axial XES) to avoid the strong absorption of the signal by the DAC. This extends the range of measurable energies as low as 4 keV, permitting electronic measurements of 3d, 4f, and 5f elements. All x-ray spectroscopy measurements use the third-generation synchrotron at the Advanced Photon Source (APS) at Argonne National Laboratory.

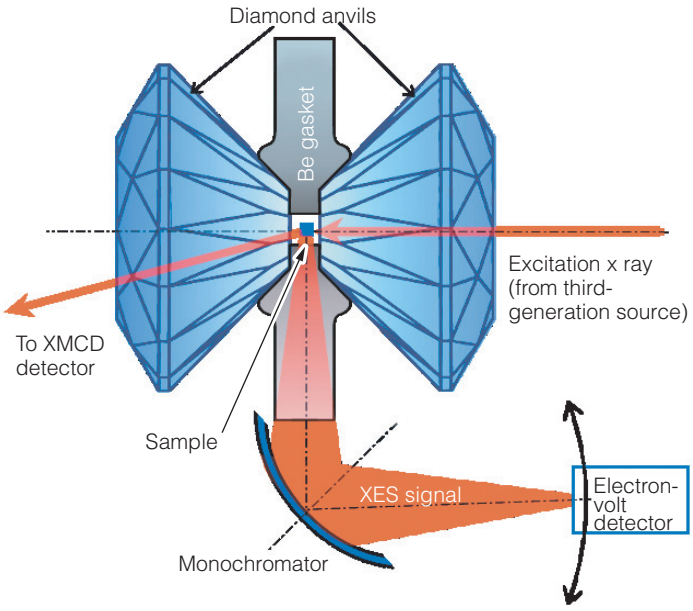

A diamond-anvil cell (DAC) combining x-ray emission spectroscopy and x-ray magnetic circular dichroism to measure simultaneously the electronic and magnetic properties of a metal sample subjected to high pressures by the DAC and heated to high temperatures by x rays. Our use of a beryllium (Be) gasket in the side-access DAC extends the energy range for in situ spectroscopic measurements to ~4 keV.

In FY2002, we performed our first XES experiments on Fe, Co, and Ni at APS and confirmed the feasibility of using axial XES for electronic-structure measurements at high pressures inside the DAC. For Fe, results show quenching of the spin polarization of the valence band in the high-pressure phase, confirming that the alpha–epsilon structural transition is accompanied by a high- to low-spin transition, i.e., the high-pressure phase (epsilon-Fe) is nonmagnetic. For Co, K-beta XES measurement of a mixed hexagonal close-packed–face-centered-cubic sample partially transformed by heating to 1800 K at 20 GPa reveals electronic changes associated with the transition, suggesting that the high-pressure–high-temperature phase may be nonmagnetic. With the observed loss of Fe magnetism at high pressure, this result would verify the proposed systematics of the magnetism–structure correlation in 3d-band transition metals. Confirming these findings requires measurement at higher pressures (>150 GPa).

In FY 2003, we will (1) perform XES measurements on Co and Ni at >100 GPa to confirm quenching of the 3d magnetic moments at high pressures and (2) develop in situ XMCD measurements using a new high-pressure beamline built by LLNL and others. The data will be corroborated with first-principle calculations to help quantify the effect of magnetic interactions on phase stability in 3d electron systems.

Exchange coupling in magnetic nanoparticles composites to enhance magnetostrictive properties

H. B. Radousky, W. Choe, M. W. McElfresh, A. E. Berkowitz, N. Nersessian, G. P. Carman

The goal of this project is to investigate and improve the magnetostrictive response of magnetorheological elastomers, which are composites made up of viscoelastic solids consisting of natural or synthetic rubber filled with magnetic particles that change in length when a magnetic field is applied. This change is on the order of 10 parts per million for elements such as iron (Fe) or nickel (Ni) and on the order of 1000 parts per million for compounds such as (DyTb) Fe_2, known as Terfenol D, which are called giant magnetostrictive materials. The induced length change results in the ability to use these materials as magnetic actuators and sensors. Magnetorheological elastomers have applications to LLNL's national security missions that use magnetic sensors and magnetic actuators, and to vibration damping for automobiles, buildings, and bridges.

Our objectives are to validate the concept of using nanoparticles in magnetorheological elastomers and to understand the underlying physics of the nanoparticle interactions. Using spark erosion, we plan to produce spherical Ni and Terfenol-D particles ranging in size from a few micrometers to 10 nm, study their basic structural and magnetic properties, and produce/characterize magnetoelastomer composites incorporating these spherical particles.

A versatile and economic method for producing particles of virtually any type of material that has a nominal conductivity, the spark erosion process uses a pulsed power source to generate sparks between pieces of material that are immersed in a liquid or gaseous dielectric. In FY2002, we concentrated on using Ni as an ideal model system, both for improving the spark erosion process that produces the nanoparticles and for understanding the basic magnetic properties of small magnetostrictive particles.

We have been optimizing the spark erosion process by spark eroding Ni particles as a function of specific gap distances, different dielectrics, and by varying the frequency, duration, and amplitude of the sparks. The purpose of this study is to generate an empirical model which allows us to predict particle size and particle yield as a function of these parameters.

By varying the dielectric liquid, we were able to produce Ni particles (see Figure) that appear to be hollow under certain conditions. In addition to the hollow shells visible in the Figure, the density of the "hollow" particles was substantially reduced from those that appear to be solid Ni.

In FY2003, we will be making magnetoelastomer composites out of both the solid and "hollow" particles to compare their properties. We will also be applying the knowledge gained from the spark erosion studies on Ni to produce usable quantities of Terfenol-D for the magnetoelastomer composites.

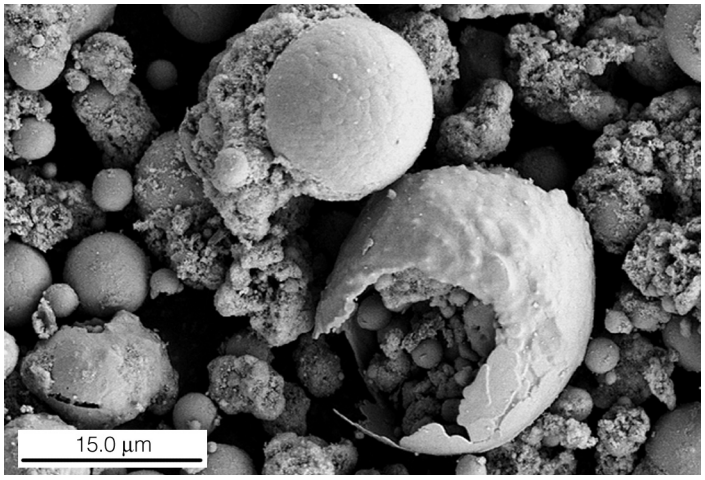

Scanning electron microscope image of nickel prepared by spark erosion. Note the formation of spherical particles, including some that appear to be hollow.

Direct imaging of DNA–protein complexes

A. Noy, R. W. Friddle

Complex interactions between DNA and DNA-repair proteins are central to protecting the genetic information in living cells. Common sources of DNA damage include free radicals and carcinogens from tobacco smoke, improperly cooked food, or even chemotherapy. If DNA damage is not repaired or is repaired with errors, it can lead to tumor-causing events. Learning how cellular proteins process damaged DNA on a molecular level is essential to understanding and controlling cancer initiation.

The mechanisms of DNA packaging—folding, compaction, and extension—are an important aspect of DNA integrity. During the cell life cycle, DNA is stored in compact structures for protection and is intermittently extended to allow transcription and repair. Together with DNA repair, DNA packaging maintains genomic integrity. The purpose of this project is to use single-molecule imaging techniques to study the mechanism of DNA binding and DNA damage recognition for proteins that are active in the initial stages of DNA repair. This project enhances the scientific understanding of DNA repair and DNA–protein interactions in general, and LLNL's capabilities in nanoscale instrumentation in support of DOE's biotechnology mission.

(a)

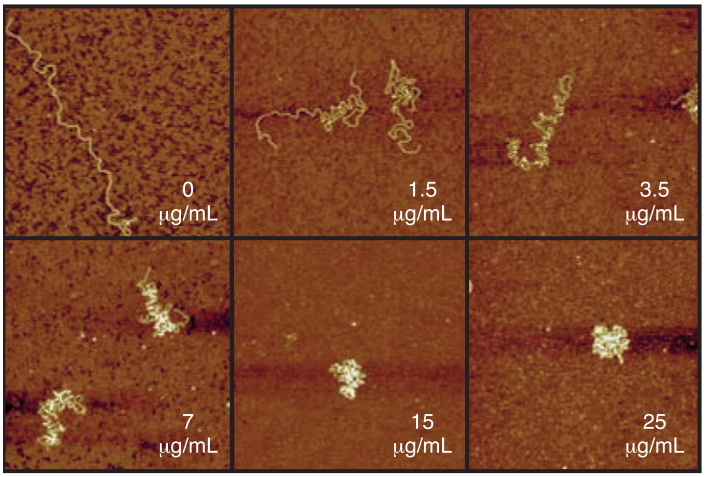

(b)

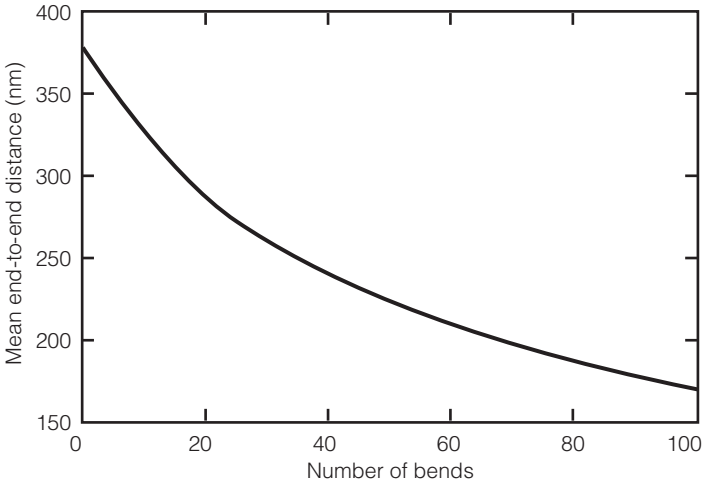

(a) Atomic force microscopy images of yeast mitochondrial DNA compacting in the presence of increasing concentrations of the protein ABF2p. (b) Compaction of DNA predicted by our computational model as a factor of the number of bends in the DNA double helix induced by ABF2p.

In FY2002, we used experimentation and computational modeling to investigate the actions of ABF2p, a yeast mitochondrial protein believed to be primarily responsible for DNA packaging in mitochondria. To directly observe compaction on a single-molecule level, we used high-resolution atomic-force microscopy (AFM), in which a sharp probe tip scans a sample and tracks its topography. Results showed that addition of ABF2p greatly changes DNA backbone geometry, leading to overall compaction. Significantly, we observed a similar mechanism for compaction of both linear and relaxed circular DNA. We believe that the protein causes compaction by inducing sharp bends in the DNA double helix—our images indicate that the average angle for these bends is 102°—and that this action neither depends on the supercoiling of DNA nor utilizes topological constraints of the circular DNA.

To quantitatively understand our results, we developed the "bent worm-like chain" model, which describes properties of the DNA molecule with regular sharp bends along its length. The model showed that the average end-to-end distance of a DNA molecule in solution decreases as more bends appear, demonstrating that introduction of such bends in the DNA helix is sufficient to cause compaction (see Figure). Our model predicted a DNA persistence length of 49 nm—in excellent agreement with published data. We also used our model to determine the binding constant of ABF2p to DNA and obtained a value of 1.4 μM, in good agreement with the results of circular dichroism measurement.

Based on our results, we propose the following mechanism of DNA compaction byABF2p: (1) The protein binds to the DNA double helix and induces sharp bends in the DNA. (2) These bends cause the molecule to compact. (3) Once a certain amount of the protein is bound, the DNA collapses into a tight bundle resembling a nucleoid. This mechanism does not appear similar to any known DNA packaging mechanism (e.g., histone or protamin packaging) and therefore represents a new mode of DNA packaging.

Developing new capability for precise elastic-moduli measurements at high pressure

P. A. Berge

The focus of this project was to perform wave-propagation modeling to determine the feasibility of developing a high-frequency ultrasonic interferometer capability at LLNL. Our goal was to determine what precision and sample sizes and types would be possible, and what frequency range would be appropriate for precise measurements of elastic properties at high pressure and temperature for various materials of interest to earth and planetary science and to stockpile stewardship.

The project used data from the literature, including material properties from extrapolation of prior measurements and theory, and performed wave-propagation modeling, assuming various sample thicknesses and pressures, to find the effects of attenuation, frequency range, and sample geometry on measurement precision. From the literature, we also obtained comparative information for various experimental methods used for measuring elastic constants at high pressures, and investigated the state-of-the-art for ultrasonic interferometry. The team brought expertise in wave-propagation analysis methods developed in geophysics, experience with static high-pressure elastic properties measurements, and knowledge of recent innovations in gigahertz ultrasonics to carry out this project.

Shear wave velocities are important since the precision of quantities derived from the observed travel times and amplitudes require good shear and compressional wave information. Precision is expected to be about 1 part in 1000 or better for velocities, elastic constants, and equation-of-state (EOS) information; and 1 part in 100,000 for compressional wave travel times but less precise for shear wave travel times. We found that interface effects and path effects may be less important than some other factors. For example, effects of heterogeneity in the sample could be significant for measurement uncertainty but may be mitigated by repeating measurements on similar samples or by careful sample preparation practices. Stress-induced anisotropy may produce slightly elliptical rather than spherical wavefronts, and is likely to have a greater effect on shear than on compressional waves. This must be taken into consideration if wedge-shaped buffer rods are used for converted waves to obtain shear-wave information.

Based on our FY2002 study, we recommend (1) using a range of sample sizes (e.g., 10 to 50 mm) to quantify sample size effects in diamond-anvil-cell experiments; (2) using the multi-anvil cell for measurements on polycrystalline samples to find properties of real materials and for measurements at high temperatures; and (3) obtaining shear-wave and compressional-wave information for a given material to fully characterize the isotropic elastic properties and to reduce the uncertainty in properties estimates derived from raw amplitude and travel-time data.

We conclude that it would be feasible to develop an ultrasonic interferometer at LLNL and produce high-precision elastic-properties information at high pressure. The Figure shows a schematic diagram of such an apparatus. A comprehensive modeling and experimental capability would support the NNSA national security mission by providing a new capability for high-precision EOS measurements at high pressures and temperatures for materials relevant to stockpile stewardship. Such data could facilitate development of comprehensive numerical models of explosions, incorporating effects that presently are combined in parameters used in phenomenological approaches. The new capability would also enable the Laboratory to attract collaborators and postdocs for basic earth- and planetary-sciences research.

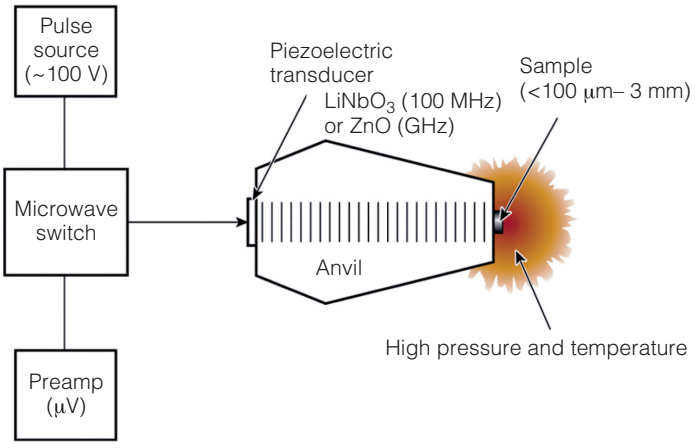

Schematic of apparatus for GHz ultrasonic interferometry. The pressure/temperature environment can be created in a diamond anvil cell, multianvil cell, or other configuration.

Computational design of novel, radiation-resistant fusion materials

A. Kubota, M. J. Caturla, B. D. Wirth and J. Latkowski

The promise of fusion as a viable twenty-first-century energy source requires the development of advanced structural and optical materials that are capable of withstanding the incredibly harsh environments expected to occur in a fusion reactor. Design challenges include damage from radiation and high concentrations of insoluble helium and reactive hydrogen gases that lead to swelling and embrittlement. At present, no sets of materials are available that can withstand the radiation environment of a fusion reactor.

The scope of this study is to determine the feasibility of using atomistic simulations to predict the radiation response of novel materials that are engineered with self-healing properties to survive in radiation environments over long time scales. One such class of materials shows promise. Nanocrystalline materials are made up of small grains on the order of several to tens of nanometers in size, and a consequent high-grain-boundary density. Experimental evidence suggests that these grain-boundary networks can act as sinks for defects and hence promote self-repair.

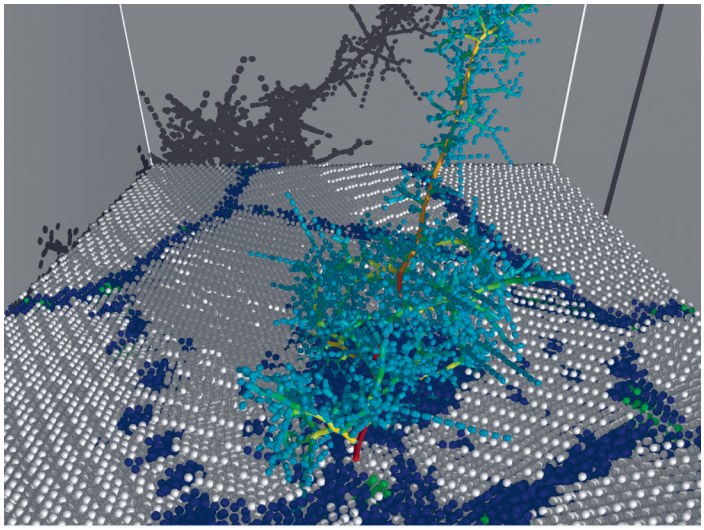

A 20-keV recoil cascade (light-blue to red) and defect (blue) structure in 10-nm grain nanocrystalline copper irradiated by a 20-keV recoil. The large amount of disorder and initial defect formation is attributed to the large cascade structure. The interaction of cascades and cascade-generated defects with grain boundaries is a fundamentally important yet poorly understood process relevant to nuclear materials and stockpile stewardship.

The goal of this study is to perform classical molecular-dynamics simulations to understand the response of nanocrystalline materials to radiation damage. Recent experiments of ion-irradiated metals have shown regions of decreased defect densities around grain-boundaries. During FY2002, we performed large-scale molecular dynamics simulations to understand the behavior of defects produced by energetic recoil atoms with up to 20 keV of kinetic energy. The Figure shows the large cascade track produced by a 20-keV recoil atom in nanocrystalline copper (Cu). This cascade track defines the extent over which initial disorder is produced. From this disorder and defect production, we observed later in the simulation, the enhanced annihilation of vacancy and interstitial defects near grain boundaries, compared to results in single-crystal copper. Moreover, our initially simplified understanding of radiation damage in nanocrystalline Cu was complicated by the observation of dislocation and stacking fault generation and interaction with grain boundaries. We now view radiation damage in nanocrystals as a much richer and more complex problem, with a great deal of fundamental physical processes yet to be learned and uncovered.

Additionally, during FY2002, we began to develop the code needed to parameterize embedded-atom-form helium interaction potentials based on equation-of-state data and electronic structure calculations. These potentials will allow us to understand the role of grain-boundary networks on helium transport in nanocrystalline metals.

This work is relevant to the LLNL and NNSA's missions in the areas of nuclear and stockpile materials. We hope this work will lead to much further experimental and computational studies on the fundamental processes of radiation damage in nanocrystalline materials. Continued work will lead to an increased understanding of the behavior and kinetics of the interactions of point defects with extended defects that are critical to furthering areas such as plutonium aging and fusion energy materials development.

Artificial microstructures for internal reference of temperature and pressure

M. Kumar, J. Colvin, A. Jankowski, J. McNaney, G. Campbell

Static high-pressure phase transitions and the associated equations of state (EOS) have been established for many elements, most of them pure metals. This study examines the case of dynamic loading of the microstructure to very high pressures and strain rates, a regime where the available data are sparse, and particularly so for the case of shock-induced melting. Usually the melting of the material has been inferred from "unexpected" deviations in the in situ diagnostic signals.

Our goal was to determine shock-compression melting of metals through post-mortem examination of the microstructures. Successful completion of this study will result in a diagnostic tool for spatial resolution of the thermal and pressure history. Such measurements are critical for scientific and stockpile stewardship efforts aimed at understanding phase transformations and constitutive response of materials under extreme conditions

The study had three parts: (1) fabrication and characterization of the sample with embedded nanothermometers, (2) design of a laser experiment to test the feasibility of the concept, and (3) execution of the experiment and microscopic examination of the recovered sample.

The aluminum–tin (Al–Sn) system was chosen for the targets as the phase relationships of these two metals are well understood under unshocked conditions. Also, the nearly complete immiscibility of the two elements under equilibrium conditions allows a high degree of control of the microstructure. A third advantage is that Sn has a low melting point and is in the range of the calculated temperature rise due to adiabatic heating.

The samples were deposited from an electron beam evaporation source onto a heated mica substrate maintained at an elevated temperature. The weight fraction of the Sn in Al was successfully varied from less than 1 wt% to about 30 wt%. The final objective was a dilute system of small particles of Sn in a homogeneous Al matrix so that the presence of the Sn—the "diagnostic" material—did not unduly change the characteristics of the traveling shock waves.

The design of the laser experiment was quite challenging. To allow the melting of the Sn particles to be used as a temperature reference, the Al matrix had to stay in the solid state during both shock compression and release. The submicrometer (<200 nm) size of the particles [Fig. (a)] allowed the hydrodynamic equations to be solved only for the EOS of Al; the calculations also assumed that the islands of Sn stayed in thermodynamic equilibrium with the surrounding Al. The compression and melt behavior of Sn was accounted for separately in the design calculations using LASNEX, a hydrodynamic code that includes details of laser–materials interactions and formation of the plasma that results.

In the LASNEX design, a 3ω laser light, with 43 J of energy deposited in a 1.5-mm-diam spot over 1 ns, is used to drive a shock that allows the Sn to melt only on release [Fig. (b)]. This design provides a maximum temperature reference for this depth into the target that can then be metallographically examined for evidence of Sn melting. Other designs allow the Sn to be melted on release over a greater spatial depth. Both these designs will be tested on the Omega laser at the University of Rochester. These experiments are slated for November 2002 as ride-along experiments at no cost.

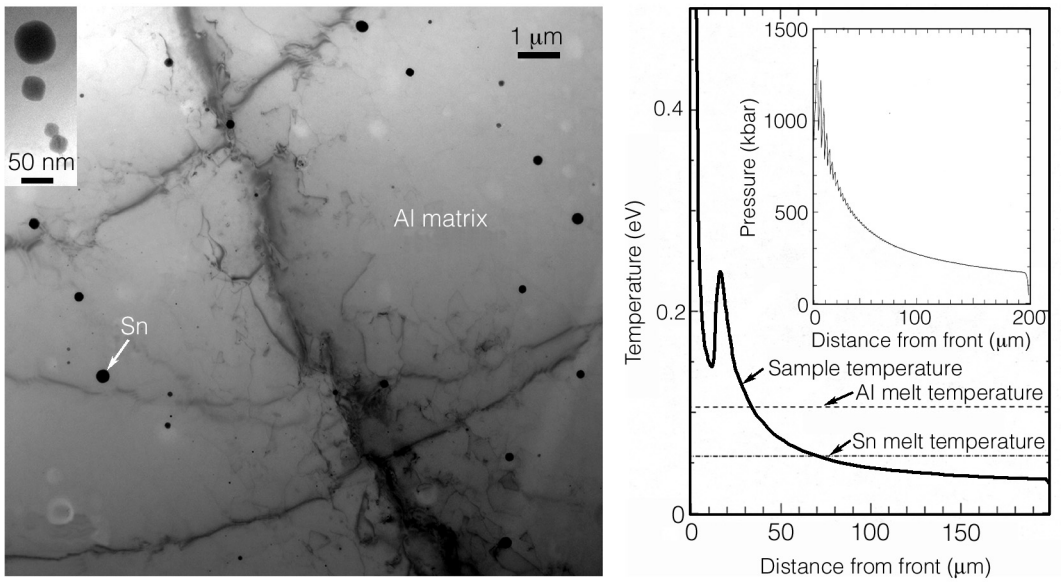

(left) TEM image of tin (Sn) nanoparticles embedded in the aluminum (Al) matrix, and (right) LASNEX design showing the expected temperature and pressure (inset) profiles.

Determining phonon-dispersion curves for plutonium and its alloys

J. Wong, A. Schwartz, H. Hong, T. C. Chiang

Pure plutonium (Pu) metal exhibits six solid state phase transitions with large volume expansion and contraction along the way to the liquid state: $\alpha>\beta>\gamma>\delta>\delta'>\varepsilon>$liquid. The face-centered cubic (fcc) δ-phase has desirable mechanical properties such as ductility and machinability, whereas the monoclinic a phase is quite brittle and difficult to machine. To overcome these challenges, Pu can be stabilized to the δ phase by alloying with Group III metals such as aluminum and gallium (Ga). This alloying expands the δ-phase field (region of space) from about 2 to 8 at.% Ga at room temperature and below. Retention of the δ-phase at room temperature makes alloying of great engineering significance.

Phonons or lattice vibrations are elementary excitations in solids. The variations of phonon frequencies, ω, together with crystal momentum, q, i.e., the so-called phonon dispersion curves (PDCs), are fundamental to a host of material properties including force constants, sound velocity, elastic constants, thermodynamic, thermal, phase stability, and interatomic potentials. However, PDC measurements on Pu and its alloys with conventional inelastic neutron scattering (INS) are hindered by two factors: (1) Pu has a high neutron absorption cross-section and (2) INS requires at least a 1-mm cube of single-crystal Pu, and nothing that size is available. As a result, until this study, the PDCs for Pu and its alloys remained undetermined.

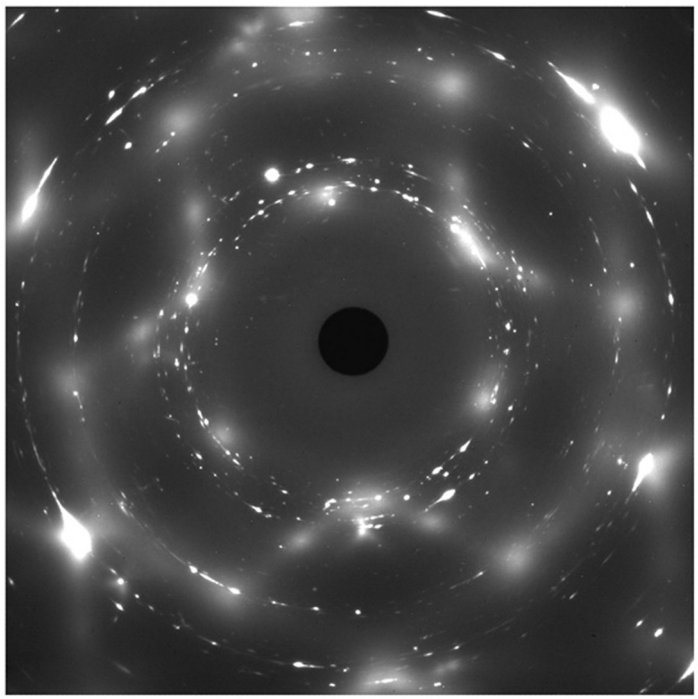

Thermal diffused scattering (TDS) image from a [111] domain in a 2 mm-diam, 30-μm-thick sample of Pu–Ga alloy. The image, recorded with a 25-μm beam at 18 keV, clearly shows a 3-fold symmetry. The bright spots in the TDS image are points on the Ewald sphere of high acoustic phonon population.

With the advent of high-brightness, third-generation synchrotron x-ray sources, we proposed an exploratory effort to establish the feasibility of measuring the PDCs of δ-phase Pu–Ga alloys using a combination of state-of-the-art synchrotron techniques of thermal diffused scattering (TDS) and high resolution inelastic x-ray scattering (HRIXS) such as those located at the Advanced Photon Source (APS) at Argonne National Laboratory and the European Synchrotron Radiation Facility (ESRF) in Grenoble, respectively. These techniques, which were recently shown as proven alternatives to INS for PDC measurement, are particularly suitable for small samples or materials with a high neutron absorption cross-section such as Pu.

A two-prong approach employing TDS and HRIXS has been taken because since these two techniques are complementary, particularly for acoustic phonons. The choice of δ-phase Pu alloys was made because of the simpler fcc crystal structure compared to the more complex low-symmetry crystal phases of Pu and because of the relevance to Pu metallurgical processing, which is critical to LLNL's stockpile stewardship mission.

The scope of our FY2002 work included (1) designing and fabricating large-grain-domain polycrystalline specimens of δ-phase Pu–Ga specimens, (2) designing sample chamber and scattering geometry for Pu TDS measurements at the APS, (3) performing exploratory TDS experiments at APS on δ-phase Pu–Ga alloy, and (4) extending and modifying our TDS design for future HRIXS experiments at ESRF on these alloys. We accomplished all these tasks and succeeded in determining TDS images along two of the three principal directions in the fcc lattice. The Figure shows the result for the [111] TDS image.

Mathematics and Computing Sciences

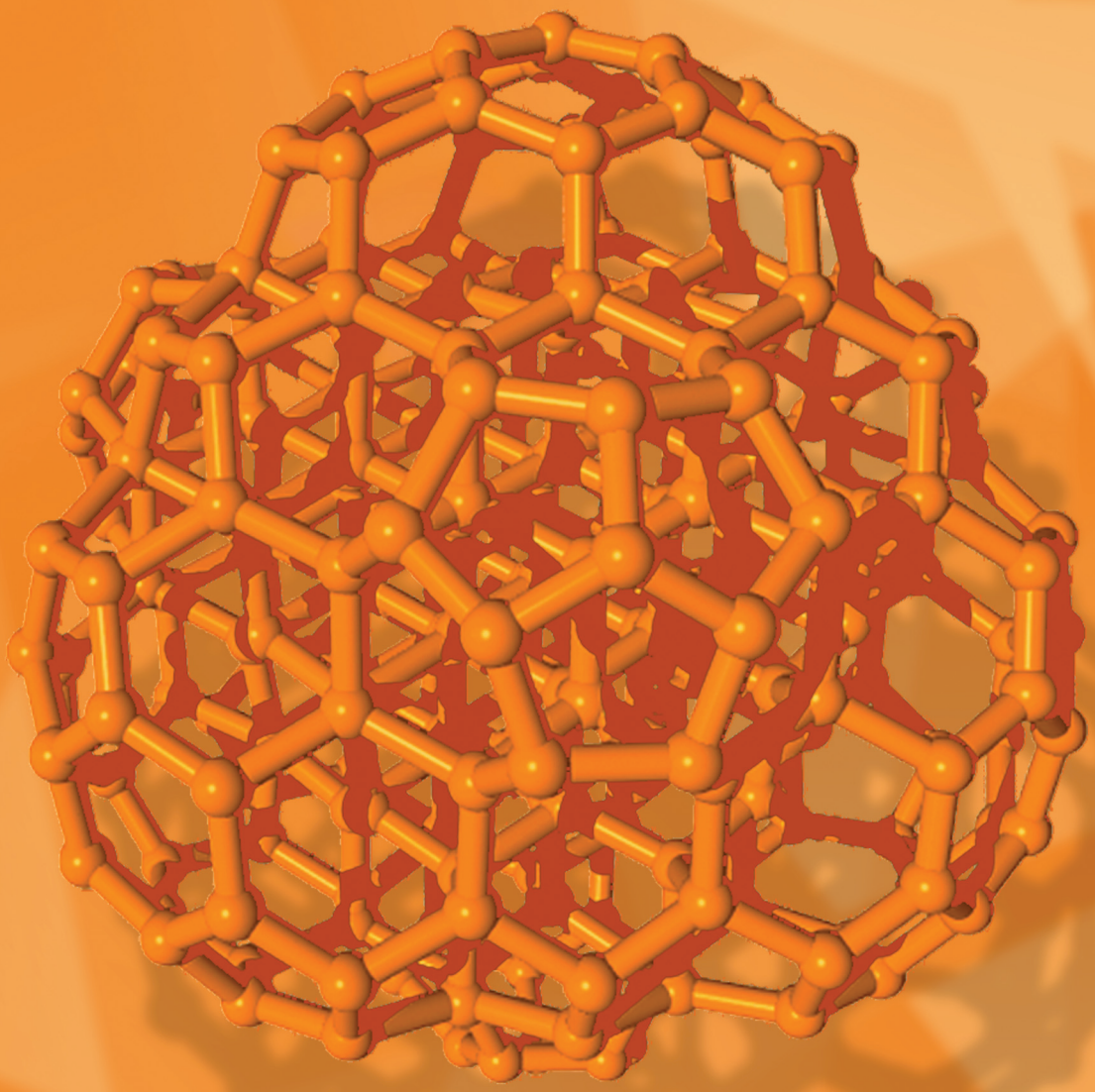

Section 8

Section 8 — Mathematics and Computing Sciences

Scientific component technology initiative

S. Kohn, B. Bosl, T. Dahlgren, T. Epperly, G. Kumfert, S. Smith

Numerical simulations play vital roles in DOE's science mission as basic research tools for understanding fundamental physical processes. As simulations become increasingly sophisticated and complex, no single person—or even single laboratory—can develop scientific software in isolation. Instead, computational scientists must construct simulation software by combining separate software modules developed by experts in physics, chemistry, mathematics, and computer science. Often, combining these software packages in a single application is difficult because of differences in implementation language, programming style, or calling interfaces.

To address problems of complexity, re-use, and interoperability for simulation software, we are developing software component technology for high-performance parallel scientific computing. Our research focuses on the unique requirements of scientific computing on Advanced Simulation and Computing (ASCI) and ASCI-class parallel machines—such as fast, in-process connections among components, language interoperability for scientific languages, and data-distribution support for massively parallel components. This work supports DOE and LLNL missions in national security, energy technology, and environmental stewardship.

In FY2002, we continued developing our Babel language interoperability tool for high-performance parallel scientific software. Our Babel tool generates "glue" code that allows a software library to be called seamlessly from any supported language. Babel currently supports Fortran 77, C, C++, and Python; support for Java and Fortran 90 is being developed. A number of features were added this year at the request of users, including routines that automatically translate between Fortran and C array ordering, Fortran interface descriptions, method overloading, and initial support for Fortran 90. We also analyzed Babel overheads, improved performance, and significantly increased the robustness of our software using an extensive regression test suite with over 6000 tests.

In collaboration with the Adaptive Laser Plasma Simulator (ALPS) project, we demonstrated the use of Babel in ALPS, an adaptive mesh refinement simulation code used to investigate laser–plasma interaction for inertial-confinement fusion. Our Babel-modified ALPS code combines C++ and Fortran with Python, which is used as the scripting language. For example, from the Python scripting layer, we can call the application framework (written in C++), which in turn calls a numerical routine written in Fortran, which in turn calls a laser boundary condition module in Python. This interoperability allows a scientist to rapidly prototype new boundary condition modules in Python without recompiling or linking.

Finally, we collaborated on community technology standards with DOE's Common Component Architecture (CCA) working group (see http://www.cca-forum.org). The DOE Office of Science has selected the CCA as one of the recipients of a Scientific Discovery through Advanced Computing (SciDAC) award, a 5-yr research effort consisting of DOE laboratories and academic partners and intended to deliver component technology to computational simulation programs within the DOE. Babel will serve as a foundation of the CCA infrastructure and will link SciDAC numerical and meshing libraries—typically written in C or C++—with SciDAC applications written in Fortran 90.

The component technology developed under this project is playing a critical role in efforts for interoperable scientific applications.

The stochastic engine: Improved accuracy in predicting the behavior of unobservable features in geologic environments

R. Aines, J. Nitao, W. Hanley, A. Ramirez, R. Newmark, S. Carle, V. Johnson, R.Glaser, K. Dyer

Complexity is an ever-present element in many LLNL programs. We are often asked to answer important questions—for example, determining the underground connectivity that allows contamination to move through the ground—by combining computer simulations with sparse data from many sources. Similar issues arise in imaging rapidly evolving systems, utilizing diverse intelligence data, or quickly evaluating the internal flaws in a large structure. A rigorous approach is not always available.

In this project, we are developing a new approach that allows us to use all the data available in these problems by integrating accurate simulators with a probabilistic method that accounts for error in both data and models. The answer obtained is very different from conventional solutions and allows decision makers to weigh various courses of action or determine what new data would be required to reach a decision with sufficient confidence. We call this combination of probabilistic and deterministic approaches the "stochastic engine." In addition to enhancing LLNL's support of DOE's environmental restoration mission, this methodology will find applications in programs that support LLNL's antiterrorism, nonproliferation, and stockpile-stewardship missions.

Accurate simulators and fast computers make this methodology possible, but the root technology is importance-based Monte Carlo sampling. The method rapidly chooses among a very large number of hypothesized states of the system, and the final selected states are those consistent with all the data. In our Earth Science application, we transform uncertainty in a sample space (e.g., lithology or permeability) to uncertainty in a measurement space (e.g., temperature or electrical current). Predicted measurements from a simulator are used to estimate the likelihood of actual measurements, which in turn reduces the uncertainty in the original sample space via conditional probability (Bayesian inferencing). A highly efficient, staged Metropolis-type search algorithm is used to address extremely large, multidimensional state spaces.

In FY2002, we extended our work to three-dimensional imaging of fluids in the earth. At DOE's Hanford Site, operations personnel want to know the certainty with which they can determine if the tanks stored at that site are intact, and, if some liquid escaped from the tanks, how much entered the soil and how far it traveled. The Figure, a probabilistic image of an experimental leak at a Hanford test facility, was generated using electrical resistance tomography data, which can be combined with pressure- and moisture-sensor data to provide a robust monitoring method.

In FY2003, we plan to combine this approach with the soil representation demonstrated last year, providing the first multisensor images of tank leaks at the Hanford site and steam injection at the Savannah River site. We plan to extend the concept of a "hypothesized object in a geologic background" to locate underground facilities and tunnels. Demonstrations will be conducted that apply the stochastic engine to diverse intelligence data interpretation and to structural-flaw analysis of buildings and complex mechanical devices. These real-world applications use LLNL's large-scale computing capability, which allows us to analyze extremely large amounts of data composed of millions of subunits and to continuously upgrade the analysis as new data become available.

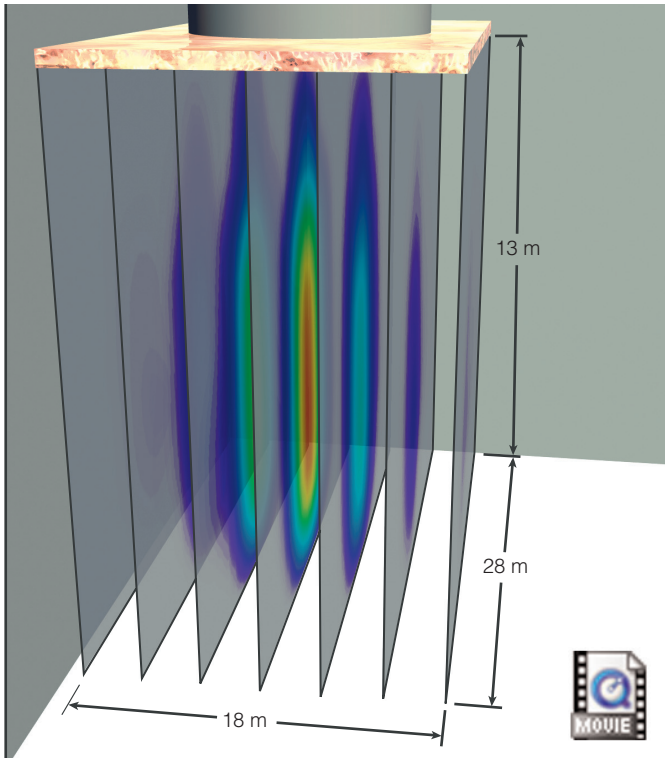

Probabilistic image of a water-infiltration experiment at the Hanford nuclear waste tanks. Red indicates >0.6 probability of fluid presence.

Adaptive methods for laser–plasma simulation

M. R. Dorr, F. X. Garaizar, J. A. F. Hittinger

The ability to predict and control the interaction of laser light with plasmas is important in the design of laser-driven fusion experiments. For instance, under certain conditions, the beat wave of beams crossing in a plasma flow can resonate with an ion acoustic wave in the plasma, resulting in a transfer of energy from one beam to the other. Such problems are of potential relevance to the National Ignition Facility (NIF), in which beams entering the hohlraum containing the target capsule will cross in a region of substantial plasma flow. If a sufficiently large resonant region occurs, the resulting transfer of beam energy could affect the uniformity of radiation pressure on the target. Predictive computational models validated with experiments provide an effective tool in understanding laser–plasma interactions and will play an important role in the success of experiments performed at NIF.

The objective of this project is to develop new adaptive mesh refinement (AMR) algorithms and a research code called Adaptive Laser Plasma Simulator (ALPS) for simulating laser–plasma interactions. This work supports Laboratory missions in national security, such as stockpile stewardship and high-energy-density science.

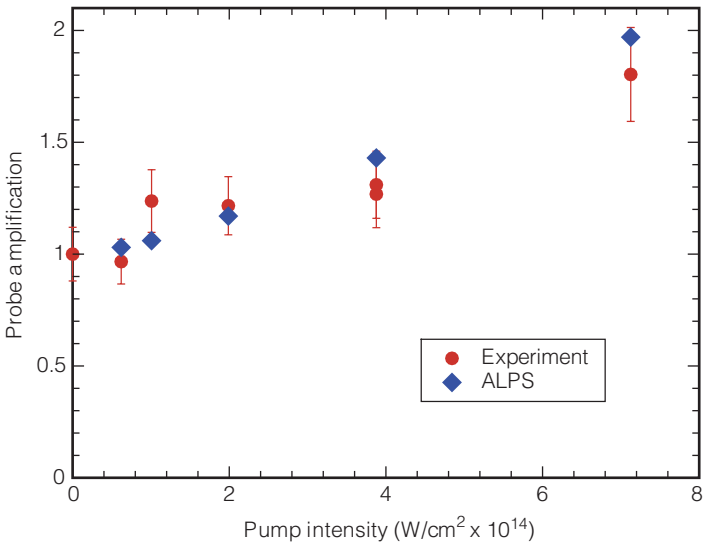

Graph showing agreement between predictions and experimental measurements of probe beam amplification by pump beams of varying intensities. Predictions were made with Adaptive Laser Plasma Simulator, a fully parallel research code for simulating laser–plasma interactions on massively parallel computer systems for the National Ignition Facility.

Our AMR algorithms focus computational resources on portions of a simulation region requiring high resolution, without wasting grid cells in regions that can be adequately resolved using coarser grids. Because the cost of numerical simulations is directly related to the number of grid cells, efficient grids can achieve substantial savings in execution time and memory utilization. This approach can also solve crossing-beam problems, in which the interaction region requires substantially higher resolution than the surrounding plasma flow.

The ALPS code involves an adaptive computational grid consisting of Cartesian grid patches of varying resolution. The location and degree of resolution of the grid patches is dynamically changed to follow important solution features according to user-specified criteria. On these adaptive grids, ALPS solves plasma-fluid equations coupled to a paraxial-light model. The code is fully parallelized to run on LLNL's massively parallel computer systems.

In FY2002, the idealized, proof-of-principle capability initiated in FY2001 was extended by adding the additional physics capabilities needed to predict an actual crossing-beam experiment. ALPS was then applied to a variety of test problems to study the scaling of energy transfer with beam intensity and gradients in the transverse flow. This included problems representing experiments performed at the Omega facility at the University of Rochester Laboratory for Laser Energetics. For example, the Figure shows ALPS predictions and experimental data obtained on Omega for amplification of a probe beam by pump beams of varying intensities crossing in a plasma generated by an exploding foil. Comparisons of our ALPS calculations with other experimental and theoretical predictions also helped demonstrate the existence of a nonlinear saturation mechanism that reduces the amount of energy transferred between sufficiently intense beams in plasmas.

This project has advanced the Laboratory's computational capabilities in the area of AMR algorithms and their application to laser–plasma interaction problems.

Rapid problem setup for mesh-based simulation

D. L. Brown

Many simulation projects at LLNL involve the solution of partial differential equations in complex, three-dimensional (3-D) geometries. A significant bottleneck in carrying out these simulations arises in converting some specification of a geometry, such as a computer-aided design (CAD) drawing to a computationally appropriate 3-D mesh that can be used for simulation and analysis. Even using state-of-the-art mesh-generation software, this setup requires weeks or months, which is often much longer than required to carry out the computational simulation itself.

The objective of this project, called Rapsodi, is to reduce this setup time to less than a day by developing rapid-setup technology for computational physics and engineering problems. This technology consists of tools and algorithms that represent complex geometry using mixed-element unstructured meshes, overset meshes, or Cartesian embedded-boundary (EB) meshes. By developing automation tools with immediate applicability in computational physics and engineering problems—such as those relevant to stockpile stewardship—this project supports LLNL's national security mission.

Although completely automatic mesh generation is extremely difficult, the amount of manual labor required can be significantly reduced. By developing novel, automated, component-based mesh-construction procedures and automated CAD geometry repair and cleanup tools, Rapsodi will significantly reduce the amount of hand crafting required to generate meshes for scientific simulation codes.

During FY2002, we improved upon the tools developed in earlier years of this project. These include tools for (1) simplifying CAD geometries by removing unwanted details or extracting a subset of the model and (2) interactively repairing structural errors in CAD geometries, such as invalid trimming curves and duplicate or missing surfaces. We also developed an algorithm to determine connectivity and generate a global triangulation for CAD geometries that consist of up to hundreds of trimmed surface patches. This algorithm automatically repairs most topological errors in the model, such as gaps and overlaps between surfaces. In addition, a fast algorithm that uses global triangulation to project points onto the CAD surface was developed and incorporated into our hyperbolic surface grid generator.

These algorithms can also be used to generate a water-tight representation of a complex surface, either with global triangulation or a set of conforming, trimmed spline patches. This representation can then be used to produce an EB mesh. The Figure is an application of Rapsodi tools to a high-energy accelerator waveguide cavity.

We also completed a fast, robust 3-D mixed-element mesh generator; built a tool that produces a water-tight surface triangulation from a CAD geometry; and used this tool with NASA's CART3D software to create the capability to produce EB meshes from complex CAD geometries.

The software developed in this project has been installed on LLNL computers for evaluation in nuclear-physics applications and is being prepared for use in simulations involving heavy-vehicle aerodynamics and aerosol transport.

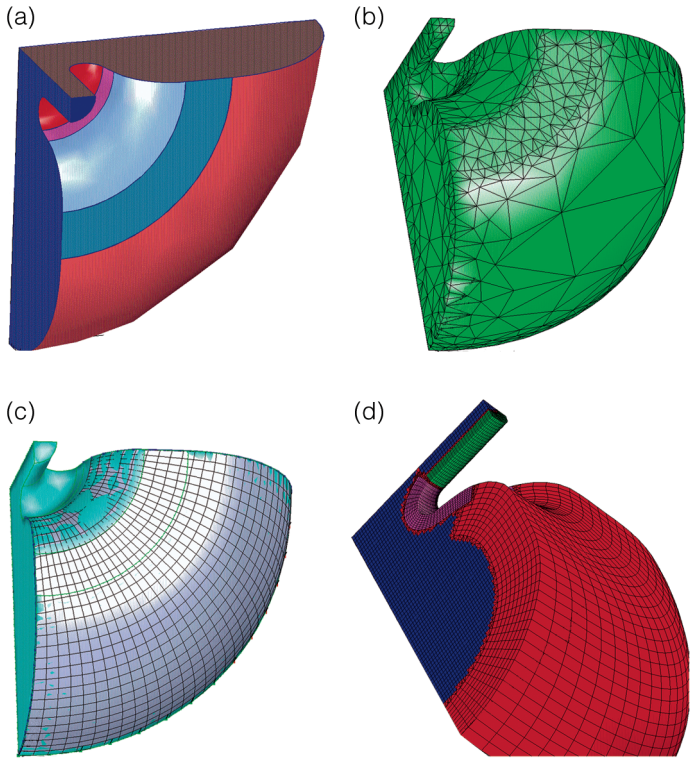

This project is developing rapid-setup technology for computational physics and engineering problems that require representation of complex geometry. Starting from (a) a broken CAD geometry of a high-energy accelerator waveguide cavity, Rapsodi tools (b) repair the surfaces, determine the connectivity, and build a global surface triangulation. Next, (c) surface meshes are constructed and used to build structured-volume meshes. These are connected with regions of unstructured tetrahedrons and pyramids to form the (d) final mixed-element computational mesh.

New directions for algebraic multigrid: Solutions for large-scale multiphysics problems

V. E. Henson

Computer simulation of extremely large multiphysics problems is increasingly important in the Advanced Simulation and Computing (ASCI) program and in disparate topics investigated at LLNL, such as climate modeling, porous-media flow, and atomic substructure. Such problems require the use of thousands of processors and, consequently, computational algorithms that are scalable—the computing time required to solve the problem must remain constant as the size of the problem and the number of processors increase. Many of these problems are also highly ill conditioned and extremely difficult to solve by any known methods.

This project focuses on algebraic multigrid (AMG) methods, which are commonly used to solve unstructured-grid problems for which conventional methods are unsatisfactory. Conventional multigrid methods are provably scalable for many problems, but constructing the solver requires geometric information about the physical problem and often entails complicated design work. By contrast, algebraic methods use only the operator matrix, require no geometric information, and construct the solver automatically. By developing practical, scalable AMG methods for solving large-scale multiphysics problems relevant to stockpile stewardship, this project contributes to LLNL's mission in national security.

Multigrid methods work by recursively applying a two-grid method. Two-grid methods are based on the discovery that "smooth" errors—those that cannot be reduced by standard iterative methods, such as Gauss-Seidel, Jacobi, or conjugate gradients—can be accurately represented and efficiently eliminated on a coarse grid. The key to creating an effective AMG algorithm is to algebraically characterize smooth errors and build operators that represent them accurately.

We devised new AMG algorithms and implemented them into efficient parallel codes. These codes are a mainstay of LLNL's advanced-computing software library and also form a research platform for deeper investigation into advanced, multilevel solver technology. In FY2000, we integrated a parallel AMG code into two of LLNL's major simulation codes (ALE3D and Kull) and developed the concept of element-based AMG (denoted AMGe) for effectively treating especially difficult problems in mechanics and elasticity. The AMGe concept is founded on the realization that individual finite-element stiffness matrices contain critical information about the smooth-error components. In FY2001, we developed AMGe methods and discovered new interpolation, coarsening, and coarse-grid operator schemes that attain superior results on many problems, especially elasticity and convection diffusion.

Results in FY2002 include developing parallel AMGe and another approach, the spectral AMGe method. Unlike other AMG methods, spectral AMGe makes no assumptions about the character of smooth-error components. Instead, the nature of these components is determined directly, by solving a series of local problems for the eigenvectors of the element-stiffness matrices.

The results of this project have been implemented into codes used regularly by numerous researchers in the ASCI and high-explosives research programs at LLNL. The DOE Office of Science has also selected this work for a Scientific Discovery through Advanced Computing (SciDAC) award. The SciDAC program is a 5-yr effort consisting of DOE laboratories and academic partners and intended to deliver component technology to computational simulation programs within the DOE.

Our research has made LLNL one of the world's leading centers of AMG research, increasing the Laboratory's visibility and importance in the worldwide scientific community.

Numerical technology for large-scale computational electromagnetics

R. M. Sharpe, D. White, N. J. Champagne, M. Stowell

The key bottleneck of implicit computational electromagnetics (CEM) tools for large complex, geometries—such as those addressed in the Advanced Simulation and Computing (ASCI) program—is the solution of the resulting linear system of equations. The goal of this effort is to research and develop critical numerical technology that alleviates this bottleneck for large-scale CEM by greatly reducing the time required to solve the associated hybrid linear systems of equations.

The mathematical operators and numerical formulations used in this arena of CEM yield linear equations that are complex valued, unstructured, and indefinite. In addition, simultaneously applying multiple mathematical modeling formulations to different portions of a complex problem (hybrid formulations) results in a mixed-structure linear system, further increasing the computational difficulty. Typically, these hybrid linear systems are solved using a direct solution method, which was acceptable for Cray-class machines but does not scale adequately for ASCI-class machines. In addition, LLNL's existing linear solvers are not well suited for the linear systems that are created by hybrid implicit CEM codes.

Activities in previous years of this project focused on establishing a test suite of samples matrices to evaluate the solver research; extending the ISIS++ solver framework to treat complex-valued, hybrid linear systems by supplementing the native iterative methods in the package with several direct solvers; and implementing a Shur-complement approach for solving block-structured hybrid linear systems. We also identified the need for both matrix- and operator-based preconditioners. Matrix-based methods can be applied to any linear system of equations after the matrix has been assembled.

In FY2002, work on sparse approximate inverse preconditioners and on incomplete lower/upper preconditioners was completed and incorporated into the final solver package. Research on direct operator-based methods, initially performed with R. J. Adams of the University of Kentucky, recasted integral equations of the first kind into integral equations of the second kind. Preliminary results indicate improvement in the basic conditioning of the linear system that reduces solution time by two orders of magnitude for some systems of equations. The Figure is an example of a hybrid matrix for a coupled finite element–boundary element solution of Maxwell's equations.

Previous work on a single-level multipole algorithm—a method shown to reduce the operation count from N*N to N*log(N) for linear systems to which they apply—was extended to a multilevel algorithm, which further improved the solution performance and increased computational speed. All of the results from this LDRD project are being incorporated into LLNL's solver framework for researchers involved in CEM.

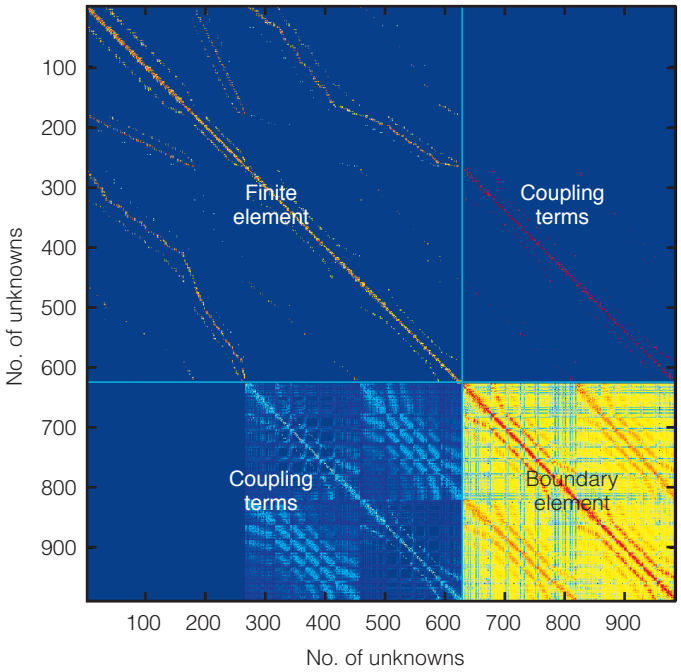

Example of a hybrid matrix for a coupled finite element–boundary element solution of Maxwell's equations. Blue represents zero matrix values. The finite element represents a discretization of the Helmholtz equation, and the boundary element represents a discretization of the electric-field integral equation.

Hydrogen bonding and molecular dissociation at high pressure: Low-Z liquids and liquid mixture

G. Galli

Hydrogen bonds are the most prominent "weak" interactions in solids, liquids, and gases. They determine the crystal packing of many organic molecules, the three-dimensional structure of biological macromolecules, and the bonding properties of water. However, the nature of hydrogen bonds and their changes under pressure are largely unknown.

In this project we investigated the structural and dynamical properties of low-atomic-number (low-Z), hydrogen-bonded liquids and liquid mixtures under pressure, using molecular dynamics simulations. The data obtained are relevant to the performance of inertial fusion targets for stockpile stewardship and also to models describing the interiors of planets, which have physics regimes similar to those found in nuclear weapons.

In FY2002, we completed our study of hydrogen metallization under pressure and of compressed liquid oxygen, and we also started an investigation of two new low-Z solids and liquids under pressure: carbon dioxide (CO_2) and lithium hydride (LiH).

By using both density functional theory and quantum Monte Carlo calculations, we found that along the 3000 K isotherm, the optical gap of liquid hydrogen vanishes at 9-fold compression and that the liquid conductivity is that of a poor metal. This is in agreement with gas-gun experiments that reported metallization of hydrogen at the same compression several years ago. However, the computed metallization pressure is slightly smaller than that measured in shock-wave experiments, and the conductivity is significantly larger (by a factor of 3 to 4). We found that in liquid hydrogen the insulator-to-metal transition (ITM) is dissociation and not disorder driven, contrary to earlier assumptions. While the fraction of dissociated molecules in metallic liquid hydrogen close to the ITM transition is more than 50%, this fraction is very small in liquid oxygen. We found liquid oxygen to metallize in a state which is almost entirely molecular. The ITM transition in liquid oxygen occurs at a pressure close to that of the solid, contrary to hydrogen where the ITM in the liquid is at a much lower pressure than in the solid. The peculiarity of oxygen is the spin triplet state of the molecule composing the low pressure liquid.

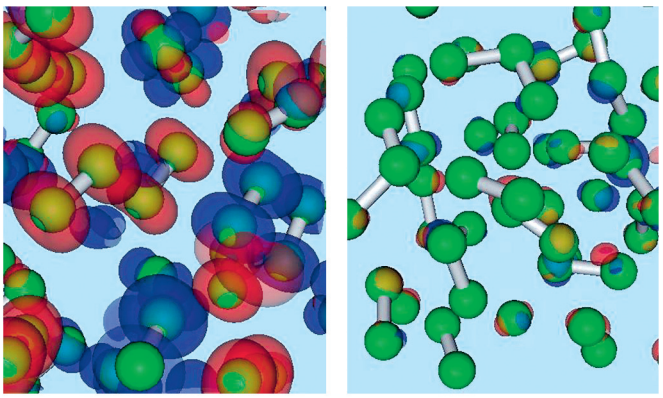

Charge-density difference between spin up and down in (left) low- and (right) high-pressure liquid oxygen. Under pressure, spin fluctuations are suppressed (see text). Positive and negative regions of charge density are represented by red and blue isosurfaces. Green spheres represent the positions of oxygen atoms.

One interesting aspect highlighted by our simulations is the suppression of spin fluctuations under pressure. This is illustrated in the Figure, in which the difference in charge density between spin up and down is shown at two different pressures. While at low pressure (~ 30 GPa) the difference shows that there are well-defined molecules in a triplet state in a disordered geometrical arrangement. At high pressure, the molecules are no longer in a triplet state and the difference between spin-up and spin-down density goes to zero throughout the liquid.

In addition to hydrogen and oxygen, we investigated the high-pressure molecular phases of CO_2. After the exciting discovery of a polymeric phase of CO_2 under pressure (~ 45 GPa) by Yoo et al., which is similar to the SiO_2 quartz structure, several other CO_2 phases were proposed, which are intermediate between the low-pressure molecular solid and the high-pressure quartz-like structure. These were proposed on the basis of x-ray and Raman data taken for samples between 15 and 35 GPa. We carried out a series of ab initio calculation, which showed that all the available experimental data can be very well accounted for by strictly molecular phases. In these phases, the CO_2 molecules are arranged differently from the low-pressure structure. However, these molecules retain the same bonding character as at ambient conditions; in particular, their bond lengths do not change.

Finally we carried out a detailed study of melting of LiH under pressure using a two-phase technique, which we applied within the context of ab initio simulations for the first time.

Generalized methods for finite-element interfaces

M. A. Puso, E. Zywicz

With the increasing complexity of finite-element models, it has become essential to mesh individual parts of a finite-element model independently such that nodes at part boundaries are not aligned. Current finite-element techniques for connecting (i.e., gluing, tying) these dissimilar meshes together at the boundary often cause serious errors in a stress analysis. Aware of this fact, engineering analysts work to avoid dissimilar meshes—often to no avail. Furthermore, the trend for teams of analysts to work independently on different weapons subassemblies makes the need for accurate dissimilar-mesh connection more acute.

The goal of this project is to solve the problem of connecting dissimilar meshes through research in accurate numerical methods that will eliminate the need to produce conforming meshes. If successful, this new technology can potentially save vast amounts of time and money across the DOE Complex. For example, a large weapons model often takes a month to build, and will undergo many revisions over a matter of years. Analysts estimate that a method for connecting dissimilar meshes may save up to 25% of their time in meshing over the course of a project, without sacrificing accuracy. In addition, similar numerical problems occur when interfacing meshes slide with contact. Our new "mortar method" techniques are now being applied to improve contact-surface modeling. This project enhances LLNL's competency in computational mechanics in support of stockpile stewardship.

The mortar method for connecting two-dimensional (2-D), flat interfaces has been extended to connect arbitrary 3-D, curved meshes so that optimal convergence is achieved. In this way, refinement of the dissimilar mesh will have the same asymptotic convergence rate as the conforming mesh—dissimilar meshing will not compromise mesh quality. This method requires solving surface integrals involving Lagrange multiplier fields for traction and displacement. Such surface integrals are straightforward for 2-D, flat interfaces but complicated for 3-D, curved surfaces. In FY2001, we developed a closest-point projection-type algorithm for 3-D surface integrals and used simple Lagrange multiplier fields to demonstrate optimal convergence on 3-D models with curved, tied interfaces.

In FY2002, we further developed our theory for stability conditions; implemented a dual formulation for the Lagrange multiplier fields, which sped calculation times by a factor of 7 over our previous results; and began work on the mortar method for contact. Mortar contact resolves the mortar-averaged gap function into normal penetration and frictional slip, provides vastly superior convergence behavior, and eliminates the locking associated with the standard contact methods in high-pressure environments, as seen in the Figure.

In FY2003, we plan to finish mortar normal contact, incorporate friction into contact simulations, and apply our methods to discretizations involving higher-order elements.

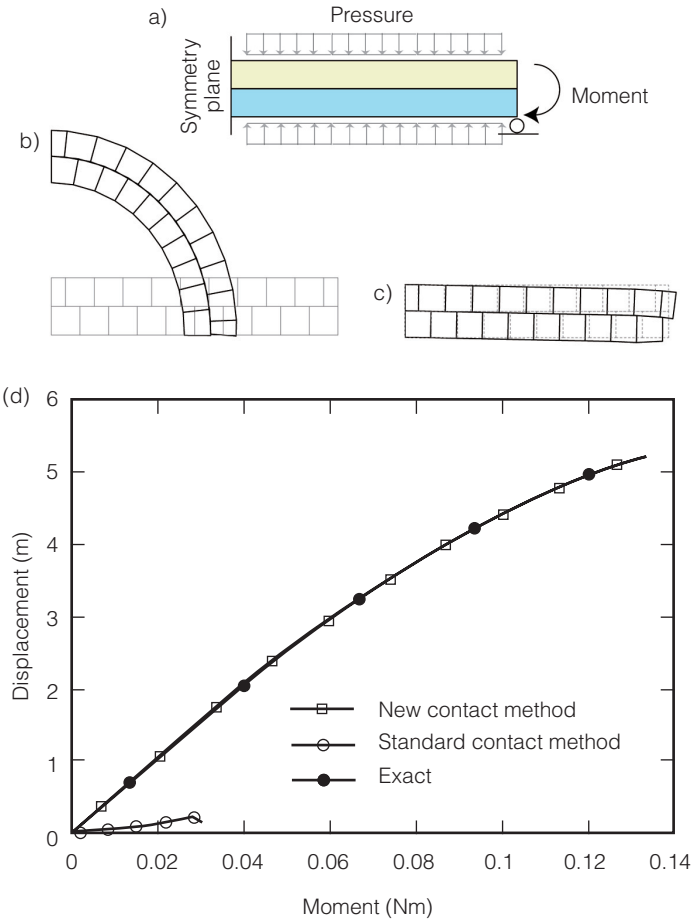

Our "mortar method" can connect arbitrary 3-D, curved meshes and eliminate the need to produce conforming meshes. These examples illustrates how, under high pressures, standard contact locks, whereas mortar contact yields nearly exact results. (a) Contacting beams with ambient pressure and applied moment. (b) Resulting deformation using new mortar contact. (c) Pathological locking behavior demonstrated by standard contact. (d) Simulated results versus analytically exact solution.

Exploratory research into the extended finite-element method

R. M. Sharpe, K. D. Mish

The finite-element method has become the standard tool of computational mechanics in the national laboratory community and accounts for the vast majority of computational analyses in LLNL's engineering work. General-purpose finite-element LLNL physics codes such as DYNA3D and ALE3D represent the pinnacle of simulation in mechanical engineering.

Unfortunately, conventional unstructured finite-element applications are optimized for designing idealized mechanical systems, whereas LLNL missions such as stockpile stewardship are more concerned with as-built systems. Tools optimized for general mechanical design can, with sufficient effort, provide efficient mechanical analysis of as-built systems. However, considerable discrepancies between idealized and as-built configurations can render analyses based on idealized configurations woefully inadequate.

The goal of this project is to develop extended finite-element (XFEM) techniques by improving conventional finite-element modeling so that the actual configuration of as-built systems can be subjected to a broader range of mechanics simulations. This will remedy some of the most onerous limitations of finite-element modeling relevant to LLNL, such as localization and singular response near cracks and imperfections. This project will substantially extend LLNL's core competence in computational science and engineering and its capabilities in nuclear weapons engineering and manufacturing technologies in support of DOE's national security mission.

During FY2002, previous results in crack propagation and material interface were extended to integrate XFEM techniques into computer-aided engineering. Additional capabilities essential for computer-aided problem setup goals—such as automation of mesh generation—were also demonstrated. Several promising new techniques developed to automate the analysis process include (1) radial basis functions—a new technique for implicit surface definition originally developed for computer graphics rendering—for determining the boundaries of a mechanical system; (2) improved integration techniques for evaluating the governing XFEM equations over regions with irregular material boundaries, cracks, or contact surfaces; and (3) new enrichment functions for modeling voids and other localization phenomena commonly found in weapons materials.

Validation of the XFEM techniques included using these new methods to analyze problems with closed-form solutions. Figure (a) shows a typical validation problem, in which a spherical inclusion is modeled in an otherwise uniform and isotropic body—represented with a structured XFEM mesh—subjected to uniaxial tension. Figure (b) is the model's boundary-value problem description. Convergence tests demonstrate that both structured and unstructured XFEM solutions converge at the same rate as conventional finite-element methods, which means that these XFEM techniques can be used to construct meshes for analysis with less effort but without compromising accuracy.

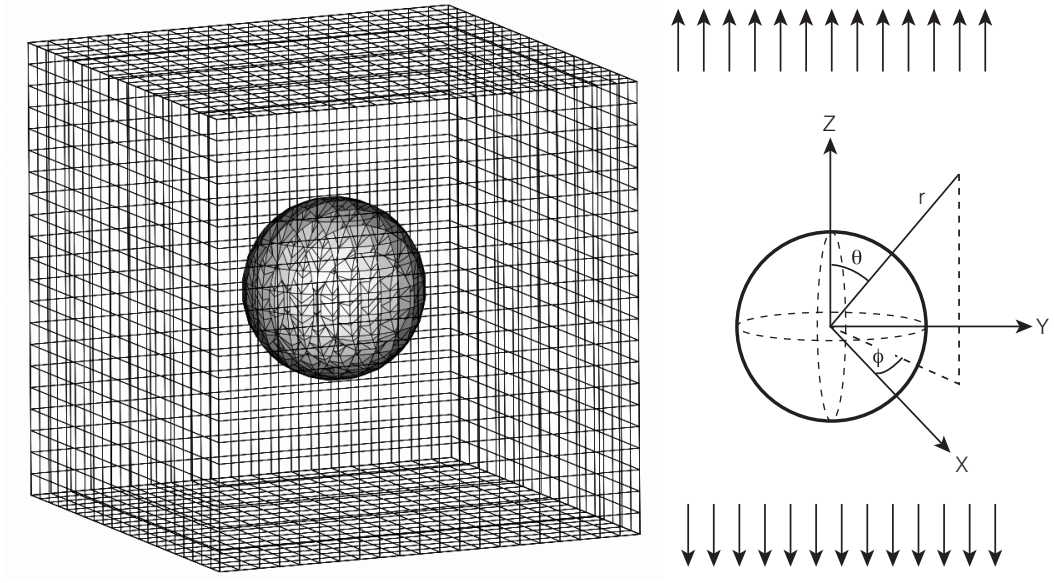

Validation of extended finite-element (XFEM) simulation techniques intended to extend the applicability of the finite-element method to as-built mechanical simulations. (a) A spherical inclusion modeled in an otherwise uniform and isotropic body—represented with a structured XFEM mesh—subjected to uniaxial tension. (b) The model's boundary-value problem description, in which arrows indicate the direction of tension.

Hyperspectral image-based broad-area search

D. W. Paglieroni

From the standpoint of the national security and nonproliferation missions of LLNL, two of the most important tasks faced by human image analysts are broad-area search (reconnaissance) and site monitoring (surveillance). In each, the objective is to detect targets of interest—typically solid, manmade objects such as buildings and moving vehicles or gaseous phenomena such as plumes. A broad-area search involves static images of large swaths of land, whereas site monitoring involves analyzing smaller images in a time sequence. Detection is often a time-critical task in which image analysts face growing volumes of image data collected with increasingly sophisticated imaging sensors.

Hyperspectral (multiband) images consist of hundreds of single-band images stacked on top of one another, each corresponding to a different frequency band. They provide a much greater context for both spatial and spectral signatures than conventional single-band images, and are potentially far more useful for broad-area searches and site monitoring. Unfortunately, image analysts do not always have time to analyze all the conventional single-band imagery presented to them, let alone on voluminous hyperspectral imagery.

The goal of our hyperspectral image-based broad-area search (HIBAS) project is to improve image analysis throughput, without sacrificing detection performance, by developing and testing fast image-analysis algorithms that extract objects from images, allowing image analysts to focus on regions containing objects matching the target's properties. The algorithms process large images one block at a time and comprise two types: (1) segmentation algorithms, which first divide images into regions containing pixels that are clustered together—suggesting a single object—and (2) spatial signature-analysis algorithms, which then detect regions or groups of connected regions that have spatial properties similar to the target.

In FY2002, we found that image-segmentation quality is affected as much by algorithm parameters as by choice of algorithm. Rather than developing a fundamentally new segmentation algorithm, we developed a generic self-calibration process that applies to many segmentation algorithms and that can automatically determine the parameter settings that produce the best result (see Figure). The self-calibration process was applied in experiments on a number of hyperspectral images from different sensors using two core-segmentation algorithms: (1) a region-growing algorithm that grows regions from seed pixels in accordance with a spectral homogeneity constraint parameter; and (2) the K-Means Re-Clustering algorithm, which automatically groups pixels into one of several spectral classes that are learned automatically, according to a parameter that specifies the number of classes.

An algorithm and an efficient implementation for spatial signature analysis based on area correlation were developed; these have potential applications to detecting objects of known shape in remotely sensed imagery and gas plumes in matched, filtered images.

The HIBAS spatial-signature-analysis algorithms developed in this project apply to various problems related to national security and nonproliferation. Issues remaining include image-segmentation algorithms that are free of problematic parameters whose values are difficult to set, model-based signature analysis techniques for detection of objects with known physical models, and more flexible spatial signature-analysis techniques capable of detecting objects of known shape.

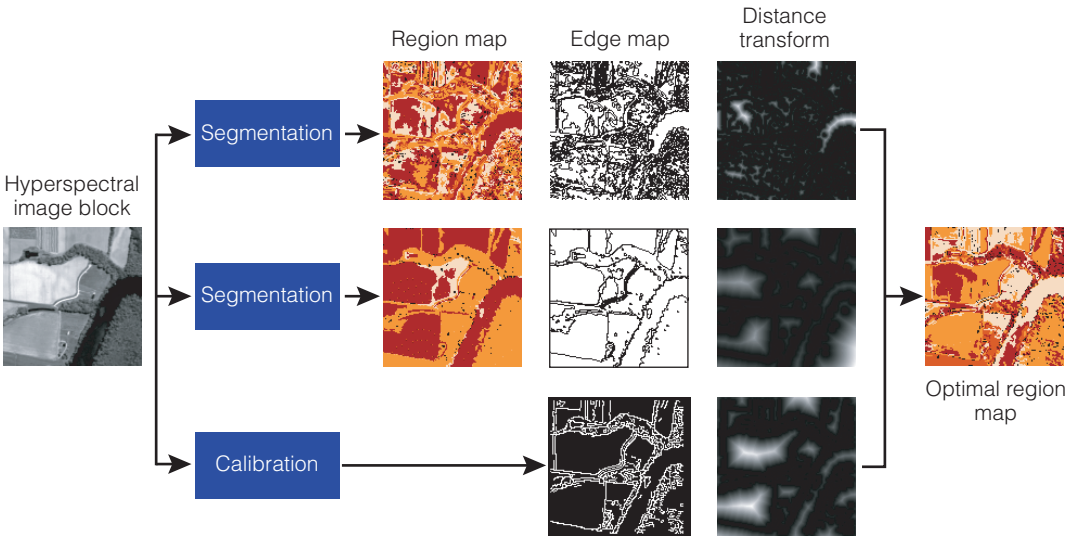

Graphical depiction of our self-calibration process for image segmentation. A hyperspectral image is segmented by a core-segmentation algorithm with different parameter settings, such as a region grower with a region homogeneity parameter. Each parameter setting has an associated region map whose borders are compared to edges independently extracted for calibration. Comparison uses the distance transform, which captures the distance from each pixel to the nearest edge pixel. The parameter setting for which the region boundaries most closely match the calibration edges is used.

Modeling-tools development for the analysis and design of photonic integrated circuits

T. C. Bond, J. K. Kallman, G. H. Khanaka

Photonic integrated circuits (PICs), which use light (photons) rather than electricity to process information, are predicted to be the next generation of high-speed processing chips. Recent advancements in material processing and device engineering are leading to integration of various optical components on a single chip. Such an optical chip could potentially enable highly compact, low-latency, wide-bandwidth, ultrafast, secure information systems. PIC design tools are needed to advance all-optical logic systems for data transmission and signal processing by reducing development time and cost, but commercial software is limited to a restricted suite of problems. The goal of this project is to create sophisticated PIC simulation tools that will benefit LLNL missions in national security, including stockpile stewardship, weapons component miniaturization, high-bandwidth diagnostics, remote sensing, high-performance computing, and secure communications.

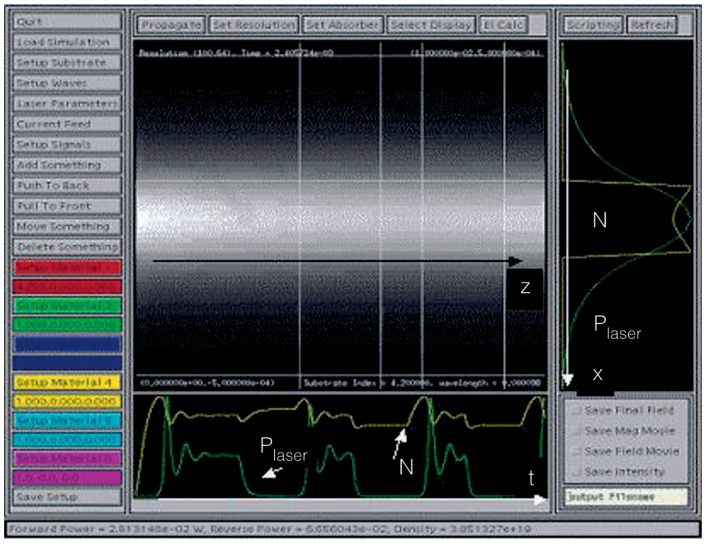

Screen capture of the two-dimensional time-domain code simulating the Boolean NOR operation for analyzing and designing photonic integrated circuits. First one control is on, then two controls are on (deeper valleys). Central window: longitudinal distribution of photons (white) at a chosen time, showing the effect of gain-guiding. Side window: Cross-sectional distribution of power (green) and carrier density (yellow), demonstrating diffusion of the carrier. Bottom window: time distribution of power and carrier density. When two controls are on, modulation is deeper and faster as expected.

We focused on novel lasers and nonlinear devices—such as logic gates—for all-optical digital circuits and signal processing, and highly sensitive sensors for analog and digital operations. For instance, the Boolean logic on which computer technology is based can be realized in PICs by integrating laser gain elements with dielectric waveguides as both optical inputs and outputs.

In FY2002, we generated frequency-domain and time-domain (TD) codes for the analysis and design, respectively, of laser-based digital gates in their steady and dynamic states. Both one-dimensional (1-D) and 2-D codes were developed using several methodologies, e.g., the Runge-Kutta and Brent's methods, finite-difference TD, and the beam propagation method tool. The codes—written in Java or C++, validated against existing data, and provided with a graphical user interface (GUI)—were used to accurately investigate the effects of gain leverage, gain quench, and other critical physical effects on gate efficiency for a wide range of geometries and material parameters, such as current applied, length, and mirror reflectivity. The 1-D models are capable of treating wavelength dependence of the gain and spectral hole burning and were used to analyze simple standard lasers and to validate the 2-D codes. The 2-D codes allow multimode structures analysis, are inherently scalable to a vectorial formulation, and include carrier diffusion, which is critical for analyzing spatial hole burning and gain guiding.

The Figure is a 2-D TD simulation of a NOR operation in a three-section, optically controlled, Fabry-Perot edge-emitting gallium–arsenide multiquantum well laser. This and other simulations indicate that higher gain (fan-out) and deeper modulation depth (signal restoration) are obtained with longer control regions and wider lasers operating close to threshold, and that operating frequencies (clock rate) up to a few gigahertz could be achieved at the expense of the applied current, above which switching is possible but level restoration is insufficient.

Goals for FY2003 are to complete, package, and deliver the suite of 2-D models for designing PICs.

Simulating fine-scale atmospheric processes: A new core capability and its application to wildfire behavior

M. M. Bradley, C. H. Hall, M. J. Leach, C. M. Molenkamp, L. E. Neher, L. Wilder,

This project focuses on developing, testing, and prototyping a unique simulation capability that couples weather-prediction models spanning a wide range of spatial and temporal scales with a state-of-the-science, physics-based combustion model developed at Los Alamos National Laboratory (LANL).Our scientific goal is to understand wildfire processes and to represent that knowledge in computer models; our humanitarian goal is to protect lives, property, and natural resources. The wildfires in 2000 that threatened DOE facilities at Los Alamos, Hanford, and Idaho Falls with possible releases of radioactive materials underscore the relevance of this work to DOE's national security missions.

The models developed in this project simulate both wildfire behavior and local weather, taking into account their mutual interactions and the effects of complex terrain. The fire model represents the chemistry, thermodynamics, radiation, and turbulent processes that occur within wildfires. The atmospheric models represent the large temperature and wind differences and the turbulence that occur near fires. A geographic information system (GIS) was used to process model input data and to analyze the human and economic consequences of predicted fire behavior.

During FY2002 we integrated the latest versions of LANL's high-gradient flow solver, HIGRAD, and its combustion simulator, FIRETEC, with our operational regional weather prediction model, the Coupled Oceanographic and Atmospheric Mesoscale Prediction System (COAMPS) on LLNL's TeraCluster 2000 computer. As a proof-of-concept demonstration, we simulated the early stages of the October 20, 1991 Tunnel Canyon wildfire in Oakland, California, which claimed 25 lives and destroyed 3000 dwellings.

Using global reanalysis weather data from the European Center for Medium-Range Weather Forecasting to provide initial and boundary conditions, COAMPS was run with up to six nests—a modeling technique analogous to the Russian matrushka nesting dolls. The COAMPS technique starts with coarse-resolution weather data over a large geographical area and "zooms in" with ever-smaller-domain, finer-resolution versions of the model to produce a very high-resolution simulation of the weather over a small area.

For the simulation, we researched pre-fire fuel conditions and acquired information on the 1991 fire history. The COAMPS nests provided atmospheric conditions at a horizontal resolution of ~148 m for the HIGRAD/FIRETEC fire simulations, which, in turn, used 10-m resolution. With the assistance of local firefighters, we accomplished the first-ever GPS survey of the 1991 fire ignition locations. We simulated wildfires using estimated East Bay Hills vegetative fuels for 1991 and high-resolution observed fuel data for 1993, which were collected on the ground, lot by lot and parcel by parcel. As part of a sensitivity study on the effects of wind speed and of fuel types and characteristics, we completed numerous COAMPS and HIGRAD/FIRETEC interactive fire–weather simulations for the early phase of the Tunnel Canyon fire. The Figure shows results from a simulation of the Tunnel Canyon fire, assuming the fuel to be uniform coyote bush as a best estimate for what covered the hillside before the fire on October 20, 1991.

The primary evaluation metric of our work has been the ability of the models to replicate observed fire behavior, as provided by historical data and eyewitness accounts of fire-fighting professionals, who have affirmed the accuracy of our simulation. An interagency urban–wildland fire physics workgroup has just been established, with our model as its core capability.

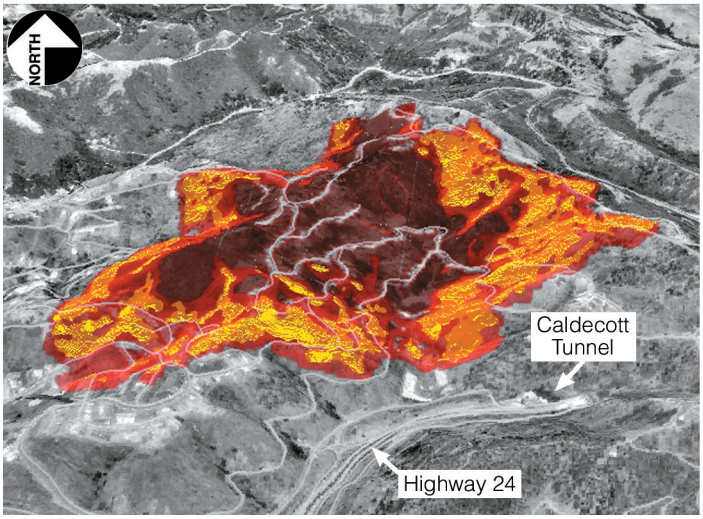

Simulation of the Tunnel Canyon fire (October 20, 1991) in Oakland, California 10 min after ignition, superimposed on an aerial photograph of the landscape. The "flames" are average temperature contours from the simulation: yellow indicates 700°C and red indicates 200°C. Blackened areas show that the vegetation fuel has been consumed by the simulated fire.

Overcoming the memory wall in symmetric multiprocessor-based systems

B. R. de Supinski, A. Yoo, S. McKee, F. Mueller, T. Mohan

Both central processing unit (CPU) and computer memory speeds are increasing at exponential rates. However, memory hardware is slower than CPUs, and memory speeds are not increasing as rapidly as CPU speeds. This increasing gap will exacerbate an already serious problem: memory access in general dominates performance for codes with large memory footprints, including many codes heavily used at LLNL. Many researchers anticipate hitting a "memory wall," at which memory access will impose an absolute performance limit, regardless of advancements in CPU performance.

This project is extending dynamic access optimization (DAO) techniques originally designed for uniprocessors to symmetric multiprocessors (SMPs). These techniques use memory more efficiently by (1) changing the execution order to exploit memory hardware features, such as interleaved memory banks, or (2) changing the apparent locations of memory accesses from those generated by the issuing program to increase significantly cache-hit ratios. Because SMP-based systems are common at LLNL, our SMP-aware DAO techniques will significantly decrease the run times of many ASCI simulation codes that are essential for the Stockpile Stewardship Program, in support of LLNL's national security mission.

Implementing DAO techniques for SMPs is more difficult than for uniprocessor systems because multiple processors may access the same physical address through different apparent locations. This aliasing of the actual physical address with other apparent physical addresses creates a remapping-coherence problem, a variant of the cache-coherence problem. SMP-aware DAO techniques must ensure that the results are consistent with those that occur without remapping. The hardware mechanisms, such as cache invalidations, used by SMPs to solve the cache-coherence problem cannot solve the remapping-coherence problem because these mechanisms are keyed on physical addresses and are not automatically invoked for all aliases created through remapping.

In FY2002, we designed three distinct mechanisms for solving the remapping-coherence problem. The first and most promising technique modifies the coherence controller to account for remapping. This hardware-based solution ensures that coherence operations are invoked on all aliases of a physical address, so that the memory semantics are identical to those of the original machine. An algorithm quickly identifies unaliased addresses while executing with operations already required to maintain coherence and access main memory. Consequently, the cost of accessing unaliased locations remains essentially unchanged.

Second, we designed virtual pinned memory, a novel mechanism—derived directly from SMP-aware DAO—for providing true zero-copy message passing. Ordinarily, exchanging data between nodes in cluster-based systems requires memory copies to gather the data from and scatter them into the user memory locations; even contiguous user data must be copied to and from system buffers. With virtual pinned memory, DAO-based scattering, gathering, and alias translation mechanisms are used to copy user data directly to the network interface, without locking the data into physical memory.

Third, we continued our work on understanding the memory-access regularity of applications. We developed a novel tool that gathers regularity statistics for threaded applications. These regularity statistics strongly indicate what memory optimizations will improve an application's performance. Our results demonstrate that applications with irregular access patterns, including many ASCI codes, would benefit from our SMP-aware DAO mechanisms.

This project developed novel techniques to improve memory performance in SMP-based systems for applications important to LLNL. Our achievements include the design and implementation of a tool set to analyze memory-access patterns of applications, the exploration of regularity metrics and their use to classify code behavior, and a set of microbenchmarks to assess and quantify the performance of SMP memory systems. Our mechanisms to maintain memory coherence in SMP-based systems could significantly improve the performance of many ASCI applications.

First-principles molecular dynamics for terascale Computers

F. Gygi, J.-L. Fattebert

First-principles molecular dynamics (FPMD) is a simulation method for studying the properties of matter at the atomic scale. FPMD does not depend on empirical parameters and is an extremely important tool for simulating physical systems for which experimental data are limited. In addition to atomic trajectories, FPMD simulations also provide the time evolution of electronic properties and therefore yield a complete microscopic picture of the system under study. This simulation approach has been successfully applied to several areas of research at LLNL involving extreme high-temperature or high-pressure conditions, such as equation-of-state (EOS) calculations of molecular fluids, high-pressure phases of solids, and biomolecules in solution.

This project is developing high-performance FPMD simulation software that exploits the unique large-scale computing facilities available at the Laboratory. The main goal of this project is to extend the size and variety of systems that can be simulated with FPMD. We will accomplish this by developing (1) new parallel implementations of existing algorithms to make optimal use of LLNL's most powerful computers, and (2) new algorithms that reduce the numerical cost by introducing controlled approximations. The Stockpile Stewardship Program will be a major beneficiary of these enhanced simulation capabilities.

In FY2002, we added several features to GP, an FPMD simulation code, including a new algorithm for the efficient calculation of maximally localized Wannier functions (MLWFs), which are used in the computation of physical properties such as electronic polarization and conductivity. In addition, code for simulating transition metals accurately was added to GP and used to begin simulations of the optical properties of cadmium selenide nanoparticles. Simulations of transition metals are complicated by the localized nature of d electrons but were made possible with semilocal pseudopotentials, which are more accurate than conventional, fully nonlocal potentials but keep computational costs relatively low.

To improve the scalability of FPMD simulation codes, we explored new strategies to develop distributed software components based on electronic-structure algorithms; began developing new algorithms that achieve linear scaling in FPMD calculations through controlled-accuracy approximations, which systematically reduce errors introduced by the localization of electronic orbitals; demonstrated the scalability of our real-space, finite-difference electronic structure code (MGMOL) with a cluster of 250 processors; and achieved linear scaling in a simulation involving 560 carbon atoms on the Frost computer platform.

Plans for FY2003 include continuing to develop the MGMOL code to include the capability of molecular dynamics simulations with moving localization domains, and exploring ways to further extend the applicability of FPMD simulations to several thousand atoms on thousands of processors, in preparation for terascale computation at LLNL.

Computational methods for collisional plasma physics

D. W. Hewett, A. B. Langdon, D. J. Larson, B. F. Lasinski, C. H. Still

Modeling the high-density, high-temperature plasmas produced by intense laser or particle beams requires accurate simulation of a large range of plasma collisionality. Although current simulation algorithms accurately and efficiently model collisionless and collision-dominated plasmas, the important regime between these extremes—semicollisional plasmas—has been inadequately addressed to date. Accurate simulation of such plasmas is important for efforts to understand and harness high-energy-density physics phenomena for stockpile stewardship.

The goal of this project is to develop a computer model that allows accurate simulation of the full range of collisional plasma physics by developing (1) a new adaptive-resolution, smart, particle-in-cell (PIC) algorithm, called kinetically extended hydrodynamics (KEYDRO), which expands the function of point particles in traditional plasma PIC models by including finite size and internal dynamics; and (2) a robust, three-dimensional (3-D), massively parallel plasma-production code (Z3) with collisional extensions. This project will enhance LLNL's competency in computational plasma physics and plasma modeling. The computational models developed will be applied to plasma problems—such as semicollisional behavior in hohlraums and the physics of high-altitude nuclear explosions—relevant to stockpile stewardship, in support of LLNL's national security mission.

In FY2002, we conducted the world's largest fully electromagnetic PIC calculation by running Z3 on the Advanced Simulation and Computing (ASCI) White system. This calculation simulated an entire laser-illumination speckle, bringing new realism to laser–plasma interaction simulations. The simulation, which is directly applicable to laser-target physics, produced, for the first time, magnetic fields driven by Raman scattering. In addition, a momentum-conserving electron-collision algorithm was developed and added to the code. The portability of Z3 across diverse massively parallel platforms enabled the LLNL computing community to effectively utilize advanced new computational resources.

Efforts in KEYDRO produced a merging capability that exhibited conservation of phase-space volume in the collisionless limit. This economy was obtained by using large particles to represent the bulk of the distribution function. We also developed a new Coulomb-collision algorithm that reproduces known partially collisional, counterstreaming ion beam behavior while requiring fewer particle pairings per time step. In addition, 2-D embedded curved boundaries (ECBs) were installed in the code and tested.

In FY2003 we will (1) continue to develop and implement collision algorithms in Z3 for application to laser–plasma interactions in long- and short-pulse lasers; (2) benchmark collisional simulations with experimental data; (3) investigate the applicability of KEYDRO collisions to Z3; (4) incorporate finite-size KEYDRO particles into our new partially collisional algorithm; (5) begin the connection to full electrostatics; (6) study the 2-D behavior of finite-size particles near KEYDRO ECBs; and (7) use test problems with known results as benchmarks to develop a fully 3-D KEYDRO model.

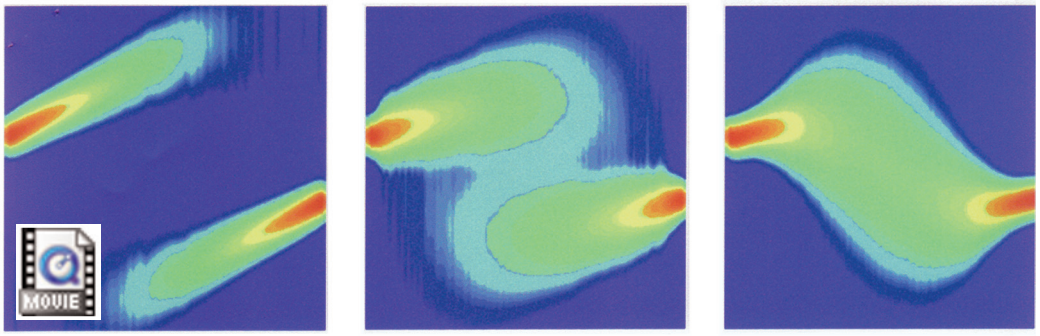

Phase-space plots of two colliding aluminum plasma beams at (a) 500, (b) 700, and (c) 900 ps, illustrating the interpenetration of partially collisional plasmas.

Radial reflection diffraction tomography

S. K. Lehman and S. J. Norton

Consider a wave-based measurement system (either acoustic or electromagnetic) in which a single transducer rotates about a fixed radius in a "pitch-catch" multimonostatic mode, i.e., at each successive angular location about its center, the transducer launches a field into its surrounding medium (the pitch) and subsequently records the backscattered field from that medium (the catch) (see Figure). We developed a diffraction tomography (DT) algorithm, a technique based on a linearized version of the forward field-scattering equation, to form planar slice images of the medium surrounding the transducer. The theory and imaging technique are referred to as radial reflection diffraction tomography (RRDT) because of the radial configuration of the transducer and the tomographic paradigm used to reconstruct the structure of the surrounding medium from reflected waves.

As a minimally invasive nondestructive evaluation tool, RRDT has the potential to improve intravascular ultrasound techniques used for imaging plaque buildup on arterial walls. It also has applications to the Laboratory's stockpile stewardship mission.

Our forward field-scattering equation and inversion algorithm are based on a 2.5 dimensional-scattering model in which the medium does not vary in the third (or z) dimension. This is a reasonable approximation, given the goal of achieving planar reconstructions. During development of the theory, we discovered that it is not mathematically possible to reconstruct fully complex images, i.e., maps for both object velocity and attenuation; only velocity maps can be achieved.

Under the constraint that the object function is real, we successfully derived an inversion expression that reconstructs planar velocity slices of the object and the Fourier Diffraction Theorem for this geometry, which dictates the resolution limit of the reconstruction. Numerical implementation of the inversion algorithm, however, has been hindered by the existence of a reciprocal of a Bessel function of the first kind in the integrand of the inversion integral. The multiple zeros of the Bessel function cause the integrand to diverge. These Bessel function zeros in the denominator can be viewed as poles along the real axis, and it is natural to attempt a complex integration, replacing the integral by the sum of the integrand residues at the poles. We derived and implemented such a method but have not yet had success at forming images due to the behavior of the some of the terms in the integrand in the complex plane.

In FY2003, we will develop a numerical inversion method based on a recently derived generalized tomographic inversion method that can be easily implemented numerically. This fully complex inversion method will yield reconstructions of both sound speed and attenuation.

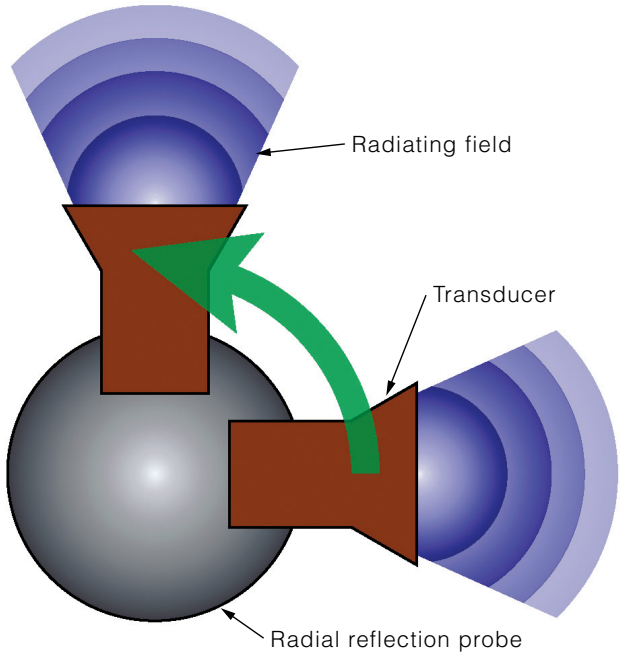

Radial reflection probe with the transducer shown launching a field at two angular locations.

Multiscale modeling of the chemical reactions in the cell

C. Melius, E. Garcia, A. Golumbfskie, J. Quong

The post-genomics revolution has witnessed the transition from gene sequencing to systems biology—the understanding of how cells carry out their functions through extremely complex interrelationships among their biological pathways. Our project is developing a multiscale computational framework to model the chemical reactions of the biological pathways within the cell.

The framework combines deterministic processes (defined by ordinary differential equations) with stochastic processes (random events) to simulate the complex chemical-reaction mechanisms involved in the signaling, metabolic, and regulatory pathways. The model treats intercellular processes involving simple proteins and metabolites, and complex protein machines such as flagella and membrane transporters.

Each of the metabolites or protein complexes is treated as a chemical species. Because of its multiscale design, the framework can also treat the biological cells themselves as chemical species interacting with each other and with the environment, through the exchange of chemicals produced by the cells. As a test of this computational framework, we are modeling the chemotaxis process in microbial cells. Our chemotaxis model couples the metabolic pathway with the signaling process that controls the direction of flagella motion.

In FY2002, we designed an object-oriented-programming-based multiscale framework to represent the cellular pathways. The basic design involves chemical species, reactions, and processing objects (see Figure). The processing objects (reactors) contain a model defining how the reactions are applied, a solver to integrate the model, and a substance (defining the chemicals and reactions contained in the reactor).

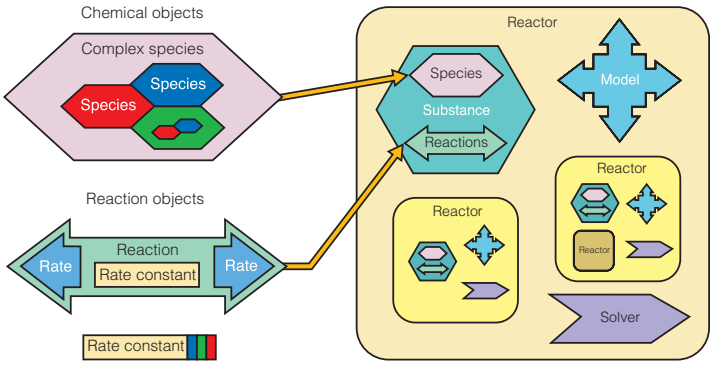

This recursive design for modeling chemical reactions enables multiscale physical processes to be treated within the same computational framework. A chemical system consists of complex species, reactions, and processes. Reactions are the rules relating species; processes (reactors) carry out the rules.

The reactions are composed of reaction rates and rate constants. The chemical species, the reaction rates, and the reactors have hierarchical, recursive designs, and the computational objects representing them can contain internal species, reaction rates, and reactors, respectively. These objects can be called recursively, providing multiscale representation of the physical objects and processes.

Dependency and effector lookup tables efficiently couple reactions and species. Specific reaction-rate objects were developed for various enzymatic reaction types. In addition, several single-step and variable-step integrators and a kinetic Monte Carlo integrator (used in the solvers for the reactors) were developed and validated. The implementation of the basic chemical and reaction objects was validated against standard chemical kinetics codes.

To test our framework design, we created a reactor containing two inner reactors to represent the cell. The first inner reactor, representing the flagella, treated the random activation processes involving the flagellum proteins and solved its chemical reactions using a stochastic Monte Carlo integrator. The second inner reactor, representing the cytosol of the cell, treated the chemical species involved in the phosphorylation of the signaling proteins and solved its chemical reactions using an ordinary differential equation integrator. We also coupled the detailed phosphotransferase system reaction mechanism into the general glycolysis reaction mechanism and identified the phosphoenol-pyruvate/glucose ratio as a sensitive variable that can affect the chemotatic signal.

In FY2003, the computational framework developed in this LDRD will be applied to the gene regulatory system involving pathogen–host interactions in support of LLNL's mission in countering bioterrorism for homeland security and to the spread of viral infections among humans. Understanding the behavior of diseases at both the cellular and the human levels will lead to better emergency response.

Automated imagery data exploitation

J. A. H. Futterman, C. Kamath, D. Poland, S. K. Sengupta

Automated techniques for searching satellite images of broad areas to detect human-made structure and other objects of interest will benefit the defense and intelligence communities, as well as efforts to monitor the Earth's population. At the intersection of these interests is the quest to produce and update detailed digital maps of the Earth's population, which can be used to minimize the consequences to civilians of military actions, such as those related to counterproliferation.

Our goal is to develop a technique for producing such maps from satellite images that is fast and robust enough for the maps to be updated annually. We have developed a multi-stage approach that uses spectral (color) information with edge and corner detection to select areas containing built structures. This promises to provide reliable detection with a low rate of false positives. Once the regions containing built structures are isolated, population counts can be assigned to them from other sources, such as the LandScan population model.

A problem frequently encountered in automated image analysis is that a technique developed for one geographic region is not accurate for other regions because of the great variability in landscape, patterns of settlement, and methods of construction across the globe. Consequently, we will most likely need to divide the globe into various topographic and cultural sections, each with its own set of control parameters, such as thresholds for statistical measures of spatial or color inhomogeneity—which indicates a candidate area containing built structures—and the sensitivity of edge and corner detection.

Because population is determined from the presence of buildings and other human-made structures, the project focuses on regions containing such structures as indicators of human settlements and workplaces. Each image for these regions is searched using multiple stages of multispectral (color) and morphological (shape) analyses. First, 4-m-resolution IKONOS satellite multispectral images are segmented into regions of relatively homogeneous and inhomogeneous color. We then use another set of algorithms to search the corresponding IKONOS panchromatic image (which has a 1-m resolution) for edges and corners. Areas with a sufficient density of edges and corners are selected as candidates to contain built structures. A logical AND operation is then used to find the areas selected as candidates in both panchromatic and multispectral processing. These areas are combined to yield a final image as shown in the Figure, in which areas of built structures in an IKONOS satellite image are colored light red. Finally, a computer extracts each area's boundaries and exports them to a commercial digital mapping or geographic information system (GIS).

In FY02, we developed and experimented with our multistage analysis technique. We found a single set of control parameters to work well over the California–Mexico border and Omaha, Nebraska. However, a different set of parameters was needed for Afghanistan. We also demonstrated the feasibility of exporting our results into ArcView, a commercial GIS used for the Laboratory's Counterproliferation Analysis and Planning System.

In FY03, we hope to evaluate the effectiveness of decision-tree algorithms instead of (or in combination with) the statistical algorithms we explored in FY02, and to establish the robustness and scalability of our techniques in preparation for packaging our techniques as a digital map production capability. We will also investigate extensions of our basic methods for finding specific types of structures or objects. Given the success of this timely and important project, this work will also be continued as part of a new Strategic Initiative.

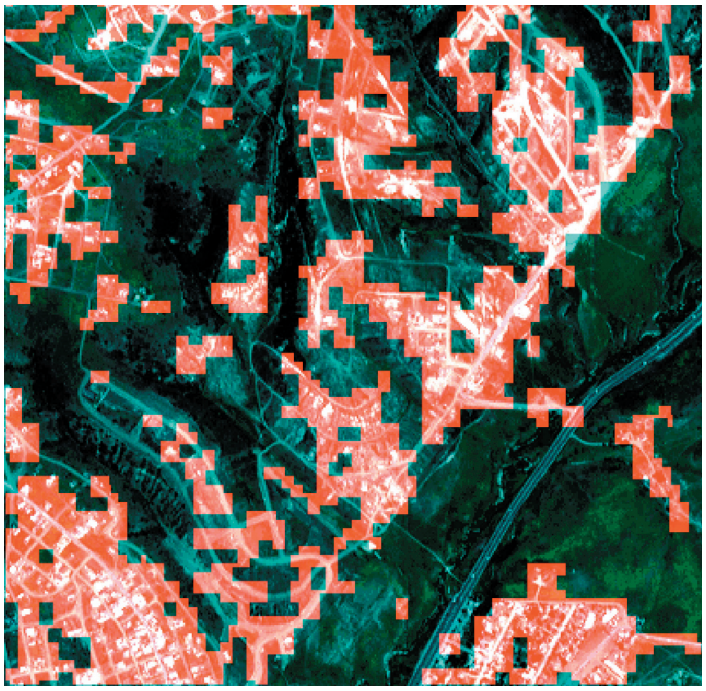

A 400 × 400 pixel portion of a multispectral IKONOS satellite image overlaid with extracted regions containing human-made structures (light red).

Atomically controlled artificial and biological nanostructures

G. Galli, T. van Buuren

Nanotechnology has become one of the most prominent interdisciplinary fields, encompassing a number of different disciplines such as biology, physics, chemistry, and engineering. The technology of "small matter" holds great promise for many applications, from semiconductors to medical research, disease diagnosis, and national security. However, for a successful development of nanotechnology, many key challenges in nanoscience must be tackled first, and a number of fundamental problems are yet to be solved. Plenty of room exists for practical innovation to understand the key physical rules governing phenomena occurring at the nanometer scale.

In this project, we are addressing a set of specific nanoscience problems to develop new capabilities for designing semiconductor nanostructures with desired labeling and sensing properties by using advanced simulation and experimental techniques. The scientific capabilities developed in this project will enable the development of novel sensing and labeling devices that LLNL can exploit to address specific problems in national security and environmental monitoring. One example is the development of rapid, in-the-field analysis of chemical and biological warfare agents.

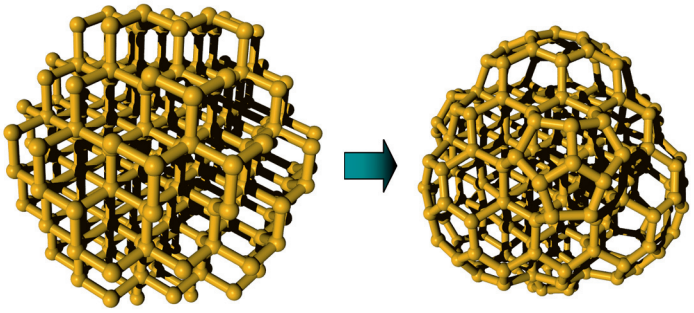

The transformation from (a) a diamond core with ideally terminate surfaces to (b) a "bucky diamond," which occurs in first principle molecular-dynamics simulations at about 300 K.

We are using state-of-the-art first-principles simulations methods and characterization techniques to investigate the structural, optical, and transport properties of group IV semiconductor nanostructures with desired labeling and sensing properties. To this end, we are (1) focusing on silicon (Si) and germanium (Ge) quantum dots, which offer advantages—such as biocompatibility—over cadmium-containing nanoparticles; (2) using ab initio simulation techniques to microscopically model interfaces between these quantum dots and specific chemical and biological media; and (3) combining computational tools with state-of-the-art experimental spectroscopic techniques to establish an effective scientific paradigm for designing semiconductor nanostructures on the atomic scale.

In FY2002 we carried out a combined experimental and theoretical investigation of nanodiamond, resulting in the identification of a "bucky diamond" (see Figure), a new type of carbon nanoparticle with a diamond core and a fullerene-like surface. Our extensive ab initio investigation of Si and Ge nanoparticles focused on how their optical properties are affected by surface contaminants. In addition, ab initio simulations of the attachment of small organic molecules to Si nanoclusters and the effect of cluster excitation on the probability of attachment resulted in suggested experiments to improve the selective attachment of molecules to Si dots 1 to 2 nm in diam.

Our chemical-synthesis efforts and investigation of carbon nanostructures were carried out in collaboration with Professor A. P. Alivisatos at UC Berkeley and with a group led by Professor H. Dai at Stanford, respectively.

Multiscale atmospheric dispersion modeling

W. P. Dannevik, S. T.Chan, M. J. Leach, A. A.Mirin

Urban areas are the most likely locations for release of toxic material into the atmosphere, whether by accident or terrorist act. The DOE and the Department of Defense are supporting efforts to develop urban modeling capabilities for emergency response and risk assessment applications. Such models must address turbulence and other phenomena. However, classical approaches for representing turbulence with simplifying assumptions are not valid in regions with complex building configurations and terrain.

The goal of this work is to advance the theoretical and empirical basis for simulating transport and dispersion at urban and local scales by (1) testing sub-grid-scale (SGS) turbulence approximations in a high-resolution building-scale model, and (2) designing procedures for information transfer from a mesoscale model to a building-scale model, including parallel implementation. The project uses LLNL's combination of advanced modeling capability and terascale computing resources.

The highly turbulent atmospheric flow in urban areas implies that a large-eddy simulation (LES) approach is necessary at such scales. As the resolution of a model changes, the size of the resolved (large) eddies necessarily changes. Consequently, the resolved flow features, including turbulence and dispersion patterns, can be expected to converge to the true solution as the model resolution is refined.

In FY02, we conducted mesh-refinement studies to optimize resolution in SGS modeling and developed protocols and software for coupling the models we are using—a finite element model, FEM3MP, and a mesoscale model, COAMPS. Optimum resolution and coupling are critical for simulating flow and dispersion at small scales. Coupling involves information passing only from COAMPS to FEM3MP—called one-way nesting. Time-dependent profiles of wind velocity and turbulence kinetic energy from COAMPS were used to generate, with interpolation when necessary, initial and boundary conditions for FEM3MP.

In addition, we used FEM3MP to simulate a Prairie Grass field experiment and compared the predictions with actual data—to our knowledge, the first successful simulation of both the flow field and tracer dispersion for this type of experiment using the LES approach. Figures (a) and (b) show predicted instantaneous velocity and tracer concentration (with contour levels in logarithmic scale) on two representative planes. Figure (c) is a comparison of predicted peak concentration, measured data from the experiment, and results from a Gaussian model. The agreement between the LES results and the data, especially as compared to the Gaussian model results, is excellent. This example illustrates that a sophisticated computational fluid dynamics model is needed, even for a case involving flat terrain, to obtain accurate results in the near field, let alone in the case of an urban area involving variable terrain and many buildings.

In FY03, we will extend COAMPS's capabilities by including an LES option to facilitate the coupling between COAMPS and FEM3MP. In addition, the modeling system will be tested using datasets from experiments in more complex environments.

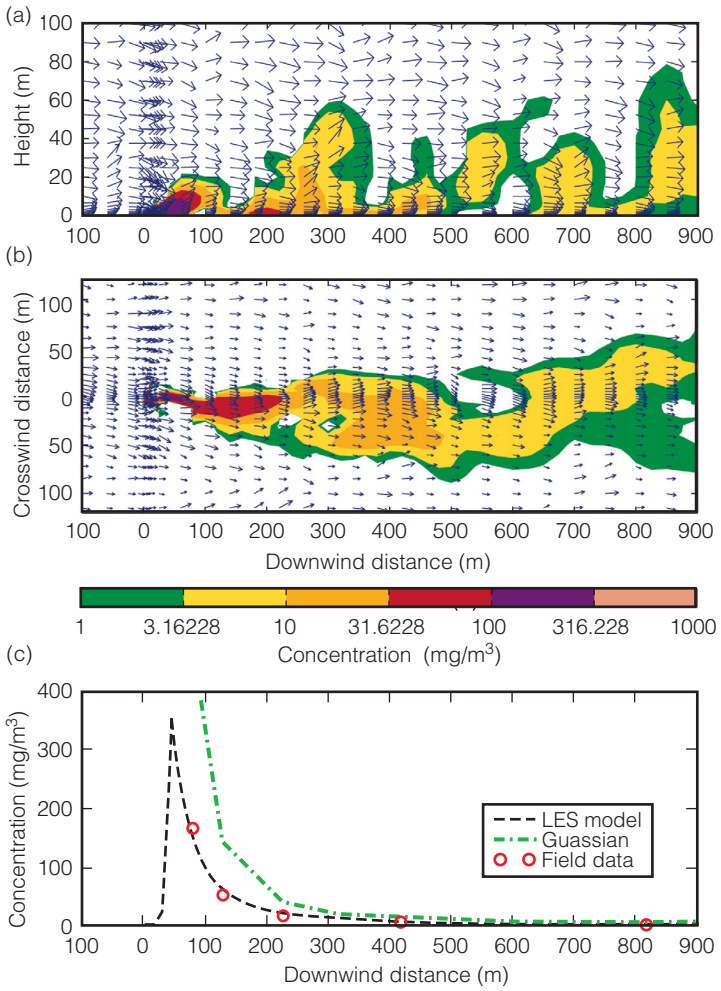

Simulated wind velocity and material concentration (mg/m^3) in a (a) vertical plane and (b) horizontal plane 600 s after release of a hypothetical toxic material. This is, to our knowledge, the first successful simulation of both the flow field and tracer dispersion for this type of experiment using the large-eddy simulation (LES) approach. (c) A comparison of peak downwind concentration predicted by LES and Gaussian model with experimental data, showing the accuracy of LES.

ViSUS: Visualization streams for ultimate scalability

V. Pascucci

Modern scientific simulations and experiments produce increasingly large amounts of data that traditional tools are not able to visualize in real time, especially on regular desktop computers, which creates a frustrating slowdown in the overall process of scientific discovery. Use of innovative, high-performance visualization techniques that allow interactive display of very large data sets on simple desktop workstations and the monitoring (or steering) of large parallel simulations will have applications to several LLNL missions—including stockpile stewardship, energy and environment, nonproliferation, biology, and basic science—that use large-scale modeling and simulations.

In the ViSUS project, we are developing a unified, scalable system that will allow visualization of large (>1 terabyte) scientific data sets on a single desktop computer, a cluster of personal computers, or heterogeneous computers distributed over a wide-area network. The main focus of this project is to develop a data-streaming infrastructure based on a suite of progressive and out-of-core visualization algorithms, enabling the interactive exploration of large data sets. Our goal is to develop a prototype of this streaming infrastructure to demonstrate the practical flexibility and scalability of our approach and increase visualization performance by several orders of magnitude in two primary settings: (1) interactive visualization on desktop workstations of large data sets that cannot be stored locally and (2) real-time monitoring of a large scientific simulation with negligible impact on the computing resources available.

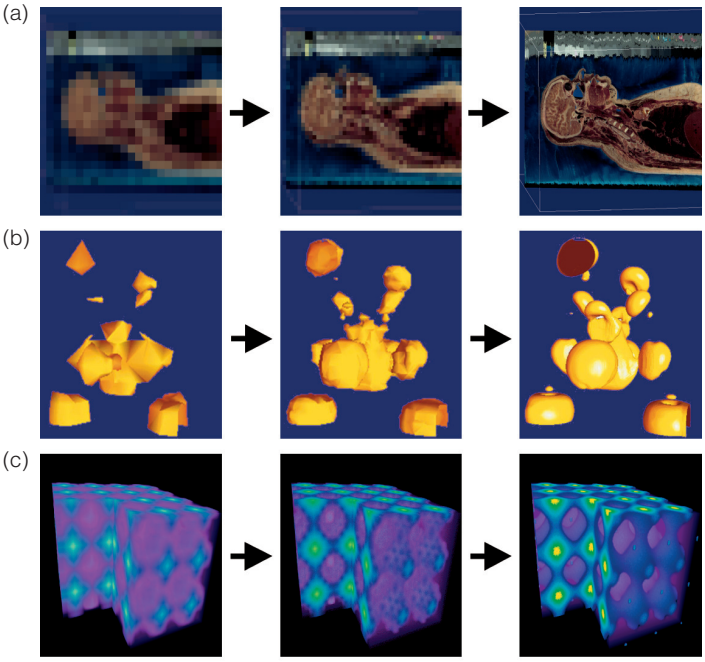

The ViSUS system enables the interactive, progressive display of large scientific data sets. Examples of progressive refinement for the three scientific visualization algorithms considered in ViSUS: (a) slicing (in a medical-imaging application), (b) isocontouring (of a high-potential iron protein), and (c) volume rendering (in a first-principle molecular dynamics simulation).

The ViSUS methodology aims to optimize globally the data flow in a pipeline of processing modules, with each module reading the input and producing the output in multiresolution format. Multiresolution methods provide the necessary flexibility to trade speed for accuracy in data visualization. Maximum coherency and minimum delay in the data flow are achieved by extensive use of progressive algorithms (see Figure) that continuously convert local geometric updates of the input stream into immediate updates of the output stream.

During FY2002, we (1) implemented a new progressive slicing technique that computes planar cross sections of rectilinear grids with arbitrary orientation; (2) designed a new data layout allowing real-time geometric queries for rectilinear grids and tested a practical implementation for meshes with up to 0.5 trillion nodes; (3) developed a novel multiresolution representation that simplifies the real-time extraction of minimal adaptive models; (4) introduced the first subdivision method for unstructured meshes of any dimension and cells of virtually any type; and (5) tested the basic network components of our streaming infrastructure.

In FY2003 we will (1) build a prototype of a remote viewer that interactively slices data sets retrieved from a remote storage system; (2) implement a direct-streaming infrastructure prototype that connects the nodes of a scientific simulation to a set of data servers used for permanent storage; (3) develop parallel preprocessing of the input grids, which should improve data reordering in our storage layout by one order of magnitude; (4) compute, in external memory, multiresolution representations of triangulated surface meshes; (5) define and implement multiresolution wavelet models to be combined with a new volumetric subdivision scheme; and (6) explore new image caching mechanisms for decoupling the display process from the image-rasterization process.

Enabling large-scale data access

T. Critchlow

The World Wide Web is the preferred method for distributing scientific data because the Web makes it easy to develop a customized interface that provides scientists from around the world access to colleagues' results with the click of a mouse. This information revolution has the potential to advance scientists' ability to perform research by enabling large-scale data exploration, improving communication among groups, increasing academic scrutiny of results, reducing duplication of effort, and encouraging collaborations. Unfortunately, these goals are floundering because scientists are overwhelmed by the hundreds of custom interfaces they must use to access the data they need.

This project is developing an architecture capable of identifying, categorizing, and wrapping (i.e., writing code to interact with) these interfaces, which will allow us to provide scientists with a single interface to access hundreds of data sources. This single interface will simplify scientists' interaction with the data and enable them to answer more complex questions than currently possible. This work supports all Laboratory missions by providing scientists direct and efficient access to more external data such as scientific publications, chemistry databases, material descriptions, production techniques, weather data, and urban planning information.

Our proposed architecture uses service-class descriptions to describe interfaces that are of interest to our scientists, a spider (i.e., a program that parses web pages and follows HTML links) capable of identifying instances of these interfaces when they are encountered, a spider-generated interface description that details how to interact with an interface of interest, and a wrapper generator to take the interface description and generate code capable of interacting with the interface. For the wrapper generator, we are expanding on the Xwrap Elite program developed by our collaborators at Georgia Institute of Technology.

Our project will implement the architecture through a series of increasingly complex prototypes. Each successive prototype will improve access to real-world data sources, with the final one capable of categorizing several dozen complex, scientific data sources. Scientific staff will access the resulting wrappers through a customized graphical query interface. This approach will allow us to evaluate alternative strategies in a realistic environment while quickly transferring the technology to the scientists who need to access data on the Web.

In FY2002, we (1) wrote an initial specification of the interface description format, which will be used once the spider has determined how to interact with it; (2) designed an extension to the existing XWrap Elite architecture to generate wrappers for complex interfaces; and (3) wrote a simple spider that takes a set of input pages and goes through each page sequentially, identifying all of the links contained on the page and queuing the links for traversal. The current implementation of the spider is able to identify those pages that use Web-forms to provide data input, but is not yet capable of categorizing web pages.

For FY2003, we will (1) write a specification for the service-class descriptions; (2) complete initial development of the XWrapComposer program; (3) create a version of the Web spider program capable of automatically categorizing simple interfaces; and (4) provide our scientists with access to new data sources through prototype interface.

New approaches to quantum computing using nuclear magnetic resonance spectroscopy

M. E. Colvin, V. V. Krishnan

Over the last few decades, computer speeds have doubled every few years due to continual miniaturization of a computer's most elementary component, the transistor. As transistors become smaller, more can be integrated into a single microchip, and so computational power is increased. However, this miniaturization process is now reaching a limit—a "quantum threshold," below which transistors will cease to function. Present state-of-the-art components possess features only a few hundreds of nanometers across. Miniaturization to the scale of tens of nanometers would cause transistor operation to be disrupted by quantum phenomena, such as electrons tunneling through barriers between wires. Quantum computing—an alternative to transistor-based technology—would actually utilize such quantum effects and enable the science of computing to progress further.

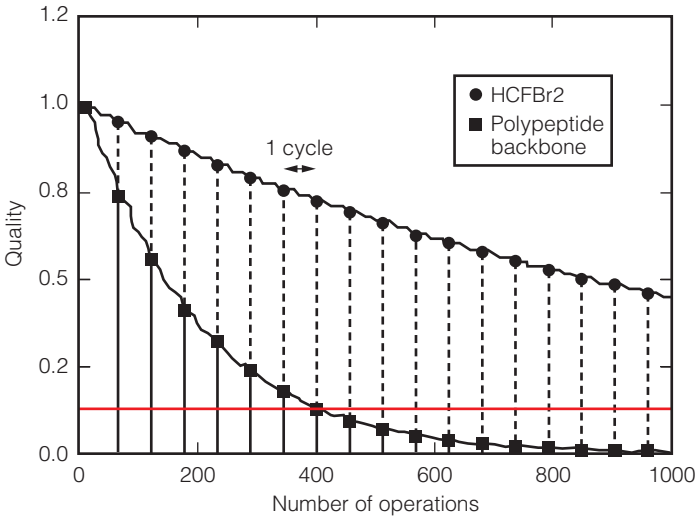

An as example of quantum computing, we implemented a three-quantum-bit Grover's algorithm in two different molecular systems, the chlorofluorocarbon HCFBr2 (circles) and polypeptide backbone (squares). These results demonstrate that HCFBr2 provides better quality in quantum-computing applications due to its long coherence length. The red line represents the approximate detection threshold.

Just as a traditional computer encodes information in bits, a quantum computer manipulates quantum bits (qubits) by executing a series of quantum gates, each a unitary transformation acting on a single qubit or pair of qubits. In applying these gates in succession, a quantum computer can perform a complicated unitary transformation on a set of qubits in some initial state. The qubits can then be measured, with this measurement serving as the final computational result. Quantum computers offer superior computational power for solving certain problems that are currently intractable by using classical computers.

Nuclear magnetic resonance (NMR) spectroscopy is uniquely capable of constructing small quantum computers. A nearly ideal physical system that can be used as a quantum computer is a single molecule, in which nuclear spins of individual atoms represent qubits. Using NMR, the spins can be manipulated, initialized, and measured to perform quantum computation.

The objective of this project is to develop theoretical and experimental techniques to perform small-scale quantum computations using NMR spectroscopy. By enabling the next generation of high-speed computing, this work will benefit the Stockpile Stewardship Program and other high-speed computation research in support of LLNL's national security mission.

In FY2002, we (1) implemented several experimental algorithms on a system containing oriented molecules, (2) developed an algorithm (QCatc) to measure the actual time cost of quantum computing, and (3) continued simulations with a general-purpose quantum-computing simulator (enQC-lator) developed in FY2001. The Figure demonstrates the performance efficiency of two different three-qubit NMR quantum computers running Grover's search algorithm.

This project has created a base of technical expertise in quantum computing at LLNL that will provide a foundation for subsequent research projects in this exciting area.

Discrete differential forms: A novel methodology for robust computational electromagnetics

D. A. White

Electromagnetic design and analysis are critical to the success of Laboratory programs as diverse as magnetic fusion energy, wireless communications, and biomedical instrumentation. LLNL has long tradition of developing computer programs to simulate electromagnetic phenomena, but much research still needs to be done in the area of computational electromagnetics (CE). Cartesian-grid finite-difference methods for electromagnetic problems are simple, stable, and work quite well for rectangular geometries but require a prohibitively fine mesh for quantitative field predictions on large electromagnetic problems with nontrivial geometry. In addition, these methods are incompatible with the unstructured-grid finite-element methods used for thermal and mechanical analyses.

To overcome these limitations, we are investigating advanced discrete differential forms (DDFs), a new methodology for numerical solution of partial differential equations on three-dimensional (3-D) unstructured grids. The key idea is that different DDFs are used to represent different physical quantities. For example, 1-forms are used to represent field-like quantities (electric field), and 2-forms are used to represent flux-like quantities (electric current).

Our research should yield a provably stable, provably conservative, higher-order accurate method for electromagnetics and coupled electrothermomechanical systems. Such methods exist for other disciplines such as computational fluid dynamics, but because of the unique characteristics of Maxwell's equations, no established comparable method exists for CE. Our DDF methodology will be a key component of the Laboratory's next-generation, unstructured-grid electromagnetic simulation codes and will lead to a coupled electrothermomechanical modeling capability, which has applications in remote sensing, nondestructive testing, and biomedicine in support of LLNL's missions in national security and bioscience to improve human health.

In FY2002, we designed and implemented an object-oriented C++ class library—named FEMSTER—that contains a wide variety of elements, basis functions, quadrature rules, and bilinear forms. These classes provide all the necessary functionality to construct arbitrary-order discretizations of the divergence, gradient, and curl operators on 3-D unstructured grids. We have demonstrated that these discretizations can be combined to yield arbitrary-order discretizations of electromagnetic equations such as Laplace's equations, Helmholtz's equations, and Maxwell's equations. The advantages of higher-order discretization are illustrated in Figure (a), which shows the error of the computed solution of the vector Helmholtz equation versus grid spacing h for different polynomial order p. This figure demonstrates we can achieve a computed solution accurate to 10 significant digits using a computational mesh with a few thousand elements if we use a polynomial order of $p = 5$, whereas the standard linear basis ($p = 1$) would require billions of elements.

An example of an important application of our DDF methodology is the microstrip coplanar waveguide simulation shown in Figure (b). The waveguide, a type used in state-of-the-art radio-frequency integrated circuits, consists of three thin strips of metal on a semiconductor substrate: two finite ground planes (outer strips) and a signal line (inner strip). The illustration shows that although most of the electromagnetic energy is confined between the conductors, some energy radiates into the surrounding substrate and could couple to adjacent devices. This simulation was performed on a 3-D unstructured computational mesh using our 1-form basis functions for the electric field and 2-form basis functions for the magnetic field.

To summarize, we (1) developed a unique DDF methodology for numerical solution of partial differential equations that is particularly well suited for CE, and (2) designed and implemented a C++ class library that contains all the finite-element components required for arbitrary-order discretization of gradient, divergence, and curl operators on 3-D unstructured grids. This library has been used to compute solutions to Laplace's equation, Helmholtz's equation, and Maxwell's equations.

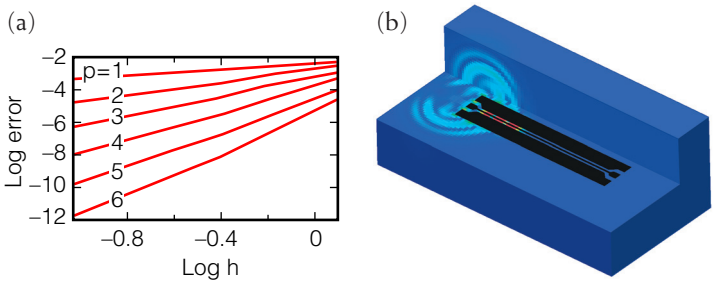

(a) Validation of convergence rates for our higher-order discrete differential forms basis functions. With a polynomial basis of order p = 5, we can achieve a computed solution accurate to 10 significant digits using a mesh with only a few thousand elements. (b) Computed solution of a Gaussian pulse (red) propagating along a microstrip coplanar waveguide (black) on a semiconductor substrate (blue). This simulation, performed on a three-dimensional unstructured mesh, shows that some energy radiates into the surrounding substrate and could couple to adjacent devices.

Quantum vibrations in molecules: A new frontier in computational chemistry

K. R. Glaesemann, L. E. Fried

A highly accurate, fundamental understanding of the structure and properties of most molecules has eluded scientists. Such information would have implications for both defense applications (e.g., the properties of detonation products) and fundamental science. One basic aspect of molecular behavior is molecular vibration. Although the vibration of a molecule is a quantum-mechanical phenomenon, the current treatment of molecules in quantum chemistry is usually based on the harmonic oscillator approximation. However, wide classes of molecules (e.g., molecules with significant proton transfer) do not behave as simple harmonic oscillators because of very strong interplay between electronic effects and anharmonic quantum vibrations.

Our research approach is the first to employ simultaneously a fully quantum computational treatment of both the nuclei and electrons in a molecule. This fully quantum picture will provide new insights into molecules that are directly relevant to LLNL's stockpile stewardship mission. In addition, our work on chemical systems such as carbyne, carbene (CH_2), water (H_2O), and nitrogen hydride (NH) is useful in calculating chemical kinetic rates, which will add to knowledge about conventional explosives important to stockpile stewardship. We have found the results of our fully quantum calculations to differ significantly from those of the simple harmonic approximation. In some, cases the energy difference is greater than 2 kcal/mol.

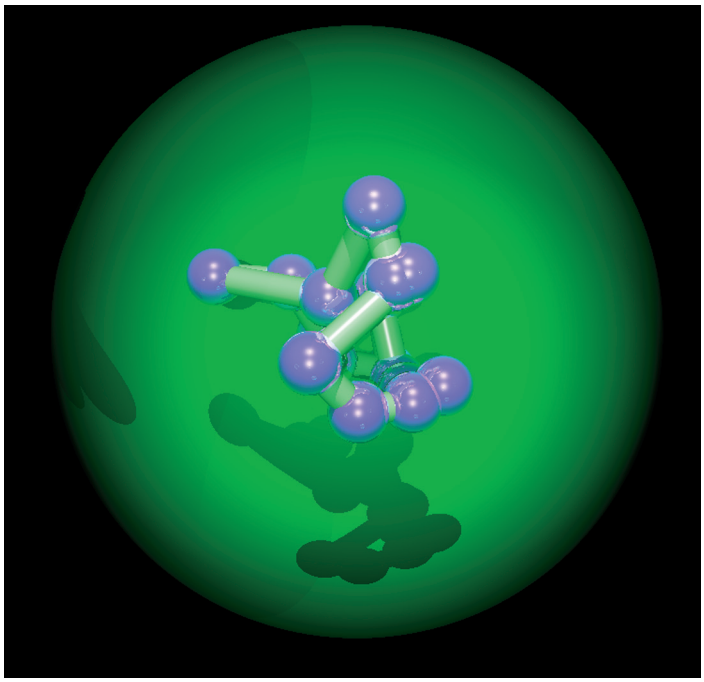

Computer-simulated quantum delocalization: Each atom of argon (Ar_6) is converted into a fractal path (green) along points (purple) using path-integral Monte Carlo (PIMC) code. Quantum delocalization—without which each atom would have only one point—greatly improves the accuracy of calculated molecular properties.

For the quantum treatment of nuclei, we generated in FY02 an efficient, massively parallel path-integral Monte Carlo (PIMC) code, which is now being used to explore, for the first time, quantum effects in a variety of chemical systems—the behavior of hydrogen in a carbon nanotube, proton-transfer reactions, rotational barriers, and ultracold molecular clusters. The code provides a capability to study fundamental scientific questions about structure and bonding.

For example, using the PIMC code to incorporate quantum delocalization in accordance with the Heisenberg uncertainty principle—which states that particles do not have well-defined positions—results in the proper calculation of the melting temperature of argon (Ar_6). The Figure shows a single step during a Monte Carlo calculation for Ar_6.

Regarding the quantum treatment of electrons, our research is the first to use a high-level treatment of electron correlation through methods such as Møller–Plesset perturbation theory, allowing us to perform fully ab initio simulations of proton transfer and other problems involving long-range electron correlation.

Achievements in FY02 included (1) writing an efficient, massively parallel PIMC code combining high-order quantum-mechanical propagators with highly efficient estimators for energy and heat capacity, achieving up to 100 times greater computational efficiency than the methods already available; (2) linking our PIMC code to a caching code for greater performance with smaller chemical systems; (3) performing calculations on several molecules, such as H_2O, including initial ab initio calculations on the CH_2 molecule; and (4) submitting a paper about our new PIMC energy estimator that was accepted by the *Journal of Chemical Physics*.

In FY03, we will apply our PIMC code and theoretical methods to additional chemical systems to gain thermochemical knowledge, and develop additional methods for increasing efficiency.

Nuclear Science and Engineering

Section 9

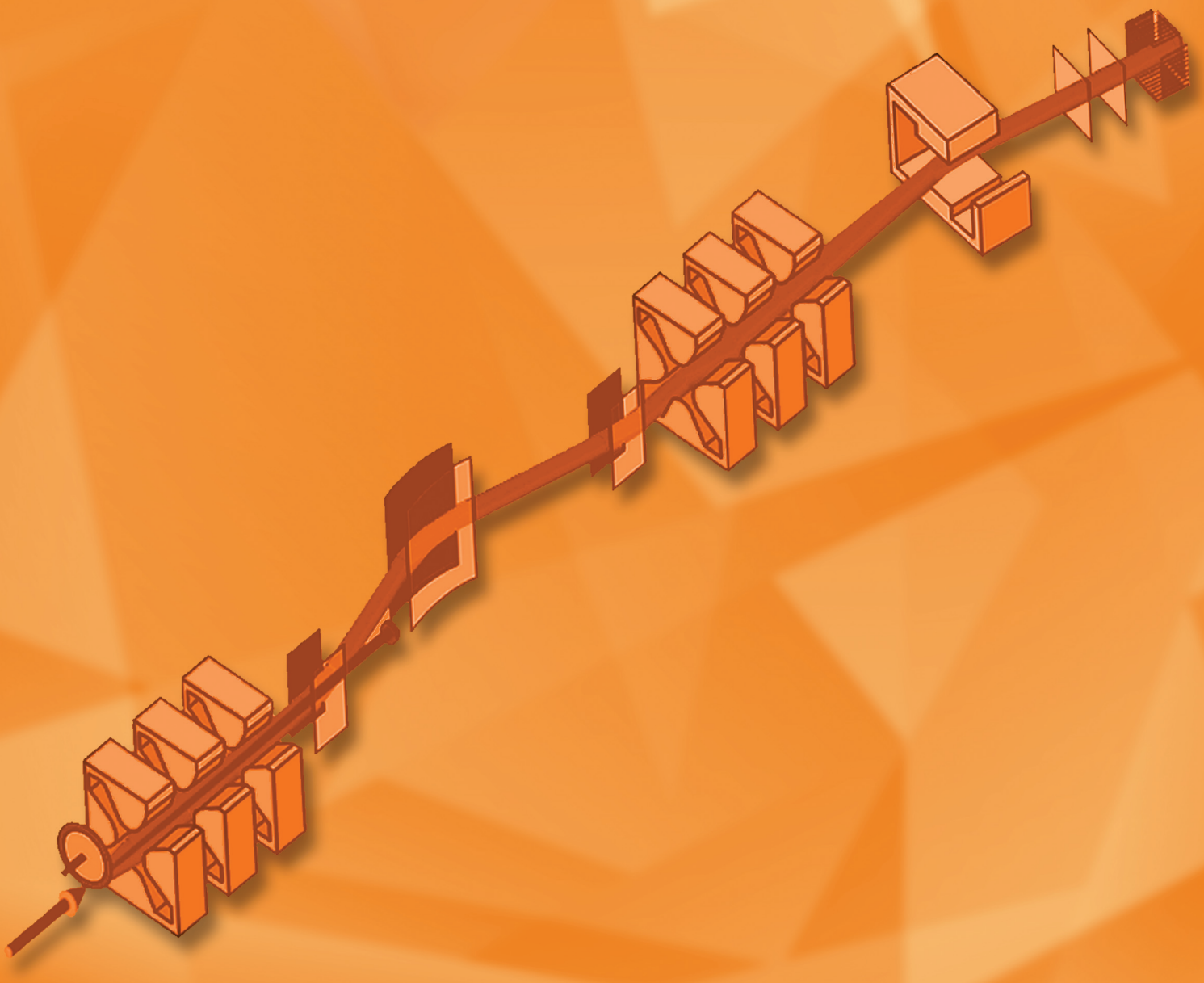

Section 9 — Nuclear Science and Engineering

Double-shell target design and experiments at Omega: Nonlinear mix studies for stockpile stewardship

P. Amendt, J. Colvin, M. J. Edwards, J. Milovich, H. Robey, L. Suter, R. Tipton

Large laser systems, such as Omega at the University of Rochester, represent unique testbeds for stockpile stewardship. Many of our laser–target experiments at Omega employ single-shell capsules designed to have relatively low levels of hydrodynamic instabilities. Single-shell capsules are designed to demonstrate ignition and high gain but are not well suited as a testbed for studying highly evolved, nonlinear mix. Double-shell targets are commonly viewed as inherently more hydrodynamically unstable but offer the advantage of not requiring elaborate methods for controlling target entropy. Moreover, recent advances in increased laser–target coupling seem to indicate that double shells offer increased robustness in performance.

This project explores the devlopment of a double-shell target capsule alternative by finding methods for mitigating the sources of instability so that ignition with double-shells appears achievable. Developing a simulation and diagnostic capability for understanding highly evolved mix in such an igniting target would provide an essential role for high-power lasers in stockpile validation. In addition, the dual use of double-shell targets as both a vehicle for ignition and as a testbed for stockpile-relevant studies provides a unique opportunity to study nonlinear mix under the extreme physical conditions of thermonuclear burn.

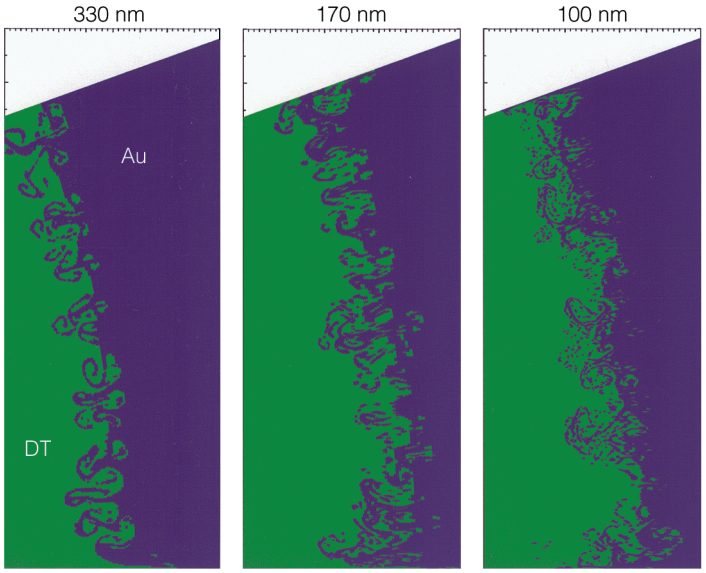

Fuel–shell interface in a double-shell ignition target at the instant of thermonuclear burn for three realizations of initial surface roughness using progressively smaller wavelength cutoffs. The deuterium (DT) fuel is shown in green and the gold (Au) shell in blue.

During FY2002 we made outstanding progress in exploring the robustness of our double-shell target design to hydrodynamic growth of short-wavelength surface perturbations. To understand the effects of this growth, we conducted detailed computer simulations of the mixing process with unprecedented spatial resolution. The Figure shows the results of several simulations at the instant of peak thermonuclear burn, using progressively smaller perturbation wavelengths. The smallest wavelengths considered are on the order of 100 nm, which is near a theoretical cutoff value that we derived based on the stabilizing effects of atomic diffusion between the fuel and high-Z inner shell. This demonstration opens the possibility of performing integrated and detailed simulations of ignition double shells and provides a meaningful testbed for NNSA-sponsored stockpile stewardship research.

In FY2003, we will conduct a double-shell experimental program on the Omega laser to validate and refine our nonlinear mix models. We expect to field ten double-shell targets to investigate double-shell implosion physics and to provide a baseline understanding of double-shell ignition physics. One goal is to mimic the proposed National Ignition Facility double-shell ignition design in as many relevant aspects as possible, despite the energy limitations of the Omega laser. We also plan to perform state-of-the-art three-dimensional simulations of double-shell instability growth using the HYDRA.code

Stellarator divertor studies

M. E. Fenstermacher, A. E. Koniges, T. D. Rognlien, M. Umansky

Modeling the physics of magnetized plasma in full three-dimensional (3-D) geometry, without any axes of symmetry, remains one of the grand challenges of plasma physics research. Applications range from atmospheric studies to thermonuclear-fusion reactor design. LLNL has had an ongoing set of research projects to help develop controlled fusion energy because of fusion energy's potential as both a clean, abundant energy source and as a neutron source that could transmute present radioactive material into much safer products.

Most of the modeling to date has assumed at least one axis of symmetry for equilibrium plasma parameters, but the National Compact Stellarator Experiment (NCSX)—to be built at the Princeton Plasma Physics Laboratory—is a toroidal device with no axis of symmetry. We are using LLNL's recognized expertise for computational simulation of the edge plasmas in axisymmetric tokamaks to produce the fully 3-D modeling capability that is needed for more geometrically complex configurations like the stellarator and for other 3-D magnetized plasma applications. The NCSX project will maintain our robust international presence and provide LLNL with a unique tool within the U.S. fusion program for 3-D studies of boundary plasmas in magnetic fusion devices.

The two major components of this project are to (1) collaborate in the development of 3-D transport and field-line tracing codes, and (2) join in the NCSX design activities and become strong participants in the international stellarator community.

Field-line tracing is our first step in analyzing the edge plasma. However, our long-term goal is to build-up LLNL's core competency in state-of-the-art computer modeling by collaborating with the five-person team at the Max Planck Institute for Plasma Physics (IPP) in Greifswald, Germany on the development of BoRiS, a multispecies, 3-D, magnetized-plasma-fluid simulation code. This capability will give LLNL the 3-D computational techniques needed to design the plasma-interaction hardware (the divertor) for stellarators and other nonaxisymmetric plasma devices.

During FY2002, we completed our field-line tracing studies for the NCSX baseline design, including models of turbulent heat diffusion, and contributed our numerical expertise in implicit solvers, interpolation methods, and fluid neutrals models to the development of the BoRiS fluid code. The field-line tracing calculations identified the regions of the NCSX material surface where concentrated heat and particle deposition are expected, and thus where protective armor must be included. When fully developed, the BoRiS simulations will give self-consistent plasma solutions from the interior edge to the plasma–material interaction surfaces. We have implemented a 3-D neutrals model in the BoRiS package and performed multiple benchmarking tests of the code against UEDGE, our mature 2-D edge-plasma transport code.

The Figure shows our initial predictions of the distribution of neutral deuterium atoms around the periphery of the NCSX 3-D plasma as a result of localized gas recycling from wall support ribs. Neutrals are confined well to the boundary plasma on the inner side of the thick bullet-shaped cross section. The neutral density in the thin banana-shaped cross section is substantially reduced (by a factor of 100), a very positive result since neutral penetration into the thin banana-shaped core plasma could lead to excessive cooling of the hot plasma in the NCSX experiment.

Although this LDRD project ended in FY2002, our work will continue in FY2003 with DOE support. We plan to continue our participation in developing the BoRiS code, which will be used to guide the NCSX design project.

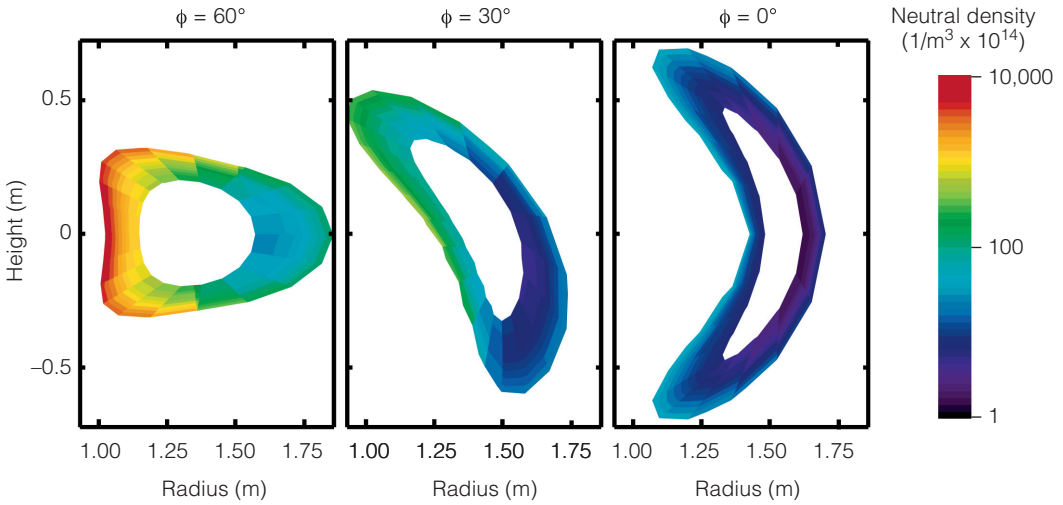

Modeling of two-dimensional, neutral-deuterium-atom density at three NCSX toroidal locations. The neutral density resulted from localized gas recycling on inner midplane support ribs located at the bullet-shaped cross section (ϕ = 60°).

Investigation of the shores of the Island of Stability

K. J. Moody, J. F. Wild, M. A. Stoyer, N. J. Stoyer, C. A. Laue, D. Shaughnessy, J. Patin, R. Lougheed

Calculations performed over the period of more than 30 yr predict a substantial enhancement in the stability of heavy nuclei when approaching closed spherical shells where the proton number (Z) is 114 and the neutron number (N) is 184. We reached the edge of this "Island of Stability" in 1998 when thin-foil targets of plutonium-244 (^{244}Pu) were bombarded with beams of calcium-48 (^{48}Ca) and cesium-248 (^{248}Cm), which produced isotopes of elements 114 and 116 with half-lives of seconds to minutes. The decay properties of the new nuclides confirmed theoretical predictions and can be considered proof of the existence of enhanced stability in the region of heavy elements.

We are investigating the topography of the southwest edge of the Island of Stability by bombarding americium-243 (^{243}Am) (half-life = 7370 yr) with ^{48}Ca ions at the U400 cyclotron in Dubna, Russia. The goal of this experiment is to synthesize the as-yet undiscovered element 115, with the added advantage that, should the isotope decay by alpha emission, element 113 will also be discovered. The alpha decay of element 115 isotopes directly probes the influence of the closed proton shell where Z is 114. For the first time, except for the extremely neutron-deficient bismuth (Bi) isotopes, alpha decay across a closed proton shell can be studied. These experimental data will provide valuable information for bound-shell model calculations of the ground-state properties of the heaviest elements. In addition to its scientific importance, this work supports the Laboratory's national-security mission and provides nuclear and radiochemical expertise that can be applied to stockpile stewardship, nonproliferation, and issues related to nuclear power production and the safe disposal of radioactive materials.

With our collaborators in Dubna, we plan to irradiate a target of ^{243}Am with ^{48}Ca ions to produce element 115 and possibly, subsequent to alpha decay, a second new element, element 113. The half-life predictions for element 115 nuclides are on the order of milliseconds, which are ideal for the experimental setup in Dubna. The spontaneous fission (SF) and alpha-decay hindrance factors for odd-Z nuclides suggest that the signature for the decay of an element 115 isotope will be a 2- or 3-member alpha-decay chain, eventually terminated by SF when the decay leads to the edge of the region of stability. From the expected reaction cross section, the intended target thickness, and the predicted performance of the Dubna electromagnetic separator (see Figure), we anticipate being able to detect an atom of element 115 every four weeks of beam on target.

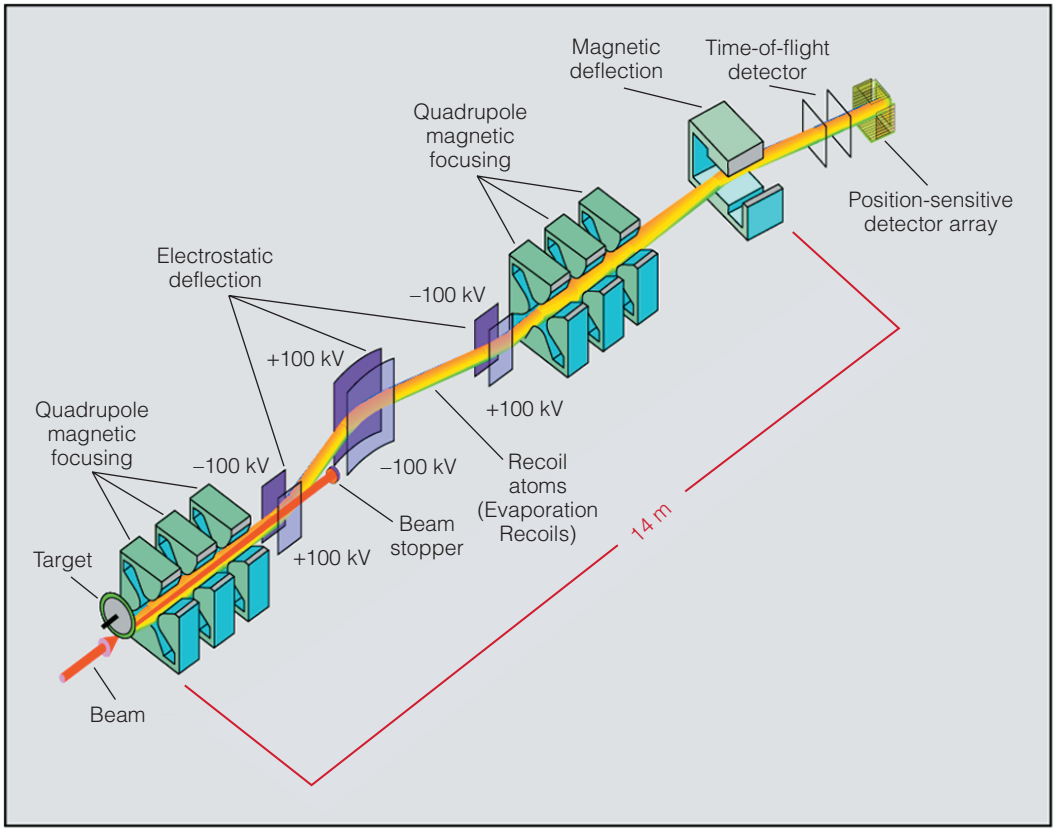

The Dubna electromagnetic separator is used to transport products of heavy-ion fusion reactions to the detector array and suppresses unwanted reaction products.

During FY2002, we completed experiment planning details and traveled to Dubna to carry out preliminary bombardments and to test new equipment. We acquired, purified, packaged, and shipped 20 mg of ^{243}Am to Dubna, along with the electronic modules acquired for upgrading the detector system.

In FY2003, we will complete the production run using the Dubna electromagnetic separator and analyze the resulting data.

Modeling in support of maritime cargo-container interrogation with neutrons

K. Sale and J. K.Wolford

Using computer simulations of various concepts and laboratory experiments, this project is exploring the potential use of active neutron interrogation for detecting clandestine weapons of mass destruction (WMD) materials entering the U.S. in cargo containers. To detect special nuclear materials, active interrogation uses neutrons to irradiate the target to induce fissions that produce prompt radiation and fission products. These products will continue to emit neutrons and gamma rays for several minutes. Measurements of this delayed radiation are used to infer the presence and quantity of the fissionable material.

Detecting high explosives or chemical weapon agents relies on neutron activation, which ultimately produces characteristic gamma-ray spectra. While these concepts are well established, their application to the detection of WMD materials in realistic environments remains technically challenging for several reasons: (1) lack of knowledge about the potential target material and the amount and nature of the other substances shielding it inside the container, (2) delivering sufficient flux of neutrons through the intervening material to the target of interest, and (3) detecting sufficient radiation relative to the background.

In this, project we use LLNL's Advanced Simulation and Computing Program (ASCI) Pacific computers to simulate experiments and proposed detection scenarios, which included various sources, detectors, experimental configurations and data-analysis methods for a range of possible combinations of cargo content and target materials.

In FY2002, we began by modeling experiments in various programs at LLNL that are relevant to this problem. The modeling characterized the difficulty of detection for thick absorbing or scattering layers and established thresholds for mass detection in various scenarios, including comparison to simple passive detection. Modeling efforts concentrated on the most definitive signature—radiation derived from delayed neutron emission—and established a maximum allowable value for the neutron source leakage between pulses. It also guided the design, content and placement of cargo simulants within the experiment, and provided estimates of dose to experimenters. The Figure (bottom) shows the predicted neutron flux into a helium-3 slab detector from an active neutron experiment, and (top) a simulated vertical section of the cargo container contents, target, and detector configuration.

The enhanced modeling capability resulting from this project will ultimately serve as a computational testbed for predicting the expected real-world performance of prospective active neutron-interrogation systems for detecting clandestine WMD materials entering the U. S. in cargo containers.

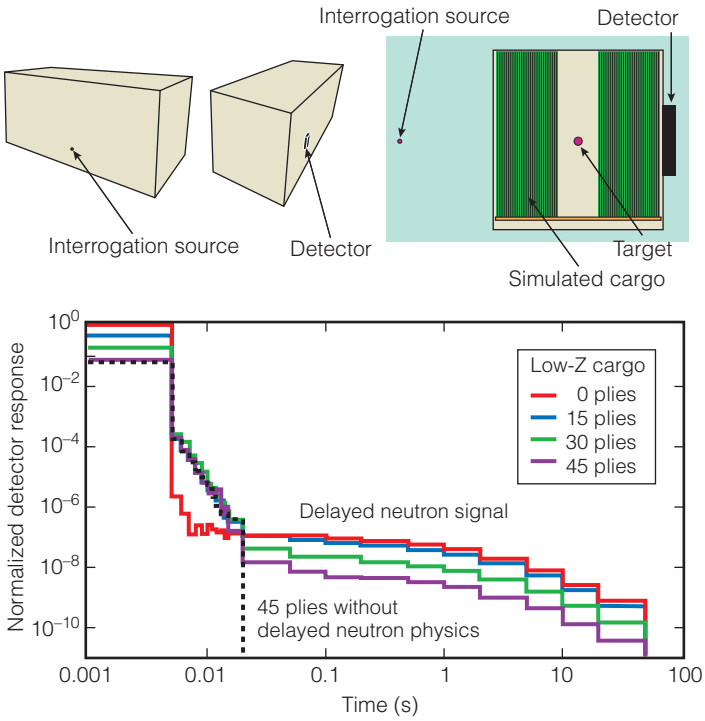

Simulated geometry of the active neutron experiment showing simplified cargo and predicted delayed neutron flux into the surface of a helium-3 slab detector.

Physics

Section 10

Section 10 — Physics

High-energy physics at the Next Linear Collider

J. B. Gronberg, K. A. van Bibber, D. Asner, E. Cook, W. Stein, J. Early

The current theory of particle physics, the Standard Model, is incomplete, lacking an explanation of the origin of mass and the mechanism of electroweak symmetry breaking. Indirect measurements at previous high-energy physics (HEP) experiments, such as the Large Electron Positron Collider, suggest that new particles are waiting to be discovered just outside the energy reach of current experiments. The new data from the Large Hadron Collider (LHC), currently under construction at CERN in Geneva, is expected to bring the first observation of new particles such as the Higgs boson or supersymmetric particles. However, the full study of these particles, which would elucidate the underlying theory, requires high-precision data. The international physics community has determined that the full exploitation of this new physics will require a teraelectron-volt, electron–positron linear collider. The Next Linear Collider (NLC), based on a normal-conducting X-band (11.424 GHz) design, is being developed as a candidate for this future machine.

This LDRD research project focuses on two main elements: (1) developing the technology for the NLC main linear accelerator (linac) systems to ensure affordability and reliability and (2) analyzing the physics capability and research and development needed for the preliminary design of a photon–photon collider.

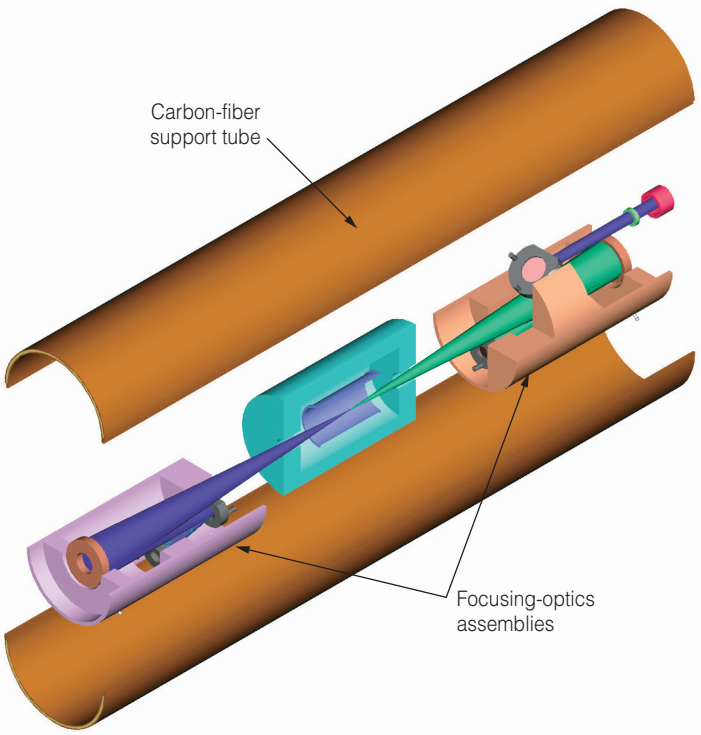

The focusing optics for the photon collider interaction region integrated with the accelerator vacuum system.

High-energy photons are produced through Compton backscattering of short-pulse, high-intensity laser light from the high-energy electron beam available at the NLC. High-energy photon–photon collisions open new production channels and allow the polarization of the initial state to be controlled. This would enhance the ability of the NLC to explore new physics.

The NLC's 20-km-long main linac system requires efficient and reliable production of about 100 MW of radio-frequency (rf) power. The rf system has four main subcomponents: (1) a modulator to convert AC electrical power into fast, high-voltage pulses; (2) klystrons to convert the pulsed power into rf power at the X-band frequency; (3) a compression system to increase the peak power of the rf pulses; and (4) accelerator structures where electron bunches "surf" the rf to reach their ultimate energy. Under this LDRD, LLNL has developed the modulator technology (1) and precision machining techniques for accelerator structures (4), while partner labs have worked on the other systems.

This project produced a solid-state prototype modulator that greatly improved efficiency and performance compared to the previous technology. This work was enabled by LLNL's expertise in pulsed power gained from construction of induction accelerators for stockpile radiography. Expertise in pulsed-power technology will have application to any accelerator-based program, including proton radiography for stockpile stewardship and the basic science mission of the NLC. In FY2002, the solid-state modulator prototype was upgraded with an improved fault-protection circuit to increase its reliability and became the keystone of the NLC full systems rf prototype, where it will provide pulsed power in FY2003.

In FY2002, we performed a Monte Carlo analysis that demonstrated the ability of a photon collider to observe charged and neutral supersymmetric Higgs bosons in theoretical scenarios where both the electron–positron collider at the NLC and the proton collider at the LHC would be blind. We also developed a preliminary design for integrating photon collider hardware components with the linac systems. This design could form the basis of a proof-of-principal demonstration at the Stanford Linear Collider that would produce gamma–gamma collisions at energies up to 30 GeV.

This work has been presented at numerous national and international meetings and published in refereed journals. The consensus of the international HEP community is that the option to produce photon collisions at the NLC should be retained and further study devoted to determining its full potential.

Short pulse: Enabling relativisitic applications for inertial confinement fusion and stockpile stewardship

M. Key, C. P. J. Barty, J. Caird

This Strategic Initiative aims to develop enabling technologies to generate and use high-energy petawatt (HEPW) laser pulses of ~5 kJ and ~5-ps pulse duration. Via relativistic laser–matter interactions, pulses of this type can be used to generate picosecond bursts of energetic (100 keV to MeV) electrons, protons and x rays.

High-energy petawatt lasers will allow heating solid-state media to temperatures and densities relevant to the Stockpile Stewardship Program (SSP), inertial fusion energy science, and laboratory-based astrophysics. They will also greatly enhance the scope of radiographic measurements used in SSP experiments at the National Ignition Facility (NIF). Targets in these experiments will be approximately 1000-times larger volume than those used in previous Nova laser experiments at LLNL or current Omega laser experiments at the University of Rochester. The plasmas in NIF experiments will be opaque to traditional, nanosecond, laser-generated, thermal x-ray sources in the 5-keV spectral region. The 20 to 100-keV, nonthermal, K_α x rays produced via collisional ionization from HEPW-laser-driven relativistic electrons would have sufficient brightness for this critical imaging task.

Work in this project in FY2002 included research and development in HEPW-enabling technologies, short-pulse optical damage studies, and evaluation of HEPW science opportunities. The project concentrated on developing damage-resistant diffraction gratings for multikilojoule-pulse compressors and compact-pulse compressor designs.

In conventional short-pulse amplification systems, a short-duration seed pulse is passed through an optical delay line to produce a long-duration, positively chirped pulse (optical frequency increasing linearly with time). After amplification up to the intensity-dependent damage limit of the amplifier, the chirped pulse is passed through an inverse delay line consisting of parallel pairs of diffraction gratings to remove the chirp and produce a short-duration, high-energy pulse. Intensity-dependent damage of gold-coated compressor gratings has limited previous short-pulse systems to energies of ~0.5 kJ. This project has explored a new grating technology based on multilayer dielectric (MLD) coatings and has optimized MLD grating designs to obtain a predicted efficiency near unity and damage resistance approaching that of bulk dielectric materials—an order of magnitude beyond the damage threshold of gold-coated gratings.

During FY2002, the project developed tools for production of 5-cm-diam test gratings, constructed a damage-test work station and conducted preliminary damage tests, which verified initial models for short-pulse damage. A new, folded-compressor design was invented that reduces overall compressor dimensions by ~500%. Normalizing to experimental data from the Office of Fusion Energy Sciences program in fast ignition, Monte Carlo modeling was performed to identify laser requirements for K_α sources. Monte Carlo modeling was also used to identify scattering limits in proton radiography.

At LLNL's Janus ultrashort-pulse laser facility, a significant breakthrough was made in a collaborative experiment that demonstrated the first ballistic focusing and isochoric heating by laser-generated protons. The Figure shows the experimental arrangement and the key result. Protons were focused to a 50-μm spot and a solid, 10-μm-thick aluminum foil was isochorically heated to a rear surface temperature of 23 eV, with the focused proton beam relative to 4 eV with the unfocused beam.

In FY2003, the project will research technologies for scaling HEPW components to the meter-scale dimensions required to support multikilojoule pulses, develop new broadband seed-pulse technologies, and continue to evaluate advanced radiographic and dense-plasma applications of HEPW pulses.

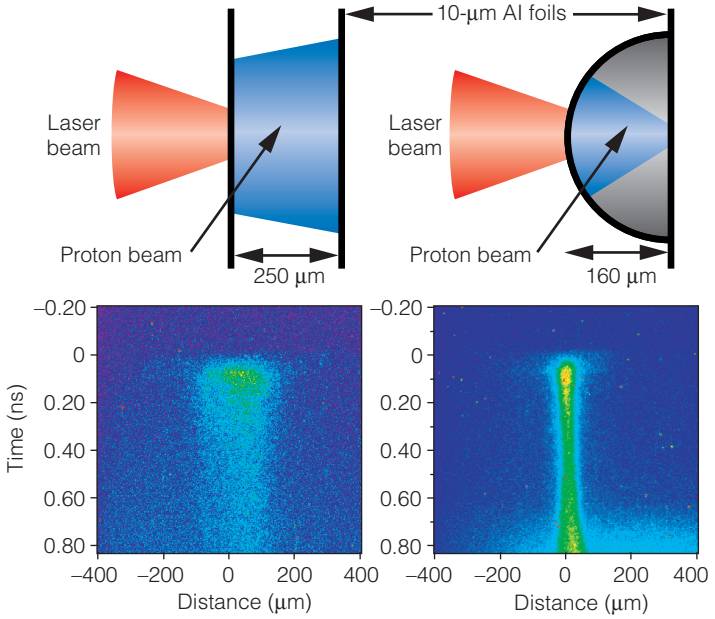

a) The experimental arrangement generating (left) unfocused and (right) focused proton beams on aluminum (Al) foils. (b) The corresponding streak camera images of Planckian emission due to proton isochoric heating, showing a 200-μm-wide heated region narrowed to 50 μm with ballistic focusing.

Modeling and experiments for theater-missile-defense agent negation

G. T. Nakafuji, T. G. Theofanous, R. A. Greenman

The threat of ballistic missiles carrying chemical, biological, or nuclear payloads is driving the development of new, high-altitude, theater ballistic-missile-defense (BMD) systems that are designed to intercept incoming ballistic targets at altitudes in excess of 30 km. However, the BMD community lacks vital knowledge required to understand the post-intercept survival and fallout of chemical-warfare (CW) agents.

Our goals are to address issues involving the hydrodynamic breakup of a CW agent following a successful, high-altitude (>30-km) intercept of a missile bearing that agent. Our project has both computational and experimental components and includes a strong collaboration with scientists at the University of California, Santa Barbara (UCSB). This research will enhance LLNL's capabilities to model BMD intercepts and their outcome and will aid in developing new counterproliferation and demilitarization methodologies to support LLNL's national-security mission.

In FY2002, we experimentally characterized the aerodynamic breakup of non-Newtonian surrogate fluids in supersonic flows in a vertical, supersonic, blowdown wind tunnel at UCSB. The wind tunnel had a 1.8-m-long glass test section allowing optical imaging with several high-speed cameras and a copper-vapor laser as backlight. This technique allowed examination of the time evolution of fluid breakup, as well as its end state—the final size distribution of masses. To simulate CW agents, we used a variety of fluids, which were thickened with polymers of varying molecular weights at different concentrations. Drops ranging from 2 mm to 1.5 cm in diameter were subjected to flows of up to Mach 3 (see Figure). Operating conditions in the wind tunnel were varied to simulate breakup at altitudes ranging from sea level to ~70 km. Computational fluid dynamic simulations were used both to quantify the operating conditions in the wind tunnel and to investigate the dynamic pressure loading of liquid masses.

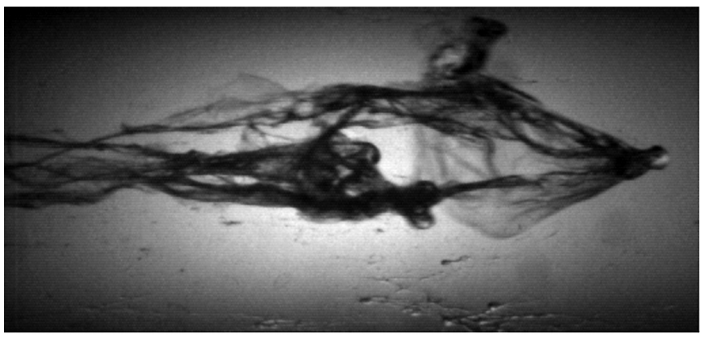

Aerodynamic response of a viscoelastic fluid in Mach 3 flow conditions.

The experiments revealed that viscoelastic fluids—fluids that exhibit both solid and liquid behavior—break up in a two-stage process. In the first stage, the fluid mass tears into filaments collinearly aligned with the direction of flow. This occurs on time scales of milliseconds in both subsonic and supersonic flow regimes. The fluid filaments rapidly decelerate due to aerodynamic drag forces and become suspended in the flow, then drift and settle at the prevailing settling velocity. The initial formation of threads was observed occurring over an increase in ambient pressure of four orders of magnitude—from 10^{-4} to 1 bar.

In the second stage, the filaments reach a zero-strain state, in which the relative velocity between the filament and air is negligible. With aerodynamic forces minimized, the surface-tension force of the filaments begins to dominate. Perturbations in the filaments may lead to surface-tension-driven instabilities that can cause the filaments to break up into particulates. Filament behavior varies depending on the polymer thickener's concentration, molecular weight, and physicochemical characteristics.

The observed process of viscoelastic fluid breakup directly contradicts current models used to calculate drop-size distributions for bulk fluids. The results of this project and its implications for aerosol applications are being used to reexamine and redirect scientific efforts involving chemical dispersal for applications in national security and other fields.

X-ray optics and applications for fourth-generation light sources

A. Wootton, R. Bionta, J. Kuba, R. London, D. Ryutov, R. Shepherd, V. Shlyaptsev

The DOE is funding the Linac (linear accelerator) Coherent Light Source (LCLS), a fourth-generation light source that will operate as a free-electron laser (FEL). The LCLS will produce a 0.8- to 8-keV, transversely coherent x-ray beam with a 200-fs pulse length and unprecedented brightness—10 orders of magnitude greater than existing third-generation sources. The LCLS will present opportunities—not available since the end of nuclear tests—to investigate nonlinear optics at x-ray wavelengths, as well as demanding requirements and innovative design opportunities for the optical systems, diagnostics, and components to transport the beam to experiments.

Our goals are to (1) develop new optical methods to control, manipulate, and measure LCLS-relevant x-ray-beams; and (2) understand the damage that occurs when an LCLS beam meets optics, diagnostics, and targets. We are using a combination of theory and computer codes to model these interactions and experimentation to benchmark these calculations in totally new regimes. Results from this project are relevant to any x-ray source but are particularly important to the future of the LCLS, which has potentially large benefits for stockpile stewardship and for the Laboratory's biology and biotechnology research.

In FY2002, we performed three types of simulations to determine the x-ray beam characteristics needed for designing the optics and diagnostics: (1) Monte Carlo to simulate photons shot through the optical elements in the beam, as well as the photon absorption, refraction at interfaces, and Compton scattering; (2) a wave model to calculate far-field distributions for generating spontaneous photons; and (3) other wave models to calculate distributions for generating FEL photons.

These simulations were used to develop novel schemes for minimally invasive imaging of x rays of extreme brightness, including Compton scattering off a thin solid foil (for x-ray energies greater than a few keV) and photoluminescence induced in a thin gas jet immersed in an axial magnetic field (for lower x-ray energies). The Figure illustrates a third concept—an apparatus in which a small fraction of FEL light is directly reflected off a thin, polished beryllium foil and strikes the surface of a 100-μm-thick crystal doped with a 5-μm-thick scintillating layer of cerium. Visible light reflected from the crystal is then collected by a microscope objective and forms a magnified image on a charge-coupled device (CCD) camera.

Using the fabricated apparatus, we studied photon–material interaction by measuring subpicosecond photon-induced damage at multiple wavelengths: 800 nm (a visible laser), 14.7 nm (an x-ray laser), and 1.0 to 0.15 nm (K_α sources driven by visible lasers). In the visible-laser experiments, damage occurred at ~0.1 J/cm^2—50 times lower than predicted from linear absorption. X-ray laser experiments used a novel multilayer target to demonstrate pulse length and focusing control. K_α experiments, which used two ~10-μm-thick foils separated by ~20 μm to control fast electrons, showed indications of both x-ray and proton damage.

As a consequence of this project, LLNL is now responsible for LCLS optics, diagnostics, and beam transport. The conceptual design review for these components was successful, and initial funding has already started.

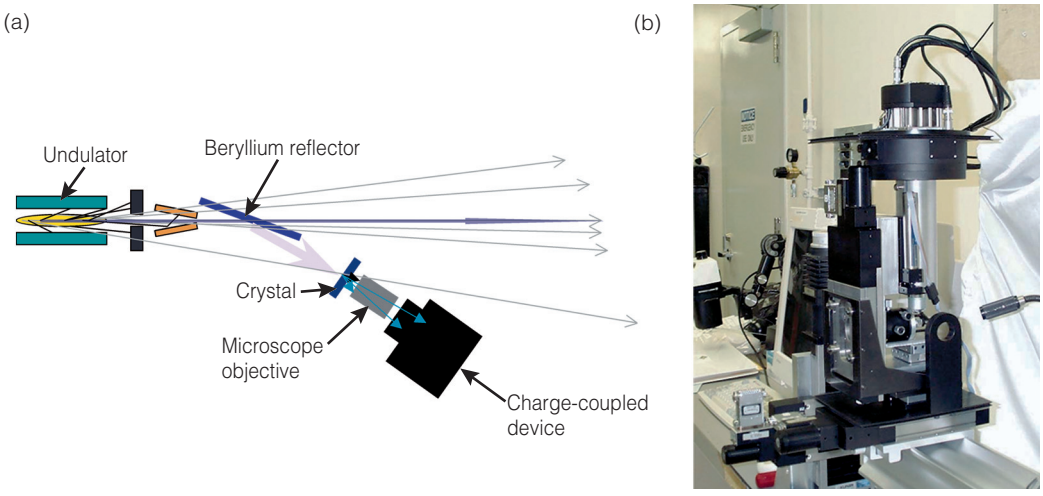

(a) Layout and (b) photograph of an apparatus for minimally invasive imaging the type of high-brightness x-ray beams that the Linac Coherent Light Source will produce.

Quantum chromodynamics at the Relativistic Heavy Ion Collider with two-particle correlations

R. A. Soltz, S. C. Johnson, E. P. Hartouni, M. Heffner, J. Burward-Hoy

The quantum chromodynamics (QCD) theory of the strong interaction between elementary particles predicts that—at sufficiently high temperature or baryon density—nuclear matter will exist as a gluon–quark plasma (QGP). Detecting and studying this new phase of matter is the purpose of the Relativistic Heavy Ion Collider (RHIC), a DOE facility at Brookhaven National Laboratory (BNL). Relativistic heavy-ion collisions provide the only laboratory available to study high-temperature QCD, a topic of enormous interest to the nuclear physics community and to the DOE Office of Science.

The Pioneering High Energy Nuclear Interaction Experiment (PHENIX), one of two large experimental programs at RHIC, detects and measures many different physical probes of the matter created in these collisions. Measuring the dimensions of the hot nuclear fireball produced in a relativistic heavy-ion collision presents an extraordinary challenge as the size of the fireball is so small, on the order of 1 to 10 fm, and lives for such a brief time, about 10^{-23} s.

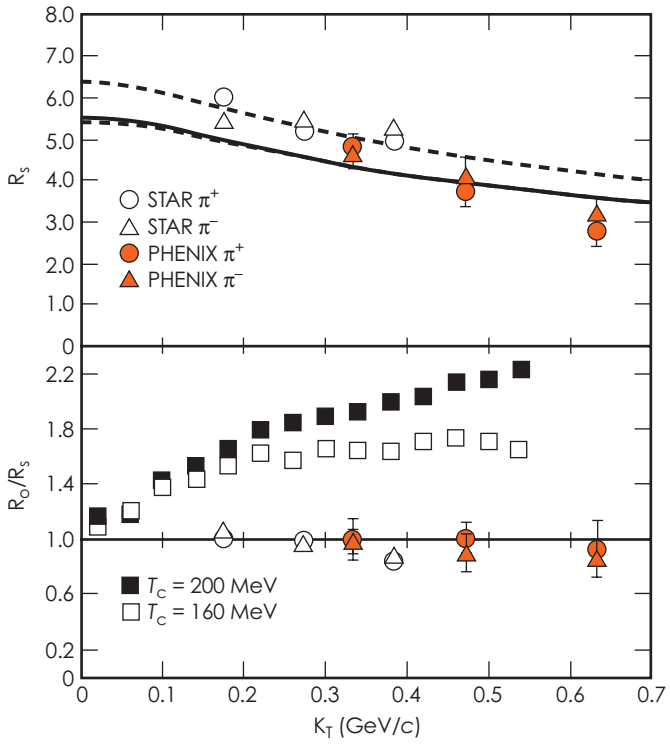

Measurements of the ratio of the outwards radius (parallel to the momentum of the pions) to sidewards radius (perpendicular to both pion and beam momenta) (R_O/R_S), shown as triangles and circles, are close to unity, indicating that the particles are produced very quickly during the collision. Theoretical calculations predicted a much larger ratio (open and filled squares), indicating a longer-lived fireball.

An analysis of two-pion correlations provides the only means of extracting the space–time information for the collision at RHIC. This information is needed both as a signature of the creation of a new form of matter—the QGP—and to understand the physical processes of high-temperature QCD. In this project, the LLNL team, using Monte Carlo calculations on LLNL's supercomputing cluster, led the analysis of two-pion correlations within PHENIX to extract spatial and temporal information in these collisions.

In FY2002, our first results on pion correlations from PHENIX were something of a surprise. As the Figure shows, the experimental ratio of the outwards radius (parallel to the momentum of the pions) to sidewards radius (perpendicular to both pion and beam momenta), shown as filled triangles and circles, is close to unity, indicating that the particles are produced very quickly during the collision. However, the theoretical calculations, which presume that a QGP was created, predicted a much larger ratio (open and filled squares), indicating a longer-lived fireball. This has presented the field of relativistic heavy-ion physics with a puzzle that has yet to be explained. Preliminary results have also been obtained with kaons and protons. While of lower statistics, results from both are consistent with the pion analysis.

The remainder of FY2002 was spent analyzing a higher-statistics dataset that will allow for a more unified analysis of the two-pion correlations and single-pion momentum distributions. We expect this approach will help to unravel the current puzzle regarding the short time scale for particle production in heavy-ion collisions. We also continued to carry out Monte Carlo simulations for the PHENIX experiment. Over 50,000 h of processing time were needed to understand background corrections in these and other PHENIX analyses. Work in FY2003 will also include completing the analysis of the kaon and proton data, the latter requiring more corrections due to strong interaction effects.

In summary, this project contributed a crucial measurement of one signature for the creation of a QGP. The result is in disagreement with current expectations and has paved the way for future theoretical inquiry while data for other potential signatures continue to be collected.

Ab initio nuclear structure from helium to oxygen

W. E. Ormand, P. Navrátil

The goal of this study is to answer a long-standing question in nuclear physics: Do we really know how nuclei are put together? Starting with our knowledge of the fundamental interaction between two nucleons, our goal is to achieve an exact description of nuclear structure and compare that with experimental observation. Due to advances in many-body theory and computational capabilities, it is now possible to realize this goal for nuclei more massive than helium. With the exceptional computational power of Advanced Simulation and Computing (ASCI) facilities at LLNL, this study is using effective interaction theory within the framework of the nuclear shell model to push the frontier to oxygen

Effective interaction theory is a powerful tool that is capable of yielding exact solutions within a computationally manageable framework primarily through "mapping" the interaction. The main feature of this mapping is that it contains terms that act between pairs of nucleons and triplets, quartets, etc. This is true even if the fundamental interaction is only pair wise.

In FY2001, we carried out the first-ever calculations that included triple terms in the effective interaction for nuclei more massive than helium-4. With this significant new capability, in FY2002 we observed a serious disagreement between the experimentally observed spectrum for the nucleus boron-10 and the calculated spectrum derived from the fundamental nucleon–nucleon interaction. This is shown in the Figure, where the calculated spectrum obtained with an effective interaction, including triplets derived from the realistic Argonne AV8′ two-nucleon force, is compared to experimental results. The primary disagreement is exhibited by the fact that the first two states are inverted in the calculated spectrum. We conclude that the nucleon–nucleon interaction by itself is insufficient to describe the structure of light nuclei. Although it has been known that so-called "true" three-nucleon interactions are needed to provide extra binding in nuclei, our results are the first compelling evidence that the three-nucleon interaction also plays an important role in determining the structure of low-lying nuclear states.

In FY2002, we also carried out calculations including a realistic three-nucleon force. In this case, we chose the Tucson-Melbourne interaction, whose form is dictated by symmetries in the strong interaction. The excitation spectrum obtained from these calculations is also shown in the middle spectrum in the Figure, and better overall agreement with experiment was achieved. In particular, the correct ordering of the first two states is obtained. For the most part, the exact form of the three-nucleon interaction is not yet known, and in a follow-on to this project, we will employ our method to map out the form of the three-nucleon interaction.

During FY2002, we carried out several systematic studies of the properties of light nuclei. In particular, we studied nuclear structure predicted by different formulations of the nucleon–nucleon interaction. In addition, we initiated a systematic study of light nuclei ranging from lithium-6 to carbon-13 with nucleon–nucleon and three-nucleon interactions. This study will be completed mid-FY2003.

With the new methods developed at LLNL, an accurate description of the structure of light nuclei is possible, and research at LLNL will take a leading role. This project has also achieved the important goal of re-establishing a nationally recognized nuclear theory program at LLNL. In the future, we plan to use the foundation of this project to develop a new reaction formalism to describe thermonuclear reactions that are important in stellar astrophysics and Laboratory programs, such as the NIF.

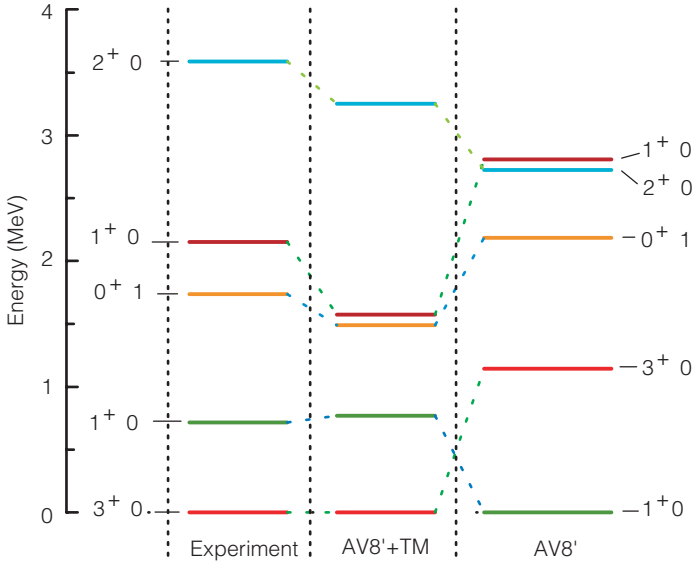

Calculated and experimental spectra for boron-10: (left) experimental data, (middle) calculated spectrum with AV8′ and the realistic Tucson-Melbourne (TM) three-nucleon interaction, and (right) calculated spectrum with the Argonne AV8′ nucleon-nucleon interaction.

Planetary interiors in the laboratory

R. Chau

The recent discovery of extrasolar planets whose masses are comparable to the giant planets in our own Solar System has focused attention on the nature of planets such as Jupiter and Uranus. To understand the formation and properties of these planets, we must determine the composition and nature of the hot, dense fluids within their interiors. For example, the very complex magnetic fields of Uranus and Neptune are generated by the convective dynamo motion of electrically conducting fluids in their interiors. Unfortunately, the extreme conditions within the planets and their great distances from Earth make direct probes of the planetary interiors impossible; ground-based observation and space probes provide only limited information.

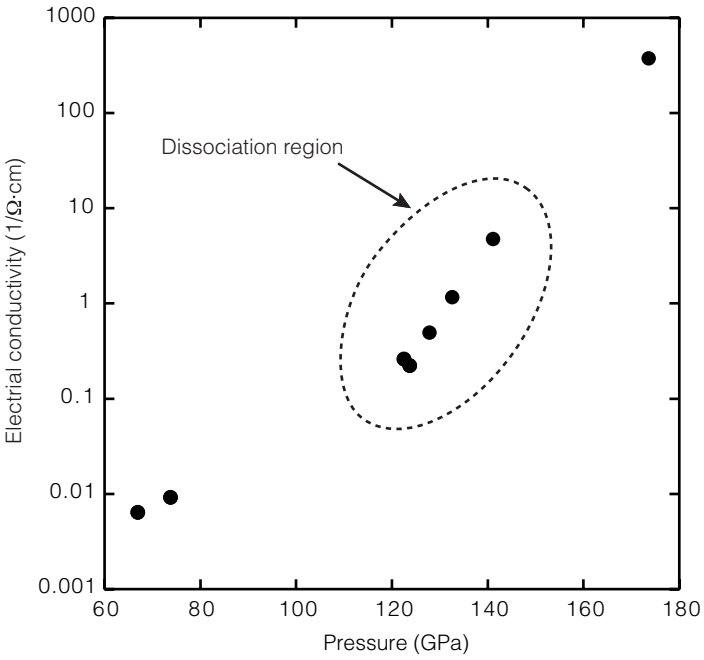

Molecular dissociation of methane (CH_4) in a narrow range above 120 GPa. Dissociation of CH_4 and other materials is believed to occur under the high-temperature and -pressure conditions in the interior of extrasolar planets.

In this project, we are simulating conditions within the interiors of giant planets by using gas-gun drivers to generate—for a short time—high temperatures (7000 K) and high pressures (200 GPa). Coupling dynamic generation of high pressures with real-time measurement of electrical conductivity provides information about the concentrations of electrons and ions. This in turn indicates chemical composition and the equations of state of planetary matter.

This project builds on and enhances experimental capabilities in the shock physics of low-Z materials for stockpile stewardship. Planetary materials such as hydrogen, methane (CH_4), and water are also important to work in inertial confinement fusion and energetic materials, in support of LLNL's energy-security mission.

In FY2002, measurements of the electrical conductivity of nitrogen and oxygen showed that the nonmetal-to-metal transition first observed in hydrogen is a general phenomena in disordered, dense fluid systems. A model explaining the mechanism for this transition was developed and predicts that carbon monoxide and many other materials found in planets also undergo a metallic transition.

In addition, we completed measurements of CH_4, a more complex system; confirmed the chemical dissociation first observed in FY2001; and showed that the kinetics and timescale of dissociation are highly dependent on pressure and temperature. Dissociation of CH_4 as a function of electrical conductivity is shown in the Figure.

This project has provided a complete database of the electrical conductivity of planetary materials up to 200 GPa. Moreover, we have demonstrated that the electrical conductivity of most simple planetary materials can be understood using a simple model; chemical effects occur in more complicated planetary materials, such as CH_4; and understanding high-pressure and -temperature chemistry is the next step in the laboratory study of planetary interiors.

Soft-x-ray line emission from comets

P. Beiersdorfer

The surprise discovery of x-ray emission from comets in 1996 by various x-ray satellites has far-reaching implications for understanding the interaction of comets with the inner Solar System. This discovery has opened up a new wavelength band for probing the solar wind—space weather—in real time, studying interactions between comets and the Sun, and understanding the composition of cometary atmospheres. Charge transfer of solar-wind heavy ions has been proposed as the comet's main x-ray production mechanism. This process is poorly understood. Models of charge-transfer-induced x-ray emission are based on best-guess estimates, precluding a proper description of the interaction of comets with the Sun.

Understanding cometary x-ray production is a prerequisite for describing this natural phenomenon in the solar system. It broadens LLNL's expertise in modeling short-wavelength radiation and benefits LLNL's core mission in high-temperature plasma and atomic physics.

The goals of this project were to (1) simulate, in a controlled laboratory setting, the conditions that cause comets to emit x rays, (2) produce the necessary experimental database for describing charge-transfer-induced x-ray emission in low-energy collisions of highly charged ions with atoms and molecules, and (3) incorporate our results into models that accurately describe x-ray emission by comets.

Our project uses Livermore's electron beam ion trap facility to produce the relevant heavy ions found in the solar wind, such as bare and hydrogenlike carbon, nitrogen, and oxygen. The ions were allowed to interact with gases found in cometary atmospheres. We used a high-resolution magnetically cooled x-ray calorimeter to perform spectrally resolved measurements of the resulting x-ray emission. This calorimeter is a one-of-a-kind detector built at the Goddard Space Flight Center as part of the Astro-E satellite mission, which made possible a breakthrough in data collection.

In FY2002, we probed the dependence of the x-ray emission on the interaction gas. We installed an atomic hydrogen beam to study charge exchange with the simplest atomic system available. Moreover, we used a variety of gases found in cometary atmospheres, such as carbon dioxide, methane, alcohol, and nitrogen. Our measurements provided the first detailed spectroscopic evidence that the x-ray emission depends on the interaction gas. This discovery may be used to probe the chemical composition of cometary atmospheres.

Our FY2002 measurements completed the data needed to describe charge-exchange-induced x rays from comets. Our measurements were used in FY2002 to model satellite observations of comet Linear (see Figure), the first time that a realistic charge-exchange-induced x-ray emission model was used to simulate the x-ray emission from a comet. The good agreement between our model based on laboratory data and the spectrum from comet Linear is the first unequivocal demonstration that charge exchange can produce x-ray emission from comets.

In FY2002, we also completed the construction of the first radiative-cascade model that accounts for all transitions from and between the atomic levels populated by charge exchange. New applications of this model have been identified in DOE's Fusion Energy Program. Our radiative-cascade model was successful in describing x-ray observations from charge exchange between argon tracer ions and a neutral hydrogen beam used to heat the plasma in magnetic fusion experiments. This application demonstrates that answers to basic science problems can significantly affect Laboratory programs and DOE missions.

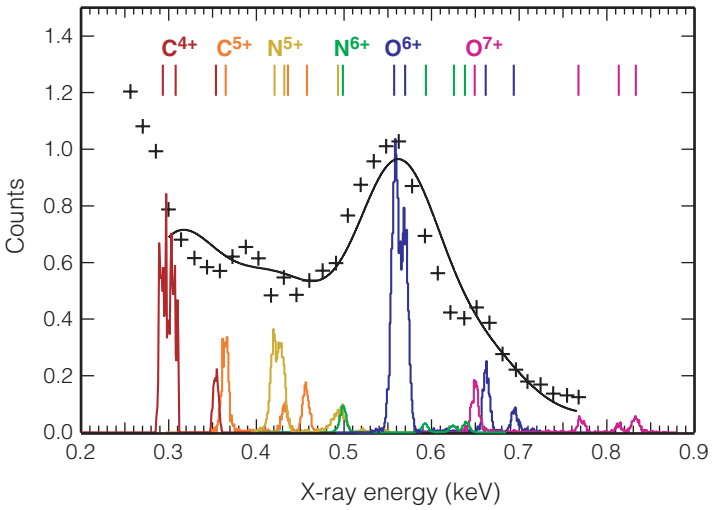

X-ray spectrum of the comet Linear (crosses) and best fit to that spectrum by modeling (solid line), using as input measurements of cometlike charge-transfer-induced measurements (colored peaks) from Livermore's electron beam ion trap.

First physics from BaBar

D. Wright, D. Lange, V. Brigljevic

Cosmological models of the early universe require a charge/parity (*CP*) violating process to produce our matter-dominated universe; however, a plausible source for this *CP*-violating effect has yet to be discovered. Current particle-physics theory contains such a process, but it does not resolve the cosmology problem, and until recently could not be experimentally tested. Discoveries in the late 1980s led to the realization that *CP* violation could be observed in the decays of neutral *B* mesons. LLNL was a founding member of an international collaboration at the Stanford Linear Accelerator Center to construct a new accelerator and detector, called BaBar, dedicated to *B* meson and *CP*-violation physics.

This project directly benefits LLNL programs in accelerator-related science and technology supporting stockpile management. The project also provides LLNL researchers with the opportunity to produce high-profile results at the frontier of physics and attract top-notch physicists to the Laboratory. Our achievements in this project have led to new program opportunities in DOE's linear collider project.

The *CP* violation asymmetry appears as a perturbation in the time dependence of *B*-meson decays. The most sensitive tests of *CP* violation can be made from the K_S decay channel where the *B* meson decays into a short-lived kaon and a pair of charm quarks—a mode that is easy to detect and has low background. Equally sensitive but more challenging to detect is the K_L decay channel, in which the K_S is replaced by the long-lived kaon. Because the K_S and K_L have opposite *CP* properties, the effects in each decay mode will be equal but opposite. To make a convincing discovery, BaBar should observe the appropriate signal in both channels.

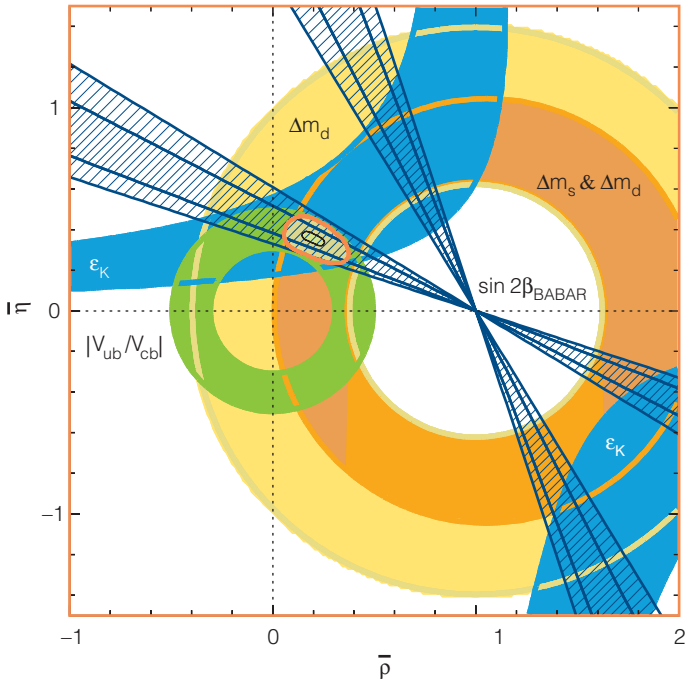

Change/parity measurement from BaBar (blue region) compared to expectation from theory (red) in terms of the fundamental theory parameters ρ and η. The BaBar result strongly establishes a non-zero value for the parameter η, which implies the existence of a large violation of matter/anti-matter symmetry.

Within the BaBar collaboration, LLNL plays a leading role in the *CP* analysis. In the first year, this project developed the software tools to find the signal and measure the *CP* asymmetry in the K_L decay mode; K_L events are difficult to reconstruct and have large, complicated backgrounds. To handle this background, we developed a sophisticated, general-purpose fitting algorithm, which resulted in our taking the lead in fitting all of the *CP* modes. We have produced results for all of the BaBar publications on *CP* violation.

In FY2002, we included a new, complex *CP* channel in the fitting software, modified the K_L detection algorithm to increase the signal efficiency, improved the simulation of muon and K_L interactions in the detector, and took the lead in the *B*-meson tagging group. We also participated in the effort to improve the muon/K_L detector hardware, including building a data-acquisition system and cosmic-ray test stand, which we used to test 132 replacement detector modules that were installed this summer.

BaBar achieved high-luminosity running by mid FY2000 and has steadily improved accelerator luminosity since then. In March 2001, we published the first tantalizing results and subsequent measurements with larger data sets, and improved analyses have established the existence of a *CP* asymmetry by about ten standard deviations (see Figure). Although the new results are in agreement with theoretical expectations, the experimental errors are still too large to constrain the theory significantly.

Although the combined results are statistically significant, with the expected increases in accelerator luminosity we can make a clean measurement of the *CP* violation parameter in the K_L channel alone. This is an important systematic check, since the K_L mode is a completely different *CP* state than that of the other high-precision (K_S) channel. From these *CP* studies and other precision measurements, the BaBar experiment will make stringent tests of the current theory and possibly detect the presence of new physics.

Positrons and positronium in insulators

P. A. Sterne, P. Asoka-Kumar, R. Q. Hood, A. L. R. Bug

Positrons in insulators pose a wide range of outstanding physics questions. In metals, the theory of positrons is well established, and first-principles calculations of positron characteristics are routinely used to identify defects. In insulators—in addition to the delocalized and defect-trapped states seen in metals—the positron can also bind with an electron to form positronium, an electron–positron "atom." Because this complicated behavior is not captured in existing theories, there is currently no general theory for interpreting positron experiments on insulators.

In this project, we are developing a detailed, predictive quantum-mechanical description of positrons in insulators. The combination of experimental capabilities, extensive computational resources, and advanced quantum-simulation computer codes makes LLNL uniquely suited for this project. The project's successful conclusion will create opportunities to solve defect-related problems in a wide range of insulators with potential applications to the Stockpile Stewardship Program and high-power laser programs.

In FY2002, we used the path-integral Monte Carlo (PIMC) approach that we developed in the previous year to predict the behavior of positronium in solid argon and in a vacancy in argon. The calculations yielded the experimentally testable prediction that the positronium wave function will be smaller in solid argon because of the confining potential of the argon atoms. Because this change in wave function reduces the positron lifetime, understanding this effect is important for correctly interpreting experimental results.

We completed experiments on a set of zeolite-y samples baked in vacuum to remove water and other gaseous contaminants. By measuring the changes in positron lifetime resulting from liquids of different molecular sizes added to the samples, we identified lifetime components associated with three distinct structural cages in the zeolite structure. Each cage was expected to have a corresponding positron-lifetime value determined by cage size, but surprisingly no lifetime component was observed at the value expected for the largest cage structure in zeolite-y. Our preliminary PIMC calculations suggest that the positron is spread over both large and small cages in the structure, resulting in an intermediate lifetime value close to that observed experimentally.

Using a positron microprobe at another facility, we mapped positron lifetimes around a laser-damage spot in a sample of silica (SiO_2), a material that shows a strong tendency to form positronium. In the Figure, the damage region clearly exhibits a reduction in positron lifetime due to the defect trapping of positronium. These results demonstrate the sensitivity of positrons to defects associated with laser damage, and highlight the need for further theoretical development to identify the specific defects produced by laser damage.

We also began development of a powerful quantum-mechanical approach based on variational and diffusion Monte Carlo (VMC and DMC), completing preliminary calculations for electron-only systems and performing a series of electron–positron calculations on small systems. This work demonstrated the ability of our VMC–DMC approach to calculate positron lifetime and other observable factors.

In FY2003, we will complete development of the VMC and DMC methods for positronium in insulators and use them in calculations on two systems with dramatically different positronium behavior—SiO_2, in which positronium forms readily, and diamond, in which no positronium has been observed experimentally—and implement a novel age–momentum technique for measuring the momentum distribution associated with different lifetime components.

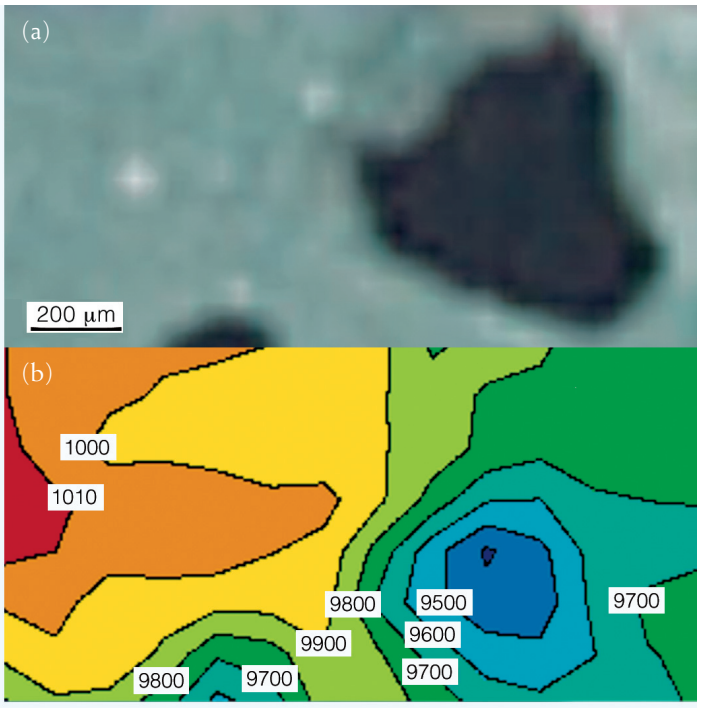

(a) Optical image of a laser-damage region in silica. (b) Positron microprobe image of mean positron lifetimes (in picoseconds) around the defect. These results demonstrate the sensitivity of positrons to defects associated with laser damage.

Smart nanostructures from computer simulation

J. C. Grossman, A. J. Williamson, G. Galli

Recent rapid growth of interest in nanoscience has been inspired by breakthroughs in the production of high-quality semiconductor and metallic nanostructures. A growing literature reports promising technologies at the nanoscale, such as recording devices only 1 nm across, nanomanipulation devices that could inject drug molecules directly into DNA, and nanosensors designed to detect biowarfare agents. The ability to (1) control the critical dimensions of individual nanoparticles and (2) assemble multiple particles into organized structures raises the possibility of constructing a new generation of nano-electronic devices, such as lasers, single-electron transistors, and photovoltaic materials.

Computer simulation can play a central role in studying nanostructure physics. However, current nanostructure simulation methods face the difficulties posed by the large range of size scales of different nanostructure systems—from single nanoparticles comprising as few as 20 atoms, to three-dimensional (3-D) arrays containing several million atoms.

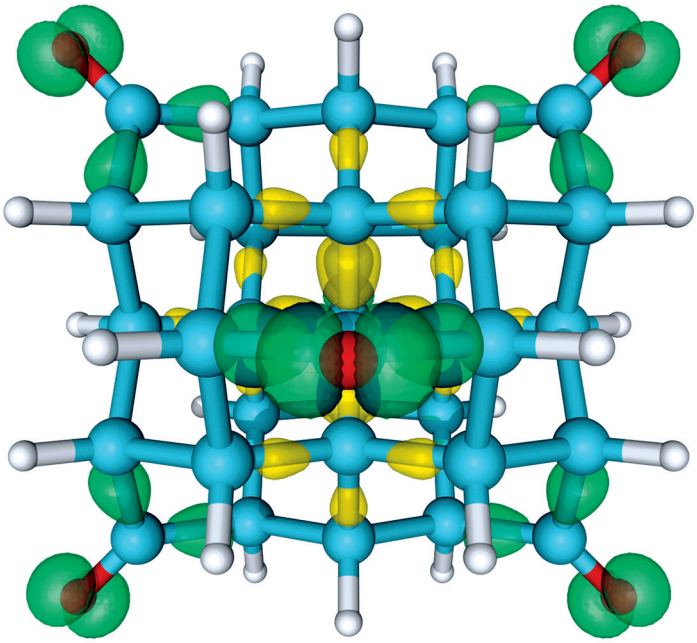

We are developing computer-simulation techniques for simulating nanostructures over a large range of size scales—from single nanoparticles comprising as few as 20 atoms, to three-dimensional arrays containing several million atoms. This isosurface plot shows electronic charge density (green and yellow surfaces) around a silicon quantum dot terminated with oxygen (red atoms).

The goal of this project is to develop computer-simulation techniques capable of performing simulations over this large range of size scales. This capability will facilitate the design of smart nanostructures with tailored physical properties, a technology that will support LLNL missions in countering the threat of bioterrorism and in bioscience to improve human health.

In FY2002, we studied the optical effects of different passivant molecules on the surface of silicon quantum dots, demonstrating that the optical gap—the energy of light absorbed upon excitation—is significantly reduced by oxygen and fluorine atoms on the surface. The results of our study are important because oxygen is a common contaminant in the synthesis of nanoparticles. Examining the relative stability of different structural relaxations on the facets of silicon nanoparticles, we (1) successfully identified possible relaxations using knowledge of reconstructions on the surface of bulk semiconductor materials, (2) calculated which of these relaxations produce the most stable nanoparticles, and (3) used these stable structures to calculate the reduction of the optical gap.

Significant advances were made in algorithms for quantum Monte Carlo (QMC) formalism. By implementing a localized basis set efficiently evaluated using cubic spline interpolation techniques, we enabled our calculations to scale linearly with the number of electrons in the calculation. These improvements expanded the range of problems we can address within QMC by an order of magnitude.

In FY2003, we plan to continue investigating the structural effects of adhering different surface passivants to nanoparticles; provide theoretical interpretations of measured optical properties, such as quantum-confined valence- and conduction-band edges, excitonic band gaps, and charging spectra; and study the behavior of groups of nanoparticles acting as an "artificial molecule"—in particular, how the electronic states of individual nanoparticles result in coupling into small clusters or fully 3-D, closely packed arrays.

Direct characterization of the electronic structure of shocked and heated materials

A. J. Nelson, J. Dunn, A. W. van Buuren, R. F. Smith

Detailed knowledge of how materials respond to strong shocks or other extreme conditions on rapid timescales (such as laser heating) are relevant to LLNL missions of national security and stockpile stewardship. This project is developing and demonstrating a new pump-probe characterization capability for investigating ultrafast changes in the chemical and electronic structure of materials under extreme conditions with picosecond time resolution.

The project utilizes a unique tabletop x-ray laser facility at LLNL—the Compact Multipulse Terawatt (COMET) laser—to perform photoemission spectroscopy (PES) and to study the surface chemical and electronic structure of various types of matter, including metals, semiconductors or organic materials undergoing fast laser excitation or shocking. The 85-eV x-ray source properties of the COMET laser, including high photon flux (10^{12} photons per pulse), high-energy monochromaticity ($\Delta E/E \sim 10^{-4}$) and fast (2 to 5-ps pulse duration), are ideal for studying chemical and electronic structure changes due to fast laser excitation when combined with time-of-flight (TOF) photoelectron spectroscopy. This combined technique results in unique, direct, time-resolved measurements of the electronic structure of the material and will provide insight into the dynamic process and final states.

In FY2002, we overcame several major scientific and technical challenges to validate the x-ray laser PES technique by measuring tantalum 4f and tungsten 4f core- and valence-electron spectra from room-temperature bulk materials (see Figure). We installed an argon ion gun in the dedicated x-ray-laser beamline ultrahigh-vacuum chamber for sputter-cleaning samples in situ to remove surface oxides and contaminants. This improved the surface purity and corresponding core-level and valence-band photoemission intensity. To meet the novel requirements of single-pulsed x-ray-induced PES spectra, we improved the data-acquisition electronics for fast time resolution by optimizing the TOF analyzer performance using fast (3 GHz), transient, digitizing oscilloscopes.

Previously, we completed and tested the third COMET laser arm for high-contrast, frequency-doubled output. This arm will be the optical pump in the dynamic experiments for creating sample melts. The beam (1.2-J, 500-fs pulse, at 527 nm) can be delivered simultaneously and in synchronization with the other two laser arms generating the x-ray laser probe.

In FY2003, the pump-probe x-ray laser photoelectron spectroscopy experiments will continue with further refinements. We will proceed to measure the shallow 3d core (39.3 eV binding energy) and valence-electron spectrum from room-temperature bulk germanium (Ge) using x-ray-laser-induced PES and investigate size- and phase-dependent changes in 3d core and valence electronic structure of Ge nanostructures. Also, we plan to perform the first dynamic pump-probe experiment of heating bulk Ge with a 500-fs laser pulse up to and beyond melt to determine the time-resolved changes through the intermediate and final phase conditions of the sample.

The project will then focus on a number of more exotic materials that are of interest at LLNL and in the scientific community. We plan to compare theoretical models with experimental results to enhance our understanding of these scientific phenomena.

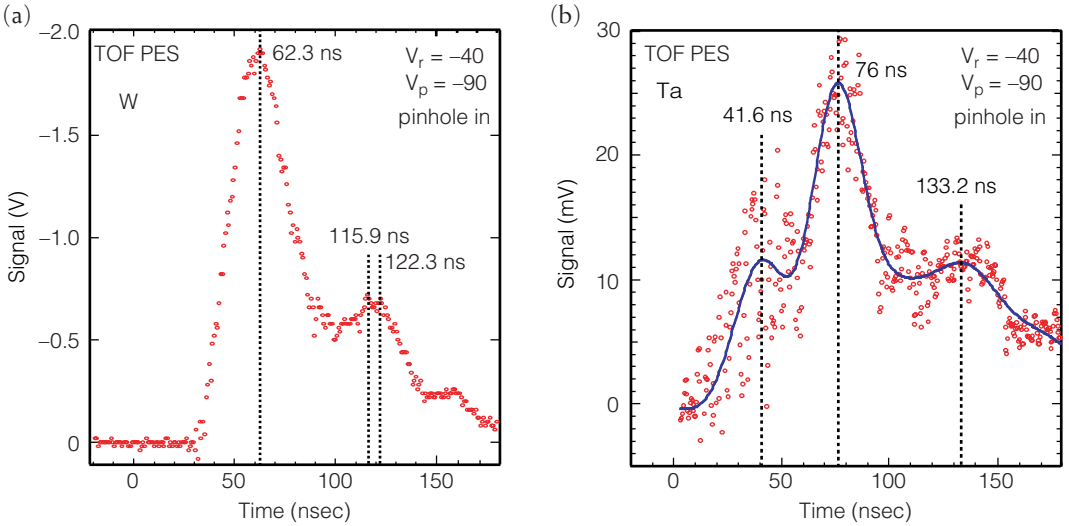

The first demonstration of using the COMET x-ray laser to perform time-of-flight (TOF) photoemission spectroscopy (PES), showing the 4f core-level and valence band for (a) tungsten (W) and (b) tantalum (Ta). The blue line in (b) is the best fit to all the data points.

Multimegabar metal equation-of-state and material-property data using high-explosive pulsed power

R. Cauble and D. B. Reisman

The experimental determination of high-energy-density equations of state (EOS) and properties of plutonium and other metals is central to Stockpile Stewardship Program applications. These applications require EOS and material models that must be tested by experiment and constrained by data. For many applications, data in the few- to tens-of-megabar regime are needed. Strong shocks can generate these pressures but produce unwanted high temperatures.

"Squeezing" a sample on an isentrope produces lower temperatures than shocking it to that pressure, but squeezing is extremely difficult to do at high pressures without producing an unwanted shock. In earlier work with Sandia National Laboratories (SNL), we developed isentropic compression experiments (ICE) on SNL's Z Accelerator—a large, pulsed-power system that produces an intense magnetic field, which in turn generates magnetic pressure to squeeze samples to high pressure. However, pulsed-power machines have limitations: the maximum pressure is only about 1 Mbar, the current pulse cannot be easily modified, and actinide sample materials are prohibited.

High-explosive pulsed power (HEPP) is a relatively mature technology that uses a set of explosives to provide a very large electrical current for a few microseconds and another set of explosives to shorten the current pulse to less than 1 μs. Although HEPP had never been previously considered for ICE, HEPP ICE has the potential to overcome the limitations of machine-based ICE, including the use of actinide samples.

Our goals in this project are to (1) establish, in collaboration with Los Alamos National Laboratory (LANL), the use of HEPP for ICE; and (2) design and field an improved diagnostic, called a velocity interferometer system for any reflector (VISAR), for our measurements. By providing EOS and material-property data to benchmark models now in use, and by developing improved VISAR diagnostics, this project furthers stockpile stewardship in support of LLNL's national-security mission.

In FY2002, VISAR was completed, and target configurations designed in FY2001 were implemented in HEPP firing tests at LANL. Although the tests proved the HEPP ICE concept, the constraints of ICE involved HEPP regimes in which HEPP specialists had no previous experience. In addition, two partial tests in FY2001 and two full tests in FY2002 indicated that progress on ameliorating arcing problems in the HEPP device was slow. Furthermore, investigating and correcting these problems was deemed to be beyond the scope and scale of this project. However, the project did develop novel, high-efficiency probes that can be used with any of the many VISARs in use. These probes have higher light-gathering capability than standard probes, significantly improving signal-to-noise ratios.

High-pressure, high-strain-rate materials effects

D. H. Kalantar, E. Bringa, K. Budil, J. Colvin, M. Kumar

Time-resolved dynamic x-ray diffraction provides a technique for studying the response of a crystal lattice under shock compression as the shock passes through the sample. Compression of the lattice spacing is observed as a shift of the Bragg diffraction angle, and a broadening of the signal may be characteristic of the dislocation and stacking fault density in the material. By recording x rays diffracted from multiple lattice planes simultaneously, this technique provides information on the state of the shocked sample as it is compressed and subsequently relaxed. Optical and electron microscopy are used on recovered shocked samples to investigate the residual deformation structure that remains in the sample following the release of the shock.

The goal of this project is to study the possible correlation of the lattice response under compression with this residual deformation microstructure. This research will provide information on how the microstructure affects the material response under shock loading at extreme conditions. The results of experimentation—performed primarily at the Janus, Omega, and Vulcan laser facilities—will directly benefit future experiments involving materials properties on advanced lasers and aid the development of improved models of the properties of shocked materials of interest to the Stockpile Stewardship Program.

In FY2002, we focused on obtaining information on the lattice response of shocked materials using a new wide-angle detector to record x rays diffracted from multiple lattice planes. This detector—designed for shock experiments with the Omega laser at the University of Rochester—consists of three film holders positioned to subtend a π-steradian solid angle around the target. Using the device, we performed single-crystal silicon (Si) and copper (Cu) shock experiments to record x rays diffracted from approximately 12 different lattice planes simultaneously. The Figure is an example of the diffraction pattern from Si. Such images show diffraction signals from both unshocked and shocked lattice planes, providing information on the detailed lattice response. Free-surface velocity measurements were made with similarly shocked materials, and analysis was begun to interpret the lattice information and correlate it with the more traditional wave profile measurements.

Continuum and molecular dynamics modeling were also started to model the experiments. Continuum modeling will calculate the pressure in the shocked samples to compare with the free-surface wave profile measurements, and molecular dynamics modeling will help understand the broadening of the diffraction signals that results from shock loading. We also made progress in selecting a model potential that is consistent with the shock Hugoniot results for our single-crystal Cu experiments; began developing a dislocation model; and started developing procedures for postprocessing to simulate the Bragg diffraction signals.

The combination of these techniques and simulations will provide information on the dynamic response of the lattice during shock compression, and enable a comparison with the residual state as characterized by postshock microstructural analysis.

In FY2003, we plan to continue experiments with shocked single-crystal Si, Cu, and iron (Fe) samples to study the time dependence of lattice response under shock loading. These different materials respond on different time scales, from microseconds (Si) to picoseconds (Cu). In the case of Fe, a phase transition occurs on a ns timescale. In addition, work will continue on molecular dynamics and postprocessing simulations for comparison with experimental diffraction-signal broadening measurements.

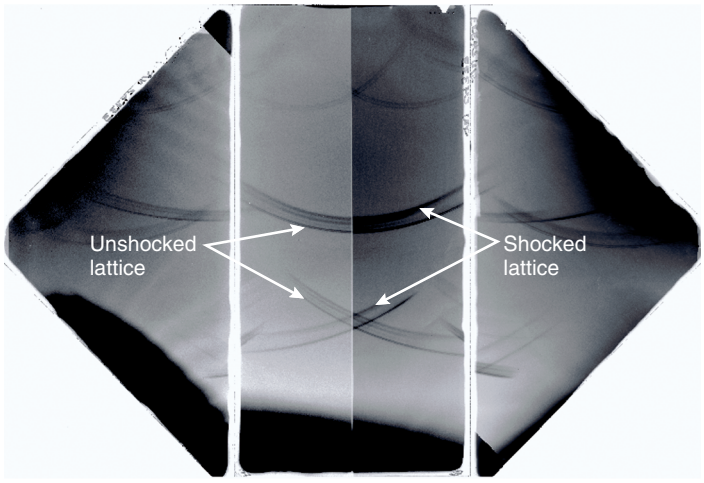

An example of the x-ray diffraction pattern of silicon (Si) on film planes wrapped around an Si target. Such images show diffraction signals from both unshocked and shocked lattice planes. Analysis will interpret the lattice information and correlate it with the more traditional wave-profile measurements to better understand the response of a Si crystal lattice under shock compression.

Developing a radiative-shock testbed

J. Greenough, H. Robey, B. Remington, T. Perry, M. Herrmann, P. Drake, A. Mizuta

Radiative precursor shock occurs when the flux of ionizing photons radiated forward from the shock front exceeds the flux of atoms approaching the shock front. A dramatic example of radiative shock occurs in the localized emissions emerging from the impact of Supernova 1987A ejecta with the supernova's circumstellar ring nebula. This display of radiative hydrodynamics is occurring in Earth's nearest neighbor galaxy, the Large Magellanic Cloud, which is 160,000 light yr away. Astrophysical shocks, when they become cool enough, enter a radiatively collapsing phase in which their density can increase several orders of magnitude. Radiation leaving from behind the shock cools the plasma, lowering the pressure, in response to which the density increases. This density increase enhances the radiative cooling, which lowers the pressure still further, and so on, leading to a "radiative collapse". All supernova remnants eventually pass through this phase. Such shocks arise in a number of both astrophysical and earthbound high-energy-density contexts.

To interpret radiative shock events, this project combines Advanced Simulation and Computing (ASCI) Program state-of-the-art, numerical simulations with well-diagnosed experiments on the Omega laser (at the University of Rochester) and theoretical scaling between regimes. Our goal is to develop an experimental realization of radiatively collapsing shocks, in a way that provides a suitable testbed for the study of the radiatively preheated matter and of the dynamics of the shocked layer.

This testbed developed in this project will enable laboratory studies of hydrodynamically driven radiative shocks, which are of broad scientific interest, especially in astrophysics. The results of this research will support verification and validation of existing codes and new ASCI codes still under development for LLNL's stockpile stewardship mission.

The basic concept for the experiment was developed in FY2001, and the first experiments to test this design were conducted in FY2002. The laser target used for this purpose is a 2.5-mm-long, 600-μm-i.d. beryllium tube filled with gas using a fill tube. Argon was initially used as the fill gas, which produced visible layers, but based on improved simulations, subsequent experiments used xenon gas. The backlighter plate emits x rays that produce images called radiographs. The shocked layer is recorded as a dark band across the radiographs. Improved backlighter materials and techniques will lead to much better images in the future.

This experiment also featured a novel use of the velocity interferometer system for any reflector (VISAR) diagnostic system, using a window and mirror. The VISAR system detected signals when the shocked layer passed through viewing volume, providing an independent detection of the shock. Interpretation of the VISAR data is proceeding in FY2003 and is likely to lead to improvements in future experiments, which we hope will include a measurement of the electron density due to preheat. The data show that the shock is moving at ~100 km/s. After the shock moved 1500 μm, its thickness was less than 100 μm, which implies that its density is at least 15 times the initial gas density, and possibly much higher because of nonparallel viewing and nonplanar structure.

We are well on the way to producing the desired radiative-shock testbed. In FY2003, the target design will be optimized to produce high-quality archival data on radiative shocks. Connections will be made to astrophysics through an astrophysics shock code currently under development. Connections will also be made to the radiative-shock, noncryogenic inertial confinement fusion ignition capsule project, which uses a similar radiative shock in xenon gas, only in a spherically convergent geometry.

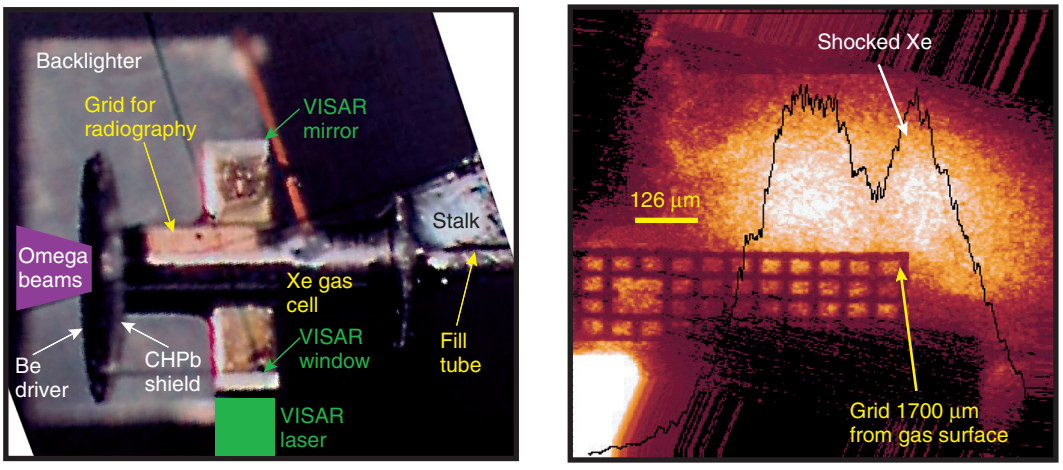

(left) Initial target used in the radiative shock experiments at the Omega laser. (right) Sample radiograph of the radiative shock traversing the xenon (Xe) gas fill, driven by the Omega laser.

High-average-power, frequency-agile fiber lasers

D. M. Pennington, R. Beach, J. Dawson, C. Ebbers, Z. Liao, S. Payne, L. Taylor

Telecommunication requirements are rapidly exceeding the bandwidth of existing erbium-doped fiber amplifiers (EDFAs), the optical amplifiers used throughout the long-haul telecommunications infrastructure. Our research will develop longer-wavelength fiber lasers that can be used to expand existing networks. When used in laser-guided adaptive optics (AO), this wavelength has both military and astronomical applications.

The goal of this project is to develop compact, versatile, high-power fiber-laser technologies based on diode-pumped fiber lasers, which can be frequency doubled or mixed in periodically poled (PP) materials to provide a spectrum of visible wavelengths. The project is developing a 920- to 940-nm neodymium- (Nd-) doped fiber amplifier (NDFA) and a 1583-nm erbium- (Er-) doped fiber amplifier (EDFA). In addition, a 589-nm wavelength can be generated by combining the EDFA and NDFA via sum-frequency mixing in a PP crystal.

This research will establish a core competence at LLNL in fiber lasers and PP materials, which have been identified as strategic, next-generation laser technologies. The fiber-laser technologies developed in this project have the potential to impact LLNL and DOE national security missions, including detecting environmental pathogens for homeland security, airborne lasers for theater missile defense, and satellite imaging for nonproliferation. Applications for energy missions include detecting atmospheric water vapor, which will assist researchers in understanding the global balance of energy and climatic issues. In addition, the NDFA can be used medically for photodynamic therapy.

In FY2002, the EDFA laser system, shown in Fig.(a), was successfully demonstrated, with 10 W of linearly polarized output [Fig. (b)] and a tuning range from 1582.6 nm to 1583.3 nm. The system is completely fiber-based, which offers robustness, compact size, and ease of operation.

Developing the NDFA presents the main technical challenge in our design. Using a combination of low-temperature operation for suppression of ground-state absorption, bend-induced losses to suppress lasing at 1088 nm, and a high-power seed source, we successfully demonstrated a core-pumped version of the 938-nm silica laser at 2.2 W, greater than 400 times the previously demonstrated value. We expect that the next generation design will yield >10 W.

For the third technology component—validating the use of PP materials at high average power in the visible—we demonstrated 28% conversion efficiency on PP potassium trihydrogen phosphate (KTP) without observable damage. Modeling was performed to determine the optimal material for sum-frequency generation to 589 nm and direct harmonic conversion of the Nd:silica laser. In FY2003, we plan to sum the 938-nm and 1583-nm fiber lasers to produce a prototype of a low-power, 589-nm source for laser-guided AO programs at LLNL; assess our ability to scale the design to higher average powers; and produce a preliminary system engineering design in FY2003.

Other work planned for FY2003 includes (1) testing the modified NDFA fiber and demonstrating a 10-W NDFA as a compact source for atmospheric measurements, (2) demonstrating higher conversion efficiency in the PP materials using elliptical formatting, (3) performing extended lifetime testing of PPKTP and other PP materials, and (4) frequency-doubling the NDFA laser using PP materials to produce a blue light source for biopathogen detection and theater projection.

(a)

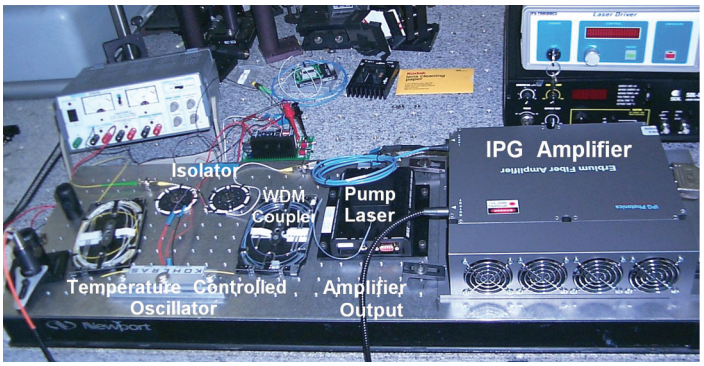

(b)

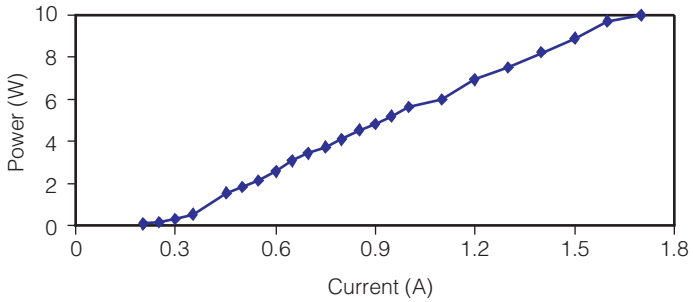

(a) Photograph of erbium-doped fiber laser oscillator and amplifier (EDFA); (b) power output of 1583-nm EDFA.

Focusing hard x rays at current and future light sources for microscopy and high-power applications

R. M. Bionta

The extreme brilliance and ultrashort duration of fourth-generation, x-ray free-electron laser (FEL) light sources will enable scientists to perform significantly new experiments in plasma physics, atomic physics, nanoscale dynamics, femtochemistry, and structural biology. Such experiments will require focusing optics that survive the extreme power loading produced by these beams.

This project is developing survivable refractive optics for focusing the beams expected from fourth-generation light sources such as the Linac Coherent Light Source (LCLS), an x-ray FEL to be built at the Stanford Linear Accelerator Center, and a similar one to be constructed at the DESY laboratory in Hamburg, Germany. Researchers from LLNL will be able to create states of warm dense matter (WDM) at the focus of these optics to obtain information of relevance to the stockpile-stewardship mission. The ultrashort focused beam will also shock samples at high pressure, extending LLNL's diamond-anvil work into new regimes of physics. Finally, even tighter focusing will allow structural biologists to decipher the structure of the many single molecules that are difficult to crystallize.

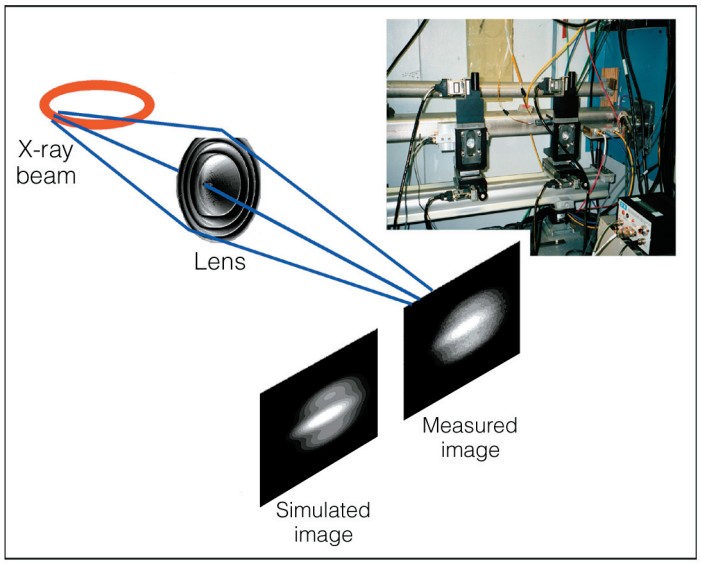

Testing low-Z refractive lenses at a synchrotron x-ray source demonstrates excellent comparison with computer simulation.

Our approach to survivable optics is to manufacture refractive lenses of materials having little x-ray absorption. A material's x-ray absorption depends mainly on its electron density, and elements at the lower end of the periodic chart (low-Z elements) tend to have the lowest x-ray absorption. Along with low absorption, these materials have low refractive power, which results in extremely concave lens designs that have been impossible to machine at a reasonable cost thus far. However, the development of target fabrication techniques for the National Ignition Facility now allows some of these designs to be realized. These techniques include diamond turning and precision milling of a variety of materials, including the hazardous low-Z materials, beryllium and lithium. We wanted to show that such low-Z refractive lenses were viable focusing elements for WDM and other experiments.

Based on a new theory for the design of these lenses and new apparatus to test them, in FY2002 we fabricated and tested several low-Z, diamond-turned lenses. These lenses were carved with a specially fabricated diamond tool into the face of a thin disk of pure aluminum. The lenses were tested in the 8-KeV x-ray beam at Stanford Synchrotron Radiation Laboratory (SSRL). Although lens performance is limited by the materials chosen and the SSRL source geometry, the measured performance closely matches the predictions, calculated from first principles, as the Figure shows.

As a result of this work, at least one fourth-generation light source plans to demonstrate refractive lenses for focusing the beam. Such demonstrations will ensure that the light source has the capability to create and study WDM.

In FY2003, we plan to extend our work to the fabrication of lenses made of beryllium and lithium.

Nonlinear saturation of parametric laser–plasma instabilities

S. H. Glenzer, D. H. Froula, L. Divol

Nuclear weapon effects and inertial confinement fusion experiments use intense laser beams that produce high-temperature, high-density plasmas. In these conditions, plasma waves are excited to large amplitudes that nonlinearly scatter the laser light. Understanding ion and electron plasma wave growth and saturation are essential to control these scattering processes for improved coupling of laser energy to targets. In this project, we directly measure the plasma wave amplitudes and frequencies allowing us to develop quantitative calculations of the laser–plasma interaction.

Our experiments are designed to test and help develop a predictive modeling capability for designing future laser-based experiments in support of the Laboratory's stockpile stewardship mission. Efficient coupling of high-intensity laser beams to hohlraums is essential to establish platforms for radiation-driven experiments and is of broad interest to defense programs, including the high-energy-density communities.

The scope of the project is to apply novel Thomson scattering techniques to investigate the plasma waves driven by the stimulated Raman scattering (SRS) and stimulated Brillouin scattering (SBS) instability. In these processes, ion acoustic waves (in the case of SBS) or electron plasma waves (in the case of SRS) are excited to large amplitudes by an incident light wave reflecting a large fraction of the incident laser energy. In the high-temperature, large-scale-length plasmas produced by the next generation of large lasers, the amplitudes of these waves are predicted to saturate due to nonlinear processes such as decay or frequency shifts.

Our objective is to discover and characterize the nonlinear processes that dominate the laser–plasma interaction using the newly commissioned 527-nm laser beam at the Omega laser facility at the University of Rochester. Full-aperture backscattering and Thomson-scattering diagnostics have been built and have provided high-quality data on the first experiments. These capabilities will be applied in large-scale-length gas-bag experiments to measure the spatial and temporal evolution of plasma waves and their correlation with time-resolved SRS and SBS reflectivity. The Thomson scattering diagnostics will be used to provide (1) independent measurements of plasma electron and ion temperature, plasma flow velocity, or electron distribution function and (2) measurements of the primary plasma wave and the secondary, nonlinear decay wave products.

In FY2002, we tested new saturation models. The detuning of three-wave coupling between the ion acoustic wave, the incident light wave, and the reflected light wave by a velocity gradient was experimentally and numerically investigated. The Figure shows the first experimental observation of the predicted frequency detuning process. This result has been quantitatively modeled with pF3D, demonstrating its importance as a saturation mechanism of SBS.

In FY2003, we will establish the limits of the various saturation models with Thomson scattering experiments at the Omega laser. We will attempt to discover a novel decay mechanism of the ion acoustic wave that is predicted to dominate the laser–plasma interaction in high-Z plasmas.

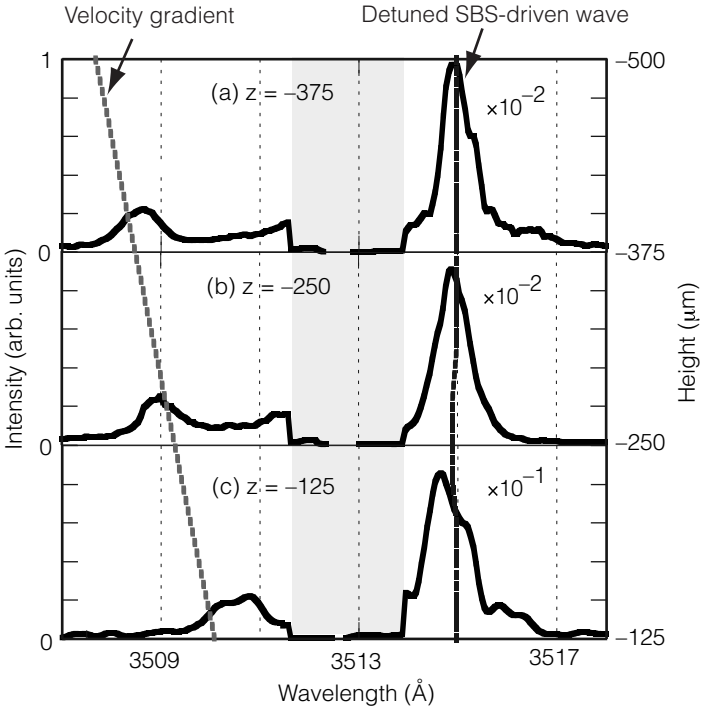

The frequencies of the stimulated-Brillouin-scattering- (SBS-) driven acoustic waves remain unchanged, not following the frequency shift of the thermal peak. This spatial detuning saturates the SBS instability at the 6% level. The solid curves are the pF3D calculations.

Structure and spectroscopy of black hole accretion disks

D. A. Liedahl, C. W. Mauche, B. F. Mathiesen

Black holes are indeed black. Drop mass onto one, however, and the surrounding warped space–time becomes the arena for a prodigious release of radiant energy. When a sufficient source of matter exists in the vicinity of a black hole—a nearby star, for example—the matter can be captured by the gravitational field of the hole, creating a disk-shaped area of matter called an accretion disk, which often mediates the infall of matter that spirals down the potential well of a black hole (see Figure). Because they convert gravitational potential energy into radiation very efficiently, quasars and other types of accreting black hole systems, taken together, actually outshine all of the stars in the Universe. Much of the radiation emerges in the x-ray band, especially that produced at small disk radii where relativistic effects prevail. Since we cannot yet image black hole environments, owing to their small angular sizes, we have come to rely on the spectral information contained in the x-ray light, which puts x-ray spectroscopy at the leading edge of black hole research.

The aim of our project, a collaboration with the Massachusetts Institute of Technology and the Harvard–Smithsonian Center for Astrophysics, is to develop a computer model that reproduces the complex physics associated with x-ray spectral formation near an accreting black hole. The project studies both the physics of disk accretion and the physics of matter affected by extreme space–time curvature,just before it plunges across the event horizon—the "one-way-ticket" boundary beyond which light and matter are forever trapped, according to Einstein's General Theory of Relativity,

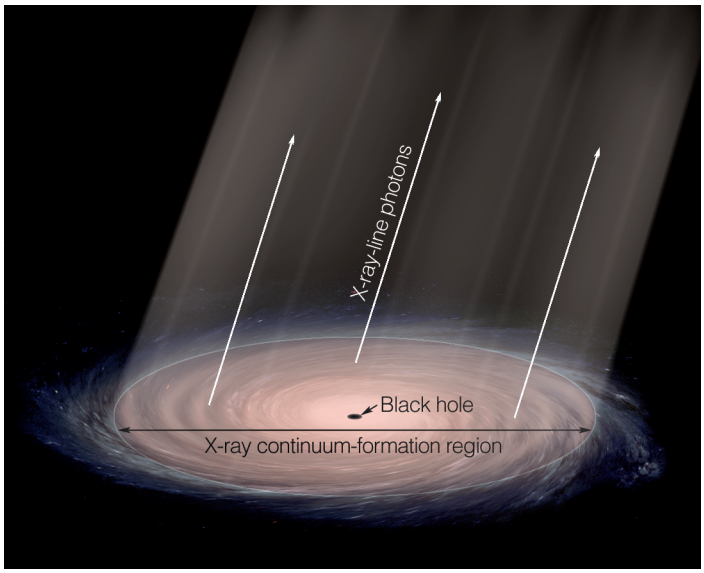

Artist's conception of an accretion disk surrounding a black hole. Matter spiraling down the potential gravitational well heats up, producing an x-ray continuum, which irradiates the disk. Atoms in the disk respond by producing x-ray-line photons through fluorescence and electron–ion recombination. These x-ray-line photons convey information about the temperature, density, and velocity structure of the disk material as it approaches the event horizon, just before it drops out of our Universe.

Our emphasis on x-ray spectroscopy couples to LLNL research in spectroscopic modeling of high-temperature plasmas. Validation of LLNL plasma kinetics codes involves their application to the widest possible range of observable phenomena. The high-energy-density environments associated with accreting black holes have important similarities to those encountered in applications to stockpile stewardship.

The computer code we are developing, called Computer Models of the Physics of Accretion Disk Structure and Spectra (COMPASS), will consist of two main components: a vertical disk structure code and a Monte Carlo (MC) photon propagation code. Each component now exists as a working prototype. When complete, a standard COMPASS run will produce a two-dimensional (2-D) physical model of the x-ray irradiated disk, which, assuming azimuthal symmetry, will be extended to a system of spatial cells in 3-D. This system will then be imported into the MC routine, which follows photon trajectories from their source to the boundary of the computational space, including a number of radiative transfer processes, special relativistic effects, and general relativistic effects.

During FY2002, we made progress in theoretical handling of the thermal instabilities that occur in the transition zone between the deep disk and the upper disk atmosphere; implemented a fully relativistic Compton-scattering algorithm, which allows for proper calculation of inelastic photon–electron interactions in high-temperature plasmas; achieved the requisite theoretical competence to manage photon trajectories in both the Schwarzschild and Kerr space–time metrics; and developed a working x-ray reflection/transmission model, including continuum opacity from 168 ionic species of 13 elements.

Work for FY2003 will center on integrating the various components now being developed in parallel. We plan to enhance the MC simulator by including a detailed line-opacity model, and build in a line-transfer capability. A geodesic ray-tracing capability in the Schwarzschild metric will be in place by the end of the year.

Reaching isochoric states of matter by ultrashort-pulse proton heating

P. K. Patel

The goal of our project is to develop a new technique to obtain—for the first time—experimental equation-of-state (EOS) data of high-pressure, off-Hugoniot material states. Our new method will use an intense, ultrashort pulse of protons to volumetrically and almost instantaneously heat a sample of material to high pressure (1 to 10 Mbar) and temperature (1 to 10 eV), while the sample remains at solid density. Such plasmas—with temperatures of a few electron volts at solid density—lie in the warm, dense matter (WDM) regime. This complex regime has long eluded a satisfactory theoretical description, creating the need for constraining experimental data.

Although methods exist for obtaining EOS data in certain regions of phase space, no method currently exists for accessing high-pressure, off-Hugoniot states on the isochore of a material. Our new technique will use an ultrashort-pulse laser to generate a highly energetic, directional beam of protons, which will isochorically heat a sample to the desired state. Our initial measurements of the proton energy flux produced on the 100-TW Janus ultrashort-pulse (JanUSP) laser indicate that this flux can heat a large volume (50 to 100 μm) of high-Z material to several electron volts. Moreover, the intensity of this beam at the target is at least three orders of magnitude greater than that of the current generation of heavy-ion accelerators. In addition to using a proton beam to create the plasma, our project will use a second proton beam to obtain two-dimensional spatial and time-resolved radiographs. This measurement will provide the first EOS data of any material on the isochore.

Our project will benefit stockpile stewardship—in support of LLNL's national-security mission—by investigating WDM and collecting EOS data in a highly complex and previously inaccessible regime. This knowledge will also benefit many core elements of LLNL's scientific program, including inertial confinement fusion target design, high-power laser experiments, planetary core physics, and high-pressure theory and molecular dynamics modeling.

FY2002 accomplishments included (1) optimizing the flux of the laser-produced proton beam, (2) resolving outstanding issues related to the proton-acceleration mechanism, (3) testing the viability of probing solid-density materials with protons, (4) developing a Monte Carlo proton-transport code to model the propagation of protons through various test objects, (5) performing the first target-heating experiment, and (6) attempting to produce a focused proton beam to attain higher proton flux densities. The initial probing experiments indicated an extremely high degree of collimation in the proton beam, enabling radiographs to be obtained at a very high spatial resolution (~1 μm). The Figure is an optical interferogram of hydrodynamic expansion in laser-heated aluminum foil.

Work proposed for FY2003 includes (1) developing a multibeam experimental capability on the JanUSP laser to perform proton heating and proton radiography of material simultaneously, (2) designing and implementing diagnostic hardware to measure the spatial and temporal characteristics of laser-heated foils, and (3) conducting the first plasma-characterization experiments of proton-heated foils. If successful, this work will enable integrated EOS experiments in FY2004 that use high-energy proton beams to isochorically heat and probe materials in WDM states.

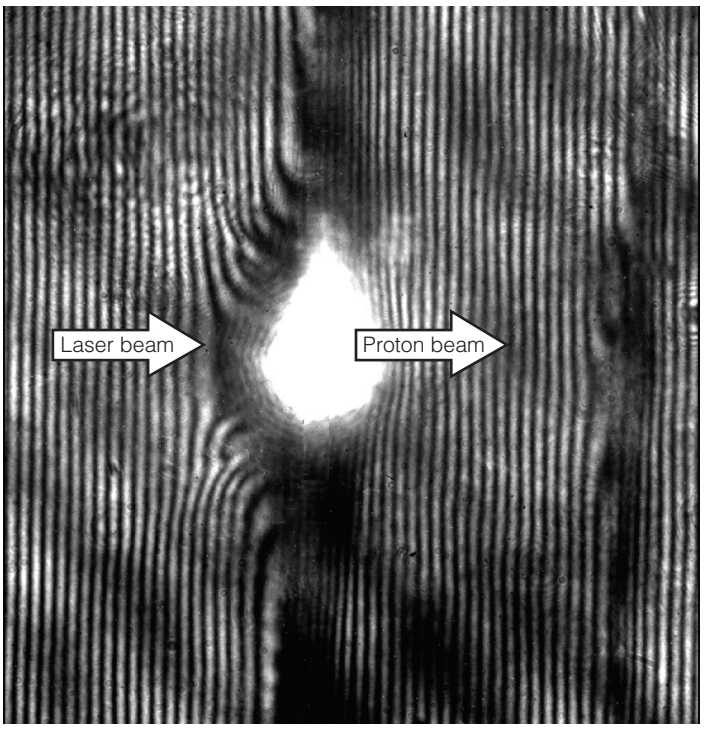

This project is obtaining experimental equation-of-state data for high-pressure, off-Hugoniot material states. An intense, ultrashort pulse of protons heats a sample of material to high pressure (1 to 10 Mbar) and temperature (1 to 10 eV), generating a plasma in the warm, dense matter (WDM) regime. This optical interferogram (600 μm × 600 μm) shows the hydrodynamic expansion of aluminum foil 180 ps after the main laser pulse. Protons from the laser-interaction plasma (bright spot) create a plasma in the WDM regime, indicated by the wide black bands near the right edge.

Proton radiography of laser–plasma interactions with picosecond time resolution

A. J. Mackinnon, P. K. Patel, D. Hicks, M. Borghesi

Dynamic proton radiography, with its microsecond timescales, was developed as a tool for time-resolved imaging of large, dense materials for stockpile stewardship. The recent discovery that high-intensity laser–matter interactions generate collimated proton beams with peak energies up to 10 MeV makes it possible to perform proton radiography on picosecond timescales. Our project has developed proton radiography techniques that can be used to diagnose plasma conditions generated by high-power laser–matter interactions.

Proton radiography allows transient electric and magnetic fields to be diagnosed directly through particle-deflection measurements, but because the magnitude and characteristics of these fields are not well understood, detailed experiments are needed to understand how beam and source characteristics affect imaging properties. This project is conducting such experiments using the Janus ultrashort-pulse (JanUSP) laser at LLNL and the more complex Vulcan multibeam facility in the U. K. These experiments will validate our proton propagation codes, which model proton interactions over a range of plasma conditions. Experimentally validated codes will help determine the feasibility of conducting experiments on large, high-density plasmas, such as those present in ignition-scale inertial-confinement-fusion (ICF) experiments where petawatt-class lasers generate the proton beams.

Our research underpins the understanding of electromagnetic fields in plasmas and supports LLNL's mission to produce ignition using high-powered lasers. In addition, our project will support LLNL's stockpile-stewardship mission by developing techniques for diagnosing the hot, dense plasmas that exist inside imploding shells.

FY2002 accomplishments included (1) demonstrating micrometer-scale resolution in targets ranging from 1 to 30 μm and demonstrating that these images are formed through the small-angle scattering of protons by electromagnetic fields of plasmas; (2) performing the first measurements of the location of the virtual source during an experiment using JanUSP; (3) showing that electron recirculation is an important factor in proton acceleration and publishing this work in Physical Review Letters; and (4) demonstrating "proton moiré," a new proton-deflection diagnostic that may make field measurements from proton beam deflections more quantitative (see Figure). Work is continuing on the development of these techniques for diagnosing fields in laser-produced plasmas.

In FY2003, we plan to conduct several experiments to test the resolution limits in high-density-laser-driven implosions and shock-heated materials. These experiments will develop the recently demonstrated proton moiré technique as a diagnostic of proton beam deflection in a variety of plasma conditions: diagnosing laser-driven electric and magnetic fields, measuring shock propagation, and diagnosing density perturbations. This work will enable us to develop a predictive capability in proton probing to diagnose fields and density inhomogeneities for ICF conditions. FY2003 experiments in conjunction with our FY2002 developments in models and simulation codes will help to determine the feasibility of using protons to measure magnetic fields in laser-driven hohlraums and other plasmas relevant to high-power lasers.

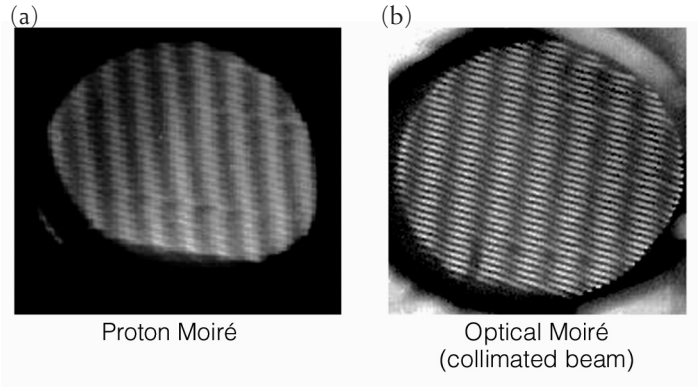

Moiré fringes are generated by passing a beam of light or particles through two identical one-dimensional gratings that are separated by a small distance and whose rulings have been rotated by a small angle with respect to each other. (a) Proton moiré: Moiré fringes, inclined at an angle of 10° counterclockwise from vertical, observed with 7-MeV protons from an ion beam produced from LLNL's Janus ultrashort pulse laser. (b) Optical moiré: Moiré fringes from collimated optical light, which are inclined 10° clockwise from vertical. This 20° difference in fringe orientation between the proton beam and collimated light shows that the protons are not collimated but instead come from a point source, so that the beam is diverging when it goes through the moiré gratings. The rotation arises because in diverging light (or protons) the shadow of the first grating is slightly magnified when it reaches the second grating. This shifts the position of the fringes, resulting in their rotation. The degree of rotation can be used to locate the proton source.

Dense-plasma characterization by x-ray Thomson scattering

O. L. Landen, S. H. Glenzer, G. Gregori, S. M. Pollaine

The full range of plasmas—from Fermi degenerate, to strongly coupled, to high-temperature ideal gas plasmas—are present at high density in a variety of laboratory and astrophysical environments. In this regime, material properties such as electrical and thermal conductivities, opacity, and equation-of-state (EOS) have been measured to resolve theoretical and calculational uncertainties. However, the usefulness of such measurements has been impaired due the lack of an independent measurement of the key plasma parameters—temperature and density. Such high-density plasmas are the principal state of matter in inertial confinement fusion (ICF) and high-energy-density physics (HEDP) research, an important component of LLNL's Stockpile Stewardship Program.

This project proposes to develop a novel characterization technique for low-atomic-number (low-Z) plasmas using spectrally resolved x-ray Thomson scattering. The technique could ultimately be used to measure the compressed ICF fuel density and temperature and provide a noninvasive internal temperature measurement in radiatively and shock-heated materials for HEDP. In addition, this project extends the development of transient hot laser plasmas as x-ray probes, which has been a key part of LLNL's experimental expertise.

In this project, we are extending the plasma-characterization technique of spectrally resolved optical photon scattering off free electrons (Thomson scattering) to the x-ray regime for providing dense plasma data unattainable by other means. Our technique uses resonance line emission from laser plasmas as a narrow-bandwidth transient x-ray probe, which scatters from sample solid-density plasmas created by volumetric heating using x rays from other laser plasmas. The shape of the collected scattered spectra provides instantaneous information on the free-electron density, temperature and charge state of the sample plasma.

During FY2002, using the Omega laser facility at the University of Rochester, we obtained improved, publishable x-ray scattering data from solid density beryllium (Be) heated to a range of temperatures up to 50 eV. The Figure shows an example of the increase in broadening in the long-wavelength component of the scattered spectra as the Be is heated. In parallel, we developed an integrated model combining x-ray scattering and dense-plasma theory for fitting the data. The model includes both elastic and inelastic scattering for arbitrary scattering wavelength, angle, and plasma degeneracy, and is valid for up to moderately coupled plasmas. The fitted data provide both temperature and ionization state information, which is beginning to distinguish between ionization balance models developed here and elsewhere. These models predict the number of free electrons per atom for a given plasma temperature, which can vary between models at high density due to differences in the calculated electrostatic field profiles between close-packed ions and electrons. In addition, the temperature information is being used to benchmark predictions by radiation-hydrodynamic simulations.

In FY2003, we will execute more experiments on the Omega laser and at other smaller facilities, further measuring the plasma EOS of low-Z solids and foams (e.g., beryllium, lithium hydride, and carbon). In addition, we will execute experiments at the Omega facility to demonstrate the extension of x-ray Thomson scattering to higher plasma temperatures (up to 200 eV) of interest to several LLNL radiation-transport and opacity projects that support stockpile stewardship.

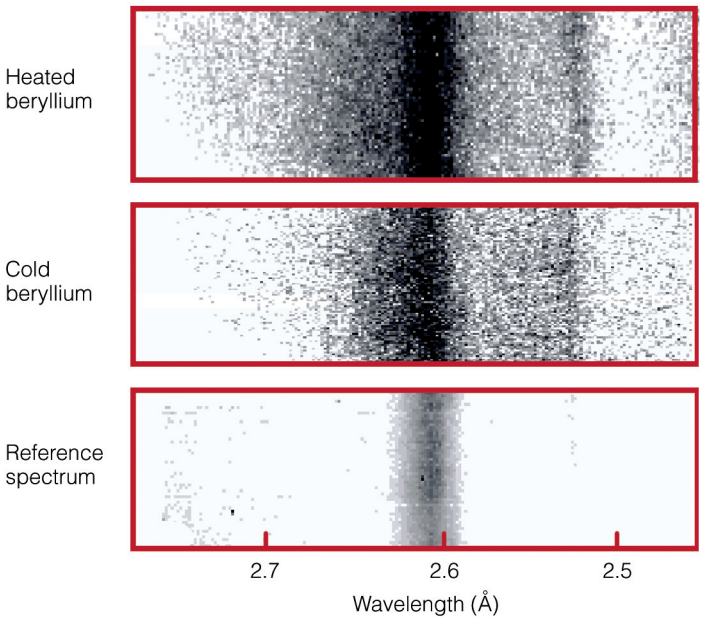

X-ray-scattered spectra from heated beryllium and cold beryllium are Compton shifted and Doppler broadened compared to the original unscattered spectrum.

Gaseous laser targets and optical diagnostics for studying compressible turbulent hydrodynamics

J. Edwards, F. J. Hansen, S. H. Glenzer, H. F. Robey, T. Dittmire

Developing models to describe compressible turbulent mixing, a complex subject with many unresolved questions, is an important research area for stockpile stewardship. Because modern computers remain orders of magnitude away from being able to compute turbulent flows from first principles, experiments must guide advances in theory and models.

Shock-tube facilities, which use optical diagnostics to generate high-resolution images, provide exquisite detail about turbulent flows. A shock-tube contains two gases, initially dissimilar in pressure, separated by a thin membrane. When the membrane is broken, a shock wave propagates into the lower-density region. However, shock-tubes drive gases only relatively weakly—the resultant shock wave has a Mach number of ~1 and is not highly compressible. High-compressibility experiments can be performed using high-power drivers such as lasers, but the established route of solid targets and the relatively low resolution of projection x-ray backlighting (higher-resolution optical or laser diagnostics are precluded by the use of solid targets) reveals only very limited information about the complex turbulent flow patterns.

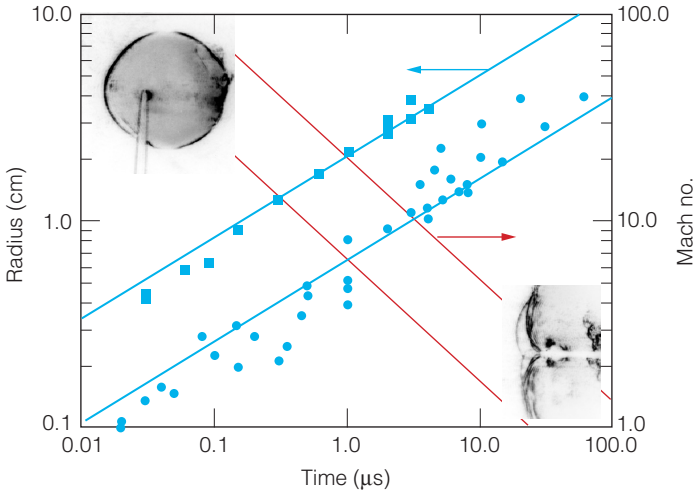

Shock wave radius vs time (blue) and Mach number vs time (red) from our experiments. The data show the large radius (3 cm) and high Mach number (~10) of the blast wave generated, demonstrating that our technique permits high-compressibility investigation of turbulence. Inserts are Schlieren images of a blast wave (top left) produced when a 1-mm-diam pin is illuminated with the Janus laser and the complex interaction between the shock wave and a rod (bottom right).

Our objective is to demonstrate a high-resolution experimental technique for studying turbulence in a highly compressible regime by combining laser-based diagnostics with a laser driver. Our experimental arrangement is very simple: using the Janus laser at LLNL, we illuminate a ~1-mm-diam pin in the center of a target chamber filled with a gas such as nitrogen at low pressure. The shock driven through the gas by the resultant blast wave then interacts with an object, such as a laminar or turbulent gas column, foam ball, or rod (see Figure). This shock–object interaction gives rise to a turbulent or other complex flow, which is imaged with a separate low-power laser using a standard Schlieren (dark-field) technique. This diagnostic is sensitive to density gradients driven by the shock wave and subsequent motions of the gas.

Gas targets not only allow high-resolution laser-based probing but also have the benefit of being ~50 times larger than solid targets, with obvious additional resolution benefits. In fact, initial estimates indicate we may be able to resolve a range of spatial scales of about 1000, which is just enough to see all the eddies existing in a flow as it transitions to a highly mixed turbulent state. The smallest scales in the flow are heavily damped out by viscosity, which converts the turbulent kinetic energy into heat.

In two experiments in FY2002 using Schlieren shadowgraphy, interferometry, and spectroscopy to characterize blast-wave evolution, we demonstrated a blast wave with a Mach number of ~10 at a radius of ~3 cm using just 100 J of the Janus laser (compared to a ~1-mm radius achieved with the traditional approach using ~10 kJ of laser energy on the Omega laser). The larger radius makes the phenomena much easier to study. We also began shock–object interaction studies using Schlieren shadowgraphy and started to build a new Schlieren system to improve resolution and field of view and allow multiple frames per shot.

In FY2003, we will concentrate on completing improvements to the Schlieren system to obtain high-quality images of turbulent flows—in particular, we will investigate using double-pulse Schlieren shadowgraphy with image correlation to try to extract crude velocity spectra, which are important properties for model development—while continuing to explore other advanced diagnostic options for obtaining more-detailed information.

Anisotropic shock propagation: Fine structure, curvature, and caustics

J. Stölken, M. Caturla, B. Remington, J. McNaney, M. Edwards

Shocks in solid materials, such as metals, have complicated wave profiles that depend on the orientation of shock propagation. This direction dependence complicates our understanding of shock-wave processes because it introduces intricate shock-front interactions and curved wave fronts that can produce singular material behavior. Our project studies the propagation of shock waves in anisotropic materials. The research objective is to establish a physics-based foundation for predictive models of shock-interaction processes.

Nearly all practical engineering alloys consist of polycrystalline ensembles of anisotropic metal crystals. Understanding shock-wave propagation in single crystals provides a foundation for understanding shock-wave interactions with microstructural features such as the grain boundaries between individual crystallites. The interactions are known to play a key role in causing failure and fracture in engineering alloys. Understanding such failure mechanisms is useful for exploring the strength and other constitutive properties of metals under extreme conditions. This area of research is important to understanding the processes governing the safety and reliability of nuclear weapons and is thus highly relevant to the Laboratory's stockpile stewardship mission.

The influence of material anisotropy on shock propagation in metals is studied through a combination of molecular dynamics and continuum models coupled to laser-driven experiments. The effects of plastic anisotropy at the grain scale on the fine structure of the shock front are investigated to better understand shock-wave interactions within materials. We are studying the influence of wave-front curvature on basic shock-physics issues. The potential for forming caustics provides the opportunity to study the extreme nonlinear behavior of materials over a broad range of conditions, from weak elastic waves to very strong shocks, all within a single experiment.

We use large-scale, three-dimensional molecular dynamics (MD) simulations to inform continuum-level theory and models by developing appropriate scaling relations that connect the MD and continuum-level simulations to the experiments. The MD simulations explore the limits of the continuum models to provide insight into their limitations and possible improvement in modeling anisotropic shock propagation, wave-front curvature, and caustic formation. The resulting models are developed with and tested against critical laser-driven experiments.

During FY2002, we completed an extensive scaling study of spherical shocks in convergent geometries (see Figure), developed and executed an initial experiment at the OMEGA laser facility at the University of Rochester, and gave three invited presentations of our MD results. The initial laser experiment explored techniques used to shock and recover spherical targets for comparison with the MD scaling study. An unexpected result of the scaling study was the identification of a void growth mechanism in spherical geometries. The mechanism consists of shock splitting induced by phase transformation.

Although this project was short lived (7 mo), we have made better-than-expected progress in understanding the self-interaction of curved shocks in metals. Both the large-scale MD simulations of spherical shocks and the proof-of-principle recovery experiment were quite successful. The MD work, in particular, gave valuable insight into the role of phase transformations in initiating void formation within spherically convergent shock geometries.

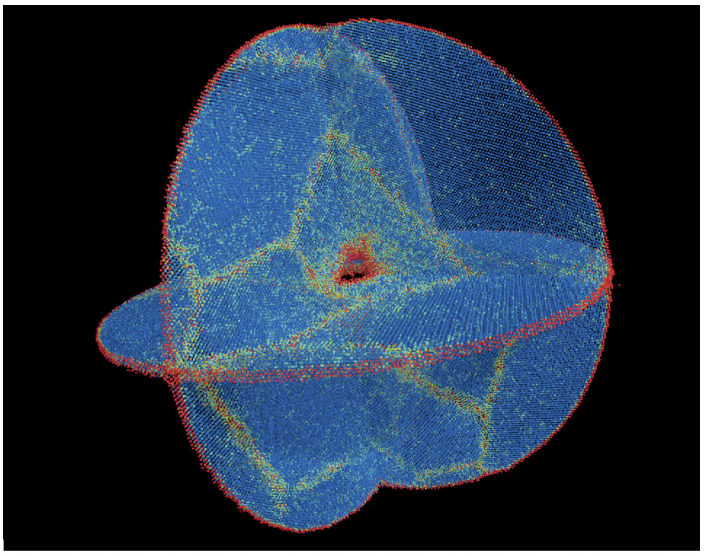

Molecular dynamics simulation of the three-dimensional cross section of a convergent shock in a nanocrystalline copper sphere.

Remote-sensing signatures for kill assessment

C. Stevens, G. T. Nakafuji

Theater and national missile-defense systems are designed to intercept an incoming ballistic target with enough mass to disassemble it and negate the payload. The intercept event will produce an expanding debris cloud containing solid-, liquid-, and gas-phase components. Successful intercept of an incoming target by a Ballistic Missile Defense interceptor, means answering several important questions: What type of warhead or RV was hit? Was the warhead or RV destroyed? and Do we shoot again?

To answer the second and third questions, the first question must be addressed by assessing the post-impact state of the incoming target using remote sensors. However, prior to investigating different remote-sensing options, unique signatures for each type of warhead must be developed to identify the intercepted target accurately. Without signature development, determining what type of warhead was intercepted is problematic and ambiguous. An extensive database of quantitative intercept and post-intercept signatures is needed for high-explosive (HE), chemical, biological, and nuclear warheads.

The scope of our project is to identify candidate signatures resulting from a successful ballistic missile intercept of a nuclear target. Examination of the post-impact state using hydrodynamic modeling and chemical analysis tools focuses on unique material behavior peculiar to the type of payload. Our objective is to quantify a range of conditions that have a strong probability of producing a signature detectable by a remote sensor. Once the candidate signature is identified, experiments will be designed to reduce the analytical uncertainties and confirm the presence of the signature source. These experiments will be carried out in LLNL's High Explosive Applications Facility.

The signature development for nuclear targets uses a two-phase approach: (1) identifying specific signatures unique to nuclear payloads through modeling and analysis of the post-impact debris, and (2) using energetic-materials experiments to systematically reduce the modeling uncertainties uncovered during phase one.

During FY2002, we discovered the presence of specific infrared signatures that may emanate from post-impact debris specific to nuclear targets. Detailed computer modeling and analysis allowed us to bound the conditions of ejected material during the post-impact phase. The analysis tracked the formation of hot, molten ejecta leading to formation of hot vapor emission.

Figure (a), which shows the output of one such calculation, reveals the temperature distribution of the surface of a molten-metal slug created at impact. Hot atomic vapor issuing from the surface of this ejecta encounters a cloud of high-explosive detonation products. These products—especially hot water vapor—react chemically with the vaporizing atoms. Within about 50 ms, the cloud density decreases and the vaporizing atoms survive long enough to emit and absorb radiation. Figure (b) shows some estimates, based on the velocity of the molten slug, for the probability of a vaporizing atom surviving long enough to emit a photon. Modeling spectral signatures of this vapor reveals signal levels bright enough to be detectable at realistic standoff distances.

The results of the FY2002 work are very promising, both in terms of detectable signal strength and the uniqueness of the signal source. In FY2003 we will design and conduct energetic-materials experiments at HEAF to reproduce certain source conditions that are expected to occur in a real intercept. These tests, using radiography and spectrometry, will benchmark modeling predictions of material ejecta velocities and temperatures.

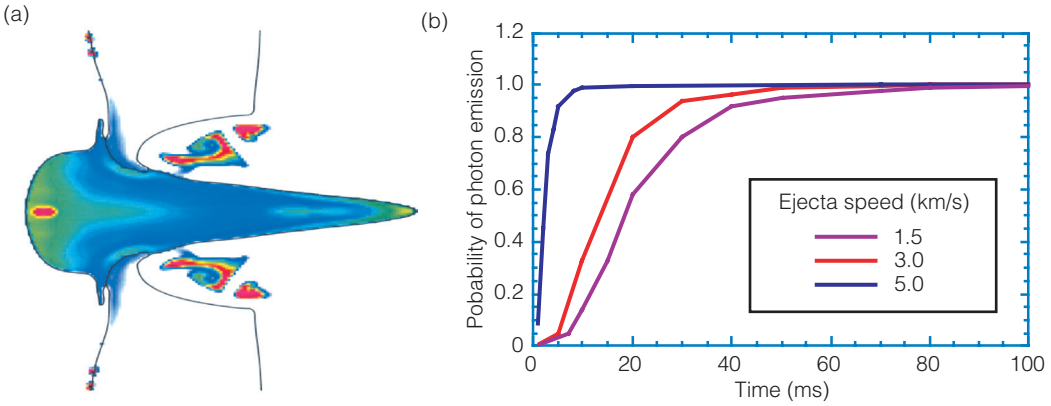

(a) Modeled formation of a molten stream of metal resulting from a high-explosive (HE) detonation. Surface temperatures range from 600 K (blue) to 1500 K (red). The velocity of the stream, its dispersion and surface temperatures are all important parameters that influence the formation of atomic vapor and its survival in the surrounding cloud of HE products. (b) Estimates for the probability that a vaporizing atom in a near-infrared excited state will emit a photon before being consumed in a chemical reaction with hot water vapor. Faster ejecta speed allows the atoms to escape the surrounding cloud sooner.

Development of a predictive computational tool for short-pulse, high-intensity laser–target interactions

M. Tabak, B. Lasinski, R. J. P. Town, W. L. Kruer

Many applications have been proposed for high-energy, short-pulse lasers, such as the fast-ignitor fusion concept for fusion energy research, production of very high-temperature hohlraums for probing material properties at high-energy density, very high-energy photon backlighters for inertial confinement fusion, and proton beams for heating and radiography. However, because no predictive, integrated computational capability exists to model the relevant physics associated with such applications, calculations have been unable to explain the results of short-pulse laser experiments.

To remedy this situation, we are investigating the physics of high-intensity, short-pulse lasers interacting with plasmas and focusing on the key issue of supercurrent electron transport in dense plasmas. The goal of this project is to provide a multiscale description of high-energy-density phenomena induced by ultrahigh-intensity lasers by validating a hybrid particle-in-cell (PIC) electron-transport code—a "hybrid" in that the PIC code is combined with a material description that includes an electrical conductivity model and equation of state—against the results of recent short-pulse laser experiments. This PIC code will then be coupled with hydrodynamic and thermonuclear burn codes. This work will support the Stockpile Stewardship Program with physical data and improved simulation capabilities, and also support LLNL's energy-security mission by furthering fusion energy research.

In FY2002, we (1) hired a mid-career scientist; (2) ported the hybrid PIC code—named Large-Scale Plasma (LSP)—to LLNL computing facilities and performed debugging; (3) modeled existing short-pulse experiments (see Figure); (4) investigated the effects of laser beam polarization and runaway electrons on transport; (5) and supported, with Lasnex calculations, the design of high-temperature hohlraums and other weapons-physics applications. Our results were reported in a paper at the Anomalous Absorption Conference and in three abstracts at the conference of the American Physical Society, Division of Plasma Physics.

In FY2003, we will continue to benchmark LSP and improve the electrical conductivities used in LSP. We will also continue to use LSP in two-dimensional (2-D) and 3-D calculations to understand the results of recent experiments, such as fast proton emission from solid-target illuminations with LLNL's Petawatt and Janus-pumped, ultrashort-pulse lasers, K-alpha electron transmission measurements with the Petawatt and a 100-terawatt laser, and plasma-heating experiments with the Petawatt laser.

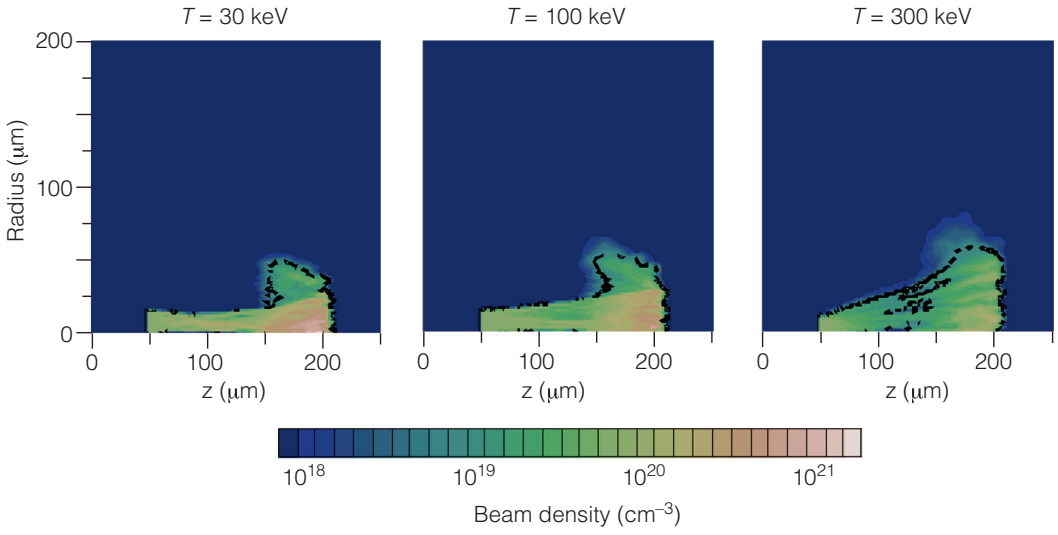

False-color representation of hot-electron density calculated using a particle-in-cell (PIC) electron-transport code to simulate irradiation of a polystyrene slab (density 1 g/cm^3; initial temperature 5 eV) with a high-intensity laser. Electrons were injected with a drift velocity corresponding to an energy of 1 MeV and a temperature (T) of 30, 100, and 300 keV. Calculations for 300 keV matched the results of recent experiments conducted under similar conditions, indicating that our PIC code can model the physics associated with applications of high-energy, short-pulse lasers.

A revolution in biological imaging

H. N. Chapman, S. Hau-Riege, R. Balhorn, R. London, B. Segelke, A. Szoke, J. Trebes, A. Wootton

X-ray free-electron lasers (XFELs) are a new fourth-generation x-ray source theoretically capable of extremely short-duration, high-fluence pulses at a brightness 10 orders of magnitude higher than current third-generation synchrotrons. XFELs promise to revolutionize the life sciences by allowing atomic-resolution imaging, by x-ray diffraction, of the three-dimensional (3-D) structure of virtually any macromolecule, including viruses and proteins. Because the function of a molecule is determined by its structure, this capability will profoundly benefit structural biology and medicine, and could eventually lead to solving the entire proteome. Such light sources will also be able to image cellular components and whole cells.

This project focuses on imaging individual biomolecules. It supports LLNL missions in national security, by furthering the study of potential bioterrorism agents; stockpile stewardship, by enabling the study of changes in the atomic structure of relevant materials; and bioscience and technology to improve human health.

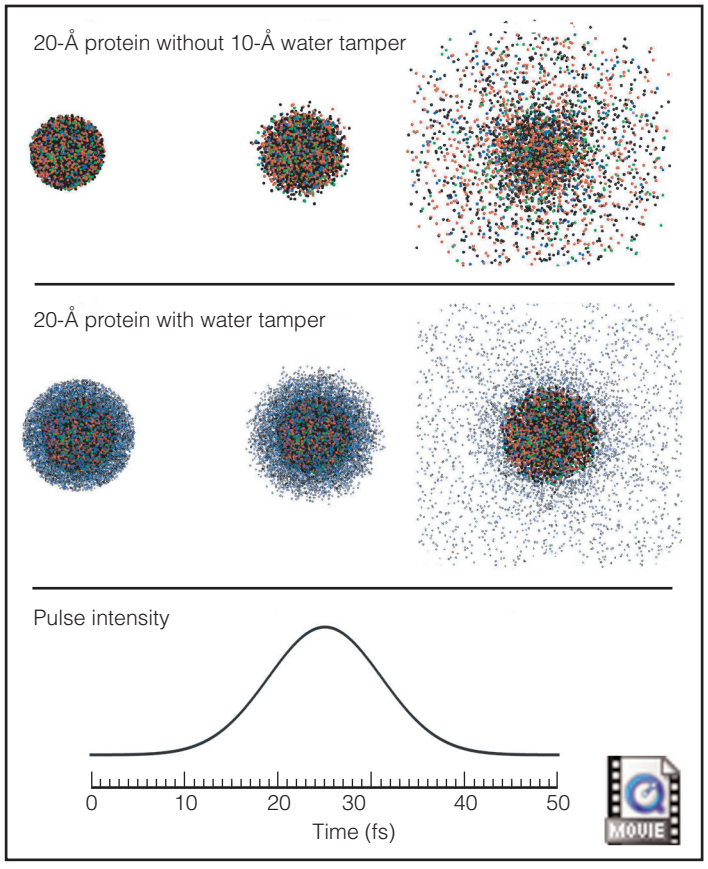

Simulation of a 20-Å protein molecule Coulomb-exploding due to interaction with an x-ray free-electron laser (XFEL) pulse (having a Gaussian time profile and a 20-fs width at an intensity of 1/e) (top) without and (middle) with a 10-Å water tamper to suppress Coulomb explosion long enough to obtain an accurate diffraction pattern.

A goal of the project is to examine the feasibility of XFELs and determine source requirements for imaging molecules and particles of various sizes at various resolutions. With x-ray pulses of sufficient intensity and sufficiently short duration, an XFEL source will enable recording of a diffraction pattern from a single molecule. Although a molecule Coulomb-explodes as it interacts with the pulse, a pulse shorter than the timescale of the explosion will diffract before the explosion, generating a diffraction pattern of the undamaged molecule. In contrast, x-ray crystallography requires crystallizing the molecules, which can change the conformation of the molecules. Many types of biomolecules cannot be crystallized at all. Furthermore, the long exposure times of third-generation light sources also lead to radiation damage during measurement.

To examine the feasibility of XFELs for molecular imaging, the project uses computational modeling of Coulomb explosion, x-ray diffraction, diffraction signal detection, and image construction from diffraction signals. To determine the temporal change of the molecule, we will use a hydrodynamic model that goes beyond previously published studies by incorporating the destructive Coulomb force and the effects of trapped electrons and the time dependence of Auger decay. Images will be constructed from multiple-view, single-shot data. Computational results will be compared to synchrotron data.

Since mid-year FY2002 funding, we (1) began developing the hydrodynamic model of molecular Coulomb explosion, (2) simulated diffraction patterns for a range of macromolecules and beam parameters, (3) developed an image-reconstruction algorithm, and (4) performed an initial synchrotron-imaging experiment. A layer of water was used around the macromolecule as a tamper to suppress Coulomb explosion (see Figure) long enough to allow longer, higher-intensity XFEL pulses, which extend the range of the technique.

In FY2003, we will further improve hydrodynamic modeling and compare the results to those of molecular dynamics simulations. In addition, our image-construction algorithms will be tested on experimental x-ray diffraction data to guide us in performing detailed simulations to determine XFEL pulse requirements and the ultimate limitations on image resolution.

Single-particle nanotracking for Genomes-to-Life applications

K. Widmann

Understanding how molecular machines and other cell components function together in a living system will offer important new insights into the mechanism that governs the response of microbial and human cells to environmental changes. The importance of gaining this understanding has been acknowledged on a federal level and, with the support of the DOE Office of Science, a new initiative has been created: Genomes to Life (GtL). This research addresses a scientific goal of the GtL initiative—to identify and characterize the molecular machines of life.

In this project, we plan to conduct a proof-of-principle experiment to demonstrate our techniques for imaging single particles—proteins and viruses, for example—in real time to track single polymerase molecules as they move along a single DNA strand. Our techniques can be applied for studying the rolling-circle DNA amplification (RCA) process: as the polymerase progresses continuously around the single-stranded DNA loop, it continuously assembles the complementary strand, thereby generating new copies of the targeted genetic material that has been implemented in the DNA loop. In comparison to the commonly used polymerase chain reaction technique for amplifying DNA material, the RCA process works under isothermal conditions that are needed for in situ measurements, which are critical for pathogen and bioagent detection.

In the imaging technique we are developing, plasmon resonant particles (PRPs), metallic nanospheres approximately 50 to 100 nm in diameter, are used as optical tags for the polymerase. At this diameter range, the plasmon resonance frequency is in the visible regime, which yields an increased cross section for scattering optical photons, thus allowing us to track the polymerase around the DNA strand with a darkfield microscope and measure its velocity. The velocity is the main experimental parameter for our investigation of the dependence of the RCA process on the environmental conditions such as the temperature and pH level. Tracking single polymerase molecules also provides information on the duration of attachment of the polymerase to the DNA and on the probability of failure modes such as the sudden stop of the enzyme motion. Gathering detailed information about the RCA process is essential for optimizing this DNA amplification process, which is applicable to pathogen and bioagent detection instrumentation for homeland security and counterterrorism missions.

Since the project began in April of FY2002, we have (1) demonstrated that the relative position of the centroid of the diffraction limited image of a PRP can be determined with an accuracy of +/- 10 nm (see Figure), (2) shown that the scattering cross section of silver-enhanced gold PRPs is significantly higher than of pure gold PRPs, (3) established a protocol for preparing the glass slides so that their surface bonds the DNA loops yet avoids immobilizing the PRPs, and (4) measured the impact of the optical tagging of the polymerase on its functionality. The single-stranded DNA loop we are using for the RCA experiment has a diameter of about 1 µm, which provides the high-precision of PRP tracking that is need to determine the velocity of the polymerase enzyme experimentally.

For FY 2003, we will investigate the dependence of the RCA process on several environmental parameters such as the temperature, pH level, and DNA polymerase concentration by labeling the polymerase with a PRP; apply real-time imaging to track individual polymerase enzymes on their way around a single-strand DNA loop and measure their velocity; obtain detailed information about the RCA process in order to optimize the DNA amplification technique for pathogen-detection instrumentation; and investigate the feasibility of using phosphorescent dyes as optical tags to discriminate between the autofluorescence background and phosphorescent emission by implementing a pulsed light source and gated detection system.

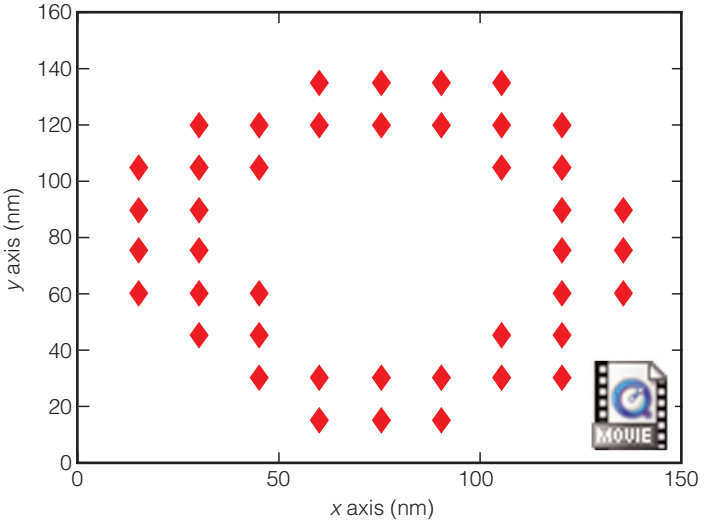

Centroid location of the diffraction-limited image of a plasmon resonant particle that has been moved in a 100-nm-diam circle by means of a piezoelectrical stage.

Simulations and experiments for assessing rapid, multipurpose cargo-scanning technologies

A. D. Dougan, D. Slaughter, J. Luke, M. Accatino

Approximately 6 million cargo containers enter U.S. ports every year. The potential for a terrorist to hide a weapon of mass destruction (WMD) in one of these containers poses a substantial threat to national security. Reliable screening techniques are needed to detect WMD in containers loaded with other cargo. The screening technique must be rapid, free of false alarms so as not to impede commerce, and proven reliable to detect significant quantities of WMD.

The goal of this project is to use a fully integrated experimental and calculational approach to determine the ultimate performance potential of active-neutron interrogation as a technique for detecting WMD, including chemical weapons materials, high explosives (HE), and special nuclear materials (SNM), in cargo containers. (The calculational work is being performed in a separate LDRD project, 02-ERD-057.) This work supports the Laboratory's nonproliferation and counterterrorism missions.

Chemical weapons materials and HE can be reliably detected using active-neutron interrogation when container geometry is simple and no other object intervenes between the material and the detector. However, a loaded container can result in false positives (i.e., nuisance alarms) from conflicting signatures, and identifying some materials may require long counting times because of increased background. For shielded SNM, active-neutron interrogation relies on detecting signatures from induced fission of the material, but the cargo in a loaded container will moderate both the source and emitted neutrons or gamma rays, creating the possibility of false negatives.

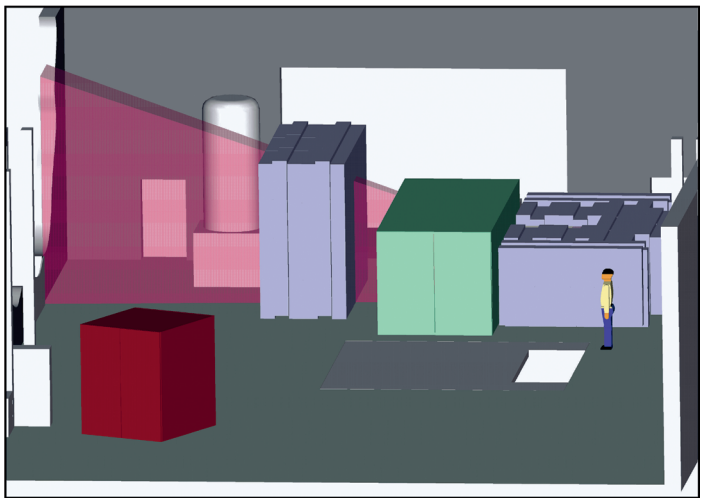

Graphic depiction of a modeling simulation of our active-neutron interrogation technique for detecting a hidden weapon of mass destruction. The maroon color depicts the neutron beam passing through a cargo container.

Current active-neutron interrogation techniques—prompt fission, delayed fission, differential die-away, and delayed-fission gamma emission—pose challenges. Prompt fission and delayed fission have low yield, differential die-away requires a long measurement time, and using delayed-fission gamma rays may be vulnerable to interference from longer-lived fission products that may be produced. The main deliverable of this project is a statement of the boundaries of feasibility of active-neutron interrogation. We plan to map out the limits of the method using carefully chosen experiments together with extensive, high-fidelity modeling. Experiments will prove that the models are dependable; calculations will permit extrapolation and interpolation between well-focused but costly experiments. This combined approach of experiments and calculations will enable us to reach a broad and solidly grounded understanding of performance that is not achievable with experiments or calculations alone.

In FY2002, we (1) conducted experiments to identify radiation signatures for different amounts of thermalization and neutron-source energy; (2) performed radiation-safety calculations by developing a complete model of a cargo container, source igloo, shielding walls, and the experimental facility; (3) performed calculations to identify signatures of SNM in cargo and cargo loading; (4) installed radiation-shielding blocks in a new laboratory dedicated to cargo container scanning technologies; (5) performed experiments to determine characteristic radiation signatures; (6) compared preliminary experiments with calculations; and (7) designed and set up experimental data-acquisition system and analysis-management system.

Our work plan for FY2003 has several specific goals: characterize radiation signatures; determine how those signatures are altered by the presence of multiple targets; study the effect of conventional cargo; and quantify, in the case of two or more distinct targets present, the effect of conventional cargo as it attenuates the signature, produces confusing interferences, and alters the background.

Fiber-optic solutions for short-pulse lasers

J. Dawson, R. Beach, and Z. Liao

Diffraction-limited fiber-optic lasers can produce high-beam-quality radiation from efficient, compact, and rugged sources for applications requiring high-intensity radiation, such as short-pulse lasers. These lasers have demonstrated average power levels exceeding 100 W, with near-diffraction-limited output, and are finding uses in both scientific and industrial applications. However, the key to achieving high power without sacrificing beam quality is the type of optical fiber used. Conventional step-index fibers are not suitable for such power levels, because when a larger-diameter core is used to increase the fibers' average power capability, multiple transverse modes occur simultaneously, resulting in non-diffraction-limited beams. Beam quality also suffers because of nonlinear effects and laser damage.

The objective of this work is to fabricate a large-mode-area (LMA) fiber capable of single-transverse-mode operation and which provides higher average and peak powers than are possible today with conventional fibers. The most important benefit of our work is the extension of chirped-pulse amplification in fibers to the millijoule level, potentially allowing the replacement of complex regenerative amplifier systems with simpler, more reliable fiber systems. This work will benefit a broad range of LLNL laser systems important to stockpile stewardship and other missions. For instance, LMA fibers will be critical to the Petawatt laser—to be used in conjunction with the National Ignition Facility—in applications such as fast ignition to boost gain and backlighter x rays for imaging dense targets. Furthermore, LMA-fiber-based chirped-pulse amplification lasers will significantly enhance laser-machining capabilities for the disassembly of nuclear weapons.

In FY2002, we engineered an LMA fiber to produce the flat-topped mode [see Fig. (a)] specified in our theoretical calculations. This mode is significant for two reasons: (1) intensity remains constant across the entire diameter of the fiber core and (2) the elevated region of the refractive index profile (corresponding to the cladding around the core) occurs in an area of declining intensity. Both improvements substantially increase the peak and average power capability of the fiber. (In contrast, standard step-index fibers result in an intensity that peaks at the fiber axis and in a high-refractive-index area that occurs in the gain region, limiting the peak and average power that the fiber can handle.)

To determine the practicality of the fiber structure, we compared its performance to that of a standard step-index optical fiber with approximately the same specifications as the custom optical fiber but without our fiber's raised ring, which provides for the flattened-mode behavior. Due to the raised ring in the fiber's refractive index profile, our fiber exhibited a large, flattened mode and a constant intensity over the entire core diameter, as Fig. (b) shows.

However, because the fiber exhibited multiple waveguide modes due to the large core diameter, we investigated the potential of using bend-induced waveguide loss to achieve operation in a single transverse waveguide mode. In theory, the higher-order modes would radiate from the bent region first, leaving only the low-order, most stably guided modes. Bend-induced waveguide loss was successful; 70% of the transmitted light was contained in the preferred flat-topped mode despite a higher attenuation resulting from preferential overlap with the gain region.

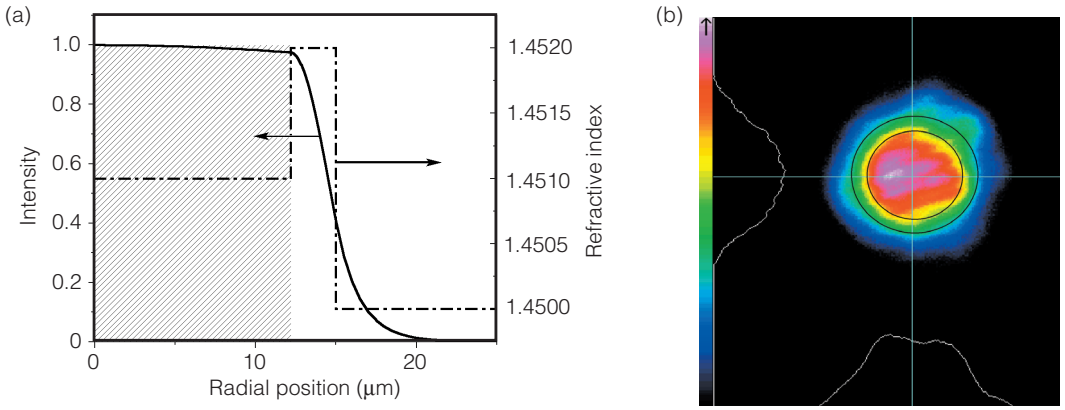

(a) The intensity (solid line) and refractive index (dashed line) of a diffraction-limited fiber for laser applications. The flat-topped intensity profile indicates that intensity is nearly constant over the gain area (shaded), i.e., the fiber core. The result is high beam quality at power levels >100 W. (In conventional fibers, intensity peaks at the fiber axis, limiting the power level.) (b) The fiber's near-field radiation image, with rings indicating the fiber boundary (inner ring) and cladding (outer ring) and crosshairs indicating the fiber center. The orange and red colors show that peak laser intensity is maintained over the entire fiber core, as is also seen in the white flat-topped intensity profiles along the horizontal and vertical axes.

Ultrafast dynamics of plasma formation and optical materials modifications under high-fluence laser irradiation

S. G. Demos, H. B. Radousky, M. Feit

Laser-induced damage is a concern in large-aperture optics for high-power, high-energy lasers such as the National Ignition Facility. However, observed laser-damage thresholds are lower than the theoretical intrinsic values by more than one order of magnitude. Various models have been proposed to explain this phenomenon, each predicting a specific wavelength and pulse-length dependence of the damage threshold. The goal of this project is to reveal the mechanisms of laser damage in transparent dielectric materials at relatively low fluences. By improving our understanding of laser damage in optics for the Stockpile Stewardship Program and inertial-confinement fusion, this project supports LLNL's missions in national and energy security.

In FY2002, we quantitatively studied the wavelength-dependent damage threshold of deuterated potassium dihydrogen phosphate (DKDP) crystals. In our experiments, the focal spot at the damage-testing region was maintained for all wavelengths at 100 ±5 μm, the temporal profile at 2.9 ±0.1 ns, and the polarization–extinction ratio at 1:100. The radiation source for the experiment was an optical parametric oscillator producing continuously tunable output from 310 to 650 nm.

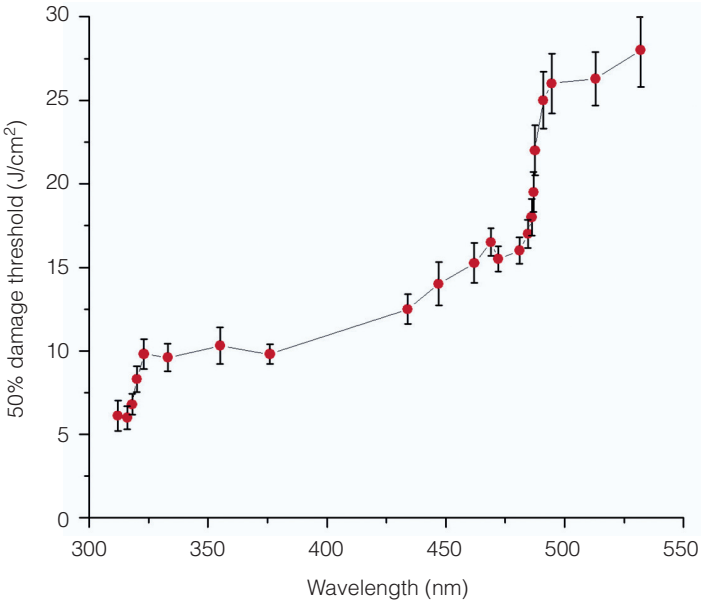

Measured 50% damage probability as a function of wavelength in a deuterated potassium dihydrogen phosphate (DKDP) crystal. Our results suggest that most damage initiation in DKDP crystals arises from material defects.

The percentage of sites with damage initiation was plotted against fluence to generate a damage probability curve (see Figure), which shows the 50% damage probability fluence as a function of wavelength. Most notably, the curve shows sharp steps in the damage threshold at 487 and 321 nm. The step width approximates the product of Boltzmann's constant and temperature. The region between steps exhibits a smooth increase in damage threshold with increasing wavelength.

We used these results to evaluate possible mechanisms of laser-induced damage in DKDP. A previous model suggests that foreign particles absorb sufficient energy to initiate damage. This model predicts a smooth, wavelength-dependant damage threshold profile, which roughly agrees with values between the steps but does not explain the existence of the steps. The results also contradict the impact-ionization model, which predicts a flat response at long wavelengths and an increased damage threshold at short wavelengths, and the pure multiphoton model, which predicts different locations for the steps, in conjunction with the band-gap of DKDP; much larger steps when the order for multiphoton absorption changes; and a much higher overall damage threshold.

Our observed data suggest a defect-assisted multiphoton mechanism. Defect states in the gap would alter the cross section for multistep or multiphoton excitation following excited-state absorption. Our model accounts for the observed sharp steps in the damage threshold, a much smaller step magnitude than the pure multiphoton model does, and the discrepancies of 0.30 and 0.15 eV in the step locations compared to the values that a pure multiphoton mechanism predicts for band-gap energy divided by order (E_g/n) when E_g = 7.2 eV. This energy can be attributed to nonradiative decay losses during population of the excited states involved. Furthermore, the wavelength-dependant damage-threshold profile indicates a band structure similar to that of pure DKDP and not of a foreign material.

The results of this project strongly suggest that most damage initiation in DKDP crystals arises from material defects. These results can help identify the defect type and devise means to passivate or eliminate them.

Starburst galaxies

W. J. M. van Breugel

Starbursts are short periods—a few million years—of intense star formation in the central regions of galaxies. The near-simultaneous explosions of millions of stars drive superwinds that enrich the intergalactic medium and feed massive black holes, which trigger high-energy jets. In the early universe, starburst galaxies provided the building blocks for larger galaxy systems. In the local universe, they provide nearby analogs of their more distant counterparts. By studying starbursts and starburst galaxies we can learn more about how galaxies form and what triggers high-energy activity from their central black holes.

This project will contribute to LLNL's stockpile-stewardship mission by stimulating and helping to validate hydrodynamic code development of galaxy formation and starburst astrophysics and laser experiments of starburst outflows and jets. Benchmarking hydrodynamic codes and laser–plasma experiments on challenging astrophysical problems, with peer-review by world experts, allows us to apply codes and experiments to nuclear weapons simulations with more confidence. In addition, this research project advances special LLNL capabilities in adaptive optics (AO) and instrumentation, and will develop data-analysis and observational techniques that are applicable to the Laboratory's nonproliferation mission. The scientific appeal of this high-visibility research will attract new talent to the Laboratory. University collaborators include researchers from the University of California at Berkeley, Davis, and Santa Cruz; the California Institute of Technology; Leiden University, the Netherlands; the Australian National University; and Cardiff University, U. K.

This research focuses on the most luminous starburst galaxies, both near and far, to obtain the best possible data. We use narrowband filters for emission-line imaging of jets and superwinds, and high resolution AO imaging of their central galaxy morphologies. The best way to identify the most luminous starburst galaxies is with bright, extragalactic radio sources. Such sources are powered by supermassive black holes, which are uniquely associated with the most massive galaxies. We have developed an effective method for finding such galaxies using large surveys such as the Faint Images of the Radio Sky at Twenty Centimeters (FIRST) survey at the Very Large Array in New Mexico.

Observations at several wavelengths were used to determine the relationships between the cold gas (60 K) in young forming galaxies, their star-forming regions, and outflowing hot gas (10,000 K) from their central starbursts (see Figure). The cold gas and dust are found in two regions, which straddle the central part of the galaxy. The hot line-emitting gas escapes along the path of least resistance, the minor axis of the galaxy system. This gas is probably from supernova explosions of young stars that had formed earlier during a large burst of star formation. The cone-shaped outflow cleared away the gas from the central region. Our observations are the best evidence to date that massive forming galaxies exhibit many of the same phenomena as nearby starburst galaxies, although on a 10 to 100 times larger scale. Also, a string of star-forming regions along the interface between the hot and cold gas suggests that the superwind may have induced additional star formation by driving shocks into the cold cloud.

In FY2003 we will (1) complete our detailed studies of giant emission-line halos around a few massive forming galaxies; (2) determine how they are ionized and whether they contain nuclear fusion material produced by the starbursts; (3) complete our AO studies of nearby starburst galaxies to determine the causal connection between galaxy collisions and starbursts; (4) perform numerical simulations to investigate the effects of jets and radiation on star formation, and the chemical enrichment in galaxies and their environment.

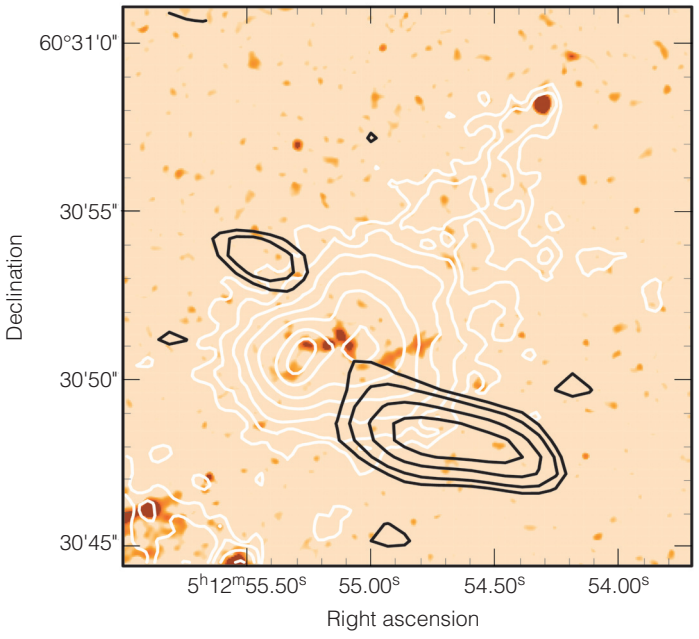

Hubble Space Telescope image of the starburst galaxy 4C60.07 (false color) showing hot gas (white contours) blown from center of cold gas in the forming galaxy (black contours).

A tunable, monochromatic, 1-angstrom, Compton-scattering x-ray microfocus for multi-wavelength anomalous diffraction experiments

F. V. Hartemann, W. J. Brown, H. A. Baldis

The goal of this project is to demonstrate the microfocus, multiwavelength anomalous diffraction (microMAD) concept. In microMAD, tunable, monochromatic, 1-Å x rays are produced by a compact, femtosecond Compton-scattering microfocus for such applications as x-ray protein crystallography [i.e., determining a protein's three-dimensional (3-D) structure from x-ray diffraction]. Our experiment will be the first anomalous x-ray diffraction experiment performed using a Compton-scattering source.

In addition to x-ray protein crystallography, the microMAD concept also has the potential to revolutionize femtosecond material physics and advanced medical imaging. For example, protein crystallography based on microMAD could reveal the detailed 3-D structure of proteins specific to a pathogen identified as a potential bioterrorism agent. Such information would help detect, identify, and protect against that pathogen, contributing to the homeland security mission of the Laboratory.

In FY2002, we used a 3-D code developed under a previous project (99-ERI-008) to model in detail the x-ray output of the Picosecond Laser–Electron Interaction for the Dynamical Evaluation of Structure (PLEIADES), a high-peak-brightness x-ray facility. This will enable us to benchmark the code in great detail against the measured output of PLEIADES and to determine accurately the modifications needed to generate tunable radiation of approximately 1 Å (12.8 keV) for our microMAD experiment. We also extensively modeled the electron beam using the particle dynamics code PARMELA and began a full characterization of the photoelectron beam produced by an S-band radiofrequency gun and accelerated by a linear accelerator (linac) at LLNL. Detailed measurements include emittance, energy, energy spread, optical transition radiation profiles, and x-ray flux [Figs. (a)–(d)]. We also developed a 3-D time-domain Compton code.

Key issues that largely determine the ultimate brightness of the x-ray source are timing jitter and synchronization between the femtosecond drive laser pulse (produced by the Falcon laser) and the subpicosecond photoelectron beam. To address this issue, we designed a new electro-optic diagnostic to obtain subpicosecond timing jitter data; identified the 180° interaction geometry as optimal for minimizing the impact of timing jitter on the x-ray flux [Fig. (c)]; and designed a novel optical mirror–x-ray window that enables head-on collisions (180° interaction) between the laser pulse and electron beam (a patent is pending).

In FY2003, the spatial, temporal, and spectral properties of the high-peak-brightness, ultrashort x-ray flashes of PLEIADES will be fully characterized and the results compared with those predicted with our 3-D code. This analysis, supplemented by PARMELA calculations, will be used to design the microMAD experiment scheduled for FY2004. In connection with the Linac Coherent Light Source project, we will also develop a fully 3-D time-frequency domain x-ray code to model chirped x-ray pulses. Close collaboration with Jefferson Laboratory (JLab) and Columbia University will continue. Using JLab's superconducting linac and a free-electron laser producing femtosecond light pulses, we plan to demonstrate gains of 3 to 5 orders of magnitude in average x-ray brightness compared to other x-ray microfocus tubes, as well as the required tunability.

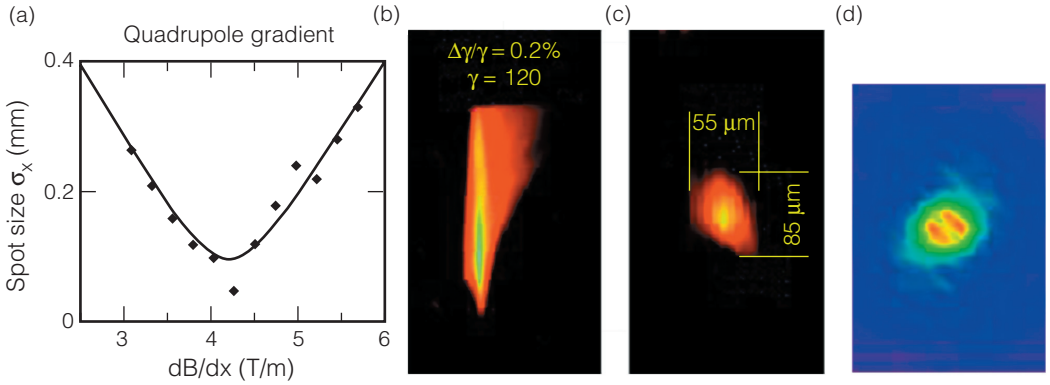

Some results demonstrating the microfocus, multiwavelength anomalous diffraction concept. (a) Electron beam emittance measurements showing beam spot size (σ_x) as a function of the focusing quadrupole gradient (dB/dx). We achieved good agreement with the values predicted with PARMELA. (b) Magnetic spectrometer of the focused electron beam. For a normalized beam energy (γ) of 120, relative energy spread ($\Delta\gamma/\gamma$) was only 0.2%. (c) Optical transition radiation photo of the focused beam. (d) Compton x-ray angular map of x-ray flux as a function of solid angle for a 1-eV spectral window below the spectral maximum on-axis (10 × 10-mrad frame). The two x-ray lobes reflect the kinematics of Compton scattering.

Fermion Monte Carlo

M. H. Kalos

This research in fermion Monte Carlo proposes to find a numerical method for solving the Schrödinger equation for many-fermion systems that contains no uncontrolled approximations. The Schrödinger equation for many-fermion systems has been under study for six decades, but no accurate methods without uncontrolled approximations have emerged for this important problem, which underlies the physics of molecular structure, equations of state (EOS), and other applications of interest to stockpile stewardship. The key difficulty of this problem is that of dimensionality. Monte Carlo methods in particular have been impeded by the "fermion sign problem"—wave functions must be antisymmetric in the exchange of identical particles—which has been one of the major unsolved problems in computational quantum mechanics.

Our research in fermion Monte Carlo at LLNL has demonstrated a new class of methods capable of overcoming this difficulty. Central to these new methods is the use of correlated random walks for objects that carry algebraic signs. These new methods that build on well-known techniques of diffusion Monte Carlo, along with future extensions, will provide LLNL with advanced computational tools to treat many scientific challenges for LLNL's stockpile stewardship mission, including atomic structure, EOS, properties of condensed matter, nuclear structure, and chemical binding.

An important algorithmic question for fermion Monte Carlo is the dependence of the computational time required to achieve a given statistical accuracy upon the particle number. It has been conjectured that the time will necessarily grow exponentially with the number of particles. We believe that the behavior, within our method, is polynomial or better, and an important issue is to demonstrate that the calculations are practical for systems of increasing size. Thus, demonstrating success with systems of 10 and 23 electrons and with 54 helium-3 (He^3) atoms is an important validation.

In FY 2002, we made substantial methodological and practical advances—our codes were rewritten and made considerably more efficient. A long-standing error in the program for treating systems of He^3 was corrected. New forms of importance functions were devised, studied, and optimized. The long-standing algorithmic question of how to incorporate the Monte Carlo technique of "acceptance–rejection" into our correlated random walk was solved, and the revised codes appear to be significantly faster as a consequence.

We have completed a sequence of computations for the lithium (Li) and beryllium (Be) dimers and have begun computations on the boron (B) dimer. The Figure shows results for the Li dimer. The calculations of the 54-body system of He^3 atoms have produced both strongly stable behavior and credible numerical answers. Finally, the program for the last system has been adapted to study the two-dimensional electron gas, about which there is some uncertainty in the phase diagram. This research, although just started, is going well, exhibiting Monte Carlo stability and credible results for a 26-body system.

The use of a shadow-wave function based on fixed-node functions was proposed to improve first-stage importance functions in our code. To make this feasible, we solved a long-standing technical problem connected with using shadow functions as importance functions. Our collaborations continued with professors at the University of California, Berkeley; the University of Trento, Italy; the University of Granada, Spain; and the University of Illinois at Urbana-Champaign.

For FY2003 we plan to accelerate the performance of the dimer code by more than an order of magnitude using improved methods of linear algebra, novel Monte Carlo stratification, and careful code optimization. The new code will be used to compare results for the B dimer with experiment. The program for treating systems of He^3 will be speeded up as well. Based on our results, which show that the quality of the computational results depends upon the nature of the "guiding functions" used, we plan to examine alternative mathematical forms.

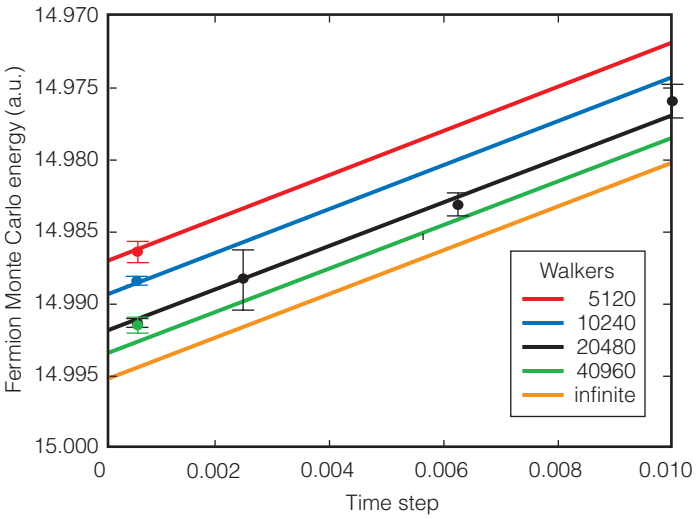

The computational results for the lithium dimer, as a function of the time step and of the population of walker used. Fits to the data permit extrapolation to zero time step and infinite population. The extrapolated result is 14.9954(6) a.u., which agrees with experiment.

Study of the ionization dynamics and equation of state of a strongly coupled plasma

R. Shepherd, P. Audebert, J. P. Geindre, J. Dunn, S. Moon, M. Foord, C. Iglesias, F. Rogers

Understanding radiation cooling of white dwarfs is important to estimating the age of star clusters. Because the majority of stars, including our Sun, will end their life as white dwarfs, knowing the number of white dwarfs as function of brightness within a star cluster and the brightness as a function of evolutionary track allows one to infer the star cluster's age. However, the age estimate is strongly dependent on understanding the internal cooling dynamics of white dwarfs. The internal structure of a white dwarf consists of strongly coupled matter, which is of relatively low temperature (1 to 100 eV) and high density (>10^{23} g/cm^3). Matter becomes strongly coupled when the potential energy of the particles becomes large compared to the kinetic energy—a ratio of potential to kinetic energy [known as gamma (Γ)] greater than 1 indicates strongly coupled matter. A thorough understanding of radiation transport through strongly coupled matter is necessary to understand the cooling of white dwarfs. Although an abundance of theoretical models exist for this regime, experimental data to test the models are scarce.

The goal of this project is to test models of radiation transport in strongly coupled matter by utilizing the unique capabilities of ultrashort-pulse (<1 ps) lasers and fast x-ray detection pioneered at LLNL. The technique relies on generating high-density, low-temperature plasma using ultrashort-pulse lasers. This project, the first application of this technique to understanding energy-loss mechanisms in matter, will contribute to the Laboratory's national-security mission by furthering our understanding of matter under extreme conditions.

High-density, low-temperature plasmas are formed by illuminating a thin aluminum foil with an ultrashort-pulse laser. Because of inertia, little expansion occurs as the foil absorbs the short burst of laser energy. Heat conduction rapidly distributes the energy through the target as the surface layer expands and cools. Because expansion takes place on a time scale that is long relative to the conduction heating time, a high-density (>0.1 g/cm^3), low-temperature (<100 eV) plasma forms briefly. The time histories of temperature and density are inferred by measuring the target's expansion velocity using Fourier domain interferometry (FDI), which works like extremely sensitive radar (see Figure). Radiation transport is studied by back-illuminating the heated target with a long burst of x rays created with a laser pulse. The x rays are dispersed in energy and time resolved with an ultrafast x-ray streak camera combined with a crystal spectrometer. The x-ray absorption data are compared to models used to calculate the energy balance in white dwarfs.

During FY2002, we completed characterization of the aluminum-foil targets using FDI. The targets were illuminated with laser intensities between 5×10^{14} and 5×10^{15} W/cm^3. The data showed a temperature of ~20 to 50 eV, with an average density of ~10^{23} e/cm^3, producing a maximum Γ of ~7. The temporal and spectral characteristics of the x-ray back illuminator were measured, and the first x-ray absorption data were collected and are being analyzed for comparison to opacity code simulations.

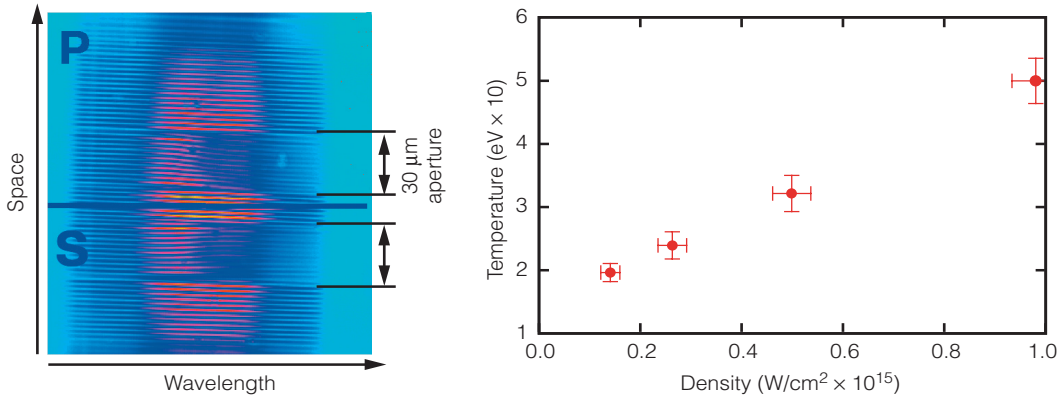

We are studying radiation transport by back-illuminating a short-pulse-laser-heated target with a long burst of x rays created with a laser pulse. The x rays are dispersed in energy and time resolved with an ultrafast x-ray streak camera combined with a crystal spectrometer. The x-ray absorption data are compared to models used to calculate the energy balance in white dwarfs. (a) Fourier domain interferometery (FDI) image, in s and p polarizations, showing the fringe movement of a heated target. (b) For a given laser intensity, these data are used to determine the power density (assuming isothermal expansion) and temperature of the target.

Absorption measurement requires precise alignment of the x-ray back-illuminator to the fast x-ray streak camera and the short-pulse-laser-heated target. Although data collection was initially limited by the extremely laborious alignment process, we redesigned the target holder to simplify alignment.

In FY2003 we plan to use our redesigned target holder to speed collection of a comprehensive data set for aluminum, silicon, and selenium.

Beta-decay experiments and the unitarity of the Cabibbo–Kobayashi–Maskawa matrix

P. E. Garrett, W. E. Ormand

The unification of the electromagnetic force and the weak nuclear force—two of the four basic forces of nature—by the Standard Model of electroweak interactions has been one of the most successful and important scientific breakthroughs of the 20th century. The Standard Model remains unscathed by many experimental attempts over the past 30 yr to discover physics that would require its extension. The goal of this project is to perform precise measurements of superallowed Fermi beta decay to investigate a possible nonunitarity in the Cabibbo–Kobayashi–Maskawa matrix of the Standard Model. Findings suggest that the sum of squares of the matrix's first row differs from unity at the 98% confidence level. If the results of our testing support these findings, it would be the first indication of physics beyond the Standard Model, a result of major scientific importance.

The scope of our project is simple in principle: use a large-scale gamma-ray spectrometer to measure half-lives and branching ratios for superallowed Fermi beta-decaying nuclei such as argon-34 (^{34}Ar), gallium-62 (^{62}Ga), and rubidium-74 (^{74}Rb). Small correction factors to be applied to the data are then calculated. Accurate and precise (>99.9%) half-lives and decay branching ratios will be measured for nuclei for which different sets of calculated corrections give divergent results. These measurements are being performed at Canada's Triangle University Meson Facility (TRIUMF) using the 8π spectrometer, the world's most sensitive gamma-ray spectrometer dedicated to decay studies (see Figure). At TRIUMF, our role in the collaborative effort is to define and build the data acquisition system and to provide the theoretical calculations necessary to interpret the results.

The sophisticated data-acquisition-system technology developed in this project will have applications in various areas of research at other DOE laboratories, e.g., in neutron cross section measurements undertaken at the LANSCE facility at Los Alamos. The refinement of techniques used in nuclear-physics calculations will also have a major impact in basic science, and on quantities relevant for the Stockpile Stewardship Program. Such calculations require new nuclear-structure computational codes that are at the forefront of research in nuclear physics.

In FY2002, we (1) designed, built, and debugged the data-acquisition system; (2) designed and fabricated a precision clock (accuracy greater than 1 part per billion) to allow the accurate half-life measurements; (3) incorporated the precision clock into the data-acquisition system and performed testing; (4) successfully tested the system with a radioactive sodium-26 (^{26}Na) beam; and (5) performed preparatory work for new calculations of the Coulomb correction factors.

In FY2003, we will (1) measure the half-life of ^{34}Ar; (2) expand the data-acquisition system to incorporate different detector types, which is necessary for accurate branching-ratio experiments; (3) perform the branching-ratio measurement on ^{34}Ar and the initial study of ^{74}Rb; (4) carry out calculations for the theoretical correction factors for ^{34}Ar, manganese-50, and cobalt-54; and (5) analyze data from the experiment on ^{26}Na and include the analysis in a paper about the new data-acquisition system.

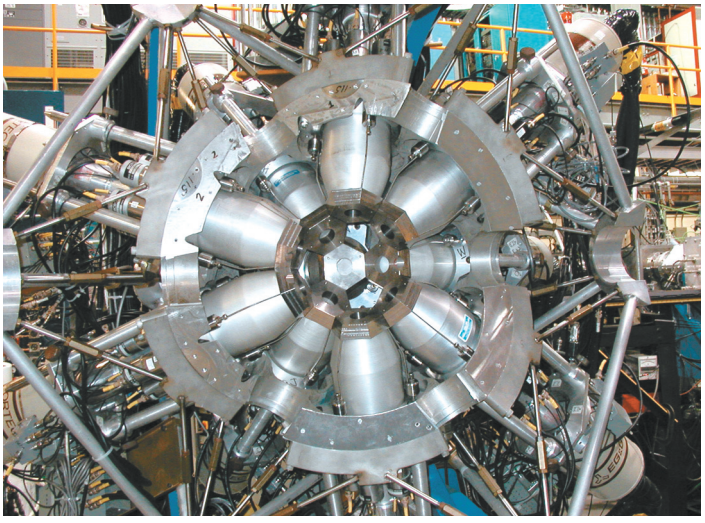

The 8π spectrometer at Canada's Triangle University Meson Facility (TRIUMF). We used the 8π—the world's most sensitive gamma-ray spectrometer dedicated to decay studies—to investigate a possible nonunitarity in the Cabibbo–Kobayashi–Maskawa matrix. If proven, this nonunitarity would be evidence of physics beyond the Standard Model.

Tests of quantum field theory in strong fields

P. Beiersdorfer, M.-H. Chen, K.-T. Cheng, J. Sapirstein

Quantum field theory forms the underpinning of most of modern physics and has been extremely successful in describing natural phenomena. The theory has been thoroughly validated in low electric fields, yet questions remain about the completeness of the theory in ultrahigh electric fields (>10^{14} V/cm), found only in the vicinity of heavy nuclei. Such questions have far-reaching implications, from the validity of the Standard Model to the details of the Big Bang model. The goal of this research is to refine theoretical quantum field calculations for ultrahigh electric fields by incorporating recent breakthroughs, then compare calculated values with actual measurements to test quantum field theory. Our research utilizes LLNL's unique capabilities in ion sources and atomic spectroscopy and a theory collaboration between LLNL and the University of Notre Dame.

This work directly affects DOE programs in high-energy physics research, because a breakdown of quantum field theory in strong fields would imply the existence of new elementary particles. The research also affects DOE missions in atomic, molecular, and chemical sciences and weapons physics, which are based on atomic physics and rely heavily on the correctness of atomic calculations.

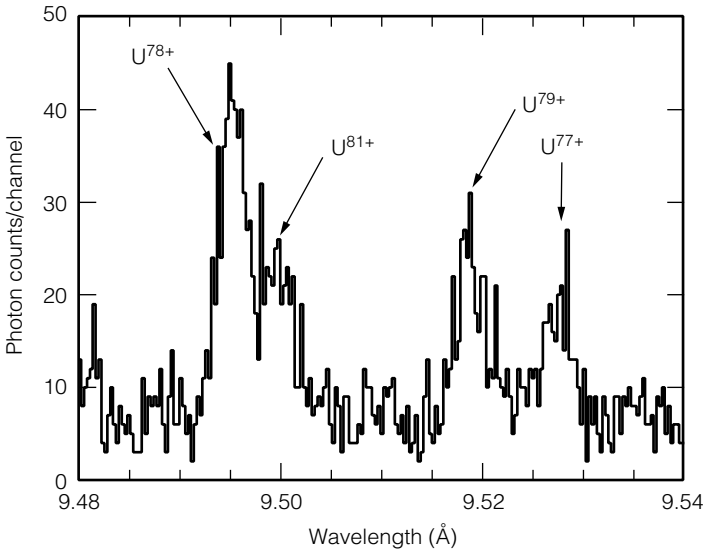

Measured x-ray emission spectrum of the 3s–3p transition in highly charged uranium ions. Measurements were made with a high-resolution Bragg crystal spectrometer at LLNL's electron beam ion trap facility. Our enhanced ab initio calculations achieved far better agreement with such measurements than was possible before, helping validate quantum field theory for ultrahigh electric fields.

The energy of electronic transitions is our basis for comparing calculations and measurements. Measurements, conducted with the Livermore electron beam ion trap device, focused on using high-resolution spectrometers to determine the wavelength of the 2s–2p and 3s–3p transitions in very heavy ions. Because the highest electric fields exist near very highly charged nuclei, uranium ions in particular provide a natural test bed for quantum field theory. Our measurements established benchmarks of the quantum field effects for different heavy ions—such as barium, lead, and uranium (atomic number Z = 56, 82, and 92, respectively)—and represent the best such measurements ever performed.

Our calculations focused on providing the most accurate ab initio values from quantum electrodynamic theory for direct comparison with measurements. The comparison enables us to quantify contributions of the elusive two-loop self-energy term and to assess the validity of quantum electrodynamics. Because the ions of interest have more than one electron, the calculations become very elaborate. We also focused on transitions in which multi-electron physics dominates to test separately the validity of the calculations associated with these effects.

Incorporating such effects into our ab initio calculations made possible excellent agreement with measured results. In FY2002, testing included the 3s–3p transitions in sodium-like U^{81+} and neighboring charge states of uranium (see Figure). For example, the transition energy of the line in U^{79+} near 9.52 Å was measured to be 1302.55 ± 0.02 eV, whereas the value we calculated was 1302.53 eV. Before our project, such a precise test of theory was unheard of, nor could calculations of such complex multi-electron systems (this particular one has 13 electrons) be made with such accuracy. In fact, the accuracy of both our calculations and our measurements exceeded those performed earlier by more than an order of magnitude. Similarly excellent agreement between calculations and measurements was obtained for other measured transition energies.

Our results indicate that multi-electron physics is now well under control and that extremely accurate tests of quantum electrodynamics are now possible.

Appendix

Appendix

Publications

The publications listed here report on LDRD research conducted in FY2002. Publications are listed by Section, and within each Section by project tracking code in the same order that the corresponding article appears in the text. The unique document number (beginning with UCRL) at the end of each publication reference indicates that the document was published under the auspices of the DOE in compliance with Contract W-7405-Eng-48.

Section 1 Advanced Sensors and Instrumentation

01-SI-010

Johnson, G. W. et al. (2002). "Characterization of gigabit ethernet over highly turbulent optical wireless links." *Proc. SPIE* **4821**, 283. UCRL-JC-146490.

Thompson, C. A. et al. (2002). "Free space optical communications employing MEMS adaptive optics." *Proc. SPIE* **4821**, 129. UCRL-JC-150017.

Wilks, S. C. et al. (2002). "Modeling of adaptive optics-based free-space communications systems." *Proc. SPIE* **4821**, 121. UCRL-JC-146575.

02-SI-005

Fitch, J. P. et al. (2002). *Biosignatures of pathogen and host*. Presented at the Workshop on Genomic Signal Processing and Statistics (GENSIPS). UCRL-JC-149741 Abs.

Milanovich, F. et al. (2002). *Mechanisms of pathogenicity*. LLNL Science Day Expo. UCRL-MI-150058.

Sokhansanj, B. A. et al. (2002). *Fuzzy rule-based modeling of* Yersinia*-host interactions*. Presented at the DIMACS, Workshop on the Pathogenesis of Infectious Diseases. UCRL-JC-150426 Abs.

01-ERD-023

Cunningham, C. T. and R. S. Roberts. (2001). "An adaptive path planning algorithm for cooperating unmanned air vehicles." *Proc. IEEE Intl. Conf. on Robotics and Automation* **4**, 3981–3986. UCRL-JC-140415.

Jones, E. D., R. S. Roberts, and T. C. Hsia. (2003). *STOMP: A software architecture for the design and simulation of UAV-based sensor networks*. Presented at the IEEE Intl. Conf. on Robotics and Automation. UCRL-JC-150771.

Roberts, R. S., C. A. Kent, and E. D. Jones. (in press). "UAV cooperation architectures for persistent sensing." *Proc. SPIE Conf. on Sensors, and C3I Technologies for Homeland Security*. UCRL-JC-150006 Abs.

01-ERD-108

Bogen, K. T. (2002). *Homogeneity of proportions estimated from pairs of correlated compound-binomial counts that are stochastically censored*. UCRL-JC-149327.

Bogen, K. T., A. A. Marchetti, and T. A. Brown. (2002). "Use of a correlated compound-binomial model to assess absence of non-counting noise in Pu-isotope ratios measured by AMS at LLNL." *Proc. 9th Intl. Conf. on Accelerator Mass Spectrom.*, September 9–13, Nagoya, Japan. UCRL-JC-148648 Abs.

02-ERD-010

Quarry, M. J. (in press). "Design of a phased array for guided wave mode tuning." *Nondestructive Matls. Char.* **XI**. UCRL-JC-148725.

02-ERD-023

Edwards, J., H. F. Robey, and A. J. Mackinnon. (2001). *Application of gaseous laser targets and optical diagnostics to study high mach number unstable plasma flows*. UCRL-ID-143428.

01-ERI-001

McElfresh, M. et al. (2002). "Combining constitutive materials modeling with atomic force microscopy to understand the mechanical properties of living cells." *Proc. Natl. Acad. Sci.* **99**, 6493. UCRL-JC-145763.

02-ERI-001

Baesu, E. et al. (in press). "Continuum modeling of cell membranes." *J. Nonlin. Mech.* UCRL-JC-150482.

Rudd, R. E. et al. (2002). "Modeling the deformation of living cells induced by atomic force microscopy." *Proc. ICCN 2002*. UCRL-JC-146706.

02-FS-015

Esposito, A. P. et al. (in press). "Analysis of single bacterial spores by micro-Raman spectroscopy." *Appl. Spectrosc.* UCRL-JC-150162.

Section 2 Biological Sciences

01-SI-002

Fitch, J. P. (2002). *Chemical and Biological National Security Program Update*. UCRL-PRES-147771.

Fitch, J. P. et al. (2002). "Biosignatures of pathogen and host." *Proc. 2002 Workshop on Genomic Signal Proc. and Stat.* UCRL-JC-149741.

Fitch, J. P. et al. (2002). "Rapid development of nucleic acid diagnostics." *Proc. IEEE*, Nov. 2002. UCRL-JC-148118.

Forde, C. E. et al. (2002). "A rapid method to capture and screen for transcription factors by SELDI mass spectrometry." *Biochem. and Biophys. Res. Comms.* **209**, 1328–1335. UCRL-JC-146363.

Forde, C. E. et al. (2002). *Identification of transcription factors responsible for* Y. pestis *virulence using SELDI-MS*. Presented at the 1st Ann. N. Am. Protein Chip Tech. Users Group Meet. UCRL-JC-147406 Abs.

McCutchen-Maloney, S. L. et al. (2001). "Cancer proteomics and differential protein profiling by SELDI mass spectrometry." *Proc. 5th Intl. Symp. on Mass Spectrom. in the Health and Life Sci*. UCRL-JC-144156 Abs.

McCutchen-Maloney, S. L. et al. (2002). "Cancer proteomics and SELDI mass spectrometry." *Proc. 2nd Ann. Human Proteome Project Forum*. UCRL-JC-146493 Abs.

McCutchen-Maloney, S. L. et al. (2002). *Proteomics, genomics, and national security*. LLNL Family Days Poster. UCRL-MI-150060.

Motin, V. L. et al. (2002). "DNA microarray analysis of differentail gene expression in *Y. pestis*." *Proc. 8th Intl. Symp. on* Yersinia. UCRL-JC-148073 Abs.

Motin, V. L. et al. (2002). "Genome-wide expression profiling of Y. pestis during low-calcium response." *Proc. 102th Gen. Meet. Am. Soc. for Microbio.* UCRL-JC-146479 Abs.

Rocco, J., C. E. Forde, and S. L. McCutchen-Maloney. (2002). *Real-time protein expression of virulence factors in* Yersinia pestis. LLNL Summer Student Intern Poster Session. UCRL-MI-149532.

Sokhansanj, B. A. and J. P. Fitch (2002). "Interpreting microarray data to build models of microbial genetic regulation networks." *Proc. SPIE Photonics West 2002*. UCRL-JC-144382.

Sokhansanj, B. A. et al. (2001). "Mathematical modeling of the base excision repair pathway." *Proc. 1st SIAM Conf. on Life Sci*. UCRL-JC-146306-PT-1.

Sokhansanj, B. A., G. R. Rodrigue, and J. P. Fitch, "Scalable fuzzy modeling of gene regulation." *Proc. 2001 Intl Conf. on Systems Bio.* UCRL-JC-144149.

01-SI-012

Balu, N. et al. (2002). "Modified guanines representing O^6 alkylation by the cyclophosphamide metabolites acrolein and chloroacetaldehyde: Synthesis, stability, and ab initio studies." *Chem. Res. in Toxicol.* **15**, 380–387. UCRL-JC-145823.

Colvin, M. E. and J. N. Quong. (2002). "DNA-alkylating events associated with nitrogen mustard based anticancer drugs and metabolic byproduct acrolein." *Advances in DNA Sequence-Specific Agents* (G. B. Jones, ed.) **4**, 29–46. UCRL-JC-146483.

Cosman, M. et al. (2002). "Identification of novel small molecules that bind to two different sites on the surface of tetanus toxin C fragment." *Chem. Res. in Toxicol.* UCRL-ID-146919.

Lau, E. (2002). "Improving delivery of radionuclides to cancerous cells using computational chemistry." Presented at the 8th Ann. Cancer Res. Symp. at the UC Davis Cancer Center, Sacramento, CA. UCRL-MI-150071.

Leininger, M. L. et al. (2002). "Complete basis set MP2 binding energies for stacked uracil dimmers." *J. Phys. Chem. A* **106**, 3850–3854. UCRL-JC-145822.

Mundy, C. J., M. E. Colvin, and A. A, Quong. (in press). "Irradiated guanine: A Car-Parinello molecular dynamics study of dehydrogenation in the presence of an OH radical." *J. Phys. Chem. A.* UCRL-JC-145509.

Nguyen, D. H. et al. (2002). "The dynamic structure, and free energy profile of proline-containing antifreeze glycoprotein." *Biophys. J.* **82**, 2892–2905. UCRL-JC-142598.

Nguyen, D. H., W. H. Fink, and M. E. Colvin. (2002). "Molecular dynamics simulations of nitrogen mustand crosslinked DNA." Presented at the Ann. Biophys. Soc. Meet., San Francisco, CA. UCRL-JC-145926 Abs.

Sasaki, J. C., R. S. Fellers, and M. E. Colvin. (2002). "Metabolic oxidation of carcinogenic arylamines by P-450 monooxygenases: Theoretical support for the one electron transfer mechanism." *Mutation Res.* **506–507**, 79–89. UCRL-JC-137235 Rev1.

Sawicka, D. et al. (2002). "Structural predictions of RAD51 paralogs and the complexes they form." Presented at the 8th Ann. Cancer Res. Symp. at the UC Davis Cancer Center, Sacramento, CA. UCRL-JC-150043 Abs.

Schwegler, E. (2002). "First principles simulations of ion solvation." Presented at the 85th Canadian Soc. for Chem. Conf., Vancouver, Canada. UCRL-PRES-148730.

Tran, N. L. et al. (2002). "Experimental and simulation studies of heat flow and heterocyclic amine mutagen/carcinogen formation in pan-fried meat patties." *Food and Chem. Toxicol.* **40**, 673–684. UCRL-JC-142434.

Venclovas, C., M. E. Colvin, and M. P. Thelen. (2002). "Structural model of the clamp loading mechanism." Presented at the Keystone Symp. on Molec. Mech. of DNA Repl. and Recomb., Snowbird, UT. UCRL-JC-146899 Abs.

Venclovas, C., M. E. Colvin, and M. P. Thelen. (2002). "Molecular modeling-based analysis of interactions in the RFC-dependent clamp-loading process." *Protein Sci.* **11**, 2403–2416. UCRL-JC-147562.

Venclovas, C., M. E. Colvin, and M. P. Thelen. (2002). "Molecular mechanism of the 9-1-1 checkpoint response to DNA damage based on protein structure prediction." Presented at the 9th DOE Genome Contractor and Grantee Workshop, Oakland, CA. UCRL-JC-146883 Abs.

Wheelock, C. E. et al. (in press). "Use of ab initio calculations to predict the biological potency of carboxylesterase inhibitors." *J. Medicinal Chem.* UCRL-JC-147934.

00-ERD-006

Heidbrink, J. L., et al. (2002). *Structural characterization of protein-DNA noncovalent complexes*. Presented at the 50th Ann. Am. Soc. for Mass Spectrom. Conf. UCRL-JC-147452.

Shields, S. J. and R. L. Balhorn (2002). *Protein-ligand complexes: Binding sites and conformation changes*. Presented at the 50th Ann. Am. Soc. for Mass Spectrom. Conf. UCRL-JC-147451.

Shields, S., et al. (in press). "Mass spectrometry and non-covalent protein-ligand complexes: confirmation of binding sites and changes in tertiary structure." *J. Am. Soc. Mass Spectrom.* UCRL-JC-151116.

01-ERD-045

Beernink, P. T., B. W. Segelke, and M. A. Coleman (2003) "High-throughput, cell-free protein expression screening using RTS 100." *Biochemica 2003* **1**, 4–5. UCRL-JC-150785.

Beernink, P. T., B. W. Segelke, and M. A. Coleman. (in press). "High-throughput, cell-free protein expression screening using RTS 100." *Roche Applied Sciences*, Application Note. UCRL-JC-150785.

Krupka, H. I. et al. (2002). "The high-speed Hydra©-plus-one system for automated high-throughput protein crystallization." *Acta Crystall. D* **58**, 1523–1526. UCRL-JC-147970 Ext Abs.

Rupp, B. et al. (2002). "The TB Structural Genomics Consortium Crystallization Facility: Towards automation from protein to electron density." *Acta Crystall. D* **58**, 1514–1518. UCRL-JC-147969 Ext Abs.

01-ERD-111

Cosman, M. et al. (2002). "Identification of novel small molecules that bind to two different sites on the surface of Tetanus Toxin C fragment." *Chem. Res. in Toxicol.* UCRL-ID-146919.

Perkins, J. et al. (2002). "Synthetic antibodies." *Abs. of Papers of the Am. Chem. Soc.* **223**, 005. UCRL-PRES-146007.

01-ERD-114

Jones, I. M., C. B. Thomas, and D. O. Nelson. (2002). *How human lymphocytes are handled affects Comet assay estimates of endogenous damage and repair of damage induced by ionizing radiation*. UCRL-JC-150395.

01-ERI-006

Hillegonds, D. J. et al. (2002). *Carbon isotope dilution accelerator mass spectrometry*. UCRL-JC-149406 Abs.

02-LW-003

Barsky, D. and A. Zemla. (2002). *From bubonic plague to foot-and-mouth disease: employing a holistic approach to homology-based protein structure prediction*. Presented at the 46th Biophys. Soc. Ann. Meet., Feb. 23–27, San Francisco, CA. UCRL-JC-147333 Abs.

Fitch, J. P. et al. (2002). "Rapid development of nucleic acid diagnostics." *Proc. IEEE* **90** (11), 1708–1721. UCRL-JC-148118.

Miller, K. et al. (2002). *Analysis of RAD51 paralog complexes*. Presented at Maintenance of Genomic Integrity, Oct. 15–18, Houston, Texas. UCRL-JC-150531 Abs.

Rupp, B. et al. (2002). "The TB structural genomics consortium crystalization facility: Towards automation from protein to electron density."*Acta Crystall.* **58**, 1514–1518. UCRL-JC-147969 Abs.

Sawicka, D. et al. (2002). *Structural predictions of RAD51 paralogs and the complexes they form*. Presented at the 8th Ann. Cancer Res. Symp. at the UC Davis Cancer Center, Sept. 19–20, Sacramento, CA. UCRL-JC-150043 Abs.

Segelke, B., A. Zemla, and B. Rupp. (2002). *Towards automated molecular replacement with adaptive template generation and effective bias removal*. Presented at the Am. Crystall. Assoc. Ann. Meet., May 25–30, San Antonio, TX. UCRL-JC-147052 Abs.

02-FS-006

Kulp, K. S. et al. (in press). "Dietary constituents affect estrogen receptor activation and cell proliferation in MCF-7 cells." *Mol. Biol. Cell*. UCRL-JC-150105 Abs.

Section 3 Chemistry

01-ERD-063

Beller, H. R. (2002). "Anaerobic biotransformation of RDX (hexahydro-1,3,5-trinitro-1,3,5-triazine) by aquifer bacteria using hydrogen as the sole electron donor." *Water Res.* **36**, 2533–2540. UCRL-JC-141362.

Beller, H. R. (2001). "Anaerobic metabolism of RDX (hexahydro-1,3,5-trinitro-1,3,5-triazine) by aquifer bacteria using hydrogen as the sole electron donor." *Proc. Am. Soc. for Microbio. 101st Gen. Meet.* UCRL-JC-141362 Abs.

Beller, H. R. (2002). "Analysis of benzylsuccinates in groundwater by liquid chromatography/tandem mass spectrometry and its use for monitoring in situ BTEX biodegradation." *Environ. Sci. & Tech.* **36**, 2724–2728. UCRL-JC-147921.

Beller, H. R. (2001). "Detection of distinctive indicators of intrinsic RDX metabolism in groundwater at an Army Ammunition Plant." *Proc. Tri-Service Environ. Tech. Symp.* UCRL-JC-142677 Abs.

Beller, H. R. and K. Tiemeier. (2002). "Use of liquid chromatography/tandem mass spectrometry to detect distinctive indicators of in situ RDX transformation in contaminated groundwater." *Environ. Sci. & Tech.* **36**, 2060–2066. UCRL-JC-143125 Rev1.

Beller, H. R. et al. (2002). "Biochemical and genetic evidence of benzylsuccinate synthase in toluene-degrading, ferric iron-reducing *Geobacter metallireducens*." *Proc. Am. Soc. for Microbio. 102nd Gen. Meet.* UCRL-JC-146414 Abs.

Kane, S. R. et al. (in press). "Biochemical and genetic evidence of benzylsuccinate synthase in toluene-degrading, ferric iron-reducing *Geobacter metallireducens*." *Biodegradation*. UCRL-JC-146414.

01-ERD-064

Gates-Anderson, D. D., C. A. Laue, and T. E. Fitch. (2002). "Development of a waste treatment process to deactivate reactive uranium metal and produce a stable waste form." *Proc. Waste Mgmt. 2002*. UCRL-JC-147189.

Laue, C.A., D. D. Gates-Anderson, and T. E. Fitch. (2002). "Deactivation of pyrophoric uranium metal—attempts to elucidate the chemical reaction mechanisms." *Proc. Am. Chem. Soc. 2002 Rocky Mountain Regional Meet.* UCRL-JC-149443.

01-ERD-103

De Pater, I. (in press). "Keck adaptive optics images of Uranus and its rings." *Icarus*. UCRL-JC-147365.

Fried, L. E. and R. H. Gee. (2003). "Ultrafast crystallization of polar polymer melts." *J. Chem. Phys.* **188**(8), 3827–3834. UCRL-JC-147887.

Gee, R. H. et al. (2002). *Theoretical study of intermolecular interactions in the molecular crystal of TATB*. UCRL-JC-150607.

Gee, R. H., S. Roszak, and L. E. Fried. (2002). "Theoretical studies of interactions between TATB molecules and the origins of anistropic thermal expansion and growth." *Proc. 33rd Intl. Conf. ICT*, 30. UCRL-JC-146807.

02-ERD-015

Balasubramanian, K. (2002). *Theoretical study of aqueous uranyl carbonate (UO_2CO_3) and its hydrated complex*. UCRL-JC-150618.

Majumdar, D., K. Balasubramanian, and H. Nitsche (2002). "A comparative theoretical study of bonding in UO_2^{++}, UO_2^{+}, UO_2, $OUCO_1$, $O_2U(CO)_2$ and UO_2CO_3." *Chem. Phys. Lett.* **242**, 143–151. UCRL-JC-148500.

Majumdar, D., K. Balasubramanian, and H. Nitsche. (in press). "Theoretical study of aqueous uranyl carbonate (UO_2CO_3) and its hydrated complexes." *Chem. Phys. Lett.* UCRL-JC-145545.

02-ERD-021

Sutton, M. and S. R. Burastero. (2002). *Beryllium chemical speciation in elemental human biological fluids*. UCRL-JC-150385.

Sutton, M. and S. R. Burastero. (2002). *Examining beryllium chemistry with modern analytical techniques*. UCRL-JC-147978 Abs.

Sutton, M. et al. (2002). "Modern chemistry techniques in the medical chelation of beryllium." *Pharmacologist* **44**, A174. UCRL-JC-147010 Abs.

02-ERD-027

Glaude, P. A. et al. (in press). "Detailed chemical kinetic reaction mechanisms for incineration of organophosphorus and fluoro-organophosphorus compounds." *Proc. Combustion Inst.* UCRL-JC-146563.

00-LW-010

Hope-Weeks, L. J. (2002). *Preparation and functionalisation silicon nanocrystals via a solution synthesis.* Presented at the Chemistry and Materials Science Directorate Post Doc Symp. UCRL-PRES-149681.

Hope-Weeks, L. J., B. R. Taylor, and G. A. Fox. (2002). "Preparation of colloidal germanium nanocrystals with novel surface termination." *Abstr. Pap. Am. Chem. Soc.* **223**, 383. UCRL-PRES-146217.

Hope-Weeks, L. J., B. R. Taylor, and G. A. Fox. (2002). "Preparation of functionalised silicon nanocrystals." *Abstr. Pap. Am. Chem. Soc.* **223**, 045. UCRL-PRES-146058.

Taylor, B. R. et al. (2001). "Solution preparation of Ge nanoparticles with chemically tailored surfaces." *Sci. & Eng. B* **96**(2), 89–92. UCRL-JC-145430.

01-LW-018

Vance, A. L. et al. (2002). "XAS and XPS characterization of monolayers derived from a dithiol and structurally related disulfide-containing polyamides. *Langmuir* **18**, 8123–8128. UCRL-JC-145977.

Vance, A. L. et al. (2003). "XAS and XPS characterization of a surface-attached rotaxane." *Nano Lett.* **3**, 81–84. UCRL-JC-149987.

01-LW-039

Baumann, T. F., B. R. Hart, and J. H. Satcher, Jr. (2002). *Template-directed preparation of periodic macroporous organic and carbon aerogels*. UCRL-JC-149721.

Section 4 Earth and Space Science

00-SI-004

Eggleton, P. P. (2002). "Envelope ejection: an alternative evolutionary process for some early Case B binaries." *Astrophys. J.* **575**, 1037. UCRL-JC-147726.

Eggleton, P. P. (2002). "Three incomprehensible binaries, exotic stars as challenges to evolution." *IAU Coll. 187* (ASP Conf. Ser.). UCRL-JC-147735.

Eggleton, P. P. and L. Kiseleva-Eggleton. (2002). "The evolution of cool algols." *Astrophys. J.* **575**, 461. UCRL-JC-148457.

Eggleton, P. P. and L. Kiseleva-Eggleton, (2002). "Orbital evolution in binary and triple stars, with special reference to SS Lac." *Astrophys. J.* **562**, 1012. UCRL-JC-145927.

Keller, S. C. and K. H. Cook (2003). "Variable Red Giants—the MACHO View Relation." *Proc. 201st Meet. of the Am. Astronom. Soc.* UCRL-JC-151332.

Keller, S. C. and P. R. Wood. (2002). "Large Magellanic cloud bump cepheids: probing the stellar mass-luminosity relation." *Astronom. J.* UCRL-JC-148958.

Keller, et al. (2002). "Blue variable stars from the MACHO database." *Astronom. J.* UCRL-JC-148953 Pt1.

Keller, S C. et al. (2002). "UBVI and H (alpha particle) photometry of the H and X Persei Cluster." *Astronom. J.* UCRL-JC-143309.

Richard, O. et al. (2002). "Models of metal-poor stars with gravitational settling and radiative accelerations: I. Evolution and abundance anomalies." *Astrophys. J.* **568**, 979. UCRL-JC-146578.

Turcotte, S. (2002). "Djehuty: A code for modeling whole stars in three dimensions." *IAU Coll. 185* (ASP Conf. Ser.) **259**, 72. UCRL-JC-145807.

Turcotte, S. (in press). "Mixing and accretion in lambda Bootis Stars." *Astrophys. J. Lett.* UCRL-JC-148660.

Turcotte, S. and O. Richard. (in press). "On variability, or its absence, in HgMn Stars." *Asteroseismology*. UCRL-JC-150091.

Turcotte, S., C. Aerts, and P. Knoglinger. (in press). "Searching for line profile variations in HgMn Star." *Asteroseismology*. UCRL-JC-150094.

Turcotte, S. and R. F. Wimmer-Schweingruber. (in press). "Possible in situ of the evolution of elemental and isotopic abundances in the solar convection zone." *J. Geophys. Res.: Space Phys.* UCRL-JC-149653.

01-SI-008

Duffy, P. B. et al. (in press). "High resolution simulations of global climate using the CCM3 atmospheric general circulation model." *Climate Dynam.* UCRL-JC-149235.

Govindasamy, B., K. Caldeira, and P. B. Duffy. (in press). "Geoengineering Earth's radiation balance to mitigate climate change from a quadrupling of CO_2." *Global and Planetary Change*. UCRL-JC-140243.

Govindasamy, B., P. B. Duffy, and K. Caldeira. (2001). "Land use change and Northern Hemisphere cooling." *Geophys. Res. Lett.* **28**, 291. UCRL-JC-137478.

Govindasamy, B. et al. (in press). "High-resolution global simulation of the climatic effects of increased greenhouse gases." *Climate Dynam.* UCRL-JC-148726.

Govindasamy, B. et al. (in press). "Impact of climate stabilization schemes on the terrestrial biosphere." *Geophys. Res. Lett.* UCRL-JC-149732.

Govindasamy, B. et al. (2001). "Limitations of the equivalent CO_2 approximation in climate change simulations." *J. Geophys. Res.* **106**, 22593. UCRL-JC-34980.

99-ERD-065

Wurtz, R. et al. (in press). "LIFTS: An imaging Fourier transform spectrograph for astronomy." *ASP Conf. Ser*. UCRL-JC-147937.

00-ERD-011

Kersting, A. B. et al. (2002). *Colloid-facilitated transport of low-solubility radionuclides: A field, experimental and modeling investigation*. UCRL-ID-149688.

00-ERD-049

Bauman, B. J. et al. (2002). "Proposed multiconjugate adaptive optics experiment at Lick Observatory." *Proc. SPIE* **4494**, 81. UCRL-JC-145061.

Bauman, B. J. et al. (2002). "Update on optical design of adaptive optics system at Lick Observatory." *Proc. SPIE* **4494**, 19. UCRL-JC-145173.

Bogdanovic, T. et al. (2003). "Near-IR imaging and spectroscopy of NGC 6240 with adaptive optics." *Bull. Am. Astronom. Soc.* **199**, 49.03. UCRL-JC-151216 Abs.

Brotherton, M. S. et al. (2002). "Hubble Space Telescope imaging of the poststarburst quasar UN J1025-0040: Evidence for recent star formation." *Proc. Astronom. Soc. of the Pacific* **114**, 593. UCRL-JC-151352.

Christou, J. C. et al. (2002). "Preliminary measurements of residual tip-tilt motion and Strehl ratios for laser guide star compensation at Lick Observatory." *Proc. SPIE* **4494**, 317. UCRL-JC-151687.

Gates, E. L. et al. (2002). "Observations of quasar hosts with the Lick adaptive optics system." *Bull. Am. Astronom. Soc.* **200**, 05.13. UCRL-JC-151351.

Gavel, D. T. (2003). "Suppressing anomalous localized waffle behavior in least squares wavefront reconstructors." *Proc. SPIE* **4839**, 972. UCRL-JC-147287.

Gavel, D. T. and D. Wiberg. (2003). "Toward Strehl-optimizing adaptive optics controllers." *Proc. SPIE* **4839**, 890. UCRL-JC-147283.

Gavel, D. T. et al. (2002). "Recent science and engineering results with the laser guide star adaptive optics system at Lick Observatory." *Proc. SPIE* **4839**, 354. UCRL-JC-147284.

Max, C. E. et al. (2001). "Adaptive optics observations of the core of Cygnus A." *Bull. Am. Astronom. Soc.* **199**, 68.02. UCRL-JC-146661 Abs.

01-ERD-013

De Pater, I. (in press). "Keck adaptive optics images of Uranus and its rings." *Icarus*. UCRL-JC-147365.

Gibbard, S. G. et al. (2002). "High-resolution infrared imaging of Neptune from the Keck Telescope." *Icarus* **156**, 1. UCRL-JC-135712.

01-ERD-023

Berryman, J. G., P. A. Berge, and B. P. Bonner. (2002). "Estimating rock porosity and fluid saturation using only seismic velocities." *Geophys.* **67**, 391–404. UCRL-JC-135507.

Berge, P. A. and B. P. Bonner. (2002). *Seismic velocities contain information about depth, lithology, fluid content, and microstructure*. UCRL-JC-144792.

Farber, D. L. et al. (2002). "Observations of a water induced transition from brittle to viscoelastic behavior in nanocrystalline swelling clay." *Eos, Trans. Am. Geophys. U*. UCRL-JC-145246 Abs.

Toffelmier, D. et al. (2002). "Load dependence of ultrasonic velocities for sand and sand/clay mixtures." *Eos, Trans. Am. Geophys. U*. UCRL-JC-145264 Abs.

01-ERD-065

Kane, S. R. et al. (2001). "Aerobic biodegradation of methyl tert-butyl ether by aquifer bacteria from leaking underground fuel tank sites." *Appl. and Environ. Microbio.* **67**, 5824–5829. UCRL-JC-143865-DR.

02-ERD-044

Larsen, S. C. (2002). *Las Vegas Basin Seismic Response Project: 3-D finite-difference ground motion simulations*. Presented at the Am. Geophys. U. Fall Meet. UCRL-JC-149756 Abs.

Rodgers, A. J. and D. B. McCallen. (2002). *Las Vegas Basin Seismic Response Project: Overview and site response*. Presented at the Am. Geophys. U. Fall Meet. UCRL-JC-149853 Abs.

Shen, J. H. J., A. Astaneh-Asl, and D. B. McCallen. (2002). "Use of deep columns in special moment resisting frames." *Steel Tips of the Structural Steel Education Council*. UCRL-JC-148802.

02-ERD-052

Wurtz, R. E. et al. (in press). "Astronomy with a visible-band imaging Fourier transform spectrometer." *ASP Conf. Ser.* UCRL-JC-147937.

Wurtz, R. E. et al. (in press). "Gallery of datacubes obtained with the Livermore imaging Fourier transform spectrometer." *Proc. SPIE*. UCRL-JC-150958.

00-ERI-009

Benedetti, L. et al. (2002). "Post-glacial slip history of the Sparta fault (Greece) determined by ^{36}Cl cosmogenic dating: Evidence for non-periodic earthquakes." *Geophys. Res. Lett.* **28**, 87-1–87-4. UCRL-JC-146922.

Murphy, M. A. et al. (2002). "Structural evolution of the Gurla Mandhata detachment system, southwest Tibet: Implications for the eastward extent of the Karakoram Fault system." *Geol. Soc. Am. Bull.* **114**, 428+. UCRL-JC-146944.

Van der Woerd, J. et al. (2002). "The November 14th, 2001 Mw = 7.8 Kokoxili Earthquake in Northern Tibet (Qinghai Province, China)." *Seismolog. Res. Lett.* **73**, 125–135. UCRL-JC-146848.

00-ERI-010

Reimer, P. J. et al. (2002). "An integrated approach to understanding controls on soil carbon sequestration." *Proc. 9th Intl. Conf. on Accel. Mass Spectrom.*, Sept. 9–13, Nagoya, Japan. UCRL-MI-150577.

01-ERI-003

Carilli, C. L. et al. (2002). "The x-ray/radio alignment in the z = 2.2 radio galaxy PKS 1138-262."*Astrophys. J.* **567**, 781. UCRL-JC-146227.

Dawson, S. et al. (2002). "A galactic wind at z = 5.190."*Astrophys. J.* **570**, 92. UCRL-JC-146228.

De Breuck, C. et al. (2002). "Optical and near-IR imaging of ultra steep spectrum sources." *Astron. J.* **123**, 637. UCRL-JC-145778.

De Breuck, C. et al. (2002). "Radio AGN surveys." *IAU Colloq.* **184**. UCRL-JC-148807.

de Vries, W. H. et al. (2002). "Deep Westerbork 1.4 GHz imaging of the Bootes Field." *Astron. J.* **123**, 1784. UCRL-JC-145797.

de Vries, W., W. van Breugel, and A. Quirrenbach. (in press). "Adaptive optics observations of three powerful radio galaxies." *SPIE Conf. Proc.* UCRL-JC-149438.

van Breugel, W. (2002). *Starbursts forever*. Presented at LLNL Science on Saturdays, March 2, 2002. UCRL-JC-147264.

van Breugel, W. et al. (in press). "BRIGHT lights, BIG City: Massive galaxies, giant Ly-a nebulae, and proto-clusters." *SPIE Conf. Proc.* UCRL-JC-149640.

01-ERI-004
Amelin, Y. et al. (2002). "Lead isotopic ages of chondrules and calcium-aluminum-rich inclusions." *Science* **297**, 1678. UCRL-JC-149449.

Krot, A., I. D. Hutcheon, and K. Keil. (2002). "Plagioclase-rich chondrules in the reduced CV chondrites: Evidence for complex formation history and genetic links between CAIS and ferromagnesian chrondrules." *Meteoritics and Planet. Sci.* **37**, 155. UCRL-JC-146346.

01-ERI-009
Guilderson, T. P., D. P. Schrag, and M. A. Cane. (2002). *Surface water mixing in the Solomon Sea as documented by a high-resolution coral-^{14}C record*. Presented at the 2002 Ocean Sciences Meet., Feb. 11–15, Honolulu, HI. UCRL-JC-142826 Abs.

02-LW-022
Glaesemann, K. R. and L. E. Fried, "An improved heat capacity estimator for path integral simulations." *J. Chem. Phys.* **117**, 3020. UCRL-JC-147423.

Glaesemann, K. R. and L. E. Fried, "An improved thermodynamic energy estimator for path integral simulations." *J. Chem. Phys.* **116**, 5951. UCRL-JC-144960.

Glaesemann, K. R. and L. E. Fried. (in press). "A path integral approach to molecular thermochemistry." *J. Chem. Phys.* UCRL-JC-149046.

Guilderson, T. P. (2002). *Radiocarbon as a diagnostic of ocean circulation and the marine carbon cycle*. Presented at the Am. Chem. Soc. Ann. Meet., Orlando, FL. UCRL-JC-140481.

Section 5 Energy Supply and Use

00-ERD-059
Cherepy, N.J. and Fiet, K.J. (2003). *Direct conversion of carbon fuels into electricity in a molten carbonate fuel cell: Final report*. UCRL-JC-151539.

Cherepy, N. et al. (2002). *Direct carbon fuel cells: Technology feasibility plan*. UCRL-ID-150103.

Steinberg, M., J. F. Cooper, and N. Cherepy. (2002). "High efficiency direct carbon and hydrogen fuel cells for fossil fuel power generation." *Proc. AIChE Spring Meet. 2002*, 78f. UCRL-JC-146774.

01-ERD-089
Heller, A. (2001). "Probing the subsurface with electromagnetic fields." *LLNL Sci. and Tech. Rev.,* Nov. 2001, 12–19. UCRL-JC-52000-01-11.

Kirkendall, B. and J. Roberts. (2002). "Reservoir characterization: Electromagnetic imaging of CO_2 for EOR processes." *Proc. DOE-SPE Improved Oil Recovery Conf.*, 2. UCRL-JC-155231.

Kirkendall, B. and J. Roberts. (2001). "Reservoir management of sequestrated CO_2 using borehole electromagnetic tomographic imaging." *Proc. Intl. Gas Res. Conf.*, 12. UCRL-JC-144655.

01-ERD-091
Caldeira, K., M. E. Wickett, and G. Rau. (2002). "Comparing pH impacts and ocean CO_2 storage from atmospheric CO_2 release, oceanic CO_2 injection, and injection with carbonate dissolution." *Proc. 2002 Am. Geophys. U. Spring Meet.*, May 28–31, Washington, DC. UCRL-JC-147567 Abs.

Hoffert, M. I. et al. (in press). "Advanced technology paths to global climate stability energy for greenhouse planet." *Science*. UCRL-JC-144122.

Caldeira, K. (2002). "Monitoring of ocean storage projects." *Proc. IPCC Workshop on Carbon Separation and Storage*, Nov. 19–21, Regina, Canada. UCRL-JC-150681 Abs.

Caldeira, K., M. E. Wickett, and G. Rau. (2002). "Atmospheric CO_2 concentrations and ocean pH impacts resulting from atmospheric CO_2 release, ocean CO_2 injection, and accelerated carbonate weathering." *Proc. 2002 Am. Geophys. U. Fall Meet.*, Dec. 6–10, San Francisco, CA. UCRL-JC-149771 Abs.

01-ERD-100
Chen, H. P. (2002). *Electron productions from short-pulse laser plasma interactions*. Presented at the 44th Ann. Meet. Div. of Plasma Phys., Orlando, FL. UCRL-JC-149722 Abs.

Chen, H. P. et al. (in press). "A novel compact electron spectrometer for hot electron measurement in pulsed laser solid interaction." *Rev. Sci. Instr.* UCRL-JC-149724.

Chen, H. P. et al. (2002). *Short-pulse laser produced hot electron measurement using a novel compact electron spectrometer*. Presented at the 14th Topical Conf. on High-Temp. Plasma Diag., Madison, WI. UCRL-JC-148355 Abs.

McLean, H. S. et al. (2002). *FLIRT: A field line tracing diagnostic for self-organized, magnetically confined plasmas*. Presented at the 14th Topical Conf. on High-Temp. Plasma Diag., Madison, WI. UCRL-JC-148674 Abs.

McLean, H. S. et al. (2001). "FLIRT: A magnetic field topology diagnostic for self-organized magnetically confined plasmas." *Bull. Am. Phys. Soc.* **46**, 159. UCRL-JC-144624 Abs.

McLean, H.S. et al. (2002). "Injection of high-energy electrons into a spheromak to map our magnetic field lines." Presented at the 44th Ann. Meet. of the Div. of Plasma Phys., Orlando, FL. UCRL-JC-149195 Abs.

McLean, H. S. et al. (in press). "A laser-based diagnostic for tracing magnetic field lines in spheromaks and other self-organized magnetically confined plasmas." *Rev. Sci. Instr.* UCRL-JC-149196.

Ryutov, D. D. (2001). "The dynamics of fast electrons in a spheromak." *Bull. Am. Phys. Soc.* **46**, 159. UCRL-PRES-144605.

Ryutov, D. D. (2002). *Space-charge effects in the emission of fast electrons generated by a short laser pulse*. UCRL-JC-144196.

02-ERD-056
Van Dam, C.P., et al. (2002). *Computational design and analysis of a microtab based aerodynamic loads control system for lifting surfaces*. UCRL-JC-150324.

01-ERI-007
Buchholz, B. A. et al. (2001) "Isoptopic tracing of fuel component carbon in the emissions from diesel engines." *SAE Tech. Paper* 2002-01-1942. UCRL-JC-145698.

Buchholz, B. A., A. S Cheng, and R. W. Dibble. (2001). "Isotopic tracing of bio-derived carbon from ethanol-in-diesel blends in the emissions of a diesel engine." *SAE: Research in Alt. Fuel Devel.,* SP-1716, 37. UCRL-JC-146603.

Buchholz, et al. (2001). "Tracing fuel component carbon in the emissions from diesel engines." *9th Intl. Conf. on Accel. Mass Spectrom.* UCRL-JC-149036 Abs.

Buchholz, B. A., et al. (2002). "Tracing fuel component carbon in the emissions from diesel engines." *9th Intl. Conf. on Accel. Mass Spectrom.* UCRL-MI-149036-poster.

02-LW-043
Post, R. F. (2003). "The Kinetic Stabilizer: Further calculations and options." *Fusion Tech.* **43**, 195. UCRL-JC-148763.

Post, R. F. (in press). "The Kinetic Stabilizer: Issues and opportunities." *Plasma Phys. Reports.* UCRL-JC-146667.

02-FS-020
Kesler, O. and R. L. Landingham. (in press). "Improvements in mechanical behavior of SOFC anodes." *Proc. Matls. Res. Soc. Fall 2002 Meet.* UCRL-JC-148801.

Section 6 Engineering and Manufacturing Processes

01-ERD-005
Castillo, P. et al. (in press). "A discrete differential forms based framework for electromagnetism." *Comp. Modeling in Sci. and Engr.* UCRL-JC-149836.

Koning, J. and D. White. (2002). *A discrete forms framework for optical waveguides*. Presented at the SIAM Ann. Meet. U CRL-MI-148820.

White, D., P. Castillo, and R. Rieben. (2002). *FEMSTER Documentation*. <http://www.llnl.gov/casc/femster>. (Retrieved March 2003). UCRL-WEB-147600.

White, D. and R. Rieben. (2002). *Generalized high order interpolatory 1-form bases for computational electromagnetics*. Presented at the IEEE APS Symp. & URSI Meet. UCRL-JC-146726.

01-ERD-080
Morse, J. et al. (2002). "A MEMS-based fuel cell for micropower energy conversion." *Proc. Electrochem. Soc. Spring Symp.*, May 2002. UCRL-ID-147074.

01-ERD-087
Dinh, L. N. et al. (2002). "Properties of GaAs nanoclusters deposited by a femtosecond laser." *J. Matl. Sci.* **37**, 3953–3958. UCRL-JC-142798.

Section 7 Materials Science and Technology

01-SI-004
Hsiung, L. M. and D. H. Lassila. (2002). "Initial dislocation structure and dynamic dislocation multiplication in Mo single crystals." *Comp. Model. in Eng. and Sci.* **3**, 185. UCRL-JC-138788.

Lassila, D. H., M. M. LeBlanc, and G. J. Kay. (2002). "Uniaxial stress deformation experiments for validation of 3-D dislocation dynamics simulations." *J. Eng. Mat. and Tech.* **124**, 290. UCRL-JC-146808.

Lassila, D. H. et al. (2001). "Dislocation dynamics validation experiments." *Plasticity 2002*. UCRL-JC-145290 Abs.

Moriarty, J. A. et al. (2002). "Quantum-based atomistic simulation of materials properties in transition metals. *J. Phys.: Condensed Matter* **14**, 2825. UCRL-JC-146608.

Tang, M. and L. P. Kubin. (2001). "Boundary conditions for dislocation dynamics simulations and stage 0 of bcc metals at low temperature." *Matl. Res. Soc. Proc.* **AA1.2**. UCRL-JC-143692.

Yang, L. H. and J. A. Moriarty. (2001). "Kink-pair mechanisms for a/2 <111> screw dislocation motion in bcc tantalum." *Matl. Sci. and Eng. A* **124**, 319. UCRL-JC-136573.

Yang, L. H., P. Soderlind, and J. A. Moriarty. (2002). "Atomistic simulation of defects in bcc tantalum." *Proc. CIMTE-2002*. UCRL-JC-148128.

01-SI-007

Baldis, H. et al. (2002). *Numerical simulations of attosecond x-ray strobe light produced by colliding laser pulses*. Presented at the Ann. Meet. of the Am. Phys. Soc. Div. Plasma Phys. UCRL-JC-149372.

Brown, W. et al. (2002). "RF phase stability & electron beam characterization for the PLEIADES Thomson x-ray source." *Proc. 27th IEEE Intl. Conf. on Infrared and Millimeter Waves*. UCRL-JC-147968.

Gibson, D. J. et al. (2002). *Design and characterization of a TW-class hybrid chirped pulse amplification system for production of x rays via Thomson scattering*. Presented at the Ann. Meet. of the Am. Phys. Soc. Div. Plasma Phys. UCRL-JC-149375 Abs.

Jovanovich, I. and C. P. J. Barty. (2002). *Hybrid chirped amplification*. Presented at the 2002 Conf. on Lasers and Electro-Optics. UCRL-JC-146224.

Jovanovich, I., C. A. Ebbers, and C. P. J. Barty. (2002). "Hybrid chirped amplification." *Opt. Lett.* **27**, 1622. UCRL-JC-146224 Rev3.

Springer, P. et al. (2002). "Electron beam production and characterization for the PLIEADES Thomson X-ray source." *Proc. Workshop on Adv. Accel. Concepts 2002*. UCRL-JC-149374.

Tremaine A. and P. Springer. (2002). "Ultrafast materials probing at PLEIADES, a subpicosecond x-ray source at the LLNL electron linac." *Proc. XXI Intl. Linac Conf.* UCRL-JC-147864.

00-ERD-031

Bonev, S. et al. (2002). *High-pressure molecular phases of carbon dioxide.* UCLR-JC-151202.

Hood, R. Q. and G. Galli. (2002). *Insulator to metal transition in fluid hydrogen.* UCRL-JC-146651 Abs.

Militzer, B., F. Gygi, and G. Galli. (2002). *Structure and bonding of dense liquid oxygen for first principles simulations.* UCRL-JC-151201.

01-ERD-018

Ehrenfreund, P. et al. (2002). "Astrophysical and astrochemical insights into the origin of life." *Reports Prog. Phys.* **65**, 1427–1487. UCRL-ID-148252.

01-ERD-022

Becker, R. et al. (2002). "How metals fail." *LLNL Sci. and Tech. Rev.* July/August 2002, 13–20. Reprinted as "Understanding Metal-Failure Dynamics." *Industrial Heating,* November 2002. UCRL-52000-02-7/8.

Rudd, R. and J. Belak. (2002). "Void nucleation and associated plasticity in dynamic fracture of polycrystalline copper: An atomistic simulation, computational materials." *Science* **24**, 148–53. UCRL-JC-144339.

01-ERD-026

Campbell, G. H. and M. Kumar. (in press). "Effect of laser shock processing on the microstructure and mechanical properties of pure Cu." *Zeitschrift für Metallkunde*. UCRL-JC-150085.

01-ERD-028

Balazs, G. B. et al. (2002). "Damage mechanisms of filled siloxanes for predictive multiscale modeling of aging behavior." *MRS Spring 2002 Meet. Abs.* UCRL-JC-145943.

Balazs, G. B. et al. (2002). "Techniques for the analysis of aging signatures of silica-filled siloxanes." *MoDeSt Conf. Abs.* UCRL-JC-146413.

Maxwell, R. S., and G. B. Balazs. (2002). "Residual dipolar coupling for the assessment of crosslink density changes in gamma-irradiated silica-PDMS composite materials. *J. Chem. Phys.* **116**, 10492. UCRL-JC-145154.

01-ERD-029

Blobaum, K. et al. (2002). *Investigating the delta/alpha' martensitic phase transformation in Pu-Ga alloys*. Presented at the 2nd Intl. Workshop on Orbital and Spin Magnetism of Actinides. UCRL-MI-149588 Abs.

Haslam, J. J. et al. (2002). *Investigation of differences in morphology and transformation mechanisms of alpha formed from delta plutonium at low temperatures*. Presented at the 2003 TMS Ann. Meet. UCRL-JC-149061 Abs.

Krenn, C. R. et al. (2002). *Effects of local solute ordering and plasticity on the delta to alpha transformation in gallium stabilized plutonium alloys*. Presented at the 2nd Intl. Workshop on Orbital and Spin Magnetism of Actinides. UCRL-JC-149837 Abs.

Krenn, C. R. et al. (2002). *Influence of local solute ordering and plasticity on the martensitic transformation kinetics of plutonium alloys*. Presented at the 2003 TMS Ann. Meet. UCRL-JC-149178 Abs.

Krenn, C. et al. (2002*). Phase field modeling of metal hydride growth in a plastically deforming matrix*. Presented at the 2003 TMS Ann. Meet. UCRL-JC-149179 Abs.

01-ERD-030

Allen, P. G. et al. (2002). "Vibrational properties of Ga-stabilized delta-Pu by extended x-ray absorption fine structure." *Phys. Rev. B* **65**, 214107. UCRL-JC-146442.

01-ERD-036

Jackson, D. D. (in press). "Magnetic susceptibility measurements at high pressure using designer diamond anvils." *Rev. Sci. Instr.* UCRL-JC-149345.

01-ERD-042

Asoka-Kumar, P. et al. (2002). "Composition and magnetic character of nanometer Cu-precipitates in reactor pressure vessel steels: Implications to nuclear power plant lifetime extension." *Phil. Mag. Lett.* **82**, 609. UCRL-JC-145328.

Marian, J. et al. (2002). "Dynamics of self-interstitial cluster migration in pure α Fe and Fe-Cu alloys." *Phys. Rev. B* **65**, 144102. UCRL-JC-144102 Rev1.

Wirth, B. D. et al. (2002). *Characterization of nonstructural features in irradiated reactor pressure vessel model alloys*. Presented at the 10th Intl. Symp. on Environ. Degradation of Matls. in Light Water Reactors. UCRL-JC-145544.

01-ERD-054

Hart, B. R. et al. (2002). *Development of an enzyme-based photoluminescent porous silicon detector for CW*. Presented at the Am. Vacuum Soc. Topical Conf. UCRL-MI-148261 Abs.

Hart, B. R. et al. (2003). "New method for attachment of biomolecules to porous silicon." *Chem. Comm.* **3**, 222. UCRL-JC-150438.

01-ERD-082

Howard, W. M. (2001). *Modeling of shock waves in silica aerogel.* Presented at the 12th Intl. Detonation Symp. UCRL-JC-144970.

Howard, W. M. (2002). *Warm dense matter in colliding shock compressed silica aerogel*. Presented at the 1st Intl. Conf. on Warm Dense Matter, June 2002, Hamburg, Germany. UCRL-JC-147603.

Howard, W. M. et al. (2002). *Shock propagation and instability structures in compressed silica aerogel*. UCRL-JC-146894.

Molitoris, J. D. et al. (2002). *Measurements of shock propagation in silica aerogels for the generation of warm dense matter*. Presented at the 12th Intl. Detonation Symp. UCRL-JC-145033.

Molitoris, J. D. et al. (2002). *Measurements of shock propagation in silica aerogels for the generation of warm dense matter*. Presented at the 1st Intl. Conf. on Warm Dense Matter, June 2002, Hamburg, Germany. UCRL-JC-148416.

Molitoris, J. D. et al. (2001). *Shock propagation and instability structure in silica aerogels*. Presented at the 54th Meet. of the APS Div. of Fluid Dyn. UCRL-JC-145032.

Molitoris, J. D. et al. (2002). *Warm dense matter with energetic materials*. Presented at the 1st Intl. Conf. on Warm Dense Matter, June 2002, Hamburg, Germany. UCRL-JC-148417 Abs.

01-ERD-085

Niew, T. G., C. A. Schuh, and J. Wadsworth. (in press). "Strain rate-dependent deformation in bulk metallic glasses." *Intermetallics* **10**(12). UCRL-JC-146890.

Schuh, C. A., T. G. Nieh, and Y. Kawamura. (2002). "Rate dependence of serrated flow during nanoindentation of a bulk metallic glass." *J. Matl. Res.* **17**, 1651–54. UCRL-JC-146730.

Schuh, C., T. G. Nieh, and T. Yamasaki. (2002). "Hall-Petch breakdown manifested in abrasive wear resistance of nanocrystalline nickel." *Scripta Materialia* **46**, 735–40. UCRL-JC-146358.

01-ERD-086

Noy, A., et al. (2002). "Fabrication and imaging of luminescent nanostructures and nanowires using dip-pen nanolithography." *Nano Lett.* **2**, 109. UCRL-JC-145323.

Weeks, B. L. et al. (2002). "Importance of dissolution kinetics in controlling feature size during dip-pen nanolithography." *Phys. Rev. Lett.* **88**, 255505. UCRL-JC-146855.

02-ERD-039

Minich, R. W., C. A. Schuh, and M. Kumar. (2002). "The role of topological constraints on the statistical properties of grain boundary networks." *Phys. Rev. B* **66**, 052101. UCRL-JC-147509.

Section 8 Mathematics and Computing Sciences

00-SI-002

Bernholdt, D. et al. (2002). *A component architecture for high-performance computing*. Presented at the Workshop on Perf. Optimiz. for High-Level Lang. and Lib. UCRL-JC-148723.

Kumfert, G. (2002). *Understanding the CCA standard through decaf*. UCRL-MA-148390.

01-SI-003

Aines, R. D. et al. (2002). *The stochastic engine: Improving prediction of behavior in geologic environments we cannot directly observe*. UCRL-ID-148221.

00-ERD-016

Hittinger, J. A. F. et al. (2002). "Theoretical model and numerical simulation of energy transfer between crossing laser beams in an expanding plasma." *Proc. 2002 Anomalous Absorption Conf.*, 1–6. UCRL-JC-148435 Abs.

Kirkwood, R. K. et al. (in press). "Observation of saturation of energy transfer between co-propagating beams in a flowing plasma." *Phys. Rev. Lett.* UCRL-JC-148550.

Kirkwood, R. K. et al. (2002). "Scaling of energy transfer between crossing laser beams with beam intensity and plasma density and temperature." *Proc. 2002 Anomalous Absorption Conf.*, O1–2. UCRL-JC-148991 Abs.

Williams, E. A. et al. (2002). "Saturation of crossed beam and SBS interactions by trapping induced frequency shifts." *Proc. 2002 Anomalous Absorption Conf.*, O1–1. UCRL-JC-148398 Abs.

00-ERD-017

Fast, P. and W. D. Henshaw. (2002). *Applications involving moving grids and adaptive mesh refinement on overset grids*. Presented at the 32nd AIAA Fluid Dynamics Conf. AIAA Paper 2002–1411. UCRL-JC-147263.

Henshaw, W. D. (in press). "An algorithm for projecting points onto a patched CAD model." *Eng. with Computers*. UCRL-JC-144016.

Henshaw, W. D. (2002). "Generating composite overlapping grids on CAD geometries." *Proc. 8th Intl. Conf. on Numerical Grid Generation in Comp. Field Sim*. UCRL-JC-147161.

Henshaw, W. D. (2002). "Overture: An object-oriented framework for overlapping grid applications." *Proc. 32nd AIAA Conf. on Appl. Aerodynam.* UCRL-JC-147889.

Petersson, N. A. (2002). *Applying Overture to CFD computations for ships*. Presented at Chalmers University of Technology. UCRL-JC-150390 Abs.

Petersson, N. A. (2002). "Overlapping grid generation on CAD models." *Proc. 6th Overset Meet.* UCRL-PRES-149939.

Petersson, N. A. (2002). "A software demonstration of 'rap': Preparing CAD geometries for overlapping grid generation." *Proc. of 8th Intl. Conf. on Numerical Grid Generation in Comp. Field Sim.* UCRL-JC-147260.

00-ERD-018

Chartier, A. J. et al. (in press). "Spectral AMGe." *SIAM J. Sci. Comp.* UCRL-JC-146369.

Vassilevski, P. S. (2002). "Sparse matrix element topology with application to AMG(e) and preconditioning." *Num. Lin. Algebra with Appl.* **9**, 429-444. UCRL-JC-147872.

01-ERD-004

Laursen, T. A., M. A. Puso, and M. Weinstein. (2002). "Practical issues associated with mortar projection in large deformation contact/impact analysis." *Proc. 5th World Cong. Comp. Mech.* **1**, 651. UCRL-JC-14894.

Puso, M. A. and T. L. Laursen. (in press). "Mesh tying on curved interfaces in 3D." *Eng. Comp.* UCRL-JC-148193.

Puso, M. A. and T. L. Laursen. (2002). "A 3D contact smoothing method." *Proc. 5th World Cong. Comp. Mech.* **1**, 525–535. UCRL-JC-148192.

01-ERD-008

Meyer, A., D. W. Paglieroni, and C. Astaneh. (2003). *K-means reclustering: algorithmic options with quantifiable performance comparisons*. Presented at SPIE Photonics West 2003, January 25–31, San Jose, CA. UCRL-JC-151259.

Paglieroni, D. (2003). *A self-calibrating multi-band region growing approach to segmentation of single and multi-band images*. Presented at SPIE Photonics West 2003, January 25–31, San Jose, CA. UCRL-JC-150988.

01-ERD-024

Bradley, M. M. (2001). *A national wildfire behavior prediction initiative: Full-physics models on supercomputers*. Presented at California 2001 Wildfire Conf. UCRL-JC-147051 Abs.

Hanson, H. P. et al. (2000). "The potential and promise of physics-based wildfire simulation." *Environ. Sci. and Policy* **3**, 161–172. UCRL-JC-147078.

Heller, A. (2002). "This model can take the heat." *LLNL Sci. and Tech. Rev.*, Nov. 2002. UCRL-52000-02-11.

Wagoner, R., M. M. Bradley, and R. R. Linn. (2001). *Roadmap for a national wildland fire research and development program*. Presented at Am. Meteorolog. Soc. 4th Symp. on Fire and Forest Meteorology. UCRL-JC-151907.

01-ERD-043

Marathe, J. et al. (2003*). METRIC: Tracking down inefficiencies in the memory hierarchy via binary rewriting*. Intl. Symp. on Code Generation and Optimization, March 23–26, San Francisco, CA. UCRL-JC-151497.

01-ERD-044

Fattebert, J.-L. and F. Gygi. (2002). "Density functional theory for efficient ab initio molecular dynamics simulations in solution." *J. Comp. Chem* **23**, 662. UCRL-JC-143326.

01-ERD-073

Hewett, D. W. (in press). "Fragmentation, merging, and internal dynamics for collisional PIC simulation with finite size particles." *J. Comp. Phys.* UCRL-JC-148430.

Larson, D. J. (in press). "A Coulomb collision model for PIC plasma simulation." *J. Comp. Phys.* UCRL-JC-148993.

02-ERD-034

Kamath, C. et al. (2003). "Use of machine vision techniques to detect human settlements in satellite images." *Proc. Image Processing: Algorithms and Systems II, SPIE Electronic Imagery* **5014**, January 2003. UCRL-JC-150218.

Sengupta, S. K. et al. (2003). "Detecting human settlements in satellite imagery." *Proc. Optical Engineering at the Lawrence Livermore National Laboratory, SPIE Lasers and Applications in Science and Engineering* **5001**, January 2003. UCRL-JC150220.

02-ERI-003

Gregorski, B. et al. (in press). "Interactive view-dependent rendering of large iso-surfaces." *IEEE Visualiz. 2002*. UCRL-JC-146819.

Lindstrom P. and V. Pascucci. (2002). "Terrain simplification simplified: A general framework for view-dependent out-of-core visualization." *IEEE Trans. on Comp. Graphics* **8**(3), 239–254. UCRL-JC-147847.

Lindstrom P. and V. Pascucci. (2001). "Visualization of large terrains made easy." *IEEE Visualiz. 2001*, 363–370. UCRL-JC-144753.

Lindstrom P. and C. Silva. (2001). "A memory insensitive technique for large model simplification." *IEEE Visualiz. 2001*, 121–126. UCRL-JC-144550.

Pascucci, V. (2002). "Slow growing subdivision (SGS) in any dimension: Towards removing the curse of dimensionality." *Comp. Graphics Forum* **21-3**, 451–460. UCRL-JC-144257.

Pascucci V. and K. Cole-McLaughlin. (in press). "Efficient computation of the topology of level sets." *Algoritmica*. UCRL-JC-149277.

Pascucci, V. and R. J. Frank. (in press). "Hierarchical indexing for out-of-core access to multi-resolution data." *Hierarchical Approximation and Geometrical Methods for Scientific Visualization*. UCRL-JC-140581.

02-ERI-007

Anderson, J. and T. Critchlow. (2002). *Design of wrapper integration within the DataFoundry bioninformatics application*. UCRL-ID-149835.

Crtichlow, T. (2001). *Challenges in microbial database interoperability working group position paper*. UCRL-ID-146327.

Critchlow, T. (2001). *DataFoundry data warehousing and integration for scientific data management*. UCRL-TB-127593.

Critchlow, T. (2001). *Enabling large-scale data access*. UCRL-PROP-143828.

Lehman, S. K. and S. J. Norton. (2002). *Radial reflection diffraction tomography*. UCRL-ID-149016.

Liu, L. et al. (2002). *BioZoom: Exploiting source-capability information for integrated access to multiple bioinformatics data sources*. UCRL-JC-146952.

Rocco, D. and T. Critchlow. (2002). *Discovery and classification of bioinformatics web services*. UCRL-JC-149963.

01-LW-068
Castillo, P. et al. (2002). "A discrete differential forms based framework for electromagnetism." *Comp. Model. in Sci. and Engr.* UCRL-JC-149836.

Koning, J. and D. White. (2002). *A discrete forms framework for optical waveguides*. Presented at the SIAM Ann. Meet., July 8–12, Philadelphia, PA. UCRL-MI-148820.

White, D. and J. Koning. (2002). *A discrete differential forms framework for wave equations*. Presented at the SIAM Ann. Meet., July 8–12, Philadelphia, PA. UCRL-JC-147162.

White, D. and R. Rieben. (2002). *Generalized high order interpolatory 1-form bases for computational electromagnetics*. Presented at the 2002 IEEE APS Ann. Meet., June 16–21, San Antonio, TX. UCRL-JC-146726.

White, D., P. Castillo, and R. Rieben. (2002). *FEMSTER Documentation*. <http://www.llnl.gov/casc/femster>. (Retrieved March 2003). UCRL-WEB-147600.

Section 9 Nuclear Science and Engineering

01-ERD-033
Amendt, P. et al. (2001). "Hohlraum-driven noncryogenic double-shell ignition target designs for the National Ignition Facility." *Inertial Fusion Sci. and Appl. 2002* **2**, 217. UCRL-JC-143188.

Amendt, P. et al. (2002). "Indirect-drive noncryogenic double-shell ignition targets for the National Ignition Facility: Design and analysis." *Phys. Plasmas* **9**, 2221. UCRL-JC-145878.

Amendt, P. et al. (2002). "Modified Bell-Plesset effect with compressibility: Application to double-shell ignition target designs. *Phys. Plasmas* **10**, 820. UCRL-JC-148944.

01-ERD-069
Koniges, A. K. et al. (2002). "Magnetic topology of a candidate NCSX plasma boundary configuration." *Nucl. Fusion* **43**(2), 107–118. UCRL-JC-147845.

Umansky, M. et al. (in press). "Modeling of localized neutral particle sources in 3D edge plasmas." *J. Nucl. Mat.* UCRL-JC-147590.

Section 10 Physics

00-SI-005
Asner, D. (2002). *Prospect for discovering H^0,A^0 in two-photon collisions at a linear collider*. UCRL-JC-148615.

Asner, D. (in press). "Studying standard model-like Higgs bosons in two-photon collisions at a linear collider." *Intl. J. Mod. Phys*. UCRL-JC-148614.

Asner, D., J. Gronberg, and J. F. Gunion. (in press). "Detecting and studying two-photon collisions at a linear collider." *Phys. Rev. D*. UCRL-ID-143967.

Asner, D. et al. (2002). "Higgs physics with a gamma–gamma collider based on CLIC I." *Eur. Phys. J. C*. UCRL-JC-145692.

Asner, D. et al. (2002). *New results for a photon collider*. UCRL-JC-149844.

Caturla, M. J. et al. (2002). *Report on radiation damage effects in a titanium target under photon irradiation*. UCRL-ID-149951.

Stein, W. and J. C. Sheppard. (2002). *NLC polarized positron photon beam target thermal structural modeling*. UCRL-ID-148940.

01-SI-005
Sunwoo, A. J. et al. (2002). *Characterization of W-26% Re target material.* UCRL-ID-149787.

02-SI-004
Jovanovic, I., C. A. Ebbers, and C. P. J. Barty. (2002). "Hybrid chirped pulse amplification." *Optics Lett*. **27**, 1622. UCRL-JC-146224 Rev3.

00-ERD-025

Kuba, J. et al. (2002). *X-ray optics research for free electron lasers: Study of material damage under extreme fluxes*. UCRL-JC-149090 Abs.

Kuba, J. et al. (2002). "X-ray optics research for the Linac Coherent Light Source: Interaction of ultra-short X-ray laser pulses with optical materials." *Proc. 8th Intl. Conf. on X-Ray Lasers*. UCRL-JC-147682 Abs.

London, R. A. et al. (2002). "Computational simulations of high intensity x-ray matter interaction." *Proc. SPIE* **4500**, 51. UCRL-JC-142074.

Ryutov, D. D. and A. Toor. (2001). "Optical elements based on the use of renewable liquid films with magneto-electrostatic control." *Rev. Sci. Instr.* **72**, 4042. UCRL-JC-141538.

Wootton, A. J. and D. D. Ryutov. (2003). "Compton scattering and photoluminescence for x-ray imaging." *Rev. Sci. Instr.* **74**, 1180. UCRL-JC-149563.

Wootton, A. J. and D. D. Ryutov. (2001). *Imaging weakly perturbing diagnostics of an x-ray beam at the LCLS facility (physics issues)*. UCRL-ID-145967.

Wootton, A. J. et al. (2002). "Research and development for x-ray optics and diagnostics on the Linac Coherent Light Source (LCLS)." *Nucl. Instr. & Meth.* **A483**, 345. UCRL-JC-145122.

Wootton, A. J. et al. (2002). "X-ray optics and diagnostics for the first experiments on the Linac Coherent Light Source." *Proc. SPIE* **4500**, 113. UCRL-JC-144183.

00-ERD-026

Adcox, K. et al. (2002). "Centrality dependence of +/–, p and $\bar{p}$ production from (sqrt) S_{NN} = 130 GeV Au + Au collisions at RHIC." *Phys. Rev. Lett.* **88**(24), 242301. UCRL-JC-147214.

Adcox, K. et al. (2002). "Transverse mass dependence of the two-pion correlation function in Au-Au collisions at sqrt(s) = 130 GeV/*c*." *Phys. Rev. Lett.* **88** (19), 192302. UCRL-JC-147237.

Burward-Hoy, J. M. (2002). "Centrality dependence of inclusive identified hadrons in PHENIX." *Proc. 18th Winter Workshop on Nucl. Dyn.* UCRL-JC-147945.

Johnson, S. C. (2002). "Particle correlations with the PHENIX experiment." *Proc. 18th Winter Workshop on Nucl. Dyn.* UCRL-JC-147865.

00-ERD-028

Caurier, E. et al. (2002) "Ab initio shell model for A = 10 nuclei." *Phys. Rev. C* **66**, 024314. UCRL-JC-148460.

Marsden, D. C. J. et al. (in press). "Feasibility study of a three-nucleon force in the no-core shell model: ^{3}H binding energy." *Phys. Rev. C*. UCRL-JC-148973.

Navratil, P. (2002). "Ab initio no-core shell model." *Bull. APS* **47**, 62. UCRL-JC-149305 Abs.

Navratil, P. and W. E. Ormand. (2002). "Ab initio shell model calculations with three-body effective interactions for p-shell nuclei." *Phys. Rev. Lett.* **88**, 152503. UCRL-JC-146446.

00-ERD-037

Beiersdorfer, P. et al. (in press). "Laboratory studies of the x-ray emission produced by the interaction of solar wind heavy ions with comets," *Proc. of the NASA Laboratory Astrophys. Workshop*, May 1–3, NASA Ames, Moffett Field, CA. UCRL-JC-147239.

Beiersdorfer, P. et al. (2002). "New Insights into the x-ray spectra of heliumlike and neonlike ions." *Proc. of Atomic Processes in Plasmas,* April 22–25, Gatlinburg, TN, 135–144. UCRL-JC-148356.

Beiersdorfer, P. et al. (in press). "Overview of the Livermore Electron Beam Ion Trap Project." *Nucl. Instr. Meth.* UCRL-JC-148354.

01-ERD-014

Aubert, B. et al. (2002). "Measurement of $B \rightarrow K^*\gamma$ branching fractions and charge asymmetries. *Phys. Rev. Lett.* **88**, 101805. UCRL-JC-150945.

Aubert, B. et al. (2002). "Measurement of B^0/anti-B^0 flavor oscillations in hadronic B^0 decays." *Phys. Rev. Lett.* **88**, 221802. UCRL-JC-150098.

Aubert, B. et al. (2002)."A study of time-dependent *CP*-violating asymmetries and flavor oscillations in neutral *B* decays at the upsilon(4S)." *Phys. Rev. D* **66**, 32003. UCRL-JC-150934.

01-ERD-015

Asoka-Kumar, P. R. et al. (2002). "Opportunities for materials characterization using high-energy positron beams." *Appl. Surface Sci.* **194**, 160. UCRL-JC-145018.

Denison, A. B. et al. (2002). "Observation of positron annihilation in CdSe quantum dots." *Phys. Rev. B* **66**, 041305. UCRL-JC-150685.

Eshed, A. S. et al. (2002). "Gamma spectra resulting from the annihilation of positrons with electrons in a single core level." *Phys. Rev. Lett.* **89**, 075503. UCRL-JC-145231.

Meulenberg, R. W. et al. (2002). "Positron annihilation in nanocrystal quantum dots." *Bull. APS* **47**, 1252. UCRL-JC-148538.

Sterne, P. A., P. Asoka-Kumar, and R. H. Howell. (2002). "Atomic-based calculations of two-detector Doppler-broadening spectra." *Appl. Surface Sci.* **194**, 71. UCRL-JC-144719.

Sterne, P. A. et al. (in press). "New theories for positrons in insulators." *Rad. Phys. & Chem.* UCRL-JC-148530.

01-ERD-017

Grossman, J. C. (2002). "Benchmark quantum Monte Carlo calculations." *J. Chem. Phys.* **117**, 1434. UCRL-JC-147602.

Grossman, J. C. and W. A. Lester, Jr. (2002). "Quantum Monte Carlo for the electronic structure of combustion systems." *Recent Advances in Quantum Monte Carlo—Volume II*, 159. W. Lester et al. (ed.), World Scientific Publishing. UCRL-JC-144783.

Grossman, J. C. et al. (2002). "Aromaticity and hydrogenation patterns in highly strained fullerenes." *Chem. Phys. Lett.* **356**, 247. UCRL-JC-146046.

Puzder, A. et al. (2002). *Passivation effects of silicon nanoclusters*. UCRL-JC-149129.

Puzder, A. et al. (2002). "Simulation of semiconductor nanoclusters." *Physica Status Solidi.* **233**, 39. UCRL-JC-144762.

Puzder, A. et al. (2002). "Surface chemistry of silicon nanoclusters." *Phys. Rev. Lett.* **88**, 097401. UCRL-JC-145443.

Puzder, A. et al. (2002). "Surface control of optical properties in silicon nanoclusters." *J. Chem. Phys.* **117**, 6721. UCRL-JC-148961.

Williamson, A. J. et al. (2002) *Accurate prediction of nanostructure optical gaps: Application to silicon quantum dots*. UCRL-JC-148678.

01-ERD-019

Dunn, J. et al. (2002). "A picosecond 14.7-nm x-ray laser for probing matter undergoing rapid changes." *AIP Proc. 8th Intl. Conf. X-Ray Lasers*. UCRL-JC-149104.

Dunn, J. et al. (2002). *Small-scale soft x-ray lasers for probing matter*. Presented at the APS Laser Sci. XVIII Symp. UCRL-JC-149091 Abs.

Nelson, A. J. et al. (2002). *Time-of-flight x-ray photoelectron spectroscopy with an x-ray laser source*. Presented at the 8th Intl. Conf. X-Ray Lasers, May 2002, Aspen, CO. UCRL-JC-147929 Abs.

01-ERD-031

Bringa, E. et al. (in press). "Metals far from equilibrium: from shocks to radiation damage." *Nucl. Instr. and Meth. B*. UCRL-JC-148559.

01-ERD-083

Dawson, J. et al. (in press). "983-nm Nd-doped high-power cladding pumped fiber amplifier." *2003 Tech. Digest Adv. Solid State Photonics*. OSA Topical Meeting. UCRL-JC-150354.

Dawson, J. et al. (in press). "High-power 938-nm cladding pumped fiber laser." *Proc. SPIE Photonics West Lasers and Appl. in Sci. and Eng.* UCRL-JC-148985 Abs.

Pennington, D. M. (2002). "Laser guided adaptive optics for high-resolution astronomy." *CLEO Tech. Digest* **73**, 68. UCRL-JC-146335 Abs.

Pennington, D. M. (2002). *Laser technologies for laser-guided adaptive optics*. Presented at the NATO Adv. Study Inst. on Optics in Astrophys. UCRL-PRES-150503.

Pennington, D. M. et al. (2002). "Compact fiber laser approach to generating 589-nm laser guide stars." *Proc. SPIE Astron. Tel. and Instr.* **4839**. UCRL-JC-143873 Abs Rev.

Ziao, Z. M. et al. (2001). *Turnkey fiber laser system for laser guide stars*. Presented at NSF Center for Adaptive Optics Fall Retreat. UCRL-PRES-146670.

01-ERD-097

Bionta, R.M. et al. (2002). *Research and development for x-ray optics and diagnostics on the Linac Coherent Light Source*. UCRL-JC-145122 Rev1.

01-ERD-107

Divol, L. (2002). *Workshop on the nonlinear saturation of stimulated Raman and Brillouin instabilities for plasma and laser parameters of interest to inertial fusion confinement and high-density science*. UCRL-JC-148983 SUM.

Divol, L. et al. (2002). *Nonlinear behavior stimulated Brillouin scattering in 1-D hybrid PIC simulations of a 500-μm-long Be plasma*. UCRL-PRES-148447.

Divol, L. et al. (2002). *Nonlinear saturation of stimulated Brillouin scattering for long time scales*. UCRL-JC-149983.

Froula, D. H. et al. (2002). *Laser–plasma interaction experiments in the nonlinear saturated regime.* UCRL-JC-149002 Abs.

Froula, D. H. et al. (2002). "Measurement of nonlinear growth of ion-acoustic waves in tow-ion-species plasmas with Thomson scattering."*Phys. Rev. Lett.* **88**, 105001. UCRL-JC-145688.

Froula, D. H. et al. (in press). "Observation of ion heating by SBS-driven ion-acoustic waves using Thomson scattering." *Phys. Plasmas*. UCRL-JC-145885.

Froula, D. H. et al. (2002). *Search for SBS-saturation processes with Thomson scattering experiments on ion-acoustic waves in beryllium plasmas.* UCRL-PRES-148448.

Glenzer, S. H. et al. (2002)."Anomalous absorption of high-energy green laser light in high-Z plasmas." *Phys. Rev. Lett.* **88**, 235002. UCRL-JC-145287.

Mounaix, P. and L. Divol. (2002). Near-threshold reflectivity fluctuations in the independent-convective-hot-spot limit of a spatially smoothed laser beam." *Phys. Rev. Lett.* **89**, 165002. UCRL-JC-148982.

02-ERD-012

Borghesi, M. et al. (2002). "Electric field detection in laser-plasma interaction experiments via the proton imaging technique." *Phys. Plasmas* **9**, 2214. UCRL-JC-147112.

Mackinnon, A. J. et al. (2002). "Enhancement of proton acceleration by hot-electron recirculation in thin foils irradiated by ultraintense laser pulses." *Phys. Rev. Lett.* **88** (21), 215006. UCRL-JC-145540.

Mackinnon, A. J. et al. (in press). "First observation of moiré fringes in a proton beam generated by a 100 femtosecond laser pulse." *Rev. Sci. Inst*. **74**. UCRL-JC-149131.

02-ERD-013

Glenzer, S. H. (2001). "Dense plasma characterization by x-ray Thomson scattering." *APS Div. Plasma Phys. Bull.* **46**, 325. UCRL-JC-144574 Abs.

Glenzer, S. H. (2002). *Dense plasma characterization by x-ray Thomson scattering*. Presented at Intl. Conf. on Strongly Coupled Coulomb Systems. UCRL-PRES-138258 Rev1.

Glenzer, S. H. and O. L. Landen. (2002). *Warm dense matter characterization by x-ray Thomson scattering*. Presented at Intl. Conf. on Warm Dense Matter. UCRL-JC-138258 Abs Rev.

Glenzer, S. H. et al. (in press). "Demonstration of x-ray Thomson scattering. *Phys. Rev. Lett.* UCRL-JC-149694.

Glenzer, S. H. et al. (in press) "Ionization balance measurements from solid-density plasmas by x-ray Thomson scattering." *APS Div. Plasma Phys. Bull.* UCRL-JC-149135 Abs.

Gregori, G., S. H. Glenzer, and O. L. Landen. (in press). "Theoretical model and interpretation of x-ray Thomson scattering." *Phys. Rev. E.* UCRL-JC-147395.

Gregori, G., O. L. Landen, and S. H. Glenzer. (2002). *Interpretation of x-ray Thomson scattering in warm dense matter*. Presented at Intl. Conf. on Strongly Coupled Coulomb Systems. UCRL-JC-148984 Abs.

Gregori, G. et al. (in press). "Analysis of x-ray scattered spectra for solid density plasmas." *APS Div. Plasma Phys. Bull.* UCRL-JC-149081 Abs.

Gregori, G. et al. (2002). Calculations and measurements of x-ray Thomson scattering in warm dense matter. *Proc. 16th Intl. Conf. on Spectral Line Shapes*. UCRL-JC-148076.

02-ERD-023

Edwards, J., A. MacKinnon, and H. Robey. (2001). *Application of gaseous laser targets and optical diagnostics to study high mach number unstable plasma flows*. UCRL-ID-143428.

02-ERD-024
Bringa, E. M. et al. (2002). *Shock propagation in defective single crystals*. Presented at the Conf. on Comp. Phys. 2002, Aug. 2002, San Diego, CA. UCRL-JC-149641 Abs.

Remington, B. A. et al. (2002). *Materials science at extreme pressures and strain rates*. Presented at the 44th Ann. Meet. Div. of Plasma Phys., Nov. 2002, Orlando, FL. UCRL-JC-149202 Abs.

Remington, B. A. et al. (2002). *Materials science under extreme conditions of pressure and strain rates*. Presented at 132nd Ann. Meet. Minerals, Metals & Matls. Soc. (TMS), Mar. 2003, San Diego, CA. UCRL-JC-149205 Abs.

Stölken, J. S. et al. (2002). *Atomistic modeling of spherical shocks*. Presented at Intl. Conf. on Shock Waves in Condensed Matter, Sept. 2002, St. Petersburg, Russia. UCRL-PRES-149842.

02-ERD-028
Ormand, W. E. and P. Navratil. (2002). "Recent applications of the ab initio, no-core model." *Bull. APS* **47**, 35. UCRL-JC-149304 Abs.

02-ERD-043
Bostedt, C. and T. Van Buuren. (2002). "Photoemission spectroscopy of germanium nanocrystal films." *J. Electron Spectroscopy and Rel. Phenom.* **126**, 117. UCRL-JC-149020.

Bostedt, C. and T. Van Buuren. (in press). "Electronic structure of germanium nanocluster films." *J. Electron Spectroscopy and Rel. Phenom.* UCRL-JC-148288.

Catellani, A. and G. Galli Gygi. (in press). "Physical properties of SiC surfaces." *Mat. Sci. Res. B*. UCRL-JC-136186.

Galli, G. and L. Pizzagalli. (in press). "Surface reconstruction effects on the atomic properties of germanium nanoparticles." *Matl. Sci. & Eng. B*. UCRL-JC-147182.

Raty, J-Y and G. Galli Gygi. (in press). "Bucky diamond." *Phys. Rev. Lett.* UCRL-JC-148251.

Raty, J-V, J. P. Gaspar, and C. Bichara. (in press). "Properties of molten Ge chalcogenides: an ab-initio molecular dynamics study." *J. Phys. Cond. Matter*. UCRL-JC-147931.

Raty, J-V et al. (2002). *Optical and structural properties of hydrogenated nanodiamonds*. Presented at Meet. of the Am. Phys. Soc., Mar. 2002. UCRL-JC-146691 Abs.

00-ERI-004
Demos, S. G. et al. (2002). "Application of fluorescence microscopy for noninvasive detection of surface contamination and precursors to laser-induced damage." *Appl. Optics* **41**, 1977–1983. UCRL-JC-144941.

Demos, S. G. et al. (2002). "Investigation of processes leading to damage growth in optical materials for large-aperture lasers." *Appl. Optics* **41**, 3628–3633. UCRL-JC-144946.

Demos, S. G. et al. (2002). "New evidence of the displacive feature of the ferroelectric transition in KDP-type crystals." *J. Condensed Matter Phys. C.* **14**(4): L89–L93. UCRL-JC-144361.

Jiang, H. et al. (2001). "Nanosecond time-resolved multi-probe imaging of laser damage in transparent solids." *Appl. Phys. Lett.* **81**, 3149–3151. UCRL-JC-139577.

02-ERI-004
Baldis, H. A. et al. (2001). "Experimental characterization of a high-brightness X-band photoinjector." *Bull. APS* **46**, 127. UCRL-JC-144648 Abs.

Baldis, H. et al. (in press). "Numerical simulations of attosecond x-ray strobe light produced by colliding laser pulses." *Bull. APS*. UCRL-JC-149372 Abs.

Brown, W. J. et al. (in press). "Electron beam production & characterization for the PLEIADES Thomson x-ray source." *Bull. APS*. UCRL-JC-149374 Abs.

Brown, W. J. et al. (2002). "RF phase stability & electron beam characterization for the PLEIADES Thomson x-ray source." *Proc. 27th IEEE Intl. Conf. on Infrared and Millimeter Waves*. UCRL-JC-147968 Abs.

Gibson, D. J. and F. V. Hartemann. (2001). "Experimental observation of coherent synchrotron radiation in an X-band photoinjector." *Bull. APS* **46**, 127. UCRL-JC-144646 Abs.

Gibson, D. J. et al. (in press). "Design and characterization of a TW-class hybrid chirped pulse amplification system for production of x-rays via Thomson scattering." *Bull. APS*. UCRL-JC-149375 Abs.

Hartemann, F. V. (2002). "Novel advanced x-ray source concepts based on Compton scattering and Bragg resonance channeling." *IEEE Conf. Record*, 02CH37340, 139. UCRL-JC-146925 Abs
Hartemann, F. V. et al. (2001). "Three-dimensional theory of Compton scattering." *Bull. APS* **46**, 128. UCRL-JC-144676 Abs.

Hartemann, F. V. et al. (in press). "Time and frequency-domain calculations of x-ray production for the PLEIADES Thomson x-ray source." *Bull. APS*. UCRL-JC-149373 Abs.

Kerman, A. K. et al. (2001). "Nonlinear laser acceleration in a magnetostatic field and the chirped-pulse inverse free-electron laser." *Bull. APS* **46**, 128. UCRL-JC-144647 Abs.

Springer, P. T. et al. (2002). "Ultrafast materials probing at PLEIADES, a subpicosecond x-ray source at the LLNL electron linac." *Proc. XXI Intl. Linac Conf*. UCRL-JC-147864 Abs.

02-LW-026

Garrett P. E. et al. (2002). "The new data acquisition system for the 8(pi) (gamma)-ray spectrometer at TRIUMF-ISAC." *Bull. APS* **47**, 101. UCRL-JC-149468-Abs.

Kulp, W. D. et al. (2002). "Multi-step Coulomb excitation of 152Sm studied with gammasphere plus CHICO." *Bull. APS* **47**, 93. UCRL-JC-149461 Abs.

Svensson C. E. et al. (in press). "Radioactive beam experiments with large gamma-ray detector arrays." *Nucl. Instrum. Methods B*. UCRL-JC-149024.

02-LW-042

Beiersdorfer, P. et al. (2002). "The transition energy of the 3s-3p spectral line in sodium-like uranium." *Bull. APS*. UCRL-JC-147335 Abs.

Beiersdorfer, P. et al. (2002). "X-ray emission from highly charged ions colliding with a relativistic electron beam in the SuperEBIT Electron Beam Ion Trap." *Proc. X-Ray and Inner-shell Process Conf.* UCRL-JC-149433.

Sapirstein, J. and K. T. Cheng. (in press). "Calculation of the Lamb shift in neutral alkalis." *Phys. Rev. A*. UCRL-JC-148767.

Sapirstein, J. and K. T. Cheng. (in press). "Calculation of the radiative corrections to hyperfine splittings in the neutral alkalis." *Phys. Rev. A*. UCRL-JC-150452.

Principal Investigator Index

Project Title Index

Tracking Code Index

The movie shows the diffraction-limited image of a single plasmon resonant particle (PRP) viewed through a darkfield microscope. The PRP is being moved in a circular motion (100-nm diam) by a piezoelectrically driven ultraprecise x-y translation stage.
(Click on movie frame to run movie.)

back